1967

4th U.S. NAVY SYMPOSIUM ON MILITARY OCEANOGRAPHY

THE PROCEEDINGS OF THE SYMPOSIUM

10-12 May 1967

VOLUME I

DATA LIBRARY & ARCHIVES
Institution

WHOI
DOCUMENT
COLLECTION

NAVAL RESEARCH LABORATORY
WASHINGTON, D.C.

Each transmittal of this document outside the agencies of the U.S. Government must have prior approval of The Oceanographer of the Navy, 732 N. Washington Street, Alexandria, Va. 22314.

Papers have b publication substantially
as

be requested from the
ron Station, Alexandria,

4th US Navy Symposium
10-12May 67,
graphy, D. C.
Washington,

RETURNED
22 Dec 67
5 June 68
23 Sep 76
Elroy Tallio

4th U.S. NAVY SYMPOSIUM ON MILITARY OCEANOGRAPHY

THE PROCEEDINGS OF THE SYMPOSIUM

VOLUME I

NAVAL RESEARCH LABORATORY

WASHINGTON, D.C.

MBL/WHOI
0 0301 0045419 5

SPONSOR

Oceanographer of the Navy

CO-SPONSORS

Office of Chief of Naval Operations
Office of Naval Research
Office of Naval Material
Naval Ships Systems Command
Naval Electronics Systems Command
Naval Air Systems Command
Naval Ordnance Systems Command
Naval Facilities Engineering Command Headquarters
Naval Air Development Center
Naval Civil Engineering Laboratory
Naval Oceanographic Office
Naval Ordnance Test Station
Naval Research Laboratory
Naval Underwater Weapons Research and Engineering Station
Naval Underwater Sound Laboratory
Naval Weather Service
Navy Electronics Laboratory
Navy Mine Defense Laboratory
Naval Radiological Laboratory
Naval Applied Science Laboratory
Navy Marine Engineering Laboratory
Naval Ordnance Laboratory
Supervisor of Salvage

STEERING COMMITTEE

Captain R. A. Zettel
Commander R. W. Haupt
Mr. B. K. Couper
Mr. Fred Knoop
Dr. Victor Linnenbom
Dr. Donald P. Martineau
Mr. W. H. Hymes
Mr. Murray Schefer

PROGRAM COMMITTEE

Dr. V. J. Linnenbom, Naval Research Laboratory, Chairman
Dr. N. S. Rakestraw, Naval Research Laboratory
Mr. J. Schule, Naval Oceanographic Office
Mr. M. Schefer, Naval Air Systems Command
Commander R. W. Haupt, USN, CNO (OP09B5)
Dr. H. McLellan, Office of Naval Research

TABLE OF CONTENTS

Page

OPENING ADDRESS
Honorable Robert A. Frosch vii

BANQUET ADDRESS
Honorable Robert H. B. Baldwin xiii

SESSION A - GENERAL SESSION

AN ANALYTICAL REVIEW OF LESSONS LEARNED FROM THE H-BOMB SEA SEARCH OFF SPAIN
F. A. Andrews 3

SUBMARINE TOPOGRAPHIC ECHOES FROM CHASE V
J. Northrop 29

NEL MANNED SUBMERSIBLE OCEANOGRAPHIC SYSTEM, MODIFICATION I
A. J. Schlosser 42

SESSION B - THE OCEAN BOTTOM

ENVIRONMENTAL LIMITATIONS TO DEEP SEA SEARCH
F. N. Spiess, J. D. Mudie, and C. D. Lowenstein 69

DIRECT MEASUREMENT OF BOTTOM SLOPE, SEDIMENT SOUND VELOCITY AND ATTENUATION, AND SEDIMENT SHEAR STRENGTH FROM DEEPSTAR 4000
E. C. Buffington, E. L Hamilton, and D. G. Moore 81

VARIABILITY IN DERIVED SEDIMENT SOUND VELOCITY AS A FUNCTION OF CORE ANALYSIS TECHNIQUES AND ITS EFFECT IN DETERMINING THEORETICAL BOTTOM REFLECTIVITY
J J. Gallagher 91

STRANGE HOT WATERS AND MINERALS AT THE BOTTOM OF THE RED SEA
J. M. Hunt and D. A. Ross 102

MILITARY SIGNIFICANCE OF DEEPLY SUBMERGED SEA CLIFFS AND ROCKY TERRACES ON THE CONTINENTAL SLOPE
R. F. Dill 106

SESSION C - OCEANOGRAPHIC PREDICTION

REAL-TIME OCEANOGRAPHIC DATA FOR OCEANOGRAPHIC PREDICTION
K. M. Palfrey, Jr. 121

DATA REQUIREMENTS FOR SYNOPTIC SEA SURFACE TEMPERATURE ANALYSES
R. W. James 125

LARGE-SCALE ANOMALOUS SEA SURFACE CONDITIONS IN THE NORTH PACIFIC
J. D. Isaacs 152

ENERGY SPECTRA OF THE SEA FROM PHOTOGRAPHS
D. Stilwell 171

NUMERICAL PREDICTION OF GEOSTROPHIC FLOW DERIVED FROM SEA-SURFACE TEMPERATURE
J. G. Welsh 184

THE FNWF SOUND MAP PROGRAM
CAPT P. M. Wolff, USN, LCDR P. R. Tatro, USN, and LCDR L. D. Megehee, USN 195

SESSION E
OCEAN ENGINEERING AND TECHNOLOGY

CONCRETE HULLS FOR UNDERSEA HABITATS
J. D. Stachiw 219

FIVE YEARS EXPERIENCE WITH A SHIPBOARD OCEANOGRAPHIC DATA PROCESSING SYSTEM: HINDSIGHT AND FORESIGHT
C. O. Bowin 253

CORROSION OF MATERIALS IN HYDROSPACE
F. M. Reinhart 265

SENSORS, CONTROLS, AND DISPLAYS OF THE DEEP SUBMERGENCE RESEARCH VEHICLE (DSRV)
S. K. Sezack 289

THE "FAIL-SAFE" PROGRAM FOR PREVENTION OF LOSSES OF OCEANOGRAPHIC EQUIPMENT
R. L. Stewart and G. Poudrier 294

SESSION F - MARINE SCIENCES RESEARCH

LONG RANGE OCEAN ACOUSTICS AND SYNOPTIC OCEANOGRAPHY – STRAITS OF FLORIDA RESULTS
J. G. Clark and J. R. Yarnall 309

OCEANIC TURBULENCE AND AMPLITUDE FLUCTUATION IN ACOUSTIC SIGNALS
L. C. Breaker and W. B. O'Neil, Jr. 366

SIPHONOPHORES AND THEIR RELEASED BUBBLES AS ACOUSTIC TARGETS WITHIN THE DEEP SCATTERING LAYER
G. V. Pickwell 383

MIGRATION AND TEMPERATURE STRUCTURE OF EDDIES ON THE LEEWARD SIDE OF THE HAWAIIAN ISLANDS
E. L. Smith 396

POSITIONING OF THE GULF STREAM BY MEANS OF AERIAL INFRARED RADIATION THERMOMETER MEASUREMENTS
J. C. Wilkerson 415

COMPARISON OF MINIMUM DETECTABLE LIGHT LEVELS AND THE LEVEL OF STIMULATED MARINE BIOLUMINESCENCE IN OCEAN WATERS
S. J. Neshyba 428

ADDRESS TO THE 4TH U. S. NAVY SYMPOSIUM
ON MILITARY OCEANOGRAPHY
OPENING SESSION, DEPARTMENT OF STATE AUDITORIUM
WASHINGTON, D. C. - 10 MAY 1967

by

Honorable Robert A. Frosch
Assistant Secretary of the Navy for
Research and Development

Mr. Chairman, Admiral Waters, Captain Owen, Gentlemen:

Many things have happened since the last Symposium on Military Oceanography was held a year ago at the Naval Electronics Laboratory in San Diego.

Superlatives are always suspect but I will risk one and say that the year that has passed since then has been the greatest year in the history of American oceanography from an administrative and organizational standpoint. The scientific, economic and national defense benefits that will flow from this strengthened organization in the field of oceanography cannot be far behind. Since I am talking to a most knowledgeable group of ocean scientists I need not go into detail about the events of the past year. But I will tick off a few highlights just for the record.

About a month after you last met, the so-called PSAC report was published by the President's Science Advisory Committee. It was entitled, "Effective Use of the Sea". In it the Committee alternatively "pointed with pride" and "viewed with alarm" in a report so informed and forthright that it is certain to affect the course of oceanography for many a year.

Almost simultaneously with the release of the PSAC report the President signed the Marine Resources and Engineering Development Act of 1966. This law, as you know, set up a National Council headed by the Vice President and made up of cabinet members and agency heads with a major interest in oceanography.

The law further empowered the President to appoint an advisory commission of 15 experts from the academic world industry, marine laboratories and the federal and state governments to assist the Council in working out a balanced long-range national oceanographic program.

This was followed a few months later by the National Sea Grant College and Program Act. This legislation provides grants to public and private institutions to promote both education and applied research in the oceanographic field.

Meanwhile the Secretary of the Navy, seconded by the Chief of Naval Operations, took action not only to strengthen the Navy's oceanographic program but to strengthen the Navy's ability to cooperate effectively with all other agencies and industries involved in our national oceanographic effort.

In an instruction issued in August 1966, the Secretary set up the Office of the Oceanographer of the Navy. The new head of that Office, Rear Admiral Waters, reports through me to the Secretary for policy control and directly to the Chief of Naval Operations for operational control. His job is to integrate and direct the Navy's entire oceanographic effort including research, engineering, and Fleet support.

I mention these developments, well known as they are to you, to remind you that your deliberations at this Fourth Annual Symposium are taking place against a backdrop of greatly enhanced national purpose and direction in the whole field of oceanography.

So far as our oceanographic problems are concerned they are still with us in spite of the good progress made in many areas.

The Vietnam War for instance has brought a whole new array of challenges involving both oceanography and hydrography. We have seven survey ships on rotational duty there right now. And we are concerned not only with such traditional matters as mapping and charting and oceanographic survey work in support on mine warefare, amphibious operations and shore bombardment. We are also actively involved now in river warfare all up and down the Mekong Delta. Some of the new problems involved in this kind of operation call for all of the brains and imagination we can muster.

Our first responsibility of course is to our fighting forces in Vietnam. But we must be on guard lest we shirk our responsibility for developing techniques and hardware to be ready in case of need in other types of war in other times and places. And oceanographic research must go hand-in-hand with, and in most cases precede, the development of new naval weapons systems. Although we are all hopeful of better relations with the Soviet Union we cannot ignore the fact that the Soviets continue to pursue an aggressive submarine building program. It is only reasonable to assume that their construction rate for nuclear-powered submarines will continue to increase, and that conventional submarines will eventually be phased out of their fleet.

We do know that the Soviets today have long-range, first line submarines capable of operating anywhere in the world and that this force includes ballistic missile vessels.

This means that our submarine and antisubmarine warfare programs must be given continued emphasis. I need not tell this audience that modern submarine and antisubmarine warfare and oceanography are absolutely inseparable. We must know everything about the ocean environment - and be able even to predict it in advance - if we are to hold our own in this deadly game of hide and seek.

Sound propagation is still our only reliable means for detecting enemy submarines and I am glad to be able to report that since your last meeting - where the subject came in for considerable discussion - we have strengthened our research programs in this field. We are particularly concerned with the effect that the so-called marine scatterers have on long-range sound propagation. And we are paying increasing attention to the critical influence of bottom topography and sediment structure on the newer sonar systems. This line of study will be further strengthened in the years ahead.

I can also report dramatic results from the Navy-developed satellite navigation system which is now fully operational. Our ships at sea can now position themselves with an accuracy that wouldn't have been believed a few years ago. The military advantages of this are obvious but it has wider uses and we are making the equipment to utilize the system available both to the U. S. academic community and to private industry.

Another area in which we have made great progress since your last meeting is in ocean engineering. By ocean engineering I mean all of the development efforts which center around our deep submergence program, including the Deep Submergence Systems project, the Deep Ocean Technology project and the Man-in-the-Sea program. This integrated effort involves several of the Navy's systems commands and laboratories as well as a wide spectrum of private industry.

As all the world knows since the tragic loss of the THRESHER, the Navy is operating even more complex nuclear submarines to such great depths that lives are placed in jeopardy in the event of a submerged accident. Fortunately in the long history of the Navy we have lost very few submarines except in combat. But one is one too many.

Consequently, an important part of the deep submergence program is the capability of rescuing men from disabled submarines on the ocean floor right down to the collapse depth of our most modern combatant types. Rescue will be done by mating a small deep submergence rescue vessel, a DSRV, to the hatch of the disabled submarine. The prototype DSRV is already under construction.

Plans are proceeding for the development of a 20,000 foot deep submergence research vehicle. This will also have the capability for location and recovery of small objects such as the unarmed nuclear bomb we were able to retrieve off Palomares, Spain, with the limited equipment then at our disposal. Incidentally, the 20,000 foot depth accounts for well over 90% of the ocean bottom.

The most urgent problems associated with the 20,000 foot vehicles concern hull structure and flotation materials. Fabrication techniques for welding, forming, and machining high-strength steel and titanium alloys are being developed. And we are even experimenting with massive glass.

Also within the scope of the deep submergence systems project, the man-in-the-sea program is advancing our capability for man to live and work in the oceans. SEALAB III, to be conducted later this year, will demonstrate the ability of men to live and work for extended periods of time exposed to heavy pressures almost to the edge of the Continental Shelf. Tools and equipment for performing useful work will be developed and evaluated in this program.

The deep ocean technology program which is included in the 1968 budget will advance the development of technology leading toward the occupation and exploitation of the deep ocean. Problems to be studied include:

The development of fuel cell powerplants as a prime mover for deep-diving submersibles.

The development of reliable, submersible motors, since motors presently in use are all either encapsulated or unreliable.

The advanced development of tandem propeller propulsion plants to enhance the maneuverability so vital to deep submersibles in near-bottom operation.

The development of sea water hydraulic systems to provide for improved reliability of deep ocean machinery and vehicles is also a part of the DOT program.

As an adjunct to the deep submergence systems project, the NR-1 will be the first nuclear powered deep submersible. This ship is being designed and constructed under the project managership of DSSP with powerplant development under the management of the Director, Naval Reactors Branch of the Ship Systems Command. The NR-1 will operate with a crew of five plus two scientists. In addition to demonstrating the capability of nuclear power in the deep submersible, NR-1 will be fitted with a full suit of sensors for oceanographic engineering and research.

The worldwide marine geophysical survey program begun in fiscal year 1966 will continue into 1968. These surveys, conducted under Navy contract with two commercial geophysical companies, will, when completed, have covered 16 million square nautical miles or 15 percent of the total ocean. Data are being collected on oceanographic conditions existing in deepwater masses and at the water/bottom interface.

Each of our Navy projects offers several potential applications beyond their direct military objectives: deep submergence search and rescue vehicle technology provides the basis for many uses -- mining, fishing, salvage, mechanical work, research, and data collection; sonar technology in the commercial sector can lead to considerably greater efficiency for future generations of commercial fishermen at a time when the problem of feeding the world population will have increased; man-in-the-sea may provide a key to greater and more rapid

development and exploitation of all our underwater resources.

I have taken time here to mention just a few highlights concerning some things that have happened since your last meeting as well as some ongoing programs that you will be concerned with between now and the Fifth Symposium.

Let me close by reminding you that in this business ideas are everything. Give us the ideas and the Navy-industry team can produce the hardware.

Ideas of course grow out of imagination applied to facts and you are going to hear a lot of facts in these next three days.

All I ask of anyone of you sitting here is to just give us one good idea. It would make the entire meeting worthwhile.

Good Luck.

ADDRESS TO THE 4TH U. S. NAVY SYMPOSIUM
ON MILITARY OCEANOGRAPHY
BANQUET SESSION, WILLARD HOTEL, WASHINGTON, D. C.
11 MAY 1967

by

Honorable Robert H. B. Baldwin
Under Secretary of the Navy

Captain Owen, Distinguished Guests, Ladies and Gentlemen.

I am delighted at this opportunity to speak at this banquet meeting of the Fourth Annual U. S. Navy Symposium on Military Oceanography.

I promise to be brief so that we can move on to the presentation of the awards to those who contributed to the search and recovery of the unarmed nuclear weapon off Palomares.

Though it was only three years ago that this Symposium was inaugurated, it seems already to be an instant tradition. The calibre of the delegates and the quality of the papers and the discussions make it obvious that these symposiums fill a real need and the exchange of knowledge will be of great benefit to both government and industry.

The plain truth is, of course, that modern oceanography is absolutely essential to national defense.

This is particularly true with the coming of the deep-diving, fast-running nuclear submarines with their new sophisticated and powerful underwater weapons systems.

But I don't plan, this evening, to talk very much about what oceanography can do for the military. You are spending three days doing that.

I want, instead, to say a few words about what the military can do for oceanography and what oceanography can do for the country and the world. When I say military, I refer primarily to the Navy which is responsible for virtually all of the Defense Department's oceanographic programs.

I am convinced, as I am sure most of you are, that ocean exploration and exploitation offers a challenge just as great as that posed by the current exploration of outer space. This challenge will be shared by both government and private industry working together. The discoveries which will be made by the "hydronauts" who explore ocean space will be no less dramatic than those made by astronauts--in some ways exploitations of the seas will be more vital to the future generations living on our planet.

Oceanography, of course, is an old story with the Navy--a century and a quarter old. It goes back to Matthew Fontaine Maury who was probably the world's first true oceanographer. He ran the Navy's Depot of Charts and Instruments which through several evolutions became the current U. S. Naval Oceanographic Office. He had a basic understanding of the dominant influence of the oceans on the world's weather. His studies of winds and currents enabled the fabled Clipper ships to set their astounding speed records. And his knowledge of the Atlantic Ocean and its currents was a factor in the successful laying of the first transatlantic cables.

His contemporary, Lieutenant Charles Wilkes, who headed the first scientific exploring expedition ever financed by the American Congress, was also an oceanographer of imagination and talent.

I have turned back to recall these half-forgotten Naval officers to make a point. My point is that the Navy not only has a long history of leadership in the field of oceanography but that from the very beginning it has willingly used its oceanographic skills to advance the national welfare.

I want to emphasize this point because we in the Navy must take a broader view than ever before of our responsibilities in this field of oceanography--the Navy's area of special competence.

As I stated over a year ago, the Department of Defense has an obligation to serve the national interest in any area where the Department's capabilities and the national needs are closely matched. The Department of Defense has accepted the national responsibility in ocean technology. It can also accept the national mission in ocean environmental prediction and ocean test facilities.

But this is only the beginning. Dr. Foster, DDR&E, speaking for the Defense Department, recently said that "if national oceanographic objectives require it, the Department of Defense is willing to request funds from Congress for work only marginally related to defense needs, but for which the Department of Defense is in the best position to manage because of technical skills, facilities or organization. The direction for utilization of these funds could come from a non-Department of Defense organization if this is judged to be the best course."

This is a major and significant commitment by the Defense Department to contribute in manpower, dollars, skills and facilities to our national objectives in the ocean which are determined to be the proper role of the Federal Government. The Navy concurs wholeheartedly.

First of all, our own oceanographic house is now in pretty good order. Dr. Frosch described to you yesterday the new responsibility of the Oceanographer of the Navy. The point I want to emphasize is that Admiral "Muddy" Waters administers all personnel facilities, centers and missions of our oceanographic program and is responsible for all oceanographic efforts from basic research through ocean engineering to support of the Fleet.

We recognize that without qualified people, we would not have a program. Ten years ago, we were sending only one or two Naval officers for post-graduate study in oceanography. This year we have allotted billets for 50 Naval officers to pursue post-graduate study in oceanography.

Secondly, the overall Federal oceanographic program will soon have an integrated and permanent administrative authority.

As you know, the form that this administration will take is now being worked out for Presidential and Congressional approval by the new National Council on Marine Resources and Engineering Development, chaired by the Vice President. Mr. Nitze, Secretary of the Navy, is the Defense Department nember of the Council.

The advisory Commission on Marine Science, Engineering and Resources, headed by the distinguished Dr. Julius Stratton, is vitally involved in long-range goals and organization. I am a member of the Commission and have been amazed at the wide-spread interest this Commission has evoked across the country. A friend of mine recently told me that oceanography is the sexiest thing to hit the country since the transistor.

Let me now turn to some of the areas where the Navy is contributing to the non-military exploitation of the ocean.

Our undersea technology program, with the associated Deep Submergence and Man-in-the-Sea programs, received their original impetus from the tragic loss of the THRESHER and more recently by the successful recovery of the unarmed nuclear weapon off Palomares.

Perhaps it is an oversimplification, but in my mind these programs can best be described as the development of technology leading toward the occupation and exploitation of the ocean bottom and the deep ocean. Although our primary objectives are military exploitation, the technological know-how developed by these programs is identical for all types of exploitation.

Each of our Navy's projects offers several potential applications beyond their direct military objectives:

Deep submergence search and rescue vehicle technology will provide the basis for any vehicle end use--such as mining, fishing, salvage, mechanical work, research, and data collection.

Sonar technology in the commercial sector can lead to considerably greater efficiency for future generations of commercial fishermen, as the world population doubles over the next thirty years.

Man-in-the-Sea may provide a key to greater and more rapid development and exploitation of all our underwater resources.

I have been particularly impressed by the SEALAB experiments which are just beginning to unfold the potential of man's exploitation of the continental shelf. I am fascinated by the program just being started by our own Dr. MacLean of NOTS which will enable men to live in houses on the ocean bottom at several thousand-foot depths just as we now live at home.

The NR-1, being constructed at Groton, Connecticut, and expected to be launched in 1968, will be the first true research submersible. With its nuclear propulsion, it will be able to remain submerged for several weeks, independent of surface conditions. Its ability to operate will be limited only by the endurance of its consumables. In April 1965, when President Johnson announced that the Navy and the AEC were jointly developing a nuclear-powered, deep-submerged research and engineering vehicle, the NR-1, he noted that vehicles developed to date were limited by short endurance of propulsion and auxiliary power.

This will truly be a revolutionary vehicle, able to operate at depths considerably deeper than the continental shelf.

NR-1's long endurance and its independence from the ocean surface has forced a development program which will benefit industry, the academic community, and the Navy. On surface ships, one can always reel in instruments and work on them topside. When conventional submersibles come to the surface after a day's operation for battery charging, most of the equipment is usually inoperable and must be repaired on the mother ship or ashore.

In order to fully utilize the advantage of NR-1's nuclear power and continuous operation capability, Admiral Rickover and Dr. Craven have had to embark on a significant development program in order to make the oceanographic suit reliable.

In one specific test case, we had an external electrical connector designed for a conventional submersible down at 100-200 feet only to discover it failed in a day or two. We solved this problem by eliminating this type of external connector in designing NR-1.

Our undersea technology effort is supported by wide-spread test facilities, ranging from large model basins and pressure testing facilities, to underwater test and evaluation ranges, and many specialized

Laboratories. We have several Ocean Test Ranges in operation now for the underwater testing of various types of equipment. Our new Atlantic Undersea Test and Evaluation Center (AUTEC), in the Bahamas, will go into full operation this year.

With the addition of a few new facilities, we can meet the non-military needs of both government and private industry. The Naval Civil Engineering Laboratory, for example, now cooperates with industry regularly to carry out joint tests of new industrial materials in the Lab's pressure test facilities, to the great benefit of both.

Let me mention the third field in which the Department of Defense can accept the national mission-ocean weather prediction. The Navy has been in this business for a long time and we can't operate without it. To provide this service, the Department of Defense operates a world-wide observational, collection, and communications network. Navy relies on the Coast Guard for accurate, timely, oceanographic data and services from their ocean stations, ice patrol, ice breakers, and oceanographic platforms. DOD observations are supplemented by those from merchant ships, island and coastal stations both foreign and domestic, as well as from the Departments of Interior and Commerce.

The product consists of storm warnings, weather forecasts, sea state and thermal profile production, and optimum track ship routes distributed by unclassified messages on known frequencies for use of specific military units as well as any one else.

We are making sure that marine and fishing industries will have the full benefit of the Navy's increasing knowledge in this field.

These are just a few of the areas outside the basic sciences where the Navy is contributing to the non-military exploitation of the ocean.

Let me mention one sticky point right here. Whenever Navy cooperation with the non-military community is mentioned, the subject of classification comes up. We are accused of classifying every piece of information we lay our hands on including telephone books. There has certainly been overclassification at times in the military, but Admiral Waters tells me that an estimated 90% of all raw data gathered from all our oceanographic platforms is completely unclassified.

The Navy, because the ocean is its daily operating environment, is spending over half the FY 68 Federal oceanographic budget of 462 million dollars. It not only makes good economic sense, but seems essential, that the oceanographic information and technology for which the Navy spends your money should do double duty by being made available to all other agencies and industries.

In any case there is no real separation anymore between national defense and national, and even international, welfare. The United States cannot be indefinitely safe in a hungry world anymore than we can be safe without a credible strategic deterrence. Our efforts in space should not detract us from devoting increased efforts and resources to the seas. Not only our welfare but our very existence may depend upon it.

The Renaissance was an age of geographical exploration and an age of science. It was also an age of hope in Europe after centuries of instability and violence.

We are living in a new age of exploration--of both outer space and underseas--which is dependent upon new scientific discoveries, sophisticated technology and advanced engineering. We also live in a divided world--politically, militarily and economically--which offers promise of great hope to the well-off but fears of hunger and despair to the poorer.

The exploration and exploitation of the oceans are vital to our military security, and that of our allies, until a more stable world framework evolves. Perhaps more important in the long-range, is that oceanography in the broad sense offers avenues of satisfying certain basic human needs essential to stability in future decades. It offers both avenues of world-wide cooperation and a challenge to American leadership, governmental and private, to devote our scientific, technological and management skills in furthering joint efforts.

Session A

GENERAL SESSION

AN ANALYTICAL REVIEW OF LESSONS LEARNED FROM THE H-BOMB SEA SEARCH OFF SPAIN

Part I: Search, Classification, and Recovery

F. A. Andrews
Consultant, Ocean Systems, Inc.
and Research Professor, Catholic University
Washington, D.C.

INTRODUCTION

On 17 January 1966, an unarmed nuclear weapon was lost in the Mediterranean Sea off Palomares, Spain, following the collision of two aircraft of the U. S. Air Force. The weapon was retrieved 80 days after the accident from a depth of 2,850 feet six miles off the Spanish coast by Task Force 65 of the U. S. Sixth Fleet. Inasmuch as the entire operation (named SALVOPS/MED) and the organization of Task Force 65 was "Ad hoc" and staffed by personnel ordered temporarily from other duties, it was impracticable for the Search Commander to produce the definitive type of operation report required. This task, therefore, devolved upon the so-called "Technical Advisory Group SALVOPS/MED". It was this group, sitting in Washington and meeting daily, which arranged logistic support, provided technical guidance and in general terms was "home base" for the Search Commander. Two reports and an executive summary were actually written. The first, an interim report[1] which presented a description of the operation and listed the problems encountered was published on 15 July, 1966, for immediate use by navy planners and technologists. The second, a final report[2] and a more thorough analysis which listed conclusions and recommendations from both SALVOPS/MED and a postulated recurrance was published on Feb. 15, 1967. The latter report is 1200 pages in five volumes. The executive summary[3], meant to present to executives and supervisors in both defense and industry the significant lessons and implications for the U. S. Navy found in the final report, was also published on 8 April 1967. The two reports and the executive summary are available through the Defense Documentation Center.

The actual task of drafting all reports was assigned to Ocean Systems, Inc., under contract to Captain W. F. Searle, Jr., Supervisor of Salvage, U. S. Navy, who was a key member of the

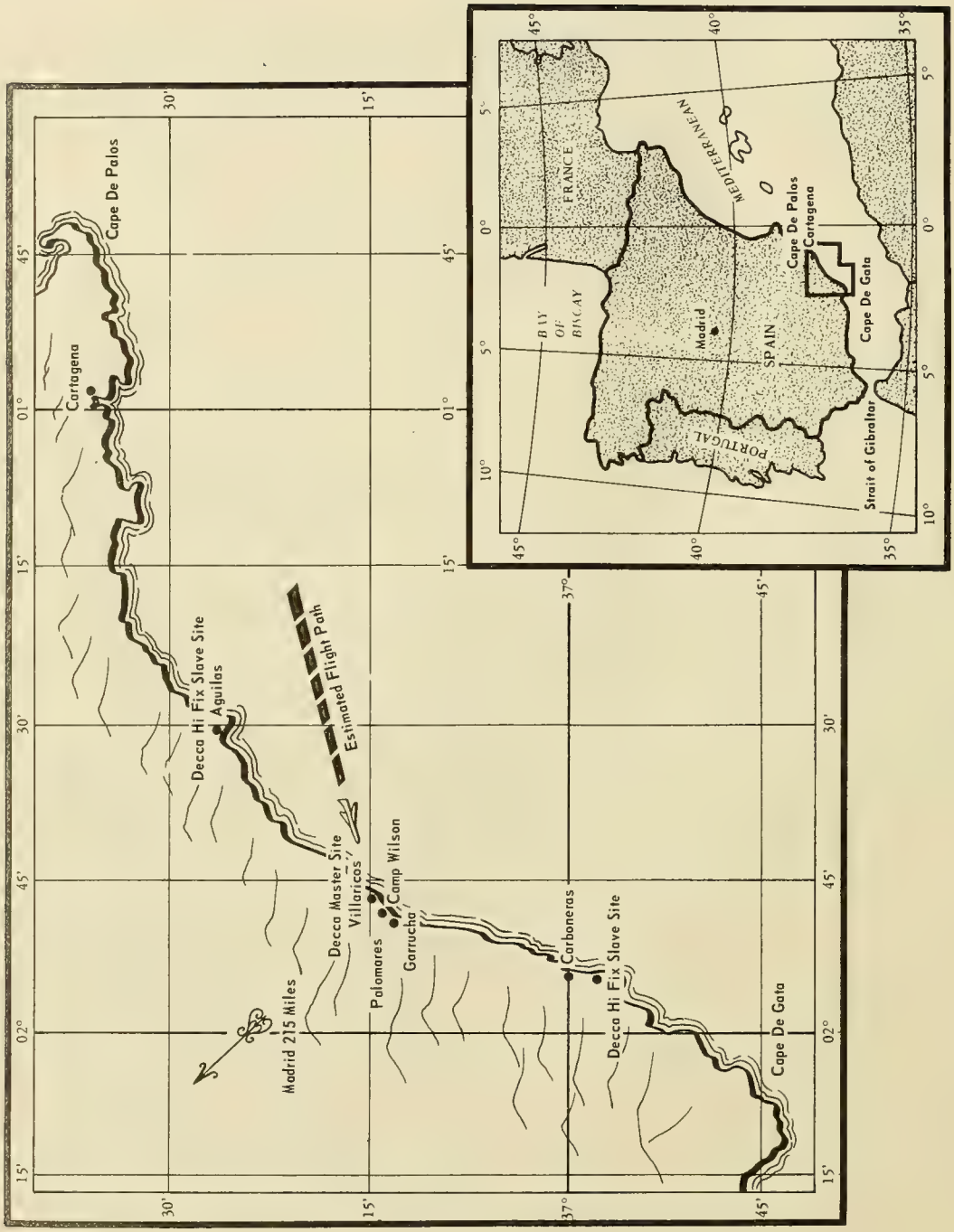

Fig. 1 - Coast of southeast Spain

Technical Advisory Group, as well as the officer responsible for the assignment of much of the technical equipment and personnel to Task Force 65. Ocean Systems, Inc., also acted as prime contractor for all commercial assistance to Task Force 65 in carrying out the H-bomb salvage operation.

The general purpose of this paper and the paper which follows is to present in brief the significant information contained in the two reports cited before, and in the executive summary report. The author of the first paper was general editor of both the interim and final report and was with Task Force 65 for 10 days assisting in the establishment of an on-scene operations analysis group. The author of the second paper was the principal writer of the executive summary.

The specific theme of this first paper will be the analysis of the Search, Identification, and Recovery phases of SALVOPS/MED. Significant lessons and recommendations derived from these phases will be listed.

A BRIEF DESCRIPTION OF THE OPERATION'S SCOPE AND ENVIRONMENT

The general area of interest is shown in Figure 1. The Naval Task Force which was collected in this area to conduct the salvage operations was ultimately composed of 25 navy ships, four research or commercial ships, four submersibles, and over 3000 men. Twenty civilian contractors were used to assist in the operation at a monetary value of effort of 2.1 million dollars.

The search areas designated by Rear Admiral Guest, Commander Task Force 65, are shown in Figure 2. The first, named Alfa I, was a circle one mile in radius, located approximately 5 miles off-shore, and centered at a point where a local fisherman sighted a large parachute and object falling into the water. The second, named Alfa II, was approximately a semi-circle with radius 4500 yards, located immediately adjacent to the beach area where three of the four weapons had been found by Air Force search parties. The other areas, named Bravo and Charlie, were defined from Air Force calculations of possible bomb splash points given various combinations of ballistic fall (without parachute) and wind-affected free fall (with parachute deployed). AI and AII were considered to be the highest priority areas; Bravo and Charlie were considered to be lowest.

The bathymetry of the area is given in Figure 3. One can note the relatively flat bottom terrain in AII, Bravo, and Charlie. The depth of water in AII ranges from 0 to approximately 300 feet. The depth in Bravo and Charlie is 400 feet slowly increasing to 3600 feet. The bottom terrain in AII was a hard, cemented gravel platform with numerous exposed black rocks. The terrain in Bravo and Charlie, on the other hand, was soft silt predicted to be as much

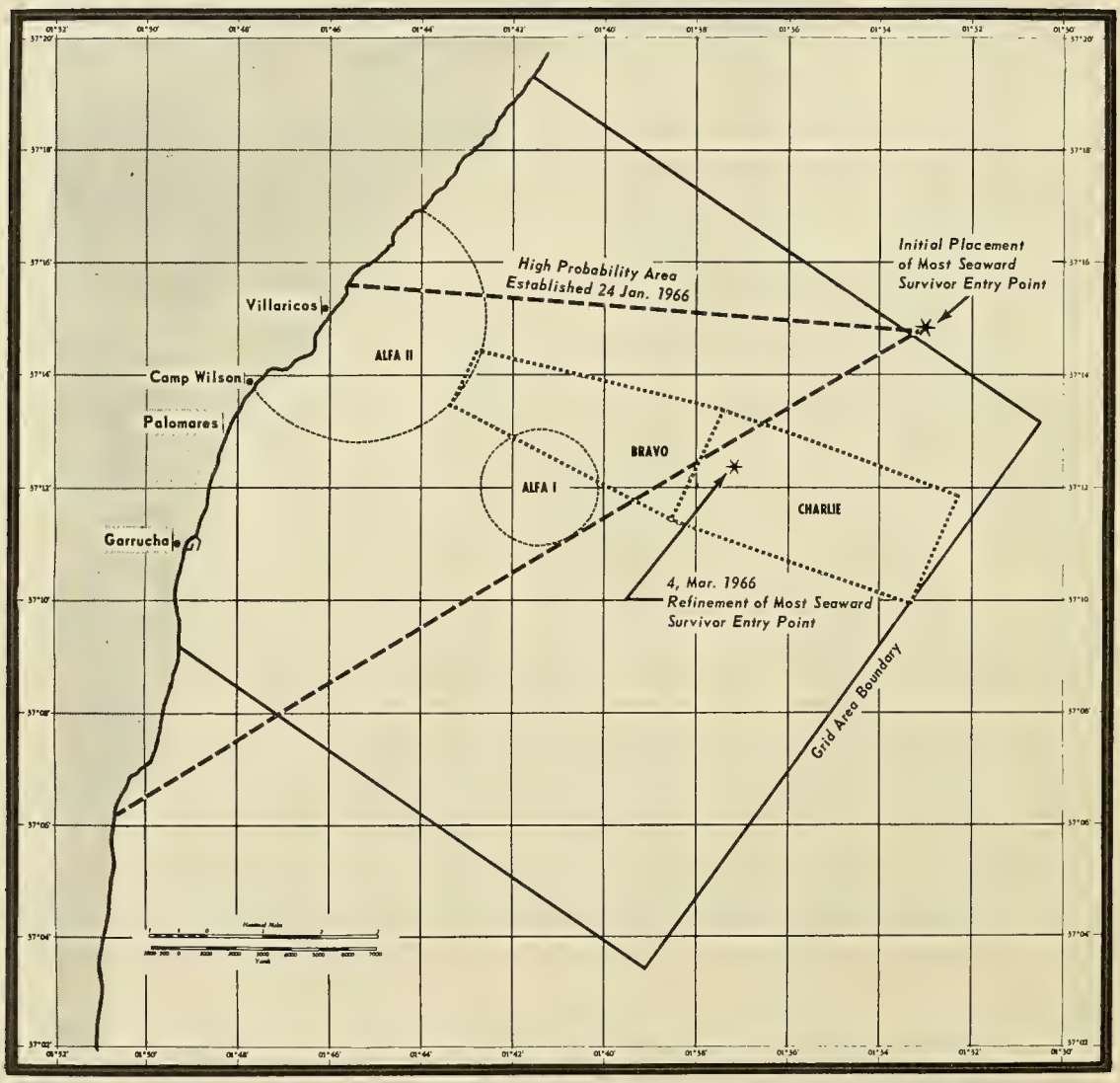

Fig. 2 - Salvops search area

Fig. 3 - Bathymetric chart

as 50 feet thick in spots. One can also note the worst possible place where a bomb might be lost, in the south part of Area AI. The northern part of AI is flat compacted silt ranging in depth from 990 to 1800 feet. From this latter depth on the terrain drops abruptly away into deep canyons. The southern half of AI is the canyon slopes comprised of bed rock and a thin intermittent covering of OOZE with heavier deposits of OOZE in the canyon floor. Depths in South Al are 1800 feet to 3000 feet. The presence of a probable ancient river bottom directed southeast from the edge of AII and passing below area AI can also be noted. As a matter of interest, the nearby land terrain was equally rugged with mountain ranges rising from a mile or two behind the shore line.

Surface currents in the SALVOPS area were generally to the southwest and reached a maximum of about 0.7 knots. Currents on the bottom in those two areas where observations were taken were also generally southwest and varied from 0.0 and 0.3 knots. In the canyon areas in the southern part of AI, the current was observed by submersible pilots to vary from southwest through south to southeast and was thought to depend somewhat on tide. The maximum bottom current observed was 1.0 knot.

Surface visibility was usually 2 miles or better with water and air temperatures never severe enough to hamper operations. The most persistent surface weather factor was an afternoon off-shore breeze which on numerous occasions necessitated the suspension of small boat operations and at times curtained submersible operations. General storm conditions prevailed for no more than 10% of the time, during which time all operations were suspended.

THE SEARCH PLAN

The stated mission of Task Force 65 was to detect, identify, and recover material associated with the aircraft collision. To carry out this mission the Westinghouse ocean bottom scanning sonar (OBSS), the Navy mine-hunter sonar (UQS-1) and the Honeywell sea scanar sonar were used for acoustic search. Navy EOD/UDT divers, television lowered on a wire, hard hat divers, and Perry Cubmarine were used for visual search and identification in medium depths. The manned and free vehicles, ALVIN and ALUMINAUT, the manned and towed vehicle DEEP JEEP, and the unmanned and towed NRL vehicle operated from USNS MIZAR, were all available and used for visual search in medium and deep depths. ALVIN and ALUMINAUT also possessed an acoustic search capability (Straza sonar on ALVIN and Westinghouse side-looking sonar on ALUMINAUT).

Outside of 80 feet the search and identification policy of the Commander Task Force 65 was; step one, search acoustically in all high probability areas reporting all acoustic contacts to the flagship, where a contact log and plot were maintained; step two, follow-up the reported acoustic contacts by sending visual

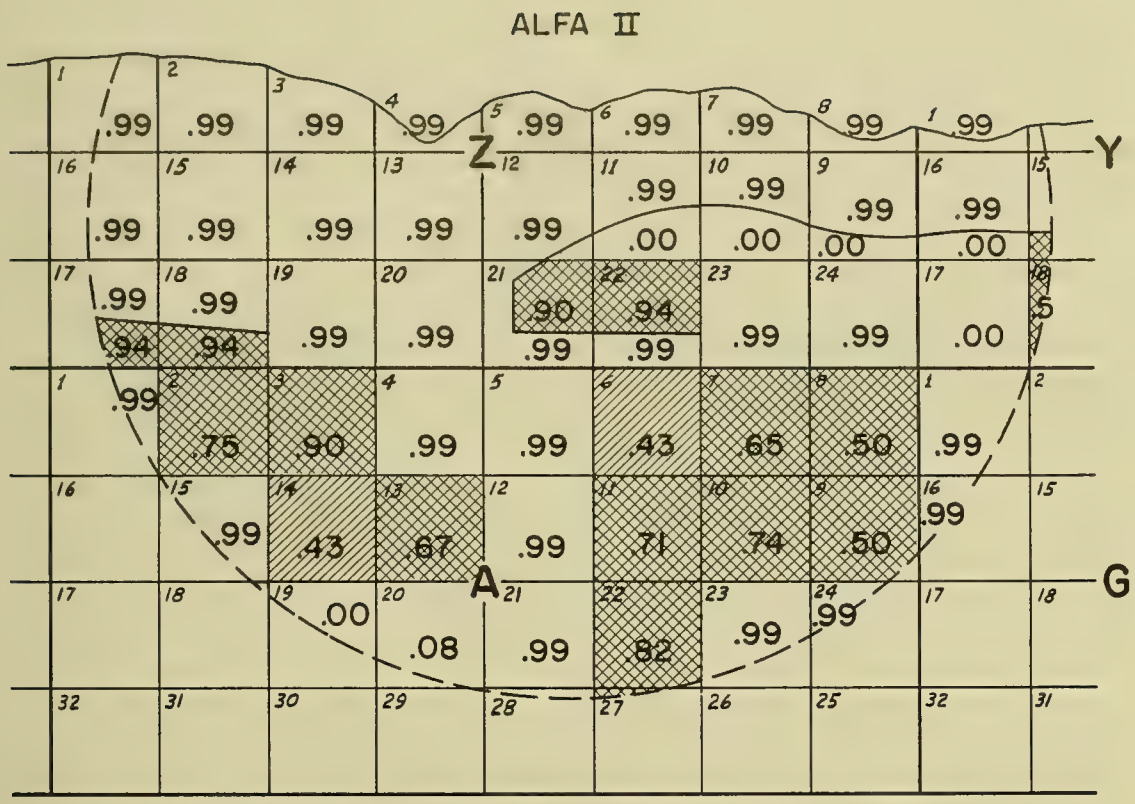

Notes: (1) SEP is given by the large bold faced numbers. The small light faced numbers give the square designation.

LEGEND

	$.95 \leq SEP \leq 1.00$
	$.50 \leq SEP < .95$
	$.10 \leq SEP < .50$
	$.00 \leq SEP < .10$

Fig. 4 - Search effectiveness probability in ALFA II (period ending 2400 on 14 March)

identifier teams to the reported position.

Inside of 80 feet EOD/UDT swimmers and scuba divers were used to search visually and simultaneously to identify. This operational group was highly successful in area AII, where they were assigned. Approximately four square miles were searched out in six weeks. 143 pieces of aircraft debris were sighted and recovered, and the search Commander could report with a degree of confidence approaching 100% that the H-bomb was not in AII inside of 80 feet. The major problem reported was a difficulty in keeping navigational bouys in place during heavy weather.

THE FIRST OPERATIONS ANALYSIS (ON-SCENE)

Two analyses of the acoustic and visual search outside of 80 feet were conducted. The first was on scene in support of the operation. Unfortunately the team which carried out this analysis did not arrive in Spain until February 22, 1966, over a month after the air collision. The dispersion of original records throughout the task force, and the lack of DECCA navigation during the early part of the acoustic search by UQS-1, OBSS, and Sea Scanar made the analysis task most difficult. Further, no measure of search effectiveness was yet developed. The second analysis was a study of reported acoustic contacts versus reported visual contacts and was conducted in Washington after SALVOPS/MED was concluded.

The definition of a measure of search effectiveness was provided by Dr. Richardson[5], a member of the on-scene analysis group. The chief method by which search was documented prior to the arrival of the analysis team was through preparation of transparent overlays showing, with different cross-hatching, the search vehicles which had been in the several areas. These overlays tended to be misleading since they did not assess the quality of effort which had been expended. The measure chosen to improve this situation was search effectiveness probability (SEP), the probability that if a target were in a particular area, then it would have been found by the amount of search effort considered. The basic inputs to the computation of SEP are initial detection probability (P_D) and the probability of correct identification (P_C) given a detection. Thus $(SEP)n = (P_D)n\ (P_C)n$ where (SEP)n is the Search Effectiveness probability in the nth area. A value for $(P_D)n$ was calculated by considering in the nth area, the sensor detection range from which sweep width (W) was obtained, the length of transit travel (L) in the nth area, and the degradation of search effort due to navigation inaccuracy. For visual search systems (e.g. MIZAR towed camera, ALVIN visual search), it was assumed that a successful identification always followed a detection. Thus $(P_C)n$ was assigned a value of unity for such systems. For the acoustic systems, a visual/identifier team had to return to the contact and attempt identification. Thus $(P_C)n$ for acoustic detection was assumed zero if no revisit had taken place or one if an effective visual revisit of a

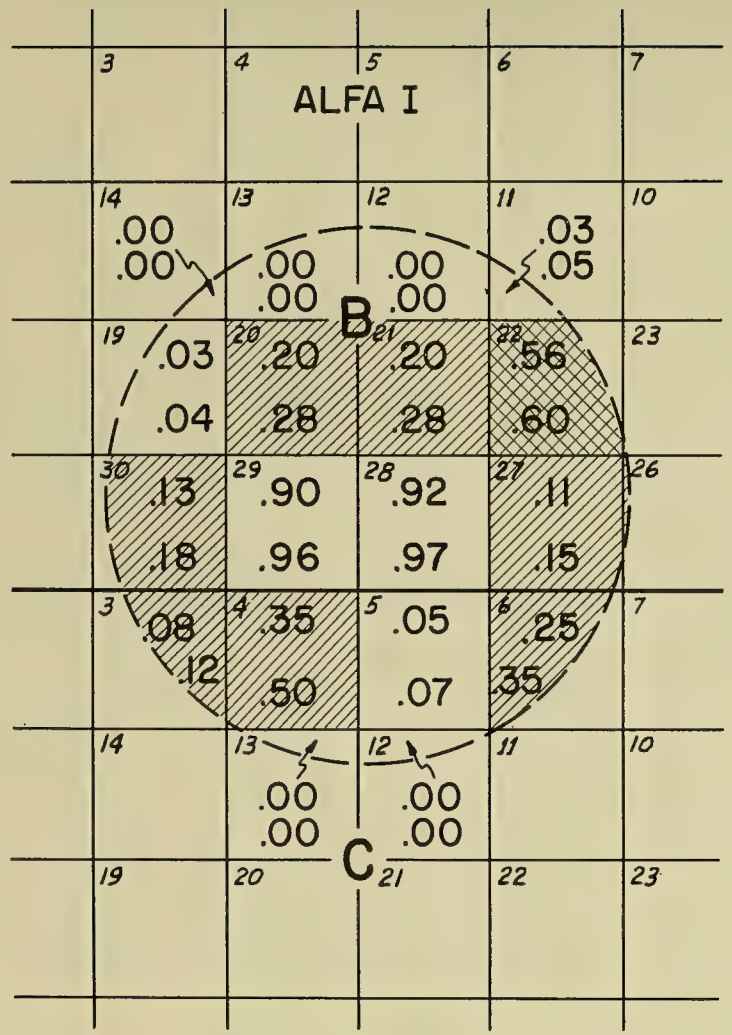

Notes: (1) SEP is given by the large bold faced numbers. The small light faced numbers give the square designation.

(2) The two values of SEP in each square result from two different assumptions about visual detection (optimistic and pessimistic).

(3) Shading is based upon the larger of the two values for SEP.

LEGEND

- $.95 \leq SEP \leq 1.00$
- $.50 \leq SEP < .95$
- $.10 \leq SEP < .50$
- $.00 \leq SEP < .10$

Fig. 5 - Search effectiveness probability in ALFA I (period ending 2400 on 14 March 1966)

reported contact area had been made. An experienced member of the analysis team, (Lt. Cdr. George Martin, former pilot of TRIESTE I) determined which of the two values to choose. Figure 4 and 5 show the values of SEP in areas AII and AI respectively the day before the weapon was found. Note in Figure 5 that search in AI was far from complete on the day the weapon was sighted in Grid C4. The effect of navigation degradation on the search is covered in detail in Part 2, Chapter V of the final report and shows amongst other factors that if one makes a random search in a given area (A), that (P_D) = 63% when W (sweep width) x L (transit distance) = A (area of nth grid) regardness of the navigation error. In fact, one can do quite well in detection by random search alone. The navigational inaccuracies will, however, impose a severe handicap if one wishes to revisit a contact which has previously been detected.

The definition of SEP and its use in the method developed on SALVOPS/MED are considered valid and most useful for future deep ocean search operations. However, the particular numbers calculated as shown in Figures 4 and 5 are considered to have unknown inaccuracies because the inputs P_D and P_C were little more than educated guesses. Thus no pre-operational test data were available, nor were any valid on-scene controlled tests performed to check the accuracies of the assumed data. For interest, the values of sweep width (W) and navigational error (σ) which were assumed are given in Fig. 6.

The major recommendation resulting from this analysis phase of the Search and Identification operation were:

- Establish an Operations Development Group which will develop search tactics, measure search parameters under realistic operational conditions, and improve further the method of operations analysis developed in SALVOPS/MED.
- Provide all search forces with a trained analysis team and adequate computing facilities.
- Improve facilities and procedures for obtaining and rapidly displaying environmental information so that the search Commander, search teams, and the analysis team can better assess day by day performance. Quantitative values of bottom currents, bottom sediment and strengths, and the charting of a micro-bathymetry survey are suggested outputs. The current measurements made by NAVOCEANO scientists were considered good, but did not cover the area sufficiently. Valid bottom strength and sediment measurements with adequate coverage were made by NCEL scientists, but they could not be processed soon enough nor displayed optimally. A bathymetry survey was made by the USNS DUTTON but showed the usual inaccuracies due to the wide directivity pattern of the UQN fathometer.

Sensor	W (Feet)	σ (Feet)
UQS-1	300	5
OBSS	416	85
MIZAR Towed Camera	50	25
ALVIN and ALUMINAUT (Visual)	30	Random Search

Fig. 6 - Assumed values of sweepwidth (W) and navigation error (σ) used in calculating SEP

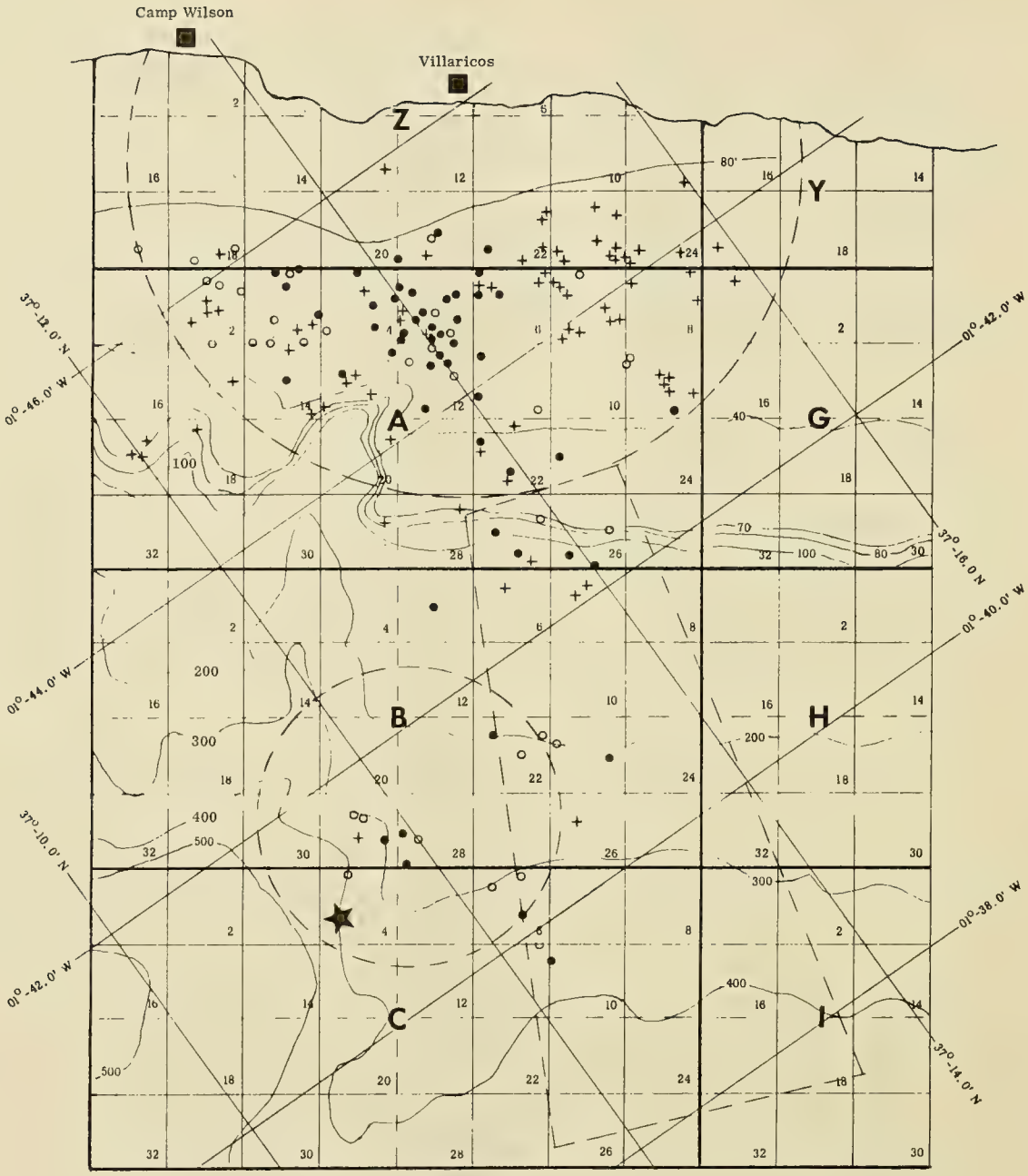

Fig. 7 - Visual sightings

THE SECOND OPERATIONS ANALYSIS (POST-OPERATION)

The second analysis, conducted after the operation, sought to determine any relation between acoustic and visual search. A plot of all visual contacts was made. This was then considered to represent the true picture of debris and rock distribution on the ocean floor off Palomares. Figure 7 shows this plot. An important point to note is the high debris density in AII and the great number of rocks also sighted in AII. The location of the nuclear weapon is shown.

With this chart and with data available from the contact logs, each acoustic contact was reviewed and placed into one of the following categories.

NF - no visual follow-up
NS - no sighting in the visual follow-up
OC - a sighting was made in the visual follow-up and its position, its depth, and for OBSS only, the approximate size of the contact correlated with the acoustic report
OD - a sighting was made but only one of the criteria sited under OC seemed to correlate with that initially reported by acoustics.

A correlation in position was considered to have occurred if the reported acoustic position was within 500 yards of the reported visual position. For depth the figure was 80 feet. For correlation in dimension, agreement within 1-2 feet for large objects and 50% for small objects was required for one dimension only. The other dimension had to agree within only an order of magnitude.

The contacts in categories OD and OC were further divided by considering (a) the availability or nonavailability of DECCA to both detection and classifier units, (b) the location of the contact in an area of high or low density as determined by the chart of visual contacts. Figure 8 gives a summary of the analysed data for the UQS-1 and OBSS Sonars. The large number of OBSS contacts in Class NF was due to lack of time to follow-up all reported contacts and the fact that many of these contacts were outside of the priority areas AI and AII.

The significant conclusions from this study were

1. The use of the OBSS sonar in SALVOPS/MED was relatively ineffective because of the tactics used, the high percentage of rocks in the operations area and the conduct of part of the OBSS search prior to the availability of DECCA.

Specifically OBSS was ordered to make single passes through an area once with a small overlap. No attempt was made to regain

Sonar	Total Contacts Reported	NF	NS	OD	OC
OBSS	256	155	22	66	13
UQS-1	45	11	2	16	16

Fig. 8 - An analysis of acoustic contacts

Identifier	(a) Sighted in Follow-up	(b) Sighted Independently	Total Sightings	Type Target		
				Aircraft Debris	Non Aircraft Debris	Natural Objects
TV	26	18	44	3	6	35
H.H. Divers	11	5	16	5	2	9
EOD/UDT	25	11	36	13	11	12
ALUMINAUT	3	14	17	8	5	4
ALVIN	2	4	6	4	1	1
CUBMARINE	10	27	37	16	10	11
DEEP JEEP	0	2	2	0	0	2
TV and H.H.	6	5	11	4	3	4
MIZAR	0	6	6	0	6	0
TOTALS	83	92	175	53	44	78

Fig. 9 - Tabulation of visual contacts

or reinvestigate any contact. Instead, if the contact looked good on the OBSS trace readout, it was reported by radio to the control ship. Thus the navigation error of detection ship and classification ship were accumulative, possible communication errors could be introduced and no opportunity was given to the OBSS operators to learn whether the targets they were reporting were good or bad. As a result there are only 13 OBSS contacts in the OC class. Of this number 9 were rocks. Of the 66 OBSS contacts in the OD category, 39 were reported or followed up by units with no DECCA, and 32 were reported in areas later determined to be high density areas (i.e. > 5 visual sightings/ 1/4 mile sq.).

2. The UQS-1 was of limited use on independent broad area acoustic search and only in shallow water (i.e. < 300 feet).

Specifically, the minesweeps with UQS-1 carried out certain mine-hunting tactics in which a contact was regained several times before it was considered a valid detection. Thus the percentage of UQS-1 contacts (16/34) in the OC category was an improvement over the OBSS. Still the inability to know whether the contacts reported were good or bad preempted any learning process by which the sonar operators could improve their skill.

A second tabulation Figure 9, shows the performance of visual identifiers. The significant conclusions from this study were:

1. Cubmarine, and the EOD/UDT divers were the leaders in sightings of aircraft debris in AII. The relative immobility of hard-hat divers and "dipped" TV, and material problems with DEEP JEEP accounts for the poorer sighting performance of these three elements.

2. The team combination of a minesweep with UQS-1 and the EOD divers or Cubmarine was a most successful method for searching acoustically and simultaneously identifying a target. Mr. Barringer, Senior Pilot of Cubmarine, indicated that Cubmarine was vectored to 75% of the contacts listed in Figure 9. This is a significant fact since it correlates with a report by COMIN DIV 84 that the ability of his UQS-1 operators to distinguish rocks from debris increased significantly when they received back an immediate report from Cubmarine or an EOD diver concerning the nature (rock or debris) of the target which had just been obtained acoustically. A tabulation of sea scanar performance (not given here) showed that this sonar mounted on a small boat and teamed with divers was also relatively effective. 31 acoustic contacts were made of which 24 visual sightings were made in the immediate follow-up. However, over 40% of the contacts sighted were rocks. A major difficulty was

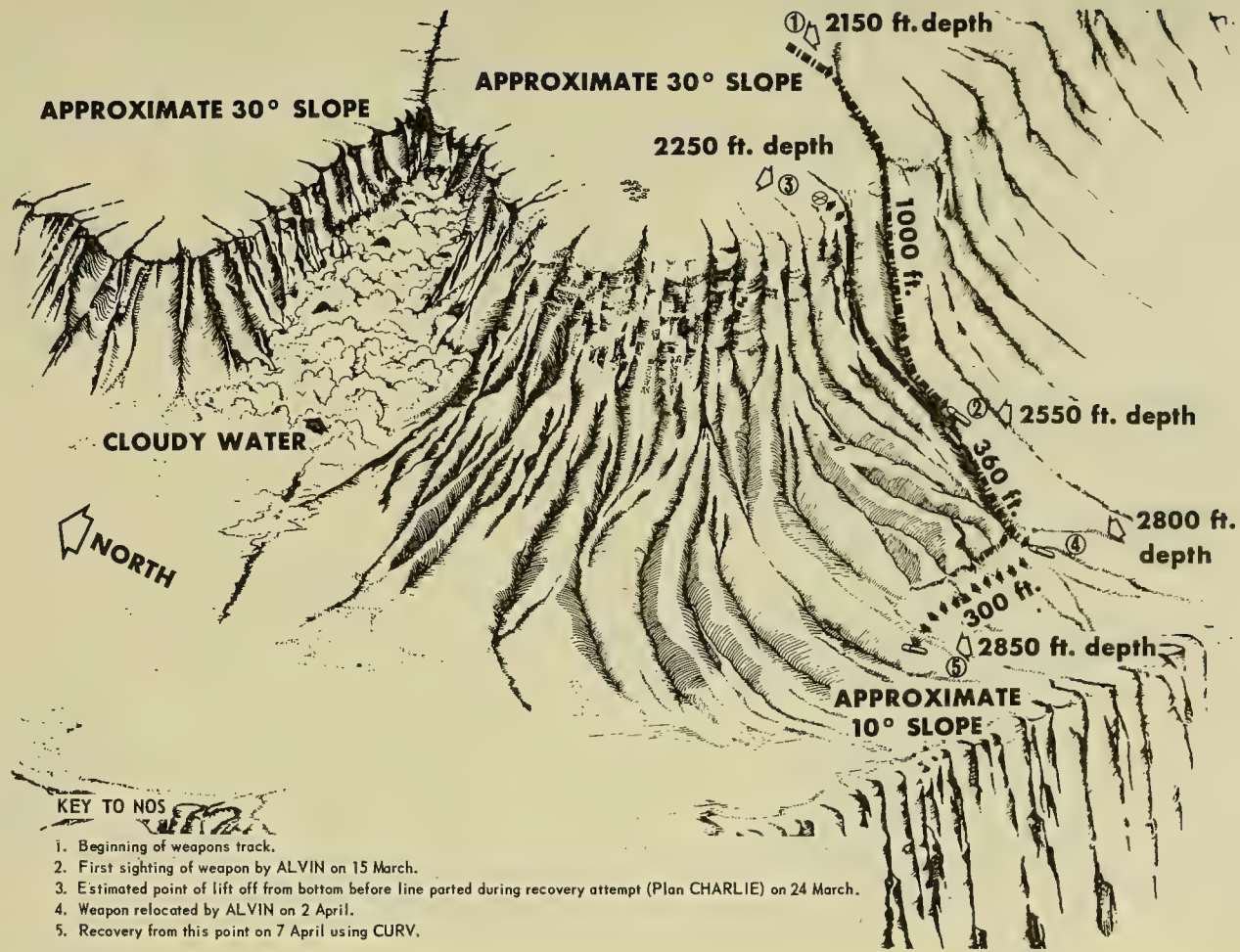

Fig. 10 - Weapon track (after R. Smith of NCEL)

in accurate navigation of the small boat, which had to be vectored into position by radar posits from the USS Boston.

3. Acoustic search in the south part of AI was totally ineffective because of the inability of sonar to receive anything but bottom reverberation in the highly discontinuous terrain. Visual search was effective even though detection ranges were rarely greater than 15 feet. The weapon was found by a modified random visual search in which a combination of fortunate circumstances counterbalanced the handicap of limited vision. ALVIN elected to search along terrain contours, and correctly deduced that the bomb might have slid some distance down one of the steep slopes, leaving a discernible track. Thus ALVIN's courses were designedly perpendicular to the track of the weapon sliding down a slope. This effectively enlarged the target to 1000 feet, the length of the track at the base of which the parachute enshrouded bomb lay. (Figure 10)

The major recommendations of this post-operation study were:

- Incorporate into the design of future search systems the target classification lesson learned in SALVOPS/MED. This lesson indicated that in the rocky terrain off Palomares, acoustic search alone was generally ineffective because of inadequate sonar classification. Future vehicles which combine the integrated use of acoustic, magnetic anomaly, visual, and other detection means are indicated. In addition, emphasis on long range research and development in acoustic classification is indicated.
- Accelerate the development of mobile hull-based and bottom mounted transducer underwater navigation systems. Efficient bottom search, the revisit of contacts previously reported, and a study of the location of a contact relative to the bottom terrain are all impossible without precise sea-floor navigation.

AN ANALYSIS OF THE RECOVERY

The extreme depth at which the bomb was lost required that the attachment of the lifting device be done remotely either from the surface, or from within a small submersible. Lifting, once the attachment was made, appeared most practical from the surface. Certain schemes involving an unassisted lift by ALUMINAUT were considered but finally abandoned because of the possible risk to the vehicle, its personnel or to the weapon and parachute.

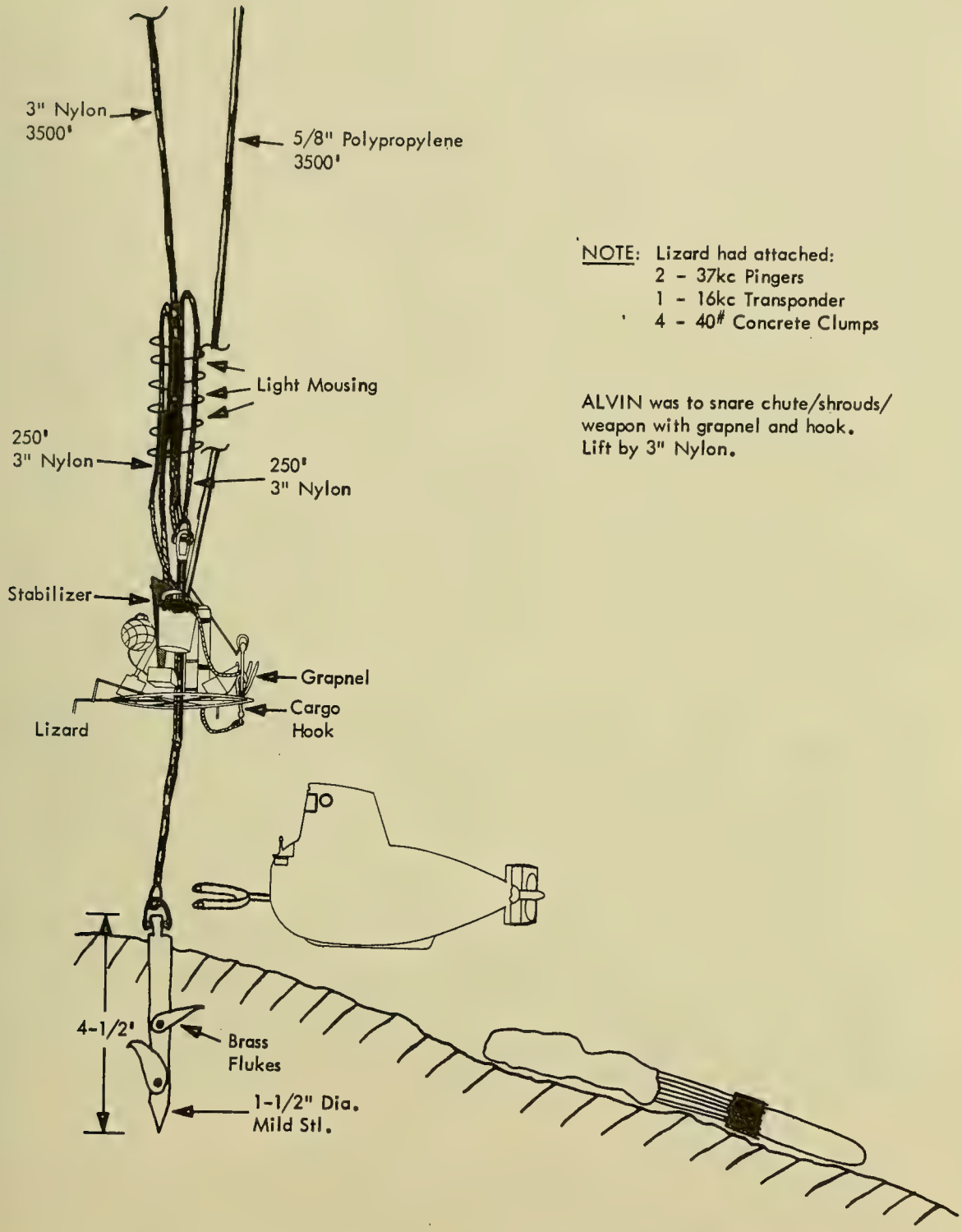

NOTE: Lizard had attached:
2 - 37kc Pingers
1 - 16kc Transponder
4 - 40# Concrete Clumps

ALVIN was to snare chute/shrouds/ weapon with grapnel and hook. Lift by 3" Nylon.

Fig. 11 - Recovery plan ALFA

Three lift plans were actually attempted using various devices constructed on scene. The first two failed, the third resulted in lifting the weapon clear off the bottom. However, the lift line parted owing apparently to chafing and the weapon fell back to the ocean floor to be temporarily lost for "9 agonizing days." The NOTS (Pasadena) controlled underwater recovery vehicle (CURV) finally brought the bomb to the surface on 7 April 1966.

The following description of the three recovery attempts (plan Alfa, Bravo, and Charlie) and the successful lift by CURV is taken largely from a memo by Lt. Com. M. MacKinnon, who participated in the operation as part of the staff of CTF65.

The initial plan (Alfa) involved the use of ALVIN to place an anchor stake in the sea floor (compacted silt) to which a small polypropylene line was attached, leading to the surface (Figure 11). A traveling "lizard" was locally constructed to slide down the polypropylene line carrying a lifting line and shorter attachment pendants. After the lizard reached bottom, ALVIN was to use her manipulator, pick up the attachment pendants and hook them into any combination of chute, shrouds, risers, and weapon. Once attached the lift was to be made from the surface using the USS Hoist (ARS-40). On 16 March, ALVIN succeeded in placing the stake in the bottom, but on 18 March when the catenary was being removed from the polypropylene line the strain imparted pulled the stake from the bottom. Only one of the two flukes on the stake had apparently taken hold.

A second plan (Bravo) was employed using MIZAR's towed sled to place the attachment pendants adjacent to the weapon (see Figure 12). The final attachment then was to be made by ALVIN in a manner similar to that of plan ALFA. A key aspect of the operation was the position keeping of MIZAR to enable close placement of the sled. This precise station keeping proved impossible and hence the plan was abandoned.

The third attempt (Charlie) again used MIZAR, but this time in conjunction with placing an anchor adjacent to the target (Figure 13). The use of a 16KC transponder and MIZAR underwater tracking system enabled the placement within 100 feet. The lizard of plan ALFA was modified and secured to the lifting system. Three lifting pendants, one on the anchor, and two on the modified lizard (now called POODL) were to be attached to the weapon by ALVIN as in ALFA and Bravo.

On 24 March ALVIN succeeded in attaching to the weapon a lift line from the anchor, by ensnaring at least 6 shroud risers. The other two lifting pendants were fouled and could not be used. The decision was made to lift, but shortly after the strain was the heaviest the lifting pendant parted.

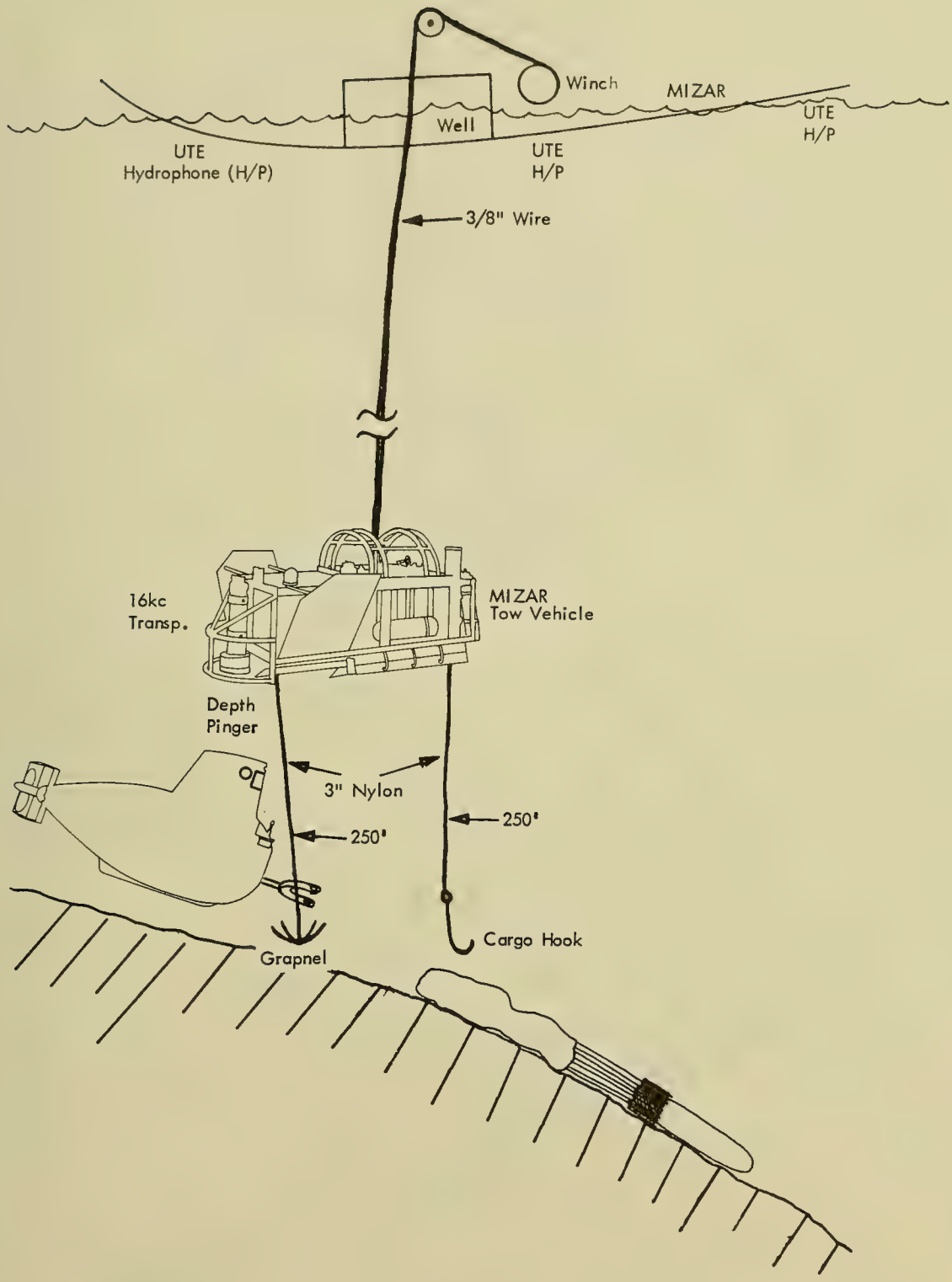

Fig. 12 - Recovery plan BRAVO

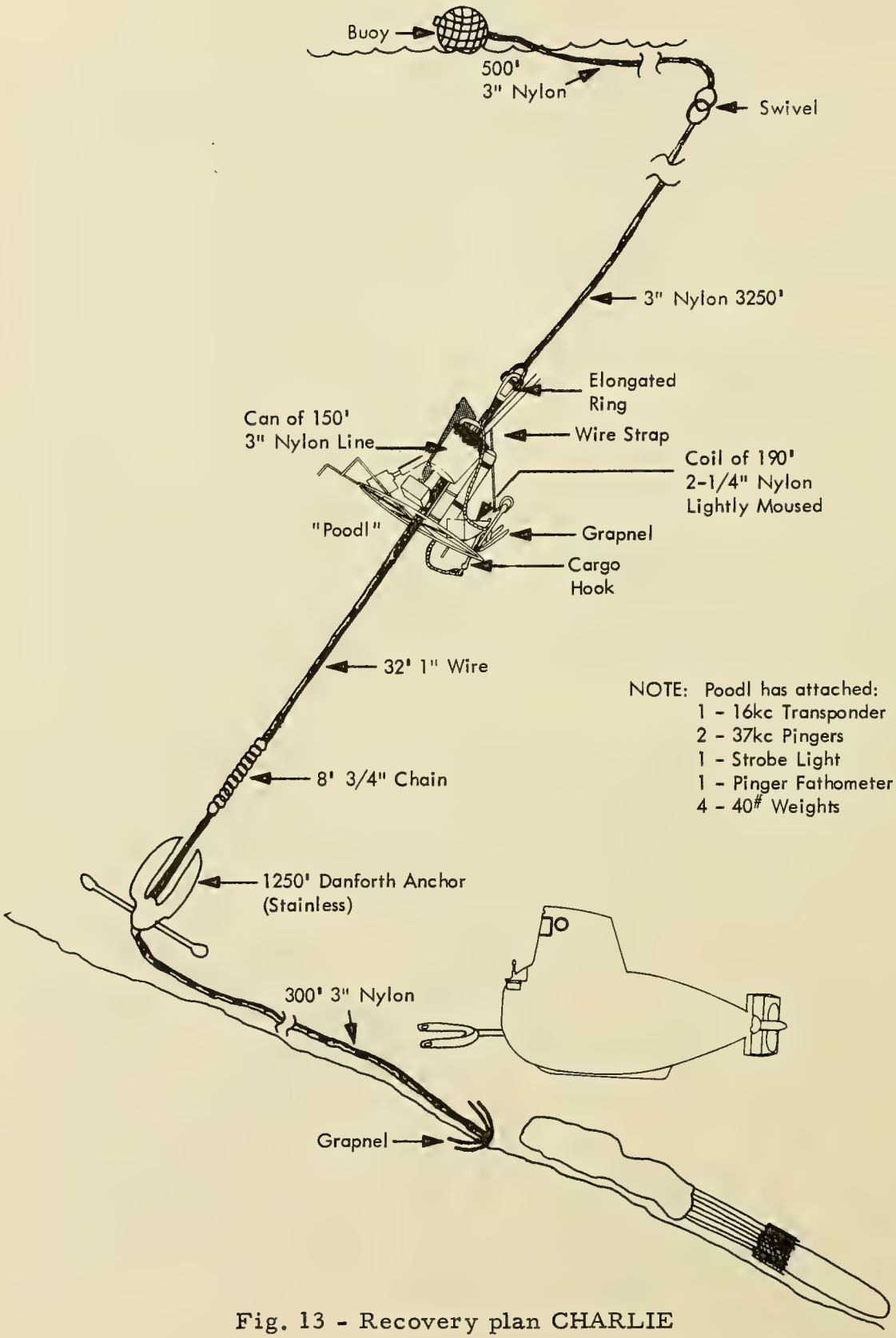

Fig. 13 - Recovery plan CHARLIE

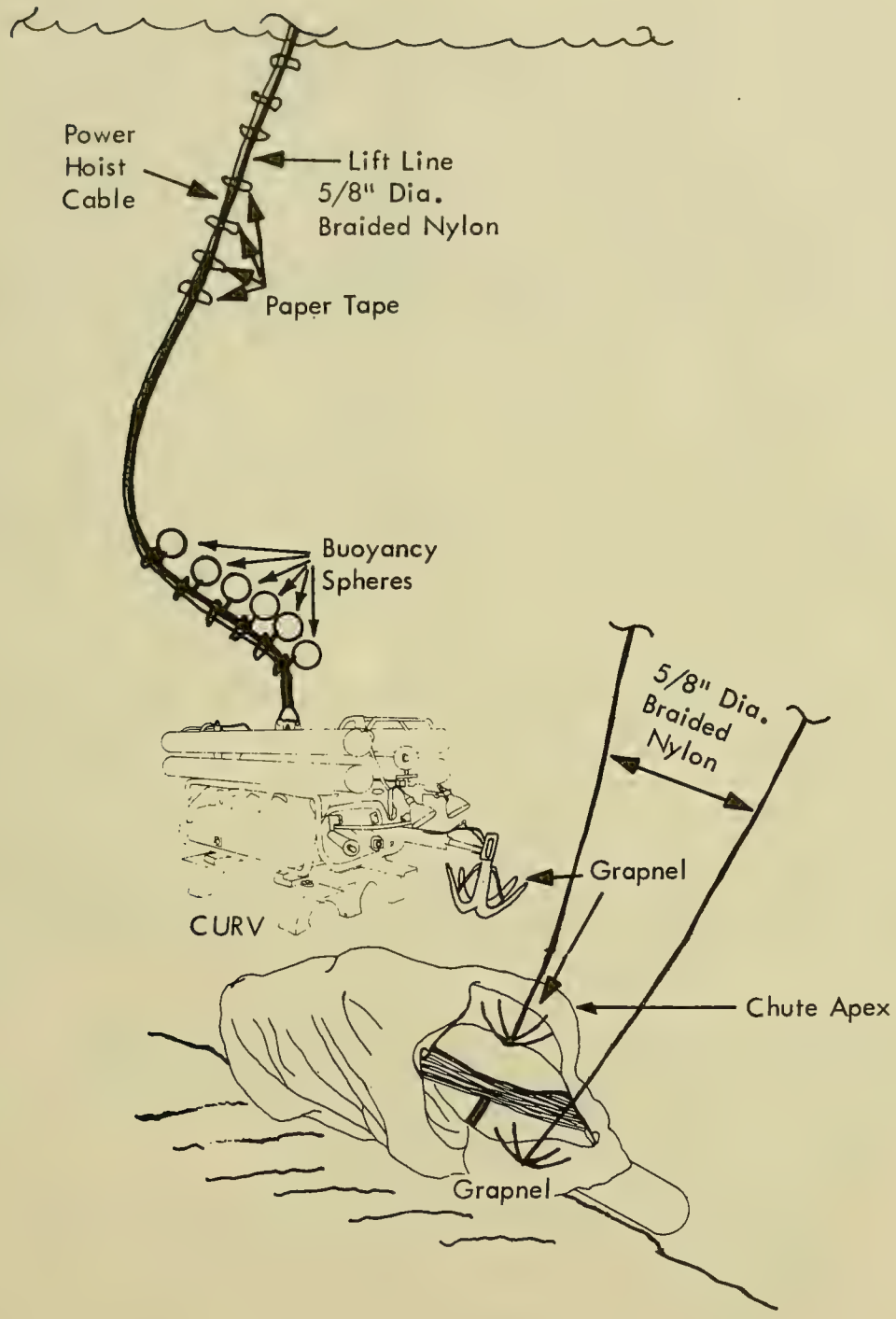

Fig. 14 - CURV recovery

CURV had been successfully tested to 2800 feet. A demonstration recovery of a dummy shape was successfully completed at a depth of 1050 feet off Palomares. CURV was to be operated to affix the lifting attachments. Three lifting lines were to be used with one of the three lines as a lazy tether long enough to remain attached should failure occur and send the weapon to the deepest canyon. In the act of attaching the third line, CURV itself became entangled in the weapon parachute. The bomb and the CURV were hauled up together. Figure 14 shows the CURV in action. CURV is an unmanned, self-propelled tethered vehicle with 5 basic systems (hydraulic, propulsion, sonar, claw, and optical) to carry out its location and retrieval function. It is described in detail in both the interim and final report.

The significant conclusions from the recovery operation were:

1. The underwater tracking system (UTE) mounted on USNS MIZAR was a vital factor in the recovery operation enabling the weapon once located to be revisited time and time again. Thus ALVIN, ALUMINAUT, the POODL, and CURV were all vectored to the site of the bomb on various occasions. UTE navigation errors were on the order of $\pm$ 80 feet.

2. The necessity to separate surface motions from the motions of the submerged recovery device, stated by Craven and Searle[6], was in evidence at all times during the recovery. For example Plan ALFA AND BRAVO failed because the systems used could not account adequately for this relative motion.

3. The use of an unmanned, remotely operated, tethered vehicle solved the relative motion problem between surface and attachment, and in addition, decreased the safety hazard one would encounter with a manned vehicle.

4. The manned vehicles were extremely useful for human observations and study of the target recovery situation. In addition ALVIN was successful at making attachments to the weapon.

The major "recovery" recommendations were:

- Continue development on methods employing an intermediate mass or other means to decouple surface action. Such development should consider both manned and unmanned vehicles.
- Develop a general purpose tool kit for both manned and unmanned vehicles to include:

  Line cutters, penetrating attachments, detachable claws with adjustable grab, latching grapnels.

- Manipulator development should emphasize dexterity, weight capability, and two handed function.

GENERAL SUMMARY

The most significant search and identification lesson learned in SALVOPS/MED is the inadequacy of sonar in classification. Improved acoustic classification, and the integration of acoustic, magnetic anomaly, visual detection, and other detection means into one package are indicated. The most significant recovery lesson is the necessity for decoupling surface motion from attachment motion. Precise underwater navigation is needed for search and recovery. Both evolutions become marginally possible to totally impossible with increasing navigation error. Finally, as for all such type operations as SALVOPS/MED, there is no substitute for at sea test and evaluation of all procedures, plans, and equipment prior to the real action.

REFERENCES

1. "Aircraft Salvops Med, Sea Search and Recovery of an Unarmed Nuclear Weapon by Task Force 65," Interim Report 15 July 1966.

2. "Sea Search and Recovery of an Unarmed Nuclear Weapon," Final Report 15 Feb. 1967.

3. "Lessons and Implications, Aircraft Salvage Operation Mediterranean," Executive Summary 8 April 1967.

4. "An Analytical Review of Lessons Learned from the H-Bomb Sea Search off Spain. Part II," by E. L. Beach presented at Fourth U. S. Navy Symposium on Military Oceanography 10 May 1967.

5. Reference 2. Part 2, Chapter V, "Operations Analysis," by H. R. Richardson.

6. "The Engineering of Sea Systems," J. P. Craven and W. F. Searle, Transactions of the 2nd Annual MTS Conference and Exhibit, June 27-29, 1966.

SUBMARINE TOPOGRAPHIC ECHOES FROM CHASE V

John Northrop
Marine Physical Laboratory of the Scripps Institution of Oceanography
University of California, San Diego

ABSTRACT

Hydroacoustic waves from the 1 kiloton CHASE V shot detonated off Cape Mendocino, California, were recorded 150 miles (240 km) north of Hawaii on FLIP. Reverberations were received for 2-1/2 hours after the direct arrival. Some of the prominent reflectors have been identified as the continental shelf of North America, the Hawaiian Arch, the Aleutian Ridge, the Emperor Seamounts, the Volshouki Ridge, the Kuril Islands, and the Japanese Islands. The reflections indicate the presence of as yet uncharted seamounts between the Emperor Seamounts and Japan in the vicinity of the Volshouki Ridge.

INTRODUCTION

A series of large (~1 kiloton) underwater explosion tests has been carried out by the Office of Naval Research under the CHASE (for Cut Holes And Sink Experiment) program. The first 4 were completed in the Atlantic Ocean and involved the demolition of surplus explosives from obsolete ships which were towed to sea, sunk, and detonated. The ammunition ship ISSAC VAN ZANDT was used for the first Pacific Ocean experiment, CHASE V. She was towed to sea and sunk at 39°28'N, 125°48'W (Fig. 1). Detonation was achieved at $05^h49^m06.85^s$ GMT on 24 May 1966. The shot depth was 3750 ft ± 250 ft and the depth of water was 12,500 ± 100 ft.[1] The yield was calculated to be 1.0 ± 0.2 kiloton from an analysis of the bubble-pulse interval (0.57 sec) and time constant of the shock wave (25 milliseconds) measured at a distance of 4.5 nautical miles.[1] The hydroacoustic waves were recorded 2000 miles (3200 km) away near the Hawaiian Islands by hydrophones suspended from the R/P FLIP (Scripps Institution), the R/V TERITU (University of Hawaii), and by both hydrophones and ocean-bottom seismographs from R/V YAQUINA (University of Oregon) during Expedition SHOW (Scripps-Hawaii-Oregon-Washington). FLIP was stationed at

23°03'N, 153°50'W in about 5 km of water; TERITU was at 22°27.8'N, 154°02.5'W; and YAQUINA was at 22°28.1'N, 153°10.1'W. Only the FLIP data will be discussed in this report.

METHOD

Three crystal hydrophones (AX-58-C) were suspended at a depth of about 250 ft (75 m) from floats connected by cable to FLIP. The hydrophones were isolated from cable-suspension noise by a series of neutrally-buoyant floats[2] and were streamed from FLIP on individual cables out to distances of from 500 to 1000 ft (150 to 300 m) (Fig. 2). This method of hydrophone suspension from FLIP has been found[3] to reduce the ambient noise level at the hydrophones to that measured for sea state two[4,5] in the frequency range of interest (4-400 cps). The hydrophone had a sensitivity of -79 dB re 1 volt per microbar. The signals were passed through a frequency dividing network[6] and split into two bands, 3-20 cps and 20-200 cps. Higher frequencies were passed on to a third stage amplifier and rectified prior to recording. Signals in the low- and intermediate-frequency bands were passed through a 40 dB (variable) amplifier. Each amplifier had high- and low-gain outputs with 20 dB separation between channels. The signals were recorded on an oscillographic camera, a pen recorder, and magnetic tape.

Analysis of Data

Arrival times and signal levels were picked on the records and total path distances computed from the elapsed time between shot and receiver, assuming a speed of sound in water of 1.47 km/sec. The events recorded after the direct hydroacoustic wave were correlated, where possible, with known submarine prominences by the use of a calibrated scale in conjunction with a 36 in. diameter globe. For each reflection travel time, one end of the scale was placed at the shot position, one at the receiver position, and an arc of possible reflectors traced. Two assumptions were made in analysis: (1) that the hydroacoustic waves traveled along great circle routes between source, reflector, and receiver with no horizontal refraction, and (2) that the main packet of energy traveled via continuously refracted SOFAR (Sound Fixing and Ranging) paths in the deep sound channel.

RESULTS

The Precursor

The earliest arrival on the FLIP records was a low-frequency (~5 cps) precursor that emerged from the background 23 sec ahead of the direct hydroacoustic wave (Figs. 3 and 4). The precursor probably corresponds to the ground wave of normal-mode propagation and the main peak to the "rider" wave of Pekeris.[8]

Similar precursors have been observed from large underwater explosions in the Pacific (C. T. Johnson, personal communication) and earthquake T phases.[9]

The Direct Wave

The main hydroacoustic wave was recorded on FLIP at $06^h25^m17^s$ GMT indicating a velocity of 1.47 km/sec, which is the speed of sound in the SOFAR channel. Although the shot depth was slightly below the depth of minimum velocity, energy was introduced into the SOFAR channel because of the sound velocity structure in the shot area (Fig. 5). The sound energy traveled outward from the source via a combination of Surface/Bottom reflected (SR/BR) paths and continuously refracted (RRR) paths. Over the long ranges utilized in this experiment, the SR/BR rays have reflection losses of 1 or 2 dB at each reflection and eventually become unimportant (the rays converge about every 35 miles, indicating at least 50 surface reflections and an equal number of bottom reflections over the path to Hawaii). Thus, only RRR sound rays need be considered in this analysis of the underwater acoustic signals received on FLIP. Sound energy was received at the off-axis FLIP hydrophones at a level of about 66 dB above background noise (Fig. 6). An oscillographic record of the direct arrival (Fig. 4) shows dispersion in the low- and intermediate-frequency bands. Peaks in the high-frequency band correspond to individual sound ray arrivals before the main (overload) arrival. After the main arrival, the first and second bubble pulse arrivals are evident in the high-frequency (rectified) trace.

Topographic Reflections

In this section, the prominent reflections are identified from arrival times and signal levels of Figs. 3 and 6. The location of these reflectors is shown in Fig. 1.

The first reflection appears on the record before the complete decay of the reverberation from the direct wave and is difficult to identify. However, the observed travel time is approximately equal to that computed for a reflection from the Mendocino Escarpment. This reflection is followed 2 min later by a long-duration return from the continental slope of the North American continent (Reflector A of Fig. 1).

The next series of reflections is from the Hawaiian Arch (Reflector B of Fig. 1). The reverberation lasts for 25 min (Fig. 6) and includes reflections from Hawaii, Maui, Molokai, Oahu, Kauai, Nihoa, Necker, and Midway islands, as well as the many reefs in the vicinity of French Frigate Shoals and Gardner Pinacles. Individual, short duration reflectors from the neighborhood of Mellish Seamount (29°N, 171°W) are also present in the data.

Reflections from the Aleutian Islands (Reflector C of Fig. 1) last for 15 min. Travel time considerations indicate that the first of this group of reflections is from the insular shelf south of Kodiak, Alaska. Continued reverberations were received from the Aleutian Ridge as far west as the insular shelf south of Adak Island.

A series of short reflections from the Emperor Seamount Chain (Reflector D of Fig. 1) account for the next set of reverberations. The first of this set of reflections is from a seamount on the southern end of the seamount chain near 32°N, 179°E. The other seamounts then cause a series of short (~10 sec) reflections on the record. Echoes were recorded from the southern seamounts before the northern ones. A reflection from the seamount near 49°N, 169°E is the last to be received because the more northern ones are in the shadow of the Aleutian Ridge. Identification of individual reflectors has been impossible because of the multiplicity of seamounts and relatively poor bathymetric charts in the area.

After 8 min of low-level noise, a series of reflections was received which lasted for 12 min. Individual bursts within this time lasted from 10-40 sec, with an average of 21 sec. The only mapped submarine topographic feature that could account for these reflections is the large (about 600 miles(960 km)long) shallow rise known as Volshouki Ridge (Reflector E of Fig. 1). This set of reflections is therefore ascribed to individual peaks on the Ridge.

Reflections from the Kuril Islands next appear on the records (Reflector F of Fig. 1). The first echo is from Long Island (46°N, 150°E), the more northern ones being in the shadow of the Aleutians for great circle paths from Cape Mendocino. The Kuril reflections all exhibit relatively low signal-to-noise ratio (Fig. 6) because of: (1) the long ranges involved (~8000 miles (1300 km)), (2) the interference of the intervening Emperor Seamounts, and (3) the onset of propeller noise from an approaching merchant vessel in the vicinity of FLIP.

The last reflection identified on the FLIP records corresponds to the submarine slope off the Island of Hokkaido, Japan (Reflector G of Fig. 1). This signal lasts for over half a minute before it is finally lost in the increasing ship noise which dominated the remainder of the record.

Signal Level

The signal level from a one kiloton charge at SOFAR depth can be calculated from the equation:

$$I_R = I_o - (71 + 15 \log_{10} R) - 0.0035 R \qquad (1)$$

where I_R is the level in dB re 1 dyne/cm^2 at a distance R in nautical miles from a shot of intensity I_o, the effective source strength (intensity at a range of 1 yd). For spectral energy within a specific frequency band, an auxiliary formula may be used:[10]

$$I_o\left(f_L \text{ to } f_U\right) = I_o + 10 \log 2/\pi \left[\tan^{-1}\left(f_U/f'\right) - \tan^{-1}\left(f_L/f'\right)\right] \qquad (2)$$

where f_U and f_L are the upper and lower frequencies respectively, and f' is the half-power frequency at the range where the pressure is 100 psi.

Using these formulas and assuming spherical spreading to a distance of 10 miles and semi-spherical spreading (4.5 dB per distance doubled) beyond (Equation (1)), a calculated level of 69 dB re 1 dyne/cm^2 is computed in the frequency band 3-20 cps. It is difficult to speculate on the observed signal level for this direct arrival because of recording system overload. From the data available, it appears that levels near 66 dB above ambient noise were recorded for the low-frequency band. The level for intermediate frequencies was about 20 dB lower because the greater part of the energy for large explosions is in the low frequencies and greater attenuation is experienced at higher frequencies (0.005 instead of 0.003 dB per nautical mile).

Discussion

Recording of topographic reflections from CHASE V was selective at the FLIP site in that the Hawaiian Arch prevented reception of reflected signals from the South Pacific. Even with this reduction of reflectors, it was still difficult with the method used to identify all of the arrivals noted. The first few returns after the decay of the main arrival were fairly easy to identify, but after that the multiplicity of targets that satisfied the travel time considerations increased. For example, the round-trip travel time shot to Vancouver to FLIP is the same as that from shot to Hawaii Ridge to FLIP. Therefore, even though multiple reflection paths (shot to Hawaii to Aleutians to FLIP for example) were excluded because of travel time considerations, the multiplicity of arrivals was such that individual targets were difficult to identify. Further identification by arrival time differences between FLIP, TERITU, and YAQUINA data were attempted to resolve these reflectors. However, the YAQUINA recorder was secured because of poor signal-to-noise ratio shortly after the Hawaiian reflection was received, and the TERITU in the interval between the Hawaiian and Aleutian reflections. Therefore, groups of arrivals with nearly the same signal level were isolated and labeled A, B, C, D, E, F, and G on Fig. 1. These general groupings are believed to be correct, although as the total travel time increased, the number of possible reflectors multiplied rapidly and errors in the later identifications are more probable than in the early ones.

Recorded signal levels for reflected sound are all below that of the direct wave because of increased spreading loss over the greater travel paths involved and because of scattering loss on bottom reflection. The signal level for Hawaiian reflectors is greater than the California Slope reflectors, probably because of the steeper slopes of the former and the lack of sedimentary cover. More distant reflectors produce levels not inconsistent with spreading and attenuation losses observed by Sheehy and Halley.[7] A curve of the level vs range computed from Equations (1) and (2) is shown on Fig. 6 to indicate the relative loss for individual reflectors.

CONCLUSIONS

1. A low-frequency seismic precursor was recorded 20 sec before the SOFAR arrival.

2. The main hydroacoustic wave was recorded at a level near 66 dB above ambient noise.

3. Topographic reflections were recorded for 2-1/2 hours after the main arrival.

4. Reflections from the continental shelf off California were 35 dB below the calculated level for a non-reflected path, whereas the other reflectors were only 20-25 dB lower.

5. Reflections from many seamounts of the Emperor Seamount Chain were received, as well as from Volshouki Ridge.

6. Reflections in the 3-20 cps band were 20-25 dB higher than in the 20-400 cps band.

ACKNOWLEDGMENTS

This work was supported by the Office of Naval Research. R. W. Raitt provided some of the records and, with P. Rudnick, gave valuable suggestions in data analysis. Information on the Ocean Bottom Seismograph results was provided by H. Bradner; the TERITU records by A. Furumoto; and the YAQUINA records by R. P. Meyer of the University of Wisconsin, and A. C. Jones of the Marine Physical Laboratory. E. W. Werner gave valuable assistance in data reduction.

REFERENCES

1. Underwater Systems, Inc., CHASE V Source Data Tech. Prog. Rep. 11, 10 pages, June 1966.

2. Raitt, R. W., Geophysical measurements, Natl. Acad. Sci., Natl. Res. Council Publ. 309, 70-84, 1952.

3. Northrop, J., and R. H. Johnson, Seismic waves recorded in the North Pacific from FLIP, J. Geophys. Res., 70, 311-318, 1965.

4. Squier, E. E., FLIP acoustical self-noise, Univ. of Calif., San Diego, Marine Phys. Lab., Scripps Inst. Oceanog., SIO Ref. 66-12, 8 pages, July 1966.

5. NDRC Summary Tech. Rep., Div. 6, Principles of underwater sound, reprinted by Committee on Undersea Warfare, National Research Council, Washington, D. C., 1946, Vol. 7.

6. Jones, A. C., Seismic equipment manual, Univ. of Calif., San Diego, Marine Phys. Lab., Scripps Inst. Oceanog., TM-143, 48 pages, January 1964.

7. Sheehy, M. J., and R. Halley, Measurement of the attenuation of low-frequency underwater sound, J. Acoust. Soc. Am., 29, 464-469, 1957.

8. Pekeris, C. L., Theory of propagation of explosive sound in shallow water in Propagation of Sound in the Ocean, Geol. Soc. Am., Memoir 27, October 1948.

9. Johnson, R. H., Spectrum and dispersion of Pacific T phases, Hawaii Inst. of Geophys. Rep. 34, 12 pages, June 1963.

10. Johnson, C. T., W. P. de la Houssaye, and T. McMillian, Hydroacoustic signals at long ranges from shot SWORDFISH, U. S. Navy Elect. Lab. Res. Rep. 1212, appendix 73-94, 10 March 1964.

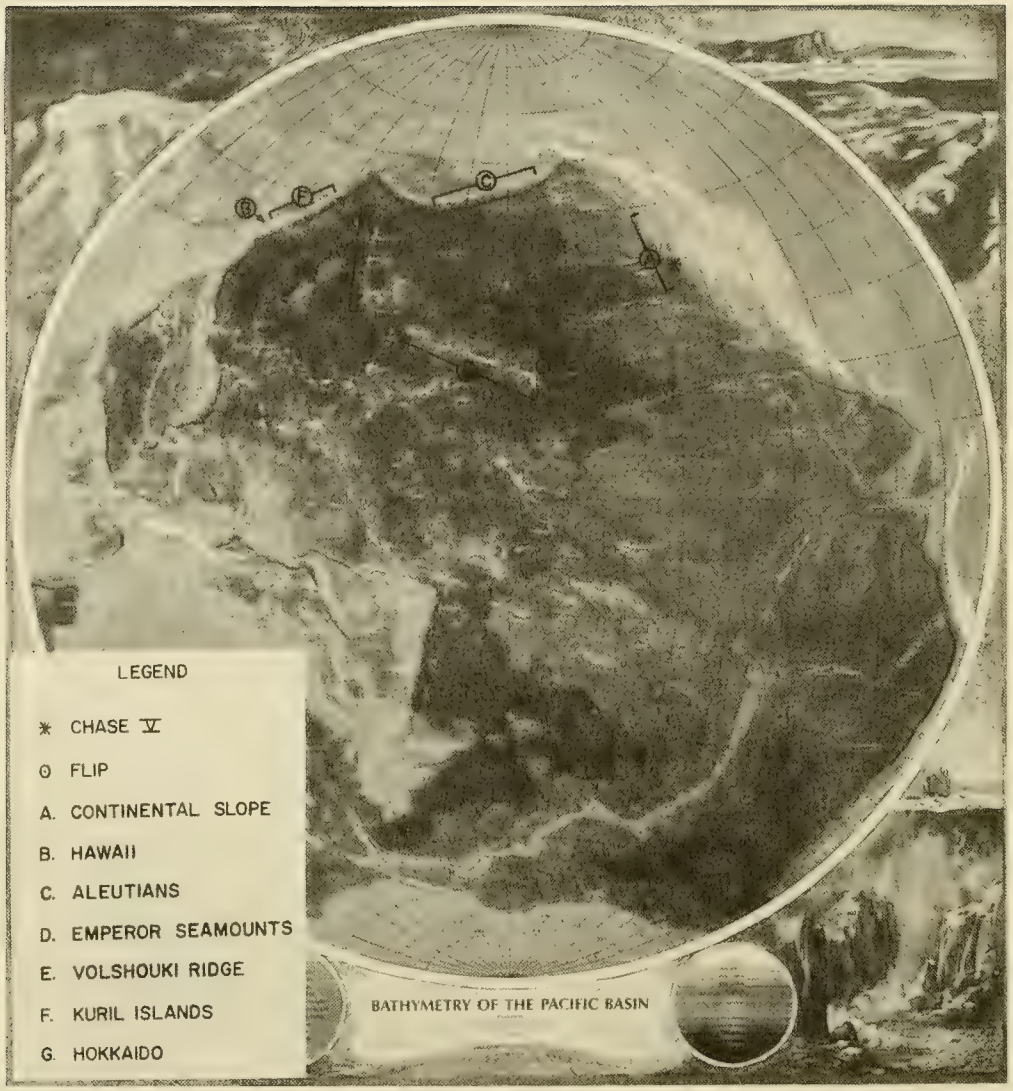

Fig. 1 - Location of area showing shot point, FLIP hydrophone position, and location of prominent reflectors

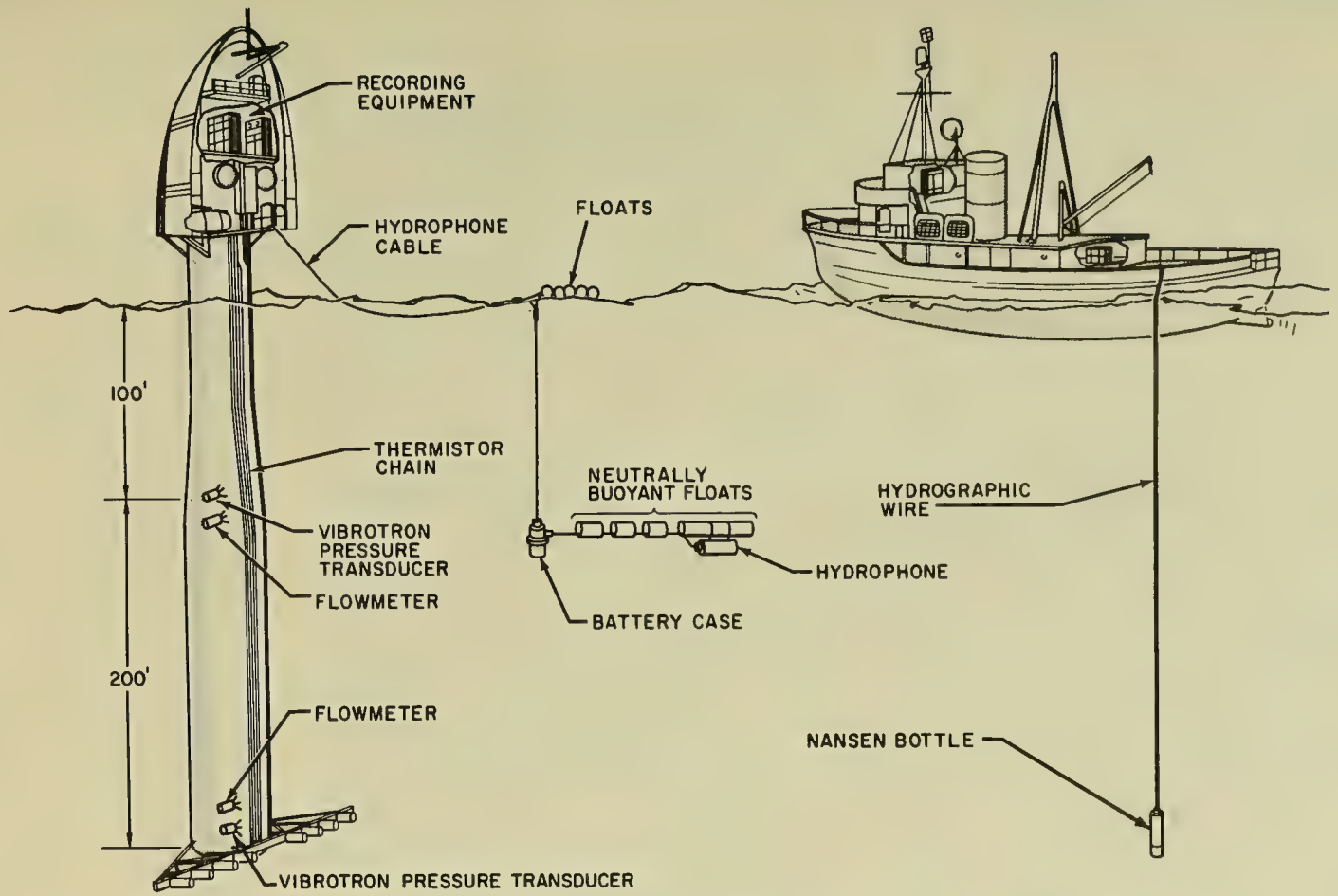

Fig. 2 - Hydrophone suspension system from FLIP

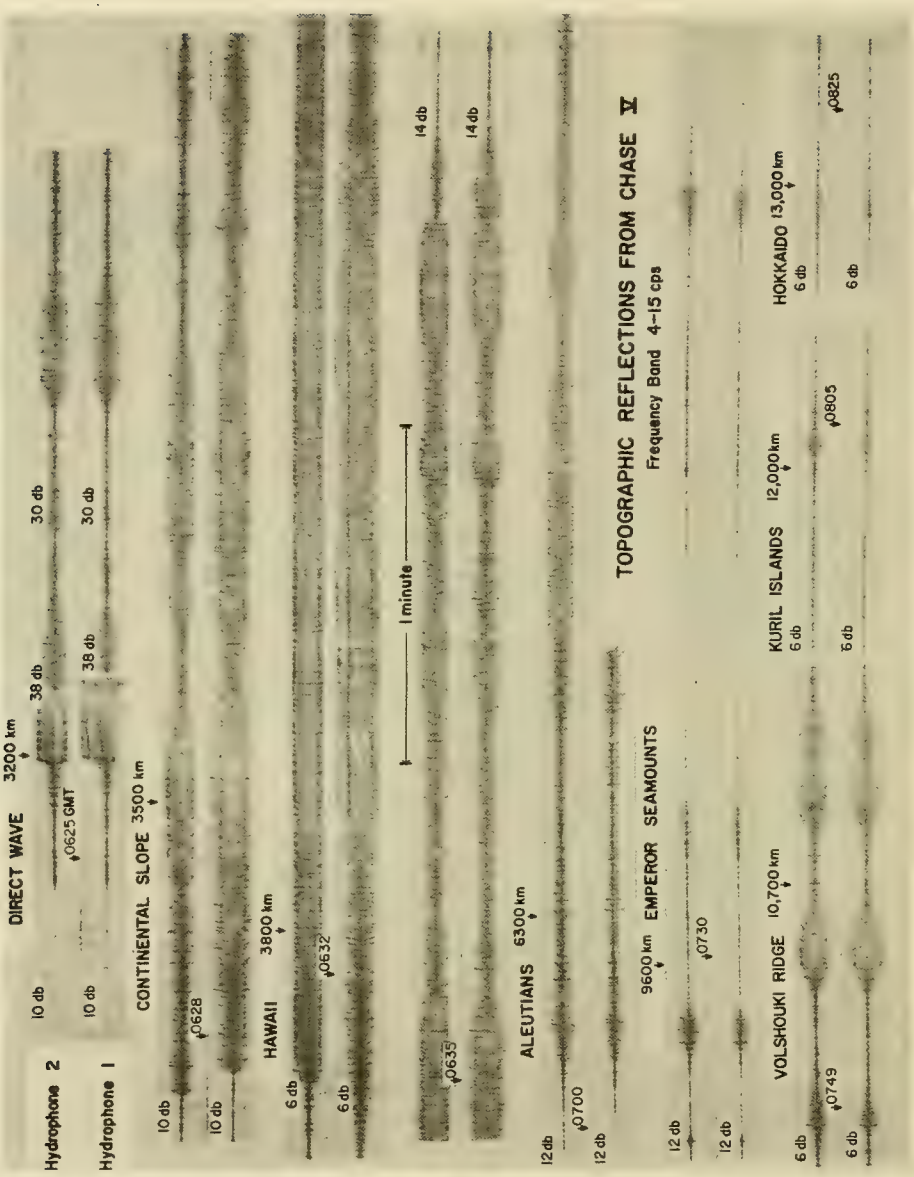

Fig. 3 - Sample brush records from two hydrophones in the frequency band 4-20 cps. The record strips are not continuous but show typical reflections from which the data of Fig. 6 were compiled.

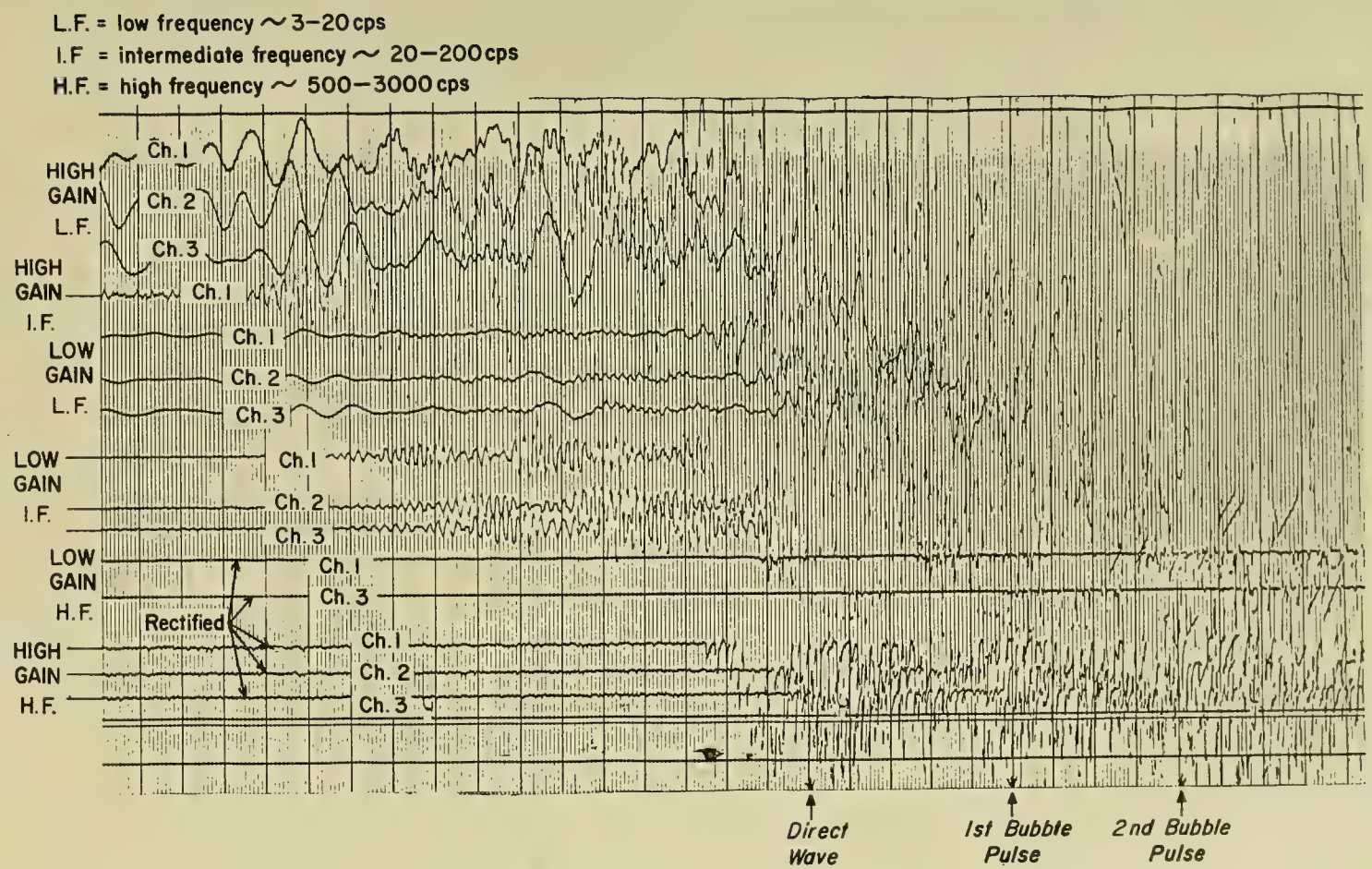

Fig. 4 - Oscillographic camera record of the main hydroacoustic wave in low-, intermediate-, and high-frequency bands

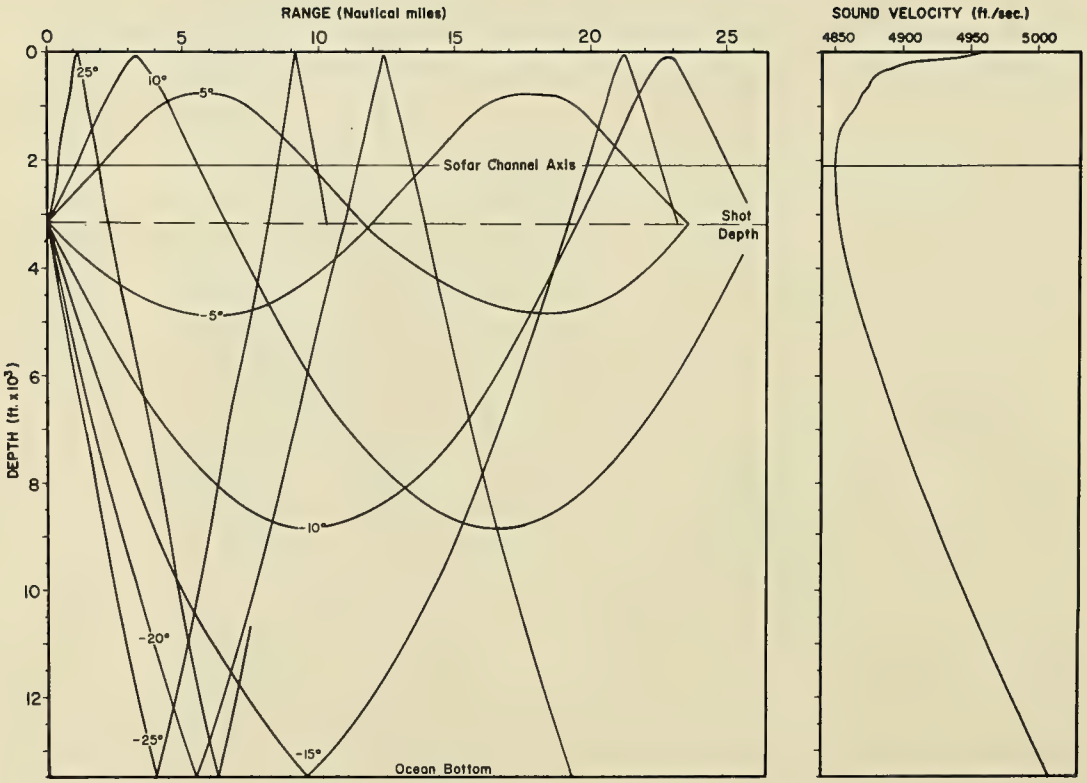

Fig. 5 - Ray diagram and vertical-velocity profile in the shot area

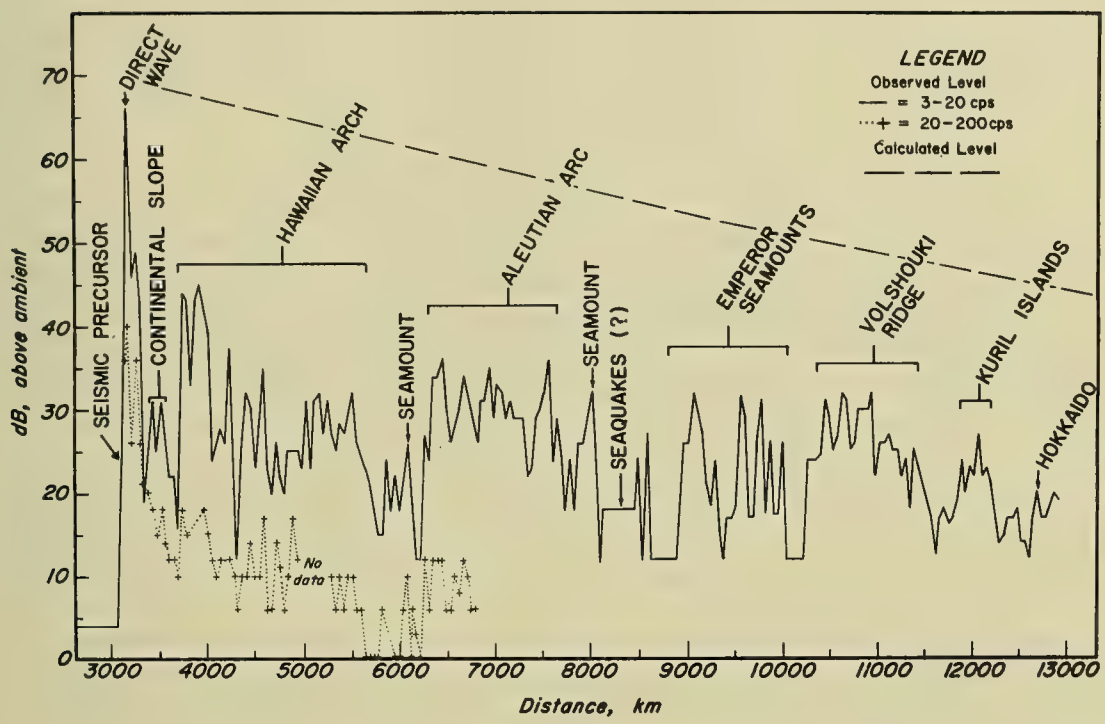

Fig. 6 - Sound pressure level vs range for CHASE V hydroacoustic waves. Pressure level is in dB above background noise. Slope of calculated curve is 4.5 dB per distance doubled (Reference (10)).

NEL MANNED SUBMERSIBLE OCEANOGRAPHIC SYSTEM
Modification 1

A. J. Schlosser
U. S. Navy Electronics Laboratory
San Diego, California 92152

Abstract: Manned oceanographic research within the Navy utilizing deep research vehicles began with the assignment of the bathyscaph TRIESTE I to the Navy Electronics Laboratory in September 1958. In June 1966 the first complete manned submersible system was established by the leasing of the Westinghouse Diving Service (DEEPSTAR DS-4000) and integrated with the scientific and professional capability established at NEL for eight years. During this eight-year period the technical and professional experience was gained from the use of the bathyscaphs TRIESTE I, ARCHIMEDE, and TRIESTE II, and the Cousteau Diving Saucer. This achievement provided an integrated and diversified system capable of conducting geological, biological, acoustical and physical oceanography investigations. Geological investigation systems involved use of coring devices, shear measurements of the sea floor, and photography of the various geological features prominent in the area. Biological investigations used listening devices, sampling methods of biological specimens and tracking of the scattering layer coordinated with echo soundings from a surface ship. Acoustical investigations were made throughout the water column measuring sound speed, pressure and temperature. Shear velocity through the bottom was measured by an explosive source and geophones. Additional investigations were accomplished by probes containing transducers implanted into the sea floor. Physical oceanography results were obtained by water-sampling temperature probes at various increments above the sea floor. The above instrumentation systems will be discussed. Manned submersibles, unique as they may be, are ineffective tools unless integrated into an oceanographic system with specific scientific mission profiles.

INTRODUCTION

Oceanographic research received a new tool with the acquisition of the bathyscaph TRIESTE in September 1958. Scientists at the Navy Electronics Laboratory began developing techniques that would allow maximum utilization of the bathyscaph for data collection. As technical competence increased the acquisition of more meaningful data was made possible by specially-developed instrumentation. Valuable knowledge was gained also from diving experience on the French bathyscaph, ARCHIMEDE, and on TRIESTE II. The minimal-payload Cousteau Diving Saucer was utilized to conduct shallow-water investigations.

Due to the payload and attachment restrictions of this latter vehicle, new instrumentation techniques were necessitated. One of the most important lessons learned was that data collection applicable to the oceanographic disciplines of acoustics, biology and geology was possible from any manned submersible if the instrumentation could be designed with a degree of flexibility to allow this interchange.

Paramount to any instrumentation system was the requirement for adequate ship facilities to support the submersible and the scientific program.

DISCUSSION

The various scientific disciplines at the Navy Electronics Laboratory engaged in the military aspects of oceanography require a submersible with a complete-facility support concept[1]. The support requirements include: (1) a surface support ship; (2) extended at-sea facilities with adequate berthing; and (3), the personnel to maintain and operate the ship and submersible. This service was best available through lease of the Westinghouse DEEPSTAR DS-4000 and its support facilities (see Fig. 1), which provided the scientific community with a highly mobile manned-submersible system and freed the technical community to concentrate on the instrumentation required for each particular scientist within his discipline.

By merging a leased diving service to a scientific program with firm mission profiles[2], a manned-submersible oceanographic system was established. The leasing service was based on "operating days" throughout the period of contract[3] in order to satisfy the quantity of dives required.

Fig. 1 - Westinghouse DEEPSTAR DS-4000 on board the support ship, BURCH TIDE (photograph by courtesy of Westinghouse)

SURFACE SUPPORT SHIP

The surface support ship was equipped with a Gifft echo sounder and recorder which was incorporated as standard instrumentation. This equipment could be trailed over the side for bottom profiles by each scientist at his discretion prior to diving at a given site. To further provide scientific support, a small shipboard van was utilized with the basic at-sea requirements for minor servicing and repair of electronic components and instruments.

INSTRUMENTING THE SUBMERSIBLE

Standard instrumentation aboard the submersible was established for the purpose of recording each mission profile. These instruments were included as part of the scientific payload, but were made removable where possible to provide payload flexibility. The movie camera was removed on many dives in order to add other scientific instruments.

External Attachments

Jettisonable instrumentation brow. The flexibility necessary for the "systems" approach called for an instrumentation-attachment device which would not only provide attachment points, but increase the payload to fulfill mission profiles. The NEL-designed, removable instrumentation brow[4], utilizing syntactic foam, provided this capability and payload was increased by 220 pounds. Shipboard changes could now be made, providing mission versatility and more efficient utilization of the submersible.

Tethering. The ability to hover at various increments of height from the sea floor necessitated development of a simple tethering device. Fig. 2 illustrates a typical tether arrangement. The procedure followed on this type of dive was for DEEPSTAR to descend full-tether distance from the bottom. By means of forward propulsion during final descent, the tether was allowed to string out aft and lay in that position as measurements were made on the sea floor. Small weights equal to the weight of the first tether were then dropped and DEEPSTAR would ascend to the desired height above the sea floor and provide a stable platform for further measurements in the desired increments of distance from the bottom.

Lighting. DEEPSTAR was equipped with external lighting conforming to specifications[1], and sufficient for visual identification and viewing.

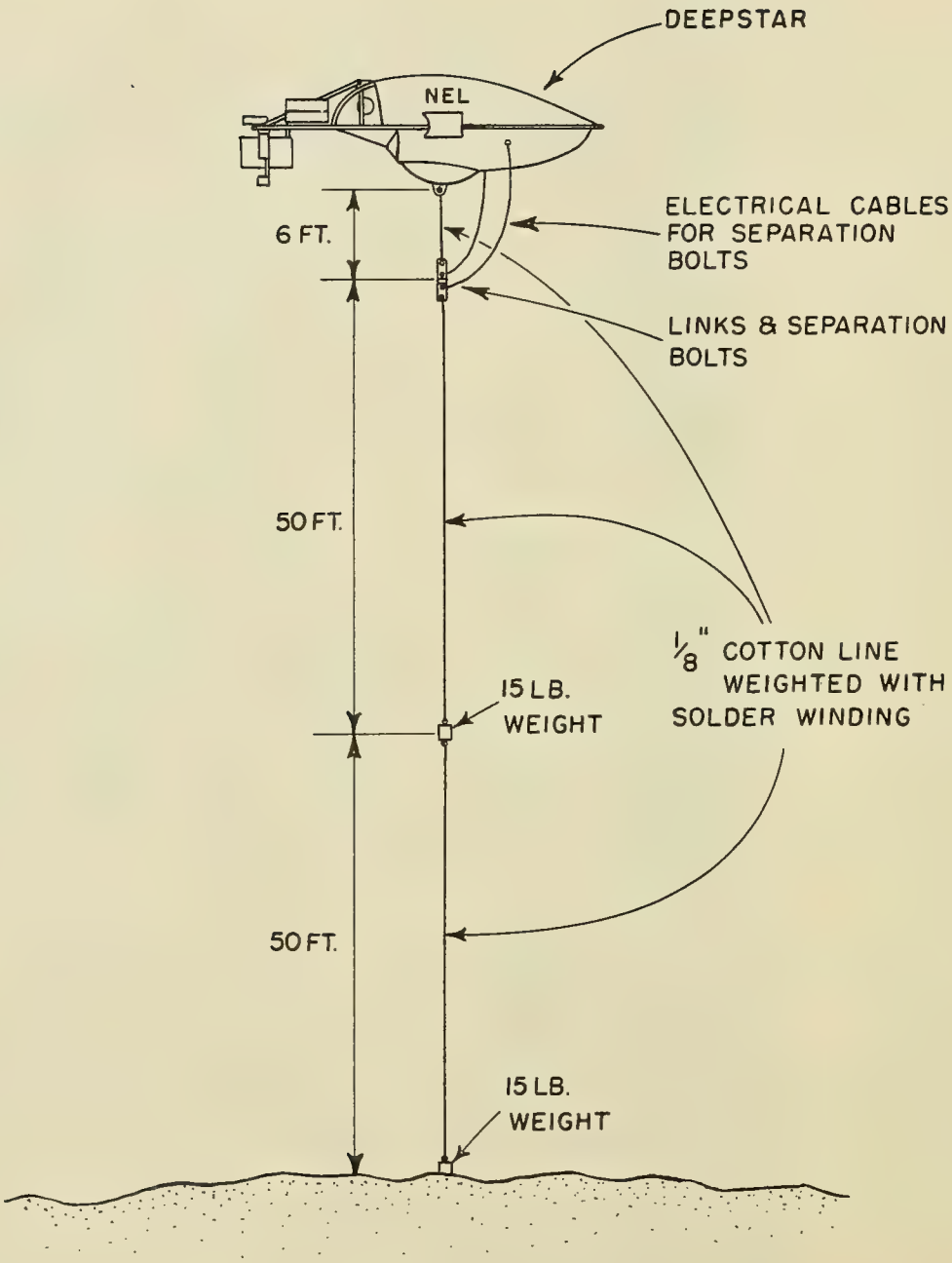
DEEPSTAR
NEL
ELECTRICAL CABLES FOR SEPARATION BOLTS
6 FT.
LINKS & SEPARATION BOLTS
50 FT.
1/8" COTTON LINE WEIGHTED WITH SOLDER WINDING
15 LB. WEIGHT
50 FT.
15 LB. WEIGHT

Figure 2

Manipulator. A manipulator, or mechanical arm, capable of collecting specimens was provided as part of the submersible. The arm was incapable of use for or adaptation to extensive core sampling but met the minimal scientific needs.

Instrumentation Power and Signal Requirements

The instrumentation power and signal requirements were made independent of the control and power supply systems of DEEPSTAR. Silvercell batteries supplied the DC power (24-28 volts). AC power was provided by static inverters. The power package was located within the personnel sphere beneath the observer's couch. Three power packages were assembled, providing two spares to be carried aboard the support ship, one of which was on recharge during each dive. A separate terminal board within the sphere consisting of 50 connections was allocated, thus allowing instrumentation changes to be accomplished without interruption to or interference with the submersible's system. Through-hull penetrations allocated to "science" from the terminal board were externally terminated in eight female connector junction boxes, located forward of the sphere and adjacent to the brow. Four junction boxes providing 32 connections were available for brow instrumentation hookups. A single eight-connector junction box was located aft of the personnel sphere. All junction boxes were Electro Oceanic-type, therefore all instrumentation was equipped with suitable male connectors. This standardization was made on all scientific equipments.

Standard Sphere Instrumentation

Standard instrumentation is that which is added on request of the user laboratory or which may be already a part of the submersible, as covered in negotiations and specified as a contract requirement. These items may vary, dependent upon mission profiles established as part of the scientific program. Fig. 3 illustrates the sphere layout. The starboard side is devoted to the scientific program.

Viewports. An observation capability to enable the scientist to view the water column, sea floor, or the performance of the external instrumentation, was a "must". To insure continuous viewing a separate viewport from that of the pilot was specified. This "instrument" obviously must be a part of the submersible.

Cameras. Mission profiles established the necessity of photographic capability, in color, for both still and motion pictures. The 300-frame, 70-mm still camera was mounted externally of the sphere

Fig. 3 - DEEPSTAR DS-4000 shpere instrumentation controls

with strobe lights providing illumination. Motion pictures were obtained by an internally-mounted 16-mm camera with a 400-foot film capacity. Film cannisters could be changed during a dive, providing unlimited motion-picture coverage. A separate camera viewport was located between those of the pilot and observer. Both the still and motion-picture cameras had the same focal point and the frame control was indexed at the observer's window. The control panel was located at the scientific observer's station, providing him complete control of the photography.

Voice tape recorder. A tape recorder was made part of the standard sphere instrumentation, providing the scientist-observer with the freedom to continue vocal observations of the sea floor or the experiment without interruption or loss of visual contact. From past experience, the recorder reliability was deemed paramount over all other basic requirements set forth for this instrument. The high humidity within the personnel sphere had, in the past, precluded any reliance on the availability of continuous and complete dive records. The recorder selected was a battery-powered Stancil-Hoffman, hermetically sealed by an "O" ring, capable of 6 hours of continuous operations. The speed used was 15/16 ips. Two recorders were used throughout the program, each containing its own rechargeable batteries. A recharge unit was carried in the equipment van aboard the support ship, which provided for one unit to be on charge at all times and insured availability of power during extended at-sea operations.

Two-channel oceanographic instrumentation package. In order to measure the temperature, pressure and sound speed through the water column, a standard suite of instruments was carried during each dive. This package was called the "2-channel oceanographic instrumentation package"[5] and provided data recorded on tape by frequency division. This information is now being correlated and will provide information on anomalies which occur within the water column at the various dive sites. This instrumentation package was located externally and aft of the personnel sphere. The sound-speed and temperature sensors were located so as to provide maximum exposure within the water column (see Fig. 4).

INSTRUMENTATION TESTING

Prior to use or installation on DEEPSTAR each instrument was tested to provide as high a reliability factor as possible. These tests, while not always sophisticated, did achieve the desired results. All electronics components were thoroughly tested within

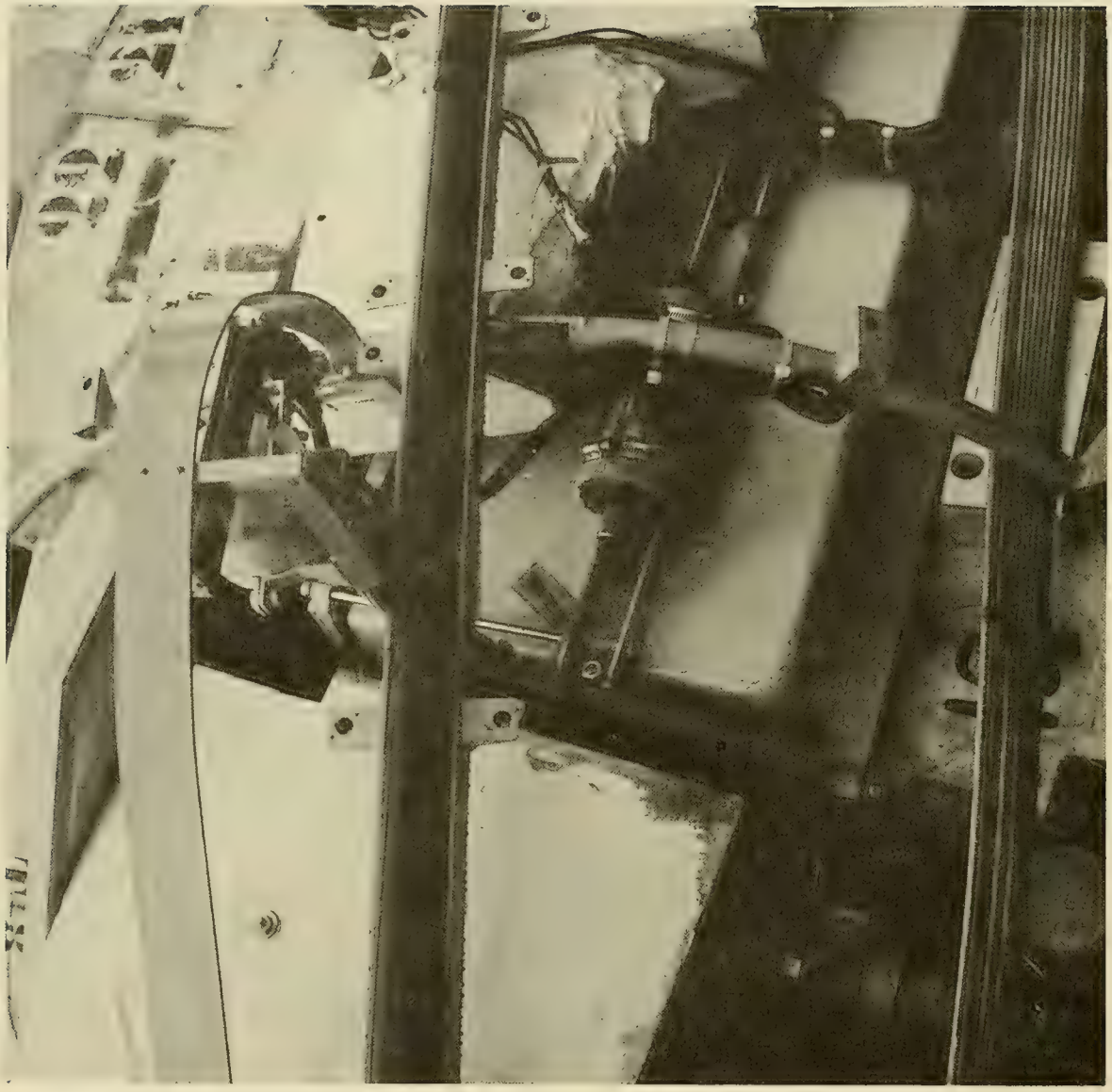

Fig. 4 - External temperature and sound-speed sensors for the 2-channel instrumentation package

the laboratory and those to be externally mounted on DEEPSTAR were then encapsulated within their individual pressure cases. All pressure cases were proofed beyond the minimums established by the Safety Certification requirements. Each component was then tested in the environment by means of a dockside evaluation. Those items performing mechanical functions were tested at pressure in a 20,000-psi pressure vessel. As each individual component tested satisfactorily, it was integrated into its particular system and a full-system test made. This latter was done as a bench check; however, a dockside test was always conducted when feasible. Upon installation of each component in DEEPSTAR, a complete functional recheck was accomplished. This thorough testing procedure provided a high confidence level in the instrumentation used.

BIO-ACOUSTICS

Bio-Acoustics aspects of the mission profiles were primarily concerned with the scattering layers[6,7]. Fig. 5 is typical of the instrumentation added to DEEPSTAR for this program. The "slurper", developed by the Mechanical Engineering Division at NEL, is a specimen-collecting device actuated by the observer within the sphere. The transducer was mounted on the brow and enabled DEEPSTAR to go below the scattering layer and obtain upward observations which could then be correlated with echo soundings made from the surface ship. All photographic equipment was utilized during scattering layer operations. For some Bio-Acoustics applications, another transducer replaced the still camera (see Fig. 6). A metal sphere suspended from the brow was used for calibration of signal strength[8].

GEOLOGY

The vehicle configuration necessary to accomplish the varied sea-floor studies[9,10,11] within the mission profiles was "bare-boat" (Fig. 7) or with the brow (Fig. 8). The brow was used to enhance lighting for motion-picture photography by the addition of two quartz-iodide lamps. The standard lighting was reconfigured for these specific dives. Core samples were taken by use of the mechanical arm which would select the core from the fairing attachment and drop it into the hydraulically-actuated specimen basket. This method was not completely satisfactory due to the deficiencies in the mechanical arm design as noted previously. However, the arm did prove valuable in collecting rock and biological samples from the sea floor.

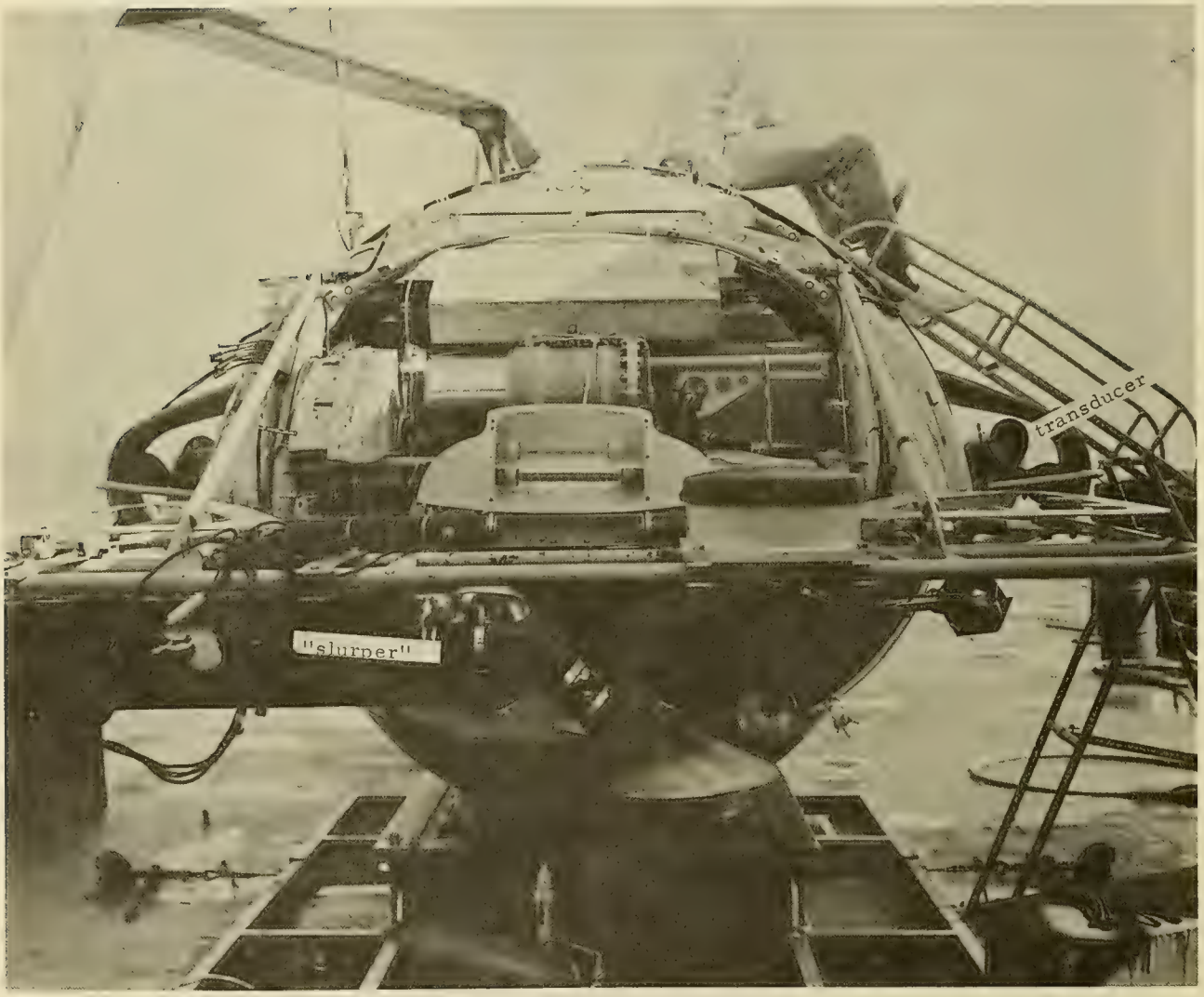

Fig. 5 - Bio-Acoustic instrumentation for scattering-layer studies

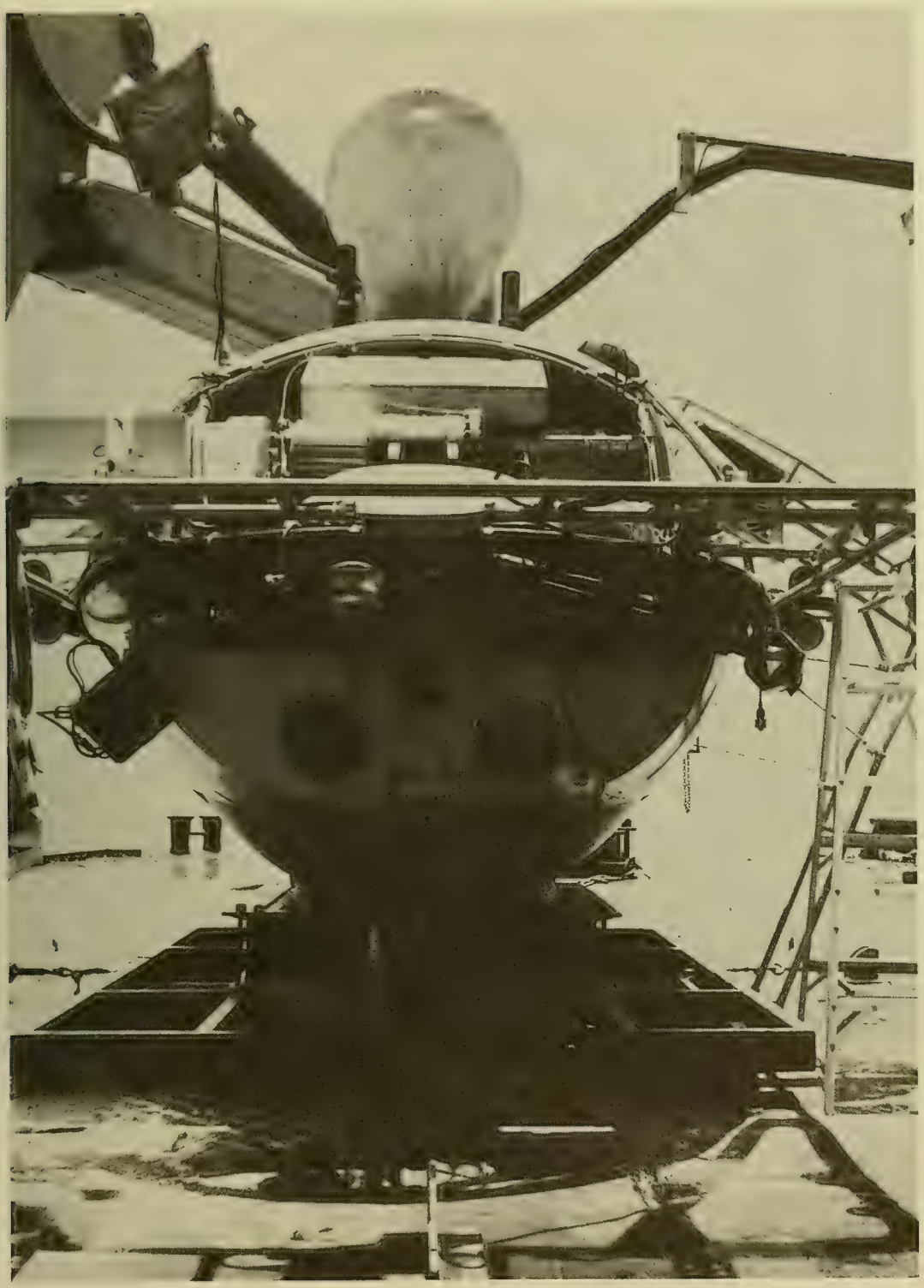

Fig. 6 - Bio-Acoustics instrumentation showing transducer replacing still camera (lower left)

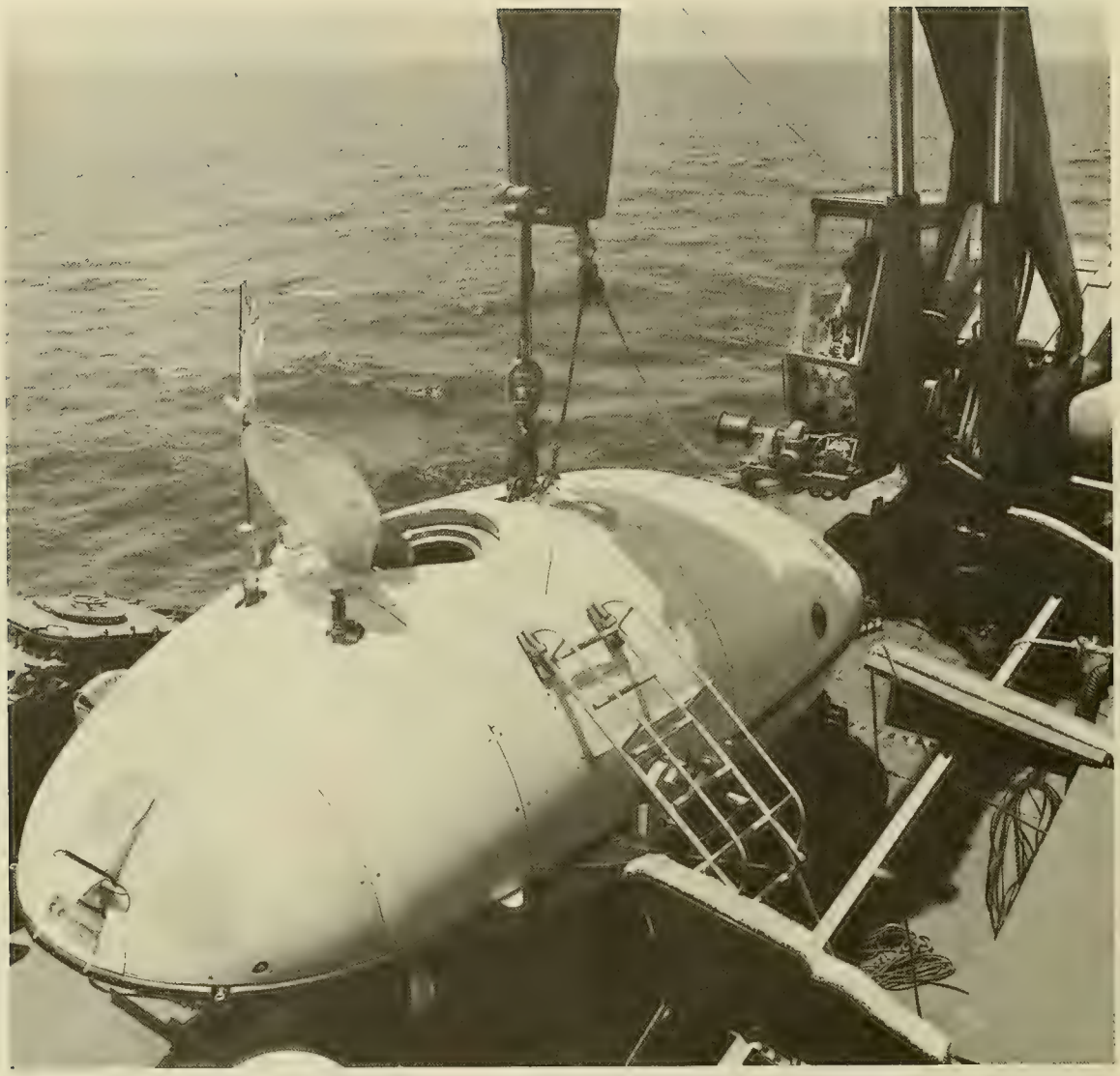

Fig. 7 - "Bare-boat" for sea-floor studies

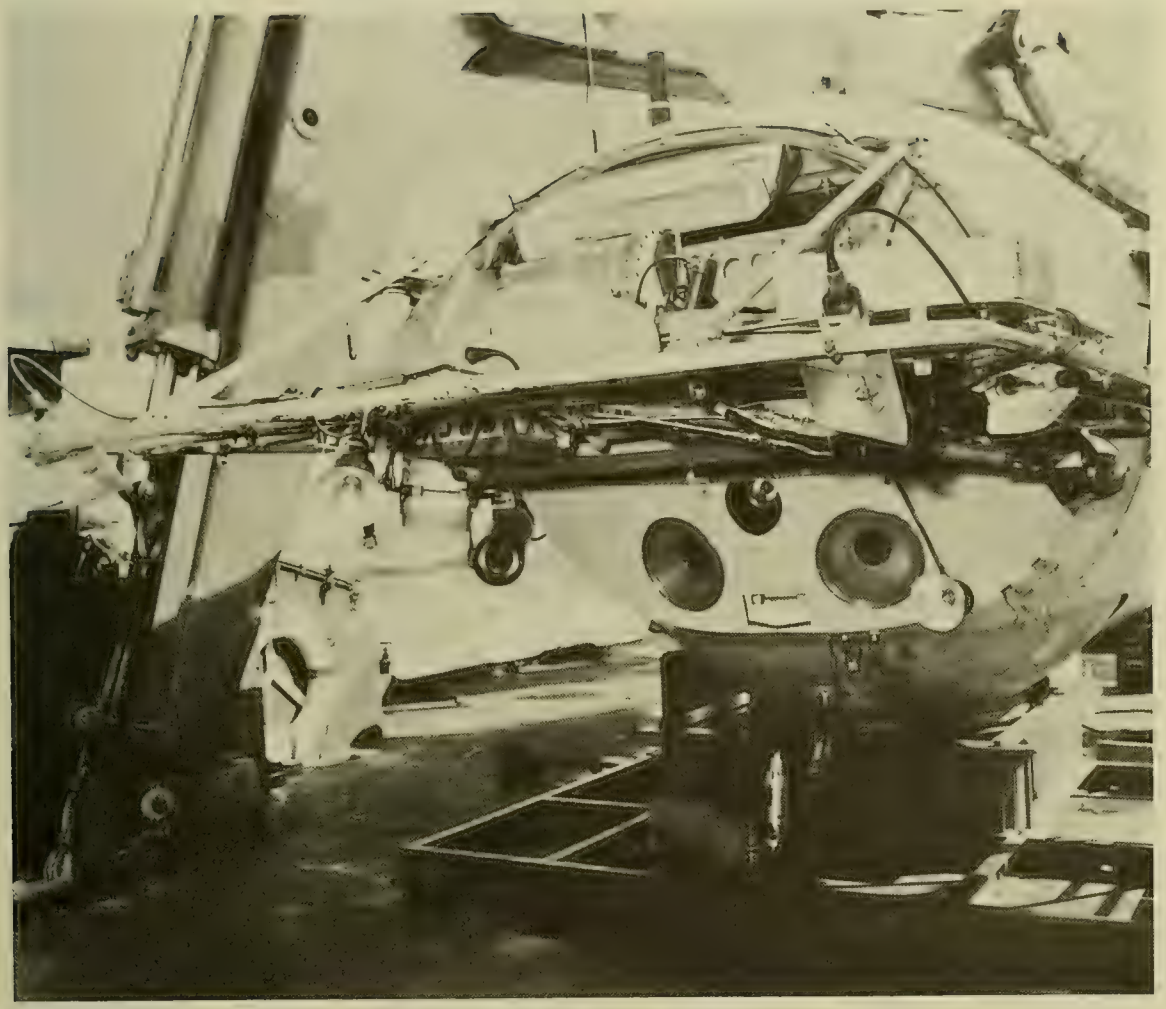

Fig. 8 - Additional quartz iodide lamps and standard lighting reconfiguration for sea-floor studies. Note fairing attachments (lower right) for sediment cores.

UNDERWATER SOUND PROPAGATION AND ATTENUATION STUDIES

One of the more challenging applications of instrumenting the DEEPSTAR vehicle was that of the Underwater Sound Propagation and Attenuation Studies[12, 13, 14]. The scientific payload of 350 pounds was not approached, but the mass of the external instrumentation presented shipboard-handling problems and the internal sphere arrangement utilized all available space. Fig. 9 shows coring tubes and probes to measure compressional wave velocity and absorption. Fig. 10 shows equipment for generating shear waves by firing dynamite caps[15], and geophones for observing them. To provide significant data, DEEPSTAR made an early-morning dive at a specified site using instrumentation shown in Fig. 9. An afternoon dive was made at the same location following an at-sea instrumentation change as shown in Fig. 10. Sea-state conditions limited diving operations in some instances, causing handling problems when geophones and dynamite caps occasionally became entangled during launching operations.

PHYSICAL OCEANOGRAPHY

Physical Oceanography studies called for specialized equipments capable of reliable performance at the 4000-foot operating depth of DEEPSTAR. The need to obtain water samples at the sea floor and at approximately 1-foot increments dictated that the design of water samplers be compatible with DEEPSTAR's maneuverability. Deep-sea solenoids developed at NEL performed reliably throughout the program. Fig. 11 illustrates the external instrumentation configuration used for this specific mission[16]. The measurement of current flow at the sea floor in "virgin water" (without interference of the vehicle hull) was accomplished by means of depositing the large bale attached to the current meter on the sea floor and backing off a distance of 10 to 12 feet for observation and recording. The signal was carried from the meter to DEEPSTAR by a retractible communication cord, similar to that used on telephones, which allowed minimal wire length and precluded entanglement during meter recovery. Temperature probes to be embedded in the sea floor were carried in a "cocked" position (see Fig. 12) so that the probes could be actuated by the scientist without disturbing the water sampling. The underwater separation bolt[15] provided an extremely simple device for actuating the probes. A dye marker was also used for current data. Dye, intermixed with sand and encased in "baggies", was released into the current upon rupture of the "baggies" by the point of the temperature probe.

Fig. 9 - Temperature probes and core samplers

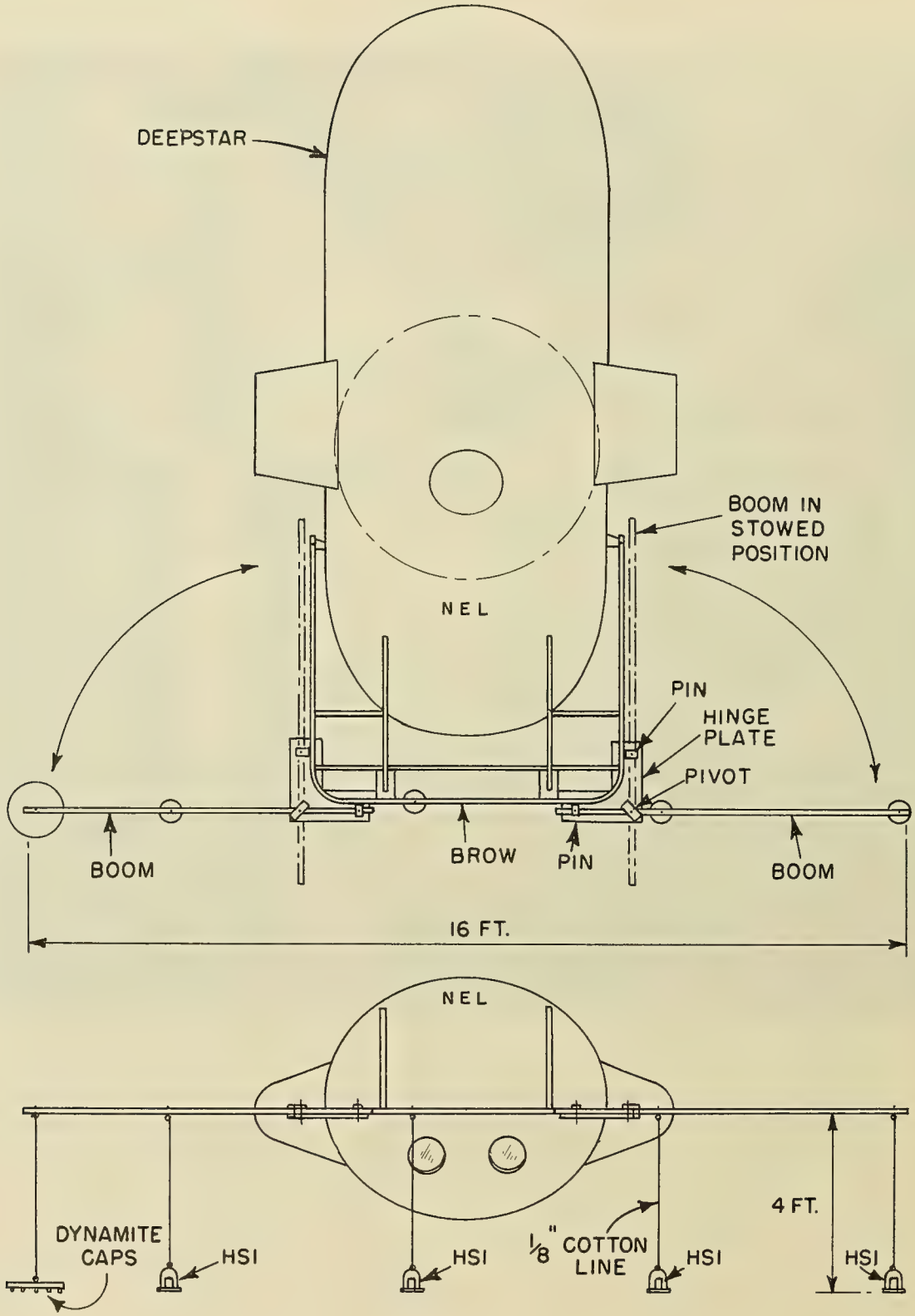
DEEPSTAR
BOOM IN
STOWED
POSITION
NEL
PIN
HINGE
PLATE
PIVOT
BOOM
BROW
PIN
BOOM
16 FT.
NEL
4 FT.
DYNAMITE
CAPS
HSI
HSI
1/8" COTTON
LINE
HSI
HSI

Figure 10

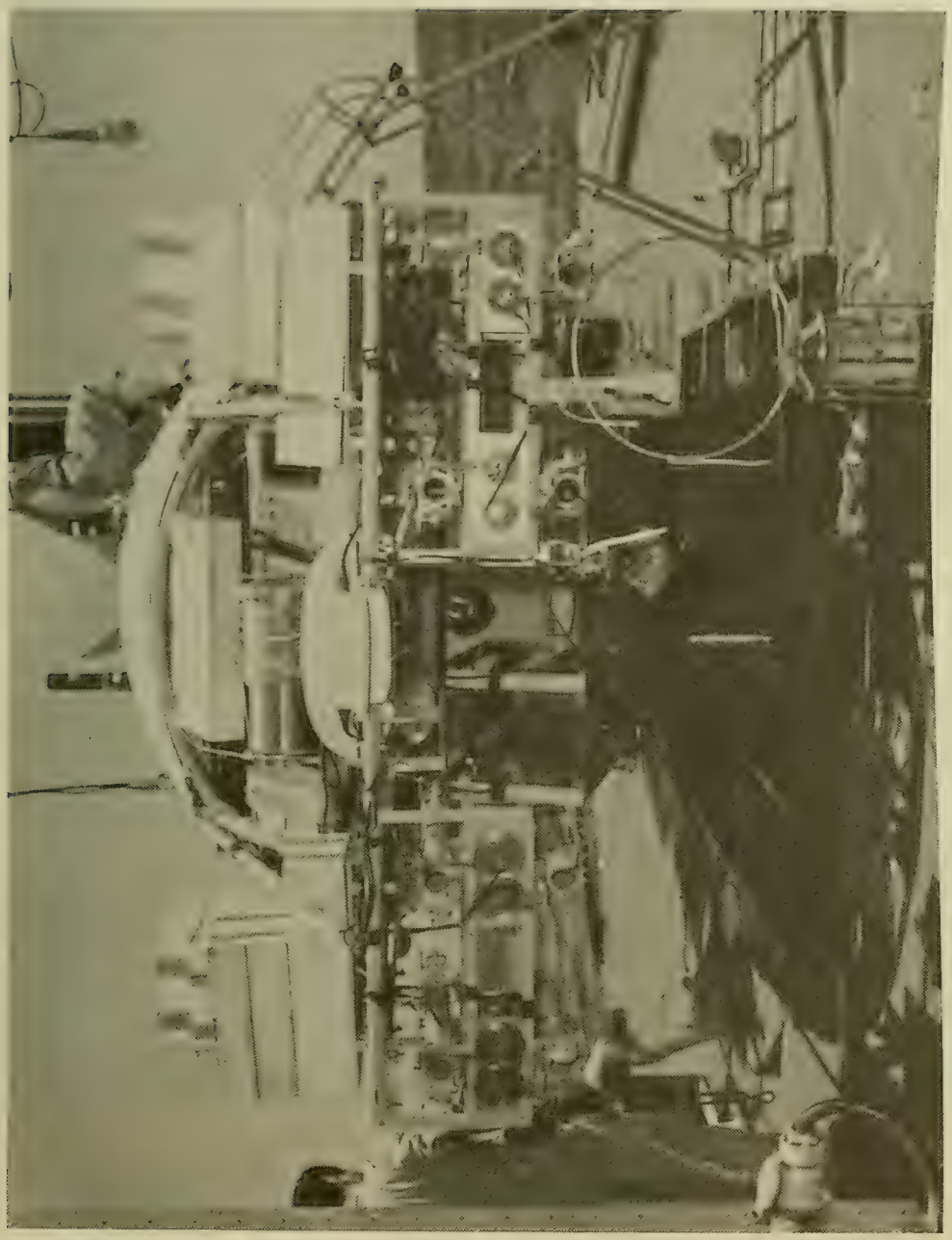

Fig. 11 - Physical oceanography instrumentation with current meter in foreground. Note "baggie" center right, containing dye. Left are solenoids and water bottles.

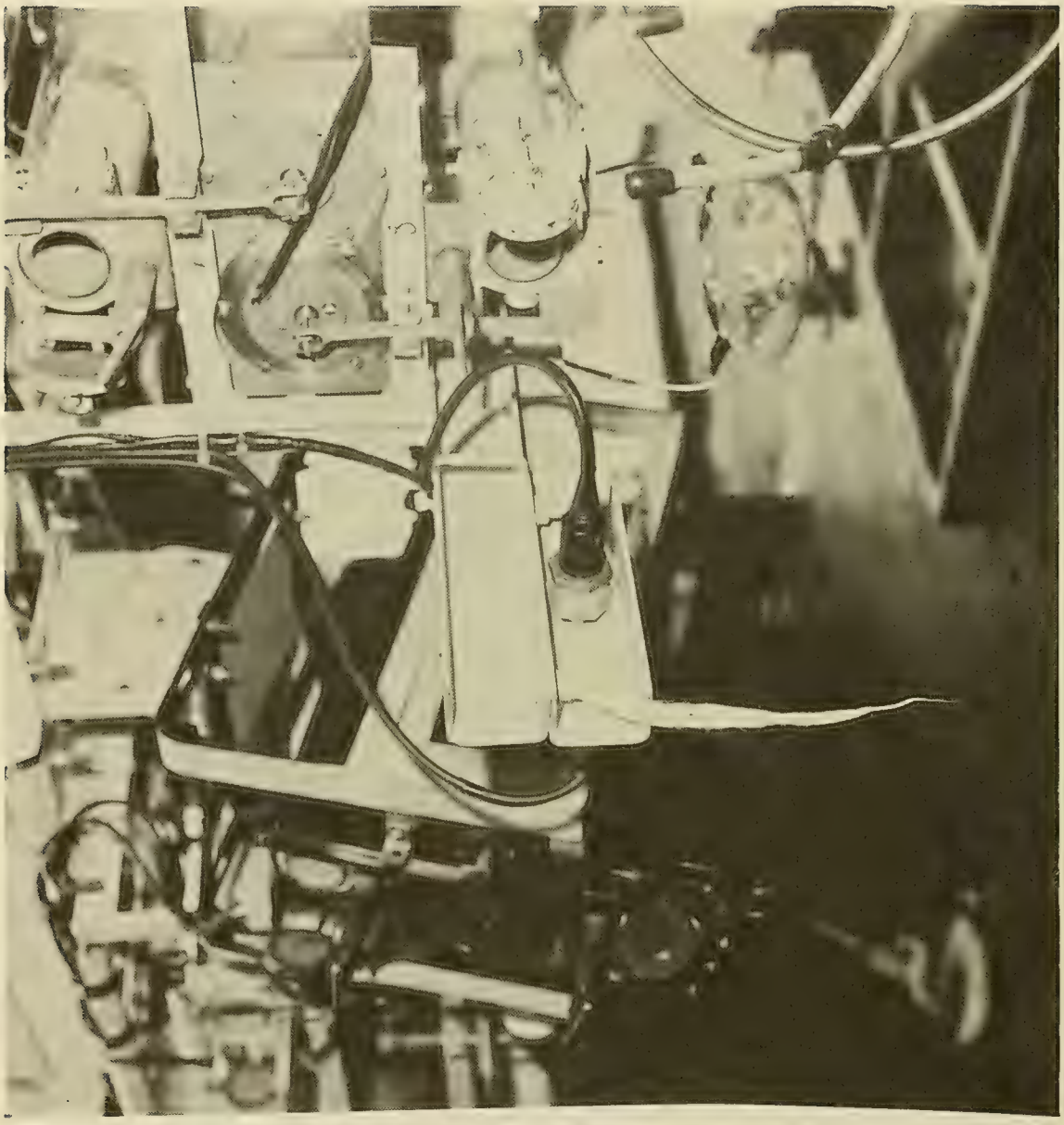

Fig. 12 - Separation-bolt release mechanism for temperature probes

ACOUSTICS

The acoustic program fully utilized instrumentation payload and available space, both within the sphere and that additional provided by the brow[17, 18]. Attachments were designed to be readily removable to allow maximum flexibility by interchanging at sea. Fig. 13 is typical of the type of instrumentation used. The water-sample bottles are of the same design and type as in Fig. 11, but are mounted vertically with reversing thermometers. A dive series of three days at sea and at different locations reflected external changes as shown in Fig. 14. The maximum payload was utilized on these dives and, in many instances, the photographic equipments were removed to allow the scientist greater versatility in the instrumentation system. Data was obtained and recorded by means of a 7-channel tape recorder. Fig. 15 shows a typical internal sphere arrangement for the acoustic mission profiles.

ACKNOWLEDGEMENTS

The author wishes to express appreciation to Dr. G. H. Curl for his assistance in reviewing this paper, to Mr. W. H. Armstrong for drafting services, and to Mrs. B. L. Hurt for editing.

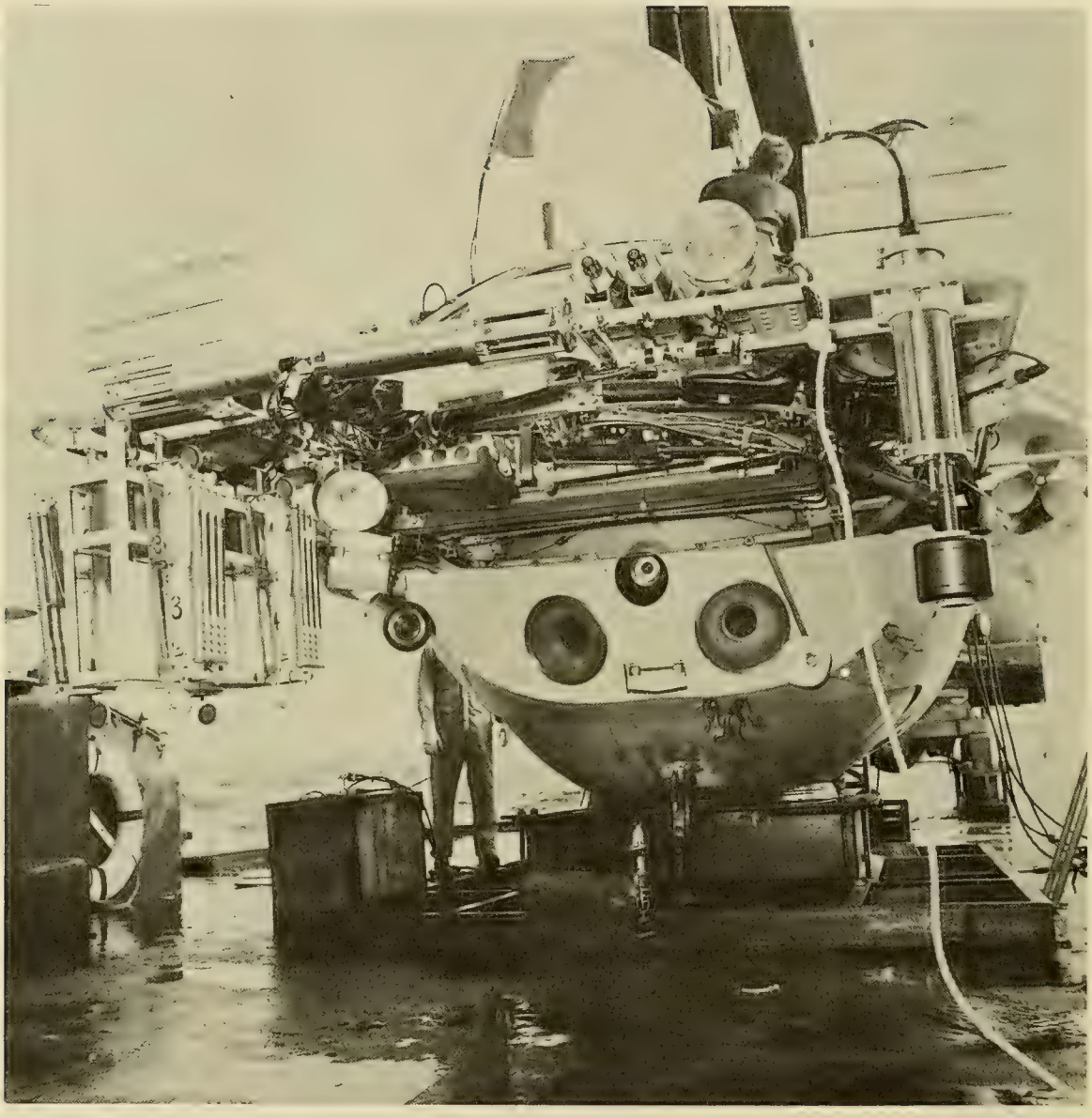

Fig. 13 - External acoustics instrumentation. Suspended at left are water-sample bottles with reversing thermometers; above left, velocimeters; top center, two temperature probes and velocimeter; and suspended at right, a salinometer.

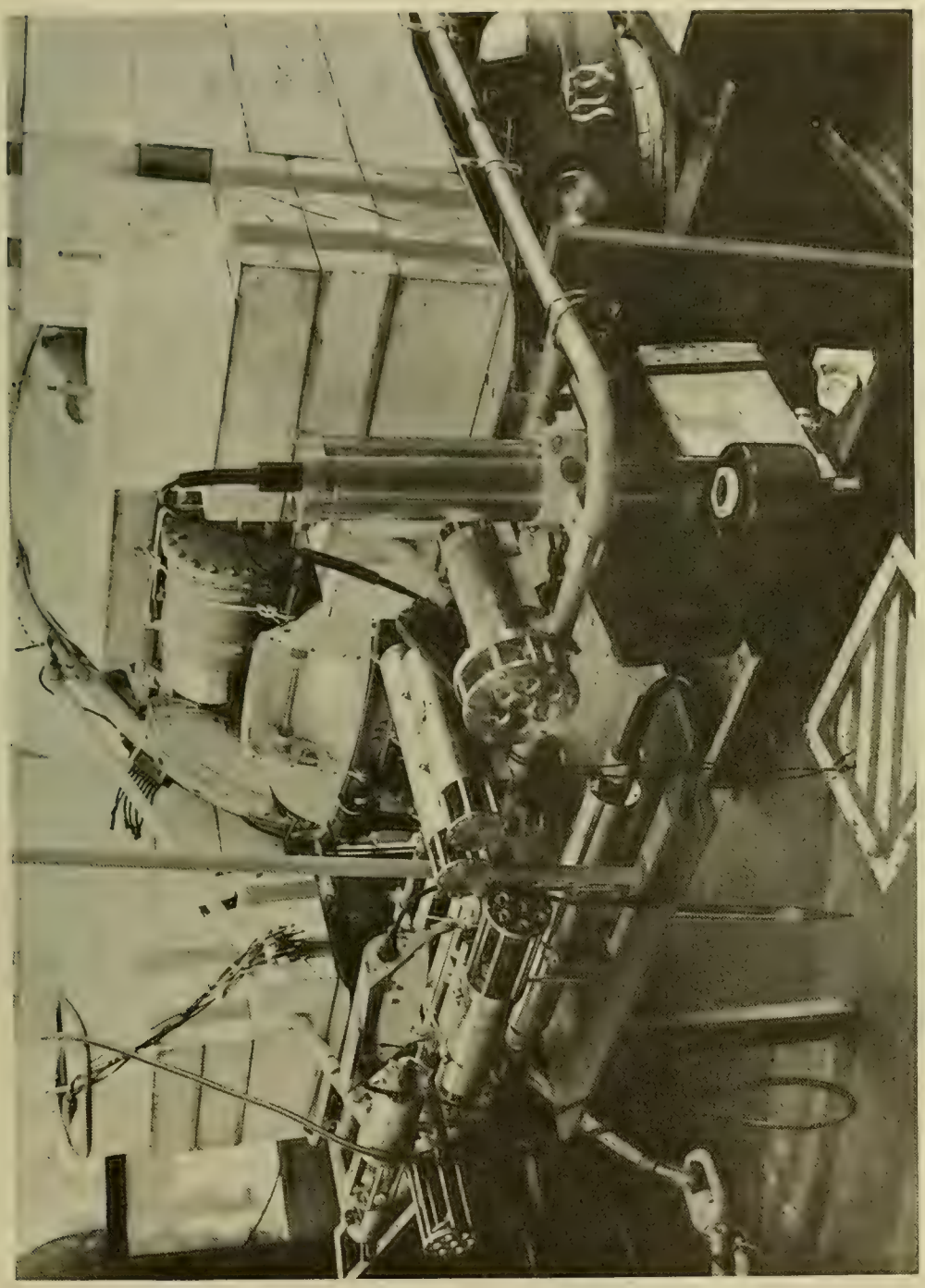

Fig. 14 - Acoustics instrumentation after 3-day dive series. Changes from that shown in Fig. 13 include removal of water samplers with thermometers, addition of large temperature probe (center), and slight relocation of salinometer.

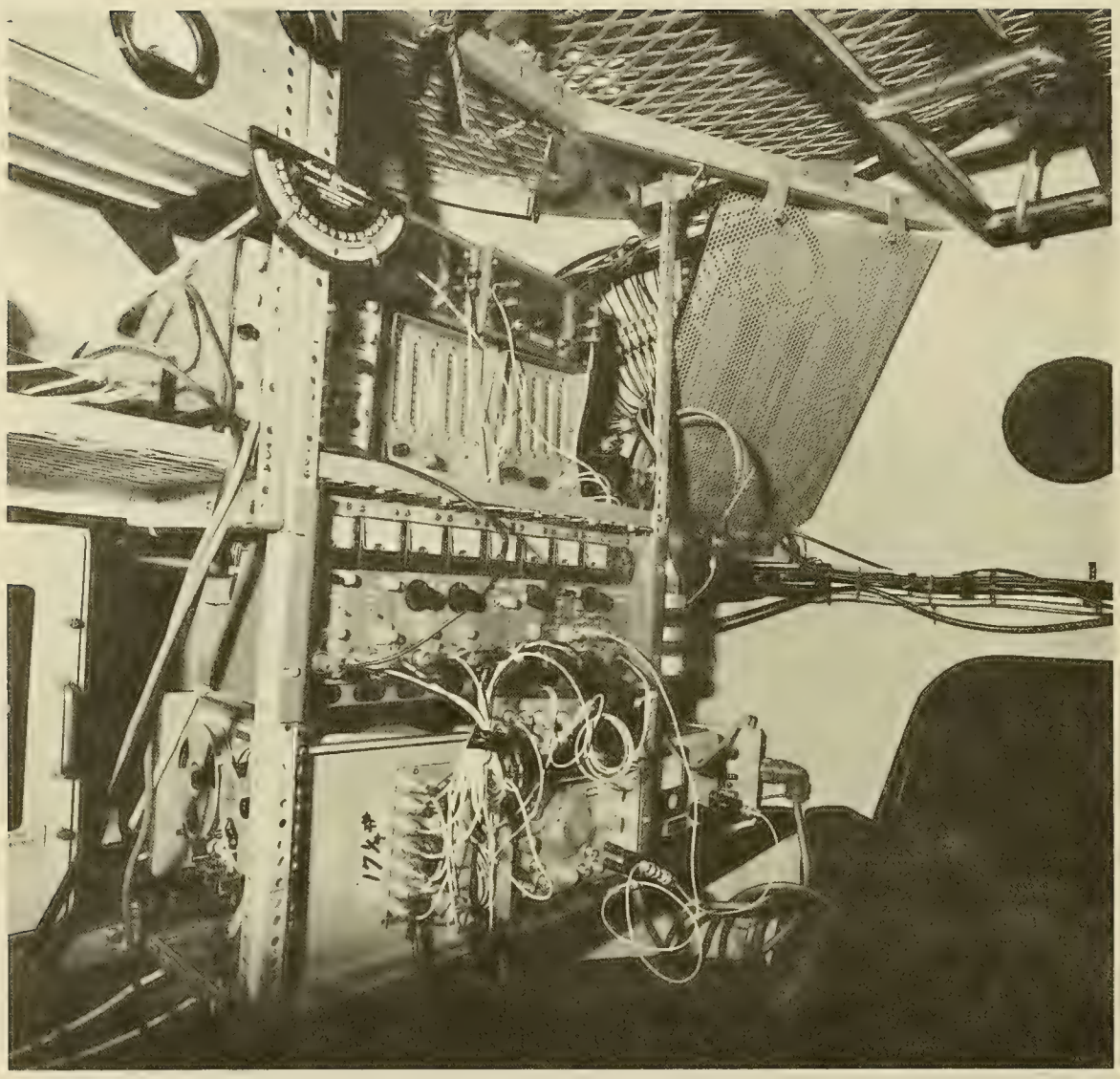

Fig. 15 - Internal sphere instrumentation for acoustics program

REFERENCES

1. "Specifications and Requirements for Lease Services of a 4,000' Submersible," NEL contract N123-(953)54016A, 13 May 1965.
2. "Appendix A: Original NEL DEEPSTAR Diving Program as Based on Scientists' Requirements (reproduction)," NEL Deep Submergence Log No. 1, August 1966.
3. Schlosser, A. J., "Submersible Diving Service Leasing for Scientific Measurements," paper presented at Workshop on Use of Deep Manned Submersibles, WHOI, Woods Hole, Mass., 21-23 November 1966.
4. Schlosser, A. J., "Instrumentation Brow for DEEPSTAR," NEL Deep Submergence Log No. 2, p. 31-34, October 1966.
5. Seeley, R. L., "Two-Channel Oceanographic Instrumentation Package," NEL Tech Memo in preparation.
6. Barham, E. G., and Davies, I. E., "Bio-Acoustics," NEL Deep Submergence Log No. 1, p. 31-38, August 1966.
7. Davies, I. E., Barham, E. G., and Pickwell, G. V., "Bio-Acoustics," NEL Deep Submergence Log No. 3, p. 47-52, February 1967.
8. Adams, R. L., "Bio-Acoustics Scattering Measurements," NEL Deep Submergence Log No. 3, p. 53-56, February 1967.
9. Beagles, J. A., "Sea Floor Studies," NEL Deep Submergence Log No. 1, p. 25-28, August 1966.
10. Buffington, E. C., "Submarine Slopes and Gullies; Topography and Structure," NEL Deep Submergence Log No. 2, p. 27-30, October 1966.
11. Dill, R. F., and Heezen, B. C., "Submerged Sea Cliffs and Rocky Terraces on the Continental Slope," NEL Deep Submergence Log No. 3, p. 61-62, February 1967.
12. Bucker, H. P., "Underwater Sound Propagation," NEL Deep Submergence Log No. 1, p. 29-30, August 1966.
13. Whitney, J. A., "Underwater Sound Propagation," NEL Deep Submergence Log No. 3, p. 57, February 1967.
14. Hamilton, E. L., "In-situ Sediment Sound Velocity and Attenuation," NEL Deep Submergence Log No. 3, p. 59-60, February 1967.
15. Schlosser, A. J., Explosive Effect on Manned Submersible Viewports, NEL Tech Memo 933, 17 May 1966.
16. LaFond, E. C., et al, "Oceanographic Research (Sea Floor Inter-face--Chemical and Physical Properties)," NEL Deep Submergence Log No. 3, p. 17-45, February 1967.

17. Mackenzie, K. V., "Deep Ocean ASW Acoustic Research," NEL Deep Submergence Log No. 3, p.63-72, February 1967.
18. Mackenzie, K. V., "Precision in-situ Sound-Speed Measurements," NEL Deep Submergence Log No. 3, p.79-99, February 1967.

Session B

THE OCEAN BOTTOM

ENVIRONMENTAL LIMITATIONS TO DEEP SEA SEARCH

F. N. Spiess, J. D. Mudie, C. D. Lowenstein

University of California, San Diego
Marine Physical Laboratory of the
Scripps Institution of Oceanography
San Diego, California 92152

During the study conducted by the Deep Submergence Systems Review Group in the aftermath of the THRESHER search it became clear that acoustic, magnetic and optical search systems should be developed to enhance our ability to find objects on the deep sea floor. It was equally clear, as we investigated hypothetical search systems, that we had no information on which to estimate, even crudely, the limitations which natural roughness of the deep sea floor would provide to the effectiveness of system operation. This limitation might be either in raising the effective "noise" level at the system output in a general way or might appear in terms of false targets.

With support of ONR and DSSP we have brought into operation a towed instrumentation system capable of observing pertinent fine scale aspects of the deep sea floor and have begun an actual program of operation at sea to determine these limitations. The system consists of an instrumented towed body which can be operated from a research ship, using an appropriate towing wire to provide both electrical and mechanical connection between the two. The observational systems which are operational at this time are precision down-looking echo sounder, up-looking sounder, bottom penetration sounder, side-looking sonar, camera and lights, and proton magnetometer. Transducers for most of these can be seen in the picture of the towed body (Fig. 1). High quality local navigation near the sea floor is provided by an acoustic transponder system.[1, 2] All outgoing signals for the acoustic systems as well as trigger signals for camera and magnetometer are transmitted from the ship down the coax core of the towing wire and all acoustic and magnetometer signals are sent back up the same line.

We have, in the past year, operated in several areas, four of which are shown on the index map (Fig. 2). In three of these (shown by circles) transponders were planted and an area of 80 to 120 square miles

was surveyed in detail. In the fourth area a long east-west traverse (105 miles) and a shorter north-south run were made. The present paper will be concerned primarily with acoustic system data from the circle areas and magnetometer data from the long straight tows (although both acoustic and magnetic data were obtained in all areas).

Magnetic search techniques are limited by inherent noise in magnetometers, noise associated with their motion or the motion of the conducting sea water in the earth's field, by ionospheric current effects and by naturally occurring magnetic effects of the rocks of the sea floor. The first few of these items lead to uncertainties of a few tenths of a gamma at most in well-designed systems. (One gamma is 10^{-5} oersted thus typically the earth's field is about 40, 000 gammas.) These imply, then, that search for iron objects up to 100 meters across must pass at least within a kilometer or so of the target and thus that such searches at sea must be conducted near the bottom. With this in mind magnetometers were towed near bottom at depths of about 2.5 kilometers in the THRESHER search. As shown in Fig. 3, taken from the paper of Maxwell and Spiess in Science,[3] and as more extensively documented by Heirtzler,[4] the natural geological background in that area, on the continental slope, was smooth. A 100 gamma anomaly, presumably due to THRESHER, is clearly visible against the gradual 30 gamma change occurring along the 1.5 km track shown in the figure.

It has long been known, however, that anomalies of several hundred gammas can be observed at the sea surface over the deep ocean. One of the best magnetic maps showing these strongly lineated anomalies is that produced by Mason and Raff[5, 6] as a result of surveys which they conducted in the middle fifties with cooperation of the U. S. Coast and Geodetic Survey. These show ridges which have north-south continuity in sections for 500 km or more and east-west wavelengths of 20 to 50 km, with amplitudes of 50 to 300 gammas.

The question as to how these anomalies look when observed near the sea floor has now been answered with the long profiles at the location shown in Fig. 2. The result (as seen from about 80 meters off bottom) is shown in Fig. 4. The long wavelength component which would be measured at the surface is barely discernible, as are the small peaks introduced artificially by adding the anomaly of Fig. 3 repeatedly every 20 km. It is clear that the naturally occurring anomalies, associated with variations of magnetization of material lying just below the thin sediment cover (50 to 300 meters), have strong short wavelength components which would make detection of ship-sized iron objects quite difficult.

Since the anomaly of Fig. 3 has significant short wavelength content we have applied a simple signal processing scheme in hope of

improving the signal-to-noise ratio. The record of Fig. 4 was high pass filtered with and without the THRESHER peaks using a cutoff wavelength of 400 meters. The result is shown in Fig. 5, in which the lower trace includes the inserted targets. In some parts of the record these show clearly but there are many similar peaks generated by the background. Even with this treatment detection would be far from easy.

Having found this strong short wavelength background in one area one may ask whether it should be expected elsewhere. The answer is that surface observations show similar lineated structures in much of the deep ocean and that the strong similarities observed among these various occurrences make it highly likely that deep observations, when they are made elsewhere, will show this same fine structure. Figure 6 shows areas which we estimate will have background of a sort which will render magnetic search difficult.

Acoustic search for objects on the sea floor can be carried out in either of two basic modes—one utilizing essentially a down-looking system and the other using more or less horizontal paths. If the down-looking mode is used in the deep sea from near the surface a reasonable sweep width can be achieved. Determination of the horizontal coordinates of suspected targets is uncertain without very sophisticated (and expensive) sonar systems. The downward looking technique can give good resolution if near-bottom equipment (towed and in future on free-running vehicles) is used. Figure 7 shows a profile over some small natural irregularities on the sea floor, at about 2200 fathoms depth 500 miles west of San Diego (area B). The upper portion shows the record of the surface-operated echo sounder over the same portion of track as that shown by the lower record from the deep tow. The lower record displays both the down-looking sounder output which gives the height of the towed body off the bottom, and (in the middle of the record) the sum of the down plus up echo sounder travel times, that is, the actual depth of the water. The small hill is very clearly discernible.

While the near-bottom use of the downward path provides good resolution, this good resolution implies a very narrow search path (typically only a few fathoms wide). In fact once one has decided to operate near the sea floor it is immediately obvious that a nearly horizontal path is much more appropriate. Under such circumstances one should naturally utilize a system in which beam width and pulse length are adjusted to provide proper resolution and employ such a beam either fixed in side-looking mode or sweeping in searchlight or scanning sonar fashion. The most natural question to ask as one proceeds with such a search system design is what one might expect in the way of false targets arising from the natural roughness of the sea floor. It is this question for which we now have the beginnings of an answer from the deep sea floor in the northeast Pacific.

In making such background observations it seemed most appropriate to use a side-looking sonar. This, operated from a deep-towed fish, gives high resolution without unduly complicating the equipment problem (no scanning motors or circuits, easy mounting of the necessarily large transducers, simple telemetry and display). At the same time results of such observations tell of the sizes of irregularities on the sea floor in a form which can be made relevant in terms of other types of sonars. We have, to date, utilized a pair of Westinghouse transducers (shown on the towed body in Fig. 1) operating in the non-focussed mode at about 230 kcps. Height off the bottom is variable depending on the circumstances but records useful for our purpose, with objects as small as 5 feet high and 10 feet across in mind as targets, can be obtained at heights off bottom of as much as 200 feet. Normally a half-second or one-second repetition period has been used and most records show useful returns to ranges of 150 to 200 fathoms (0.15 to 0.2 nautical mile). Speed of advance has typically been about 1.2 knots.

In all three of the areas of Fig. 2 a major fraction of the sea floor is essentially featureless to the side looker and would be very easy to search systematically and effectively at a rate in excess of a half square mile per hour. In every one of the areas there were, however, regions of sharp topographic relief in which the associated side-looking sonar record is patchy in a manner which would give rise to possible false targets or uncertainty as to whether or not targets were present.

Three examples can be shown of side-looking sonar records associated with rough topography. In Fig. 8 is shown a pass across a small canyon in the Hawaiian area (area D). This ditch was crossed at several points and was shown to be about 30 fathoms deep, 0.1 mile wide and at least 2 miles long. Its walls were quite steep (45°). The crossing shown here was made at an angle of about 60° to the axial line, a trend which is evident in the sonar record.

The second (Fig. 9) was made in area A as the fish was being towed down the side of a seamount at a depth of about 1900 fathoms.

Most striking from the viewpoint of possible false targets was Fig. 10 which was made close to the small hill shown in Fig. 7, in area B. In this area, along over 200 miles of track on which the total relief of two abyssal ridges was about 200 fathoms, there was only this one region, less than half a mile across, which showed other than a smooth side-looking record.

As observed with the air gun and penetration sounder there was significant sediment cover (at least 50 meters) in all these areas, except in the immediate vicinity of steep slopes. The only major exception

occurred in some portions of the Hawaiian location and in that region there were areas showing very thin sediment cover which correlated with very patchy sonar returns as shown in Fig. 11. This record is of double usefulness inasmuch as it shows the sort of roughness which the non-sediment covered portions of the sea floor can have while at the same time giving indication of the resolution of which the equipment is capable. This provides reassurance that the much more extensive smooth areas are in fact (for objects of this size) essentially featureless. In this picture the nearly round shadow at about 1157 implies an object 14 feet high and 90 feet wide along the track at a distance of about 400 feet to one side of the track.

A knowledge of general geological sea floor patterns makes it clear that one can predict that search for objects having characteristic dimensions of 10 feet or more should be highly effective in about 80% of the northeast Pacific. In volcanically controlled areas, as off Hawaii, the percentage will perhaps drop lower, with areas showing no sediment cover providing particularly difficult situations. It thus appears that any search for large objects in the deep northeast Pacific can be conducted using simple towed instruments in conjunction with small submarines with an appropriate division of effort between the two. Areas of steep terrain or those with scant sediment cover could be assigned initially for detailed search using manned craft with the towed gadgetry covering the usually much larger sediment-covered area and locating within it any possible targets or small patches of rough terrain for later manned investigation. At the present time, with only bathyscaphes available for detailed observations, this might still throw too much load on the manned portion of the system. However, as craft having greater mobility become available the combined system should approach compatibility with the environmental situation.

It should be emphasized that only a small fraction of the sea floor has been sampled in this manner thus far, although areas were chosen to allow the most significant inferences to be drawn. Further observations in areas of different geological types are still required to allow formation of a truly worldwide picture.

We would like to acknowledge the participation of the engineering staff which designed and built the equipment which made these observations possible: Messrs. M. S. McGehee, C. S. Mundy, D. E. Boegeman and M. Benson. It is also a pleasure to express our thanks to Capt. T. Hansen and the crew of the THOMAS WASHINGTON (AGOR-10) for their very effective support of our seagoing work, which was supported by ONR and DSSP.

REFERENCES

1. McGehee, M. S. and D. E. Boegeman, MPL Acoustic Transponder, Rev. Sci. Instr., 37, No. 11, 1450-1455 (1966).

2. Spiess, F. N., M. S. Loughridge, M. S. McGehee and D. E. Boegeman, Navigation: J. Inst. of Navigation, 13, No. 2, 154-161 (Summer 1966).

3. Spiess, F. N. and A. E. Maxwell, Search for the THRESHER, Science, 145, No. 3630, 349-355 (1964).

4. Heirtzler, J. R., Magnetic Measurements near the Deep Ocean Floor, Deep Sea Res., 11, 891-898 (1964).

5. Mason, R. G. and A. D. Raff, Magnetic Survey off the West Coast of North America, 32°N Latitude to 42°N Latitude, Bull. Geol. Soc. Am., 72, No. 8, 1259-1266 (1961).

6. Raff, A. D. and R. G. Mason, Magnetic Survey off the West Coast of North America, 40°N Latitude to 52°N Latitude, Bull. Geol. Soc. Am., 72, No. 8, 1267-1270 (1961).

Fig. 1 - Deep tow fish

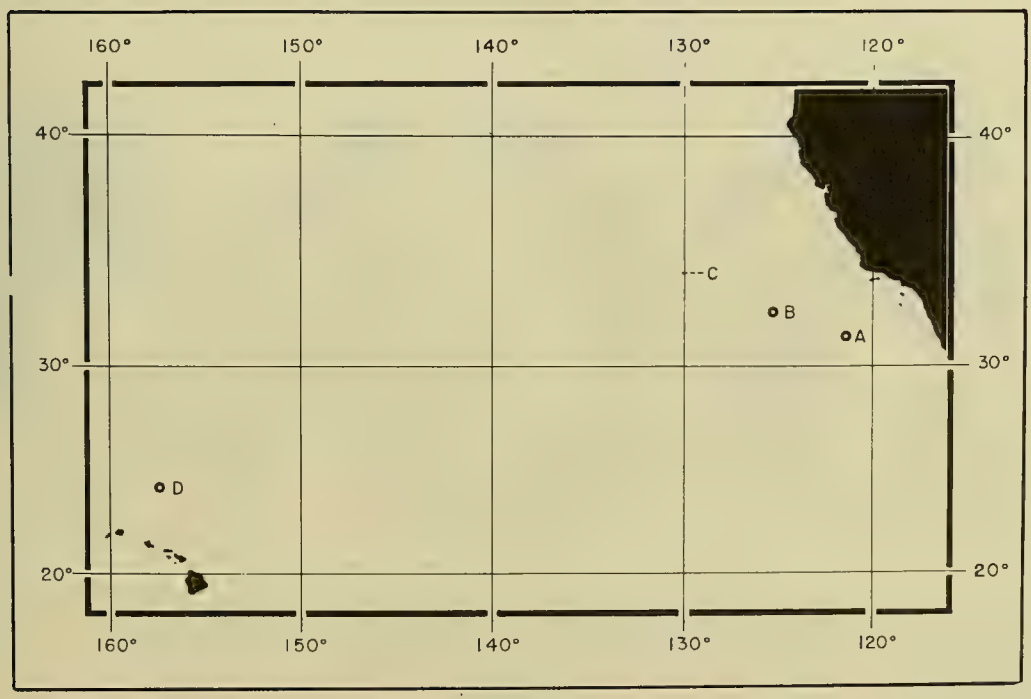

Fig. 2 - Index chart of operating areas

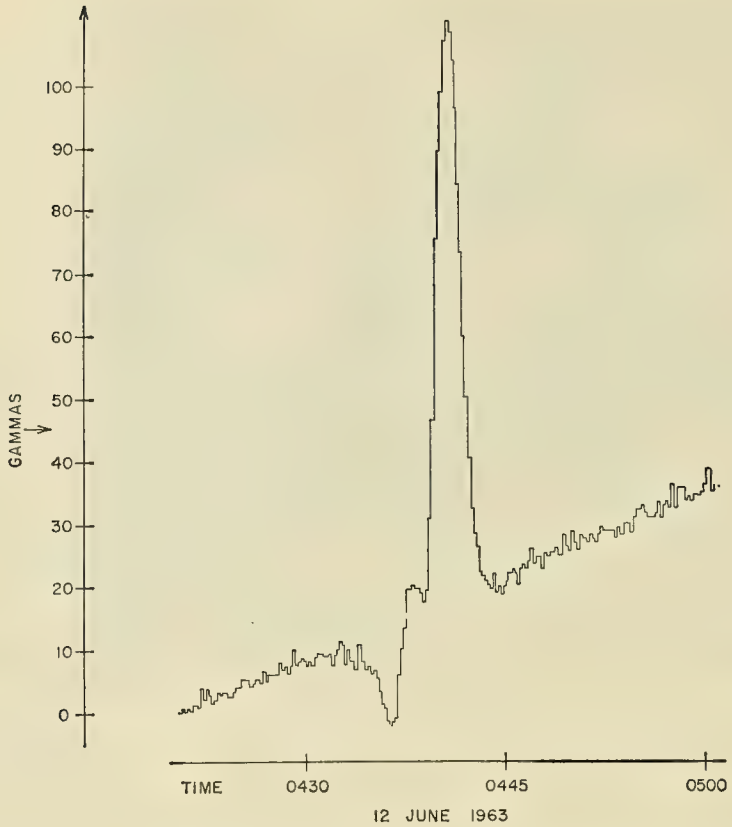

Fig. 3 - THRESHER search magnetometer trace

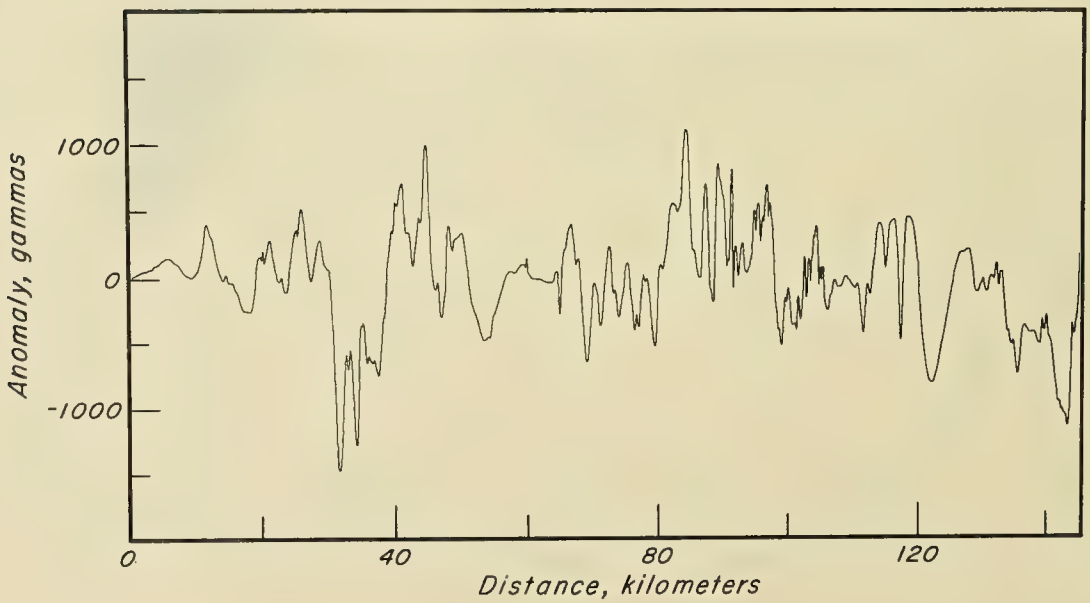

Fig. 4 - Magnetic profile at location C with trace of Fig. 3 added every 20 km

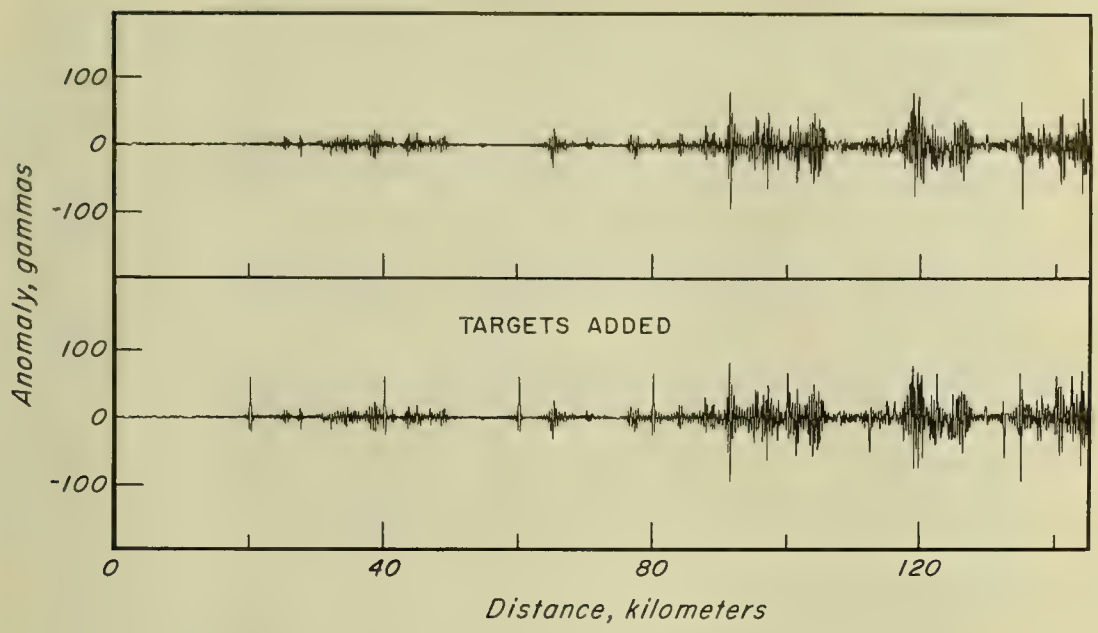

Fig. 5 - Magnetic profile at location C, high pass filtered with 400 meter cutoff wavelength. Upper trace without and lower trace with THRESHER area anomaly added every 20 km

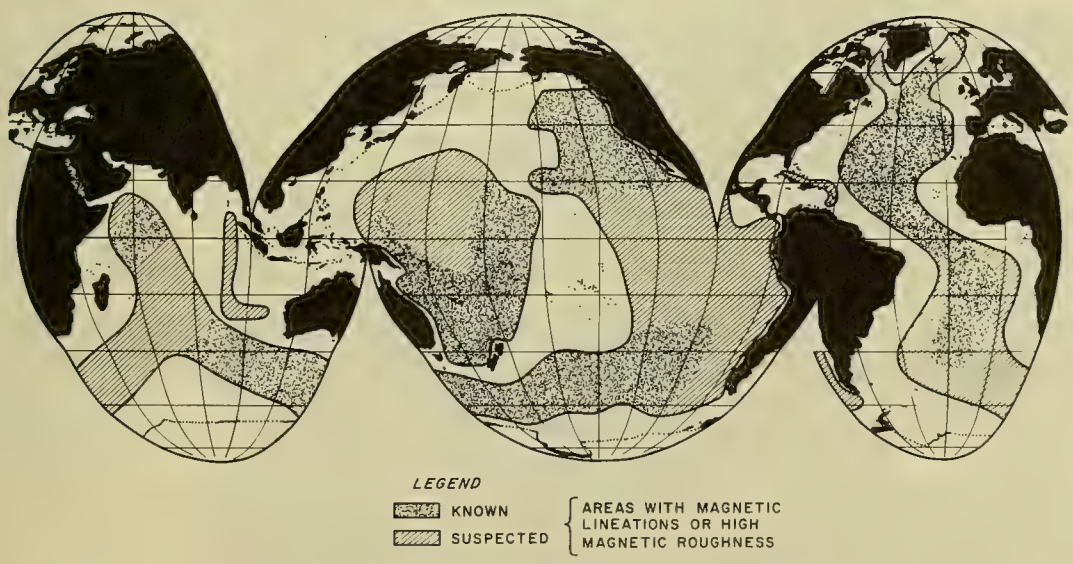

Fig. 6 - Magnetic lineations, world map

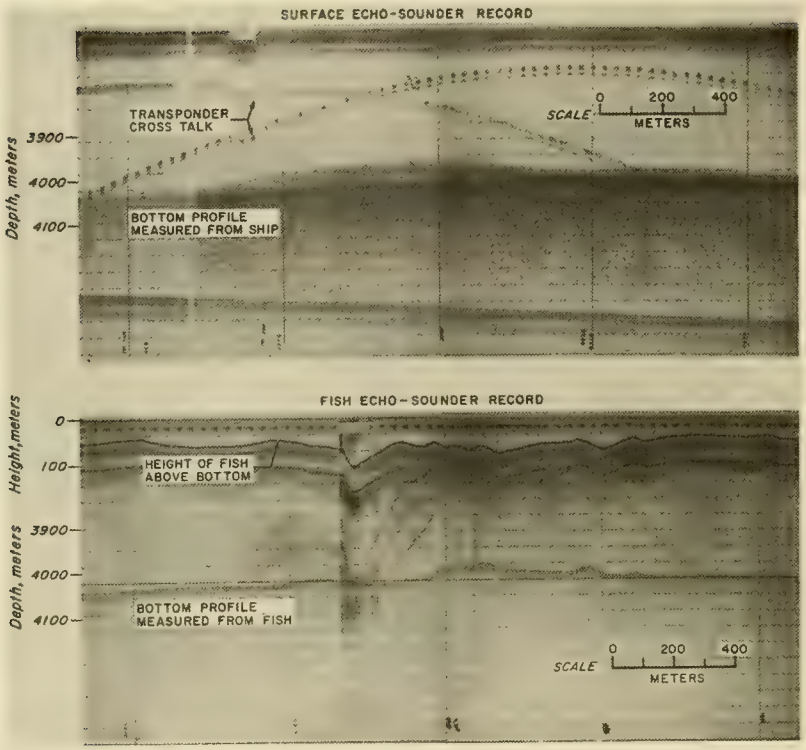

Fig. 7 - Echo sounder trace in area B. Upper record from hull mounted echo sounder, lower trace (middle of lower portion) is record from deep towed sounder.

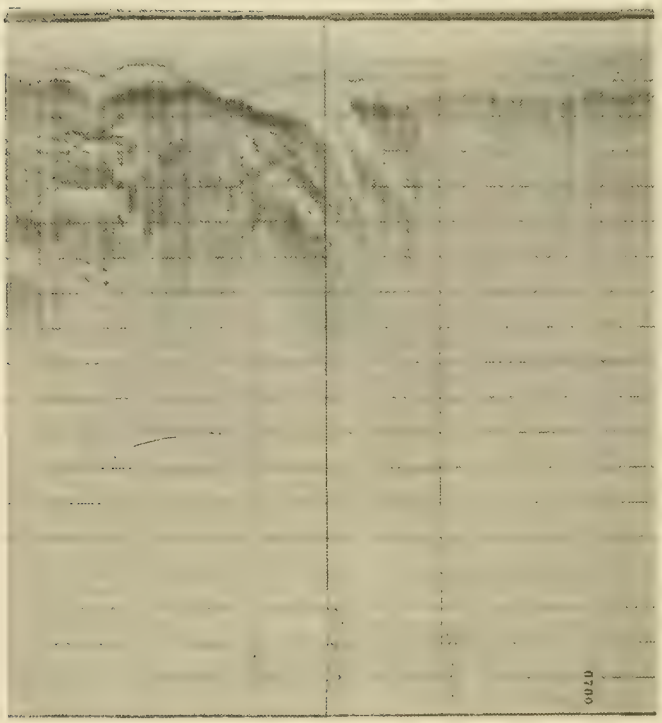

Fig. 8 - Side-looking sonar traverse across canyon in area D

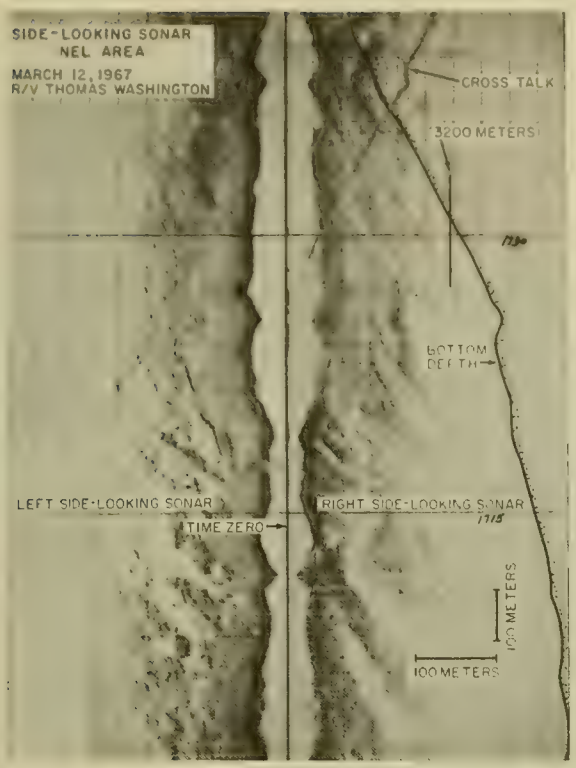

Fig. 9 - Side-looking sonar record on mountainside in area A

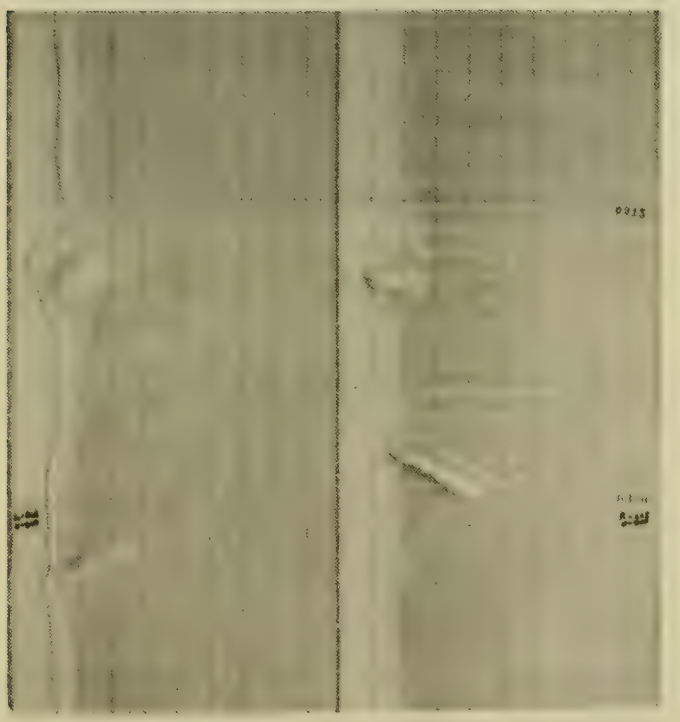

Fig. 10 - Side-looking sonar record in area B across location of sounding records of Fig. 7

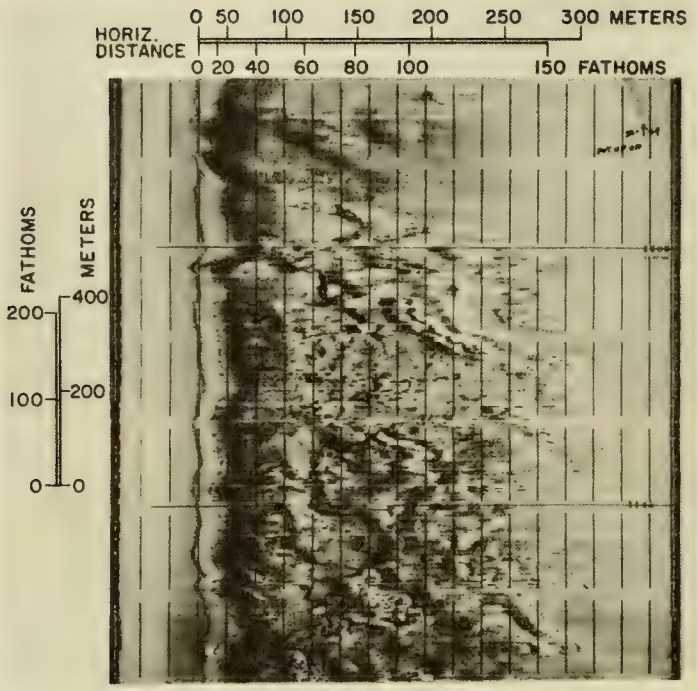

Fig. 11 - Side-looking sonar record over low-relief outcrop in area D

DIRECT MEASUREMENT OF BOTTOM SLOPE SEDIMENT SOUND VELOCITY AND ATTENUATION AND SEDIMENT SHEAR STRENGTH FROM DEEPSTAR 4000

Edwin C. Buffington,
Edwin L. Hamilton,
David G. Moore

U. S. Navy Electronics Laboratory
San Diego, California

GENERAL

Among the capabilities of deep submersibles which are especially useful, but poorly known, are those permitting types of measurements which set up, or complement, remote data customarily taken from surface ships. So much emphasis in the employment of submersibles has been toward those things which the submersible can do uniquely that frequently overlooked or, at least underpublicized, are those contributions which upgrade, calibrate, or give added significance to those data taken by wire-lowered or acoustic sensors. It is the purpose of this paper to briefly describe and discuss the significance of three such types of measurements which have been made with a high degree of success from the DEEPSTAR 4000.

DIRECT MEASUREMENT OF BOTTOM SLOPE

The sources of error inherent in echo sounding have been identified almost from the beginning, but their correction has not always been a simple matter. The two principal causes are the speed of sound in water, and the shape or character of the sound cone produced by the echo-sounder transducer. While the first cause applies at all times, and is particularly significant in deep water, whether over a flat or rugged bottom, the second applies only on slopes. And the steeper the slope and the shallower the water, the more complicated and sizable the error. Only the second cause will be discussed in this paper.

The determination of a true slope may be approached by utilizing narrow-beam echo sounders, by taking lead line soundings, or by attempting a correction of the errors inherent in a slope measured with a wide-beam echo sounder. To date, the determination of these errors has been attacked by assuming given, apical angles for the

sound cones from any given echo-sounder transducer. These angles are usually taken from a standard transducer calibration curve. Simple geometry has been developed and graphic solutions found. Acknowledging that the solutions almost certainly improve the situation, there is still no way to check the absolute error without empirical data on the slopes being measured. This empirical data can be provided by lead-line sounding, but inherent errors in this method give a very low level of confidence. This leaves only "in situ" measurements, made directly on the spot with submersibles, as the best, and perhaps the only, basis for absolute comparison or calibration.

One might expect that the measurement of a bottom slope from a submersible to be a simple matter, and indeed it is if one is content with accuracies which vary 2 or 3 degrees. Simple gravity-dependent instruments, such as pendulum or bubble inclinometers can be installed within the pressure-proof sphere in which the pilot and the observers ride. From these, inclinations can be measured to fractions of degrees. However these instruments still permit only an approximate measurement of the sea-floor slope on which a submersible rests because the pilot can only visually estimate that the horizontal plane of symmetry of the submersible, to which the interior inclinometers are adjusted and referred, is parallel to the plane of the sea floor.

In the past three years, slope measurements have been made in 16 dives with the Cousteau Diving Saucer and the Westinghouse DEEPSTAR 4000. All dives were made where the sea floor had rugged relief. The largest concentration of dives was made off the town of San Clemente, California, where specific features had been echo sounded under good navigation control, and a large number of slopes calculated from echograms. These calculated slopes ranged from 7.5° to 31.0° on the simple basis of a tangent resolved from depth differential, ship's speed, and time. In the same area, the same slopes, directly measured, ranged from 7.5° to a maximum of 43°. The accuracy of these latter measurements was circumscribed by the limitation mentioned previously; namely, the pilot's ability to estimate that the horizontal plane of the submersible was parallel to the sea floor. Even so, the difference was most striking, and underlined immediately the need for precise measurements and carefully controlled experiments.

A device for permitting a submersible to measure accurate slopes has been developed at the U. S. Navy Electronics Laboratory (NEL), and tested with DEEPSTAR 4000. It has proved successful enough so that a series of dives, designed specifically for direct and precise slope measurement and comparison with echo-sounding records under rigorously controlled conditions, is planned for the coming dive series which will get underway when DEEPSTAR is recertified.

The device is basically optical, and permits the pilot of a submersible to adjust its attitude around both a fore-and-aft and a vertical axis while heading upslope and watching two light spots projected

on the sea floor from outside the sphere. When the two spots coincide at a maximum measured fore-and-aft inclination with the thwartships axis horizontal, the horizontal plane of symmetry of the submersible is exactly parallel to the sea floor and an interior reading can be made which measures, exactly, the slope of the sea floor. The two projectors are small, simple, and fortunately, not subject to refraction problems. The details are the subject of a technical memorandum currently being published by NEL.

Fig. 1 illustrates the basic geometry involved in the installation aboard DEEPSTAR 4000. The forward of the two light projectors is mounted at maximum distance from the sphere, on the fore-and-aft axis, and is adjusted so that it projects its spot vertically downward or normal to the basic plane of horizontal symmetry of the submersible. The second projector is also mounted on the fore-and-aft axis, but next to the sphere. It is adjusted so that its beam shines obliquely, and its spot coincides with the spot projected by the vertical projector on a plane which is tangent to the bottom of the sphere and, at the same time, parallel to the horizontal plane of symmetry of the submersible.

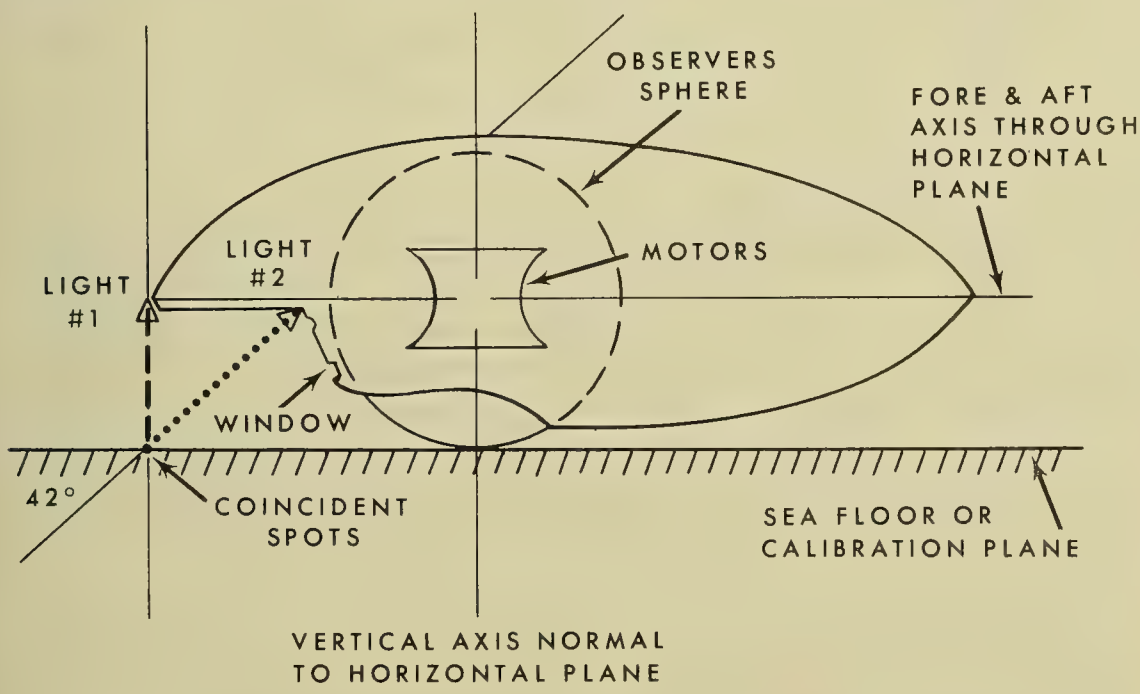

Fig. 1 - Lateral Aspect. Geometry for initial mounting and adjustment of inclinometers for measurement of a level sea floor. The horizontal plane of the submersible is parallel to the plane of the sea floor (or plane tangent to the sphere base) when the light spots coincide. This situation obtains regardless of the slope of the sea floor. The only change is angular rotation of the entire relationship with regard to absolute horizontality.

This particular geometry obtains at all times when the submersible is parallel to the sea floor and an accurate slope is being measured. If the submersible is down by the stern, the light will separate as shown in Fig. 2.

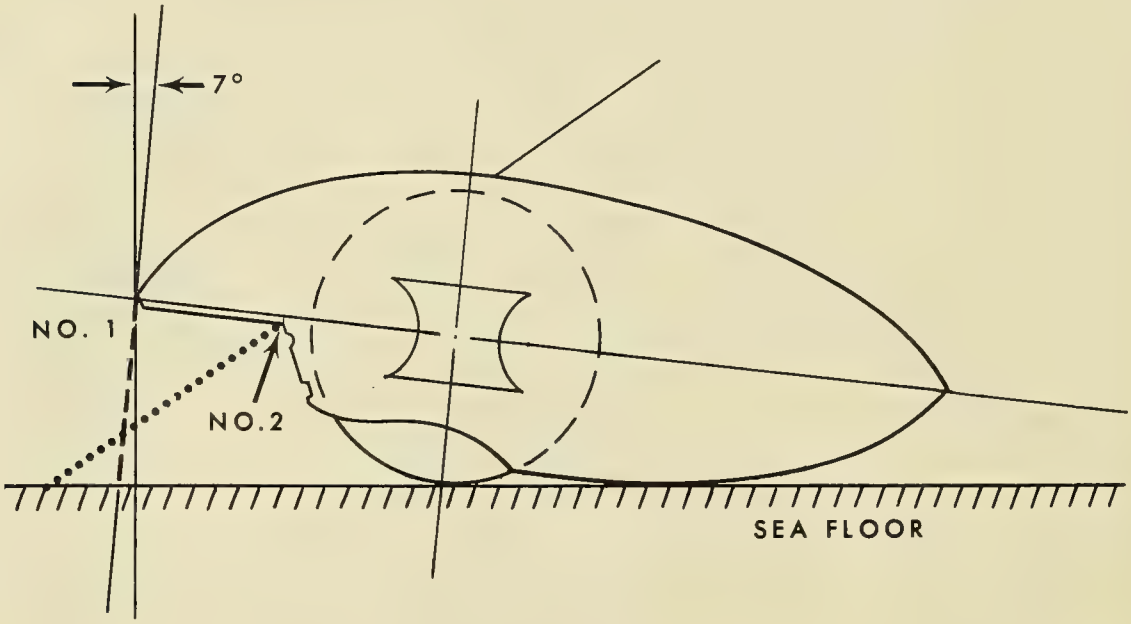

Fig. 2 - Lateral Aspect. The plane of the submersible is inclined to the sea floor stern down. Resting on its "haunches," the maximum absolute separation of the lights is about 7°. This situation obtains regardless of the sea floor slope. The only change is angular rotation of the entire relationship with regard to absolute horizontality.

Correspondingly, if the bow is down, the lights again separate, (Fig. 3) reversing their proximity to the observer's window.

Close study of the geometrical relations between the submersible and the sea floor in various situations will show that to guarantee parallelism between the horizontal plane of the submersible and the horizontal plane of the sea floor, it is necessary to control the thwartships axis running through the center of the sphere in the horizontal plane. This control can be achieved independently of any external observation or reference by simply observing the pendulum or inclinometer inside the sphere which is adjusted to measure deviations from an axis running thwartships.

In Fig. 4 we have an anomalous situation where the two spots coincide on the sea floor and the thwartship axis is horizontal. Yet

the horizontal plane of the submersible and the plane of the sea floor are not even close to being parallel, and the angle being measured is meaningless.

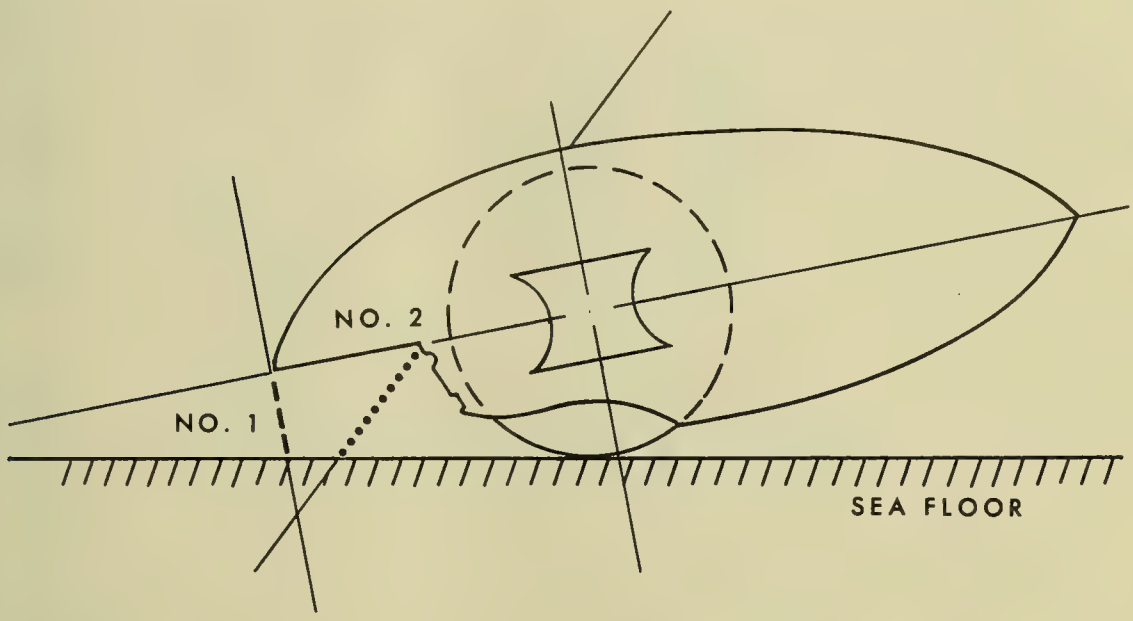

Fig. 3 - Lateral Aspect. The plane of the submersible is inclined to the sea floor, bow down. The situation obtains regardless of the absolute slope of the sea floor.

The remedy in this case (Fig. 4) is procedural. A standard part of the slope measuring procedure must include the rotation of the submersible around an axis normal to its basic horizontal plane of symmetry, while holding the thwartships axis horizontal with the two spots coinciding on the sea floor. Thus, when the submersible is facing upslope, the measured slope will decrease in both a port and starboard direction away from the azimuth of the maximum. The maximum is the true slope.

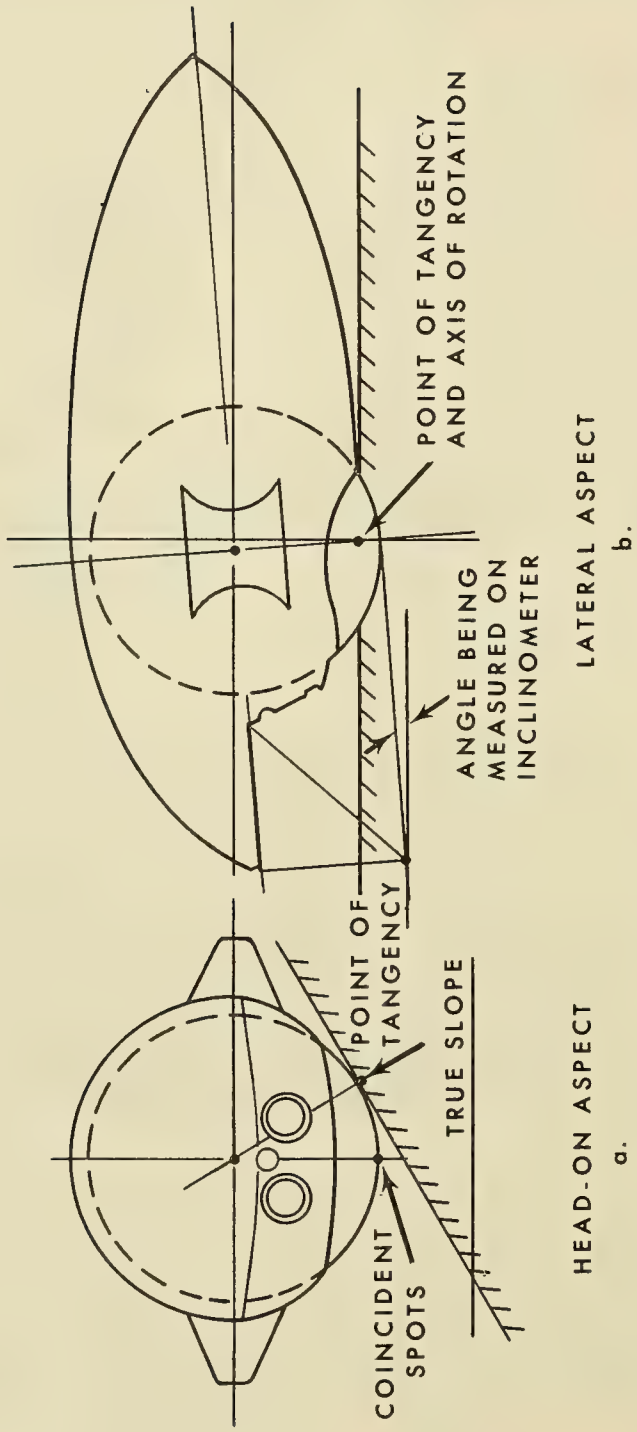

Fig. 4 - Bow (head-on) and Lateral Aspect. Submersible rests on the sea floor with thwartships axis horizontal. Point of tangency is 30° displaced from the vertical; lights coincide above the bottom (4a). Submersible is depressed by the bow, rotating around point of tangency until light sopts coincide (4b). An apparent angle is measured characterizing a slope which is defined by two points, one of which is not the sea floor. The measurement is meaningless.

MEASUREMENT OF SOUND VELOCITY AND ATTENUATION

Knowledge of sound velocity and attenuation in sea-floor sediments is now considered to be a basic requirement for experimental and theoretical studies in bottom-bounce, underwater acoustics. At the Navy Electronics Laboratory, since 1954, measurements have been made in the laboratory, and in situ by scuba divers, and from the bathyscaphe TRIESTE. The present program in the DEEPSTAR is a continuation of previous work. These in situ measurements are necessary to validate laboratory studies on sediments sampled from surface vessels, and to determine the corrections that must be made on laboratory measurements to obtain in situ values. In addition, it is necessary to measure sound velocity and attenuation in natural, undisturbed sediments in which the original sediment structural strength is present.

Successful measurements of sound velocity and attenuation were made during five dives in the present DEEPSTAR program. These stations, made from the submersible, were supplemented by 12 stations made from a diving boat (using the same equipment) with scuba divers to emplace the equipment and take sediment samples.

The equipment used for the measurements was a second model of the probes used during the TRIESTE program. The new probes allow measurements at 14, 7, and 3.5 kc/s. The equipment consists of three probes, $2\frac{3}{4}$ inches in diameter, fastened to a rigid frame in such a manner that when the frame is on the sediment surface, the probes are inserted to a variable, preset depth in the sediment; this depth varied from 6 inches to about 2 feet during the DEEPSTAR tests. The sediments were cored by plastic tubes attached to each end of the probe frame (Fig. 5).

Three barium titanate transducers, designed by NEL's Transducer Division, were used as sound source and receivers. Velocity was determined by measuring travel time over a 1-meter path length between receivers 1 and 2. Attenuation was measured relative to that in the bottom water (assumed to be zero for 1-meter). Path length between receivers was calibrated by using a water velocimeter.

The unique feature of these probes is the ability to measure sound velocity and attenuation at three frequencies (14, 7, and 3.5 kc/s) without removing the probes from the sediment.

The large diameter of the probes ($2\frac{3}{4}$ inches) was necessary to obtain measurements at lower frequencies. Insertion of the probes into the sediment to about 2 feet is necessary to obtain measurements at 3.5 kc/s, and about 1 foot for measurements at 7 kc/s. In a sediment containing appreciable amounts of sand, the DEEPSTAR could not insert the probes a sufficient depth to obtain measurements at any frequency, and even in high porosity clayey silt the probes could not be inserted a sufficient distance to measure at 3.5 kc/s. However,

successful measurements were made from DEEPSTAR at 14 and 7 kc/s, and at all three frequencies from the diving boat in water depths to 100 feet.

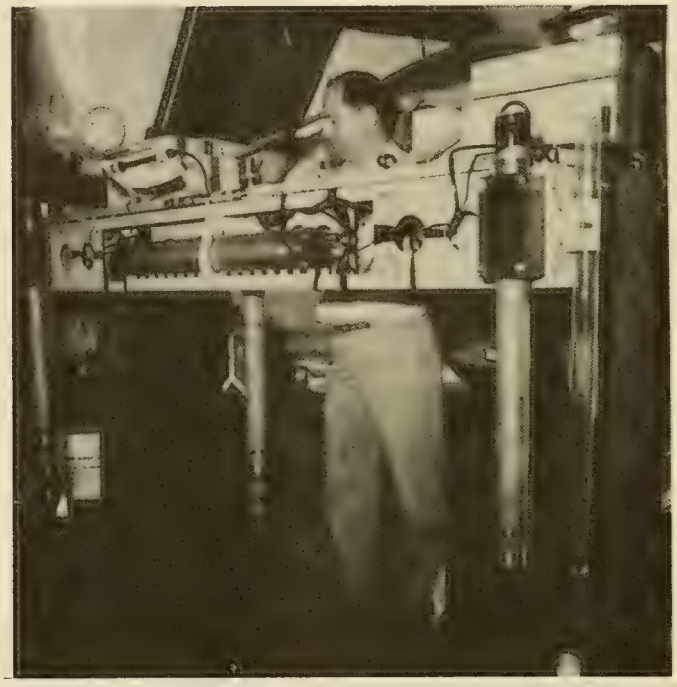

Fig. 5 - Velocity probes and core tubes mounted on the brow of DEEPSTAR 4000

Measurements of sound velocity were made in sediments having ratios of sound velocity in sediment/velocity in bottom water from 0.979 to 1.212. Sediments having sound velocities less than that in the bottom water were measured at several stations. The techniques of relating laboratory measurements of sound velocity to in situ values, determined during the TRIESTE program, were verified. There were no measurements indicating a velocity dispersion (dependence of velocity on frequency).

The attenuation measurements will be completed when the DEEPSTAR returns to NEL, and will be reported in a future paper.

DIRECT MEASUREMENT OF SEA-FLOOR SHEAR STRENGTH

The response of sea-floor sediment to imposed loads and structures is becoming increasingly important to the U. S. Navy and other organizations considering sea-floor installations. The measurement of shear strength is, therefore, of special concern. This can be done from remotely collected samples if they are undisturbed and if the validity of the measurement can be established.

To this end a carefully controlled experiment, to compare in situ and laboratory vane-shear strengths of marine sediment, was carried out in October 1966 from DEEPSTAR 4000. The tests utilized a NEL-developed vane-shear strength machine, designed for operation from deep diving vehicles. This machine was mounted as a unit including two adjacent core tubes (Fig. 6) for simultaneous collection of in situ strength data and sediment for later laboratory study. The experiment was accomplished off San Diego, California at a water depth of 365 meters in an olive gray, clayey silt.

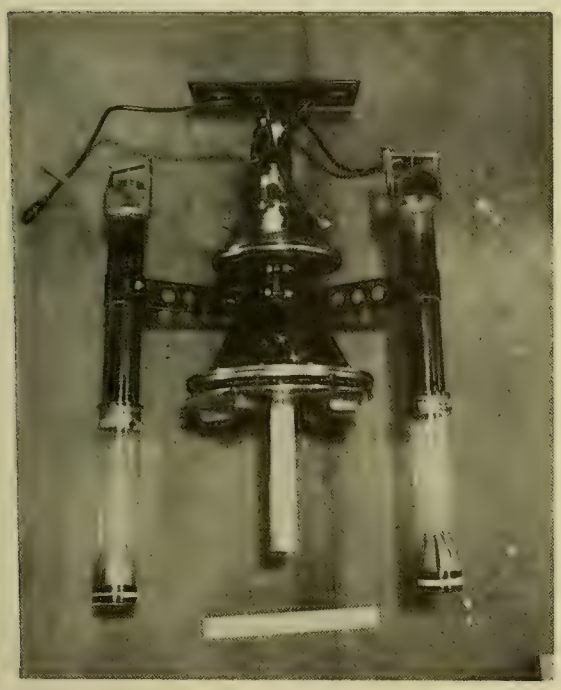

Fig. 6 - Vane-shear machine adapted for use with DEEPSTAR 4000. The white strip below the housing protecting the vane in the center is 12 inches long.

The vane-shear machine, mounted rigidly on the brow of DEEPSTAR in a frame with the two thin-walled tube samplers, operates at ambient pressures with a signal and power lead through to the pressure hull. The machine features a logarithmic accumulator which supplies torque to the vane and allows good sensitivity at a wide range of strengths. The data read-out is in electrical resistance calibrated to torque. For this test, the machine was set up to measure strength in the interval 20 to 22.5 cm beneath the sediment surface with a 2.5 × 2.5 cm vane. The tube samplers were 30-cm long with an inside diameter of 6.67 cm and were fixed at a distance of 26 cm on both sides of the vane. Thus, as the vane was inserted into the sediment for the in situ strength test the sample tubes also penetrated the sea floor and were filled. The samples were carefully handled and stored under sea water in their collecting tubes until the laboratory measurements were made.

The measurement in the sea floor gave a shear strength of 22.13 gm/cm^2 and the adjacent samples tested at exactly the same depth intervals within the sediment showed strengths of 21.81 and 27.91 gm/cm^2 when later measured with a calibrated laboratory vane-shear strength machine. It is apparent that, in this test, the variation in sediment strength between the two cores taken 56 cm apart is significantly greater than the variation between in situ and laboratory measurement of shear strength. With this limited data, the tentative conclusion is that laboratory measurements of vane-shear strength are valid on gravity type cores at least 20-cm long, assuming a well-designed core tube and proper handling between collection and testing.

For this type of comparative test, it is imperative that laboratory measurements of shear strength be made on cores collected as closely adjacent to the in situ measurement as is practical, and at exactly the depth interval in the core which corresponds to the in situ depth measurement. Without this precaution the comparisons may be meaningless as lateral variations and, particularly range in strength with depth may be great. The laboratory vane strengths of these sediments, for example, varied from 5.79 gm/cm^2, at 3 to 5.5 cm beneath the sediment surface, to the previously stated values at 20 to 22.5 cm which are about four times as great.

VARIABILITY IN DERIVED SEDIMENT SOUND VELOCITY AS A FUNCTION OF CORE ANALYSIS AND ITS EFFECT IN DETERMINING THEORETICAL BOTTOM REFLECTIVITY

James J. Gallagher
U. S. Navy Underwater Sound Laboratory
Fort Trumbull, New London, Connecticut

INTRODUCTION

Acoustic field tests have been conducted over limited portions of flat-bottomed ocean areas. Core samples were collected from these insonified bottom areas, where each area was usually about two square miles. A multilayered, absorbing, mathematical model is being used to transform the geological core data into an acoustic description of the unconsolidated ocean bottom.[1-5]

This description is supposed to provide an understanding of the influences that a nonuniform bottom exerts on an acoustic signal as it travels through that bottom. The results of the model investigations are being compared with corresponding 3.7 kHz field data to determine whether the mechanisms affecting acoustic behavior are, in truth, being explained by the model. Relationships between geologic and acoustic properties of marine sediments have been studied by other investigations.[6-10] Inasmuch as the results of these studies will not be reviewed here, it should be noted that the products of these investigations have direct application to the mathematical model studies.

The salient features of the multilayered model as currently programmed are (1) it treats up to 10 liquid layers overlying a solid layer; (2) it considers acoustic absorption; and (3) it requires a smooth, nonsloping surface.

This model is being employed as a research tool. In its present capacity disagreement between observed and predicted reflection coefficients of about 0.05, which may correspond to a change in bottom loss of several db, is considered significant. The sensitivity of this model to changes in sound velocity and layering thickness is of concern and is being explored at the present time. This report discusses the results of a preliminary investigation that was designed

to test the effects of changing sound velocity values on the values of acoustic reflection coefficients obtained over a broad range of incident angles.

DISCUSSION

Two dissimilar sediment depositional areas were considered. The sediments in the slow depositional area, the Hatteras Abyssal Plain (HAP), are characterized by fine grained particles, low carbonate content, and high porosity. Sediments in the rapid depositional area, the Tongue of the Ocean (TOTO), are characterized by medium sized particles, high carbonate content, and moderate porosity. Two cores from each area were investigated. The distance between the two cores in both the HAP and TOTO areas is 0.4 mile.

Variations in sound velocity are provided by values computed from Sutton's regression equation and from direct laboratory measurements on the core samples.

HATTERAS ABYSSAL PLAIN (HAP)

These variations are strikingly evident in core no. 1, as seen in Table 1. The measured velocities for core no. 1 should probably be viewed with caution since they are considerably higher than what the accepted sound velocity versus porosity curves indicate; the porosities lie in the 70 percent range. It is possible that a constant error existed in the laboratory measurements. However, the

Table 1

MEASURED AND SUTTON DERIVED SOUND VELOCITIES AND CORRESPONDING ACOUSTIC IMPEDANCE DATA — CORE NO. 1 — HAP

Depth Interval	Sound Velocity ft/sec		Direct Minus Sutton	Percent Difference	Impedance $\times 10^4$ lb/ft^2-sec		Direct Minus Sutton
	Direct	Sutton			Direct	Sutton	
0-1	5266	4530	+736	13	47.00	40.85	+6.15
1-2	5181	4359	+822	15	47.80	40.67	+7.13
2-3	5336	4492	+844	15	47.60	40.47	+6.59
3-4	5266	4896	+370	6	49.30	46.26	+3.04
4-5	5266	5826	-555	11		75.09	
5-6	5336	4756	+580	11	51.60	46.13	+5.47
6-7	5356	4369	+987	17	46.90	38.66	+8.24
7-8	5246	4456	+790	15	47.80	40.28	+7.52
8-9	5236	4458	+878	16	47.80	40.34	+7.46
9-10	5356	4405	+951	18	47.80	39.73	+8.07

measured sound velocity values for core no. 2, and for core no. 3, which is not included in this report, were determined with the same equipment, and both were lower. It is interesting to note that the laboratory vane shear strength values for core no. 1 were an order of magnitude higher than those determined from cores 2 and 3. During the core sampling operation it was noted that the bottom was quite hard in this general area. Core no. 1, in particular, seemed so compact that it appeared to be almost dry when it was removed from the barrel at sea. However, the porosities did lie in the 70 percent range. The 3.7 kHz acoustic field data substantiate the nonuniformity of this bottom.

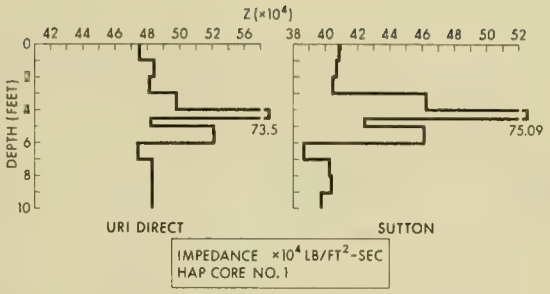

Fig. 1
Vertical Acoustic Impedance Profiles – Core No. 1 – HAP

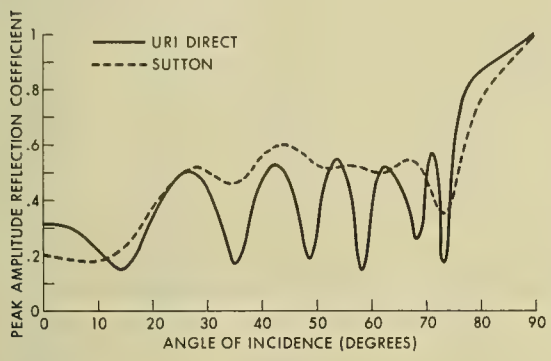

Fig. 2
Reflection Coefficients versus Incident Angles – Core No. 1 – HAP

Figure 1 denotes the impedance profiles for the directly measured and Sutton derived data for core no. 1. The number and thicknesses of the acoustic impedance layers are not altered by the sound velocity differences, but differences in the magnitudes of these layers are produced. The resulting differences in the peak amplitude reflection coefficients over increasing incident angles for core no. 1 are shown in Fig. 2. Considering the requirements imposed on this model study, the differences in bottom loss are considered significant. This is generally true for the succeeding data to be discussed.

The measured and Sutton derived sound velocities and impedance data are indicated in Table 2. Graphical differences in the impedance profiles are shown in Fig. 3. For core no. 2, the differences in the sound velocity values obtained from the two cases of interest produced differences in both the layering and the magnitudes of the impedance layers. The reflection coefficients computed from the measured and Sutton derived data for

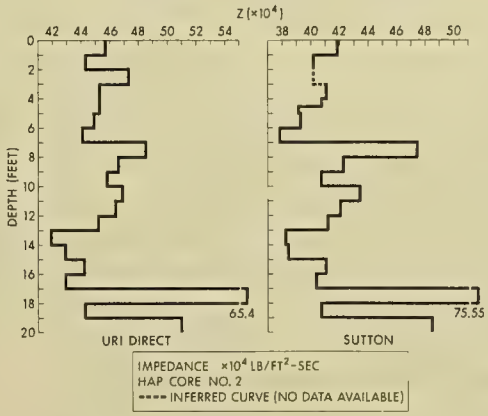

Fig. 3
Vertical Acoustic Impedance Profiles – Core No. 2 – HAP

Table 2

MEASURED AND SUTTON DERIVED SOUND VELOCITIES AND CORRESPONDING ACOUSTIC IMPEDANCE DATA — CORE NO. 2 — HAP

Depth Interval	Sound Velocity ft/sec Direct	Sound Velocity ft/sec Sutton	Direct Minus Sutton	Percent Difference	Impedance $\times 10^4$ lb/ft^2-sec Direct	Impedance $\times 10^4$ lb/ft^2-sec Sutton	Direct Minus Sutton
0-1	5026	4597	+429	9	45.70	41.83	+3.9
1-2	5041	4564	+477	10	44.30	40.16	+4.2
2-3	5046	--	--	--	47.30	--	--
3-4	5036	4564	+472	10	45.30	41.07	+4.2
4-5	5031	4464	+567	11	45.30	40.76	+4.6
	--	4413	+618	12	--	39.14	+6.2
5-6	5026	4403	+623	12	44.90	39.27	+5.6
6-7	5016	4310	+706	14	44.10	37.84	+6.3
7-8	5006	4900	+106	2	48.50	47.43	+1.1
8-9	5041	4565	+476	9	46.60	42.22	+4.4
9-10	4926	4454	+472	10	45.80	40.71	+5.1
10-11	4996	4633	+363	7	46.90	43.45	+3.5
11-12	4956	4494	+462	9	46.40	42.06	+4.3
12-13	5041	4592	+449	9	45.20	41.19	+4.0
13-14	4881	4454	+427	9	41.90	38.22	+3.7
14-15	4876	4496	+380	8	42.90	38.44	+4.5
15-16	4906	4535	+372	8	44.20	41.04	+3.2
16-17	4876	4589	+287	6	42.90	40.38	+2.5
17-18	5066	5857	-791	16	65.40	75.55	-10.1
18-19	4846	4457	+389	8	44.30	40.73	+3.6
19-20	5026	4494	+552	11	51.00	48.46	+2.5
20-21	--	--	--	--	--	42.46	--

core no. 2 are shown in Fig. 4. The bottom loss values appear to be greater in core no. 2 for the two cases than for those in core no. 1. Although it is tempting to attribute the lower losses in core no. 1 to the higher sound velocities reported, it appears that the magnitude of the sound velocity value has little influence on the value of the reflection coefficients for any given angle.

For cores 1 and 2 the lower Sutton derived sound velocity data appear to produce generally higher reflection coefficients. However, this is not

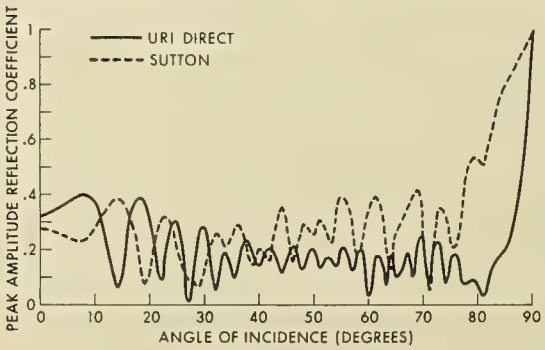

Fig. 4

Reflection Coefficients versus Incident Angles — Core No. 2 — HAP

Table 3

MAXIMUM DIFFERENCES IN REFLECTION COEFFICIENT VALUES
CORES NO. 1 AND NO. 2—HAP

Station	Incident Angle	Direct Measurement	Sutton	Bottom Loss Difference Direct Minus Sutton
Core No. 1	35°	0.17 (15.0 db)	0.45 (7.0 db)	+8.0 db
	48°	0.20 (14.0 db)	0.54 (5.4 db)	+8.6 db
	58°	0.14 (17.0 db)	0.51 (5.7 db)	+11.3 db
Core No. 2	14°	0.06 (24.5 db)	0.39 (8.1 db)	+16.4 db
	79°	0.09 (21.0 db)	0.54 (5.4 db)	+15.6 db

consistently true over all angles. The impedance values of the layers, the thicknesses of the layers, and the angles and speeds at which the sound rays are propagating through the layers apparently combine to form constructive and destructive interferences and thereby regulate the amount of acoustic energy returned to the interface.

The maximum differences in the values of these reflection coefficients, and of bottom loss, derived from the measured and Sutton data, are shown in Table 3. It is interesting to note that whereas the magnitude of the sound velocity differences between the measured and Sutton data in core no. 2 is somewhat less than that in core no. 1, larger differences in bottom loss are seen in core no. 2. These large differences may occur aperiodically over various angles, depending upon the layering effects of the model. It should be noted that the differences are smaller at other angles and at some angles there is a zero difference. It should also be noted that since the bottom loss differences are logarithmic ratios, a change in one unit of reflection coefficient at the lower range will produce a different corresponding change in db than will a change in one unit of reflection coefficient at the upper range of the scale.

Table 4 indicates the differences in bottom loss between the measured and Sutton derived data in cores 1 and 2 and the data obtained from field acoustic tests at a frequency of 3.7 kHz. Considering the suspected high measured velocity values for core no. 1, it is interesting to note that the field data report generally lower bottom losses for most incident angles. The exceptions are at 42° and at angles approaching normal incidence. In a general sense, it would be expected that even higher sound velocities would be required to produce higher impedance values in order to obtain the lower bottom losses reported by the field test data. However, in noting the previous remarks, it can be seen that this will not necessarily follow. Generally, the 3.7 kHz field test data exhibit lower bottom losses than those for both cases for core no. 2.

Table 4

VARIATIONS IN BOTTOM LOSS BETWEEN FIELD DATA AND DIRECT AND SUTTON DERIVED VALUES—CORES NO. 1 AND 2—HAP

		Core No. 1		Core No. 2	
Incident Angle	Field Values	Field Minus Direct	Field Minus Sutton	Field Minus Direct	Field Minus Sutton
42°	8.0 db	+2.5 db	+6.7 db	0	-7.8 db
50°	9.1 db	-1.2 db	+3.6 db	-5.8 db	-2.6 db
55°	5.0 db	-0.3 db	-0.2 db	-8.6 db	-3.0 db
57°	6.0 db	-4.4 db	+0.3 db	-10.5 db	-5.0 db
60°	4.4 db	-4.7 db	-1.6 db	-21.6 db	-4.4 db
62°	1.8 db	-3.9 db	-4.4 db	-14.0 db	-7.0 db
65°	3.5 db	-2.6 db	-2.0 db	-16.5 db	-8.5 db
68°	1.8 db	-9.9 db	-3.6 db	-17.3 db	-6.2 db
70°	3.1 db	-3.8 db	-3.3 db	-10.9 db	-7.9 db
75°	0.8 db	-4.4 db	-6.7 db	-14.1 db	-13.2 db
80°	3.1 db	+1.8 db	-1.0 db	-21.3 db	-2.5 db

TONGUE OF THE OCEAN (TOTO)

In contrast to the large differences noted between the Sutton derived and directly measured sound velocity values in the Hatteras Abyssal Plain cores, the differences between these values in TOTO core no. 5 are small. These data, which are shown in Table 5, present an interesting example of the caution that should be exercised in using this model for predicting in situ bottom losses. Small differences in sound velocity between in situ values and those determined from direct core measurements could be produced by mechanical disturbances in the sampling and handling processes. These differences would be produced by the alteration of the sediment aggregate structure. It may be assumed that these differences would be of the same magnitude as the differences reported for core no. 5 in Table 5.

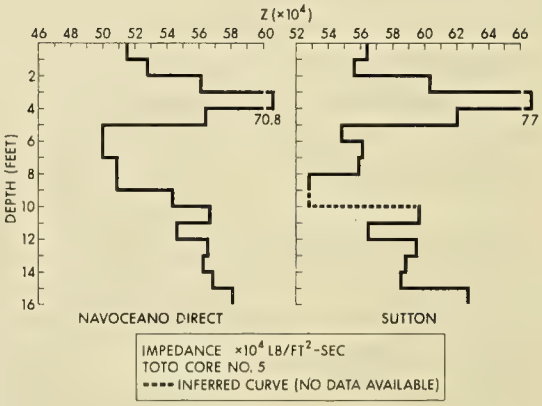

Fig. 5
Vertical Acoustic Impedance Profiles—Core No. 5—TOTO

The acoustic impedance profiles constructed from the data from these two methods are shown in Fig. 5. Changes in the magnitudes of the impedance layers

Table 5

MEASURED AND SUTTON DERIVED SOUND VELOCITIES AND CORRESPONDING IMPEDANCE DATA — CORE NO. 5 — TOTO

Depth Interval	Sound Velocity ft/sec		Direct Minus Sutton	Percent Difference	Impedance $\times 10^4$ lb/ft^2-sec		Direct Minus Sutton
	Direct	Sutton			Direct	Sutton	
0-1	4951	4970	-19	0.4	51.49	51.70	-0.2
1-2	5078	4920	+158	3.1	52.81	51.20	+1.69
2-3	5103	5030	+73	1.4	56.13	55.30	+0.83
3-4	5131	5140	-9	--	70.80	70.90	-0.10
4-5	5127	5200	-73	1.4	56.39	57.20	-0.81
5-6	4997	5020	-23	0.46	49.97	50.20	-0.23
6-7	--	4840	--	--	49.97	48.40	+1.57
7-8	4991	4720	+271	5.4	50.91	48.10	+2.81
8-9	--	4750	--	--	50.91	48.40	+2.51
9-10	5080	--	--	--	54.35	--	--
10-11	5110	5010	+100	1.95	56.72	55.00	+1.72
11-12	5104	4820	+284	5.5	54.61	51.60	+3.0
12-13	5140	4970	+170	3.3	56.55	54.70	+1.85
13-14	5116	4900	+216	4.2	56.28	53.90	+2.38
14-15	5169	4870	+299	5.8	56.86	53.60	+3.26
15-16	5142	5070	+72	1.4	58.11	55.80	+2.31

and in the number and thicknesses of the layers were effected by the small sound velocity differences. The peak amplitude reflection coefficients for both the measured and Sutton derived values over a wide range of incident angles are shown in Fig. 6.

Differences in the measured and Sutton derived sound velocity values are again large in core no. 6, as shown in Table 6. The resulting differences in the respective impedance profiles are shown in Fig. 7. These moderate differences in the sound velocity data produced changes in the number and thicknesses of impedance layers and in the magnitudes of these layers.

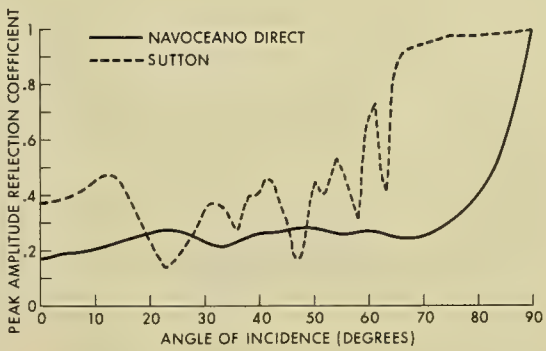

Fig. 6
Reflection Coefficients versus Incident Angles — Core No. 5 — TOTO

The reflection coefficients for both cases in core no. 6 were computed for various incident angles, and the results are shown in Fig. 8. The magnitude

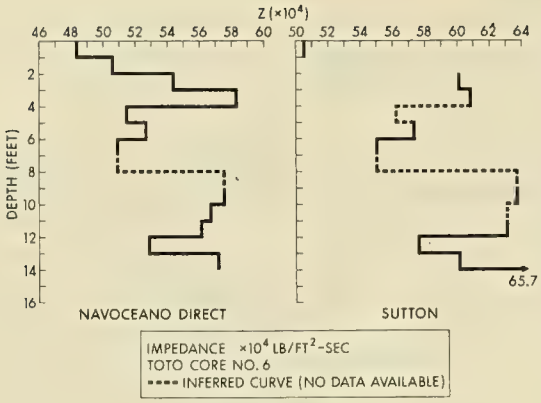

Fig. 7
Vertical Acoustic Impedance Profiles – Core No. 6 – TOTO

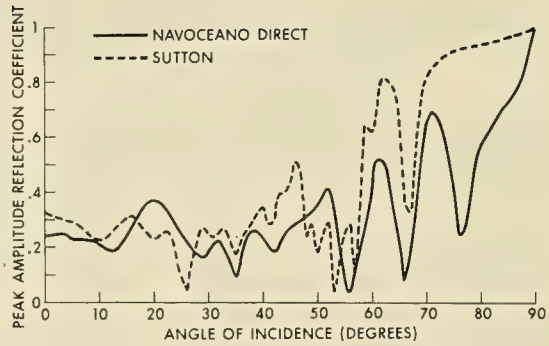

Fig. 8
Reflection Coefficients versus Incident Angles – Core No. 6 – TOTO

Table 6

MEASURED AND SUTTON DERIVED SOUND VELOCITIES AND CORRESPONDING ACOUSTIC IMPEDANCE DATA — CORE NO. 6 — TOTO

Depth Interval	Sound Velocity ft/sec Direct	Sound Velocity ft/sec Sutton	Direct Minus Sutton	Percent Difference	Impedance $\times 10^4$ lb/ft^2-sec Direct	Impedance $\times 10^4$ lb/ft^2-sec Sutton	Direct Minus Sutton
0-1	4923	5150	-227	5	48.34	50.05	-1.71
1-2	4925	--	--	--	50.62	--	--
2-3	5006	5540	-534	11	54.37	60.10	-5.73
3-4	5344	5580	-236	4	58.27	60.80	-2.55
4-5	5029	--	--	--	51.45	--	--
5-6	4954	5380	-426	9	52.71	57.30	-8.59
6-7	5015	5410	-395	8	50.91	55.00	-4.09
7-8	4949	--	--	--	--	--	--
8-9	--	--	--	--	--	--	--
9-10	5123	5680	-557	11	57.48	63.70	-6.22
10-11	5139	--	--	--	56.78	--	--
11-12	5085	5710	-625	12	56.09	63.10	-7.01
12-13	5082	5540	-458	9	52.85	57.60	-4.75
13-14	5097	5340	-253	5	57.19	60.10	-2.91
14-15	5114	5810	-696	14	--	65.70	--

of the differences in the reflection coefficient curves between the two methods for cores 5 and 6 does not necessarily reflect the respective ranges of sound velocity differences in these cores. The differences between the reflection coefficients computed from the measured and Sutton derived data for core no. 5, where the sound velocity differences are very small, are similar to those differences in

core no. 6, where the sound velocity differences are quite large. The maximum differences between the measured and Sutton derived bottom losses, occurring at various incident angles, for both cases are shown in Table 7.

Table 8 indicates the reflection coefficient values obtained from field tests at a frequency of 3.7 kHz and denotes the variations in bottom loss obtained from the core data relative to the field values. The bottom loss values obtained from the field tests are consistently greater than those obtained from the use of either method on the core samples.

Table 7

MAXIMUM DIFFERENCES IN REFLECTION COEFFICIENT VALUES
CORES NO. 5 AND NO. 6—TOTO

Station	Incident Angle	Direct Measurement	Sutton	Bottom Loss Difference Direct Minus Sutton
Core No. 5	13°	0.22 (13.2 db)	0.47 (6.6 db)	+6.6 db
	42°	0.27 (11.4 db)	0.46 (6.7 db)	+4.7 db
	54°	0.26 (11.7 db)	0.54 (5.4 db)	+6.3 db
	61°	0.27 (11.4 db)	0.74 (2.6 db)	+8.8 db
	70°	0.25 (12.0 db)	0.95 (0.5 db)	+11.5 db
Core No. 6	20°	0.365 (8.7 db)	0.23 (12.8 db)	-4.1 db
	46°	0.285 (10.9 db)	0.515 (5.7 db)	+5.2 db
	56°	0.04 (28.0 db)	0.29 (10.5 db)	+18.2 db
	62°	0.57 (4.8 db)	0.82 (1.7 db)	+3.1 db
	76°	0.25 (12.0 db)	0.93 (0.5 db)	+11.5 db

Table 8

VARIATIONS IN BOTTOM LOSS BETWEEN FIELD DATA AND DIRECT AND SUTTON DERIVED VALUES—CORES NO. 5 AND 6—TOTO

		Core No. 5		Core No. 6	
Incident Angle	Field Values	Field Minus Direct	Field Minus Sutton	Field Minus Direct	Field Minus Sutton
50°	15.4 db	+4.7 db	+14.7 db	+6.6 db	+0.9 db
55°	17.6 db	+5.9 db	+11.1 db	-5.4 db	+6.2 db
60°	17.1 db	+5.9 db	+14.0 db	+9.8 db	+12.9 db
65°	14.5 db	+2.5 db	+13.3 db	+0.5 db	+10.5 db
72°	15.9 db	+4.9 db	+15.5 db	+12.3 db	+14.6 db
75°	14.0 db	+3.9 db	+13.8 db	+7.1 db	+13.2 db
78°	15.9 db	+7.1 db	+15.7 db	+10.5 db	+15.3 db

SUMMARY AND CONCLUSIONS

The purpose of this single experiment was to test the multilayered, absorbing, mathematical model for sensitivity to changes in sound velocity. Two closely spaced cores from each of two dissimilar depositional environments were investigated. The slow depositional environment is represented by the Hatteras Abyssal Plain cores, and the rapid depositional area, by the Tongue of the Ocean cores. The sound velocity data used were values determined from direct measurements on the core samples and computed values obtained with Sutton's regression equation for the same cores.

Based on this investigation, it is concluded that for given density values higher sound velocity values will produce greater values of impedance, but they do not necessarily produce lower bottom losses over all incident angles. In addition, for given density values, the magnitude of the differences in reflection coefficients derived from two sources over various incident angles does not necessarily reflect the magnitude of the differences between the sound velocity values of these sources. The impedance values of the layers, the thicknesses of the layers, and the angles and speeds at which the sound rays are traveling through the various layers in a nonuniform bottom apparently combine to set up constructive and destructive interferences, thereby regulating the amount of acoustic energy returning to the interface.

This model is currently being employed as a research tool. In its present capacity, bottom loss differences greater than 3 db between observed and predicted values will continue to be considered significant. Differences in bottom losses of 3 db or greater over short lateral distances are evidenced by single source data obtained from two closely spaced core samples. If indeed this close range variability is widespread within a physiographic province, and there is every reason to believe that it is for some provinces, then the accurate prediction of changes in bottom loss of several db over extended distances, based on a few sample points, will be difficult. Results of acoustic measurements made at these core locations substantiate that a complex nonuniform acoustic impedance layering structure exists over small lateral distances.

The effectiveness of this model in accurately predicting in situ acoustic bottom losses over core sample lengths appears limited by the sensitivity to changes in sound velocity. The effects of small changes on layer thickness and sound velocity will continue to be sought. The problem has already been manifested by the fact that in some cores the sensitivity of the model to changes in sound velocity produced more impedance layers within a core length than the model program was capable of accommodating. Therefore, laboratory experimental model studies are being planned to simulate the mathematical model to compare measured and computed reflection coefficients for given data. Attempts will be made to alter the number of original layers, while the original mass

of sediment is retained, to note the effect of integrating the layers on the reflection coefficients.

REFERENCES

1. M. C. Karamargin, "A Treatment of Acoustic Plane Wave Reflections from an Absorbing Multilayered Liquid and Solid Bottom," USL Technical Memorandum No. 913-91-62, 16 July 1962.

2. M. C. Karamargin and B. J. Klein, "Some Theoretical Computations of Distortions at Reflection from an Absorbing Multilayered Liquid and Solid Bottom," USL Technical Memorandum No. 910-169-63, 27 August 1963.

3. F. R. Menotti, R. D. Whittaker, and S. R. Santaniello, "Analysis Procedure for the Bottom Reflectivity Measurements Program," USL Technical Memorandum No. 913-4-65, 26 January 1965.

4. F. R. Menotti, S. R. Santaniello, and W. R. Schumacher, Studies of Observed and Predicted Values of Bottom Reflectivity as a Function of Incident Angle, USL Report No. 657, 28 April 1965.

5. F. R. Menotti and S. R. Santaniello, "Observed Values of Bottom Reflectivity as a Function of Incident Angle (TOTO)," USL Technical Memorandum No. 913-286-65, 20 December 1965.

6. E. L. Hamilton, G. Shumway, H. W. Menard, and C. J. Shipek, "Acoustic and Other Physical Properties of Shallow-Water Sediments Off San Diego," Journal of the Acoustical Society of America, vol. 28, no. 1, January 1956, pp. 1-15.

7. G. H. Sutton, H. Berckhemer, and J. E. Nafe, "Physical Analysis of Deep-Sea Sediments," Geophysics, vol. 22, no. 4, October 1957, pp. 779-812.

8. G. Shumway, "Sound Speed and Absorption Studies of Marine Sediments by a Resonance Method—Parts I and II," Geophysics, vol. 25, no. 2, April 1960, pp. 451-567; vol. 25, no. 3, June 1960, pp. 659-682.

9. E. L. Hamilton, "Sediment Sound Velocity Measurements Made In Situ from Bathyscaph Trieste," Journal of Geophysical Research, vol. 68, no. 21, 1 November 1963, pp. 5991-5998.

10. E. L. Hamilton, "Sound Speed and Related Physical Properties of Sediments from Experimental Mohole (Guadalupe Site)," Geophysics, vol. 30, no. 2, April 1965, pp. 257-261.

Strange Hot Waters and Minerals at the Bottom of the Red Sea

John M. Hunt and David A. Ross
Woods Hole Oceanographic Institution
Woods Hole, Mass. 02543

During the fall of 1966, the R/V CHAIN conducted an extensive survey of the hot brine area of the Red Sea (21°10'N to 21°30'N). This survey included: detailed bathymetry using radar reflecting buoys; measurements of temperature with conventional hydrocasts and a temperature telemetering pinger; continuous seismic profiling; gravity and magnetic measurements; and a detailed sampling of bottom sediments with free-fall, gravity, piston and, box-coring techniques. This paper discusses some of the preliminary results of this survey.

The bathymetric survey showed three deeps (Fig. 1), which contain hot highly saline water. These deeps are located in the central portion of the Red Sea rift valley. The ATLANTIS II Deep is about 12 km long and 5 km wide, and contains several small topographic highs. This deep is connected to the smaller DISCOVERY Deep by a narrow channel; which is apparently sufficiently high, at present, to prevent mixing of the hot saline waters. The CHAIN Deep, which was discovered on this cruise, is situated in a saddle on this channel.

Temperature profiles of the brine areas were obtained with a temperature telemetering pinger, developed especially for this cruise by Benthos Inc. (Ross and Tyndale, 1967). This pinger emits two pings within a one second interval. The first ping is emitted every second, the second ping at a time interval after the first, this time interval is a measure of temperature. The time interval is maintained by a thermistor that produces a varying resistance which controls the telemetering electronics. Both pings were received by the ships 12 kc echo sounder and recorded on a Precision Graphic Recorder. Temperature could then be read directly from the P.G.R. In the Red Sea, a thermistor with a range of 20°C to 70°C was used. The accuracy of the measurement was ± 1.25°C. Determinations of absolute temperature were made by conventional methods using high-range thermometers. The temperature telemetering pinger

was used to define the water structure, position other equipment in certain water levels and to test other areas of the Red Sea for high temperature waters. No other areas tested contained anomalously hot water.

The highest water temperature measured was 56°C. This was from below a depth of 2040 meters in the ATLANTIS II Deep. This water had a "salinity" of about 317‰. The "salinity" was determined by a Schleicher-Bradshaw salinometer on samples diluted by volume with distilled water. Salinity values so determined assume that the brine water has the same relative proportion of salts as normal sea water. This assumption is not correct. A better estimate of salinity is total solids by evaporation to dryness at 200°C, which for the 56°C water is about 255‰ (F.T. Manheim, personal communication). The 56°C water of the ATLANTIS II Deep is overlain by a layer of 44°C water (total solids about 131‰). This 44°C water grades into normal 22°C Red Sea bottom water. The 44°C and 56°C water generally have oxygen values of 0.1 ml/l or less.

The DISCOVERY Deep has water with a temperature of 44.7°C below a depth of 2038 m, which is overlain in some instances by a layer of 36°C water. This 44.7° water has a salinity similar to the 56°C water of the ATLANTIS II Deep.

The CHAIN Deep has a maximum temperature of 34°C and a "salinity" of about 74‰. Its deepest part was not sampled.

Continuous seismic reflection profiles have not been fully analyzed at present. Field observations suggest considerable rifting and faulting in and adjacent to the brine areas. Using a recording bandwidth of 37.5 to 150 Hz some reflections were obtained from the hot brine water in the ATLANTIS II and DISCOVERY Deeps (no records were made in the CHAIN Deep area). These reflections apparently are due to density differences between the hot brine water and the overlying Red Sea water.

All gravity observations, bathymetry and navigation data were processed while at sea, and the results computed and plotted on line by the shipboard IBM 1710 computer. A gravity anomaly of about + 120 milligals is observed in the hot brine area. However, this value is within the range normally observed in the rift valley. A magnetic anomaly of - 650 gammas was observed over the ATLANTIS II Deep, and an anomaly of + 350 gammas was observed over the DISCOVERY Deep. The large magnetic gradient between these areas may be due to higher sub-surface temperatures in the ATLANTIS II Deep.

Temperature gradients in the sediments, as determined by heat flow measurements, were 10 to 20 times the world average of 1°C per 16 meters.

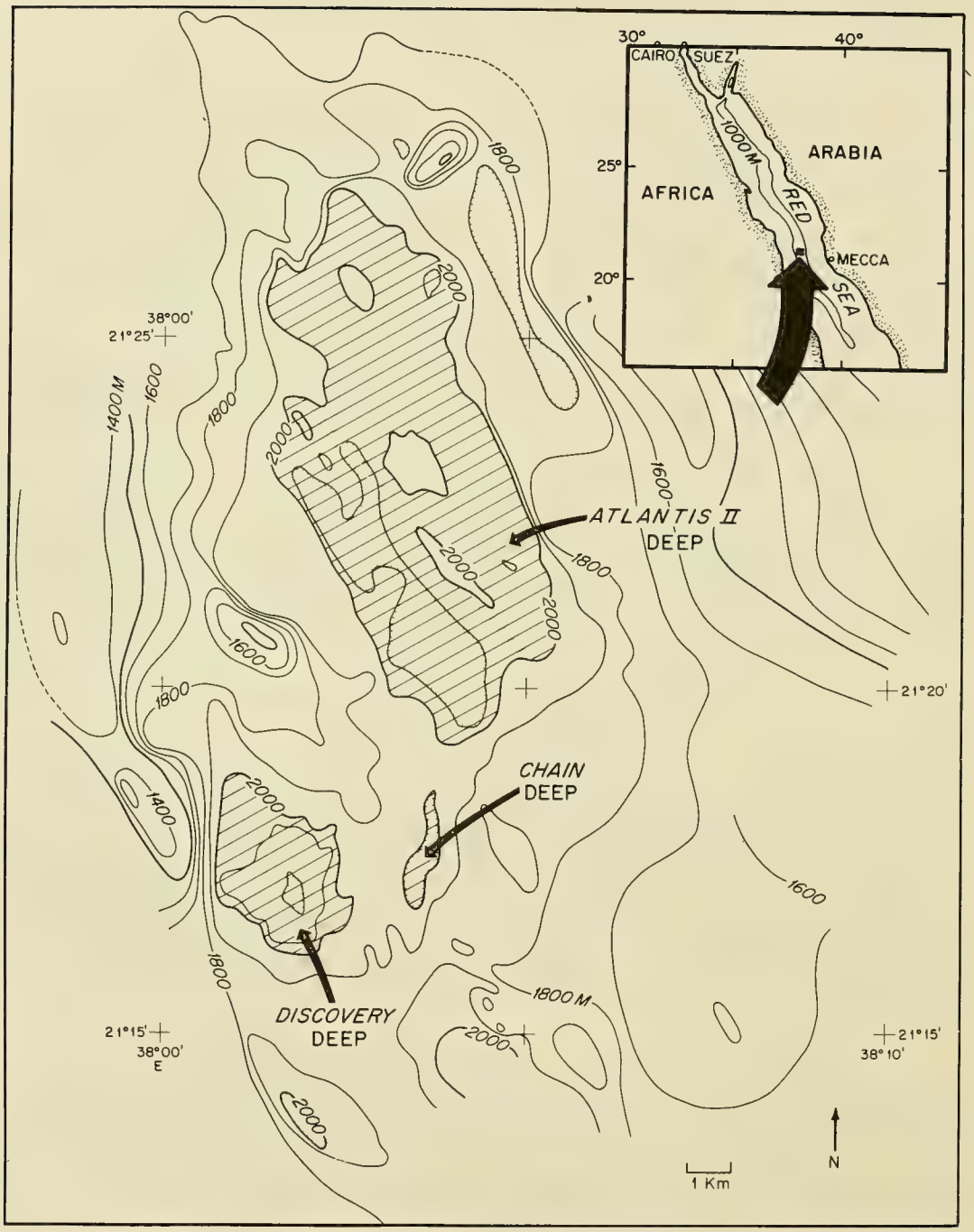

Fig. 1 - Bathymetry of the hot brine region in the Red Sea. Depth contours in meters corrected for sound velocity according to Matthews Tables. No correction has been applied for the increase in sound velocity in the hot brine water.

Extreme variations in gradients occurred along the eastern flank of the ATLANTIS II Deep, which suggests that this area may be a likely source of the hot brines.

Sediment cores obtained from both the brine and adjacent areas contained brightly colored material. The sediments generally were comprised of alternating yellow, brown, red, orange and black layers that are mainly amorphous iron oxides. Cores obtained using a square box coring device were especially impressive. These cores (4 m long x 15 cm x 15 cm) collected relatively undisturbed samples. Because of its large size, this sampler collects enough material so that many detailed chemical and geological analyses can be performed on an individual layer. These analyses are now in progress.

The preliminary interpretation is that the hot saline water and its associated heavy metals are ejected, probably forcibly, periodically from the ATLANTIS II Deep. The hot brines in the other deeps are the result of spillover. It is possible that similar brine pools may be found on the ocean floor in other parts of the world rift system.

This work was partly supported by the Office of Naval Research and by the National Science Foundation. (Nonr-4029 and GA-584)

References Cited

Ross, D.A., and Tyndale, C. A temperature telemetering pinger, in press, Geo-Marine Technology.

MILITARY SIGNIFICANCE OF DEEPLY SUBMERGED SEA CLIFFS AND ROCKY TERRACES ON THE CONTINENTAL SLOPE

Robert F. Dill
U.S. Navy Electronics Laboratory

ABSTRACT

A series of narrow, step-like, rock terraces and low sea cliffs (between depths of 325 and 1170 feet) have been observed on three DEEPSTAR dive-traverses up the continental slope off San Diego, California. The terraces are cut in bedrock and covered with coarse shelly sand of shallow water origin, and large rounded boulders. The flat terraces are less than 100-feet wide and the maximum observed relief of the adjacent cliffs is less than 60 feet. The best-developed cliff and terrace is between 600 and 700 feet (water depth), and extends at least 10 miles along the slope off San Diego. Although large when viewed from the window of a submersible, these features are usually overlooked on most echo-sounder surveys because of the lack of definition within the wide angle of the sound cone and the high speeds of the survey traverses. Restudy of existing echo-sounder and acoustic reflection profiles, especially those made with narrow beams, may show that these features are important world-wide topographic expressions. If they are related to still-stands of lowered sea-level during the Pleistocene, these terraces should be found in many areas at nearly the same depth, permitting correlation over great distances.

Acoustic reflections from the rocky cliffs and associated coarse sand and cobbles should be greatly different than those from the adjacent slopes which are usually covered with a thick mantle of fine-grained sediment. This difference must be considered in any type of ASW or lost-instrument search and recovery employing acoustic sound sources. Also, large numbers of fish were over these rock areas and may be important sources of false echos on search sonars. In addition, these terraces could afford a firm, fairly level foundation for vehicles, weapons, and equipment placed on the sea floor.

INTRODUCTION

The U. S. Navy, although capable of operating throughout all the world's oceans, conducts many of its operations over the relatively shallow waters of the continental shelves and slopes immediately adjacent to strategic land areas. The increasing reliance on sophisticated acoustic equipment for search in both ASW and Mine Hunting operations along with a requirement to retrieve lost ordnance and valuable equipment from the sea floor, makes a detailed knowledge of the bottom in these operational areas necessary. In most instances fleet personnel assigned to the foregoing tasks must rely on published hydrographic charts if they want to know the nature of the bottom over which they are working. The deeply submerged rock terraces and associated sea cliffs discussed in this paper, although capable of greatly affecting sonar search capability, do not appear on these charts. Even more critical is the fact that they do not show on most echo-sounder profiles across the continental slope when made with conventional echo-sounding equipment. (Fig. 1).

The existence of rocky areas in regions presumably covered with fine-grained sediment have been long known and exploited by fishermen. Abrupt changes in the bottom slopes recorded on echo-sounder profiles have led marine geologists (Emery and Terry, 1956; Emery, 1960; Terry, 1965; Goreau and Burke, 1966) and many others to propose the existence of deep terraces throughout the world. However, the extent that these terraces were correlatable, their size, and the nature of the sediments associated with them were unknown until world-wide surveys could be conducted with sub-bottom acoustic profilers (Moore, 1957; 1960; Buffington and Moore, 1963; Moore and Curray, 1963; Curray and Moore, 1964; Garrison and McMasters, 1966) and direct observations made from deep submersibles (Busby, 1965, Shepard and Dill, 1966). The profilers permitted a rapid survey of the relationship between the bedrock forming the continental margin and its cover of recent sediment. The submersibles permitted a visual and photographic record of bottom roughness, provided bottom samples, and allowed accurate measurements of slopes and micro-relief in the vicinity of the terraces and sea cliffs. For the first time the *in situ* factors controlling bottom reflectivity and problems associated with operating acoustic equipment in these areas could be made, and the areas could be assessed as foundations for vehicles, weapons, and equipment.

Terraces and Sea Cliffs off Southern California

The direct observation of deeply submerged terraces and sea cliffs were made during three DEEPSTAR dive-traverses up the continental slope approximately 6 miles off San Diego, California (Fig. 2). The traverses were made between depths of 325 and 1200 feet. Within this interval, 7 cobble-covered terraces and 2 small sea cliffs were found. The terraces are cut in bedrock and covered with coarse, shelly sand of shallow-water origin. Large rounded

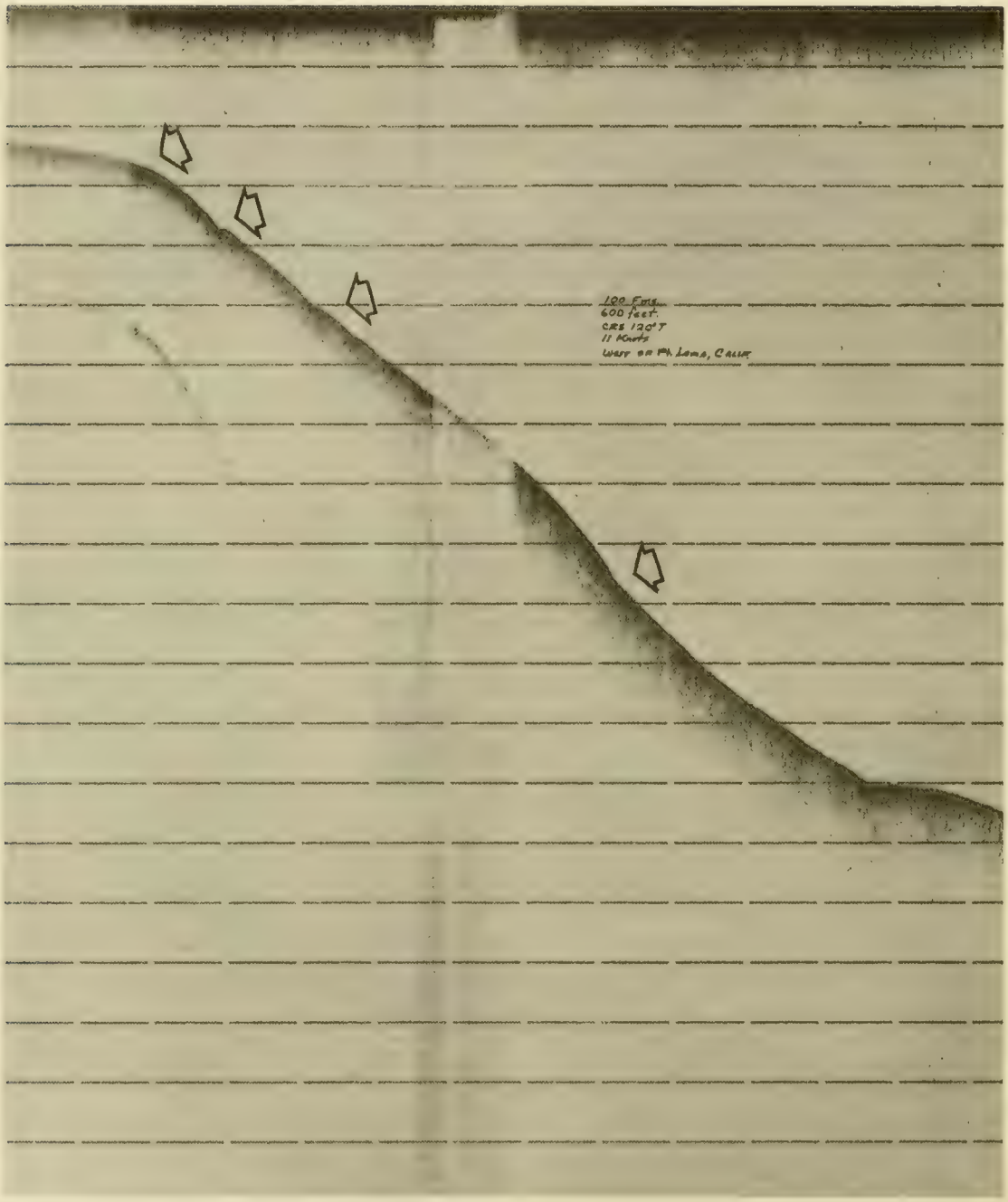

Fig. 1 - Typical echo-sounder profile across continental slope off San Diego, California and locale of terraces and sea cliffs (arrows).

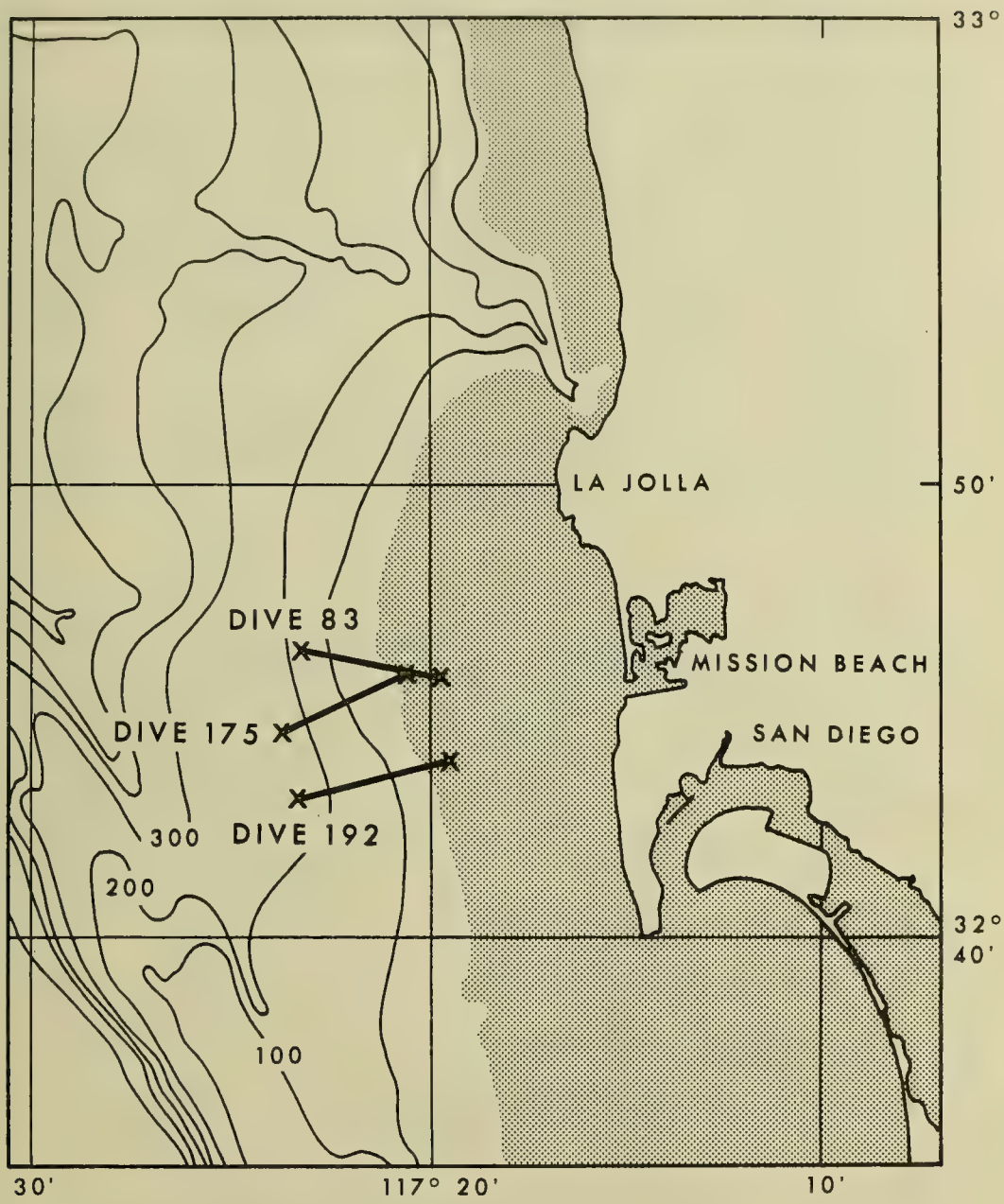

Fig. 2 - Location of DEEPSTAR dives to observe deeply-submerged terrain and sea cliffs. Shaded area continental shelf. Depth in fathoms.

boulders up to 2 feet in diameter were also observed. Exposed bedrock has been observed down to depths of 1170 feet and up to the break in slope at 325 feet (Fig. 3). The terraces are less than 100-feet across and the relief of the adjacent cliff is less than 60 feet. The best-developed cliff is between 600 and 700 feet (water depth) and is known from dredging and echo-sounding traverses to extend continuously for at least 10 miles along the continental slope off San Diego, California. Although large when viewed from the window of a submersible, the narrow terraces and rock cliffs are only barely discernible on echo-sounder traces because of the lack of definition within the wide angle of most sound cones and the relatively high speed at which most surveys are run across the continental slope. In many instances it would be difficult to differentiate between irregularities on the echo-sounder trace caused by high-sea surface swell and those caused by bottom irregularities.

The terraces and cliffs are narrow zones of acoustically different bottom that extend for great distances along the continental terrace. The bottom between the rocky zones are blanketed with a thick (over 10 feet) deposit of fine-grained, silty clays of uniform composition.

Associated Shallow Water Fossils

Dredge samples at the terrace level have been analyzed by Dr. Edwin Allison of San Diego State College who states they contain a mixture of fossil and modern species. Associations of the fossil species from a "beachrock" sample taken at a depth of 600 feet during Dive 175 (see Fig. 2) indicate water depths no deeper than 60 feet existed when they were living and that the water was colder than exists at 60 feet in the present latitude of San Diego County. The following species are indicative of the above environment:

Olivella baetica Marrat in Sowerby, 1871

Turritella cooperi Carpenter, 1864

Acila (truncacila) castrensis (Hinds, 1843).

Associated mollusks and micro-fossils from other samples taken along the continental slope off San Diego support the shallow-water origin of the fossils associated with the sea cliffs and found on the terraces. Abundant Foraminifera in the sediment collected during the DEEPSTAR dives include the following species indicative of similar shallow depths:

Casidulina tortuosa Cushman and Hughs, 1925

Cassiduling limbata Cushman and Hughs, 1925

Elphidium crispum (Linnaeus, 1758).

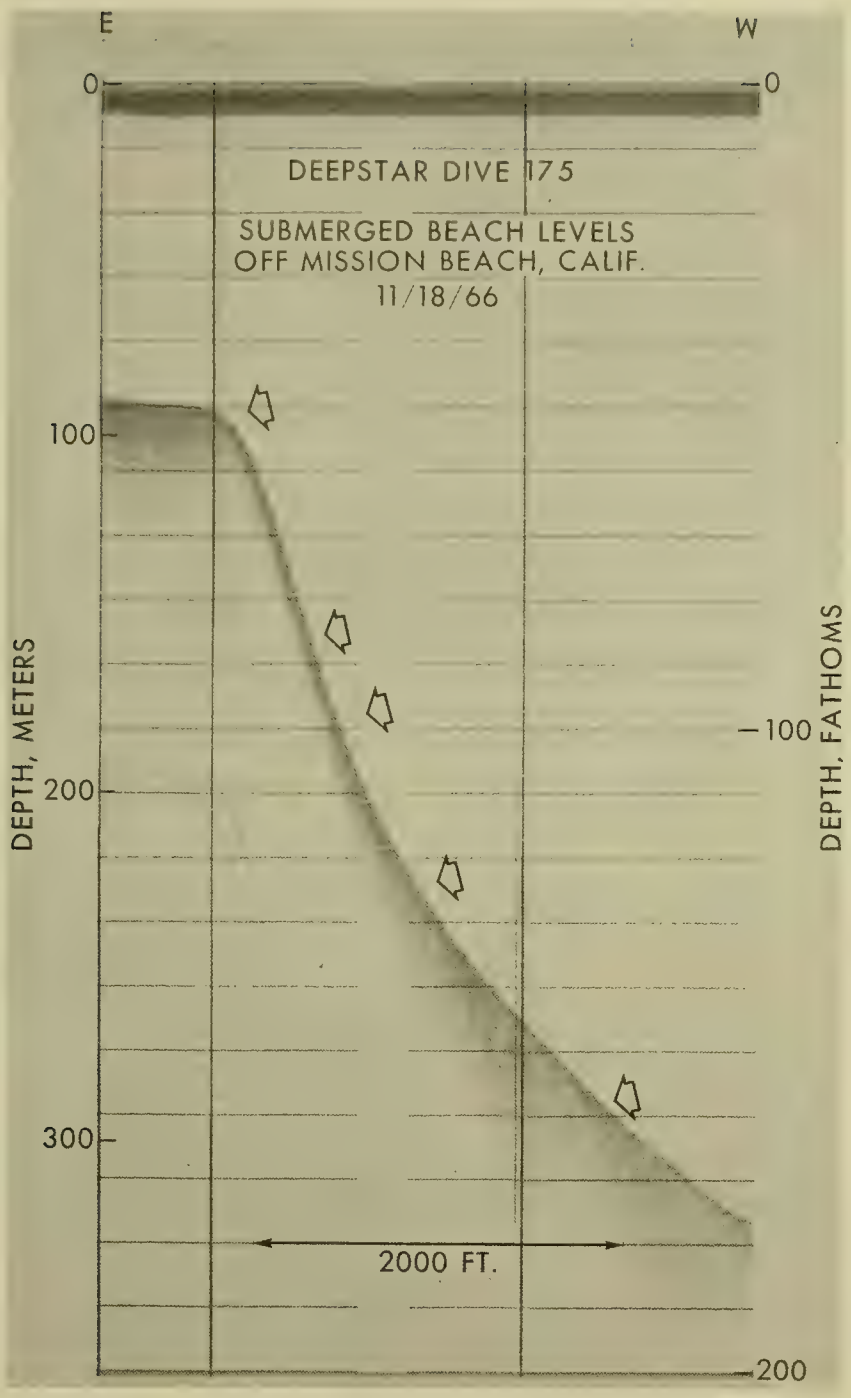

Fig. 3 - Location of sea cliffs and terraces observed on DEEPSTAR dive number 175. Note that they are not visible features on this echogram made at 12.5 Kc with a standard EDO transducer (60° sound cone) running at 4.5 knots. The sea surface was almost flat.

It thus appears that the sea cliffs were cut during the Pleistocene lowering of sea level. That such is the case is important because it permits the speculation that similar sea cliffs exist throughout the world and at similar depths, in those areas known to be relatively stable and unaffected by tectonic movements of the continental margin.

Nature of the Sediment-Covered Slope

Most of the continental slope off San Diego is covered with a deposit of fine-grained, greenish, clayey-silt. The sediment is cohesive and has shear-strength values indicating that it has built up slowly, probably as a prograding slope deposit over a considerable period of time (Moore, 1961). The benthonic Foraminifera associated with the clay are deep-water forms, characteristic of the depths in which they are found.

The slope below Dive 175 has been investigated by Hamilton (1963) in the bathyscaphe Trieste I and with cores. He reported that the bottom was composed of a sandy silt at a depth of 188 fathoms (344 m). He states that the bottom, when viewed from the window of the bathyscaphe, is relatively smooth and slopes gently toward the west. A 10.5-foot long piston core taken at a depth of 187 fathoms (342 m) cored 50 cm of clayey silt overlying 250 cm of sandy silt. This was underlain by 10 cm of silt with abundant broken shell debris.

Bottom Currents on the Slope

Bottom currents were measured during the DEEPSTAR dives that reached velocities up to 0.4 knot. In most instances they were flowing diagonally down slope. However, in one instance in the vicinity of a sea cliff, currents were observed to be flowing up slope. This might have been a counter current set up by the prevailing downslope current spilling over the upper lip of the small sea cliff. Similar counter currents have been observed in submarine canyons where there are abrupt dropoffs in the axial slope.

Another important observation was that scour depressions are frequent around large pieces of man-made junk that had been dropped on the sea floor. In one instance a bathroom sink approximately 2 feet in diameter had developed a scour depression of over 3 feet in diameter. It had settled at least 1 foot into the sediment and rested on a lag deposit of broken shells. The constrictions of flow streamlines created by this foreign object caused the erosion (or lack of accumulation) of the otherwise stable fine-grained sediments that are prograding the slope. This indicates that the sediment forming and building up the continental slope are at equilibrium with the prevailing bottom currents. Scour can therefore be expected around artifacts placed on the sediment-covered slopes; an important consideration when planning the placement of bottomed equipment if instruments must remain upright or stable.

Small objects, such as tin cans, are covered by a deposit of fine-grained sediment, showing that although larger objects cause scour, smaller ones do not. The sediment cover shows that, in general, the continental slope at the present time is an environment of deposition.

Fine-grained sediment, brought to the shoreline by rivers, form clouds of dense, dirty water that slowly spread seaward along the bottom as a turbid layer (Moore, 1960; Vernon, 1965). This material is kept is suspension by bottom currents and swell-induced surge as it crosses the continental shelf. When these suspended particles encounter the relatively quiet waters over the gently sloping continental slope (less than 10 degrees) they are no longer kept in suspension by storm surges and bottom currents, and build up as a prograding sedimentary deposit (Moore and Curray, 1963). The occurrence of relatively thick deposits of sediment have been verified by sub-bottom acoustic profiles across most of the continental slopes of the world. It is then very important to note that the terraces and sea cliffs discussed herein are not covered by such sediments. They must be older than the sediment covering most of the continental slope and yet young enough not to have been covered. In most instances the fine-grained sediments are capable of being deposited on relatively steep slopes. Submersible observations in areas of sub-bottom acoustic profiles have shown stable sedimentary deposits up to ten or even hundreds of feet thick develop on slopes of over 40 degrees, a value much greater than the average continental slope. The lack of a sedimentary cover on the terrace and sea cliffs therefore indicates there has not been a large enough supply or sufficient time to bury these features. Youth must be the other criteria for the existence of the terraces; the late Pleistocene age of associated fossils support this contention.

Significance of Terraces and Sea Cliffs

Geologically speaking, we are looking at a slope that has been formed in the last "few minutes" of earth time. A world-wide correlation of the terraces at similar depths would indicate that tectonic (mountain building) forces have not had time to warp and modify the continental edge since their formation. The occurrence of shallow-water fossils, those that lived in depths of less than 60 feet, in water ten times that depth, must indicate a greatly lowered sea level. We know that the great ice sheets that covered much of the continents during the Late Pleistocene lowered sea level; however, the deepest proposed lowering until now has been about 480 feet (Curray, 1960, 1965; Donn, et al., 1962; Shepard, 1964; Garrison and McMaster, 1966). The wide-spread, 600-foot terrace indicates a greater lowering of sea level than heretofore suspected.

Large numbers of bottom fish are associated with the rocky areas. They do not venture far from the protection of the ledges and, at high frequencies, would constitute a definite, false-echo problem because of their air bladders. Large schools of an unknown

type of fish were observed to school above the rocky regions. The schools appeared as large clouds of reflectors (on traverses over the terrace areas) on records of an echo sounder operating at a frequency of 12.5 Kc/sec. Too little is known to assess the problems of false echos in the regions of the terraces and sea cliffs but the possibility that they may exist must be investigated.

Another aspect of the biological population in the vicinity of the rocky terrace is that they constitute an abundant source of sessil organisms which could foul instruments placed on the bottom in these areas. These include sponges, corals, bryozoans, brachiopods, giant anemones, and burrowing clams.

What are the military implications of such a great change in sea level? What were its effect on the sea floor, and how can a knowledge of this occurrence benefit the Navy? Most of the new electronic acoustic equipment in use by the Navy is in some way environmentally limited. Especially if it must differentiate between a foreign object in an environment that contains similar, naturally-occurring bodies, or false echo-producing organisms. Size of the object being looked for is important because it dictates the target strength and frequency of search sonars. It is in this respect that the sea cliffs and their associated sediments become important.

It is almost impossible to find a bottomed mine, or a lost atomic bomb, by acoustic means in a boulder bed containing individual boulders that are the same size as the object being searched for (Swanson, 1967). Even more important, how is one to find a submarine nestled against or cruising, submerged, along a sea cliff 60-feet high. Could an enemy ASW group detect a submarine that is running slowly along the 600-foot contour a short distance (100 yards) away from a steep cliff? If our submarine is also equipped with a side-looking sonar using rapidly attenuated, very high-frequency sound, it could safely maneuver clear of the cliff and still be acoustically invisible to surface-search sonars. The other aspect of this problem is, could we detect an enemy submarine doing the same thing? I have been asked whether or not a submarine captain would care to venture into these rock-cliff areas. My answer is that these features were discovered by a small submarine, and that with the proper equipment (well within the state of the art), it would be no problem for a larger submarine to move with ease in the same areas. Such navigation would be much easier than an under-the-ice Polar traverse.

CONCLUSION

The great CHANGES of sea level that have taken place in the relatively recent past have greatly affected the nature of the sea floor. These changes are not visible on the charts provided the fleet. Practically nothing has been done to exploit the occurrence of terraces and sea cliffs as far as being areas of stabile rock for

bottom placement of instruments in acoustic test ranges or the tactical use of these areas as acoustic screens for hiding submarines. I'm reasonably certain that little is being done to improve the capability of acoustic equipment to differentiate natural occurring objects on the terraces and those that may be lost or placed in these areas.

We have only begun to investigate the nature of the deeply-submerged terraces on the continental slope. Their origin is complicated because they were formed during the geologic past when environmental conditions were different from those existing today. Little is known about the time necessary for them to form or their distribution throughout the world.

A preliminary review of the existing literature indicates, in addition to Southern California, that deeply submerged terraces occur in the Carribean, along the Atlantic coast, off Baja California, Mexico, in the straits of Florida, and off the Oregon coast. A well-developed terrace is indicated in sub-bottom profiles off the relatively unstable insular slope of Japan.

The acoustic reflections from the rocky cliffs, coarse shelly sands, and cobble areas associated with the terraces must be very different from those of the intervening soft muds separating the terraces. This difference has to be considered in any type of ASW or lost instrument search employing acoustic sound sources. Considerable research remains to be done before we can determine how these sea-floor features affect acoustic search and whether or not they could be utilized tactically by the fleet or as underwater construction and installation sites.

ACKNOWLEDGEMENTS

The writer wishes to thank John A. Beagles, Bruce C. Heezen, and R. F. Busby for their assistance and discussion during and before the field work. Edwin C. Buffington, Edwin L. Hamilton, and E. C. LaFond critically read the manuscript and gave many helpful suggestions.

BIBLIOGRAPHY

Buffington, E. C. and Moore, D. G., 1963, Geophysical evidence on the origin of gullied submarine slopes, San Clemente, California. Jour. Geol., V. 71 (3), 356-370.

Busby, R. F., 1962, Submarine geology of the Tongue of the Ocean, Bahamas. Tech. Report 108, U. S. Naval Oceanographic Office, Wash. D. C., 84 p.

Curray, J. R., 1960, Sediments and history of Holocene Transgression, Continental Shelf, Northwest Gulf of Mexico, in Recent Sediments, Northwest Gulf of Mexico. Am. Assoc. Petrol. Geol. P. 221-381.

Curray, J. R., 1965, Late Quaternary history, continental shelves of the United States. In Quaternary of the United States. Princeton Univ. Press, p. 723-735.

Curray, J. R. and Moore, D. G., 1964, Pleistocene deltaic progradation of continental terrace, Costa de Nayarit, Mexico, in Marine Geology of the Gulf of California - a symposium. Am. Assoc. of Petroleum Geol. Mem. 3, p. 193-215.

Donn, W. L., Farrand, W. R., and Ewing, M., 1962. Pleistocene ice volumes and sea level lowering. J. Geol. V. 70, p. 206-214.

Emery, K. O., 1958, Shallow submerged terraces of southern California. Bull. Geol. Soc. Am. 0. 69, p. 39-60.

Emery, K. O., 1960, The Sea off Southern California: A modern habitat of Petroleum. John Wiley & Sons, N. Y., 366 p.

Emery, K. O. and Terry, R. D., 1956, A submarine slope off southern California. Jour. of Geol., V. 64, p. 271-280.

Ewing, J., Luskin, B., Roberts, A., and Hirshman, J., 1960, Sub-bottom reflection measurements on the continental shelf, Bermuda Banks, West Indies Arc, and in the west Atlantic basins. J. Geophys. Res., V. 65, p. 2849-2860.

Garrison, L. E. and McMaster, R. L., 1966, Sediments and geomorphology of the continental shelf off southern New England. Marine Geology, V. 4, p. 273-289.

Goreau, T. and Burke, K., 1966. Pleistocene and Holocene Geology of the island shelf near Kingston, Jamaica. Mar. Geol., V. 4, p. 207-225.

Hamilton, E. L., 1963, Sediment sound velocity measurements made in situ from bathyscaph TRIESTE. J. Geophys. Res., V. 68, N. 21, p. 5991-5997.

Moore, D. G., 1957, Acoustic sounding of Quaternary marine sediments off Point Loma, California. U.S. Navy Elect. Lab. San Diego, Rept. 815, 17 pp.

Moore, D. G., 1960, Acoustic-reflection studies of the continental shelf and slope off southern Calif. Bull. Geol. Soc. Am. V. 71, p. 1121-1136.

Moore, D. G., 1961, Submarine Slumps. Jour. Sed. Petrol. V. 31, N. 3, p. 343-357.

Moore, D. G. and Curray, J. R., 1963, Structural framework of the continental terrace, Northwest Gulf of Mexico. Jour. Geophy. Res. V 68, 1725-47.

Shepard, F. P., 1964, Sea level changes in the past 6000 years: possible archeological significance. Science, V. 143, p. 574-576.

Shepard, F. P. and Dill, R. F., 1966, Submarine Canyons and other Sea Valleys. Rand McNally, Inc., Chicago, Ill., 381 p.

Swanson, L. U., 1967, Aircraft Salvage Operations Mediterranean, Lessons and Implications for the Navy. F. A. Andrews, general editor. Executive Summary of final report by CNO Technical Advising Group. Dept. of the Navy, Washington, D. C., 39 p.

Terry, R. D., 1965, Continental slopes of the world. Ph. D dissertation, Univ. So. Calif., Los Angeles, 648 p.

Vernon, J. W., 1965, Shelf Sediment Transport System. Report No. USC-Geol. 65-2, Coastal Engineering Research Center, U. S. Army Corps of Engr. DA-49-055-Civ. Engr. 63-13, 135 p.

Session C

OCEANOGRAPHIC PREDICTION

REAL-TIME OCEANOGRAPHIC DATA FOR OCEANOGRAPHIC PREDICTION

Kennard M. Palfrey, Jr.
U. S. Coast Guard Oceanographic Unit
Washington, D. C.

The need for oceanographic forecasting is manifold and certainly well recognized. In the field of military oceanography, particularly, oceanographic prediction is of paramount importance.

The ability to describe and predict ocean phenomena under any scheme depends in part upon time-series observations at selected control points.

Ever since the Ocean Stations were established during World War II, their potential for the collection of synoptic oceanographic data together with synoptic meteorological data has been recognized. During its first session, in 1962, the Intergovernmental Oceanographic Commission emphasised the value of the Ocean Station vessels for monitoring oceanographic conditions and recommemded that fuller use be made of their potential. The Ocean Station vessels, which are normally required to maintain station within a ten-mile square centered on each ocean station, afford opportune platforms for time-series observations. Consequently, when oceanography was added to the statutory functions of the U. S. Coast Guard, in 1962, immediate attention was given to the development of this oceanographic potential.

The high endurance cutters which had been routinely occupying the six U. S. operated Ocean Stations had been making meteorological and bathythermograph observations for years. Since passage of the 1962 law, thirty-one cutters, all those performing ocean station duty, have been equipped with oceanographic laboratories, oceanographic winches and related equipment to provide a basic Nansen cast capability.

Four classes of high endurance cutters are employed in the occupation of the four North Atlantic and two North Pacific Ocean Stations operated by the U. S. Coast Guard. These are the 327'

Secretary Class cutters, the 255' Lake Class cutters, and the 311' converted AVP Class cutters. The CGC HAMILTON, which was recently commissioned and is the first of a new 378' Secretary Class cutter, was designed and built for oceanography and will be manning North Atlantic Ocean Stations in the near future.

Since early 1963, when CGC CASCO demonstrated the feasibility of oceanographic observations by Coast Guard Ocean Station vessels, through successful completion of a pilot project at Ocean Stations DELTA and ECHO in the North Atlantic, the program has been greatly expanded. At present the Ocean Station program is functioning at forty percent of its goal of continuous observations at all six stations. The achievement of the ultimate goal has been limited solely by the availability of deep-sea reversing thermometers. A problem which is not unique to the Coast Guard. Oceanographic observations are made at all stations except ECHO on an alternate patrol basis; a patrol being twenty-one days duration. The ECHO project is currently being accomplished on a seasonal basis.

The oceanographic observation program at each Ocean Station requires a daily oceanographic station to a depth of 1500m and at least once during the patrol a daily station is extended to as near the bottom as practicable. Accepted sampling techniques and procedures are adhered to rigidly.

In 1964, the Coast Guard Oceanographic Unit was permanently established in Washington, D. C. with the mission to develop and support the total Coast Guard oceanographic program, including the time-series program at the Ocean Stations. This support includes data collection, processing and dissemination, instrument development and calibration; establishing oceanographic techniques and procedures; and liaison and cooperation with other agencies.

It was recognized quite early that the large number of vessels of opportunity involved in the Ocean Station program would prohibit scientific manning. In order to control the quality of data collected and to afford guidance to a vessel when deployed a two-fold program was established. An eight-week school was established at the Coast Guard Training Center, Groton, Conn. to provide two trained enlisted technicians as a part of the permanent crew of each Ocean Station vessel. In addition, a program of real-time quality control of data by radio was initiated.

All observed data is transmitted by radio, generally radio teletype, to the Coast Guard Oceanographic Unit where it is corrected, processed by a digital computer and checked by a trained oceanographer on a twenty-four hour a day basis. This permits rapid feed-back to the vessel so that the sampling frequency can be adjusted to better observe changing phenomena and poorly performing instruments replaced. Over 1100 oceanographic stations were handled in this manner during 1966 and a total of over 1500 is anticipated for 1967. An analysis

of transmitted data revealed an accuracy of 99.6% in comparision to original records submitted post-patrol by each vessel. It must be noted here that the high success of transmitting data is not attributed to any oceanographic scheme but rather to the tenets of security, reliability and speed which govern the Navy and Coast Guard communications system which are used.

As a result of the real-time quality control procedures of the Coast Guard, corrected and verified oceanographic data can be made available to operational and research uses within twelve hours of observation as a maximum, and generally within six hours. Since late 1965 the U. S. Fleet Numerical Weather Facility, Monterey, Cal. has been a consumer for this real-time oceanographic data and has used the information in the development of synoptic oceanographic analyses. The Coast Guard has also participated in the National Oceanographic Data Center's project "HOTLINE" using the same real-time data scheme.

The real-time data flow scheme employed by the Coast Guard requires that all data from the observing vessels pass through the Oceanographic Unit for correction and verification before reaching the ultimate data consumers. The CGC EVERGREEN and CGC ROCKAWAY, the Coast Guard's two primary research vessels, have on board data processing facilities and submit completed data direct to any consumer.

In order to more fully realize the capabilities of the Ocean Station vessels, a system of standard oceanographic sections was established in 1966. These sections were designed so as to include the areas of maximum oceanographic interest and to take advantage of the normal routes of the Ocean Station vessels. At present, most of the sections are occupied at least quarterly, mainly by an Ocean Station vessel enroute to or from station or by a primary research vessel. Pacific Standard Section One is occupied semi-annually by a station VICTOR vessel, between patrols, as a part of the Cooperative Study of the Kuroshio which began in 1965. In the Atlantic Standard Sections 2, 3 and 4 are occupied several times a month during the winter and spring to provide ocean current information for the Commander International Ice Patrol. It should be mentioned here that the Coast Guard's interest in the real-time transmission of quality data stems from many years of experience in this field in the course of providing the International Ice Patrol Service. All observations along these sections are treated as for Ocean Station data and are available in the same time frame.

An automatic salinity-temperature-depth measuring system is currently installed on EVERGREEN and ROCKAWAY, and will shortly be provided to all Ocean Station vessels by the Navy as an adjunct to ASWEPS. When the system is installed on the OSV's six-hourly observations will be made, with the data entered into the present transmission and quality control system. These observations will be made enroute as well as on station. The problem of long lead time in the

procurement of thermometers will be overcome and salinity data will be available faster.

In conclusion it is emphasised that this is only a cursory look at one system for real-time transmission of quality controlled oceanographic data. The mechanics of the Coast Guard's system are open for detailed inspection and I am sure it will holdup under the closest scientific scrutiny.

DATA REQUIREMENTS FOR SYNOPTIC SEA SURFACE TEMPERATURE ANALYSES

R. W. James
U. S. Naval Oceanographic Office
Washington, D. C. 20390

I. BACKGROUND

A common complaint voiced by analysts attempting to prepare synoptic oceanographic charts is that the present data input is insufficient to produce reliable analyses. This is reflected in the use of composite groupings of observations taken over several days and by the increased demand for ship-of-opportunity data. The constant requests for more observations, however, leads those in a planning capacity to conclude that the solution to the problem lies in saturating the oceans with observations. While it is obvious that more synoptic data are required, it is not so obvious where the observations are to come from, how they should be taken, to what accuracy, and how many are required. Funds available for increasing the quantity of synoptic oceanographic data are limited and should be carefully apportioned between possible platforms to give maximum improvement in analysis accuracies. This can be accomplished only by first ascertaining answers to the questions posed above.

This report describes the data requirements for sea surface temperature charts as deduced from a series of tests which compare accuracies of analyses based on various data inputs. These investigations are part of a continuing research effort concerning data requirements for the Navy's Antisubmarine Warfare Environmental Prediction Service (ASWEPS).

II. OBJECTIVE

The objective of this report is to establish guidelines as to the quantity and quality of synoptic observations required to ensure reliable sea surface temperature analyses. Although the study was conducted in the western North Atlantic ocean, and with ASWEPS in mind, most of the conclusions should be valid for other ocean areas.

A secondary objective is to find the point of diminishing return where the cost and efforts expended to increase the data input are not balanced by the improvement found in analysis reliability. At this point further expenditures for more data are not justified unless it can be demonstrated that an increase in operational effectiveness compensates for the additional expense.

III. PROCEDURES

A series of analysis tests were made for two areas of about 250 NM on a side. One area has a complex thermal field typical of the region just north of the Gulf Stream while the second area is representative of the rather smooth thermal gradients found in the Sargasso Sea and other areas lacking major currents. The two areas will be designated for the remainder of the report as Area A, which is complex in nature, and Area B, which has a smooth thermal field.

Basically the tests consist of starting with an assumed realistic isotherm pattern and a data field of observations over a closely spaced grid that are matched to the isotherms to produce perfect observations. Various percentages of the original data input are randomly selected and analysis made of these reduced data. Each analysis is compared to the original data field to compute the mean absolute error, and to the original analysis to ascertain the goodness of fit. Analyses were prepared both manually and by computer techniques. Error functions are introduced to vary both the quantity and quality of data utilized in a test. In all cases the data field used for analysis is considered a 24 hour data input.

Results of the tests reveal many relationships between the quantity and quality of data and the reliability of the analyses. The tests were divided into three major categories as follows:

Area A - manual analysis
Area A - computer analysis
Area B - manual analysis

For each of these major categories there were 8 to 16 individual tests. In addition, there were two special tests to determine the degrees of freedom inherent in the use of random data distributions and to compute the relative advantage of selected data points over randomly spaced data.

IV. RESULTS

Results of the tests will be described in the following sections under the three major categories and the two special tests described above.

A. Area A - Manual Analysis of Perfect Data

Area A was selected to be representative of the complex isotherm patterns found north of the Gulf Stream. Figure 1 shows the original data plot and analysis for Area A. Sea surface temperatures are considered perfect values, since the data were fitted to the isotherm pattern. The grid spacing of 12.5 NM covers an area equivalent to a five degree square but a geographic fix is not indicated since the isotherm pattern is considered typical of thermal conditions over a wide area north of the Gulf Stream. The major features of Area A are two warm tongues separated by a cold intrusion of water from the northwest. Colder water is also evident in the northeast portion of the area.

The first test was to randomly select ten percent of the grid data and to analyze this new temperature field. This procedure was followed to see if the essence of the isotherm pattern could be maintained with only ten percent of the original observations. Tables of random values were used to select the 40 observations that would be utilized in the analysis. Figure 2 shows the resulting data plot of 10 percent data by a trained analyst with no knowledge of the original isotherm pattern. Comparison of Figures 1 and 2 indicates that although some distortion occurs in the pattern the major features are well described and the more prominent tongue to the east was still drawn as the main feature. A mean absolute error was computed by overlaying the new analysis over the original data. An error of 1.30°F was obtained, which is small compared to values normally found for analyses in this area. This is not surprising in that there was an adequate input of observations and the data were of perfect accuracy.

Three more tests of this nature were made using 5, 3.5 and 2 percent of the perfect data shown in Figure 1. That is, the data plot consisted of 20, 14 and 8 observations respectively. In each case the observations utilized were randomly selected and the analyst preparing the analysis did not have a pre-conception of the pattern. Different analysts were used to avoid continuity of analysis.

Figures 3, 4, and 5 show the resulting analyses. With 5 percent of data the isotherm pattern is still well defined although the source of the cold water intrusion is misplaced. Even with 3.5 percent of data the two warm tongues are properly located, although they are considerably smoothed. For optimum sonar routing, however, the pattern shown would still be of value. Using the 8 observations available with 2 percent of data the analysis does not describe any of the original pattern. The pattern consists of one smoothed warm tongue which is not too accurately centered. Unfortunately, as it will be shown later, present sea surface temperature analyses are based on data input comparable to the 2 percent chart but of much lower quality than represented by the observations utilized in Figure 5. Only through composite groupings of observations for 3 to 5

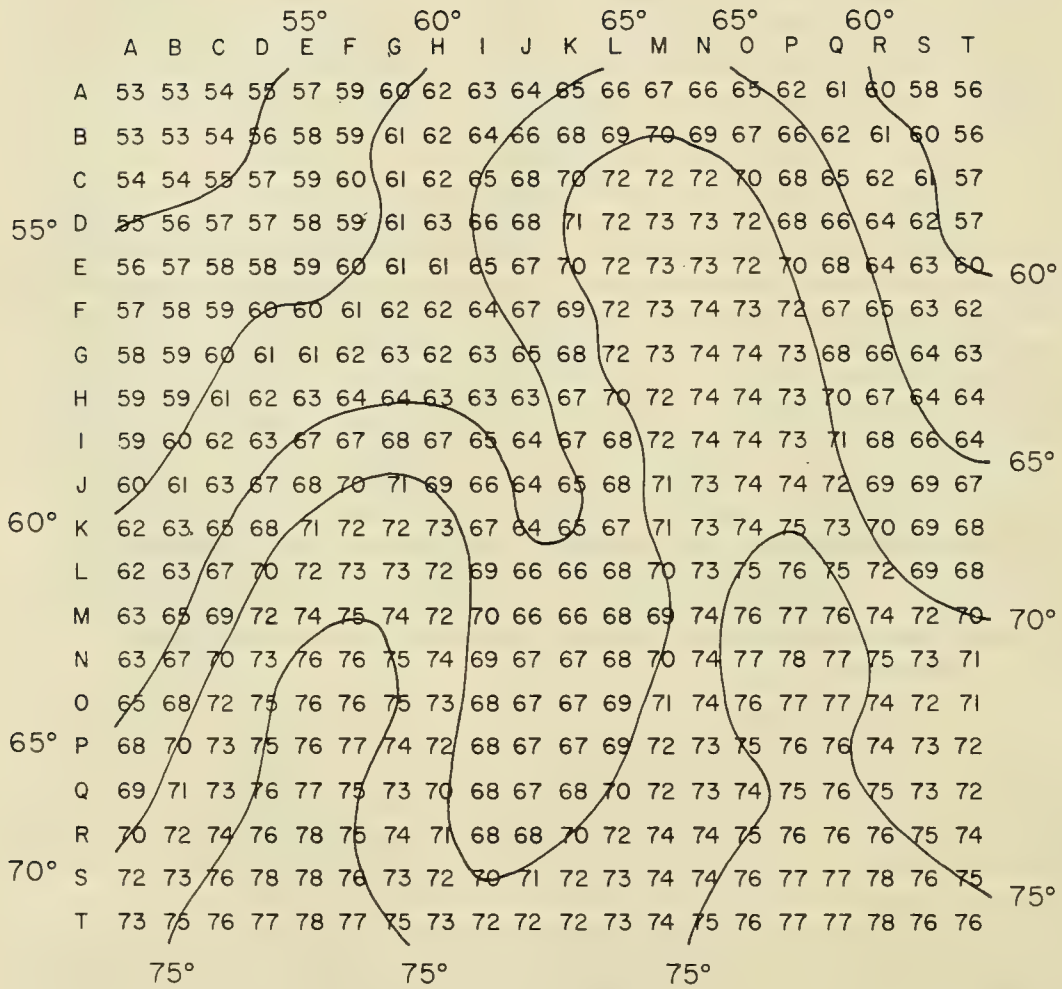

Fig. 1 - Original data and analysis

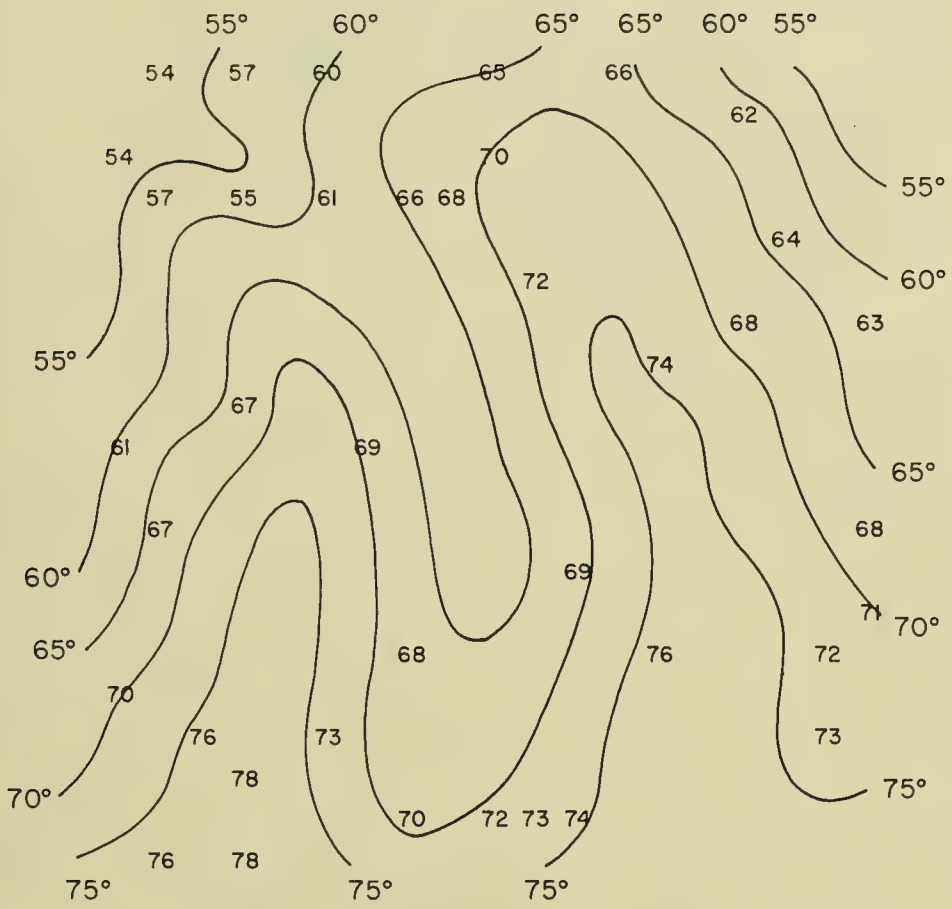

Fig. 2 - Analysis of 10 percent of data

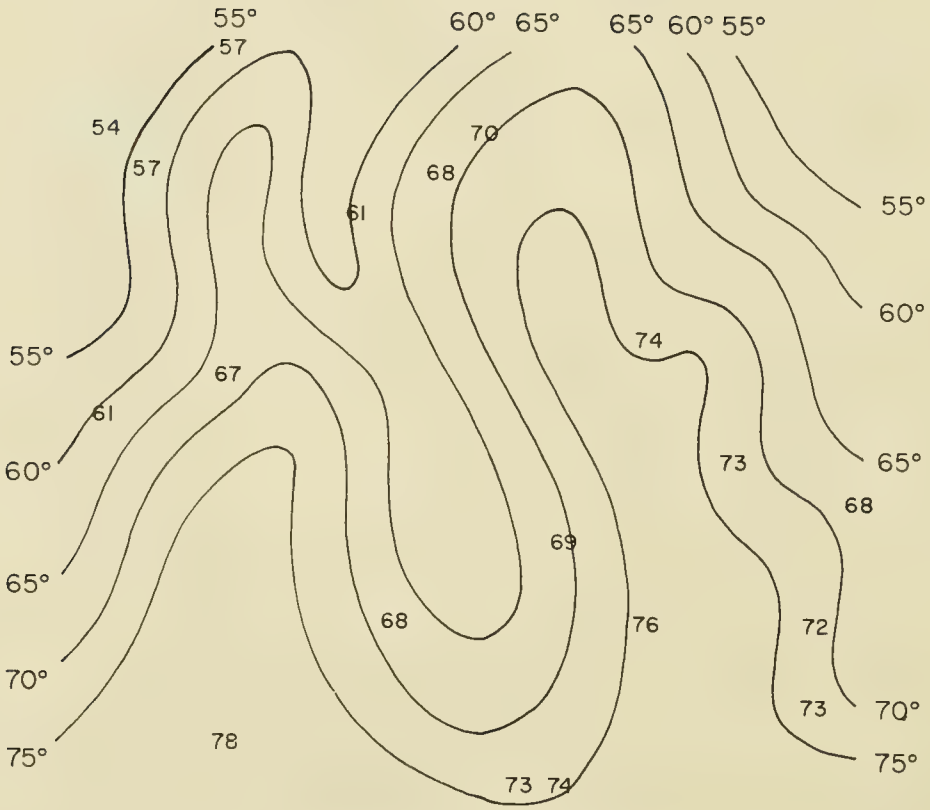

Fig. 3 - Analysis of 5 percent of data

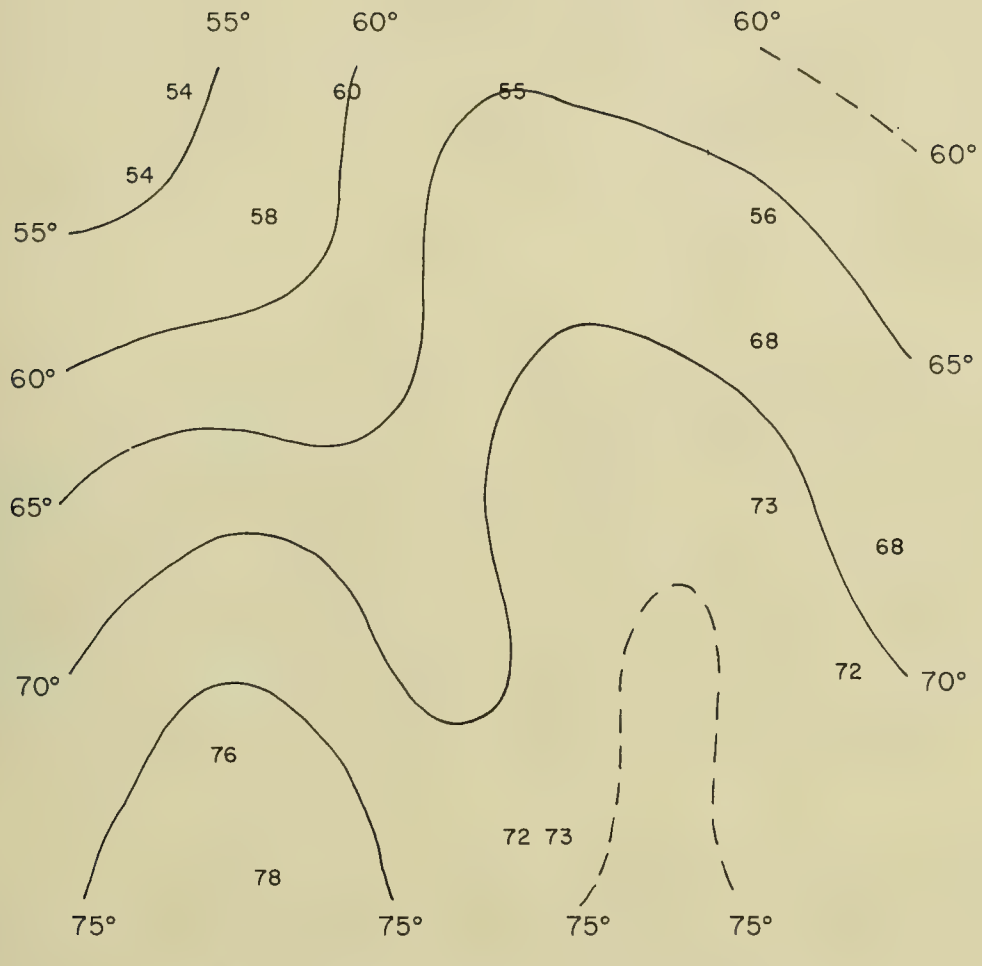

Fig. 4 - Analysis of 3-1/2 percent of data

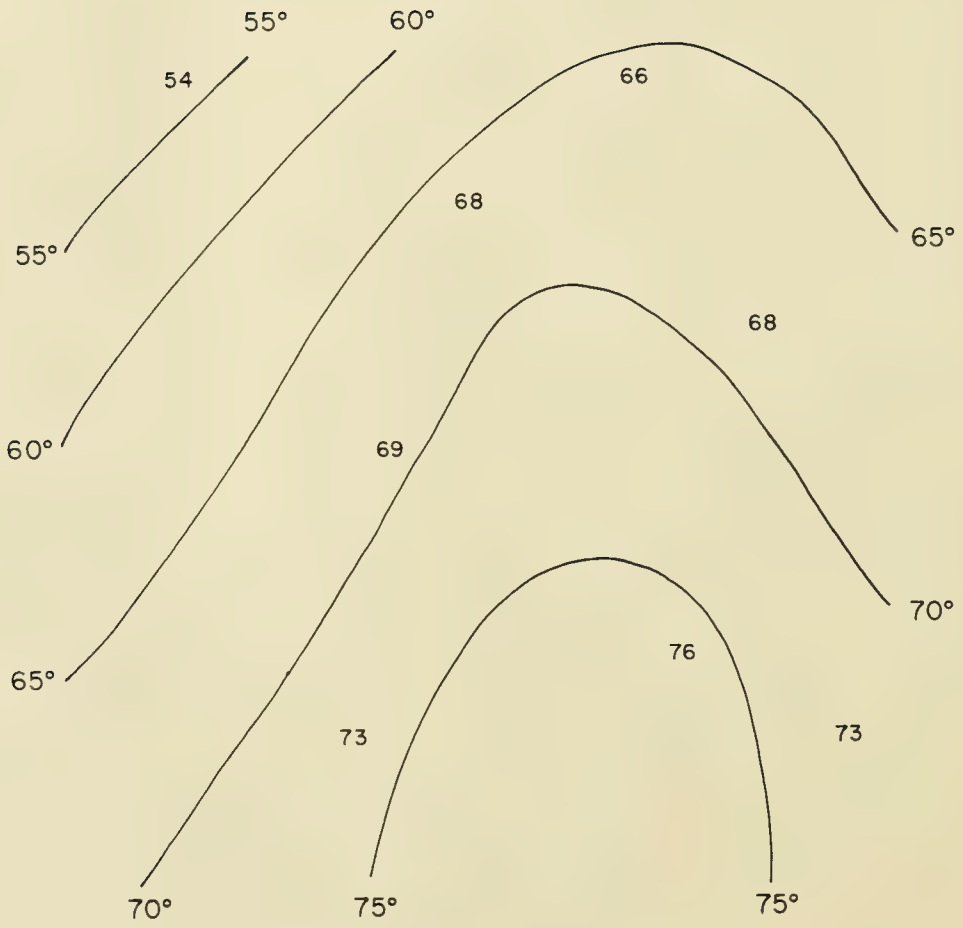

Fig. 5 - Analysis of 2 percent of data

days are sufficient observations obtained to prepare useful analyses.

Table I gives the mean absolute error for each of the analyses discussed above plus a value for 30 percent of data. At 100 percent of data the error is obviously zero since the fit is assumed perfect.

TABLE I. ACCURACY OF MANUAL ANALYSES FOR AREA A

Percent Data	Mean Absolute Error (^{o}F)
100	0.00
30	0.43
10	1.30
5	1.70
35	1.89
2	2.95

As expected the mean absolute error decreases with the increasing availability of data. Thus, by doubling the data input from 2 percent to 4 percent the analysis error is reduced by 39 percent. Tripling the 2 percent input reduces the error by 50 percent but above this point the increase of data does not produce noteable improvements in analysis reliability. For instance, although the error is reduced by half if the data is tripled it would take 12 times as much data to reduce the error by half again. Table 1 provides information concerning the quantity of data required to ensure specified analysis accuracies, assuming perfect data. Since the present data used for synoptic charts are far from perfect the mean absolute errors must be recalculated using data typical of that presently available. This was done in the second series of tests.

(1) Error Functions

For the second series of tests for Area A the perfect data were modified by introducing errors similar to those found in present ship injection temperatures. Two error functions were assumed; one for accuracy of temperature and the other for accuracy of ship position. The errors of the input temperatures were assumed to average 2°F, with a range of $\pm 7^{o}$F, and follow somewhat a normal probability distribution. With this error distribution applied to 10 percent of data, for example, there would be 6 perfect observations, 10 with $\pm 1.0^{o}$F errors, 8 with $\pm 2.0^{o}$F error, 6 with $\pm 3.0^{o}$F errors, 4 with $\pm 2.0^{o}$F errors, and 2 each of ± 5, ± 6, and $\pm 7^{o}$F error.

These errors are considered realistic based on past studies of water injection temperature reports. Saur (1963) investigated the difference between injection temperatures recorded in the log and specially observed temperatures for 6826 pairs of observations from 12 ships on 92 different trips. He found a generally normal probability distribution of errors centered around a small positive bias. Errors of 6°F were shown with a standard deviation of differences of 1.6°F. Gibson (1960) compared sea surface temperatures as reported synoptically to those that had been recorded as a log entry and found 13 percent of the observations were in error due to coding discrepancies. These errors were small, however, generally not exceeding 2°F. Other investigations of injection temperatures by Francesehini (1955), Kuhn and Farland (1963) and Beetham (1966) show the assumed error function to be realistic.

In addition to the error in the temperature observation there is also a navigation error in present ship reports, which contributes to analysis errors. This was applied by assuming that one third of the reporting ships were within the quadrangle represented by a position reported to the nearest tenth of a degree. That is, no position error within the capabilities of the code. A third of the reports were assumed to be ±6 miles from the true position and another third with a ±12 NM error. The magnitude of the movement errors were applied randomly while the direction of the deviation was uniformly distributed to the four cardinal directions.

(2) Description of Error Tests

Three cases of errors were treated using various percents of the original data. In Case I the full range of accuracy errors and movement errors were applied as described above. The resulting data plots of "bad data" are considered equivalent to the present sea surface temperature data used in preparing analyses. The Case II tests were based on data in which the error was limited to ±1°F although the navigation error was the same as in Case I. This would be equivalent to using only temperatures reported from ships with reliable instrumentation, such as the Near Surface Reference Temperature (NSRT) System described by Beetham (1966), or perhaps airborne radiation thermometer observations when carefully taken.

A third case was run where it was assumed reliable instruments were available so that the error would be ±1°F and the navigation error sufficiently accurate so that the ship is actually in the quadrangle of area reported.

An example of the three cases are shown in Figure 6 along with typical analyses. The original data are altered in value and position according to the three cases previously discussed. The product of misplaced data and inaccurate readings obviously misleads the analyst into the wrong orientation of the isotherms in some cases.

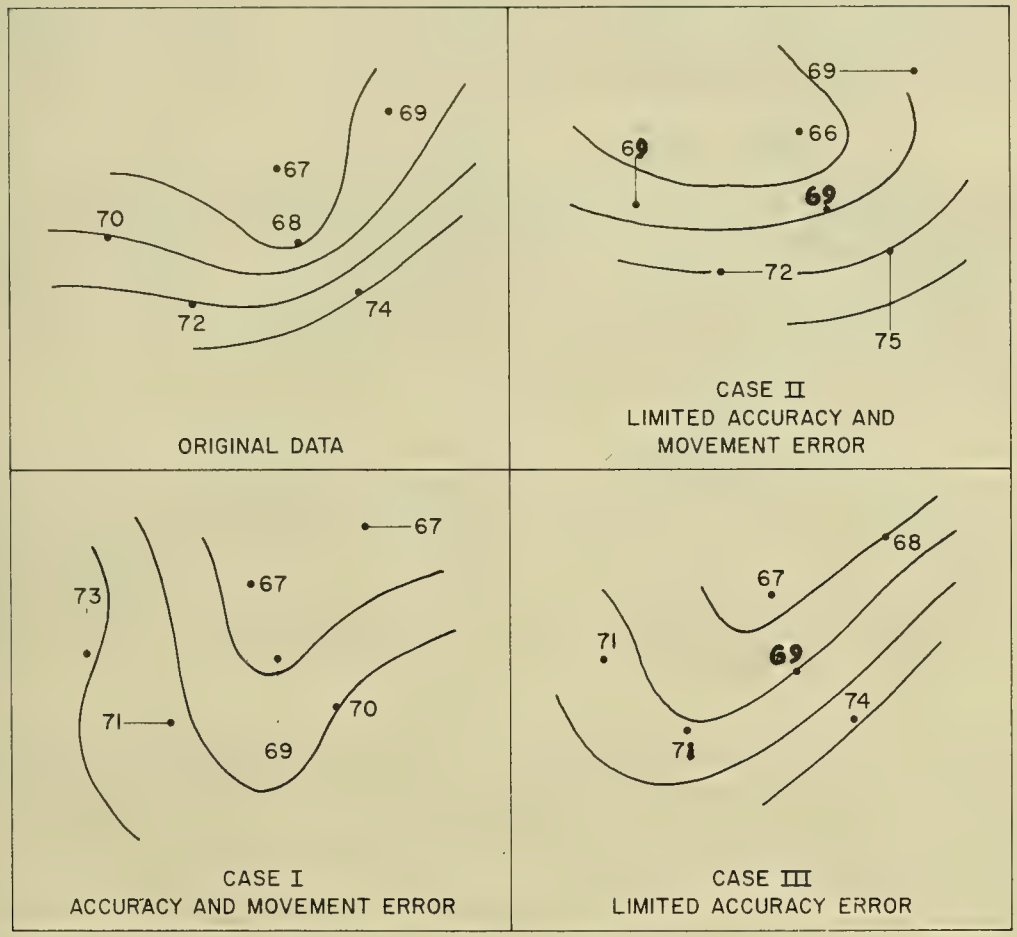

Fig. 6 - Examples of modified data field

Figure 6 is simply a model to illustrate the three error cases applied and was not part of the tests.

(3) Results of Error Tests

Figure 7 shows the analysis of 10 percent of original data which have been randomly modified by the Case I error function. This figure illustrates what happens when 40 observations of the quality presently utilized in synoptic analyses are analyzed instead of 40 perfect observations as in Figure 2. One of the two tongues is located relatively well but the cold water and the western tongue are misaligned. Gradients are also over-emphasized in some areas.

Analyses of 5, 3.5 and 2 percent modified Case I data are not shown but revealed a poorer fit to the true isotherm pattern than did analyses of the same quantity of perfect data. As would be expected analyses of the same quantities of data for the Case II and Case III errors produce isotherm patterns worse than those from perfect data and better than the analyses of Case I data. All analyses show that at 2 percent of data the isotherm pattern is not reliable but this qualitative information was not the goal of this study.

Mean absolute errors were computed for all tests and it is these values that provide quantitative answers to some of the questions posed in the objective. The mean absolute errors were plotted versus data input with a family of curves resulting as shown by Figure 8. For purposes of comparison assume that 2 percent data is our present data input; this will be justified in a later section. The following conclusions can be made from Figure 8:

(a) In all cases an increase in data produces a decrease in the mean absolute error or an increase in analysis reliability. The reliability of the analyses can be increased considerably by simply doubling the present input data. Indications are that it would be desirable to triple or perhaps quadruple the present data input.

(b) The same improvement in SST analyses can be obtained by quadrupling the data input using present type SST reports, or by only doubling the input but using more reliable data. This could be accomplished, for instance, by using only ART or NSRT data instead of the present predominantly ship of opportunity injection reports.

(c) Increases in reliability beyond 8 percent (quadrupling the data) may not be desirable owing to the small improvement per data increase.

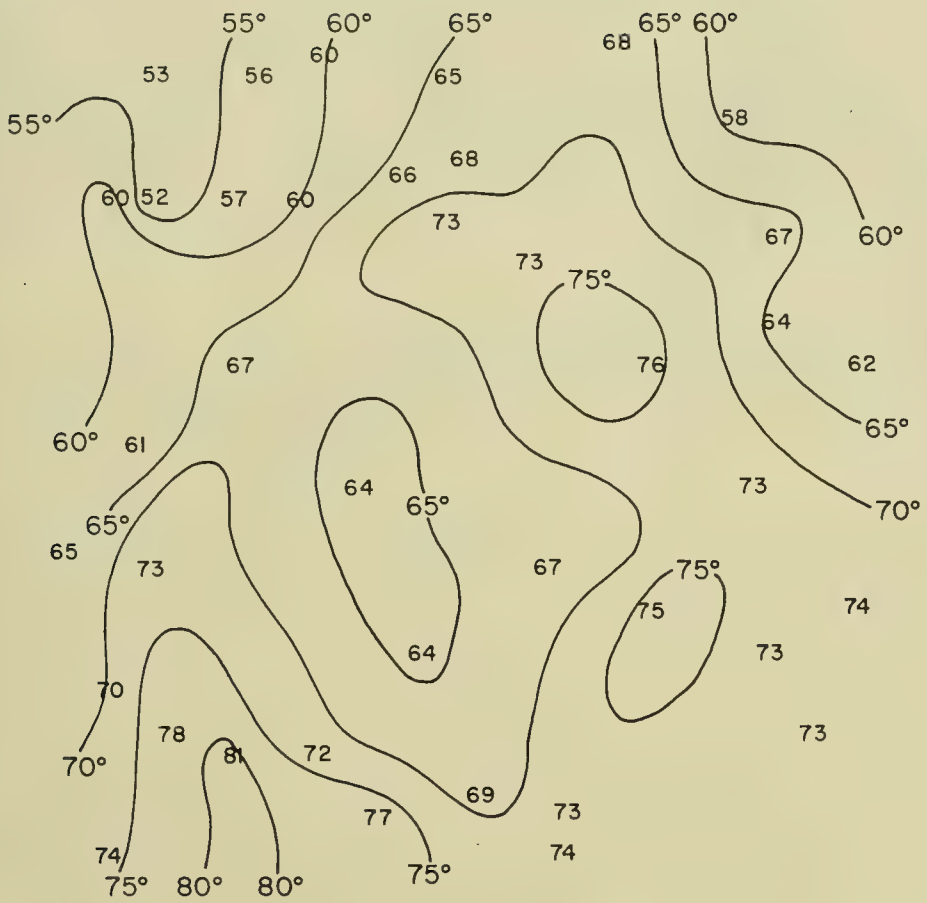

Fig. 7 - Analysis of 10 percent of modified data (case 1)

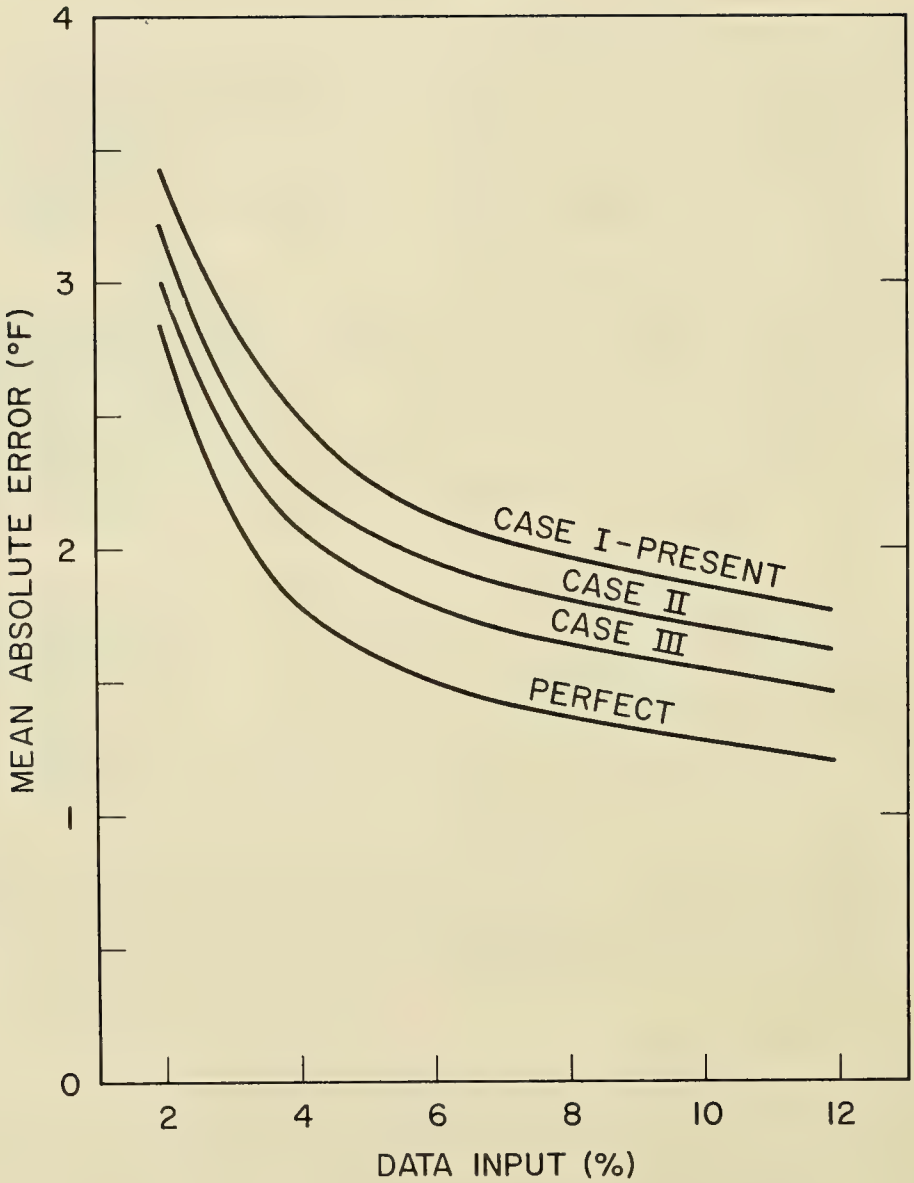

Fig. 8 - SST accuracy, manual analysis, area A

(4) Absolute Data Requirements - Area A

So far this report has dealt with quantities of data relative to the original base of 400 perfect observations. It was found that analyses of as little as 3.5 percent of these data revealed useful information concerning the isotherm pattern. With 2 percent data input it was not possible to show the detail known to be present in the isotherm pattern.

For several reasons the 2 percent data input is felt to be equivalent to the present data availability utilized in ASWEPS. The mean absolute error for the analysis of 2 percent of present data is 3.46°F. This value is close to the mean value of the mean absolute errors found in nine evaluations of present manual sea surface temperature analyses. These evaluations included 1786 individual verifying temperature observations and the mean absolute error averaged for all nine evaluations was 3.61°F. Reports by James (1966), Tuttell (1963), Shank (1966), Carman (1965) and James (1965), describe these evaluations.

The second reason for assuming the 2 percent data input is typical of present data availability is that 2 percent of the original data is eight observations and the average number of observations found per day in an equivalent area during 1966 was 7.8 observations.

On this basis 2 percent of the data used in the tests is considered equivalent to the present data input of ASWEPS. Thus from Figure 8, to reduce the analysis error to below 2°F would require 8 percent of the present type data or four times as much as presently available. This would be 32 observations per five degree square. The same analysis reliability could be obtained, of course, by doubling the data input but utilizing only accurate data as used in Case III. This would require only 16 observations. Of course the increase of data will be mostly ship of opportunity injection reports for a time and gradually the better instrumented reports will predominate. Thus, the true curve representing analysis accuracy with increasing data will slice across the three curves in Figure 8, approaching the Case III curve in time.

(5) Non-Random Data

Figure 8 shows the errors that result from analyses of various quantities and qualities of random distributions of data. If ship of opportunity data were rejected and only ART or buoy data utilized then the distribution of data could be pre-selected. To ascertain the value of specifying the data distribution instead of accepting a random field several ART tracks and buoy arrays were specified so as to give varying quantities of perfect data.

The results were that the mean absolute error was reduced by 20 to 40 percent, with the larger reduction occurring with the higher number of observations. The results of these tests are shown by Table II.

TABLE II COMPARISON OF SEA SURFACE TEMPERATURE ACCURACIES FOR RANDOM AND SPECIFIED DATA DISTRIBUTION

	Mean Absolute Error (^{o}F)	
Percent Data	Random	Specified
10	1.30	.69
5	1.70	1.08
3.5	1.89	1.39
2	2.95	2.81

The conclusion from these tests is that if more use is made of specified, reliable temperature observations instead of random ship of opportunity data the accuracy of the analyses will approach the perfect data curve of Figure 8. Routine ART flights for instance would provide data of sufficient quantity and quality, and of a specified nature, to permit analyses of less than 1°F error.

B. Area A - Computer Tests

Tests similar to those described above using manuall analyzed temperature charts were also made using computer analyses. This was done for two reasons:

(1) To verify that the family of curves shown in Figure 8 are not biased by analysts skills.

(2) To ascertain whether objective analyses introduce any special requirements or lead to difference emphasis on data requirements.

The original data input to the computer analyses was the same as used in the manual analyses and shown in Figure 1. Similar randomly distributed data inputs of 10, 5, 3.5 and 2 percent were analyzed and the mean absolute error computed. In order to maintain the same degree of pre-knowledge as in the manual analyses a flat field was used. This means that every grid point was considered zero except those at which a true observation existed. In the case of the test of 2 percent data this means there were 392 grid points of zero and eight observed values.

The computer program makes multiple passes over the grid relaxing the grid values at non-observed points until the grid field shows certain minimum differences between grid values. A description of the computer program from which this test program was drawn is given by Thompson (1966). In this case no smoothing was applied,

since the area was so small. Also no forcing function was used in order to avoid injecting prior knowledge of the isotherm pattern.

(1) Results of Computer Tests - Area A

Figure 9 shows the computer analysis of 10 percent data. Although this analysis lacks the resolution of the manual analysis shown in Figure 2 the major warm tongue is shown as is the cold water intrusion from the northwest. An interesting aspect of computer analysis is shown by Figures 10 and 11. Both figures represent analyses of 2 percent of data but one of perfect data (Figure 10) and the other of poorer quality, Case I data (Figure 11). The interesting point is that there is little difference between the analyses in spite of the great difference in the quality of observations. The same similarity was found in comparison of computer analyses of other percents of good and poor data.

This leads to the conclusion that the computer program handles imperfect data better than the manual, subjective analysis, since in the latter tests more differences are apparent. This characteristic of the computer analyses may be due to the relaxation procedures which tends to modify the temperature field around an observation without creating extreme gradients or producing distortions in the field. An analyst on the other hand tends to extend the isotherms to include high or low values far from the main warm or cold tongue.

The mean absolute errors for the computer analyses of perfect and Case I data are shown in Figure 12. For reference the curves for the same manually prepared analyses are repeated from Figure 8. Although the curves differ slightly the computer curves verify those derived from the manual analyses. No particular differences in data requirements appear to result from these tests except that computer analyses can make better use of a minimum input of poor data than can manual analyses. As expected from the similarity of their patterns, the differences in accuracy between the computer analyses of 2 percent "good" and "poor" data is small.

Although the manual analyses show slightly lower errors than the computer products this has no significance. The computer program used was not as sophisticated as that used operationally, since a simplified program was adequate to establish the curves.

(2) Effect of The Degree of Randomness on Results

In conjunction with the computer tests a test was also run to ascertain the effect of the degree of randomness in the distribution of data on the results.

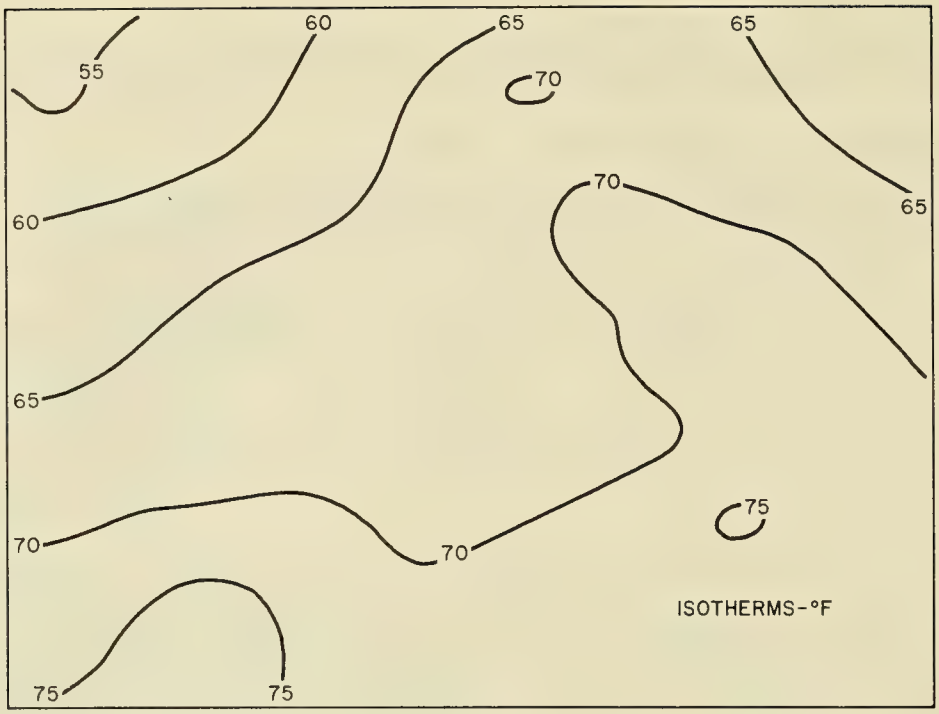

Fig. 9 - Computer analysis of 10 percent of perfect data

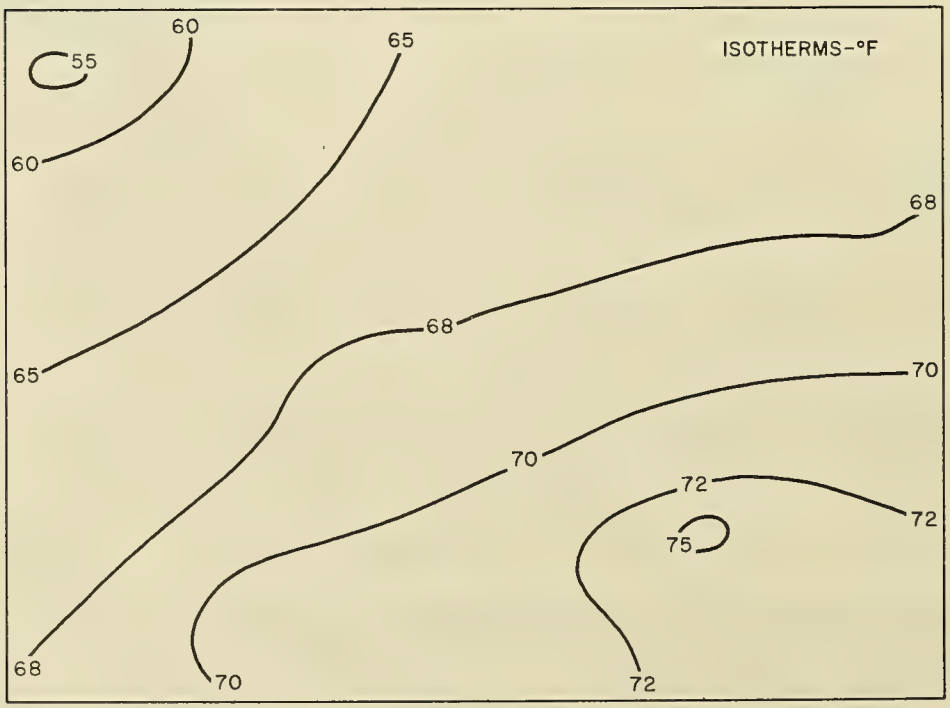

Fig. 10 - Computer analysis of 2 percent of perfect data

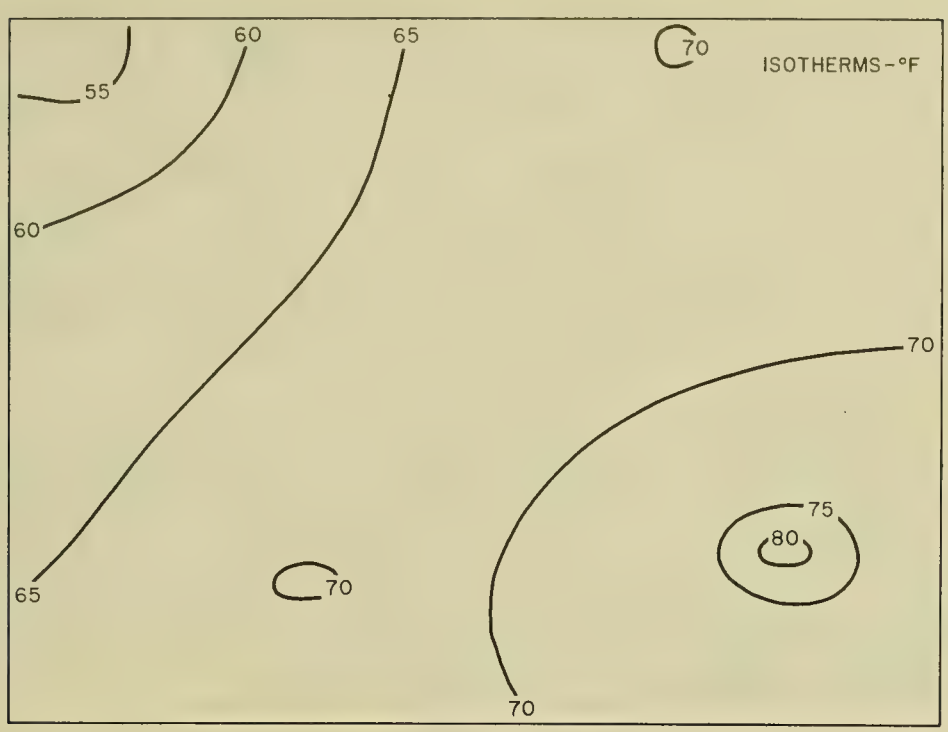

Fig. 11 - Computer analysis of 2 percent of data (case 1)

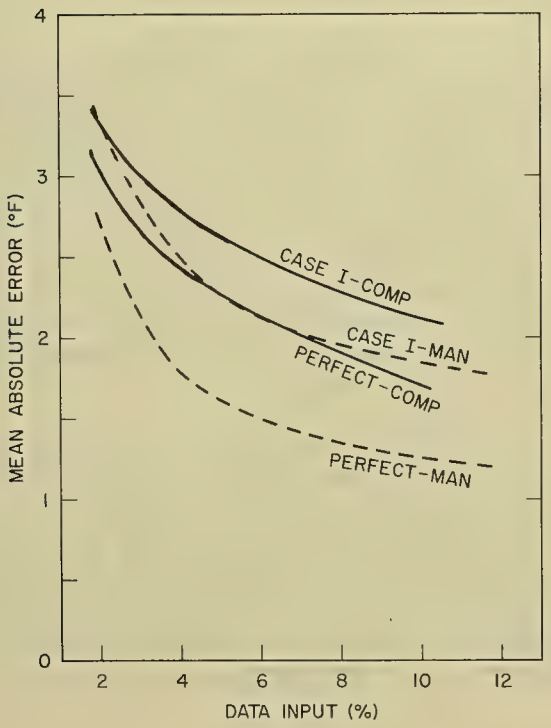

Fig. 12 - SST accuracy, computer analysis, area A

It is obvious that the accuracy of an analysis of a given random data plot is a function of not only the number of observations but also their distribution. One analysis of eight random points does not clearly establish an analysis accuracy since all the data may, in that particular case, be located in one portion of the chart. To investigate this problem various random distributions of equal numbers of observations were analyzed on the computer. The results showed that for larger number of observations, 5 and 10 percent of data, the randomness of plot makes no significant differences. That is, with a sufficient number of observations any random distribution provides some values in all quadrants of the chart. With 2 percent of data, however, the randomness does make a difference.

Eight random data plots of eight observations each were analyzed and the mean absolute errors computed. The distribution of observations varied from cases when the data was evenly distributed over the charts to one case where all eight observations were located in the eastern half of the chart. The mean absolute errors varied from 2.6°F to 4.0°F with a mean value of 3.3°F. This mean value compares well with the 3.2°F error shown in Table I for 2 percent data in the original tests. Thus, the family of curves shown in Figure 8 are considered representative of analysis accuracy.

In addition the slight smoothing necessary to establish a family of curves tends to bring the value of an individual score closer to the true mean of all random samples.

C. Area B - Manual Analyses

The tests described so far have established some facts about data requirements for complex trend areas. In order to study the requirements for data in non-complex areas a similar set of tests were repeated for a relatively smooth isotherm field. This temperature field and analyses is shown in Figure 13, and represents generally the area of a five degree quadrangle similar in size to Area A. This area will hereafter be referred to as Area B. Where Area A had a temperature gradient of 25 degrees across the area, Area B shows only a 6 degree temperature range. This is typical of areas such as the Sargasso Sea, the eastern North Pacific, eastern North Atlantic and other ocean areas away from major current systems.

With such a flat thermal field the variation in temperature between grid points is less than 1°F. A wide belt of temperatures result for a given value rather than individual whole values as in the complex field. Thus the 64°F isotherm in Figure 13 is drawn through the center of a number of 64°F temperatures. This results since the values on one side of the 64°F isotherm may represent a true value of 63.7 while a 64°F on the opposite side may represent a 64.4°F but rounding to whole degrees for coding purposes gives the same values.

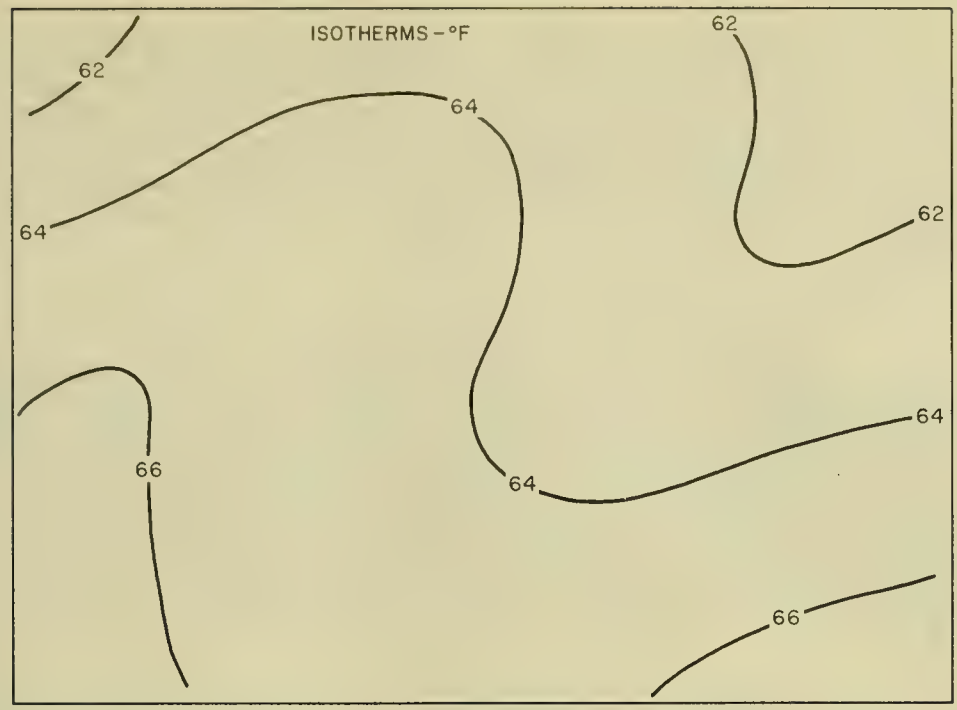

Fig. 13 - Analysis of 100 percent of perfect data, area B

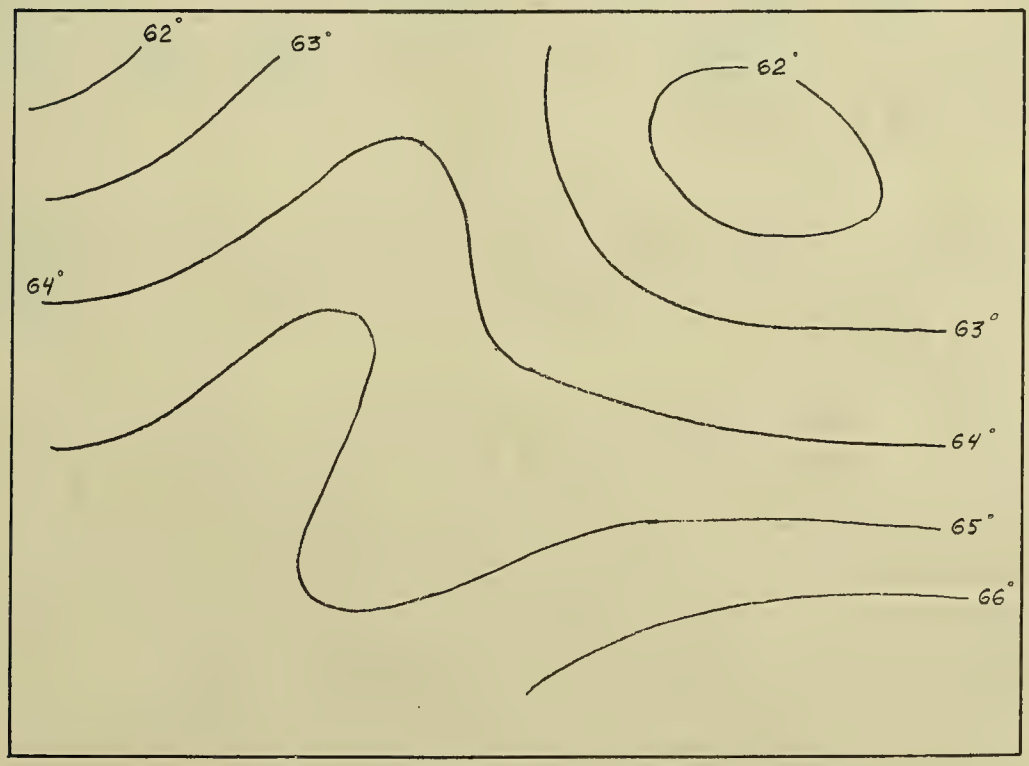

Fig. 14 - Analysis of 2 percent of data

It is obvious from this discussion that highly accurate analysis in smooth areas requires observations reported to tenths of °F. That is, to define a particular isotherm to the same exactness as is in a complex area requires more accurate data. This results simply from the fact that in Area A a 1°F temperature change occurs in 12 NM while in Area B a 1°F change may be spread over a distance of 100 NM.

(1) Results of Area B Tests

Inspection of the various analyses made for Area B reveal that excellent accuracies can be realized in relatively smooth areas with a minimum of data if the data is of high quality. Note for instance the analysis of 2 percent of perfect data as shown in Figure 14. Although there were only eight observations available the analyst was able to portray a very reliable picture of the isotherm pattern. The mean absolute error was only 0.4°F for this analysis compared to 2.95°F for eight observations in the complex Area A.

On the other hand, poor data, in any quantity, leads to very erroneous results in analyses of Area B. Applying the same error functions as previously discribed in Section IV A (1) analyses were made of present type data. Figure 15 illustrates the analysis of 10 percent of this Case I data. Numerous features are shown that do not belong there; a total of six tongues as compared to the smooth isotherm pattern actually present. Of course operationally continuity from chart to chart and grouping of data tends to reduce this problem but nevertheless poor data has a very deleterious effect on analyses of smooth areas.

The effect of poor data in deteoriating the reliability of analysis is obviously much more evident in Area B than Area A. The reason for this is that an observation of 5°F in error and 12 NM out of position may create a entirely new warm tongue in Area B while in Area A the already high horizontal gradients mask the effect of one bad observation.

Figure 16 shows the family of curves resulting from analyses of the four types of data described previously as perfect, Case I, II and III. As discussed above and shown by Figure 14 very few observations are required for reliable analyses if the observations are perfect. The perfect curve shows little improvement after 4 percent of data. Case II and Case III curves show mean absolute errors for analyses of temperature observations of 1°F accuracy but with (Case II) and without navigation errors (Case III). The closeness of the two curves indicates that the navigation error is relatively unimportant in smooth areas if the data are good. This is expected since the thermal field is so flat. The difference between reliability of analyses of a given quantity of "good" and "bad" data is very evident from Figure 16.

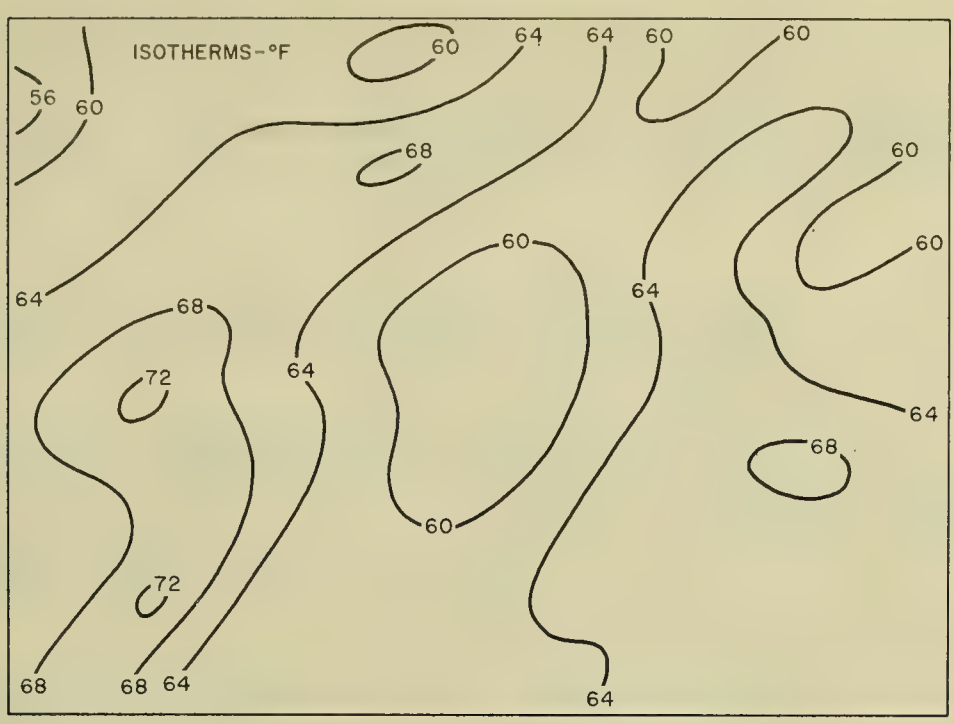

Fig. 15 - Analysis of 10 percent of data, case 1, area B

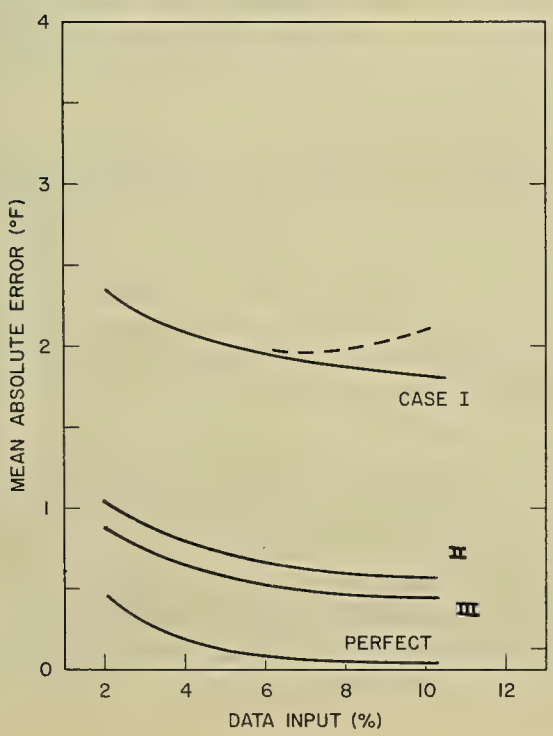

Fig. 16 - SST accuracy, manual analysis, area B

In the analysis of 10 percent of present-type data (Case I) the mean absolute error was actually larger than for 5 percent data (the solid curve shows the expected curve). This was undoubtedly due to the fact that greater quantities of poor data is more misleading than smaller quantities.

The conclusions to be drawn from the Area B tests are as follows:

(a) Very little more data is required for smooth areas than is now available but the data must be of a quality comparable to that provided by NSRT or buoys.

(b) It is not feasible to increase the data input in smooth areas with low quality data, since this leads to little improvements in analysis accuracies.

(c) The use of ART is not required in smooth areas since the need is for a small number of good observations, not a high density of data as provided by aerial survey.

(d) Buoy observations would be ideal for smooth areas since they provide both a non-random data plot and high accuracy temperature data.

(2) Absolute Data Requirements for Area B

From Figure 8 it appears that present type data should be replaced as soon as possible by more accurate data and no great effort expended on increasing ship-of-opportunity data unless it is from a NSRT system.

On the basis of the discussion in Section IV A(5) concerning selected versus random data distribution it is safe to conclude that a fixed array of buoys would give accuracies comparable to the perfect data curve shown in Figure 16. Thus, a 2 percent data input is completely adequate, which would mean eight observations or if accuracies of 1°F would be tolerated, perhaps five or six reports. Combining buoy observations and random ship reports from NSRT systems one could obtain reliable analyses from one buoy plus six to eight ship reports.

Owing to the lack of advection in smooth thermal fields it is likely that continuity would contribute highly to analysis accuracy. An occasional ART survey over the area to obtain a high data density of good accuracy would provide a highly reliable analysis which would be useful for continuity for 10 to 15 days.

D. Estimated Analysis Accuracies

In order to obtain some measure of analysis accuracy expressed as a percent score the following formula was applied to the results of the tests described in this report:

$$A = \frac{T - E}{T}$$

Where A = percent accuracy
T = total range of temperature in area, °F
E = mean absolute error, °F

This formula obviously can not be used for all cases and areas but does give a means of comparing analyses in complex and smooth areas. It considers both the degree of variation in the area to be analyzed and the mean absolute error of the analysis. A mean absolute error of 2°F may be considered good in a highly complex area but not so good in a smooth thermal field.

For Area A the temperature range was 25°F, from 53°F to 78°F. Thus the present 3.4°F error would be equivalent to an analysis accuracy of 86 percent. If the analysis error can be reduced in time to 1.4°F the accuracy score would be 95 percent.

For Area B the temperature range was 6°F, from 61°F to 67°F. Present accuracies of 2.3°F show analysis accuracies of only 62 percent. Through suitable data sources and little new data this accuracy would be improved to 97 percent.

A question that comes to mine here is what accuracy is desired? This, of course, depends upon the use to be made of the analyses but generally the charts must be reliable enough to satisfy the most stringent operator requirements. This would require accuracies of 95 percent.

V. SUMMARY AND CONCLUSIONS

This report described a series of tests designed to show what the data requirements are for synoptic sea surface temperature analyses. It was shown that data requirements are not unlimited but that a definite quantitative value can be placed on how much data are required. Data requirements for smooth and complex thermal areas were shown to be significantly different and should be so treated in planning of synoptic nets.

The number of observations required for reliable sea surface temperature analysis depends upon the area, the type of data and the reliability desired. Table III shows the data requirements estimated for various types of data input and analysis accuracies.

TABLE III NUMBER OF DAILY OBSERVATIONS PER FIVE DEGREE SQUARE

Chart Reliability	Complex Area			Smooth Area			
	85	90	95%	65	75	85	95%
Data Type							
Present Ship Injection Data	8	16	40	12	72	*	*
Random NSRT Reports Plus Some ART, Buoy	7	12	35	5	6	8	20
Mostly ART, Buoy Data Plus Some NSRT	7	8	30	5	5	6	8

*Not attainable with present type data

The results of these tests are considered valid on the basis of the number of tests conducted including computer and manual, tests for randomness, for specified data distribution and for error functions. One procedure that was not treated in these tests was the use of continuity analyses. These charts obviously help in the preparation of a synoptic chart when correct. If wrong they simple mislead the analyst. On the assumption that their popular use by all analysis groups shows a degree of corrections it is concluded that all scores would be improved slightly by their use in the tests. The slopes of the curves, however, would not be materially altered.

The major conclusions are as follows:

(1) Planning for synoptic network should emphasize high concentrations of data with average accuracies to $\pm 1.0^{\circ}F$ for complex areas. In smooth areas the emphasis should be on a few highly accurate (less than $\pm 1^{\circ}F$) fixed observations.

(2) Data should be increased about four times in complex areas and improved in accuracy. For smooth areas the quantity of data need only be improved.

(3) ART surveys should be confined generally to the highly complex areas with an occasional flight for continuity in the smooth areas. Buoy arrays should be utilized in smooth areas where their high accuracy and fixed position contribute greatly to analyses reliability.

REFERENCES

Beetham, C. V. "Test and Evaluation of the Near Surface Reference Temperature System", IM No. 66-10, Aug 1966, 14 pp.

Carman, D. R. "Comparison of U. S. Naval Oceanographic Office Sea Surface Temperature Charts with USNS GILLISS Survey Data, 2-5 March 1964", IMR 0.65-64, Jan 1965, 6 pp.

Gibson, B. A. "Note on the Reliability of Transmitted Sea Surface Temperatures", IMR No. 11-62, Jan 1960, 5 pp, NAVOCEANO.

James, R. W. "Accuracy of Sea Surface Temperature Analyses", Part III, IM No. 66-23, Sep 1966, 14 pp.

James, R. W. "A Quantitative Evaluation of ASWEPS Sea Surface Temperature and Layer Depth Charts", IMR No. 0-39-65, Sep 1965, 37 pp.

Kuhn, J. A. and Farland, R. "Sea Surface Temperature Measurement System (SURTEMS), IMR No. I-2-63, May 1963.

Saur, J. F. T., "A Study of the Quality of Sea Water Temperatures Reported in Logs of Ships' Weather Observations", Journal Applied Meteorology, Volume 2, N3, June 1963, pps 417-425.

Shank, M. K. Jr, Unpublished, "An Investigation of Grid Spacing and Data Requirements in the Preparation of an Objective Sea Surface Temperature Chart", Feb 1964, 10 pp.

Shank, M. K. Jr., "Comparisons of Analyzed Sea Surface Temperatures With Observed Data (Jan - Feb 1966)", IM No. 66-22, Oct 1966, 13 pp.

Thompson, B. J., "Numerical Techniques", SP 109, ASWEPS Manual Series, Volume 9, 1966, 26 pp.

Tuttell, J. T., "Comparison of NAVOCEANO SST and LD Charts With USNS DAVIS Survey Data, IMR No. 0-54-63, June 1963, 30 pp.

LARGE-SCALE ANOMALOUS SEA SURFACE CONDITIONS IN THE NORTH PACIFIC

John D. Isaacs
Scripps Institution of Oceanography
La Jolla, California

Aperiodic departures from the normal sea surface temperatures commonly occur throughout the world's oceans. Such anomalous fluctuations often exceed the mean seasonal or annual fluctuations of temperature in many regions, and thus constitute major features of the oceans. These changes are associated with changes in weather, currents, the distribution of marine organisms, the success of fisheries, and, undoubtedly, with the propagation of underwater sound, the background noise, and the frequency and distribution of natural targets. It is thus important to inquire into the interactions, underlying nature and causes of these changes.

It has long been recognized that ocean conditions are changeable on a time scale much more abbreviated than the broad climatic changes, such as the ice ages. Perhaps the most striking example of these abbreviated changes in the last few centuries were experienced in the North Atlantic in the years 1812 and 1813, when conditions were so frigid that some of the now existing deep Atlantic water may have been generated, and snow lay on the fields of Northern Europe all summer. We are gaining some insight into the year-to-year range of ocean conditions within the last thousand years or so from the study of certain highly stratified basin sediments.

The historical meteorological records also lend insight into the nature of these changes. The air temperatures at marine stations have been shown to follow the sea surface temperatures very closely. These records, hence allow us to extend the marine temperature record back in time for a few hundred years. In Figure I, for example, is shown the air temperatures at three Pacific Coast stations, extending to 1925. This demonstrates a number of features, anomalously high and low seasonal temperatures following one another in a complex pattern. One feature of these records, besides their variations, is the peculiar lack of fluctuation in the decade 1946 to 1956.

Such changes were long thought to be essentially local phenomena, generated by local variations in currents, winds and upwelling. Several workers, however, noted that extreme changes often occurred in the same year in areas as remote as Japan, San Francisco and Peru. This has been called teleconnection.

The work of the Bureau of Commercial Fisheries in analyzing the sea surface temperature records from surface ships has shown that the anomalies are commonly of very large scale and long persistence. Figures 2 and 3 are examples of such large-scale anomalies. A pattern similar to Figure 2 persisted in the eastern North Pacific for a period of more than eight months in 1958 and that of Figure 3 during much of 1957. Hatched areas are colder than normal and clear areas warmer.

We now believe that teleconnection is an expression of the very large scale of these features, certainly not some mysterious communication across the reaches of the sea between isolated events.

The sudden change in the conditions of the North Pacific in 1956 to 1959 and which terminated the period of persistence, demonstrated afresh the importance and magnitude of the effects of these variations. One of the deepest and most prolonged meteorological lows on record developed off Washington, remaining for three months. A strong narrow countercurrent developed along the west coast of the United States, carrying subtropical organisms as far north as Oregon, southern fish visited Alaska, the monsoon delayed its onset a full six weeks beyond its appointed time, desert isles of the Central Pacific became clothed with green, the heaviest rains in a decade dampened California, everywhere was a stirring engendered by these events.

Figure 4 exemplifies a subtropical marine organism carried far north by the narrow countercurrent, and Figure 5, from the records of the California Fish and Game, shows the invasion of tropical fishes into California waters in these times.

The ocean-air interactions related to these changes are partly understandable in a qualitative way. For example, the onset of the 1956-1959 change is most marked in the region of the Aleutians where warm Central Pacific water was carried far north of its usual position by an unusual wind pattern in the winter of 1956-57. Namias has shown that the development of the major features of the North Pacific weather can be better hindcast when the persistence from ocean-air interaction is considered.

The importance of attaining a better understanding of these events is now clear, and an approach to this understanding can be designed.

The remainder of this discussion will outline the plans at Scripps Institution for a study of these large-scale anomalies in the North Pacific.

One of the principal defects in our information about these events is the paucity of our knowledge of what is transpiring beneath the sea surface and how deeply the anomalous temperatures are distributed. We do not know whether these anomalous regions result from an unusual transport of water or from some change in cloud cover, evaporation, mixing, heat exchange or other alteration in thermal flux.

Some insight on the probable conditions has emerged from a pilot study that we have carried out. This study has brought to light a number of curious features of these changes, all of which guide us in designing a study of their nature. I will show only a few examples of these results, which, none-the-less will demonstrate the strong indications that they provide.

Figure 6 presents data for a number of North Pacific stations and shows the log ratio of the monthly temperature change (temporal gradient) at the station and the long-term average monthly temperature change for that station, plotted against the sea surface anomaly for that station. One might properly expect that the temperature change at a station at the time of an intense anomaly might depart greatly from the normal, and that it might be near normal during normal conditions. Figure 6 argues that this is by no means the case, and, if there is any trend, the regions of intense anomaly follow the normal seasonal temperature cycles more closely than do the normal regions!

Similar results emerge from the analogous relationship of the monthly horizontal temperature gradient and anomalies.

These findings argue that these large-scale anomalies result from similarly large-scale homogenous effects, with variations in the effects occurring principally at the edges. The results also allow the possibility that the "normal" conditions are unstable and that two relatively stable conditions exist, one in which temperatures are above normal and one with temperatures below normal.

Figure 7 is a plot of the relationship between the anomaly at a station for a given month and the anomaly of the monthly temperature change preceding the month. At first thought this appears to be a naive approach, and as would be expected, most warm anomalies are preceded by anomalous heating and most cold anomalies are preceded by anomalous cooling. Beyond this point, however, is a strangeness to the relationship. Warm anomalies often survive anomalous cooling, but cold anomalies very seldom survive anomalous heating. This is shown by the abundance of point in the fourth quadrant of the graph and the paucity of occasions in the second

quadrant. Keeping in mind the fact that these data are monthly and surface temperature only, the best explanation for this behavior is that there exists an anisotropy between the heating and cooling processes. Undoubtedly this results from the production of a thin stable surface layer in anomalous heating, which represents a relatively low total thermal change. Anomalous cooling, on the other hand, must involve instability and convection, requiring a much larger thermal change. Thus anomalous heating is a rapid process and anomalous cooling a slow process. In our study on monthly changes we often catch the cooling in mid-step but the anomalous heating takes place so rapidly that it is most often complete within the monthly time scale.

These two examples will serve to present the type of constraints and insights that our pilot study is providing.

I will now discuss the field program from which we hope to derive a much fuller understanding of these large-scale temperature fluctuations.

The principal tool that will be employed is the small deep-moored instrument station that has been under development for many years at Scripps. These deep-moored stations were first attempted in the Pacific Proving Grounds at the IVY event in 1951, and later deployed in larger numbers in subsequent tests for the recording of fallout and other weapons effects. Figure 8 shows a typical deployment in that period. These moorings were very successful. Depths of mooring were from 700 fathoms to greater than 3000 fathoms.

Later developments allowed a greater penetration of sensors, and our recent models record to depths of 3000 feet and are showing a very satisfactory life. Catamarans as shown in Figure 9, have all remained moored and operating in the open North Pacific for six months or more, and one survived for over two years. Two moorings placed in the equatorial Pacific two and a half months ago have just been reported to be operating and in good shape.

We thus have a number of the long deep-sea records of temperature versus depth. Figure 10 shows a spectral analysis of temperature depth fluctuations of a 100 day record taken about 600 miles off the California coast. In this record an incoherent lunar semi-diurnal fluctuation is the greatest. Curiously, the lunar and solar frequency are not significant but there is a strong unexplained coherent semi-solar periodicity. I show this analysis to point out that the moored stations are capable of yielding data that is amenable to spectral analysis and the determination of the periodicities involved in temperature-depth fluctuations.

Another essential test of these data is to determine whether they are comparable to the ships' data from which the Bureau of Commercial Fisheries has derived the delineation of the anomalous

sea-surface temperatures. Figure 11 shows the correlation between the sea-surface temperature as derived from monthly averages of hourly readings from deep-moored stations and the sea-surface temperatures from the published contoured charts from the Bureau of Commercial Fisheries for the same station and month. The relationships, unexpectedly, is excellent, with deviations between the two measurements less than 1/2° F. The prima-facie evidence is thus that the ships' data is very good and the instrument stations will delineate the same type of temperature anomaly (as well as, of course, obtaining comparable data beneath the surface).

We therefore plan that within the next two years we will establish a series of clusters of deep-moored stations, spread across the North Pacific, in some such an array as shown in Figures 12 and 13. The cluster configuration in contrast to a regular grid is required in order to ascertain the direction of any discontinuity or wave-like motion passing through the area.

The four peripheral moorings will record meteorological data, and sea-water temperatures well into the thermocline. In addition, insolation will be recorded. The central station is to be a completely submerged recorder, measuring current in the mixed layer.

Some of these clusters may also include a large telemetering station such as the Convair buoy.

In preparing for the instrumentation of this program, we are reviewing the traditional meteorological measurements to see if other measurements may more directly relate to the interaction of atmosphere and ocean. For example, measurements of humidity are related to the evaporation or condensation of fresh water. A measurement of evaporation or condensation related to the local sea water would be more direct. This, in effect, would be a wet and dry bulb measurement using sea water for the wetting agent. Of course, such a simple approach as this would not be feasible because of the changing concentrations of the wetting agent as evaporation proceeded.

Wind velocity is ordinarily recorded and converted into the square of the mean velocity for evaluating its interaction with the sea surface. Clearly the mean velocity squared of a turbulent wind may be quite different from the mean square velocity, whereas in a steady wind they will be much the same. It is perhaps more direct and meaningful therefore to measure and record V^2 rather than V.

These are some of the instrumentation problems that we hope to resolve in the near future. We plan then to launch a significant attack on the unknown nature and causes of the large-scale fluctuations in sea conditions that have been instrumental in generating much uncertainty in man's meteorological forecasts and in his fisheries, agriculture, marine transport, underwater sound

conditions, etc.

Our study of the varved sediments, to which I alluded earlier, will provide us with perspectives on the range of conditions that may be within probably future experience.

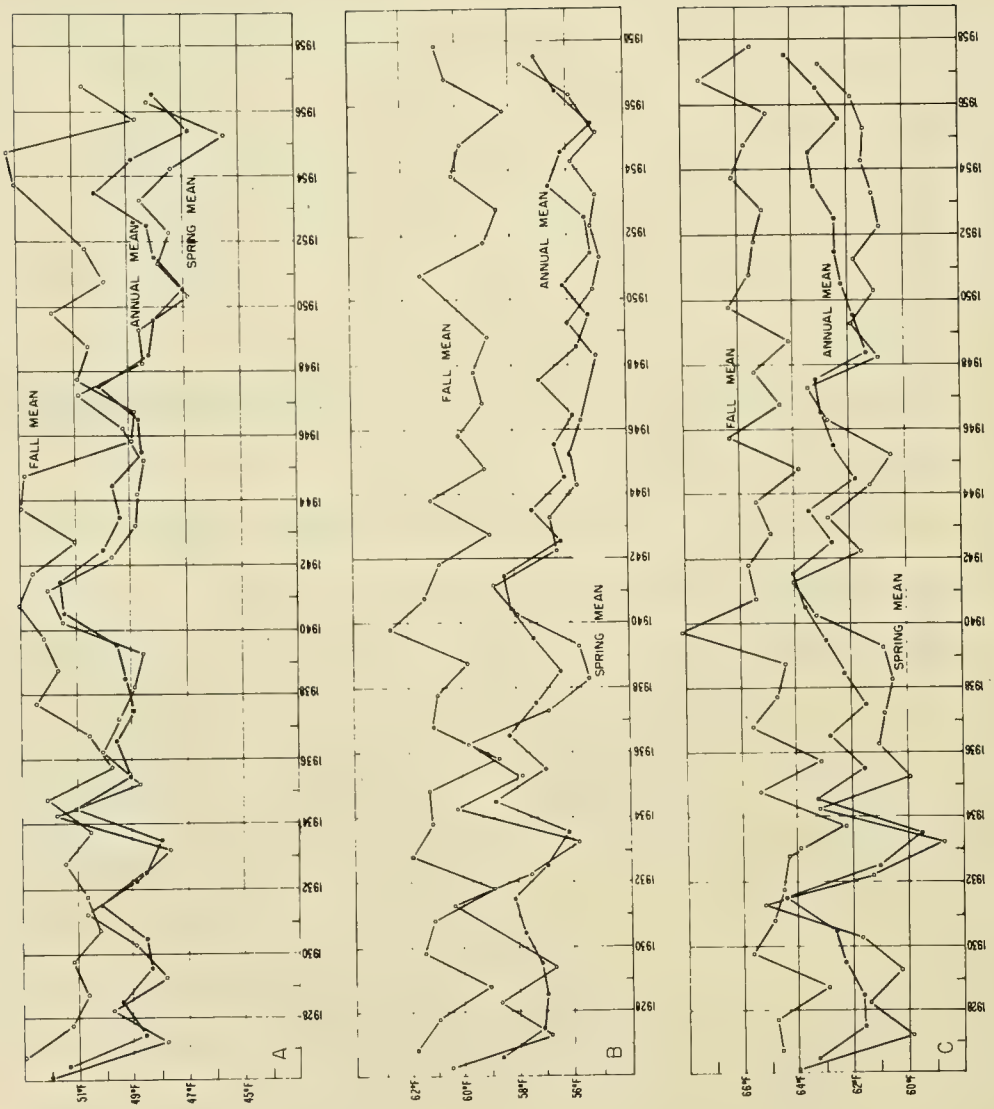

Fig. 1 - Mean air temperatures (spring, fall, annual). (a) Tatoosh Island, Washington, (b) San Francisco, California, (c) San Diego, California.

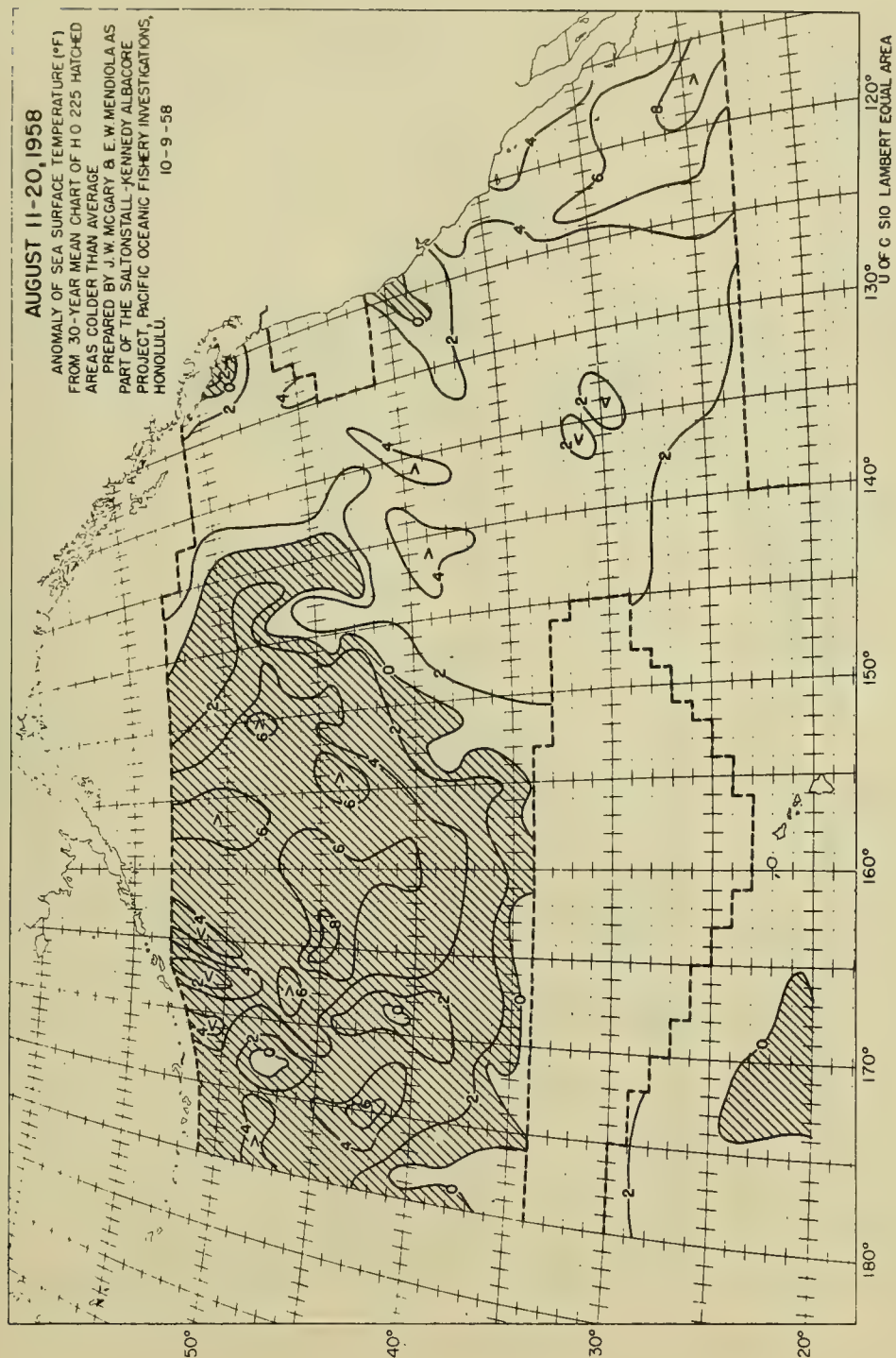

Fig. 2 - Anomaly of sea surface temperature (°F) from 30-year mean chart of H.O. 225. August 11-20, 1958.

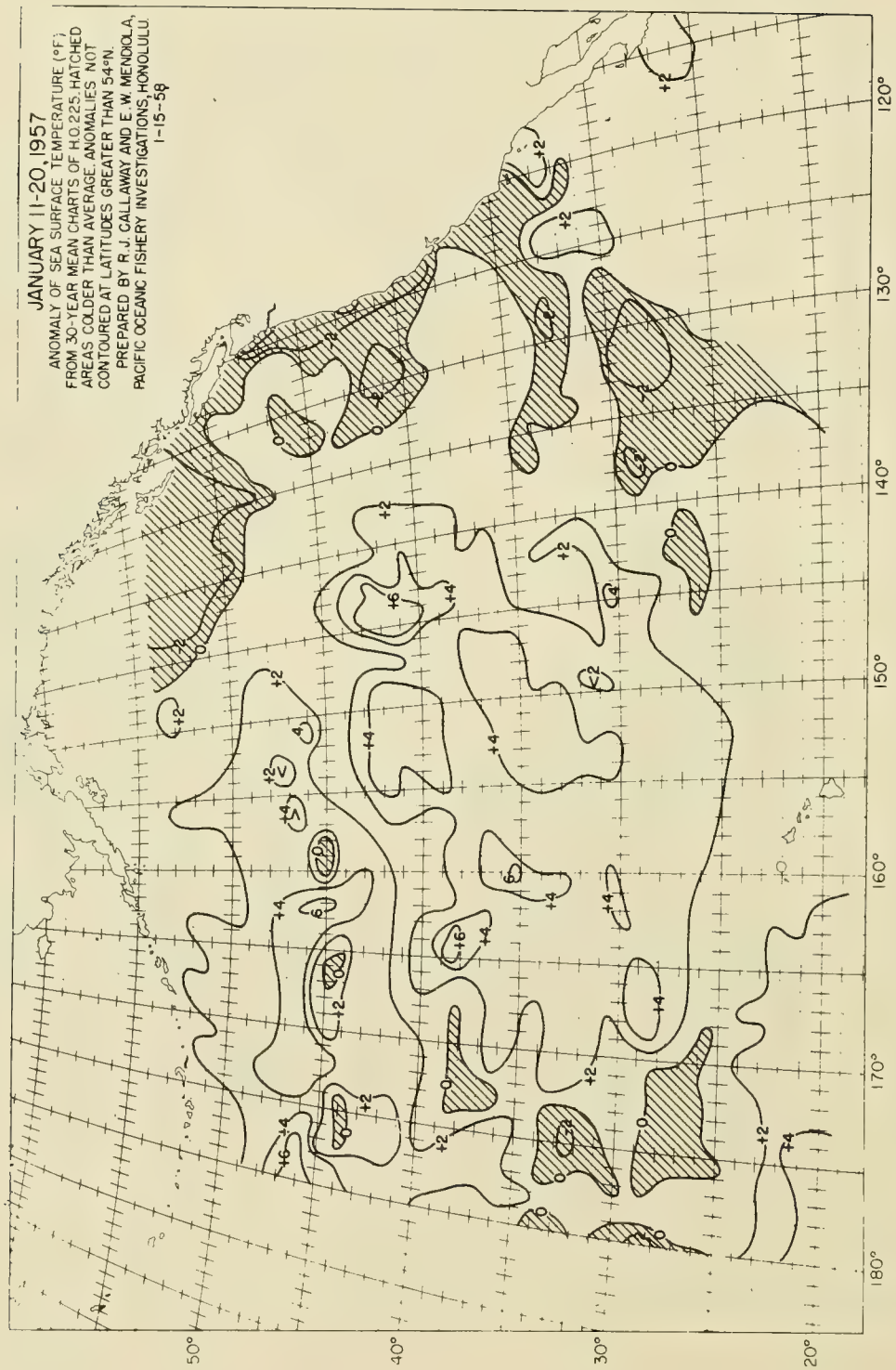

Fig. 3 - Anomaly of sea surface temperature (°F) from 30-year mean chart of H.O. 225. January 11-20, 1957.

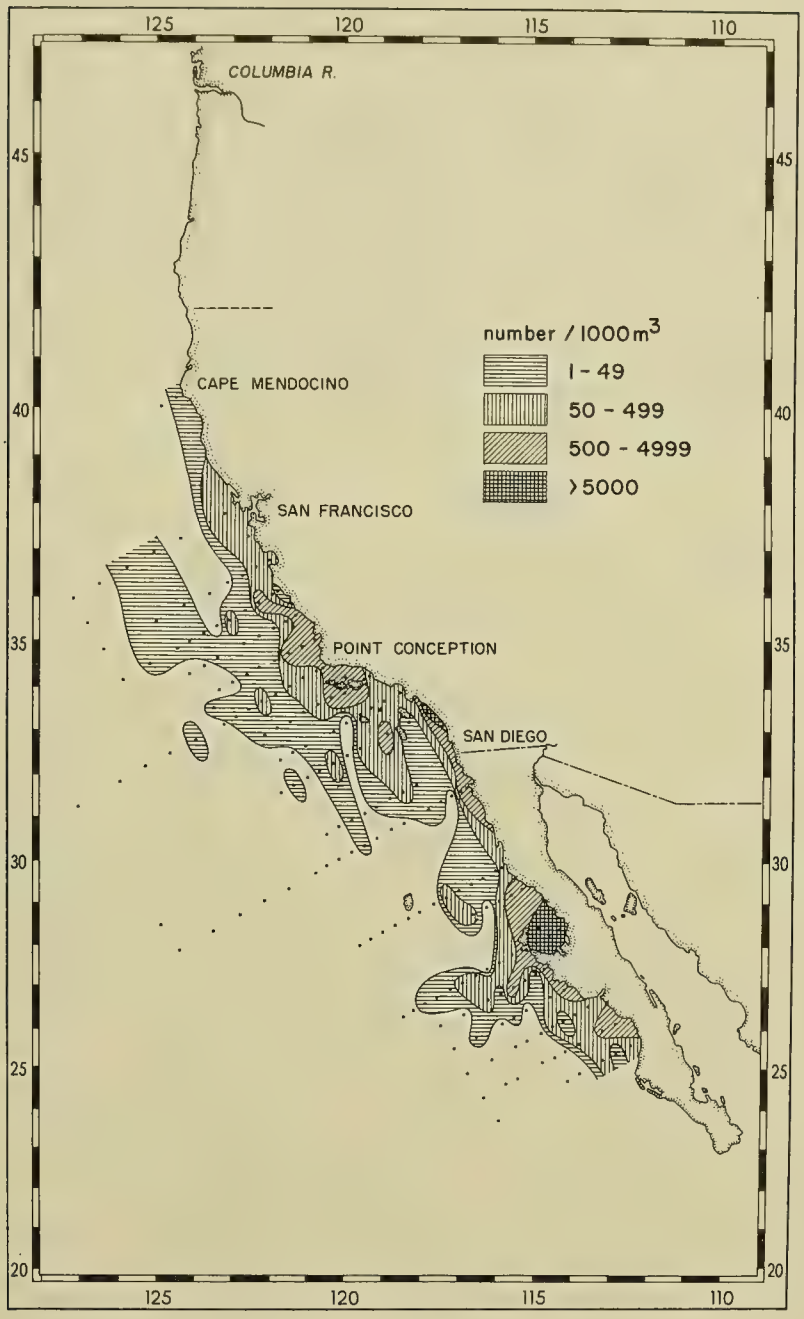

Fig. 4 - Nyctiphanes simplex, April, 1958

Year	Barracuda	Yellowtail	Bonito	Yellowfin Tuna	Skipjack	Dolphin-fish	Angler Days
1947	677,449	6,948	36,496	137	698	15	359,436
1948	384,056	13,028	14,519	18	460	0	407,757
1949	366,423	17,710	5,372	11	9	0	469,915
1950	256,367	6,971	2,359	6	31	1	544,264
1951	269,545	23,721	14,475	56	132	0	556,949
1952	336,550	59,263	7,649	34	38	2	562,898
1953	170,550	27,702	6,321	0	279	0	502,146
1954	282,552	40,872	70,078	0	50	12	532,190
1955	154,962	36,468	22,409	1	10	0	496,286
1956	87,603	29,198	61,404	78	13	2	523,063
1957 through September*	490,075	176,849	186,587	425	6,417	2,805	-

*Preliminary report

Fig. 5 - Total annual party boat catch of several species in number of fish from 1947 through September of 1957

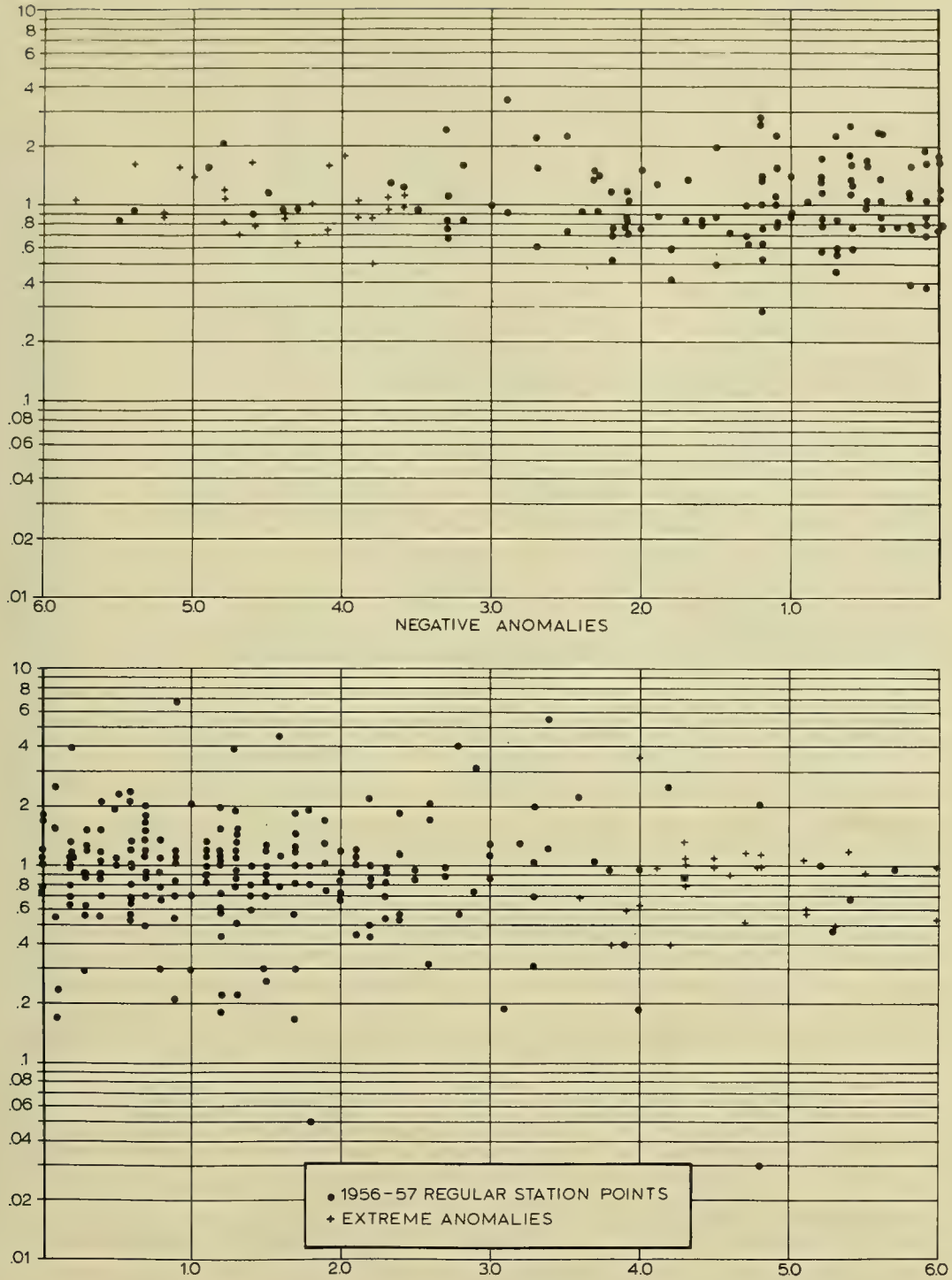

Fig. 6 - Graph of ratio of 12-year mean monthly temporal temperature gradient to monthly temporal temperature gradient versus anomaly-deviation from 12-year mean monthly temperature

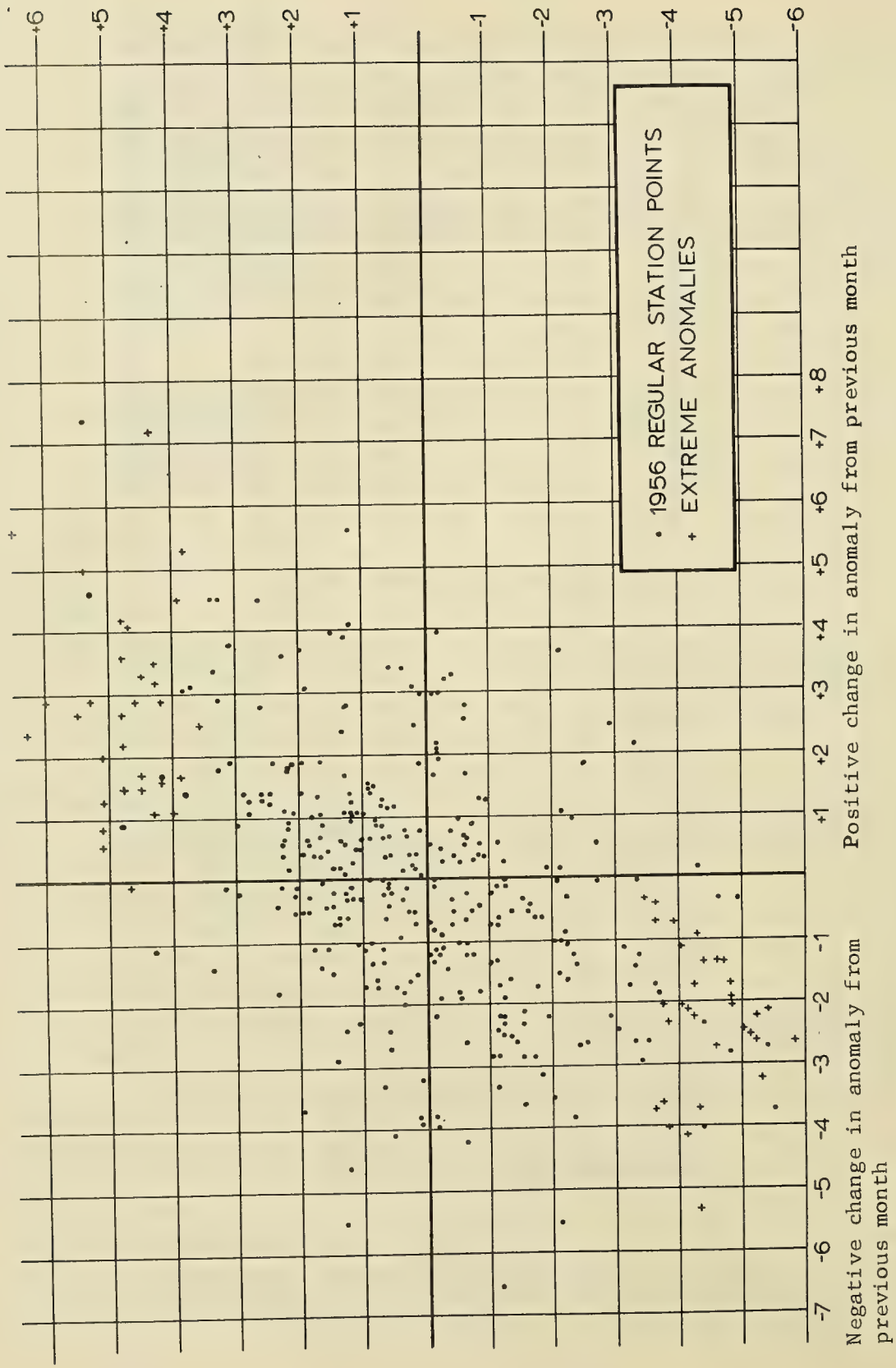

Fig. 7 - Graph of anomaly-deviation from 12-year mean monthly temperature - versus change in anomaly from previous month

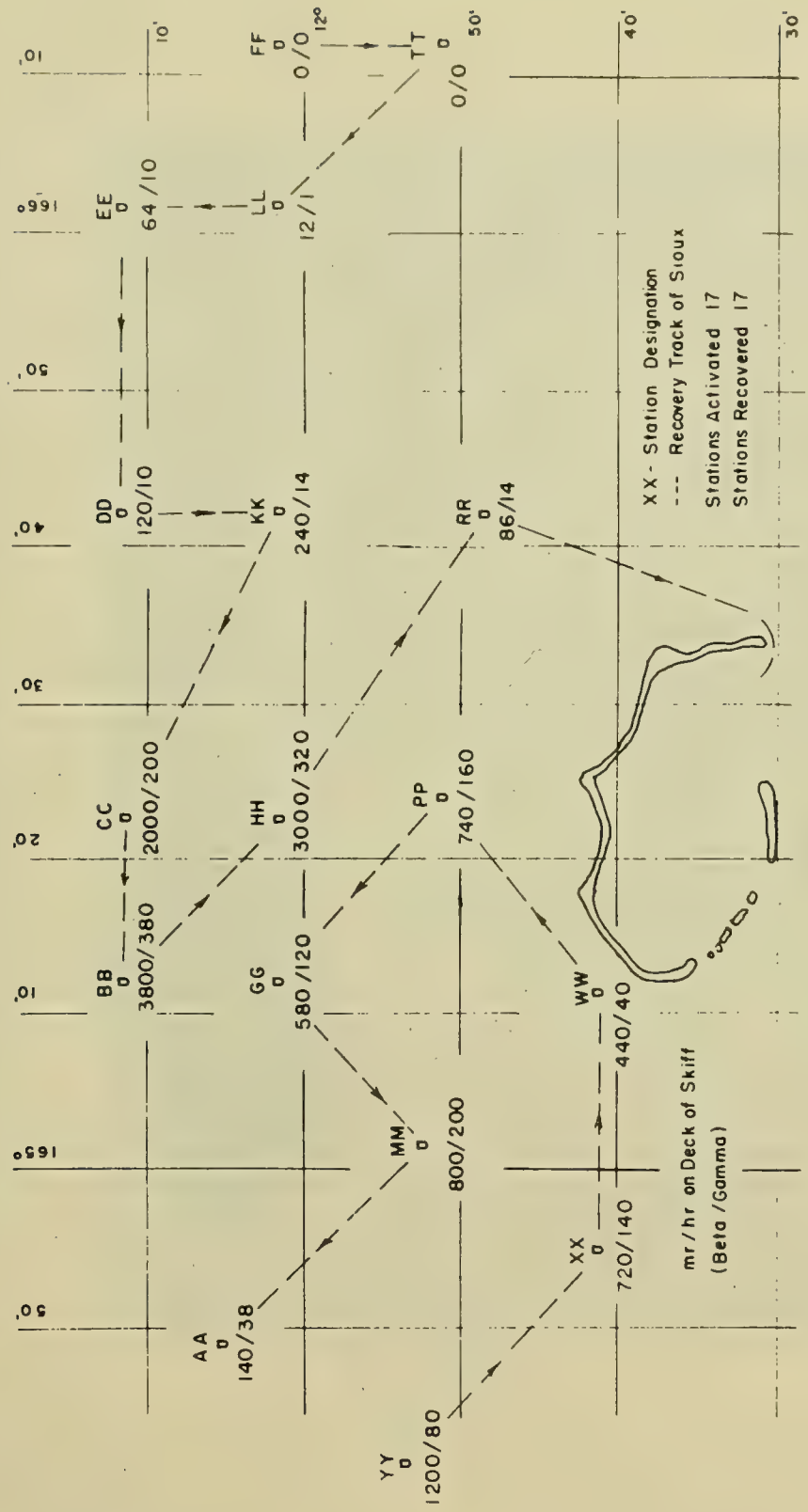

Fig. 8 - Skiff distribution and fallout contamination for TEWA

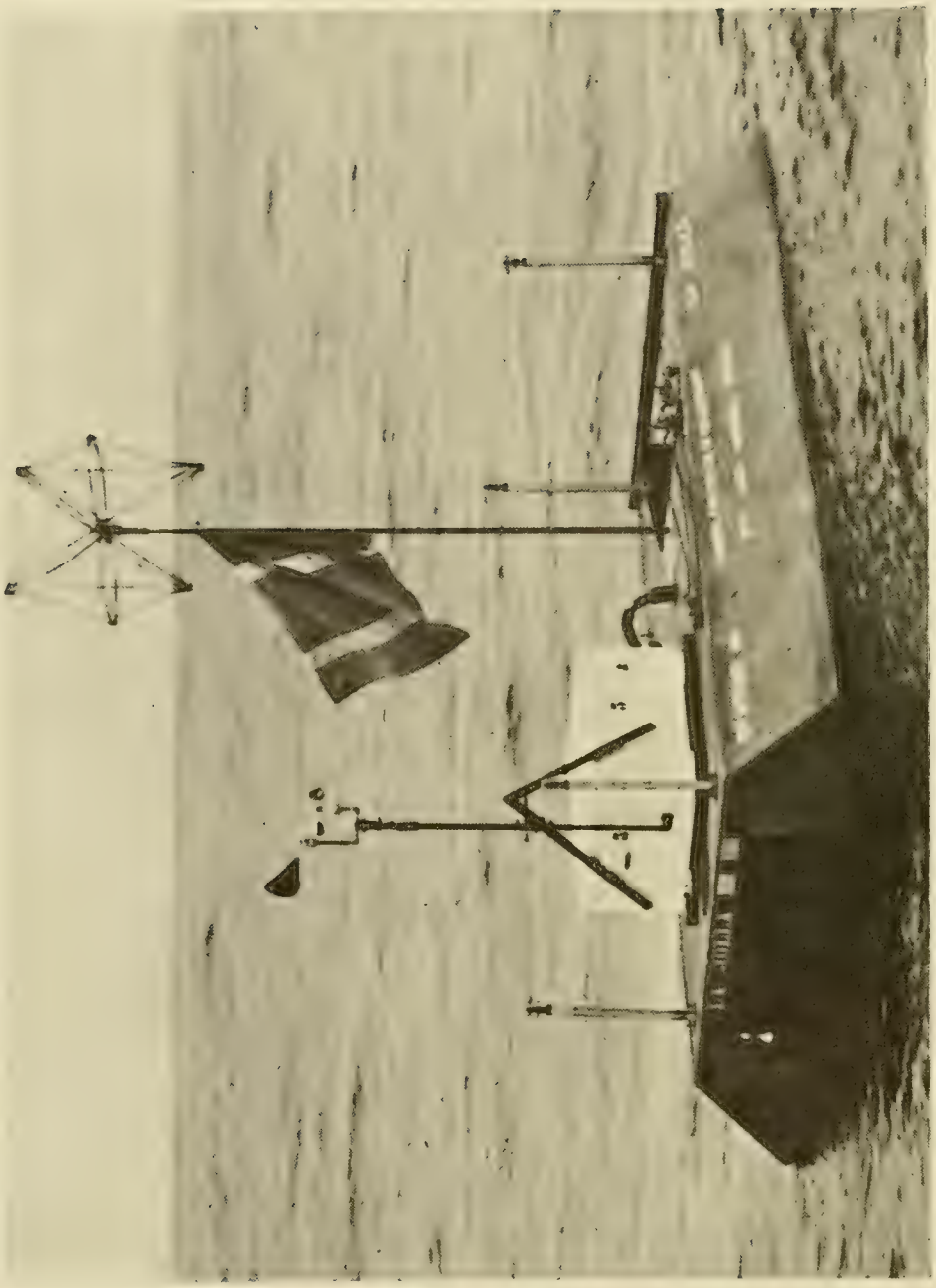

Fig. 9 - Catamaran

Frequencies (cycles-per-day)	O_1 0·93	M_1 0·97	K_1 1·00	Background 1·1	1·8	M_2 1·93	S_2 2·00
Equilibrium tides (cm^2)	85·7	0·4	209·5	0·1	1·0	332·1	54·3
Temperature at 150 m ($°C^2$)	0·091	0·135	0·085	0·080	0·011	0·046	0·015
Coherence	0·3	0·3	0·3	0·3	0·3	0·3	0·7

Fig. 10 - Energy per band (width 1 cycle/month) at selected frequencies

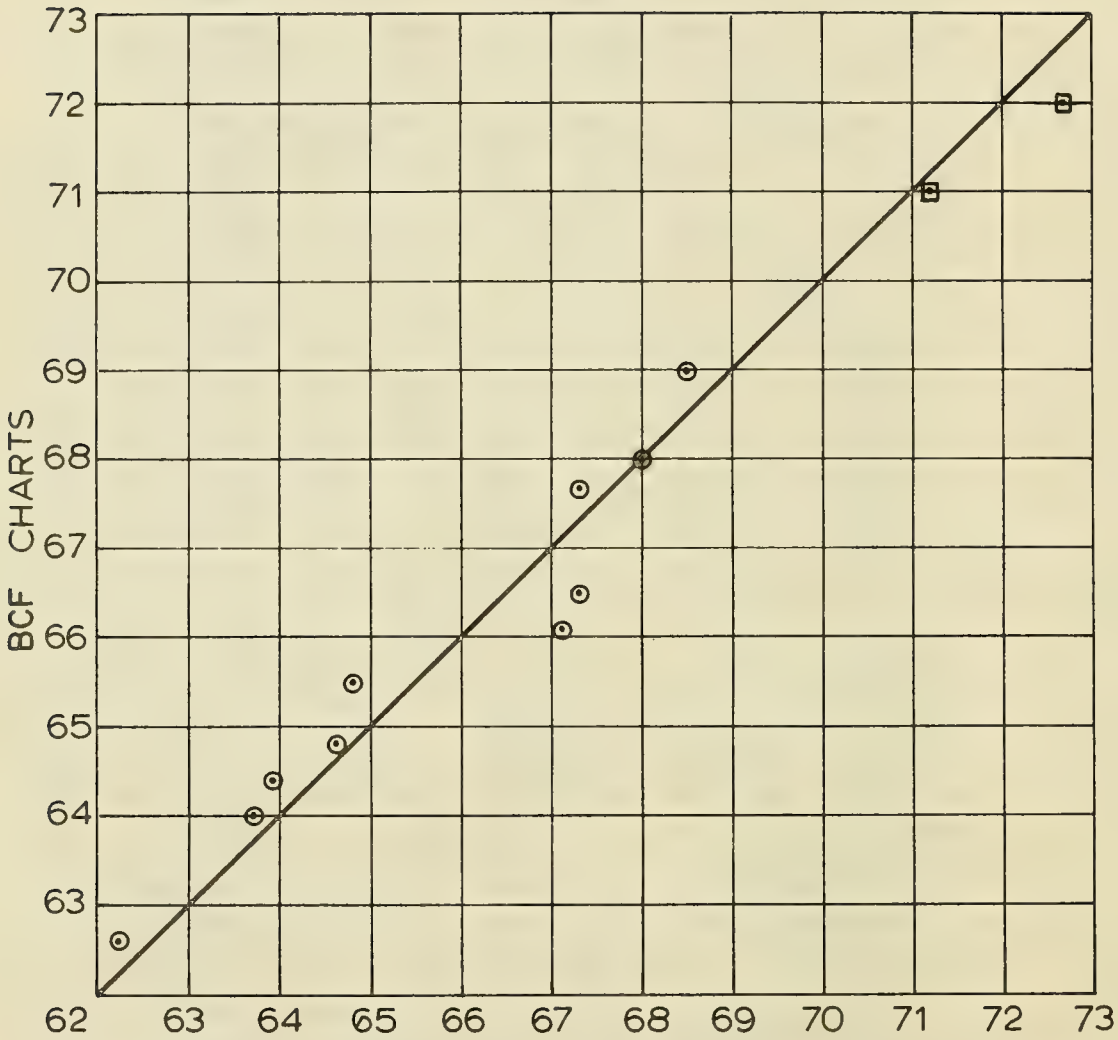

Fig. 11 - Monthly mean temperatures (°F) from SIO moorings and Bureau of Commercial Fisheries sea surface temperature charts. ⊙ - BCF sea surface temperature charts, ⊡ - weather station November.

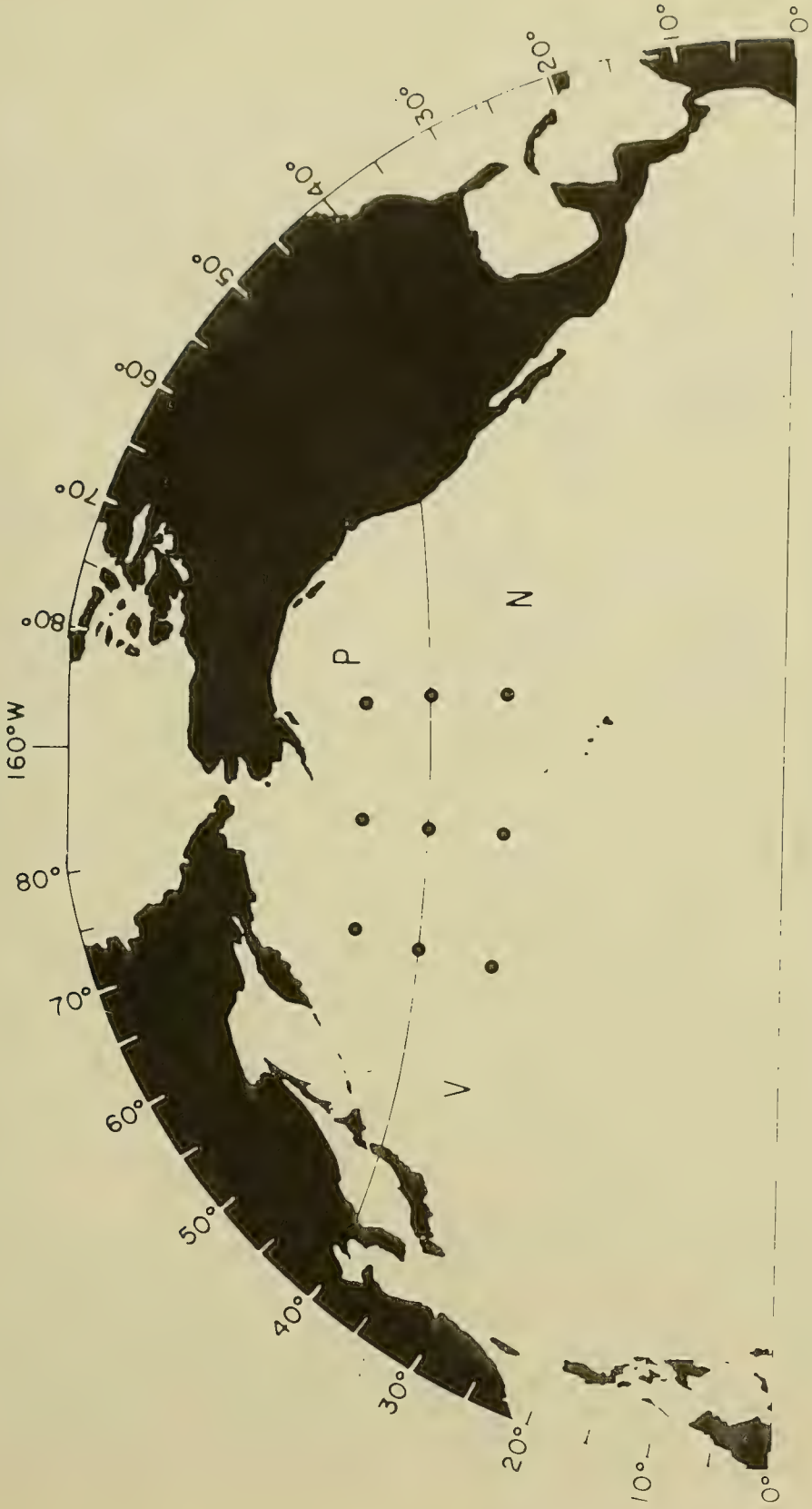

Fig. 12 - Possible locations for moored stations.
. - clusters of stations. N. V. P - weather ships.

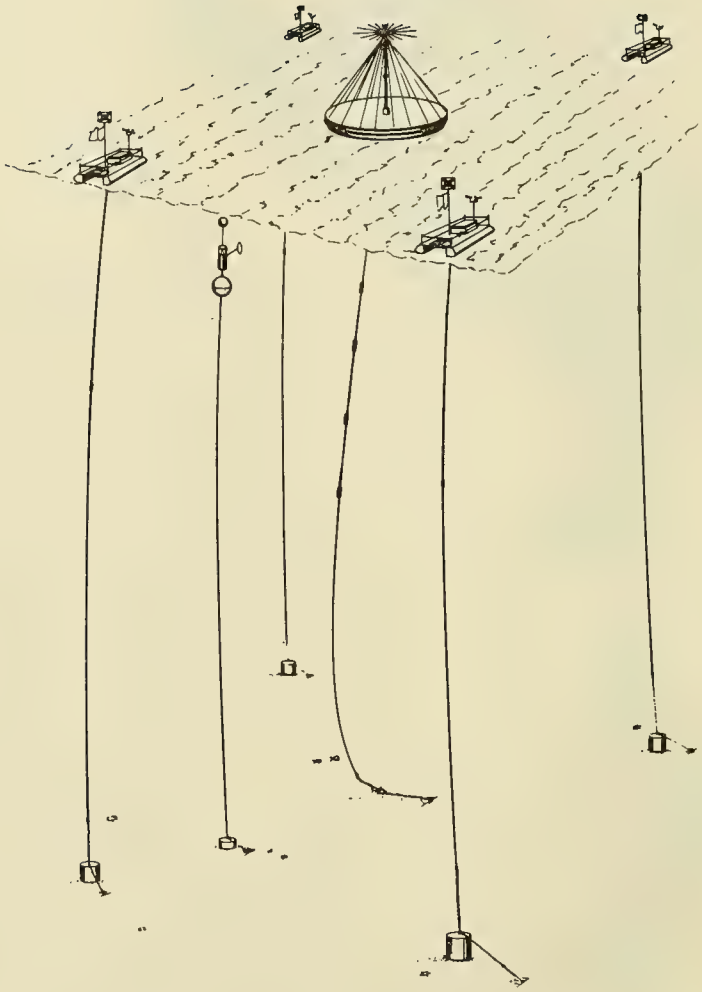

Fig. 13 - Possible locations
for moored stations

Energy Spectra of the Sea from Photographs

Denzil Stilwell
Naval Research Laboratory
Washington, D.C. 20390

BACKGROUND

The present work was undertaken to provide an independent measure of the surface conditions of the ocean in order to quantitatively correlate radar cross-sections with sea state. Previous attempts to define the sea state have been largely qualitative definitions, dependent not on direct surface measurements but on wind velocity and an observer's eye. Quantitative measurements have been made in such efforts as the SWOP program and glitter analysis, but these are not readily available techniques for the routine measure of sea clutter. Stereophotographic measurements have been attempted to supplement the SWOP data but the difficulty in its application at the very high range of the ocean spectrum (one meter wavelengths to millimeter waves) precludes it as a convenient tool. Normal oceanographic devices offer little promise of obtaining the huge amounts of information required to specify accurately the energy spectrum of a real sea, especially in the high frequency region, because of the tremendous difficulties involved in designing accurate measurements with the resolution required. Most techniques designed to obtain spectral information have one common feature, recognition of photographic recording as the only presently practical technique capable of providing a sufficiently large sample of information adequate to determine a spectrum with precision.

The technique of obtaining Fourier transforms by optical techniques[1] is particularly applicable to the present problem since the basic data are the optical intensities which expose the photograph and the analysis is performed on the light amplitudes (which are simply related to the intensities). Optical Fourier transforms arise because the basic transfer function for lens has the form of a Fourier transform and when used with monochromatic, collimated light generates a light distribution which is simply related to the desired spectrum[2]. Figure 1 illustrates the

simplest outline of an optical computer. The use of a laser is not absolutely necessary but the light intensities available from other sources are too low to be convenient. The laser beam diameter is enlarged after traversing the telescopic lens system to a size suitable for the data format, i.e., the negative size. The collimated light impinges on the transparency placed in the front focal plane (input plane) and is transformed by the lens into the output plane. The light amplitude in the output plane is proportional to the Fourier transform of the light amplitude in the input plane.

The basic problem then is to determine the relationship of the light amplitude after passing through the optical system in terms of the information on the sea as recorded on the scene photograph. To accomplish this, it is necessary to establish the correspondence between a sea parameter and the optical density on the film, determine the exact form of the transform, and to relate the recorded optical density of the transformed information to the value of the sea spectrum. In what follows the first order theory for the Fourier components analyzed optically will be presented and the conditions under which the technique is valid will be indicated.

SCENE PHOTOGRAPH REQUIREMENTS

The initial problem in the photographic analysis is to determine the relationship between the optical density at a point on the negative with some parameter of the surface point it represents. Figure 2 is a plot of the characteristic curve of photographic emulsions for which the linear range has an equation of the form

$$D = \gamma \log K \cdot u \tau \qquad (1)$$

where D is the optical density of the developed negative, γ is the slope of the straight line part of the curve, K is a constant relating to the sensitivity of the film, τ is the exposure time, and u is the power density incident on the film. Optical density is defined by the equation

$$u = u_o 10^{-D} \qquad (2)$$

where u is the light power density transmitted through the film with optical density D and u_o is the incident intensity. From these equations it is obvious that a knowledge of the light intensity leaving a point on the surface in a direction toward the camera is sufficient to determine the resulting optical density.

The camera illumination (observer direction in Figure 3) is due largely to the light reflected from the surface since light leaving the water is normally of much lower intensity. Figure 4 is a plot of the reflectivity of water with angle. Visualizing

a sinusoidal modulation of the normal angle to the wave surface, this Figure indicates that the resultant reflectivity variation would be a minimum for an observer angle of 90°, or vertical incidence. Grazing incidence would give the greatest sensitivity but the scene would be highly distorted and much of the wave surface would be obscured by the peaks of the waves. The intermediate region, that near Brewster's angle, can be used. For this region a polarizing filter is required since the vertical component would not yield a unique reflectivity with wave angle and would therefore introduce extraneous spectral components.

Reflectivity does not completely define the light directed toward the camera since the sky itself may have variations of brightness. With sky luminance entering the analysis the problem loses definiteness but certain requirements can be deduced. That part of the sky from which light is reflected into the camera must have monotonic variation of luminance if there is to be a one-to-one mapping of the surface normal angle onto the film. Thus, the sky must be either clear or uniformly overcast for the technique to work.

Denoting the product of luminance and reflectivity by g one can expand this function in terms of normal angle variations in the form

$$g(x,y) = g_o \left[1 + g'/g_o \, \varphi\,(x,y) + \ldots\right] \tag{3}$$

Noting that the power density in equation (1) is proportional to g, one can obtain

$$\frac{dD}{d\varphi} = D_\varphi = \gamma \frac{g'}{g_o} \tag{4}$$

The g_o term in equation (3) will relate to the average density of the scene negative and can be estimated by a direct measurement of this density.

The scene photograph under these conditions would consist of an increasing density in the direction away from the observer which by knowing the camera field of view would allow a measurement of density variation to yield an average of the angular gradient of density from

$$\bar{D}_\varphi = \frac{\Delta D}{\Delta \varphi} \tag{5}$$

This quantity expresses the sensitivity of the photograph density variations to the angular disturbances of the surface. It should be pointed out that waves traveling in a direction other than toward or away from the observer will not be transferred onto the

film with a density variation as large as the angular excursion would indicate using the value of D_φ obtained above. This results because only the projection of the normal angle excursions in the vertical plane directly away from the observer is effective in causing reflectivity variation of light into the camera. The sensitivity must be reduced by some function of the azimuth angle of the waves ψ to be called $p(\psi)$.

The $p(\psi)$ function can be calculated by considering the projection of arc length for a skewed wave onto a plane parallel to camera direction. The approximate equation is

$$p^2(\psi) = \mathrm{Sin}^2\ \delta + \mathrm{Cos}^2\ \delta\ \mathrm{Cos}^2\ \psi$$

where δ is the camera depression angle which for $\delta = 45°$ is

$$p^2(\psi) = \frac{1}{4}\,(3 + \mathrm{Cos}\ 2\ \psi).$$

OPTICAL ANALYSIS

The scene transparency with the properties previously described is inserted into the input plane of the optical computer and illuminated with a collimated beam of laser light. Modifying equation (2) to a form involving light amplitude gives

$$a = a_o 10^{-D/2} \tag{6}$$

Substituting in equation (1) with the power density being the g function of equation (4), one obtains

$$a = a_o \left\lfloor \{K_1 g_o \tau\}^{-\frac{1}{2}\gamma_1} \right\rfloor \left(1 + \frac{g'}{g_o}\, p(\psi)\, \varphi + \ldots\right)^{-\frac{1}{2}\gamma_1} \tag{7}$$

The quantity a_o (the incident laser light amplitude) can be written as proportional to the square root of the laser power density $(= \varepsilon \sqrt{u_o})$.

The term in brackets can be written as

$$10^{-\frac{1}{2}\overline{D}_1} \tag{8}$$

where the bar denotes an average over the area of the photo illuminated by the laser beam. The subscript 1 refers to the scene photograph to distinguish similar terms referring to different photographs occurring later in the analysis. If a small angle or density gradient assumption is made the term in parenthesis can be approximated by

$$1 - \frac{\gamma_1}{2} \frac{g'}{g_o} p(\psi)\, \varphi = 1 - \tfrac{1}{2} D_\varphi\, p(\psi)\, \varphi \tag{9}$$

The light amplitude can be seen to consist of a constant term plus a term proportional to the normal angle of the ocean wave. The constant amplitude term will transform into a finite aperture equivalent of a delta function and will contribute to the transform light intensity only near the region of zero spatial frequency and can be excluded from further consideration. The Fourier transform is then performed on the normal angle as is desired. The higher order terms ignored in writing equation (9) are less than a tenth the first order term for usual values of D_φ with wave angles up to about 40 degrees. The resultant error in the final spectrum will then be less than 5%.

Taking the light amplitude in the output plane as proportional to the Fourier transform one can write

$$u_T = q^2 \frac{F^2(a)}{\epsilon^2} \tag{10}$$

where the constant q relates to the proportionality of the transform (the light amplitude distribution being proportional to the Fourier transform) and the constant ϵ relates to the proportionality of power density and light amplitude. u_T is the intensity which will expose the film placed in the output plane to record the spectra. q can be evaluated by knowing a transform pair for the optical system. A convenient pair is just the gaussian shape of the laser amplitude with off-axis position which transforms into a gaussian shape. Then invoking the requirement that the power flow in the input and output planes must be identical, one obtains

$$\int_0^{2\pi}\int_0^{\infty} \frac{a_o^2}{\epsilon^2} \exp\left\{-\frac{r^2}{\sigma^2}\right\} r\,dr\,d\theta = \int_0^{2\pi}\int_0^{\infty} q^2 (2\pi)^2 \frac{a_o^2}{\epsilon^2} \sigma^4$$

$$\exp\left\{-\gamma^2 \xi^2\right\} \xi\, d\xi\, d\theta \tag{11}$$

where

$$\xi = (L\lambda)^{-1}\, r \tag{12}$$

and then

$$q = (L\lambda)^{-1}$$

Thus q is identical to the scale factor in equation (12) relating a sinusoidal spatial wave of spacing ξ^{-1} in the scene plane to its focal point position in the transform plane as derivable from Huygens Principle.

The power density of equation (10) exposes the film placed in the transform plane for which the equation (using an alternate form of equation (1) is

$$10^{\Delta 2} = K_2 \left[\frac{q^2 F^2(a)}{\epsilon^2} \right] \tau_2 \tag{14}$$

where Δ is the ratio of D to γ and the subscript 2 refers to the transform photograph (the second photo involved in the analysis). Thus equations (7), (8), (9), and (14) yield

$$\underline{\varphi}^2 = \frac{4\, q^{-2}\, 10^{\Delta_2 + \bar{D}_1}}{D_\varphi^2\, p^2(\psi)} \left(K_2 u_o \tau_2\right)^{-1} \tag{15}$$

where the dc term has been suppressed. (The cross product terms in the squaring operation is weighed so heavily to the delta function that they can be ignored.) This equation can be simplified by noting the term $K_2 u_o \tau_2$ is equivalent to a term like $10^{\Delta_3^1}$ in which Δ_3^1 is the optical density arising by exposing film in the scene plane to the laser intensity u_o. This film must be developed along with the transform in order that the constants K be the same. It is not always convenient to expose the third film for the same time used for the transform photo but the identity

$$10^{\Delta_3^1} = 10^{\Delta_3} \frac{u_o \tau_2}{u_3 \tau_3} \tag{16}$$

allows a different exposure time and laser intensity to be used. Thus the expression for the square of the Fourier transform is just

$$\underline{\varphi}^2 = \frac{4(L\lambda)^2}{D_\varphi^2\, p^2} \frac{u_3 \tau_3}{u_2 \tau_2} 10^{\bar{D}_1 - \Delta_3 + \Delta_2} \tag{17}$$

SPECTRUM

The photographic spectrum is obtained from equation (17) by an integration over an elemental area in the transform space as is indicated by

$$f = \int\int \underline{\varphi}^2 \, dk_x \, dk_y = q^{-2} \int\int \underline{\varphi}^2 \, dxdy \tag{18}$$

Since the finite aperture utilized in the scene plane limits the spatial frequency resolution, an elemental area in the transform plane (reciprocally related to the gaussian beam cross section in the scene plane) has constant $\underline{\varphi}^2$. Denoting that area by

$$A = \Xi^2 \pi \left(\frac{L\lambda}{\sigma}\right)^2 \tag{19}$$

The integral is trivial and one obtains the photographic spectrum

$$f = \frac{\pi \Xi^2}{\sigma^2} \underline{\varphi}^2 \tag{20}$$

The constant Ξ expresses that factor of the gaussian half width σ which is effective in the transform process. Further analysis is required to obtain the actual value of Ξ but it is of the order of $\sqrt{2}$ which is the equivalent square pulsewidth of a gaussian function.

The expression thus far derived has not involved the size of the sea photographed, only the photographic density variation. It is possible to envision a situation in which a sinusoidal wave of some fixed angular excursion propagating on the surface could be photographed and result in a photo exactly identical to a wave of different wavelength with the same angular amplitude but photographed from a different height. Using

$$\phi(\bar{k},t) = (2\pi)^{-2} \int_{\bar{x}} \overline{\eta(\bar{x}_o,t)\, \eta(\bar{x}_o+\bar{x},t)}\, e^{-i\bar{k}\cdot\bar{x}} d\bar{x} \tag{21}$$

from Kinsman[3] one can determine that the spectrum is proportional to the area analyzed. Thus the ratio of two spectra is proportional to the ratio of the respective areas. Extending this analogy to the photographic spectrum one can write that the sea spectrum is proportional to the ratio of the sea area to photograph area multiplied by the photographic spectrum. Or then

$$\phi = \alpha \beta^2 f \tag{22}$$

where β is linear reduction factor from the sea to photographic

length. The constant α can be determined by computing the spectrum for a known situation (not necessarily realizable) by equation (21) (modified to have dimensions of wave angle rather than wave height) and also by the photographic technique. The ratio of the two solutions yields

$$\alpha = (2\pi \ln 10)^{-2} \tag{23}$$

The solution for the spectrum is manifest in either equation (24) or (25).

$$\phi = \left\{ \frac{1}{\pi} \left(\frac{L\lambda}{\ln 10}\right)^2 \frac{10^{\Delta_2+\bar{D}_1-\Delta_3}}{\bar{D}^2_{\varphi} p^2(\psi)} \frac{\tau_3}{\tau_2} \frac{u_3}{u_2} \right\} \frac{\beta^2 \Xi^2}{\sigma^2} \tag{24}$$

$$= \left\{ \qquad \right\} \frac{A_s}{\pi\sigma^4} \tag{25}$$

A_s is the area of the sea analyzed and the other terms are previously defined.

EXPERIMENTAL RESULTS

Figure 5 is a composite of the scene photograph, the transform photograph, and an isodensitometer trace of the transform density contours. The photograph was taken from the South Capitol Street Bridge crossing the Anacostia River in D.C. from a height of about 30' in a wind of about 4-5 knots. Since for a given analysis equation (24) is simply a constant times the base ten power of the optical density (letting gamma be one for discussion purposes) the density contours correspond to spectral contours. The radial distance from the dc term is proportional to the wave number of the water wavelength. The spectral information is what is expected for the low wind velocity involved when the analyzed spectral region spans the minimum in the wave velocity-wavelength curve for water waves. The high frequency spectral peak is about 1.5 cm wavelength and the corresponding "gravity wave" is about 4 cm long, as indicated by the peak in the spectrum. It may be noted that the curves of velocity vs wavelength would not give the above values for paired frequencies. The surface tension on the polluted river is probably significantly larger than that for pure water which would shift the null in the velocity curve to longer wavelengths so the measurement is not unreasonable.

Figure 6 is a similar composite of data taken from Wilson Bridge across the Potomac River from a height of 50'. The wind was about 12-16 mph, blowing almost directly into the camera from the north. The bench parameters for this analysis resulted in a large magnification of the region about the dc term in order to

analyze wavelengths approaching the size of the camera field of view. The high frequency peak was beyond the camera resolution and does not show. The low frequency spectral peaking is quite evident in the region around 20 cm water wavelength.

CONCLUSIONS

The small wave theory developed here should allow a useful estimation of the spectrum of the ocean under the conditions of clear or overcast sky, camera depression angle about 45°, use of a polarizing filter, multiple photographs to reveal directional spectra and to obtain spectral smoothing, etc. The technique will have to be compared with the spectra obtained by present installations but should allow an extension of measurements into the capillary wave region. It should be useful in studying the build-up of wave systems (the transient spectral changes) and allow the study of the turbulent structure and energy transfer properties of the air-sea boundary layer. Although the technique is not applicable in all circumstances for which sea clutter data is required, it should allow a tabulation of high frequency spectral characteristics under a wide range of local wind conditions which would enable non-spectral measurements to yield a good estimate of the actual sea conditions.

REFERENCES

1. C.A. Taylor and H. Lipson, "Optical Transforms," Cornell University Press, Ithaca, N.Y., 1964.

2. L.J. Cutrona, E.N. Leith, C.J. Palermo, and L.J. Porcello, "Optical Processing and Filtering Systems," IRE Trans. on Info Theory, June 1960.

3. B. Kinsman, "Wind Waves: Their Generation and Propagation on the Ocean Surface," Prentice-Hall, Englewood Cliffs, N.J., 1965.

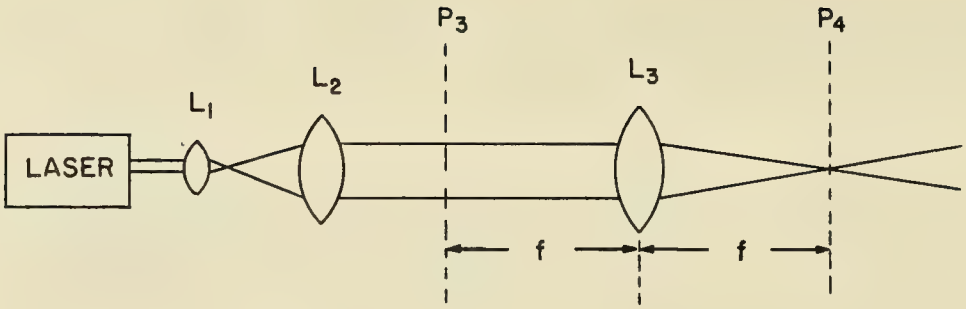

Figure 1

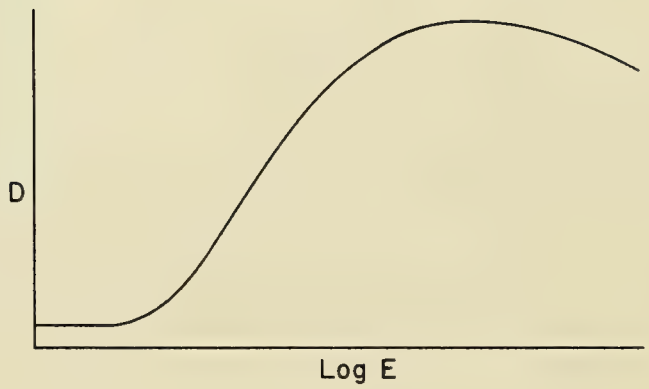

Figure 2

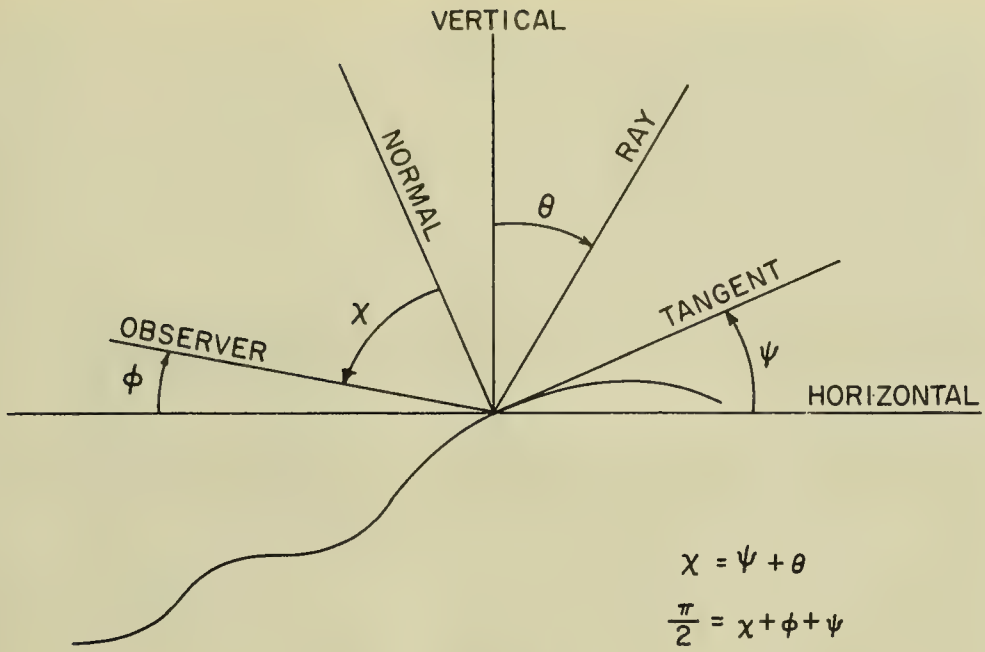

Figure 3

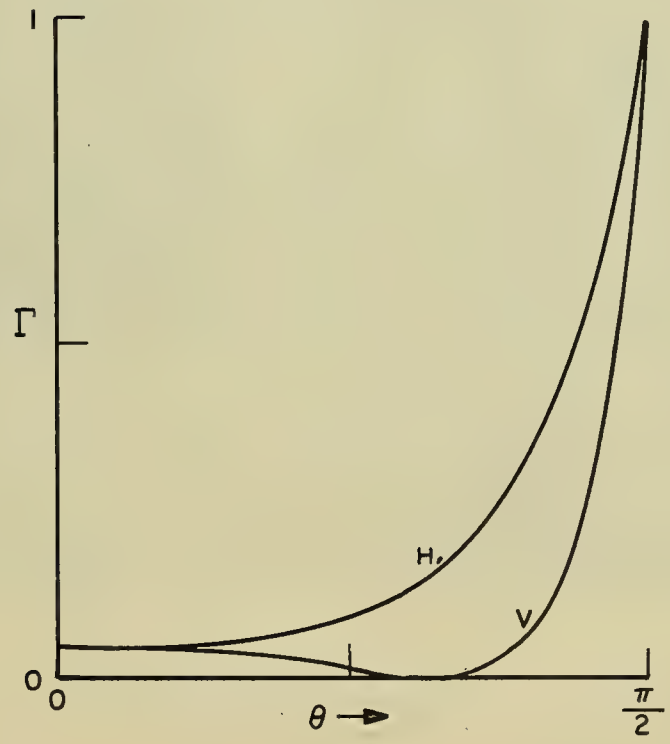

Figure 4

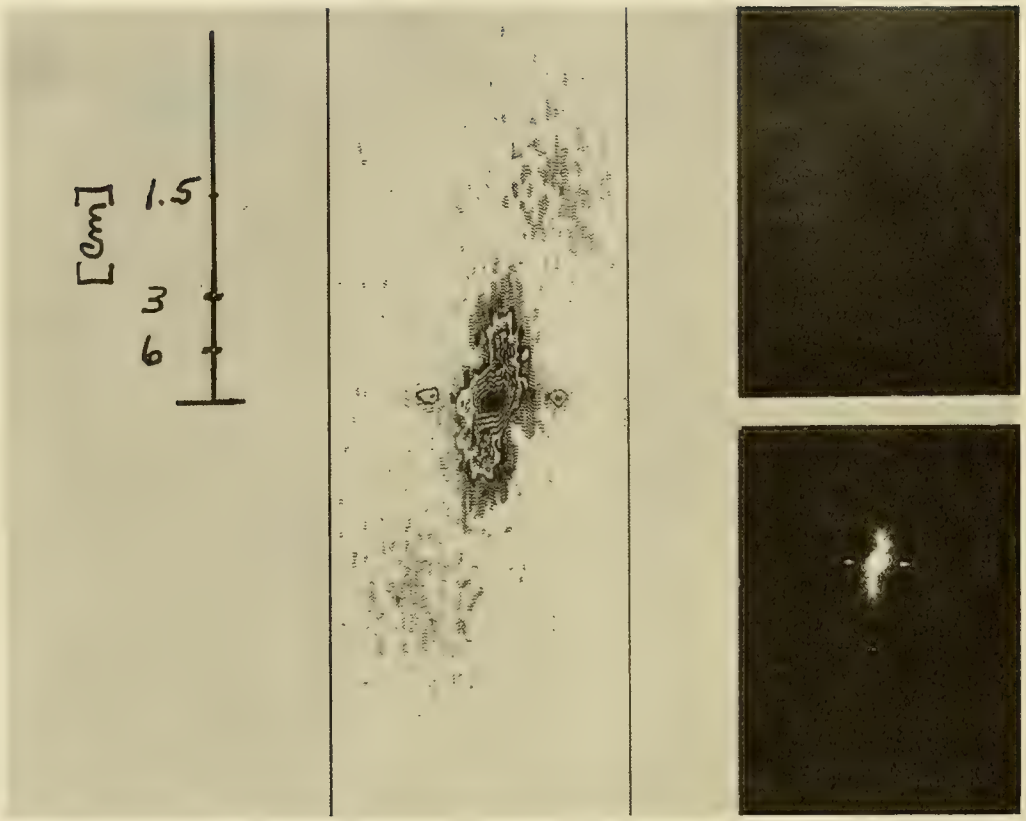

Figure 5

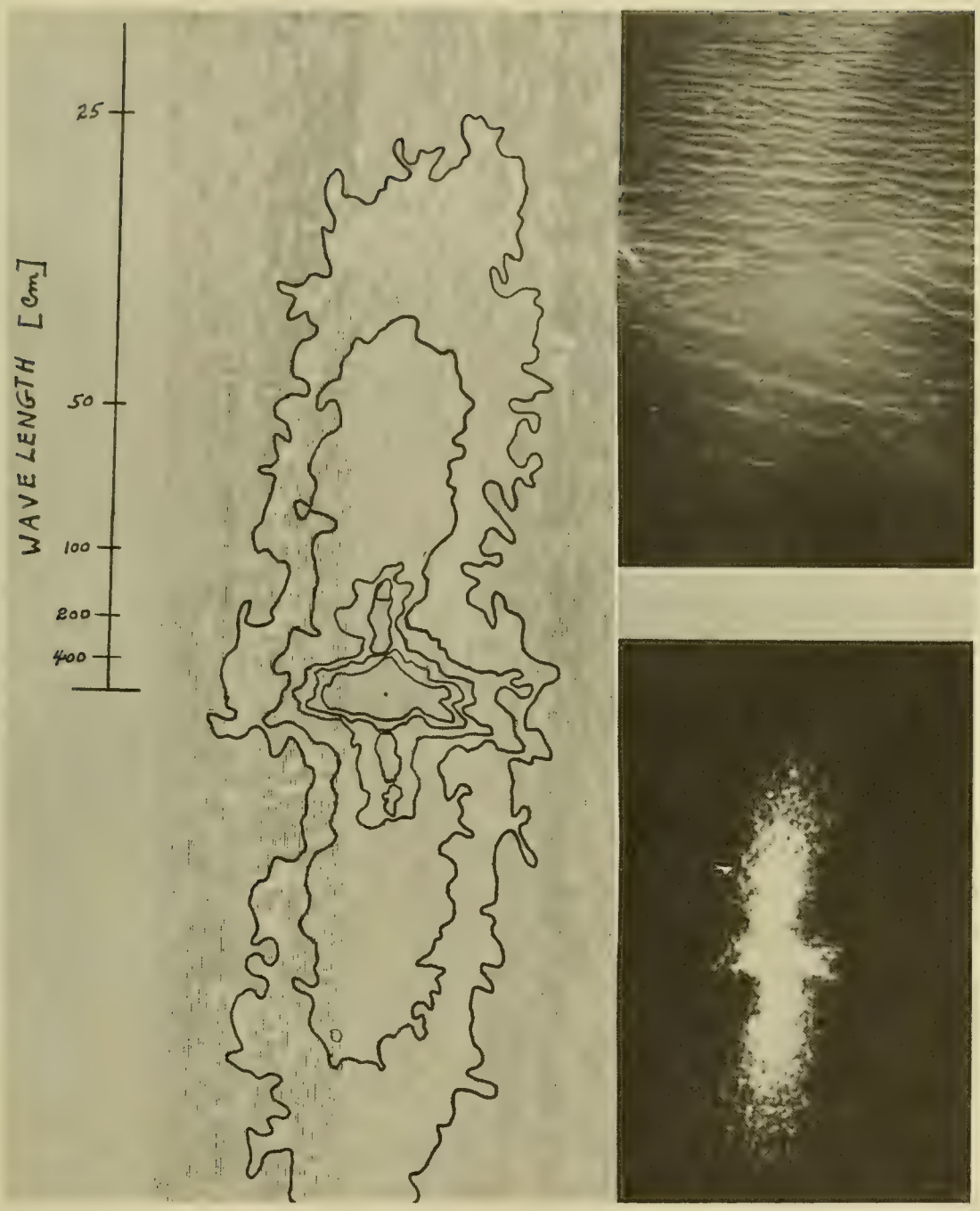

Figure 6

Numerical Prediction of Geostrophic Flow Derived from Sea-Surface Temperature

James G. Welsh
The Travelers Research Center, Inc.
Hartford, Connecticut

INTRODUCTION

The author has previously described the application of the equivalent barotropic model to an ocean of variable depth. This paper extends the model to allow sea-surface temperature prediction and to incorporate the irrotational flow associated with horizontal divergence. A simple approach to deriving a geostrophic flow field from sea-surface temperature fields is described; the inclusion of irrotational flow into the model and the nature of the derived velocity potential for the Gulf Stream are discussed, and experimental forecasts of sea-surface temperature for the western North Atlantic Ocean are shown.

GEOSTROPHIC FLOW EXPRESSED IN TERMS OF SEA-SURFACE TEMPERATURE

Geostrophic flow in the ocean can be computed when both the vertical distribution of horizontal density gradient and the actual flow at some reference level are known. For numerical prediction, these must be known for the area in which prediction is carried out. Unfortunately, it is only for sea-surface temperature that there may be adequate observations to permit a meaningful depiction of the horizontal distribution. This leaves salinity, the flow at a reference level, and the vertical variation of temperature gradient to be described. It will be assumed that salinity is constant, and the flow vanishes at the bottom.

The vertical variation of the horizontal temperature gradient ∇T will be prescribed by

$$\nabla T(z) = \nabla T_s \left(1 - \frac{z}{d}\right)^n \qquad (1)$$

where d is the depth of the ocean, T_s is the surface temperature, and n is a parameter of the model. Note that this prescribes a temperature gradient which has the same direction at all depths and, together with its $n - 1$ derivatives, vanishes at the ocean floor, for $n > 0$. The equation for the vertical shear of the geostrophic flow $\vec{V}$ can be written

$$\frac{\partial}{\partial z}\vec{V}(z) = a\frac{g}{f}\vec{k} \times \nabla T(z) \tag{2}$$

where f is the coriolis parameter and a is the linear coefficient of thermal expansion for sea water. Now Eq. (1) can be substituted into Eq. (2) and the result integrated in the vertical to yield

$$\vec{V}(z) = \frac{agd}{f(n+1)}\left(1 - \frac{z}{d}\right)^{n+1}\vec{k} \times \nabla T_s \tag{3}$$

where the assumption of zero bottom flow has been used. From Eq. (3), derive the further parameters

$$\bar{\vec{V}} \equiv \frac{1}{d}\int_0^d \vec{V}(z)dz = \frac{agd}{f(n+1)(n+2)}\vec{k} \times \nabla T_s , \tag{4}$$

$$A(z) \equiv \frac{\vec{V}(z)}{\bar{\vec{V}}} = (n + 2)\left(1 - \frac{z}{d}\right)^{n+1} , \tag{5}$$

$$\overline{A^2} \equiv \frac{1}{d}\int_0^d [A(z)]^2\, dz = \frac{(n + 2)^2}{2n + 3} , \tag{6}$$

and note that

$$A_0 \equiv A(z = 0) = n + 2 . \tag{7}$$

Furthermore, it follows from Eq. (4) that the stream function $\bar{\psi}$ of the vertically averaged flow $\bar{\vec{V}}$ is given by

$$\bar{\psi} = \frac{agh_0}{f_0(n+1)(n+2)}T_s = kT_s , \tag{8}$$

where

$$k = \frac{agh_0}{f_0(n+1)(n+2)} \tag{9}$$

is the conversion factor, and h_0 and f_0 are suitable mean values for d and f, respectively.

Figure 1 shows the profile $A(z)$ for a selection of values of the parameter n, and Table 1 lists values for A_0, $\overline{A^2}$, and k, a, g, f_0, and h_0, have been assigned the values $1.8 \times 10^{-4}\,°C^{-1}$, 980 cm sec^{-2}, 9×10^{-5} sec^{-1} and 4000 m, respectively.

Table 1

n	0	1	2	3	4	5	6	7	8	9
A_0	2	3	4	5	6	7	8	9	10	11
$\overline{A^2}$	1.33	1.80	2.29	2.78	3.27	3.77	4.27	4.77	5.26	5.76
k*	36.0	12.0	6.00	3.60	2.40	1.70	1.30	1.00	0.80	0.65

* $k \times 10^{-3}(m^2\ sec^{-1}\ °C)$

To select an appropriate value for n, we shall be guided by previous results [1]. These showed values of the vertically integrated stream function at the inflow boundary ranging from zero to 3×10^4 m^2 sec^{-1}. For comparison, the sea-surface temperature for March, 1961 at the inflow boundary ranges from 5 to 20 °C which would require a value of 2000 for the conversion factor k, corresponding to n in the range 4 to 5. After some trial and error tests, a value of 1000 for k was applied to the 31-day mean sea-surface temperature for March, 1960 to give a volume transport comparable with published values of the maximum transport, which is around 80 million m^3 sec^{-1}. Warren [2] and others have questioned whether the actual maximum transport is not somewhat higher than this figure.

THE INCORPORATION OF IRROTATIONAL FLOW

The generation of relative vorticity by horizontal divergence is significant for the numerical ocean-prediction model. In the previous report [1], it was shown that the irrotational flow associated with horizontal divergence can be derived from a velocity potential λ given by

$$\nabla^2\lambda = -\frac{1}{h_0}(\vec{k} \times \nabla\overline{\psi} + \nabla\lambda)\cdot\nabla h \cong -\frac{1}{h_0} J(\overline{\psi}, h) , \qquad (10)$$

where J is the Jacobian derivative. The prediction equation can then be written

$$\left(\nabla^2 - \frac{A_0 f_0^2}{gh_0}\right)\frac{\partial\overline{\psi}}{\partial t} + [\vec{k} \times \nabla\overline{\psi} + \nabla\lambda]\cdot\nabla\left(\overline{A^2}\nabla^2\overline{\psi} + f - \frac{f_0 h}{h_0}\right) = 0, \qquad (11)$$

in which the irrotational flow $\nabla\lambda$ is also used to advect the

Fig. 1 - Isopleths of A(z) for n = 0 to n = 10

"potential vorticity," $[\overline{A^2}\nabla^2\overline{\psi} + f - f_0 h/h_0]$. To implement the irrotational flow, the velocity potential λ is computed at each time step by solving (10). Then (11) is solved for the tendency $\partial\overline{\psi}/\partial t$.

In order to solve for λ , it is necessary to describe λ on the peripheral boundary of the prediction grid. Setting λ to zero on the boundary is not acceptable at the inflow to the prediction area, so an experiment had to be carried out to determine reasonable values. An area (see Fig. 2) was selected with the prediction area inflow well surrounded. The 31-day mean analysis for March, 1960 was used for $\overline{\psi}$, and the velocity potential λ was computed from (10) using zero values on the boundary. The velocity potential is shown in Fig. 3; the units have been converted to degrees Celsius. Note that the rotational flow is directed <u>along</u> the surface isotherms, and that the irrotational flow is directed <u>normal</u> to the λ isotherms.

Consider the velocity potential of Fig. 3. There appears to be a boundary-value distortion on the lower boundary, and perhaps a slight amount on the upper boundary, but the existence of a maximum near 36N, 74W is definite. To the southwest, beyond the computational area, the velocity potential probably is shaped like a trough which contains the Gulf Stream. Although the magnitude of the irrotational flow is an order-of-magnitude less than the rotational flow, its direction, more-or-less normal to the Gulf Stream near Hatteras, allows its effect to be significant for surpressing meander growth and stabilizing the Gulf Stream position.

SEA-SURFACE TEMPERATURE PREDICTION*

This section describes experimental sea-surface temperature (SST) predictions made with the model. The first two experiments were designed to test the flow from the SST conversion scheme. The third experiment is a series of predictions from 5-day SST analysis.

The initial field for the first two experiments was computed from 31 days of ship reports for March, 1960. This long-term analysis is smoothed some but still shows relatively small-scale features, which may or may not be real. The first experiment uses a conversion factor of $1000\ m^2\ sec^{-1}\ °C$, which gives a reasonable mass transport for the Gulf Stream. The second experiment uses $3000\ m^2\ sec^{-1}\ °C$, which corresponds to a mass transport much higher than generally suggested. The values for $\overline{A^2}$ and A_0 were taken directly from Table 1; they are shown together with the flow conversion factors in Table 2. For both experiments, predictions have been carried out to 30 days after the initial map.

---

* The quantity predicted is $\overline{\psi} = kT_s$ where T_s is the sea-surface temperature. Because k is taken to be a constant, it is convenient to label $\overline{\psi}$ in °C and to refer to it as sea-surface temperature.

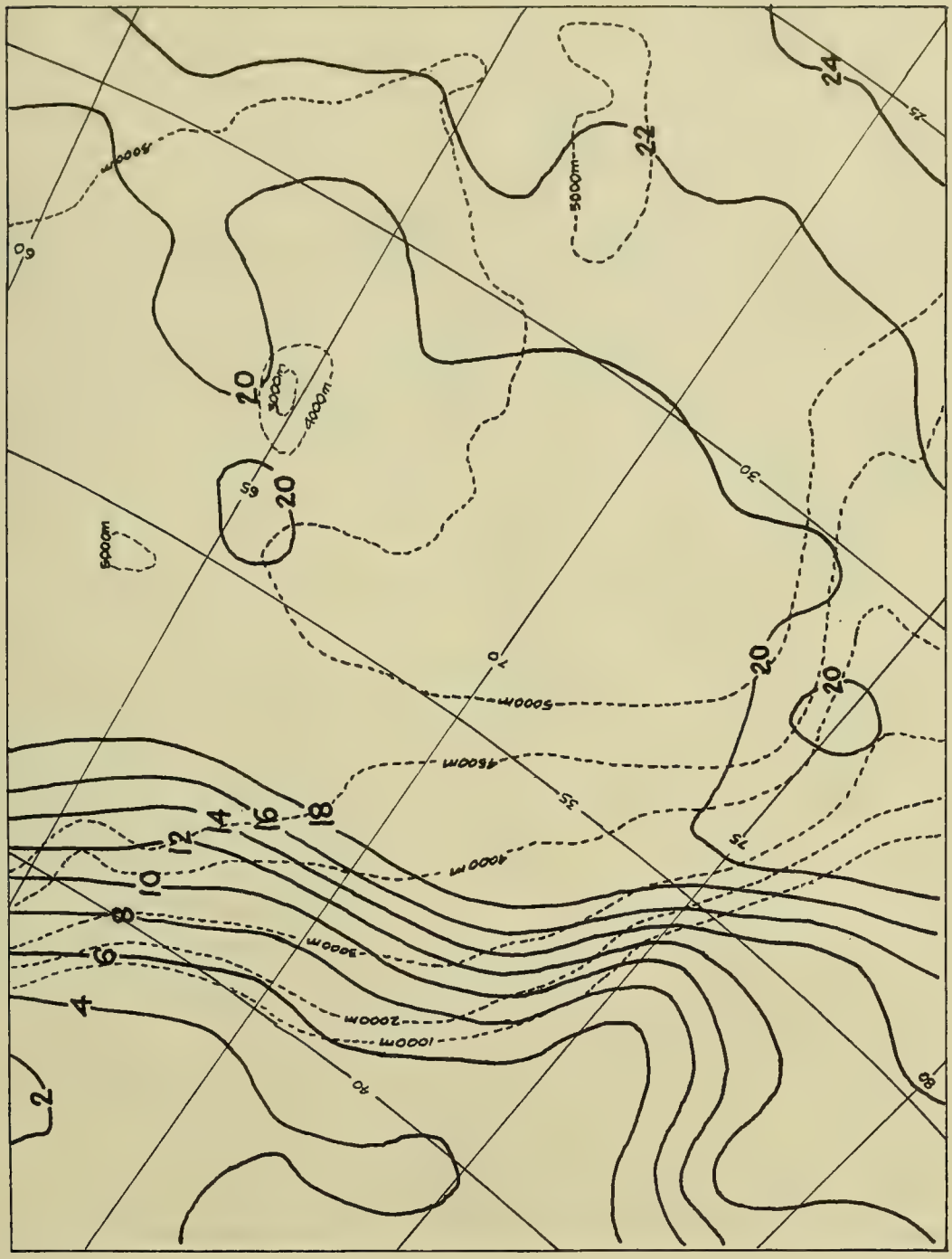

Fig. 2 - SST (°C) map from which velocity potential is computed

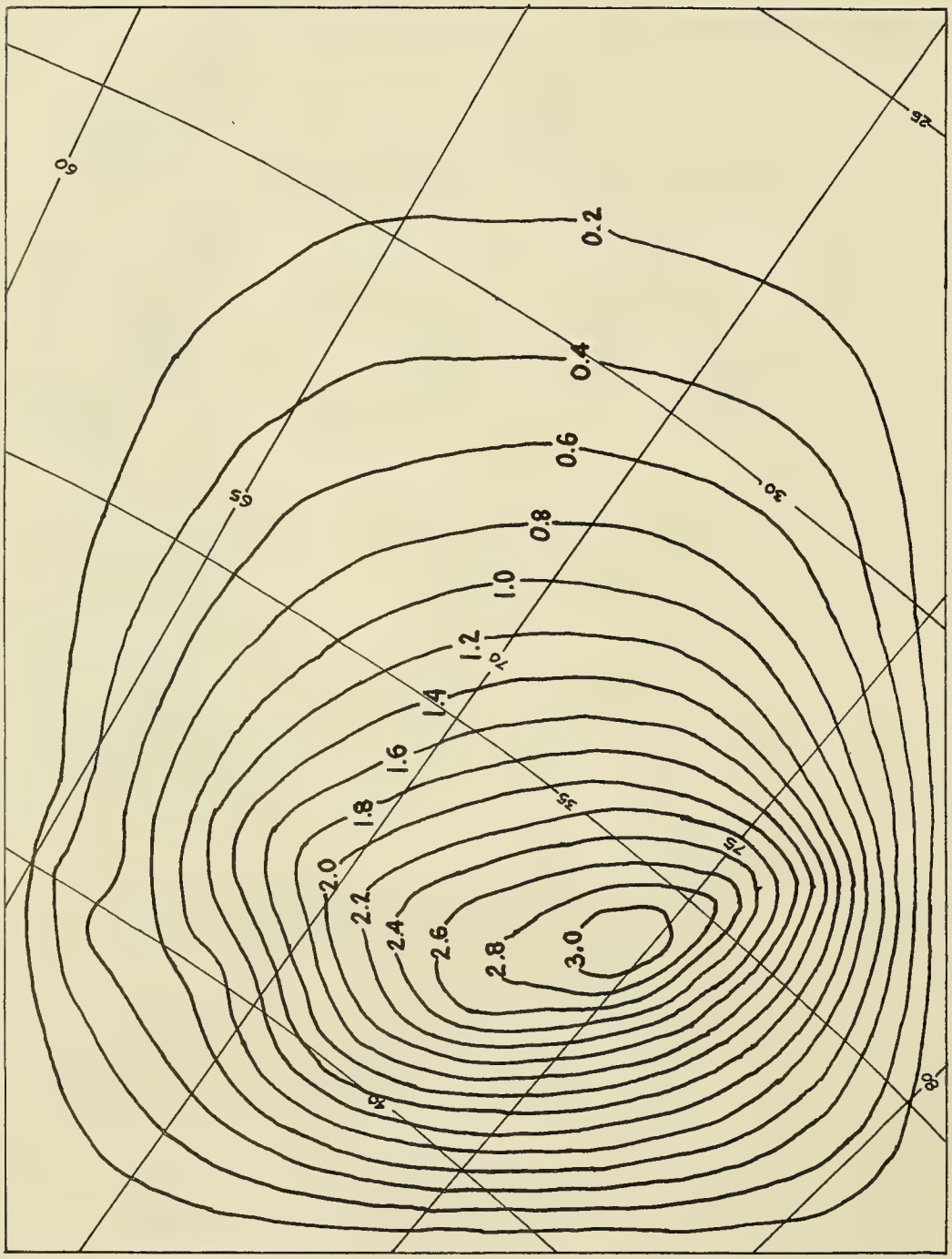

Fig. 3 - Velocity potential labelled in °C

Table 1

	$k(m^2\ sec^{-1}\ °C^{-1})$	$\overline{A^2}$	A_0
Experiment 1	1000	5	9
Experiment 2	3000	3	5.5

To appreciate the results of these experiments, I have plotted the initial and successive 5-day predicted positions of the 16°C isotherm for each experiment in Figs. 4 (Experiment 1) and 5(Experiment 2). A comparison of these two figures shows Experiment 2, with its greater transports, to produce greater development. Although our primary purpose here is only to show the general envelope of predictions, continuity between 5-day positions can be discerned in the vicinity of 65°W, where Experiment 2 clearly predicts faster movements and greater amplitude development. The indicated wave speeds in this area are about 7 cm sec^{-1} for Experiment 1 (Fig. 4) and 18 cm sec^{-1} for Experiment 2 (Fig. 5). Warren has suggested a wave speed of 5 cm sec^{-1}, with which Experiment 1 more closely agrees; as already noted, Experiment 1 gives volume transport in close agreement with accepted values.

For the third experiment, six successive, non-overlapping, 5-day SST analysis were computed for the period March 1-30, 1960. The analysis should be valid for the middle of each time period, i.e., 2.5, 7.5, 12.5, 17.5, 22.5, and 27.5 days into the month. From each analysis, a prediction was made out to day 32.5 (April 1, 1960), with prediction outputs every 5 days after the analysis time. For this experiment, the conversion factor 1500 m sec^{-1} $°C^{-1}$, $\overline{A^2} = 3.5$, and $A_0 = 7.5$ were used.

Unfortunately, the six analysis, are themselves disappointing, for they show poor map-to-map continuity. Moreover, it is the experience of the author that successive, non-overlapping periods of ship reports cannot generally be analyzed with good continuity between maps. It is not surprising, then, that the predictions in this experiment did not bear much resemblence to the verifying analysis. The analyses were simply inadequate.

For all three experiments, a computation grid with about 60 km between gridpoints and time steps of 6 hours were used. The value for f_0/h_0 on the right-hand side of Eq. (11) is 2.5×10^{-5} m^{-1} sec, which corresponds to $f_0 = 1 \times 10^{-5}$ sec^{-1} for $h_0 = 4000$ m. This represents a reduction of the effect of the bottom considerably greater than the reduction used in our previous report.

Fig. 4 - Successive 5-day positions of the 16°C isotherm for Experiment 1, k = 1000 m^2 sec^{-1} $°C^{-1}$

Fig. 5 - Successive 5-day positions of the 16 °C isotherm for Experiment 2, k = 1000 m^2 sec^{-1} $°C^{-1}$

Early experiments with SST predictions, not implementing irrotational flow, showed severe sensitivity of the inflow pattern to bottom weight. That SST should be more sensitive than the hypothetical flow field used in our previous work is probably related to the confinement of the SST gradient to a more narrow band which is also located further up the continental rise. The incorporation of convergent flow reduced the sensitivity to bottom weight and allowed more realistic development near the inflow, but the full bottom weight, $f_0/h_0 = 2.25 \times 10^{-8}\ m^{-1}\ sec$, could still not be permitted. The value $2.5 \times 10^{-9}\ m^{-1}\ sec$ for f_0/h_0 seems to give relatively undisturbed flow near the inflow boundary.

SUMMARY

Plausible predictions of sea-surface temperature can now be made using the equivalent barotropic model--plausible in that predicted wave speeds, meanders, and mass transport are close to observed values. The lack of meaningful synoptic SST analysis, however, does not allow a definitive testing of the model. Future work must be directed toward improving the analysis of sea-surface temperature.

REFERENCES

[1]Arnason, G. and J.G. Welsh, 1966: Numerical flow prediction with the equivalent-barotropic model. Part IV of "Studies of techniques for the analysis and prediction of temperature in the ocean." Interim Report, under Contract N62306-1675 with the U. S. Naval Oceanographic Office.

[2]Warren, B.A., 1963: Topographical influences on the path of the Gulf Stream. Tellus, Vol. 15, pp. 167-183.

THE FNWF SOUND MAP PROGRAM

Captain Paul M. Wolff, U. S. Navy
LCDR Peter R. Tatro, U. S. Navy
LCDR Louis D. Megehee, Jr., U. S. Navy
Fleet Numerical Weather Facility
Monterey, California

ABSTRACT

A high precision computer ray trace program developed at the Fleet Numerical Weather Facility in Monterey is used as a research tool to investigate the effects of temperature and salinity variations on the path of sound through the sea. In one case, the temperature profile as a function of depth is described in terms of its basic parameters: sea surface temperature, mixed layer depth, thermocline gradient, and 400 meter temperature. These are systematically varied, individually and in combinations, to determine their effect on convergence zone formation.

In a second case, a highly detailed cross-section of the Gulf Stream taken by XBT's is used to demonstrate the effect of water mass and current boundaries on convergence zone propagation.

INTRODUCTION

A ray tracing program developed at the Fleet Numerical Weather Facility for use on the CDC 1604, 3200 and 6400 computers has been used as a research tool to investigate the effects of oceanic variability on the paths of sound through the sea. The program is a highly sophisticated one incorporating a correction for the curvature of the earth and utilizing a time step of 1/128th of a second or less. It operates in two dimensional x - z space, and is capable of accepting any arbitrary specification of the sound velocity in x and z. This represents a significant improvement over earlier numerical ray trace programs, many of which were capable of handling only linear gradients of sound velocity or sound velocity profiles which could be

described by a particular mathematical function.

THE RAY TRACE PROGRAM

In practice, the inputs to the program are temperature and salinity as a function of depth for as many positions in x space as are desired. The program utilizes Wilson's equation to convert these variables to sound velocity. The only other variables which must be specified initially are the source depth and the bottom depth.

The program is capable of handling reflections at the air-sea and sea-bottom interfaces and of accepting an irregular bottom profile. It incorporates several options, such as terminating a ray after the first convergence zone, or after a specified number of surface or bottom reflections.

Three types of output are available from this program. Figure 1 shows the printer output showing the values for all the computed parameters at each time step. Figure 2 shows a condensed printer output which shows only the initial point, the intermediate turning points, and the end point of a ray. In this example, the terminate at end of first convergence zone option has been utilized. Figure 3 shows a plotted output. This is plotted off-line on a CALCOMP plotter. The upper box in this figure extends in depth from the surface to 500 feet, and in range from zero to 7200 yards. It displays the direct path sound field. The lower box covers the same depth range, but the horizontal range is from 50,000 to 80,000 yards. The sound which was all strongly refracted downward in the upper picture is turned at depth and often returns to the surface at a considerable range to form a convergence zone. The lower box displays the convergence zone. From any of these three forms of output it is possible to determine the range and width of the convergence zone, and from the printer output the depth of water required for convergence zone formation.

The ray trace program has been described in detail by Ayres et al (1966).

EFFECT OF SOUND VELOCITY MICROSTRUCTURE

Careful in-situ direct measurements of the sound velocity as a function of depth by means of a velocimeter lowering indicate that the sound velocity profile is not a smooth curve as it is often depicted, but rather that it has a sort of perturbation superimposed on it with an average wave length of approximately 10 meters and an

TATRO 23 INITIAL DEPTH = 00060.003 FEET

INITIAL ANGLE = +02.0000

TIME (SECONDS)	ANGLE(RADIANS)	RANGE (KYDS)	DEPTH (FEET)	N		PATH LENGTH (KY)
0030000.00000000	+000.0349065	00000.000	00060.003	3	INITIAL	00000.000
0030000.00781250	+000.0347725	00000.012	00061.349	3		00000.012
0030000.01562500	+000.0346384	00000.025	00062.707	3		00000.025
0030000.02343750	+000.0345040	00000.038	00064.040	3		00000.038
0030000.03125000	+000.0343694	00000.051	00065.386	3		00000.051
0030000.03906250	+000.0342350	00000.064	00066.718	3		00000.064
0030000.04687500	+000.0341006	00000.077	00068.051	3		00000.077
0030000.05468750	+000.0339664	00000.089	00069.371	3		00000.089
0030000.06250000	+000.0338323	00000.102	00070.691	3		00000.102
0030000.07031250	+000.0336984	00000.115	00071.999	3		00000.115
0030000.07812500	+000.0335646	00000.129	00073.306	3		00000.129
0030000.08593750	+000.0334310	00000.142	00074.613	3		00000.142
0030000.09375000	+000.0332975	00000.155	00075.907	3		00000.155
0030000.10156250	+000.0331642	00000.167	00077.202	3		00000.168
0030000.10937500	+000.0330311	00000.180	00078.483	3		00000.180
0030000.11718750	+000.0328981	00000.193	00079.765	3		00000.193
0030000.12500000	+000.0327653	00000.206	00081.046	3		00000.206
0030000.13281250	+000.0326327	00000.219	00082.315	3		00000.219
0030000.14062500	+000.0325001	00000.232	00083.571	3		00000.232
0030000.14843750	+000.0323678	00000.246	00084.840	3		00000.246
0030000.15625000	+000.0322355	00000.258	00086.096	3		00000.258
0030000.16406250	+000.0321034	00000.271	00087.339	3		00000.271
0030000.17187500	+000.0319715	00000.284	00088.595	3		00000.284
0030000.17968750	+000.0318397	00000.297	00089.825	3		00000.297
0030000.18750000	+000.0317081	00000.310	00091.068	3		00000.310
0030000.19531250	+000.0315766	00000.323	00092.299	3		00000.323
0030000.20312500	+000.0314453	00000.335	00093.516	3		00000.336
0030000.21093750	+000.0313141	00000.348	00094.734	3		00000.348
0030000.21875000	+000.0311831	00000.361	00095.951	3		00000.361
0030000.22656250	+000.0310522	00000.375	00097.169	3		00000.375
0030000.23437500	+000.0309214	00000.388	00098.373	3		00000.388
0030000.24218750	+000.0307908	00000.401	00099.565	3		00000.401
0030000.25000000	+000.0306601	00000.413	00100.757	3		00000.414
0030000.25781250	+000.0305294	00000.426	00101.949	3		00000.427
0030000.26562500	+000.0303987	00000.439	00103.141	3		00000.439
0030000.27343750	+000.0302680	00000.452	00104.320	3		00000.452
0030000.28125000	+000.0301374	00000.465	00105.486	3		00000.465
0030000.28906250	+000.0300067	00000.479	00106.652	3		00000.479
0030000.29687500	+000.0298759	00000.492	00107.819	3		00000.492
0030000.30468750	+000.0297453	00000.504	00108.985	3		00000.505
0030000.31250000	+000.0296146	00000.517	00110.138	3		00000.518
0030000.32031250	+000.0294840	00000.530	00111.279	3		00000.530
0030000.32812500	+000.0293532	00000.543	00112.432	3		00000.543
0030000.33593750	+000.0292226	00000.556	00113.560	3		00000.556
0030000.34375000	+000.0290919	00000.569	00114.701	3		00000.569
0030000.35156250	+000.0289613	00000.581	00115.829	3		00000.582
0030000.35937500	+000.0288305	00000.594	00116.956	3		00000.596
0030000.36718750	+000.0286998	00000.608	00118.071	3		00000.608
0030000.37500000	+000.0285692	00000.621	00119.186	3		00000.621
0030000.38281250	+000.0284384	00000.634	00120.288	3		00000.634
0030000.39062500	+000.0283077	00000.647	00121.391	3		00000.647
0030000.39843750	+000.0281771	00000.660	00122.493	3		00000.660
0030000.40625000	+000.0280464	00000.672	00123.582	3		00000.673
0030000.41406250	+000.0279157	00000.685	00124.671	3		00000.686
0030000.42187500	+000.0277850	00000.698	00125.761	3		00000.699
0030000.42968750	+000.0276544	00000.711	00126.837	3		00000.711
0030000.43750000	+000.0275236	00000.725	00127.901	3		00000.725
0030000.44531250	+000.0273929	00000.738	00128.978	3		00000.738
0030000.45312500	+000.0272623	00000.750	00130.041	3		00000.751

Figure 1

```
 JORDAN 03P00S 112P20W 240115Z APR 1967  INITIAL DEPTH =      14 FEET
INITIAL ANGLE = -15.0000
 TIME (SECONDS)     ANGLE(RADIANS)  RANGE (KYDS)    DEPTH (FEET)   A              PATH LENGTH(KYDS)
0000000.00000000     -000.2617993   00000.000       00013.994      0  INITIAL        00030.000
0000000.01074528     +000.2611377   00000.016       00000.000      2  SURFACE        00030.017
0000016.47847151     -000.1514654   00026.587       22801.834      2  BOTTOM         00027.524
   1 SURFACE REFLECTIONS            0 BOTTOM  REFLECTIONS

 JORDAN 03P00S 112P20W 240115Z APR 1967  INITIAL DEPTH =      14 FEET
INITIAL ANGLE = -14.0000
 TIME (SECONDS)     ANGLE(RADIANS)  RANGE (KYDS)    DEPTH (FEET)   A              PATH LENGTH(KYDS)
0000000.00000000     -000.2443460   00000.000       00013.994      2  INITIAL        00030.000
0000000.01149797     +000.2436815   00000.018       00000.000      2  SURFACE        00030.018
0000017.78520262     -000.1181790   00028.560       22801.834      2  BOTTOM         00029.733
   1 SURFACE REFLECTIONS            0 BOTTOM  REFLECTIONS

 JORDAN 03P00S 112P20W 240115Z APR 1967  INITIAL DEPTH =      14 FEET
INITIAL ANGLE = -13.0000
 TIME (SECONDS)     ANGLE(RADIANS)  RANGE (KYDS)    DEPTH (FEET)   A              PATH LENGTH(KYDS)
0000000.00000000     -000.2268927   00000.000       00013.994      2  INITIAL        00030.000
0000000.01236820     +000.2262257   00000.019       00000.000      2  SURFACE        00030.020
0000019.62944829     -000.0759828   00031.354       22801.834      2  BOTTOM         00032.854
   1 SURFACE REFLECTIONS            0 BOTTOM  REFLECTIONS

 JORDAN 03P00S 112P20W 240115Z APR 1967  INITIAL DEPTH =      14 FEET
INITIAL ANGLE = -12.0000
 TIME (SECONDS)     ANGLE(RADIANS)  RANGE (KYDS)    DEPTH (FEET)   A              PATH LENGTH(KYDS)
0000000.00000000     -000.2094393   00000.000       00013.994      2  INITIAL        00030.000
0000000.01338517     +000.2082903   00000.021       00000.000      2  SURFACE        00030.021
0000023.37243986     -000.0000000   00038.311       22511.095      3  TURNING        00039.251
0000046.73158419     +000.2080935   00076.551       00000.000      2  SURFACE        00078.430
0000047.11718750     +000.2941206   00077.215       00510.721      3 ENDOFRAY        00079.118
   2 SURFACE REFLECTIONS            0 BOTTOM  REFLECTIONS

 JORDAN 03P00S 112P20W 240115Z APR 1967  INITIAL DEPTH =      14 FEET
INITIAL ANGLE = -11.0000
 TIME (SECONDS)     ANGLE(RADIANS)  RANGE (KYDS)    DEPTH (FEET)   A              PATH LENGTH(KYDS)
0000000.00000000     -000.1919862   00000.000       00013.994      3  INITIAL        00030.000
0000000.01458942     +000.1913146   00000.024       00000.000      2  SURFACE        00030.024
0000022.93891143     -000.0000000   00037.556       21525.062      3  TURNING        00038.441
0000045.86315405     +000.1916847   00075.110       00000.000      2  SURFACE        00076.858
0000046.26562500     +000.2825782   00075.754       00507.107      3 ENDOFRAY        00077.524
   2 SURFACE REFLECTIONS            0 BOTTOM  REFLECTIONS

 JORDAN 03P00S 112P20W 240115Z APR 1967  INITIAL DEPTH =      14 FEET
INITIAL ANGLE = -10.0000
 TIME (SECONDS)     ANGLE(RADIANS)  RANGE (KYDS)    DEPTH (FEET)   A              PATH LENGTH(KYDS)
0000000.00000000     -000.1745328   00000.000       00013.994      3  INITIAL        00030.000
0000000.01605367     +000.1731823   00000.026       00000.000      2  SURFACE        00030.026
0000022.50343632     -000.0000000   00036.820       20534.245      3  TURNING        00037.630
0000044.99089229     +000.1730325   00073.516       00000.000      2  SURFACE        00073.234
0000045.41406250     +000.2704702   00074.235       00503.608      3 ENDOFRAY        00075.933
   2 SURFACE REFLECTIONS            0 BOTTOM  REFLECTIONS
```

Figure 2

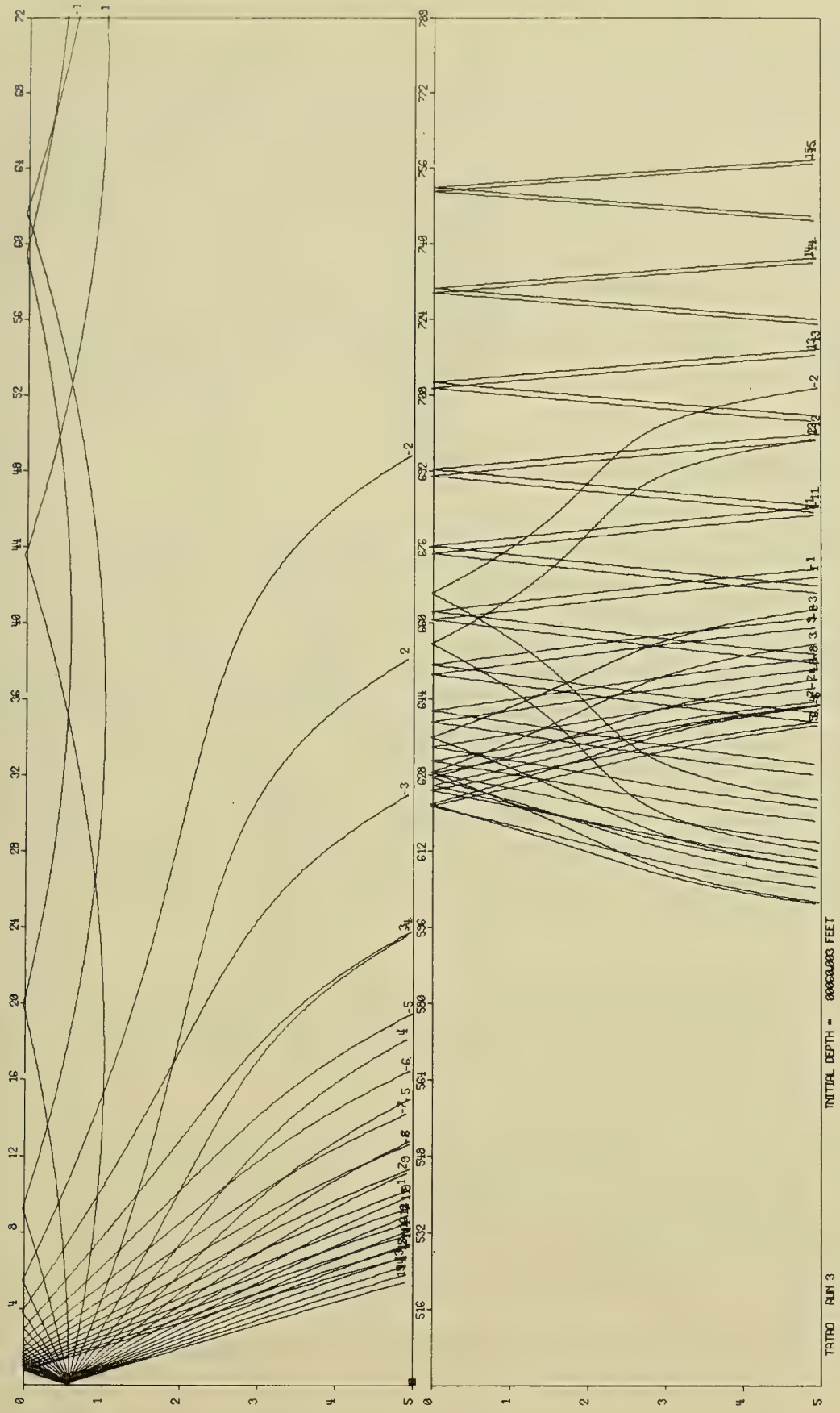

Figure 3

amplitude of approximately 1/2 meter per second (PIIP, 1963). The first question which must be answered, then, is to what extent this microstructure in the sea affects the path of sound. To answer this, a measured profile was carefully digitized using 120 points in depth which preserved all the "wiggles" and a Ray Trace run as far as the first convergence zone. Then the same profile was digitized using 54 data points, and finally 20 data points corresponding to standard oceanographic depths. Figure 4 shows a section of the basic profile and how it was smoothed by successively fewer data points. The range to the first convergence zone agreed in all three cases within less than 150 yards. It was concluded from this that a fairly smooth average profile for a point in space and time is sufficient to describe the sound field at that point.

CONVERGENCE ZONE RANGE PREDICTION

The presence or absence of a convergence zone and the range to the zone when one exists are tactically useful pieces of information. It has been shown that the ray trace program is capable of determining a very precise range; however, to run this program for enough points to adequately cover the area of interest to the Navy on a daily basis would be prohibitive in terms of computer time required. What is needed is a simpler method of prediction. It was decided to attack this problem by a variation of parameters scheme. First a rather standard "typical" temperature trace was determined. Figure 5 shows this profile. The parameters which were considered to be of importance were (1) the sea surface temperature (SST), (2) the mixed layer depth (MLD), (3) the thermocline gradient (∇T) and (4) the 400 meter temperature (T400). These parameters were varied, one at a time, while holding the others constant.

First five profiles were determined which had sea surface temperatures ranging from 14°C to 22°C (Figure 6). These were run through the ray trace program to determine the convergence zone range for a 60 foot source depth. Figure 7 shows a plot of range vs. temperature for these profiles.

Next the basic profile was modified to cover a variety of mixed layer depths, varying from 20 meters to 200 meters (Figure 8). The convergence zone ranges for these profiles were plotted on the range vs. temperature plot determined earlier, and an "equivalent temperature change" was determined for each layer depth. Figure 9 shows a plot of equivalent temperature change (ΔTMLD) versus layer depth.

The next step was to modify the basic profile to cover a range of

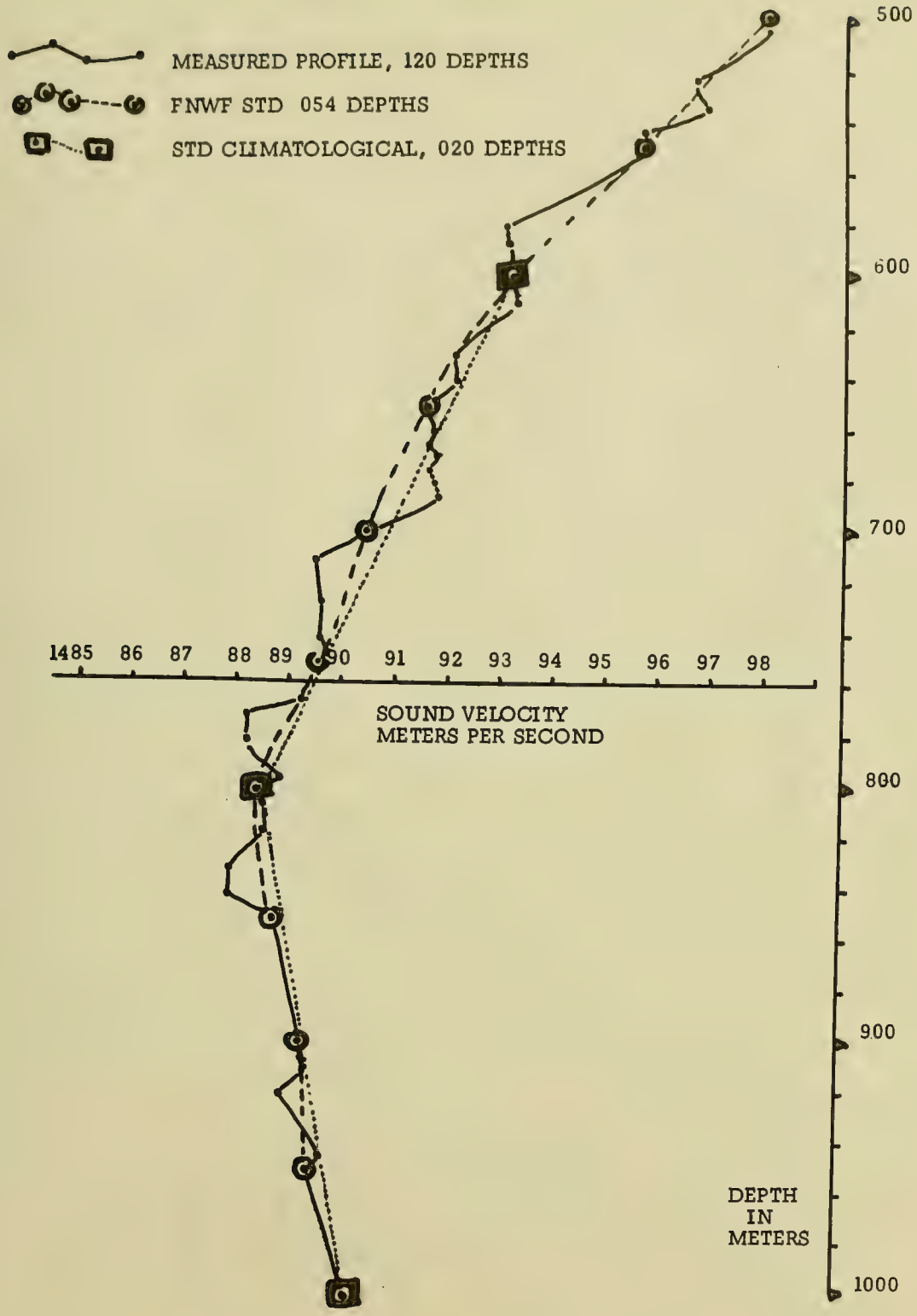
MEASURED PROFILE, 120 DEPTHS
FNWF STD 054 DEPTHS
STD CLIMATOLOGICAL, 020 DEPTHS
1485
86
87
88
89
90
91
92
93
94
95
96
97
98
SOUND VELOCITY
METERS PER SECOND
500
600
700
800
900
1000
DEPTH
IN
METERS

Figure 4

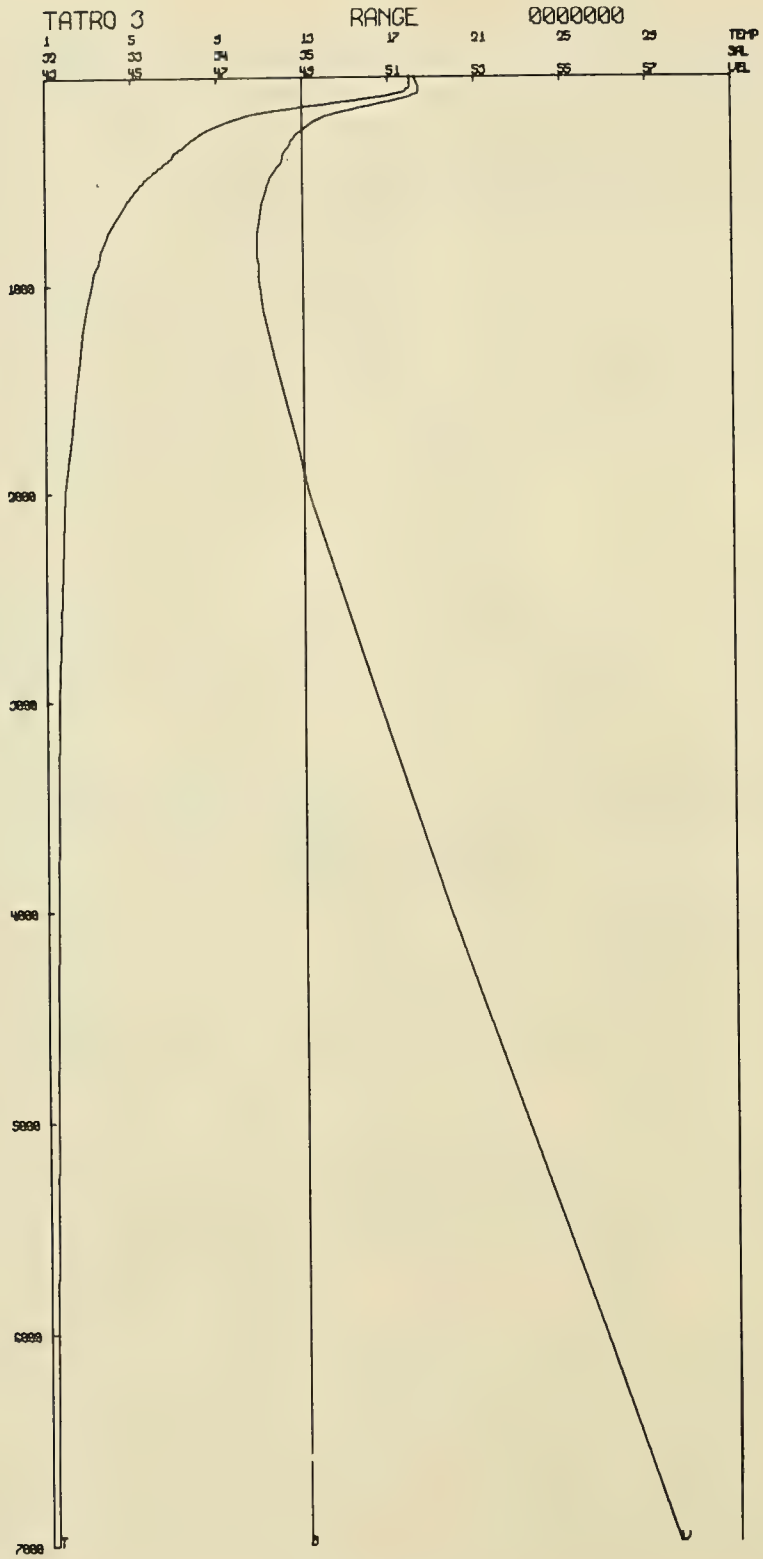
TATRO 3
RANGE
0000000
TEMP
SAL
VEL
1000
2000
3000
4000
5000
6000
7000

Figure 5

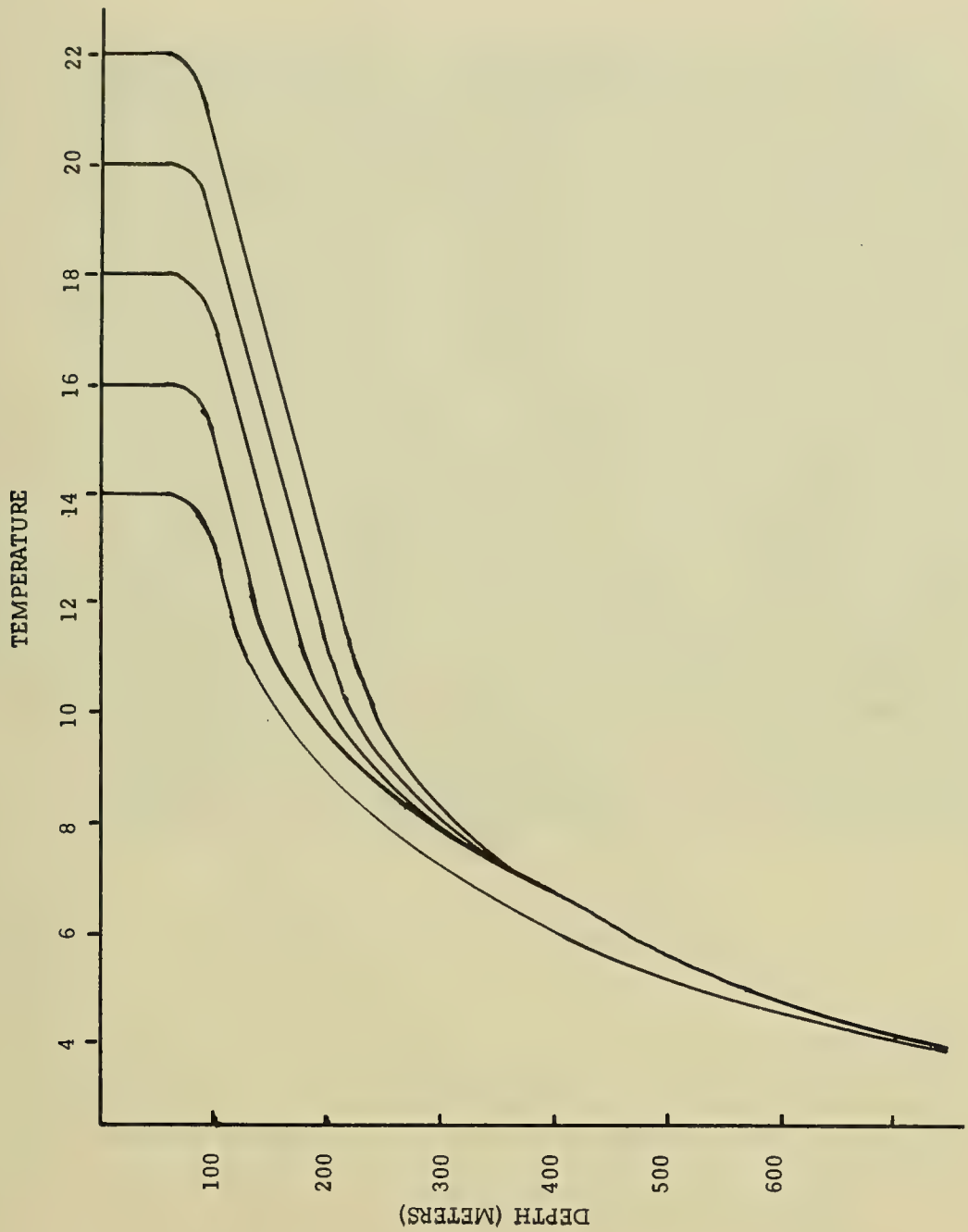

Fig. 6 - Variation of sea surface temperature

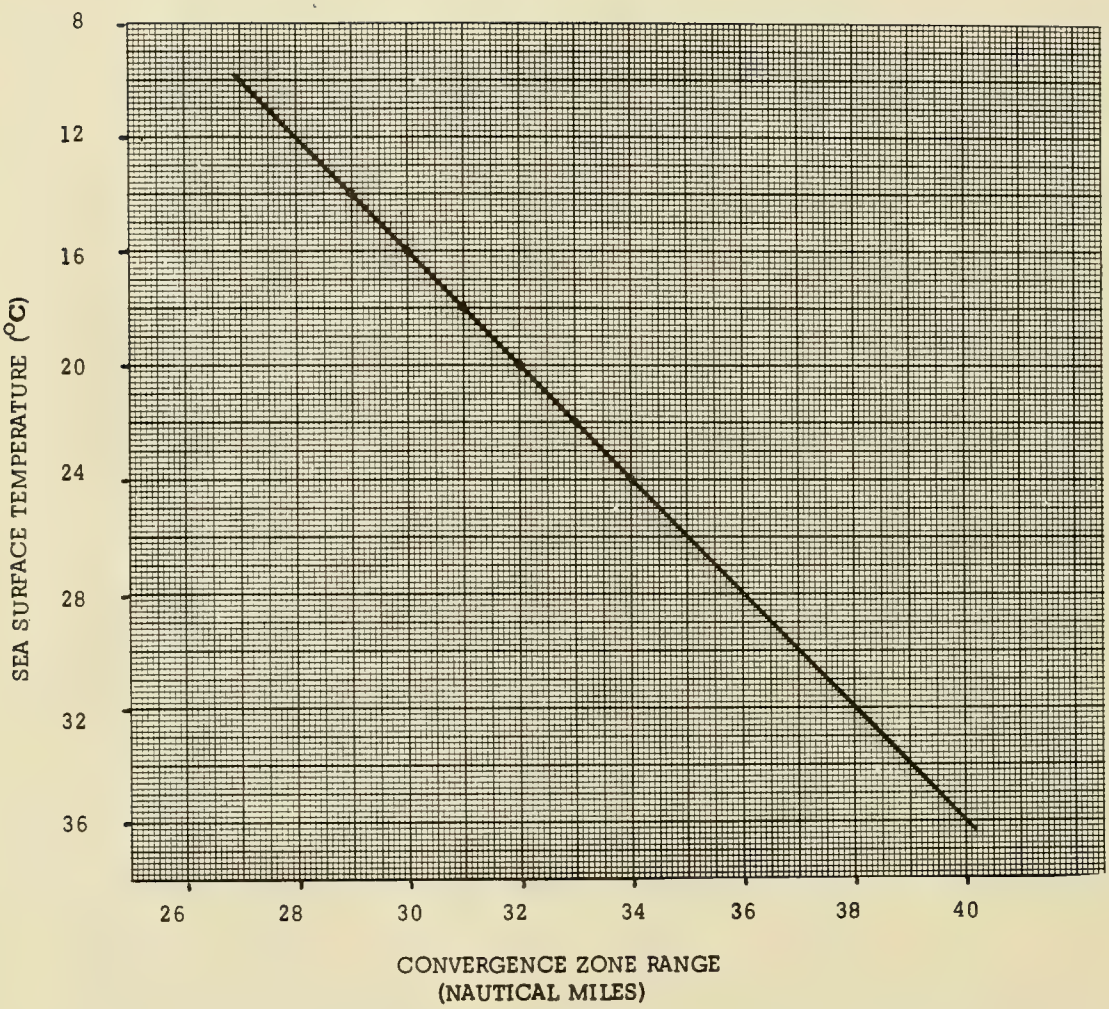
8
12
16
20
24
28
32
36
SEA SURFACE TEMPERATURE (°C)
26
28
30
32
34
36
38
40
CONVERGENCE ZONE RANGE
(NAUTICAL MILES)

Figure 7

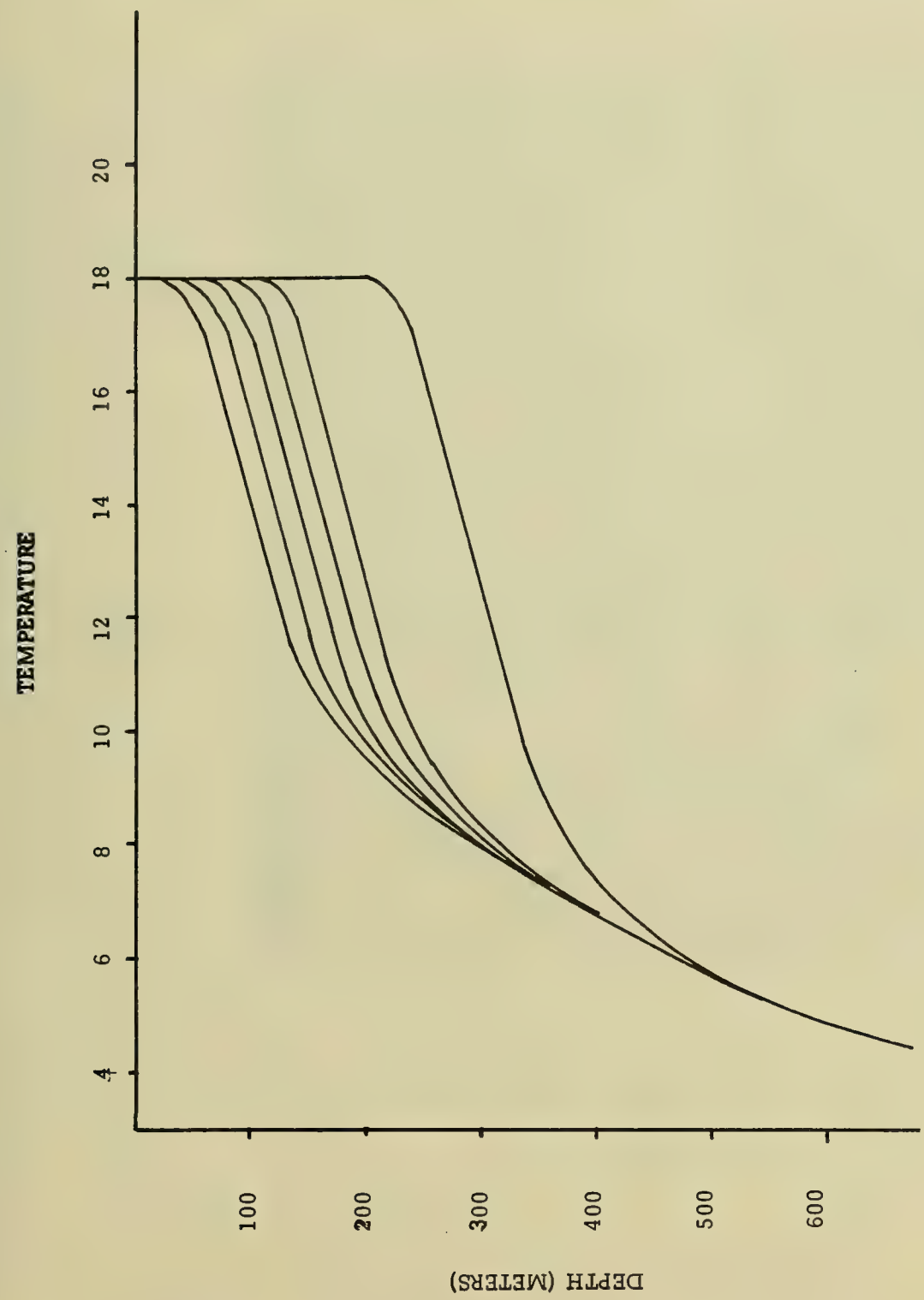

Fig. 8 - Variation of mixed layer depth

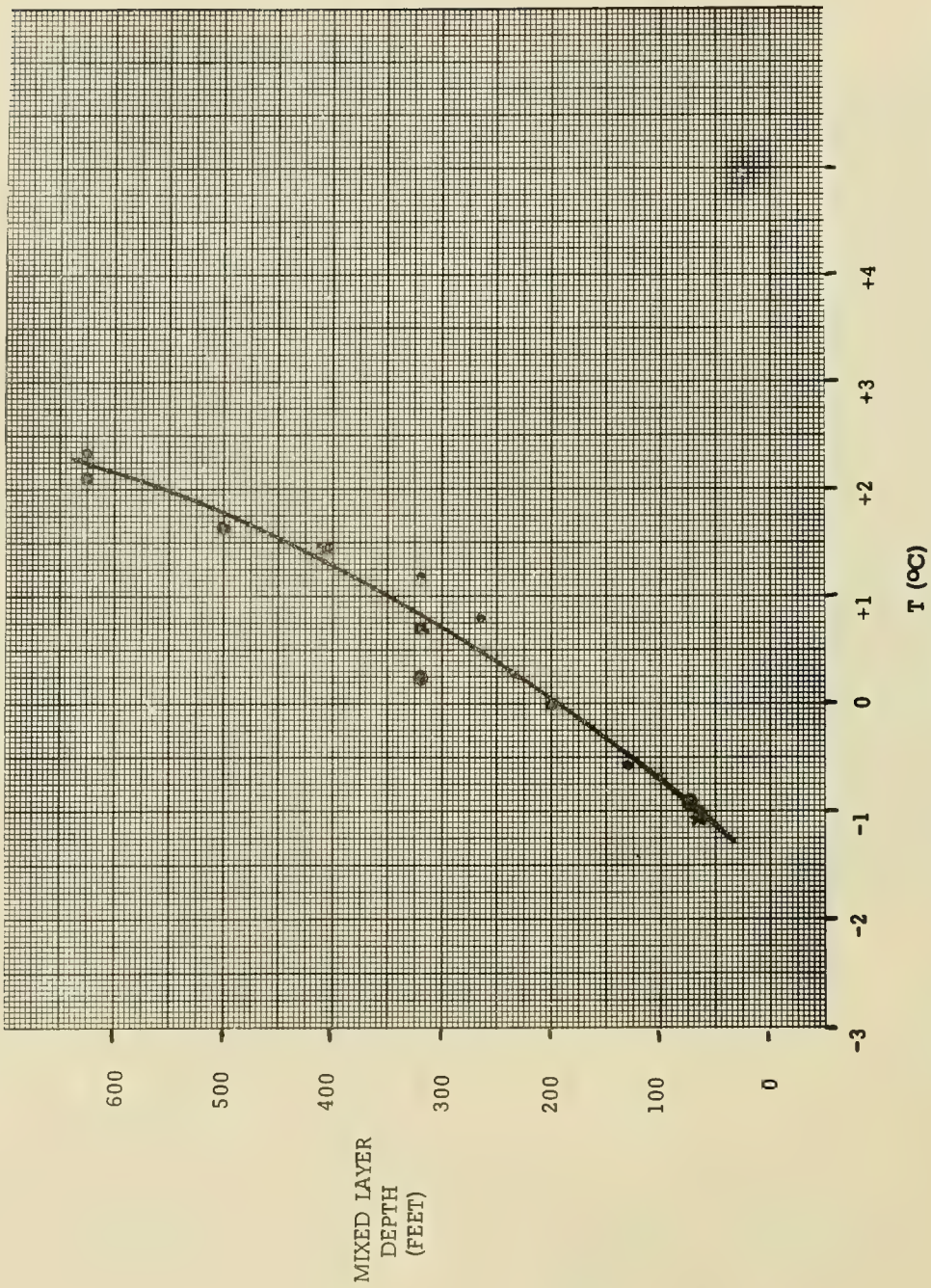

Figure 9

thermocline gradients varying from $1^{o}F$ per 100 feet to $10^{o}F$ per 100 feet (Figure 10). As before, the convergence zone ranges were converted to equivalent temperature changes and plotted (Figure 11).

Finally, the 400 m temperature was varied over a range from $5^{o}C$ to $12^{o}C$ while holding all other parameters constant. Figure 12 shows the profiles; these were run through the ray trace program, converted to equivalent temperature changes and plotted (Figure 13).

As a last step, the parameters were varied in pairs to check the interactions. The warmest and coldest sea surface temperatures were run with the shallowest and deepest layer depths, etc. All results were converted to equivalent temperature changes and compared with existing plots. In all cases they agreed quite well.

With these relationships established, it is possible to predict convergence zone range if the four critical parameters are known. It is necessary only to add the three temperature corrections to the sea surface temperature to obtain an adjusted temperature:

$$T(ADJ) = SST + \Delta T(MLD) + \Delta T\ (\nabla T) + \Delta T(T400)$$

and use this adjusted temperature to enter the Temperature versus Range plot.

VERIFICATION

To determine the accuracy of the prediction system, twenty measured temperature and salinity profiles, half from the Atlantic and half from the Pacific, were run through the ray trace program, and the convergence zone ranges obtained were compared with the ranges predicted using the series of graphs. For these 20 runs the largest error found was 1.1 nautical miles, and the mean error was 0.5 nautical miles. The prediction system tended to predict longer ranges than the ray trace showed. This is certainly due at least in part to the assumption of a constant 35 parts per thousand salinity which was made in determining the effects of the parameters. Lower salinities, at the surface which are generally the case, would result in lower surface sound velocities and shorter convergence zone ranges.

APPLICABILITY AND LIMITATIONS

The prediction scheme as derived seems to be equally applicable in the Atlantic and the Pacific Oceans. It fails

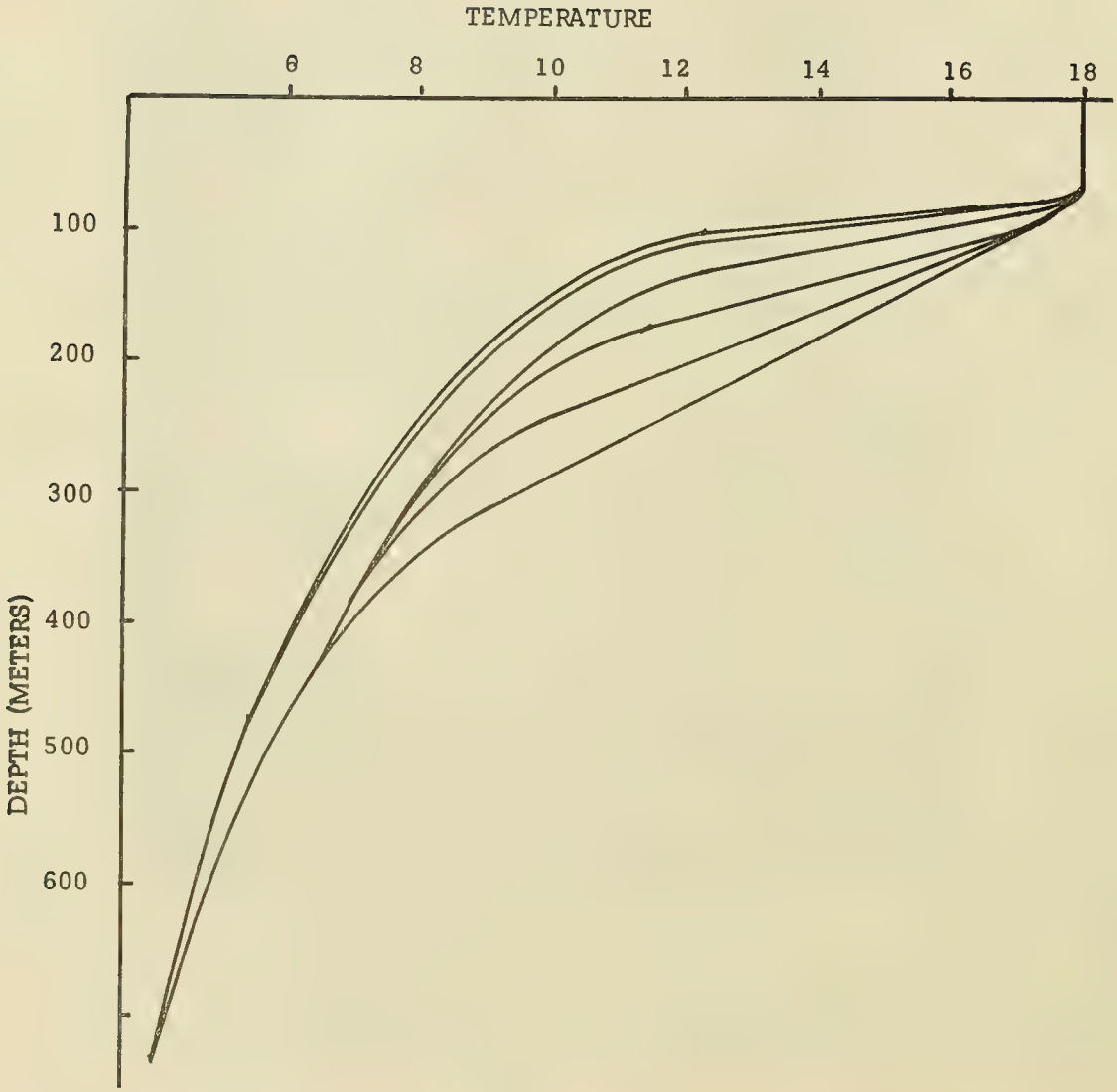

Fig. 10 - Variation of thermocline gradient

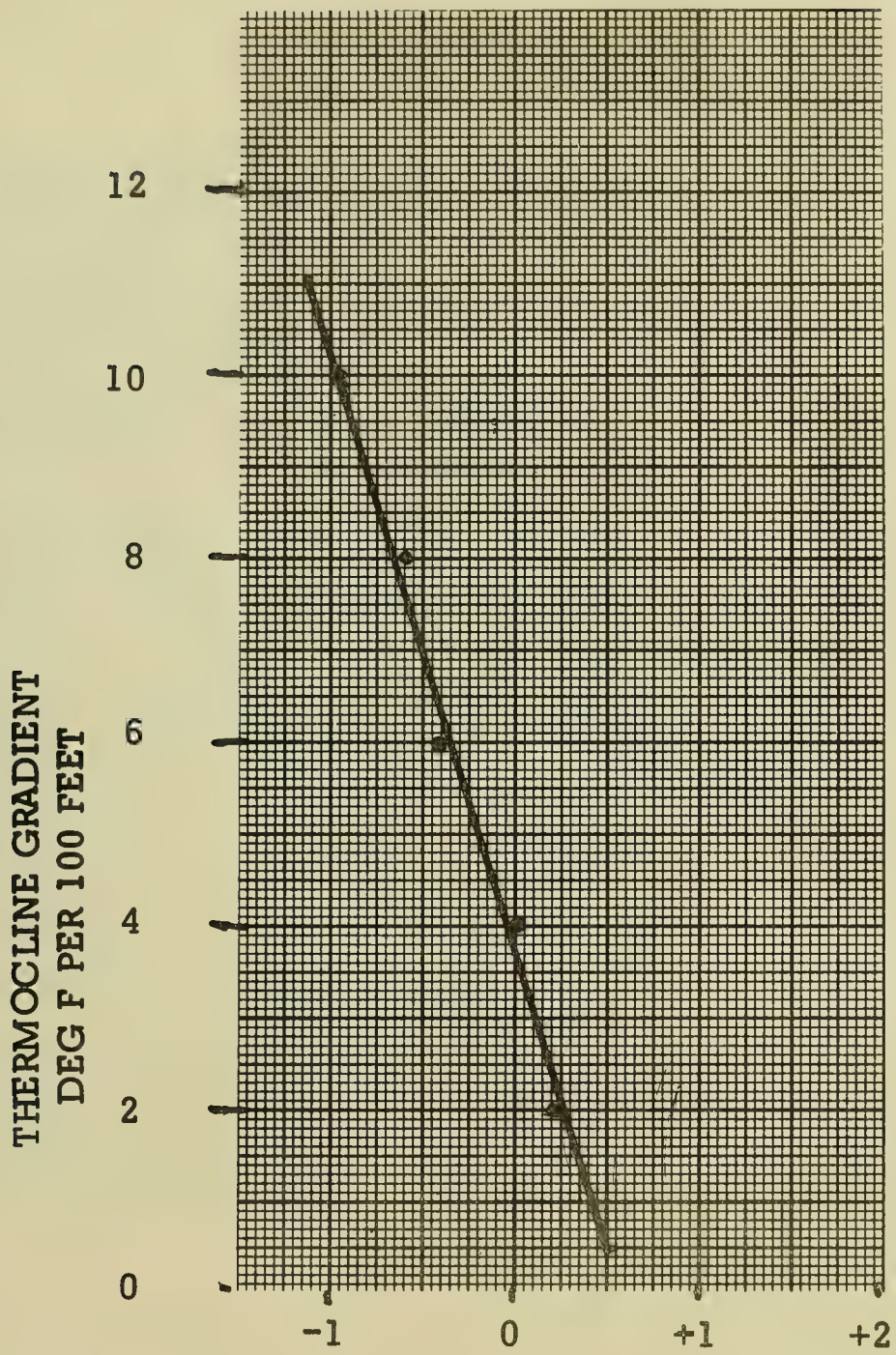

Fig. 11 - Temperature correction for thermocline gradient

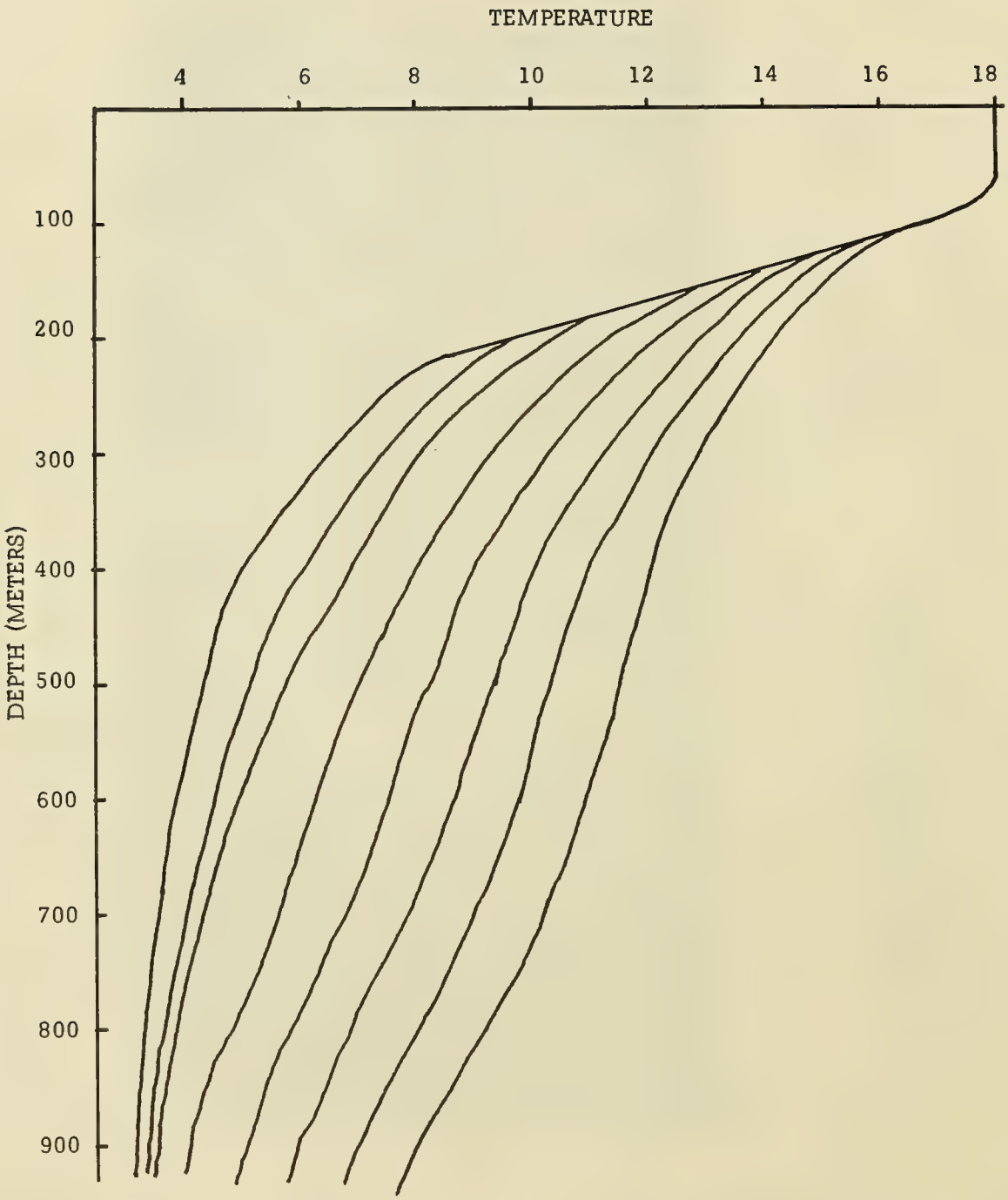

Fig. 12 - Variation of 400 meter temperature

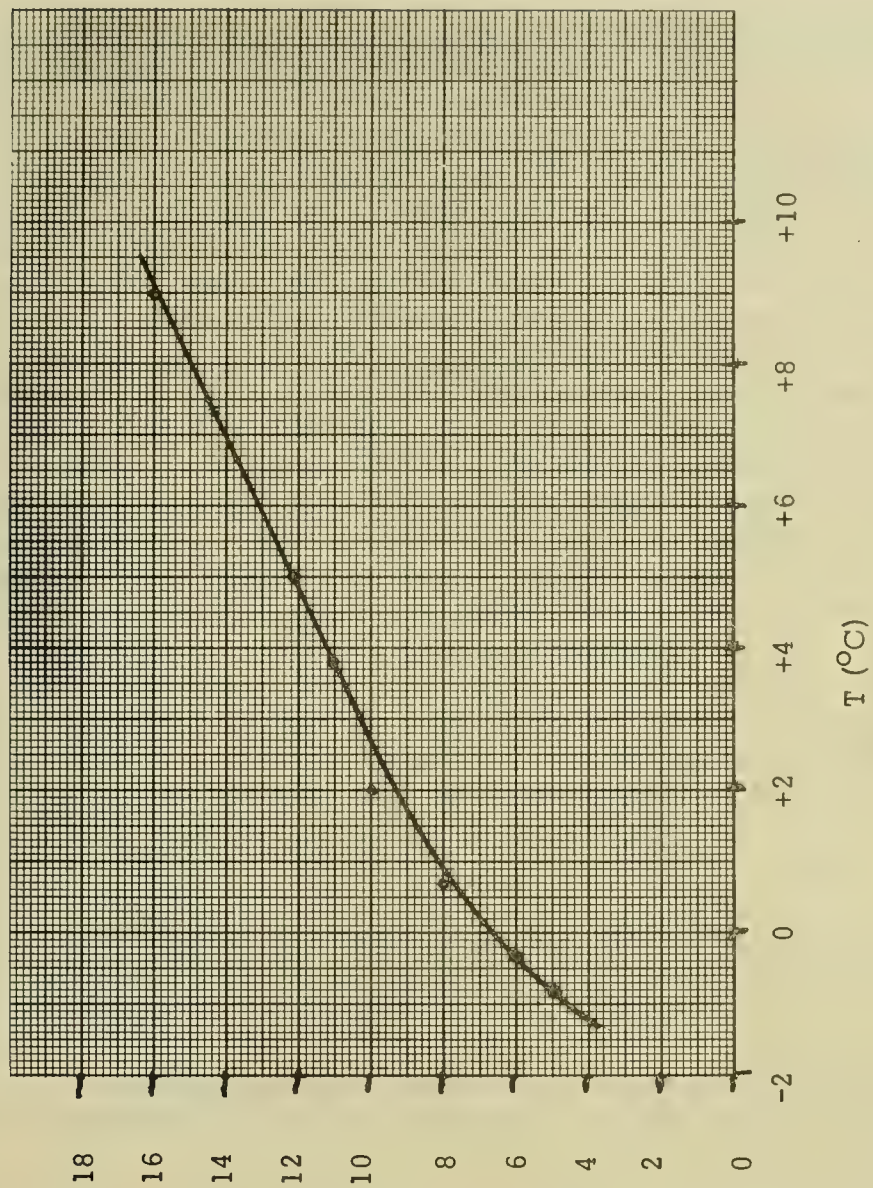

Fig. 13 - Temperature correction due to 400 meter temperature

completely, however, in the Mediterranean or any other area where the water conditions approach isothermal and a half-channel sound velocity profile results. Possibly the addition of a deeper temperature parameter will allow the extension of this system to cover these cases.

EFFECTS OF CURRENT BOUNDARIES

Near current and water mass boundaries the horizontal gradients of temperature and salinity, and thus sound velocity, become quite large. To investigate the effects of these large local gradients, a highly detailed cross-section of the Gulf Stream taken with expendable BT's by Sippican and the Woods Hole Oceanographic Institution was digitized into 71 profiles. Figure 14 shows the cross section used, and the locations of the sources which were initially considered. Sources 1 and 2 were in a cold secondary front which extended up to about 150 meters. Sources 3 and 4 were taken on the warm side of the Main Gulf Stream wall and run through the wall. Source 4 was also run away from the wall into an area of fairly homogeneous water. Sources 5 and 6 are on the cold side of the main wall and were also run through the wall. In all cases, a convergence zone was formed; however, they were generally broader and more diffuse than the well defined zones found in an area of horizontal homogeniety, and in many cases did not reach the surface. Figure 15 shows the convergence zone formed from source 4 running through the Gulf Stream wall. On this plot the depth scale is from 0 to 2000 feet rather than 0 to 500 as before. The convergence zone formed is a subsurface one at approximately 25 nautical miles. Figure 16 shows a run from the same source in the opposite direction. In this case a surface convergence zone is formed at 33.7 nautical miles.

CONCLUSIONS

Based on the Ray Trace runs which have been described here and others of a similar nature, the following conclusions have been drawn:

1. The micro-structure in the sound velocity profile is essentially self-cancelling. It does not affect the convergence zone parameters.

2. In areas of reasonable horizontal homogeniety it is possible to predict convergence zone range by empirical methods if the temperature structure is known.

3. In areas of high local horizontal gradients, convergence

zone formation is highly variable and may often be a function of the direction from the source. In these areas the only reliable method of prediction is to use a computer program.

BIBLIOGRAPHY

PIIP, Ants T. Precision Sound Velocity Profiles in the Ocean, Volume I, Technical Report No. 3, Columbia University Geophysical Field Station, 1963.

Ayres, E., P. M. Wolff, L. Carstensen and H. C. Ayres. A Ray Tracing Program for a Digital Computer, Fleet Numerical Weather Facility Informal Manuscript, 1966.

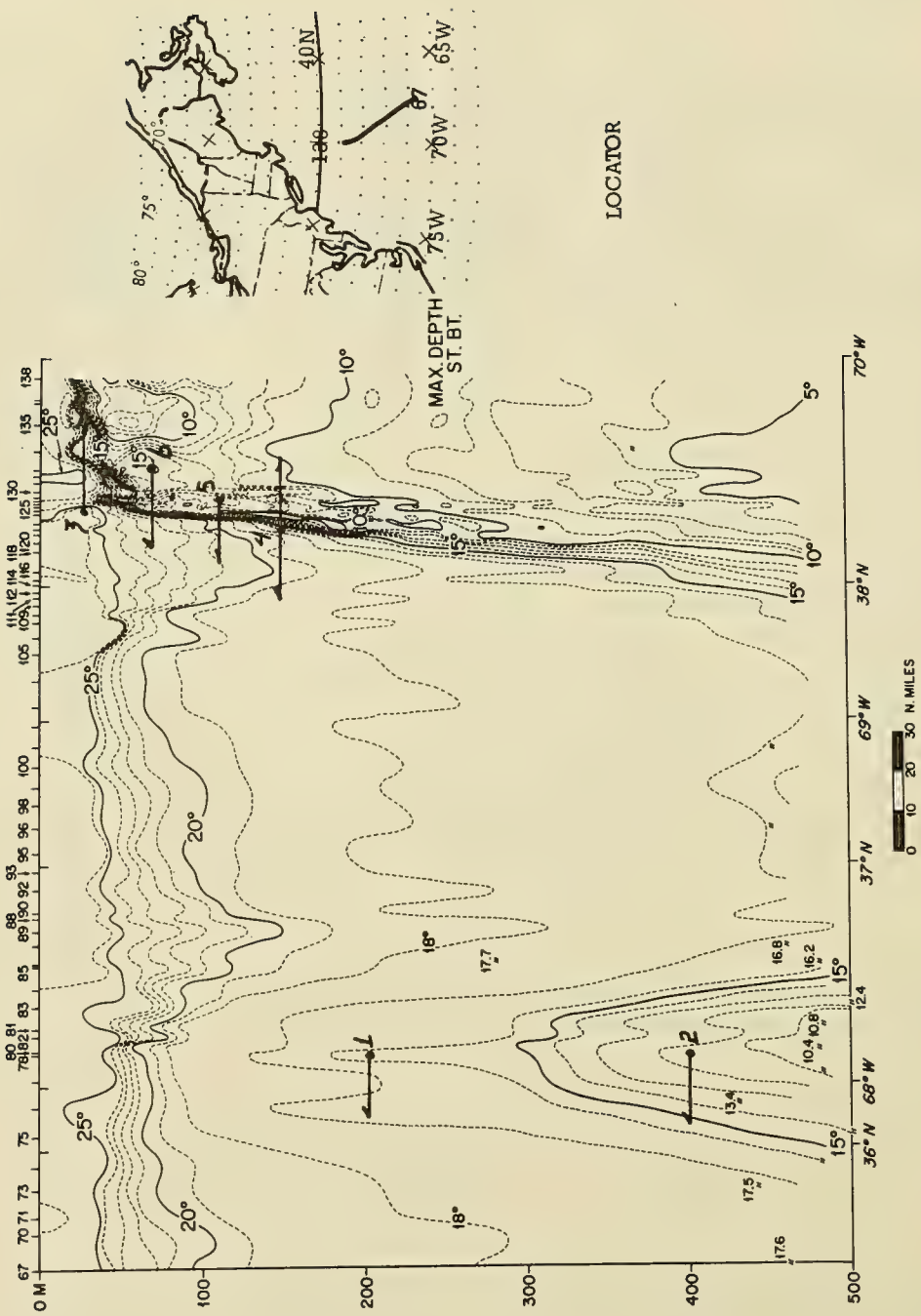

Fig. 14 - An XBT section through the Gulf Stream Labrador current boundary (courtesy Sippican and WHOI)

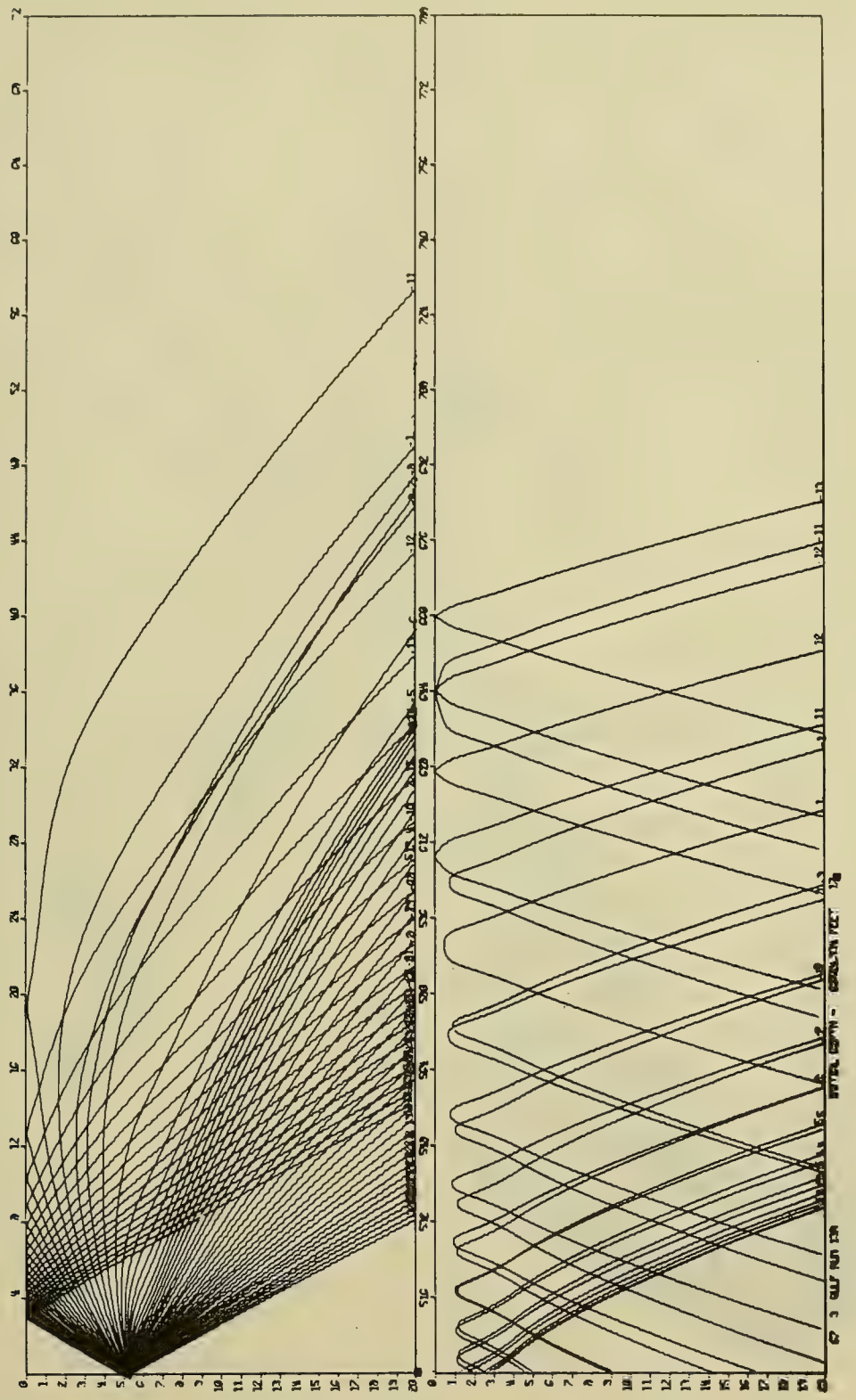

Figure 15

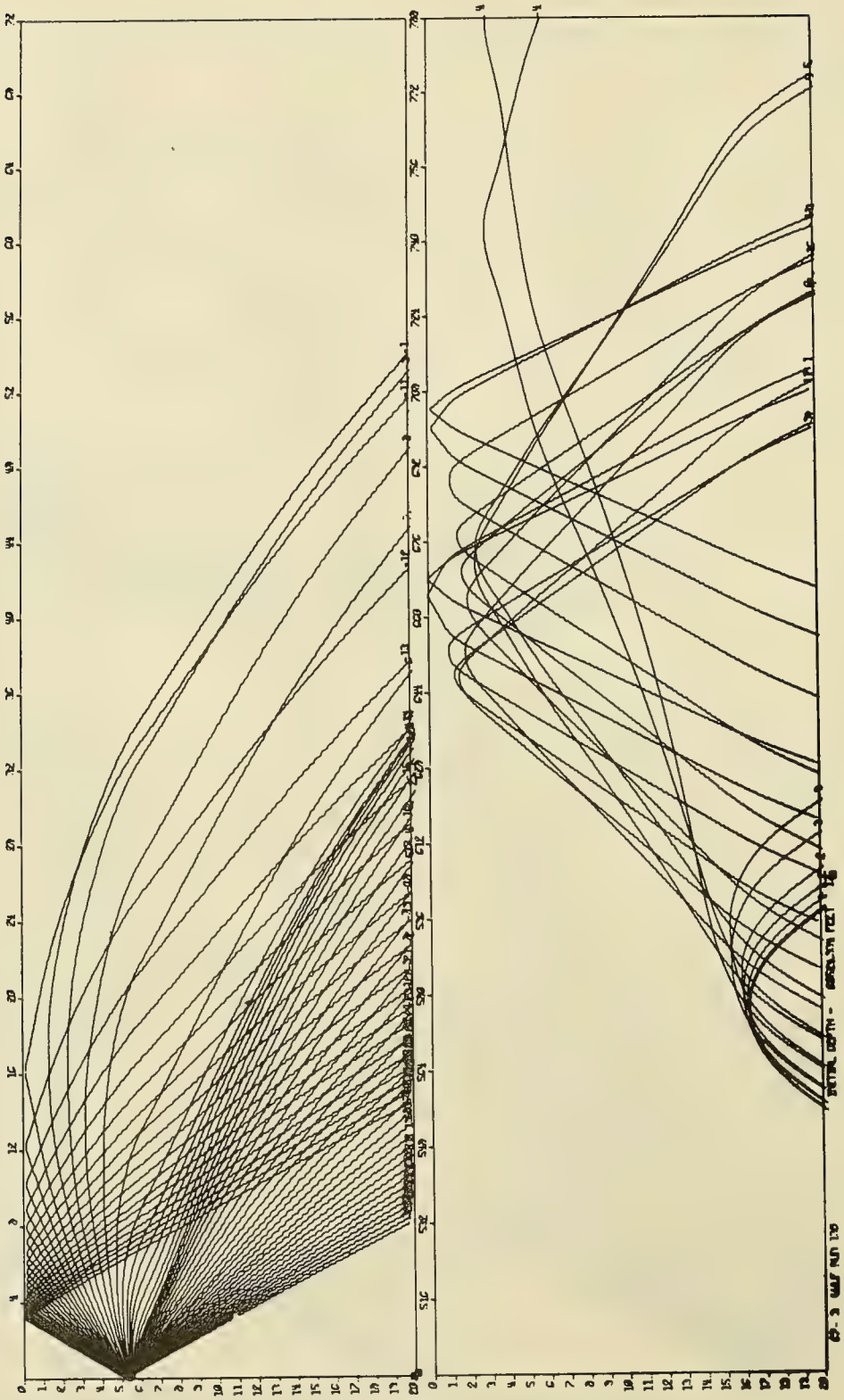

Figure 16

Session E

OCEAN ENGINEERING AND TECHNOLOGY

CONCRETE HULLS FOR UNDERSEA HABITATS

JERRY D. STACHIW
U. S. NAVAL CIVIL ENGINEERING LABORATORY
PORT HUENEME, CALIFORNIA

ABSTRACT

Exploratory experiments have shown that concrete is an acceptable construction material for hulls enclosing undersea habitats at atmospheric pressure. Models of spherical concrete hulls with and without penetrations have been built and tested to destruction in simulated hydrospace. Test results indicate that positively buoyant concrete hulls of spherical shape are feasible for location to 3500 feet depth, while negatively buoyant hulls of the same shape may be able to be placed at depths to 10,000 feet. Both economical and military considerations seem to favor concrete hulls for permanent ocean bottom installations.

INTRODUCTION

The conquest of hydrospace requires both mobile and fixed underwater structures capable of housing instruments and men for extended periods of time. There is a long history of research on the properties of materials and the design of hulls suitable for submarines; however, the research into materials and designs for static underwater hull structures is just beginning.

Although many materials developed for submarine or torpedo hulls are also applicable to fixed, ocean-bottom installations, there are materials which have not received careful study because of their manifest inapplicability to high-speed, deep submergence submarines or torpedoes. One such material is concrete.

The purpose of this paper is to describe several brief exploratory investigations into the applicability of concrete to the fabrication of structural hulls for deep submergence structures.* The scope of this series of experiments was limited to models of buoyant spherical hulls of 16 inch external diameter for 3500 feet depth cast from the same concrete mix. Variables were introduced into the study by varying the method of hydrostatic testing, as well as by incorporating into the hull different kinds of penetrations and inserts.

BACKGROUND

Concrete has been used in harbor installations for many decades, but it has not been used for the construction of underwater habitats. There are several reasons for this. Since concrete is not as desirable for submarine hull construction as other materials, no research was done on its properties under seawater hydrostatic pressure prior to the recent interest in fixed, ocean-floor installations. Furthermore, the impetus of research has been directed towards the discovery of new materials that would give buoyancy to a deep submergence hull even at greatest depths in the ocean. The most potent argument used against concrete in the past was that buoyant concrete hulls are limited by concrete's compressive strength to depths less than 5,000 feet and therefore cannot satisfy depth requirements that may arise in the future. Thus the philosophy appears to have been that since buoyant concrete hulls were definitely depth limited, there was no need to conduct research on structural characteristics of concrete as a stop-gap solution to the problem of finding suitable materials for deep submergence structures.

---

*In this paper, "deep submergence" is used to refer to depths greater than 600 feet.

Recently, materials like glass and ceramics have been discovered[1,2] to possess such high compressive strength, modulus of elasticity, and resistance to corrosion that buoyant deep submergence hulls for fixed or mobile installations can be built for any depth. Unfortunately, although glass and ceramics have the potential of providing man with hulls of ultimate depth capability, the engineering problems to be solved are formidable, and the materials are too expensive for applications in shallow depths where their use is not mandatory. Since currently available glass and ceramic materials with the ultimate depth capability have been found impractical for general use because of their high costs of fabrication and yet unsolved joint design problems, the path has been cleared for other materials with limited depth capabilities, but with an attractive cost factor and ease of applicability to large structures. Such a material is concrete which is theoretically satisfactory for buoyant hulls with an operational depth requirement of 3,000 to 4,000 feet. In addition, engineering estimates indicate that it is more economical than other available metallic or nonmetallic materials when used in large ocean bottom habitat structures.

The depth capability of 3,000 to 4,000 feet of buoyant concrete structures which can be towed to location and submerged, permits the utilization of such structures over large areas of the continental borderlands. About 12% to 14% of the ocean floor can be explored and settled using concrete as the primary hull construction material for the ocean floor installations. While the portion of ocean floor that could be made accessible through the use of concrete hulls is small in comparison to the total ocean area, in terms of importance, it is a most critical part of the total. The reason for its importance is found in the presence of large continental borderlands made up of shelves, and submerged banks in zero to 3,500 foot depth range. Since these shelves and banks are generally flat to gently sloping, and since they are also in the general vicinity of land, they make ideal construction sites.

The areas of primary interest to the United States are directly accessible from this country without transversing ocean floors that are under another country's sovereignty. By occupying the shelves and banks adjacent to the United States in the 0- to 3,500-foot depth range, the land area of the United States could be extended approximately 23%.

In summary, it can be stated that although there is a need to develop materials and structures with ultimate depth capability, development of materials and structures for depths to 3,500 feet is more important in terms of national defense and natural resources. Since concrete has been in many cases the most economical construction material on land, it should be investigated early in the search for undersea construction materials. It may also turn out to be one of the most economical materials for ocean-floor construction on continental shelves and submarine banks in the 0 to 3,500-foot depth range.

APPLICABILITY OF CONCRETE TO OCEAN BOTTOM HABITATS

There are several very good reasons why concrete will find application for the construction of ocean bottom habitat foundations and pressure hulls containing atmospheric shirt-sleeve environment. The major reasons are low cost of material, ease of forming double curvature shells, strength to weight ratio (Figure 1) equivalent to steels with a 45,000 psi yield point, and excellent resistance to corrosion. Other reasons also important, but considered minor in respect to the previously enumerated ones, are high elastic stability eliminating the need for rib stiffeners in spherical habitats for depths beyond those 100 feet (Figure 2), excellent blending in with the ocean bottom making it difficult to detect the habitat by hostile personnel with standard submarine detection gear, and excellent resistance to underwater explosions or impacts created by hostile forces.

The thick walled concrete hulls for ocean bottom habitats make it relatively easy to incorporate window, hatch, and feed-through penetration flanges without additional thickening of concrete wall around the penetrations. The low heat and sound conductivity of concrete make it unnecessary also to insulate the interior of the structure against heat losses and noise emission which is helpful in detecting the habitat by hostile personnel. Properly formulated concrete serves also as an excellent radiation shield for nuclear power generators with which future ocean bottom habitats will be equipped.

The two drawbacks that concrete possesses is its permeability to sea water and tensile strength of less than 500 psi. These drawbacks can be overcome by taking them into consideration during the design of the habitat hull, and by the use of proper steel reinforcements and waterproof coatings during the fabrication process.

Although concrete will be also used in the construction of habitat foundations and columns supporting the pressure hull, all of the discussion in this paper and subsequent experimental work has been devoted only to pressure hulls, as they represent a more demanding application for concrete.

EXPERIMENT DESIGN

Literature search failed to disclose any previous experimental work with concrete pressure hulls under external hydrostatic loading simulating deep ocean environment. Therefore it was decided first to conduct an exploratory investigation into the use of concrete hulls for deep ocean pressure environment to determine the avenues along which it would be most profitable to direct future studies. Many avenues of investigation are open in such an exploratory study. Not only may different hull shapes be selected, but also the composition of concrete mix, the thickness of the walls and types of joints. In addition, once the hull shape has been select-

ed, it can be tested for different properties, depending on the requirements of the study. Since so many alternatives were possible the approach was chosen by which only buoyant concrete hulls of maximized pressure resistant shape of the simplest construction were to be considered first.

The pressure hull shape chosen for the experimental study was a sphere as it represents the optimum pressure resistant hull. The spherical hull is also desirable for its inherent uniform distribution of stresses. Because of this uniformity of stress distribution, the strains measured at any point of the sphere's surface can be considered representative of the strains on the sphere. Knowledge of the maximum compressive strain found in simple spherical concrete hulls is extremely useful in the evaluation of future concrete hull models where the presence of inserts and penetrations will create stress risers that may lower the critical pressure of the hull.

The spherical shape is also advantageous for the determination of concrete's permeability under different levels of hydrostatic pressure. Permeability of concrete is probably related to stress level, therefore uniformity of stress in the sphere eliminates those side effects that are associated with the nonuniform distribution of stresses. A spherical hull also eliminated any anomalies caused by edge effects of the test sample, as would be found, for example, in a flat specimen mounted in some sort of a flange. Furthermore, since in a spherical hull there is also continuity of curvature, a reasonable assumption can be made that the permeability of water through the walls of the sphere will be uniform throughout, and thus only the level of water in the sphere must be known in order to determine a nominal rate of permeability through the given concrete mix.

The actual dimensions chosen for the concrete hull models were 16-inch outside diameter and 14-inch inside diameter. The outside dimension was controlled by the inside diameter of the largest vessel available at NCEL, while the inside dimension of the concrete hull was based on the requirement that the resultant concrete hull possess at most a 0.75 weight/displacement ratio. This weight to displacement ratio was considered to be the highest allowable that would permit the fully equipped concrete habitat hull to be either positively, or at worst, neutrally buoyant.

SCOPE OF INVESTIGATION

The study of spherical concrete hulls was limited, to-date, to three major phases of experimental investigation.

PHASE I - Investigation encompassed the testing to destruction of twelve identical spherical concrete hulls of 16-inch outside and 14-inch inside diameters without penetrations (Figure 3): Six of the models were waterproofed and six were bare.

PHASE II - Investigation centered around the testing to destruction under hydrostatic pressure of six 16-inch external and

14-inch internal diameter concrete spherical hull models with penetrations (Figure 4) closed by inserts (Figure 5) of different ridigities. Only two sizes of inserts, and three kinds of insert materials were experimentally evaluated. All of the models were waterproofed prior to implosion testing in simulated hydrospace facility.

PHASE III - Investigation concerned itself with the design, fabrication, and testing of two concrete habitat models (Figure 6) with 16-inch external and 14-inch internal diameters. The models were equipped with operational windows and wire feed-throughs located inside penetrations of the concrete sphere (Figure 4) reinforced by annular penetration flanges (Figure 7).

OBJECTIVES AND PROCEDURES OF THE INVESTIGATION

PHASE I - The objective of the tests was to touch upon as many facets of concrete hull's behavior under hydrostatic pressure as possible, rather than research any one of them exhaustively. Thus the hydrostatic tests on the simple concrete spheres were employed to explore ultimate compressive strength of concrete under short-term and long-term loading, the latter at hydrostatic pressures approaching the critical pressure. Experiments were also conducted to investigate the leakage of water through unprotected concrete at different hydrostatic pressure levels. Because of the exploratory nature of these tests, only one to three spheres were tested in each type of experiment. Experimental data from such a small number of test samples are considered to be indicators of the general level of magnitude of the parameters studied, but not conclusive and final evidence of these parameters. Once the general magnitude of the parameters investigated is known, an accurate plan can be drawn up for future experiments to more thoroughly evaluate and define the physical and mechanical properties of concrete under the external hydrostatic pressure of seawater.

PHASE II - The testing to destruction of the spherical hull models had as its objective a quantitative evaluation of the relationship between the size and rigidity of the penetration insert, and the critical pressure of the whole concrete hull assembly under hydrostatic pressure. The concrete spherical hull models with solid penetration inserts of different rigidity had the same dimensions and were cast from the same mix as the models without penetrations. Since it is known that the stress concentration around a penetration in the hull is to a large degree dependent on the size and on the mismatch between the rigidity of the penetration insert and that of the hull material, two sizes of penetrations and three types of insert materials were selected that represented a wide range of rigidity properties. The two selected sizes of model penetration inserts were considered to be representative of penetration inserts required for full size spherical structure. The 32°30' size insert simulated a penetra-

tion in the hull required for man-sized hatches or windows, while the 8° size insert simulated an electrical wiring or hydraulic piping feed-through on an underwater hull structure of ten to twenty feet in diameter with personnel transfer capability. The most rigid inserts selected were made of steel, while the least rigid inserts were made from polyvinyl chloride plastic; other inserts used were made from aluminum. During the hydrostatic testing to destruction of the insert-equipped models, strains were measured around the inserts and compared to strains existing in the same sphere away from the penetration inserts. In such a manner some quantitative measure of the stress concentration factors produced by inserts of different rigidities could be obtained. The comparison of the critical pressures of insert equipped spherical hulls with the critical pressures of identical hull without any penetrations would also be indicative of the effect that penetration inserts have on the overall strength of the spherical concrete pressure hull.

PHASE III - The design, fabrication, and testing of the spherical habitat model had as its objective proving the feasibility of concrete pressure hulls with usable windows, hatches, and wire feed-throughs for 3500 foot depth service. This concrete habitat model could be considered a typical example of first generation concrete habitats for ocean bottom location. The concrete hull model dimensions, concrete mix composition, and method of casting was selected to be the same as in the previous phases of concrete spherical hull feasibility study.[2] In this manner, the critical pressure of the model with penetrations reinforced by flanges could be directly compared to the critical pressure of models without penetrations. The difference between the critical pressure of the working model and of the concrete spheres without penetrations would serve as a quantitative indicator of hull strength decrease due to use of the particular type of window, hatch, and feed-through flange designs.

The pressure hull for the ocean bottom habitat was conceived as a monocoque concrete sphere resting on an aluminum cradle supported by three pad equipped legs. Three large window assemblies placed around the circumference, and one located at the bottom of the sphere would permit television or photographic cameras to observe and record the behavior of ocean floor, hydrospace, and its inhabitants. To make the habitat adaptable to different missions, it could be selectively equipped with an array of specialized subassemblies, fitting into typical large window penetrations. Such subassemblies, in the form of windows (Figure 8), a glass observation dome (Figure 9), diver transfer chamber, vehicle transfer hatch, or oceanographic instrument tower would make the basic concept of the concrete ocean bottom habitat adaptable to an almost unlimited number of mission requirements. The only requirement that would apply to all of them was that their mounting plates fit the penetration opening, and that the plate bearing lip matches the bearing lip on the penetration flange. In order to

maintain the effect of the penetration flange rigidity constant, all insert subassemblies that fit inside the penetration flanges were designed to fit with a known clearance between the exterior taper of the insert and the interior taper of the penetration flange. The only point of contact between the penetration flange and the insert subassembly was at the O-ring sealing surface located on the penetration flange lip.

FABRICATION OF CONCRETE SPHERES

Concrete hemispheres were cast in a mold and subsequently cemented together with an epoxy bonding agent. Depending on the type of test, the exterior and interior surfaces were either left untreated or coated with a waterproofing material. The concrete mix used developed after 250 days a strength of 10,000 to 11,000 psi as determined by uniaxial compression testing of solid test cylinders associated with spheres.

The treatment of the exterior surface depended upon the type of test for which the given sphere was intended. For the permeability tests, where the rate of water flow through concrete under hydrostatic pressure was under investigation, the exterior surface of the sphere was left untreated, the way it emerged from the mold. For the strain determination tests, on the other hand, where the prime objective of the test was to protect the electric strain gages from seawater, the external surface of the spheres was protected by a thin coat of epoxy resin.

HYDROSTATIC TESTING

INSTRUMENTATION - Two different types of instrumentation were employed on the concrete spheres. The permeability experiments required instrumentation designed to measure rate of permeability, while the short- and long-term stress investigations needed only strain measuring instruments.

Instrumentation for the determination of strains consisted of electric resistance strain gages attached to the concrete sphere, and an automatic strain switch and read-out unit. Two different approaches were used to measure the rate of permeability through concrete in the experimental spheres. One approach relied exclusively on electronic transducers and read-out equipment, while the other utilized only mechanical or hydraulic components. The electronic water detector, specially designed for this study, operated on the principle that a rising water level in the sphere would markedly change the resistance between two separated rods placed inside the sphere cavity. As the water rose in the sphere, it would wet more and more of the two vertical rods, decreasing the resistance between them. This voltage change could be amplified, measured, and recorded to provide a resistance versus time record. The other approach used in the measurement of permeability rate consisted of tubing inserted into the sphere, through which accumulated water in the sphere's interior could be ejected at desired

time intervals.

TESTING PROCEDURE - The testing of the concrete spheres under hydrostatic pressure was conducted in the pressure vessel of the Deep Ocean Simulation Laboratory. The spheres were either placed in a retaining cage prior to testing or were attached to end closure (Figure 10) so that they would not float in the vessel and strike the end closure when the vessel was filled with water. The vessel was pressurized by air-operated, positive-displacement pumps that raised the pressure inside the vessel at a predetermined rate until implosion occurred. Pressure and temperature sensors located inside the pressure vessel permitted recording of these two parameters on a strip chart recorder. Upon implosion of the concrete spheres, manifesting itself by a loud noise, the end closure was removed and the fragments of the concrete structure were inspected. (Figure 11).

DISCUSSION OF TEST RESULTS

PHASE I

SHORT-TERM STRENGTH OF DRY CONCRETE SPHERES - The average ultimate compressive strength of the concrete spheres under hydrostatic loading has been found to be approximately 48% higher than for the 3 x 6-inch solid control cylinders tested under standard conditions (Table 1).

Table 1. Implosion Pressure, Calculated Maximum Stress in Dry Concrete Spheres; and Average Compressive Strength of Test Cylinders Associated With These Spheres.

Item	Sphere 1	Sphere 2	Sphere 3	Sphere 8
Implosion pressure	3,100 psi	3,050 psi	3,200 psi	3,600 psi
Compressive stress 1/ on the interior of the sphere	14,080 psi	13,860 psi	14,540 psi	16,350 psi
Compressive stress 1/ on the exterior of the sphere	12,530 psi	12,330 psi	12,940 psi	14,550 psi
Average compressive strength of 3x6-inch dry test cylinders under uniaxial compression	8,990 psi	9,750 psi	9,930 psi	11,200 psi

1/ Stress calculated with Equation 1 (Figure 2).

SHORT-TERM STRENGTH OF WET CONCRETE SPHERES - The average ultimate compressive short-term strength of concrete spheres permeated by seawater has been found to be approximately 18% higher than the compressive strength of identical dry concrete in 3 x 6-inch solid test cylinders under uniaxial compression (Table 2).

Table 2. Implosion Pressure, Calculated Maximum Stress in Wet Concrete Spheres and Average Compressive Strength for the Dry Test Cylinders.

Item	Sphere 5	Sphere 12	Average
Implosion pressure	2,850 psi	2,750 psi	2,800 psi
Compressive stress 1/ on the interior of the sphere	12,950 psi	12,500 psi	12,720 psi
Compressive stress 1/ on the exterior of the sphere	11,550 psi	11,100 psi	11,320 psi
Average compressive strength of 3 x 6-inch dry test cylinders 2/	10,500 psi	11,060 psi	10,780 psi
Wetting period at 1,500 psi hydrostatic pressure	4 days	13 days	

1/ Calculated stress with Equation 1 (Figure 2).
2/ Under uniaxial compression.

TIME DEPENDENT BUCKLING OF CONCRETE SPHERES - Long term pressurization of wet and dry concrete spheres has shown that wet concrete spheres are more susceptible to static fatigue than dry concrete spheres loaded to the same fraction of their short-term implosion pressure (Table 3).

Table 3. Hydrostatic Pressure and Duration of Loading of Wet and Dry Concrete Spheres in Static Fatigue Test; and the Average Compressive Strength of the Corresponding Dry Test Cylinders

Item	Sphere 11	Sphere 6	Sphere 8
Condition of concrete in sphere	wet	wet	dry
Hydrostatic pressure	2,000 psi	2,500 psi	3,000 psi
Percent of their short-term critical pressure	71.5%	89%	83.5%
Compressive stress 1/ on the interior of the sphere	9,089 psi	11,361 psi	13,633 psi
Duration of loading prior to implosion	6 days	10 minutes	3 days 2/
Average compressive strength of 3 x 6-inch dry test cylinders	10,890 psi	10,610 psi	11,200 psi

1/ Stress calculated with Equation 1 (Figure 2).
2/ No implosion occurred during 3-day test.

PERMEABILITY OF CONCRETE SPHERES TO SEAWATER - The rate of seawater seepage into sphere at 750 psi has been measured to be approximately 2.5 milliliters per hour, while for a sphere pressurized to 1,500 psi the rate was approximately 5 milliliters per hour. When the leakage rate is divided by the surface area of the sphere, it can be expressed as 6×10^{-3} milliliters per hour per square inch of area per inch of thickness at 1500 psi hydrostatic pressure. In both cases the salinity of water siphoned from the interior of the sphere was about 20% lower than the salinity of the pressurization medium.

From this rather sparse data, it would appear that permeability of concrete to seawater under high hydrostatic pressure is quite low, and that some chemical or physical phenomena, which occurs in the concrete, results in a decrease in the salinity of the water that passes through the concrete sphere wall.

DEFORMATION OF CONCRETE SPHERES UNDER LONG-TERM LOADING - The measured strains (Figures 12 and 13) showed that dry concrete on the sphere's interior has a time-dependent strain rate, which is very large immediately after load application, but which decreases with time. That the time-dependent strain is a function of both

the compressive stress level as well as time was shown by the difference of time-dependent strain rates measured on the exterior and interior surfaces of the sphere. The interior surface of the sphere, which was under a higher stress, showed a considerably higher time-dependent strain rate than the exterior of the sphere, which was under a lesser stress.

The long-term hydrostatic loading was conducted for only 3 days, and thus it is not known how much the time-dependent strain rate decreases after loading duration of several months, or years. The data generated indicates that even at the 6,700 foot depth level to which the waterproofed concrete sphere was subjected, the time-dependent strain rate of dry concrete decreased to 0.01 microinch/inch/minute after 3 days. This would lead one to believe that at lower stress levels, corresponding to 3,500 foot operational depth, time-dependent strain would not pose any serious engineering problems for concrete spheres with a 0.0625 wall-thickness to diameter ratio.

Upon depressurization, a time-dependent relaxation strain was observed whose rate decreased to a very small value after only 3 days. The difference between the strain level at the beginning of pressurization, and the strain after 3 days of relaxation at zero pressure shows that a nonrecoverable deformation of concrete in the sphere occurred.

TANGENT MODULUS OF ELASTICITY UNDER SHORT-TERM LOADING - The tangent modulus of elasticity of concrete under short-term uniaxial compression (2,100 psi/minute loading rate) was found to decrease with increasing stress level. The axial strains on the exterior surface of solid dry concrete test cylinders under uniaxial compression show that the average tangent modulus of elasticity for concrete mix employed in the casting of spheres is 3.68×10^6 psi in the 0 to 4,500 psi stress range, but decreases rapidly at higher stress levels (Figure 14). What the magnitude of change is in the tangent modulus of elasticity under biaxial or triaxial stresses, as found in the sphere, is not known. The slope of the strain curve for the interior of the spheres shows, however, positively that a decrease in the tangent modulus of elasticity does take place. This makes it necessary to treat E_t in equation (1) as a variable, and not as a constant. Since curves for E_t of concrete under different biaxial and triaxial stress levels do not exist at the present time, E_t as determined under uniaxial compression must be used in the meantime. Since E_t under uniaxial compression appears to be larger than E_t under biaxial and triaxial stress combinations, use of E_t under uniaxial loading is a conservative assumption.

PHASE II

EFFECT OF PENETRATION INSERT RIGIDITY ON CRITICAL PRESSURE OF SPHERE - It was found that there is no significant difference between critical pressures of concrete hull models with solid penetration inserts (Spheres No. 15, 16, and 17) and model without penetration (Spheres No. 18) as long as the rigidity of the insert was equal to, or larger than, the rigidity of the concrete hull

model. When the rigidity of the penetration insert was considerably lower than the rigidity of concrete (0.5×10^6 psi for polyvinyl chloride versus 3.65×10^6 for concrete) the sphere equipped with such inserts (Sphere No. 17) imploded at a significantly lower pressure than the sphere without penetrations (Table 4).

Table 4. Implosion Pressures of Concrete Spheres With Solid Penetration Inserts.

Sphere No.	Type of Inserts	Type of Test	Implosion Pressure	Age of Concrete	Strength of Concrete*
15	Solid steel inserts	Short term implosion test; 100 psi/minute pressurization rate	3485 psi	330 days	11,205 psi
16	Solid aluminum inserts	Short term implosion test; 100 psi/minute pressurization rate	3400 psi	335 days	11,165 psi
17	Solid polyvinyl chloride inserts	Short term implosion test; 100 psi/minute pressurization rate	2675 psi	330 days	11,150 psi
18	No inserts	Short term implosion test; 100 psi/minute pressurization rate	3375 psi	320 days	11,480 psi

* Strength of concrete was determined by subjecting 3 x 6 inch test cylinders of the same mix and age as the associated concrete sphere to compression testing in an uniaxial test machine. The compressive strength shown is the average of 18 test cylinders loaded to destruction at 2100 psi/minute rate.

THE EFFECT OF PENETRATION INSERT RIGIDITY ON STRAINS AND STRESSES IN THE SPHERE - The strains at the small penetrations in the concrete were not significantly different from strains measured at locations in the sphere away from penetrations. The strains at the large penetrations in the concrete, however, were significantly higher than strains measured at locations in the sphere away from penetrations only in the sphere No. 17 containing plastic inserts in the penetrations. The strains measured there one half of an inch away from the edge of the penetration with a plastic insert were approximately 40 percent higher than the strains in the same sphere not in close proximity to the penetrations. When the strains on the

interior of the concrete hull away from penetrations are translated into stresses, the measured stresses at locations remote from the penetrations are found to be of the same magnitude as stresses derived analytically for the interior of a thick sphere.

The strains on the interior surface of the solid inserts varied inversely with the modulus of elasticity of the particular insert material (Figure 15). Stresses, calculated on the basis of the strains in insert materials, were higher than in concrete for materials with modulus of elasticity higher than of concrete. Conversely, the stresses in inserts with modulus of elasticity less than of concrete, were less than in concrete itself (Figure 16).

PHASE III

CRITICAL PRESSURE OF OPERATIONAL HABITAT MODELS - The critical pressures of the two identical habitat models were approximately the same as of the concrete sphere with identical dimensions without any penetrations (Table 5) even though one of the models was subjected prior to destructive testing to its operational depth for 200 hours.

Table 5. Implosion Pressures of Ocean Bottom Habitat Models

Sphere No.	Type of Inserts	Type of Test	Implosion Pressure	Age of Concrete	Strength of Concrete
13	Functional windows and hatches	Held at 1500 psi for 8 days, then pressurized to implosion at 100 psi/min rate	3300 psi	350 days	10,840 psi
14	Functional windows and hatches	Short term implosion test; 100 psi/minute pressurization rate	3300 psi	310 days	9,640 psi
18	No inserts	Short term implosion test; 100 psi/minute pressurization rate	3375 psi	320 days	11,480 psi

STRAINS AND STRESSES IN HABITAT MODELS - The strains and stresses in the interior of the concrete habitat models were not significantly different from those found in spheres with solid steel ($E = 27 \times 10^6$) or aluminum ($E = 10 \times 10^6$ psi) inserts, even though the rigidity of the annular steel penetration flanges was approximately the same as of a rigid insert with a 5×10^6 psi modulus of elasticity. The experimentally determined meridional and equatorial stresses on the interior of the model were in the

4400 to 4600 psi range at 1000 psi exterior pressure.

The time dependent strain rate of the model's interior under 3350 feet operational depth submersion (Figures 17 and 18) decreased from 100 microinches/hour, one half hour after submersion to 0.15 microinches/hour after 200 hours of submersion at operational depth indicating that only very little additional time dependent strain would take place in the future if the model was left at operational depth permanently.

OPERATIONAL PERFORMANCE OF HABITAT MODELS - The operational performance of the habitat models was successful. No leakage occurred through the four window assemblies, three wire feed-throughs, and the single instrumentation tower assembly. Inspection of the penetration insert assembly components after implosion of the models showed that no yielding took place in any of the components.

CONCLUSIONS

Findings based on experimental data resulting from testing to destruction of spherical concrete pressure hulls show that concrete is a reliable material and that buoyant external pressure hulls with a safety factor of two can be built from it on land that will perform successfully undersea at 3350 foot depth for at least one to two week periods of time. Whether concrete hulls with a safety factor of two will perform successfully at 3500 feet design depth for periods of time measured in years will have to be experimentally established. Indications exist that they will be able to do so successfully.

In view of the fact that concrete is a very economical material whose composition is well known, and that construction techniques of large concrete shells on land are well developed, more emphasis should be placed by the U. S. Navy on utilization of this material to permanent, or semi permanent ocean bottom installations in the 0 to 3500 foot depth range.

REFERENCES

1. Stachiw, J. D. "Glass and Ceramic Hulls for Oceanographic Applications," Second U. S. Navy Symposium on Military Oceanography, Proceedings of the Symposium Volume I, 1965.

2. Stachiw, J. D. "Solid Glass and Ceramic External Pressure Vessels," Ordnance Research Laboratory Report NOw 63-0209-C-2, Pennsylvania State University, January 1964.

3. Stachiw, J. D. and Gray, K. O., "Behavior of Spherical Concrete Hulls Under Hydrostatic Loading; Part I - Exploratory Investigation." U. S. Naval Civil Engineering Laboratory, Technical Report R 517, March 1967.

4. Stachiw, J. D., "Behavior of Spherical Concrete Hulls Under Hydrostatic Loading; Part II - Hull Penetrations." U. S. Naval Civil Engineering Laboratory, Technical Report R (under preparation).

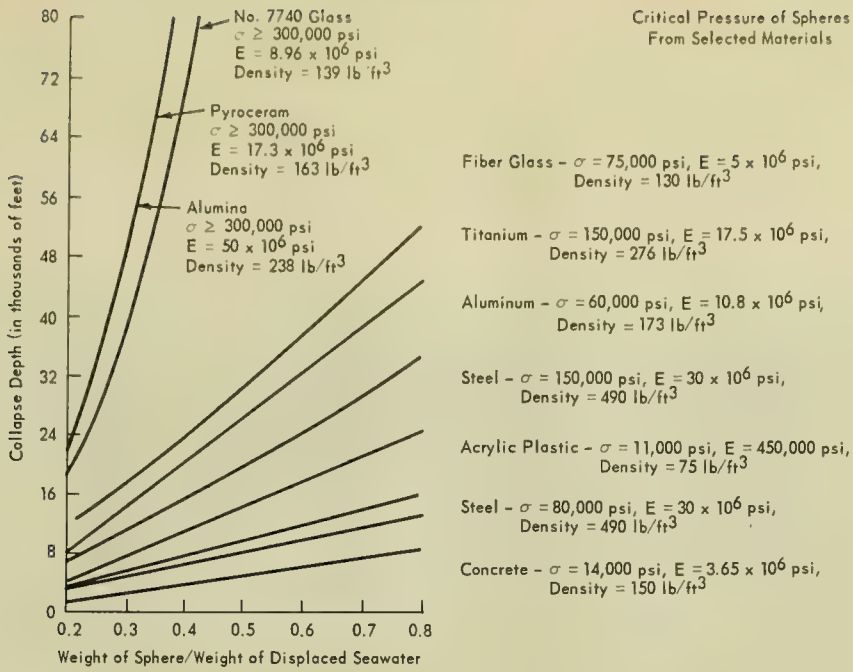

Fig. 1 - Critical pressures of spherical hulls made from selected materials

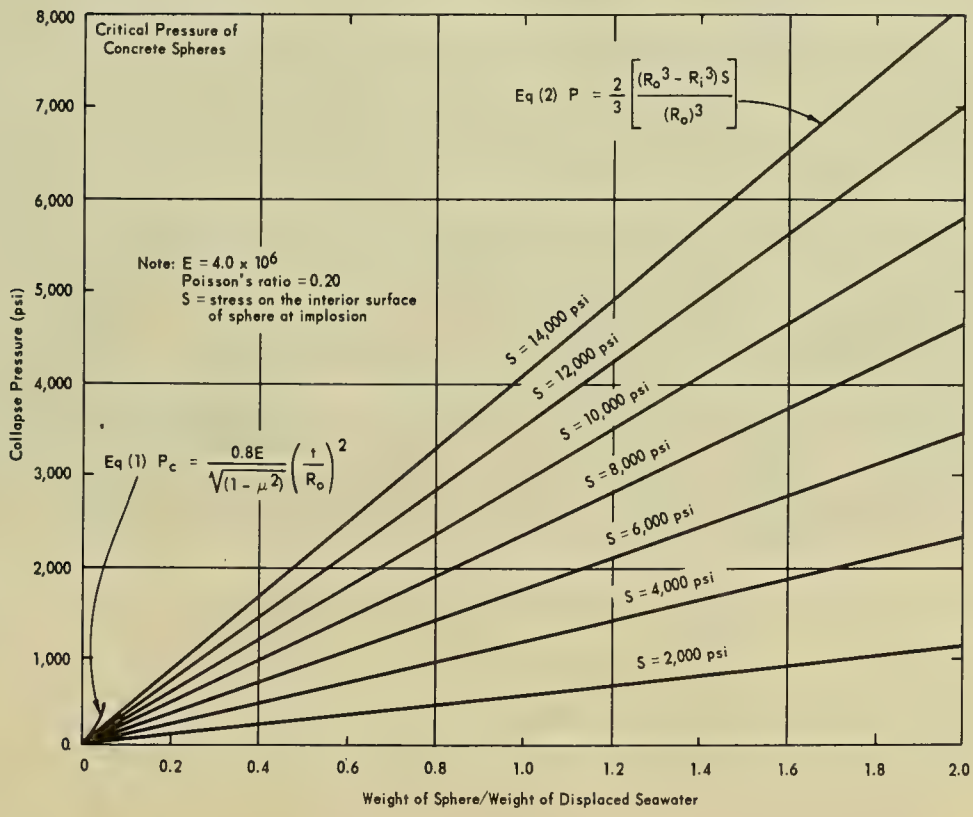

Fig. 2 - Critical pressures of concrete spherical hulls as a function of their weight to displacement ratios

Fig. 3 - Waterproofed and strain-gaged spherical concrete hull without penetration

Fig. 4 - Hull with penetrations prior to insertion and bonding of solid penetration inserts

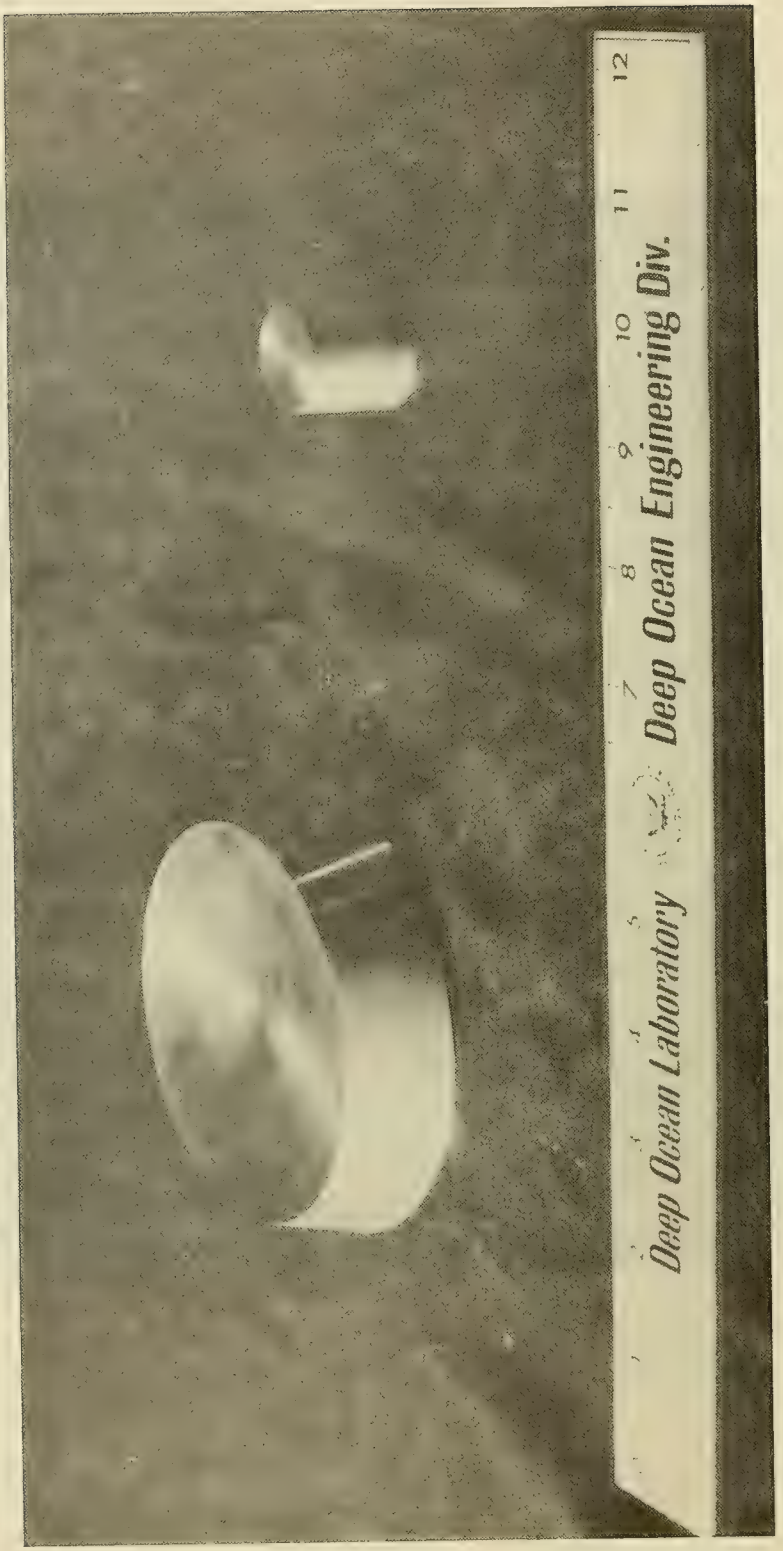

Fig. 5 - Solid penetration inserts

Fig. 6 - Concrete habitat model for 3500 ft operational depth; imploded at 7400 feet

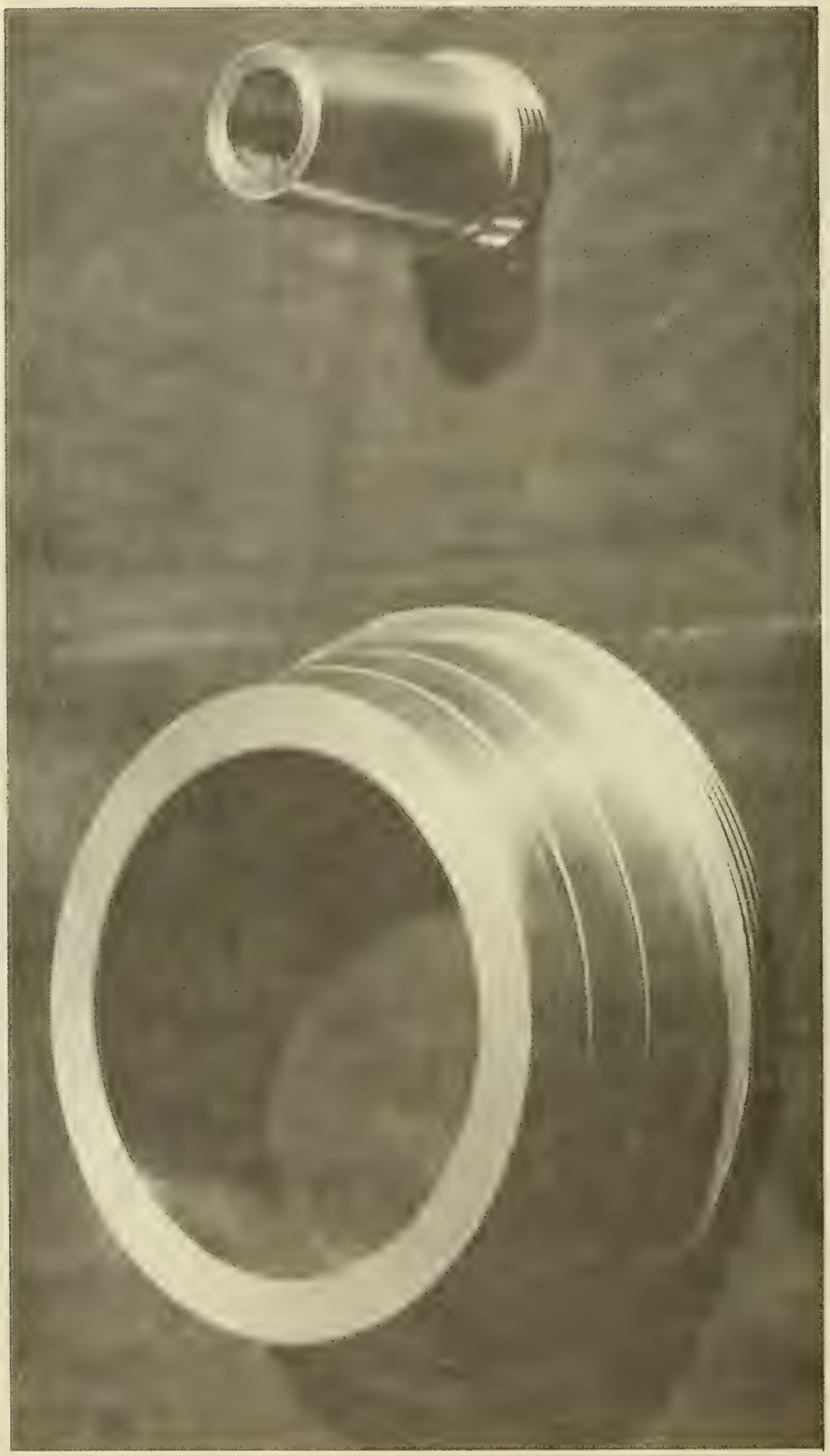

Fig. 7 - Penetration reinforcing flanges for large and small penetrations

Fig. 8 - Window assembly for the habitat model; (1) penetration reinforcing flange, (2) window seat, (3) acrylic window, (4) window retaining ring

Fig. 9 - Glass observation dome assembly for the habitat model; (1) penetration reinforcing flange, (2) dome bearing plate, (3) dome, (4) bearing plate retaining ring

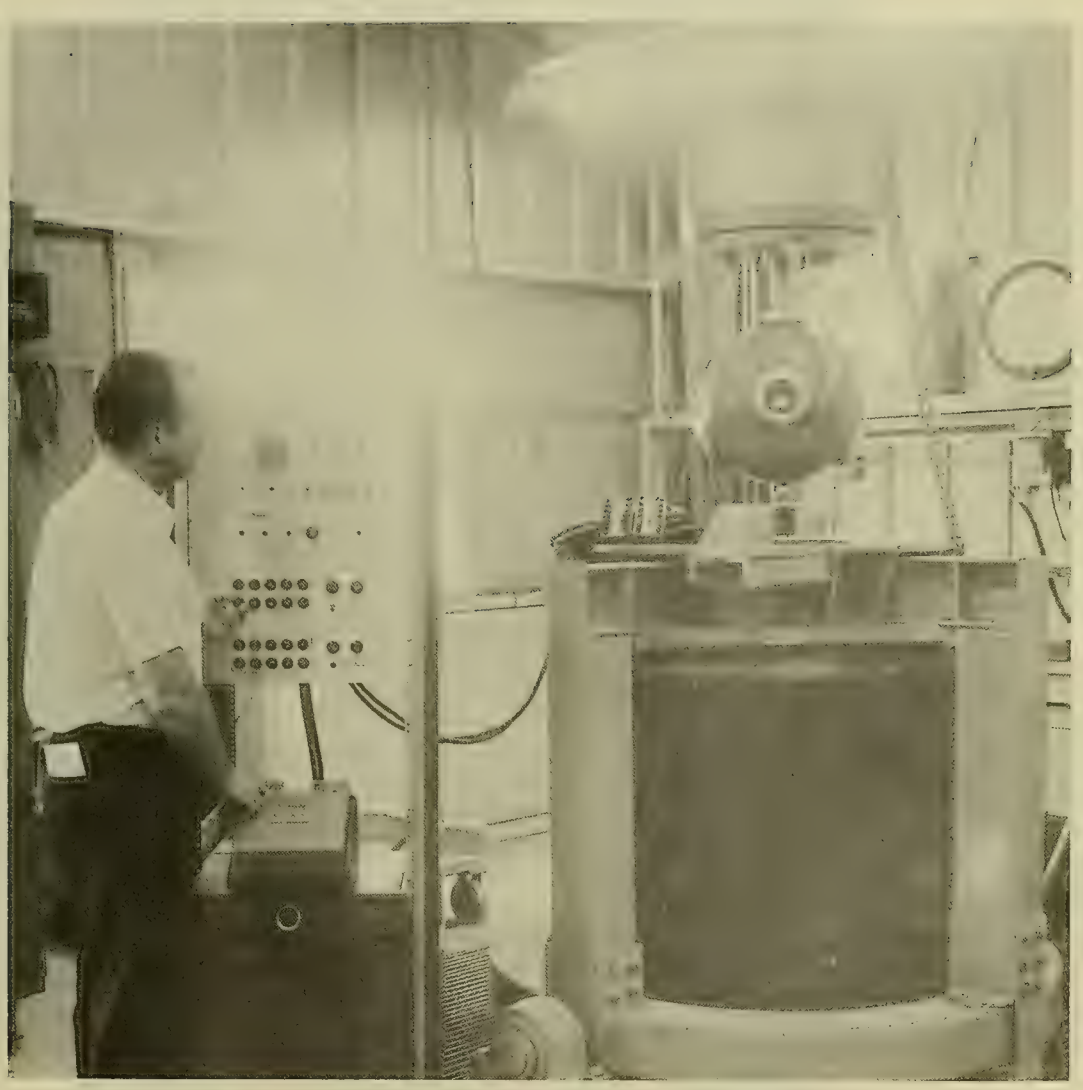

Fig. 10 - Habitat model attached to the end closure of pressure vessel used in testing the model

Fig. 11 - Fragments of the habitat model after implosion at 7400 feet simulated depth

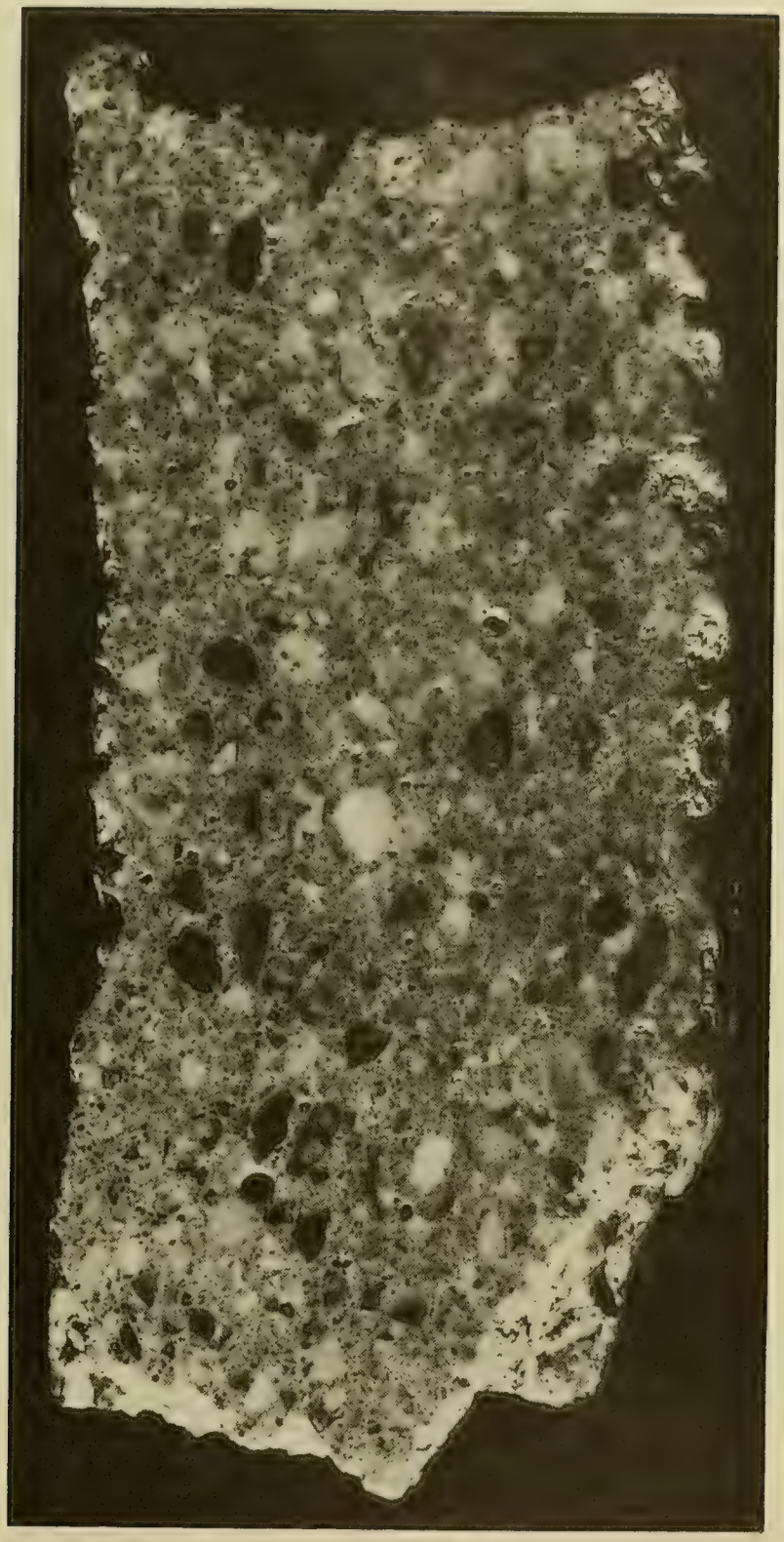

Fig. 11a - Microphotograph of the one inch thick wall section taken from the imploded concrete habitat model

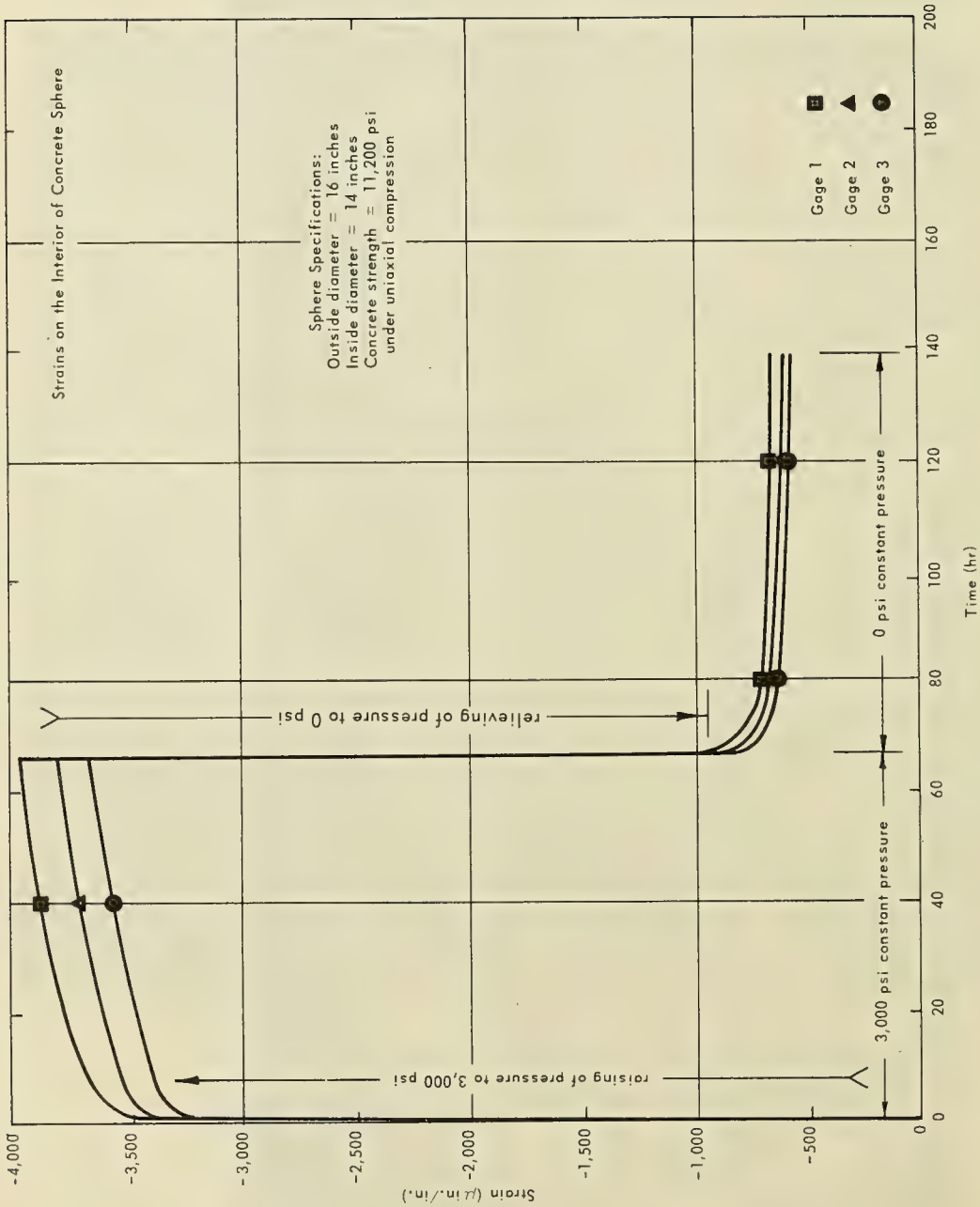

Fig. 12 - Time-dependent strains on the interior of the spherical concrete hull at 6700 feet simulated depth

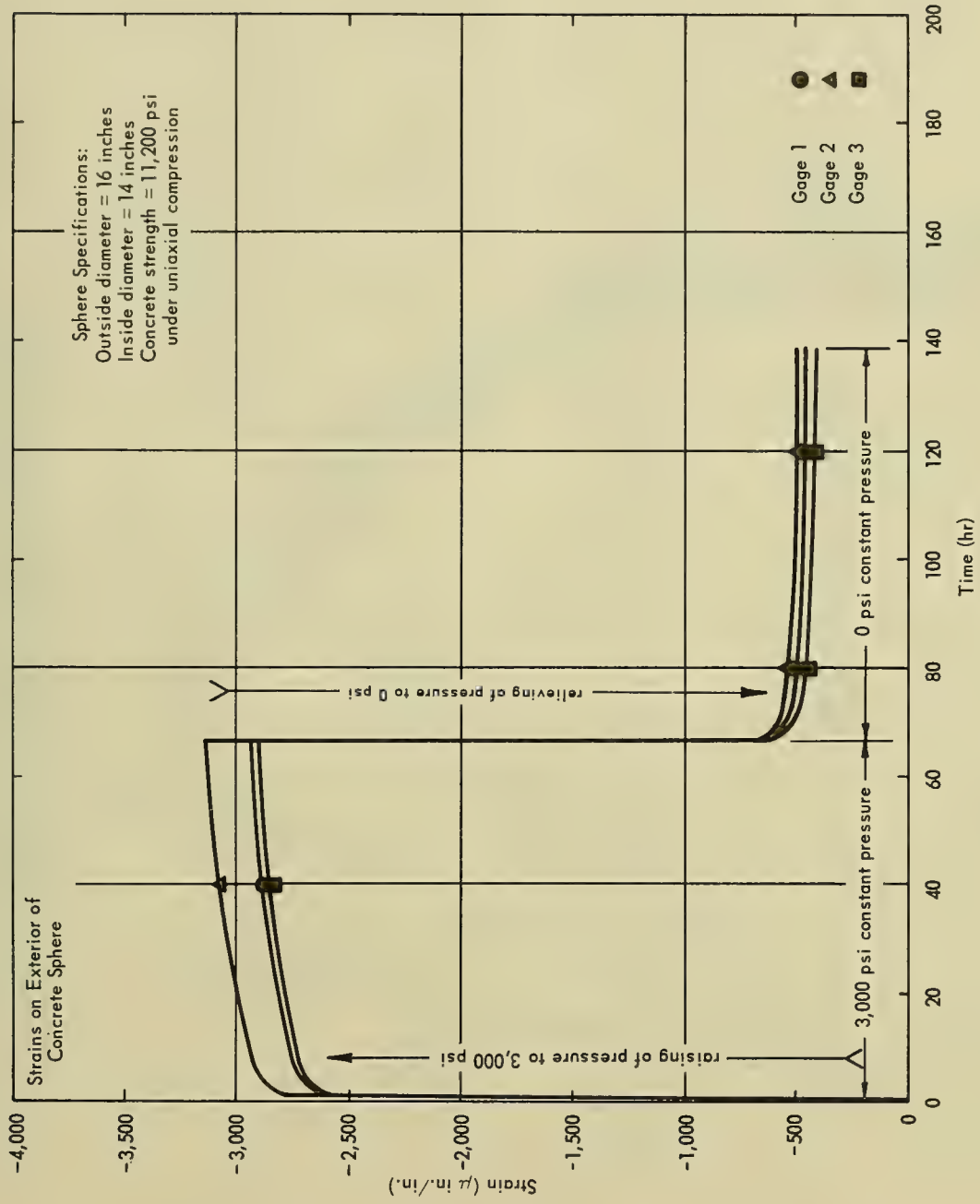

Fig. 13 - Time-dependent strains on the exterior of the spherical concrete hull at 6700 feet simulated depth

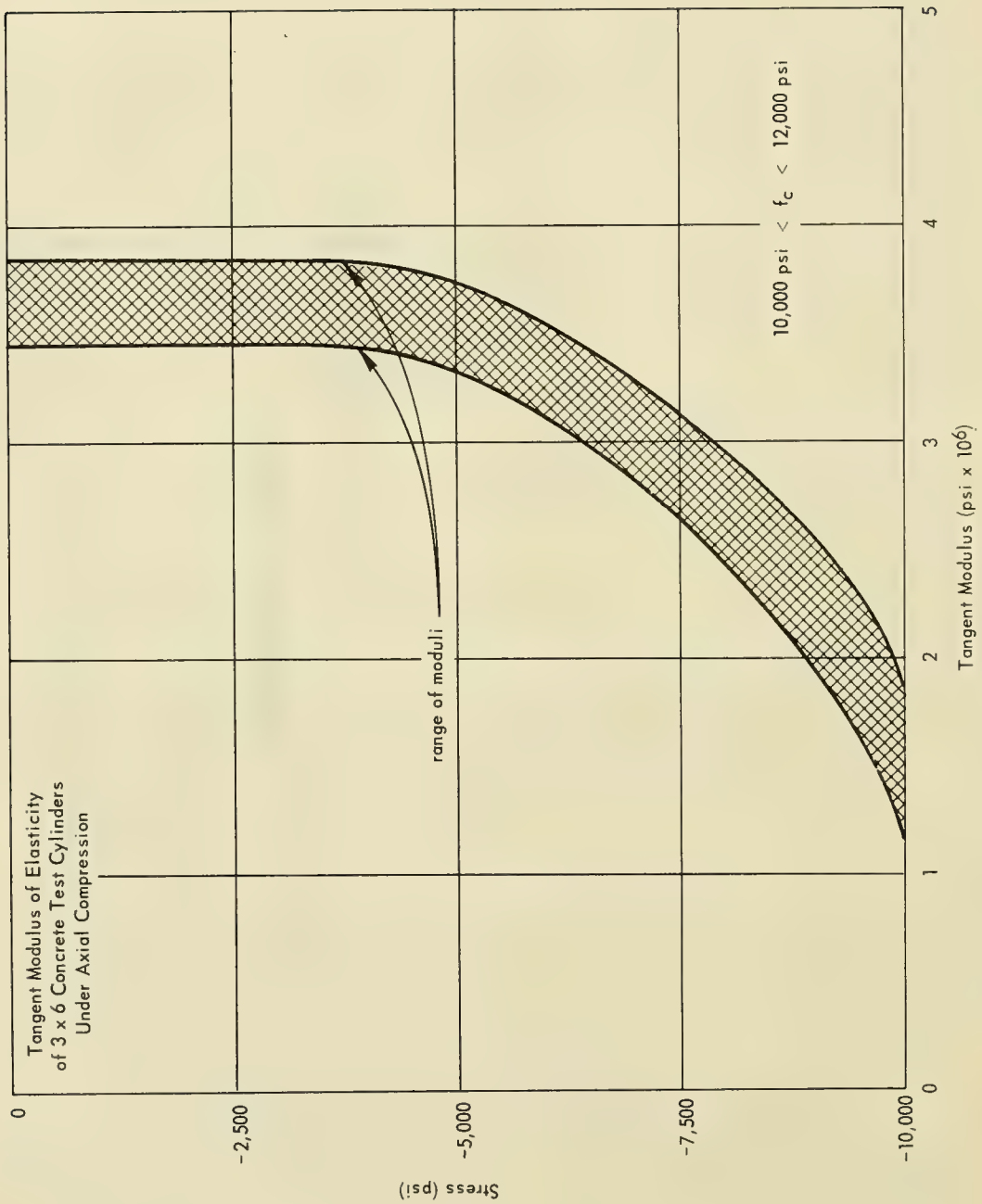

Fig. 14 - Tangent modulus of elasticity of concrete used in concrete hull models

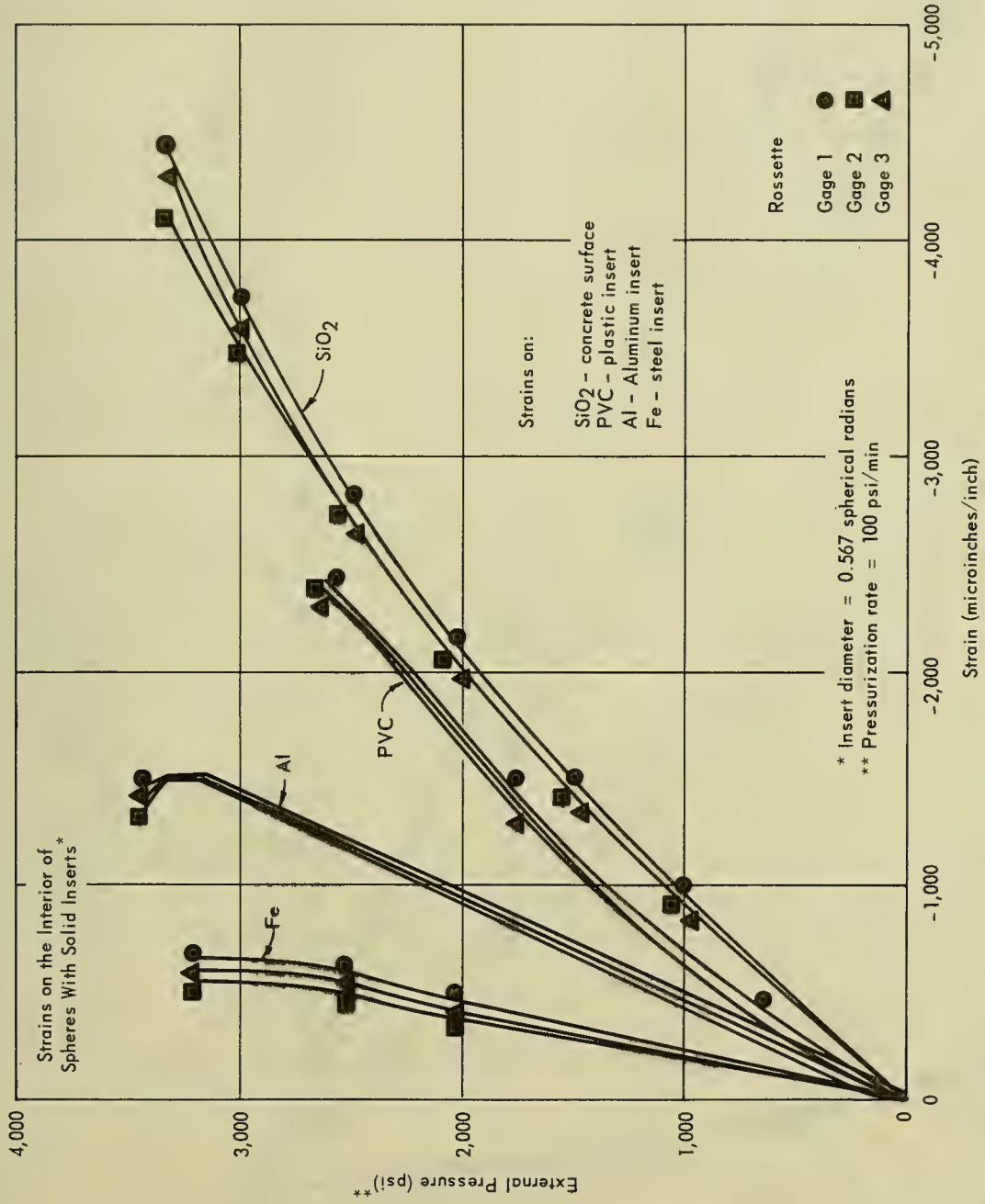

Fig. 15 - Strains on the interior of the spherical concrete hulls with solid penetration inserts

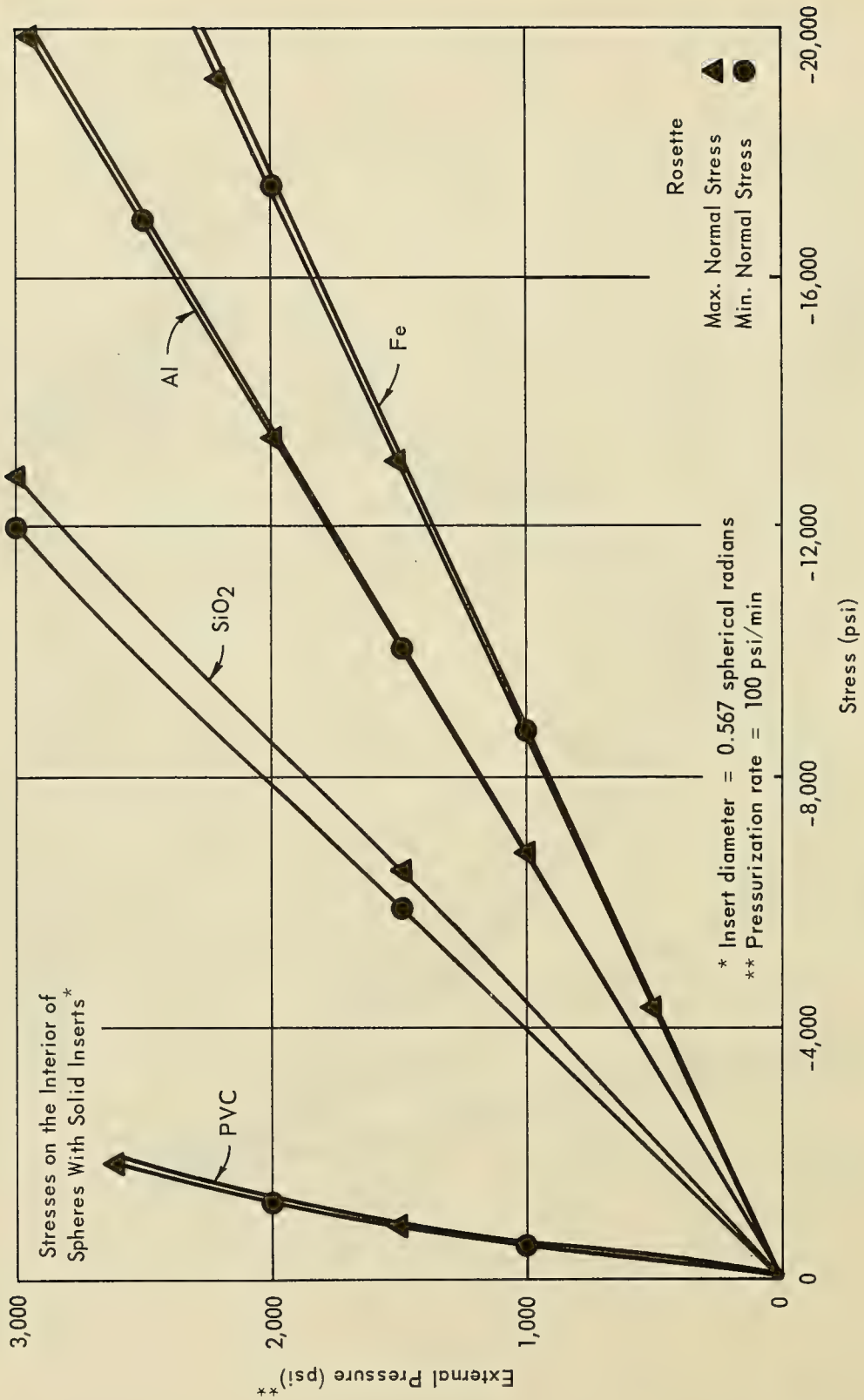

Fig. 16 - Stresses on the interior of the spherical concrete hulls with solid penetration inserts

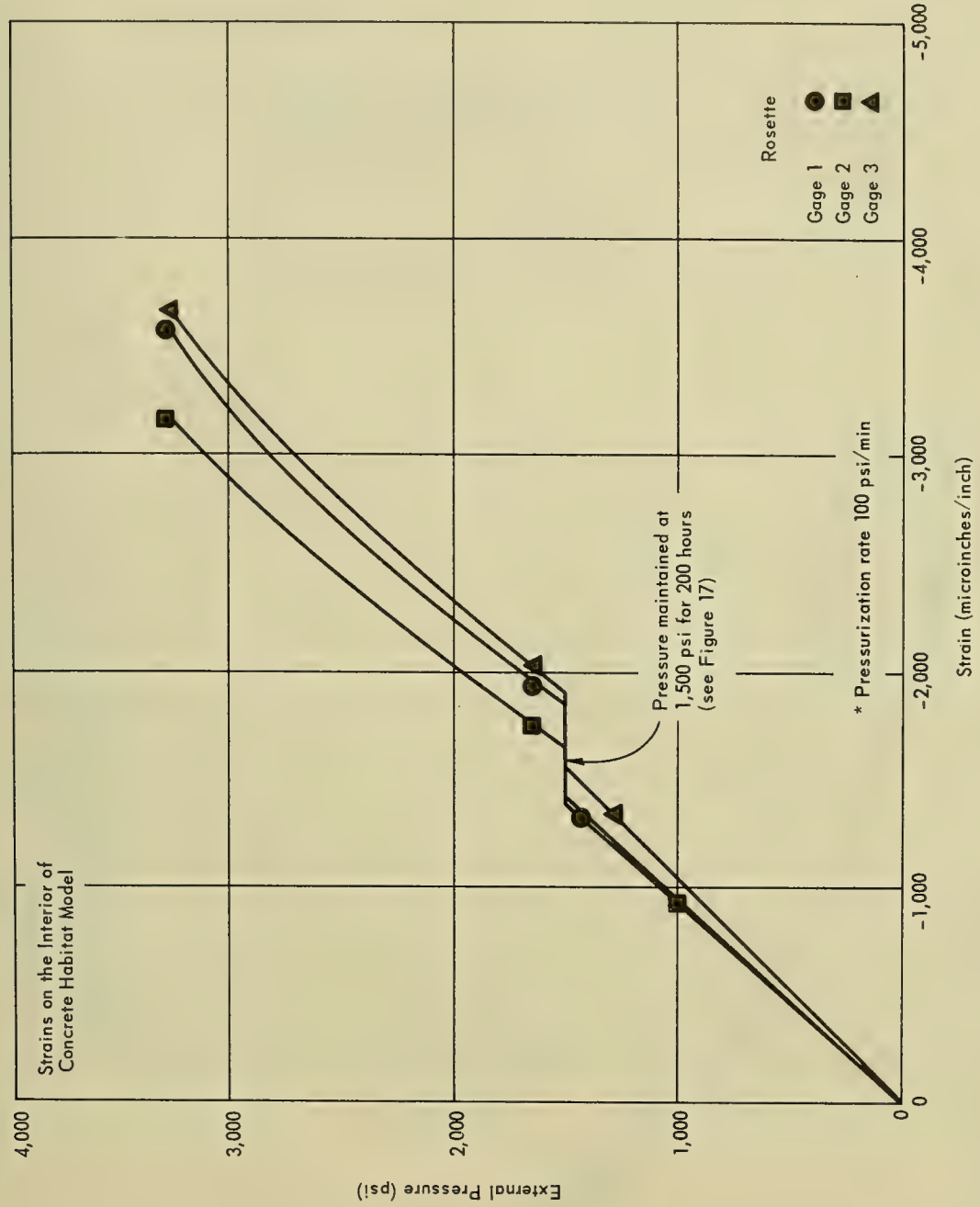

Fig. 17 - Strain history of the concrete habitat model prior to implosion

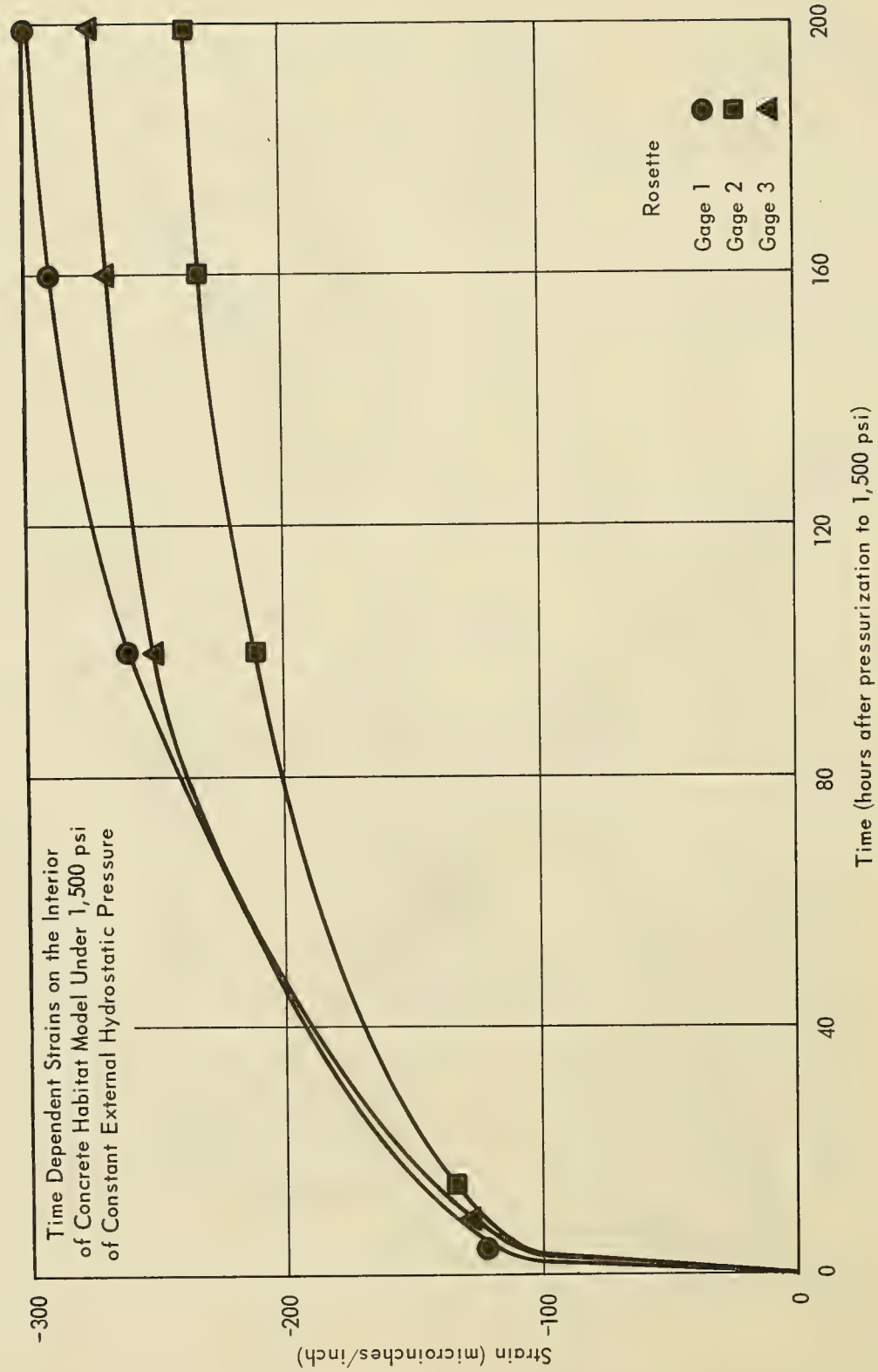

Fig. 18 - Time dependent strains on the interior of the concrete habitat model at 3350 feet of simulated depth

Five Years Experience with a Shipboard Oceanographic Data Processing System: Hindsight and Foresight *

C. O. Bowin
Woods Hole Oceanographic Institution
Woods Hole, Massachusetts

INTRODUCTION

Several years ago the Geophysics Department of the Woods Hole Oceanographic Institution recognized the need to accomplish at sea as much data analysis and interpretation as possible concurrent with the investigations. In recent years, oceanographic instrumentation developments have made it practical to collect large amounts of data during a single cruise, and the reduction of these data involves the processing of similar amounts of navigational information. The use of digital computers is a natural solution to the problem of keeping pace with an accelerating data collection capability. Data which has been collected must usually undergo a certain amount of processing or reduction to be meaningful. A researcher generally cannot evaluate data concurrent with its acquisition; this task is usually performed ashore, either manually or with the aid of a computer. Thus, scientifically interesting or significant regions may be discovered only after the data has been reduced ashore, often necessitating a return trip at great expense. Computer processing at sea eliminates this delay and expense, and allows scientists to monitor, assimilate, and evaluate the data at sea. Some data may prove worthless upon reduction at the shore

* Contribution No. 1937 from the Woods Hole Oceanographic Institution.

facility. This may be avoided, to some extent, by periodically checking important equipment voltages or parameters. With the necessary interface, the computer can be programmed to check and control scientific or navigational instruments and signal the operator when a detected abnormality exists. The scientist may thereby be released from many routine tasks to plan and direct the current research, and to interpret results. Also, by reducing the data on-line, incorrect or unreasonable data is more obvious, and a prompt check of the scientific instruments can be made. If the computer has the capability of sharing its operation between more than one task (time-sharing), general-purpose computation can be done while the main program is underway.

THE WOODS HOLE EXPERIMENT

Since June of 1962, two shipboard data processing and control systems have been implemented by the Geophysics Department of the Woods Hole Oceanographic Institution utilizing an IBM 1710 Computer System. The first system (System I) is described by Bernstein and Bowin (1963) and Bowin (1963). The second system (System II) is described by Bowin et al. (in press) and Bowin et al. (1967). These efforts were funded largely by contracts Nonr-1367 (00) and Nonr-4029(00) with the Office of Naval Research, Department of the Navy.

These systems made it possible to automatically sample, compute, and record data concerning the ship's heading and speed, latitude and longitude, water depth, acceleration due to gravity, free-air and Bouguer gravity anomalies, and the magnetic field of the earth. System II also provided on-line plotting of bathymetric, gravity anomaly, and magnetic field profiles; computer control of gravity meter spring tension; processing of surface temperature measurements and ocean sound velocity measurements; reduction of Loran C and VLF radio navigation data to latitude and longitude; display of ship's position and numerical data at remote stations aboard the ship; and malfunction detection and alarm message generation. Experiments were also made using three input/output typewriters at remote locations on the ship. A block diagram of System II is shown in Figure 1.

Presently, we are implementing a new shipboard computer system (System III) utilizing a Hewlett Packard 2116A computer. This new system gives promise of considerable expansion capability and as time, money, and personnel are available, we plan to continue development towards a multi-purpose,

multi-discipline facility. The goal is the development of a system capable of automatic sampling, computation, recording, and display of scientific information concurrent with the investigation (real-time); automatic control of scientific instruments and equipment (feedback control); and the capability of background time-sharing for compilation, assembly, off-line programs, diagnostics, and experimental on-line programs without endangering the operation of the main real-time program. How far we will be able to progress towards this goal remains to be seen. It is important, however, that our initial system (both hardware and software) incorporates the concept that someday all these objectives may be attained.

HINDSIGHT AND FORESIGHT

The operation and use of a prototype system obviously provides experience which can be obtained in no other way. The main purpose of this paper is to summarize the important aspects of that experience.

Although the details of the Woods Hole systems are by no means necessarily directly pertinent to the needs or problems of other organizations, many aspects have important relation to the general problems of shipboard data processing. Our experience from five years of development and use of a shipboard oceanographic data processing system has confirmed the value of such systems in the accomplishment of scientific investigations at sea. Most significant is the production by a digital plotter of profiles of bathymetry, gravity anomalies, and magnetic total intensity along the ship's track in real-time while the ship is traversing that part of the ocean. These records have enabled scientists aboard to better assimilate the large amounts of data being collected and thereby more effectively utilize both the ship and their time at sea.

Looking back over the last several years brings first to mind the interest, dedication, and creativity of the many people at the International Business Machines Corporation and the Woods Hole Oceanographic Institution who helped in the implementation of the system. Although a commitment on a personal level perhaps is not an essential ingredient of a successful program, the numerous demands on it during the system development suggest that it is important. It is a matter of some importance that the development of a system should be directed by the person who will use the collected data. Many possible difficulties and misunderstandings can be thereby circumvented.

A stable and reliable power supply is essential to a system. Inverters with precision frequency control were purchased for the R/V CHAIN to supply power to the computer. These inverters have several advantages. They provide a precise and stable frequency for the operation of the system. The IBM 1710 computer required a primary power frequency stability of ± 0.5 hz, which could not be met by normal ship's power. Precise frequency is also important for all clocks and recorders that have synchronous motors as their basic driving motor. The inverters were modified so as to be driven by an external oscillator, which, in our case, provided frequency control that was accurate to better than one thousandths of a hertz. In addition, the inverters were powered by the ship's DC battery which in turn is trickle-charged by the ship's DC buss. This arrangement assures continued operation during possible ship's power failures lasting up to forty-five minutes. Another advantage in operating the inverters from a battery is that large voltage transients on the ship's DC buss are in large part filtered by the battery before they reach the inverters. Our system utilized one 3 KVA inverter and one 10 KVA inverter.

An important aspect of a real-time computer system is the identification of the data which is collected. We chose to identify the data by the date and time at which it was sampled. That identification might prove to be a troublesome source of difficulty was in large part only recognized during subsequent data analysis. Errors that occurred included failures of the contacts in the mechanical clock, thereby resulting in invalid or erroneous values being supplied to the computer. Errors also occurred because the clock stopped whenever the computer power was turned off. Oftentimes during initialization of the program, the operator either would forget to enter the date and time or would enter erroneous values. In all these cases the errors proved very troublesome in processing the data later on shore. In the new system, we are endeavoring to eliminate these problems. To this end we have obtained a solid state electronic calendar clock that operates independently of the computer, and supplies the system with the day and month, and time in hours, minutes and seconds. This clock will also have its own battery backup supply in case of failure in the inverters. Whenever the system requires the time and date, it reads the clock, thereby always having accurate and reliable time. We expect this to be far superior to manually setting the time, and utilizing a counter within the computer program.

It is undesirable to subject electronic components to ambient temperatures in excess of about 90°F. Because temperatures this high, and higher, are relatively common in many parts of the world throughout much of the year, it is necessary to furnish air-conditioning for most computer systems. At the time of installation of our original system, the CHAIN was not air-conditioned. It was therefore necessary to build a room around the system in the main laboratory of the ship. Three water-cooled air-conditioners were used for cooling the room. This proved completely satisfactory. Even though difficulties with one or more of the air-conditioners was undesirably common, at least one of them was always operating. We were thereby able to maintain the computer at its required temperatures. At the same time as the system was expanded in 1963, air-conditioning was supplied to the laboratories, living quarters and messrooms of the CHAIN. Following that time, we dispensed with the room in the main laboratory that had previously sheltered the computer. Although we were no longer directly responsible for air-conditioning, it nevertheless required the suspension of operations whenever the ship's main compressor unit failed. This experience suggests that some additional independent air-conditioning capability should be provided for the computer system if the ship itself is generally air-conditioned, or that more than one air-conditioning unit should be available in any event. High humidity has not been identified as a difficulty in our past systems. The only problem encountered occurred when water actually dripped on the components of the system from either an overhead vent or from condensation upon the cooling ducts in the laboratory. Both these troubles have been corrected; one by sealing off the overhead vent and the other by coating the ducts with an insulating material.

Vibration is another concern of most people who are contemplating utilizing a computer aboard a ship. Again this has not been a serious problem in our installation. We have attributed only one failure directly to vibration when it was believed that a low voltage protection relay may have been erroneously actuated by vibration.

The central processor of the IBM 1710 computer system proved extremely reliable. In the years of operation we had only three failures in the central processor, and two of these were caused when the IBM maintenance man accidentally shorted printed circuit cards.

One failure of a printed circuit card in the analog to digital converter demonstrated a weakness of equipment diagnostic

programs. The manifestations of this failure were excessive stepping of the automatic spring tension controller for the gravity meter, water depths were changed to zero, and the digital display showed unbelievable numbers. Diagnostic programs failed to reveal any difficulties. Although adjustments of a bias voltage in the analog to digital converter helped relieve the trouble, the failing printed circuit card was not identified until the ship had returned to Woods Hole and an IBM engineer from San Jose, California worked on the system. The problem appears to have been caused by components that failed only when loaded by the computer doing multiple operations. The diagnostic tests did not reveal the trouble because they carry out only one test at a time.

We now believe that most serious difficulties during the first three and a half years of operation were the result of radio frequency interference. Now, of course, we can only surmise that many of the earlier difficulties were caused by RFI. However, the capriciousness and mysteriousness of the earlier troubles have a strong similarity to the later troubles which were positively identified to be caused by RFI and leads us to the strong supposition that this was a major source of trouble earlier. The manifestation of the interference was the alteration of values in the computer program. For example, one of the first indications of such trouble was erroneous values of ship's speed and water depth. In both these cases the trouble was identified as occurring either during the analog to digital conversion or immediately following. Somehow the interference was coming into the computer system. Many attempts were made to determine the source of these troubles; including the removal of antenna lead-in lines coming directly into the main laboratory and near the computer facility, installation of radio frequency suppression filters in the ship's radio power lines and in the 1710 system, and improvement of the system ground. These attempts usually temporarily alleviated the problem, but were not a permanent solution. In spite of these efforts, RFI problems continued which eventually developed into a mutual interference between the ship's radio and the computer system in which transmission would disturb values within the computer system. Also the units of the computer, in particular the typewriters and digital plotter, could be heard on many frequencies of the ship's radio receiver. When this interference became strong on 500 Khz (international calling and distress frequency) the problem demanded immediate correction. We tried the drastic action of removing all the personal radio receiver lines installed haphazardly throughout the ship by the scientists, crew, and officers, including the Captain's and the cook's. Older abandoned

lines throughout the ship were removed as far as possible or cut off where further removal became impractical. New antenna lead-in lines were then installed to avoid their approaching or intertwining with the systems cabling as they had previously. Following this action, which took place in the Fall of 1965, we have had practically no radio frequency interference either from the ship's radio transmitter or to the ship's radio receiver from the computer.

Our second greatest source of difficulty has resulted from operator action or misaction in performing his tasks. This will be discussed in more detail later.

The third most frequent source of trouble has been with mechanical components of the system; in particular the typewriters, and to a lesser extent the reed-relays that operate the digital display units. During the initial testing period the reed-relays exhibited frequent failures which were difficult to analyze because the trouble was intermittent and the displays were the means by which we were checking the values. However, once a good set of reed-relay cards were found, they functioned very well from then on. The typewriters broke springs, keys, and other parts which in most cases were easy to replace. The system operation was not seriously affected by these difficulties because by merely throwing a switch the output could be transferred from one typewriter to another.

One of the surprising performances was given by the IBM 1311 disc drives. These disc drives rotate on a vertical axis at 1500 revolutions per minute. These rotating discs act as gyros, and it was felt that during the rolling and pitching of the ship they would exert considerable force upon the bearings in which they rotate and thereby more rapidly wear those bearings. In four years of operation we had only one bearing fail amongst the three disc drives, and fortunately, although the spare bearing that we supposedly had aboard the ship could not be located, a bearing amongst the ship's spare parts did miraculously fit the unit and it was able to be returned to operation. We did come, however, to the practice of securing the disc drives during very rough weather. We still do not know whether this is essential or not; our only experience being that following a particularly rough storm, in which operation of the discs was continued, oxide was noted around the outside of the disc area and several scratches existed on the disc surfaces. We do not know whether these scratches were formed during the storm or were there before and only noted upon careful examination following the storm. However, this experience did cause us to

act cautiously in their operation during rough weather. The necessity of securing the primary recording units of a system is undesirable. We are hoping that we will be able to operate the magnetic tape drives of System III through all weather conditions encountered. At present, however, we do not know if this will be in fact the case.

We have found that all inputs that are entered manually by an operator, particularly routine manual inputs are unsatisfactory. All human beings will, with varying frequency, either enter erroneous values, turn the wrong switch, push the wrong button, or otherwise make mistakes. If the operator is to make an entry at a particular time, this is another potential for error. Mistakes will also occur even if the values are entered by the person who will later make use of the data, and therefore by someone who will have the most conscientious attitude towards the task. Such errors create an enormous amount of wasted time and difficulties in the correction and analysis of the data. For example, we are finding that the correction of water depth information that was usually entered manually in Systems I and II, are taking more time to correct than was spent in gathering the data. In System III we are dispensing with all routine manual inputs. Those values that are needed and their entry is not yet automated, will be digitized later ashore using conventional digitizers. Because, as mentioned previously, time and date are the means by which we identify individual data points, we have obtained a calendar clock to provide that information to the system, thereby eliminating the necessity of relying upon a person to enter such information. Should the clock or other inputs fail, we will have provision, of course, for manual input as a backup measure.

The program for Systems I and II was written in an assembly language which at the time was the only language capable of sampling analog input channels, BCD input channels, branch indicators, processing interrupts, and activating contact closures. During the development of the Systems I and II, the real-time program grew piecemeal as ideas for improvement and expansion of the computers capability developed. A complex interleaving and interconnecting of various parts of the program is a most undesirable way for the computer program to grow. In the latter stages of our utilization of System II we had reached the state where even the programmer who wrote the real-time program was afraid to make modifications or additions for fear it would jeopardize the operation of the system. One still unexplained mystery that may in part have resulted from program interaction was the inability

to originally have three input/output typewriters function properly at the same time. Any combination of two would work well, but as soon as the third one was added, typing of double letters and various other unexplained difficulties ensued. The situation was remedied merely by rearranging the priority numbers of the three typewriters. Why priority assignments should have caused the trouble in the first place, or why a rearrangement of the assignments should have been a solution, remains a mystery. All that we can do is surmise that there was some interaction between the computer program and critical timing requirements.

It is perhaps quite instructive to note that we had our most reliable operation of System II during its six months cruise to the Mediterranean immediately before being returned to IBM. The program used during this entire cruise had been checked and corrected on a prior cruise and no further modifications were made. This record suggests that program improvements are not always improvements unless they can be thoroughly tested and corrected, preferably at times when data is not of importance.

The use of a system invariably leads to ideas for improvement and expansion, and identifies errors in the original program. To meet these situations, it is very desirable that modifications to the real-time program may be made with ease and with confidence that such changes will not adversely affect other portions of the program. These requirements can be facilitated using a modular construction for the program rather than a complex interweaving of operations. It is also highly desirable that the real-time program be written by the user, or at least that he be able to easily follow the coded computer program. Neither was the case in Systems I and II which led to our dependence upon the IBM programmers for even rather simple modifications. This dependency is particularly frustrating in the years following the completion of an original contract by which such programs may have been written, and the dispersement of the programmers to new contract efforts essentially making them unavailable for further development. The facility of a user to write his own programs or to easily understand a program written by someone else is best accomplished, to date, by writing the program in Fortran. The use of an assembly language, or worse yet, machine language, only further isolates the average user from the ability to be creative in his use of the computer. Also, the larger the core memory, the more practical and convenient will be program improvement and an expansion of the tasks conducted by the system. This will be the case whether or not the system has random access

storage capability.

The tasks to which modern computer facilities may be directed lie in four categories: 1) numerical and logical analysis, 2) acquisition and collation of information, 3) display of information, and 4) control of equipment and instruments. Of these four tasks, only analysis techniques have reached a stage of implementation that could be considered young adulthood. To continue the analogy, display may be in adolescence, and acquisition and control are yet in childhood. Although notable improvements have been made in acquisition and control computers during the last five years, the implementation of these capabilities remains an effort beset by equipment specifications and timing problems; still very much dependent on the individual computer being used. The solution of these problems for one particular computer does not necessarily simplify the effort in accomplishing the same task on another computer. Developments that I expect to take place during the next several years include programming and equipment improvements that will facilitate acquisition, control, and time-sharing capabilities; reduction in the size and cost of peripheral equipment; and greater stress on reliability of commercial computer systems.

Digital computers now offer far more speed and computational abilities at lower cost then the machines of five years ago. The decision today is not whether to take a computer to sea, but which computer and how many tasks should be assigned to it. The main decision during the next several years will be in choosing between the alternatives of a large central computer system, a medium-sized central computer with small satellite computers, or many small independent computers for the accomplishment of a total program. Many factors will influence this decision including: the rate at which funding is expected; the future cost of large versus small systems; the memory size, computing power, and extent of peripheral devices desired; the degree to which future expansion capability is desired; and the degree of reliability that is required by the mission of the system.

REFERENCES

Bernstein, R. and C. O. Bowin, 1963. Real-Time Digital Computer Acquisition and Computation of Gravity Data at Sea, IEEE Trans. on Geoscience Electronics, vol. GE-1, no. 1, pp. 2-10.

Bowin, C. O., R. Bernstein, E. Ungar, and J. R. Madigan, in press. A Shipboard Oceanographic Data Processing and Control System, IEEE Trans. on Geoscience Electronics.

Bowin, C. O., W. D. Nichols, T. C. Aldrich, E. F. Dugan, G. N. Ruppert, and J. B. Zwilling, 1967. Second Supplementary Report on the Oceanographic Shipboard Data Processing and Control System (ODPCS) Aboard the Research Vessel CHAIN October 1963 - December 1966, WHOI Ref. No. 67-26 of the Woods Hole Oceanographic Institution.

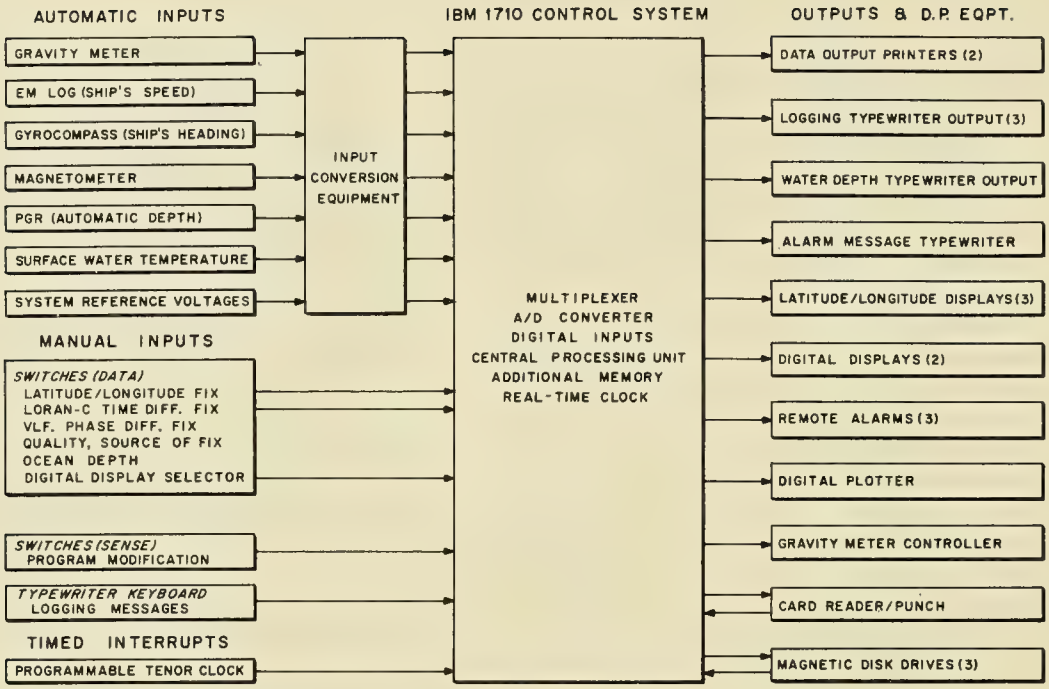

A) CONTINUOUS UNDER-WAY OPERATION

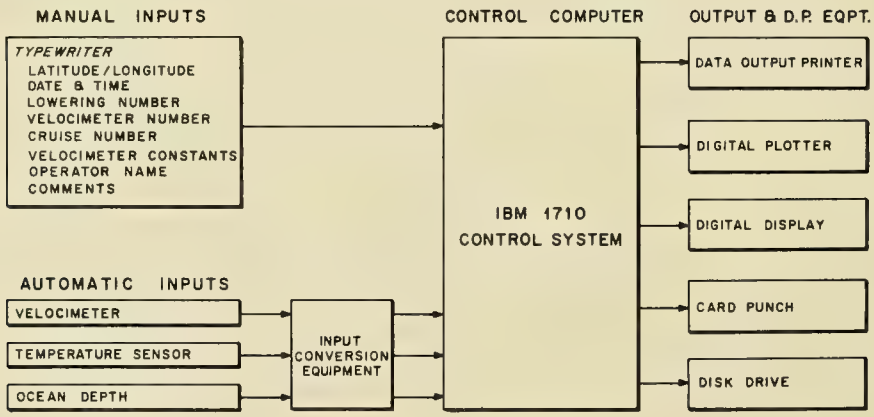

B) ON-STATION OPERATION

Fig. 1 - Block diagram of the oceanographic data processing and control system aboard the R/V CHAIN

CORROSION OF MATERIALS IN HYDROSPACE

PART I IRONS, STEELS, CAST IRONS, AND STEEL PRODUCTS

Fred M. Reinhart
U. S. Naval Civil Engineering Laboratory
Port Hueneme, California

PREFACE

The U. S. Naval Civil Engineering Laboratory is conducting a research program to determine the effects of the deep ocean environment on materials. It is expected that this research will establish the best materials to be used in deep ocean construction.

A Submersible Test Unit (STU) was designed, on which many test specimens can be mounted. The STU can be lowered to the ocean floor and left for long periods of exposure.

Thus far, two deep ocean test sites in the Pacific Ocean have been selected. Six STUs have been exposed and recovered. Test Site I (nominal depth of 6,000 feet) is approximately 81 nautical miles west-southwest of Port Hueneme, latitude 33°44'N and longitude 120°45'W. Test Site II (nominal depth of 2,500 feet) is 75 nautical miles west of Port Hueneme, latitude 34°06'N and longitude 120°42'W.

This report presents the results of the evaluations of the irons, steels, low alloy steels, alloy cast irons, metallic coated steel, uncoated and metallic coated steel wire ropes and anchor chains for six exposure periods and two nominal depths. The effect of stress on some of the materials is also reported.

INTRODUCTION

Recent interest in, and emphasis on the deep ocean as an operating environment has created a need for information about the behavior of constructional materials in this environment.

The Naval Facilities Engineering Command of the Office of Naval Materiel is charged with the responsibility for the construction of all fixed naval facilities, including the construction and maintenance of naval structures at depths in the oceans.

Fundamental to the design, construction and operation of structures, and their related facilities, is information about the deterioration of materials in the deep ocean environments. This

report is devoted to the effects of these environments on the corrosion of metals and alloys.

A test site was considered to be suitable if the circulation, sedimentation, and bottom conditions were representative of open ocean conditions.

A site meeting these requirements was selected at a nominal depth of 6,000 feet. The location of this site in the Pacific Ocean in relation to Port Hueneme and the Channel Islands is shown in Figure 1 as Submersible Test Units (STUs) 1-1, 1-2, 1-3, and 1-4.

The complete oceanographic data for Site I are shown graphically in Figure 2.[2,3] A portion of this data collected from 1961 to 1963 showed the presence of a minimum oxygen zone (as shown in Figure 2) at depths between 2,000 and 3,000 feet. Oceanographic data obtained at other sites also showed the presence of this minimum oxygen zone regardless of depth to the ocean floor.

Corrosion rates are affected by the concentration of oxygen in the environment. Therefore, it was decided to establish a second exposure site (STU II-1 and II-2) at a nominal depth of 2,500 feet. This site is also shown in Figure 1.

The NCEL oceanographic investigations also disclosed that the ocean floor at each of these sites was rather firm and was characterized as sandy, green cohesive mud (partially glauconite) with some rocks.

This report presents and discusses the results obtained from exposure of irons, steels, low alloy steels, alloy steels, unalloyed and alloyed cast irons, steel wire ropes, anchor chains and metallic coated products for six periods of time and at two nominal depths.

RESULTS AND DISCUSSION

Dr. T. P. May, Manager, Harbor Island Corrosion Laboratory of the International Nickel Company, Inc. has granted permission to incorporate his corrosion data (Reference 4), obtained from their specimens on the six STU structures, with the NCEL data.

Surface data of some alloys from the Atlantic Ocean (Reference 5) and similar to those from the Panama Canal Zone, Pacific Ocean (Reference 6) are included for comparison purposes. Deep ocean data from the Atlantic Ocean is also included to permit comparison of the different deep ocean environments, References 7, 8, and 9.

The corrosion rates of all the alloys are shown graphically in Figure 3.

Water in the open sea is quite uniform in its composition throughout the oceans;[11] therefore, the corrosion rates of steels exposed under similar conditions in clean sea water should be comparable. The results of many investigations on the corrosion of structural steels in surface sea water at many locations throughout the world show that after a short period of exposure the corrosion rates are constant and amount to between 3 and 5 mils per year.[6,12,13] Factors which may cause differences in corrosion rates outside these

limits are variations in marine fouling, contamination of the sea water near the shorelines, variations in sea water velocity, and differences in the surface water temperature.

IRONS AND STEELS

Corrosion

The corrosion rates of low carbon steels in sea water at different locations are compared in Figure 3:

a. Surface waters of the Atlantic Ocean at Harbor Island, North Carolina;[5]

b. Surface waters of the Pacific Ocean at Fort Amador, Panama Canal Zone;[6]

c. Deep Atlantic Ocean waters, Tongue-of-the-Ocean, Bahamas;[7,8,9]

d. Deep Pacific Ocean waters, Port Hueneme, California.

The corrosion rates of the steels at the surface in both the Atlantic and Pacific Oceans decrease rather rapidly with time and become relatively constant after about 2 to 3 years of uninterrupted exposure. The higher corrosion rates at Fort Amador are attributed to the difference in temperature between the two sites (27°C vs 21°C).

The corrosion rates of the steels exposed at nominal depths of 5,500 and 2,350 feet in the Pacific Ocean also decreased with time of exposure and were consistently lower than the surface corrosion rates. These lower corrosion rates are attributed to the combined effects of the differences between the variables at the surface and at the two depths; temperature, pressure and oxygen concentration.

Also, the corrosion rates at a depth of 2,350 feet were lower than those at a depth of 5,500 feet. In this case the lower corrosion rates at a depth of 2,350 are attributed to the combined effects of the differences between the variables at the two depths; temperature, pressure and oxygen concentration.

The above differences in the corrosion rates cannot be attributed chiefly to any one variable because of the interdependence of one variable on another. For example, the solubility of oxygen in sea water is increased as the pressure is increased at constant temperature but at constant pressure the solubility of oxygen decreases as the temperature increases.

The corrosion rates at a depth of 5,500 feet in the Pacific Ocean were about one-third the rate of the steels at Harbor Island after about 3 years of exposure.

The corrosion rates for a steel exposed by the Naval Research Laboratory at a depth of 5,600 feet in the Tongue-of-the-Ocean in the Atlantic were slightly higher than those in this

investigation, Figure 3. Oceanographic data reported for the Tongue-of-the-Ocean are: depth, 4,967 feet; 4.18°C and 5.73 ml/l oxygen.[14] Since the differences between the depths, pressures and temperatures are small the higher corrosion rates in the Atlantic are attributed chiefly to the difference in the concentration of oxygen between the two locations (5.73 vs 1.4 ml/l) with the possibility that some might be due to the difference in the currents (unknown in the Atlantic but practically stagnant in the Pacific). The difference between the corrosion rates on the surface at Harbor Island, N. C. and at a depth of 5,600 feet in TOTO is attributed to differences in depth (pressure, 0 vs 2520 psi) and temperature (19°C vs 4.2°C).

Corrosion rates for steel at a depth of about 4,500 feet[8,9] in TOTO were practically the same as those at the surface at Harbor Island for comparable periods of time.

The corrosion rates of wrought iron and Armco iron at depths were comparable with those of AISI 1010 steel as shown in Figure 4. The corrosion rate of wrought iron at the surface at Fort Amador in the Pacific Ocean Panama Canal Zone[10] after about 3 years of exposure was approximately 7 times greater than at a depth of 5,500 feet in the Pacific Ocean.

The corrosion rates of all the alloy steels at depths of 5,500 and 2,350 feet in sea water are shown in Figure 5. These values are shown as shaded areas encompassing most of the values. The corrosion rates for these steels decreased similarly to those for carbon steel with time of exposure at both depths. Although the corrosion rates at a depth of 5,500 feet varied between 1.9 and 6.0 MPY after 123 days of exposure they were all essentially the same after 1,064 days of exposure (0.5 to 0.9 MPY). The performance of these same steels when partially embedded in the bottom sediments is shown in Figure 6. After 1,064 days of exposure at a depth of 5,500 feet, the corrosion rates were the same as those in the sea water above the bottom sediments. However, the corrosion rates for many of the steels after 403 days of exposure in the bottom sediments at a depth of 6,780 feet were less than 0.5 MPY; this is attributed to the greater proportion of each specimen that was embedded in the bottom sediment. The specimens of these particular steels were about 2 inch diameter discs and in all probability were nearly completely embedded in the bottom sediment.

The data for all the steels was analyzed statistically. The mean curve of the corrosion rates and 95 percent confidence limits are shown in Figure 7 for the specimens exposed in the sea water. The corrosion rate curves for AISI 1010 steel and high-strength-low alloy steel #2 exposed at a depth of 5,600 feet in TOTO are also included to reveal that they are outside the 95 percent confidence limits. The fact that they are outside the 95 percent confidence limits of the corrosion rates of the steels exposed at a depth of 5,500 feet in the Pacific Ocean indicates that the environment in the Atlantic Ocean is somewhat different from the environment in the Pacific Ocean. The median curve of corrosion rates for the 2,350 foot depth is below that for the 5,500 foot depth indicating a difference in environment even though the confidence limits overlap.

The median corrosion rate curves for the 2,350 foot and 5,500 foot depths are shown in Figure 8. This figure shows quite clearly that after two years the water and bottom sediment environments are alike, with regard to their effect on the corrosion of steels. It also shows that the bottom sediment at 5,500 feet is about the same as the sea water environment at a depth of 2,350 feet. After 400 days the bottom sediment at a depth of 2,350 and the 2,350 foot level sea water environments are of equal aggressiveness in their corrosive actions.

Variations of from 1.5 to 9 percent in the nickel content of steel were ineffectual with respect to the corrosion rates as shown in Figure 9.

Stress Corrosion

Some of the steels were exposed in the stressed condition at values equivalent to 35, 50 and 75 percent of their respective yield strengths. None of these steels were susceptible to stress corrosion cracking for the periods of time exposed at the various depths.

Corrosion Products

The corrosion products from some of the steels were analyzed by X-ray diffraction, spectrographic analysis, quantitative chemical analysis and infra red spectrophotometry. The constituents found were:

Alpha iron oxide - $Fe_2O_3 \cdot H_2O$

Iron hydroxide - $Fe(OH)_2$

Beta iron(III) oxide hydroxide - $FeOOH$

Iron oxide hydrate - $Fe_2O_3 \cdot H_2O$

Significant amounts of chloride, sulphate and phosphate ions.

Anchor Chains

Two types of 3/4 inch anchor chain, Dilok and welded stud link were exposed at depths. The chain links were covered with layers of loose, flaky rust after each exposure. The layers varied from thin to thick as the time of exposure increased. Destructive testing of the exposed chain links showed no decrease in the breaking loads of the links for periods of exposure of at least 1,064 days. Hence, there was no impairment of the strength of either of the chains. The Dilok links all failed at the bottoms of the sockets where the cross-sectional area of the steel was the smallest. Rust was present in all these broken sockets indicating that sea water had penetrated the joints. Stagnant sea water in these sockets for

prolonged periods of time could result in destruction of the links due to the internal stresses created by the formation of corrosion products.

Wire Rope

A number of metallic wire ropes were exposed at various depths and for different periods of time. These were plow steel, galvanized steel, aluminized steel, stainless steel and 90 copper-10 nickel clad stainless steel ropes and cables of different types of construction.

The zinc on the 0.125 inch diameter, 7 x 19 construction, lubricated galvanized aircraft cable was completely covered with red rust after 403 days of exposure at a depth of 6,780 feet. In addition, the breaking strength had decreased by 50 percent.

The amount of zinc remaining on the other galvanized ropes varied from none in the case of the 0.094 inch diameter, 7 x 7 cable which was 100 percent rusted on the outer surfaces to considerable remaining on the 0.25 inch diameter, 7 x 19 construction cable which was dark gray. There was no loss in the breaking strength of any of these five cables.

After 403 days of exposure at a depth of 6,780 feet the smaller diameter (0.094, 0.125 and 0.187 inch diameter) stainless steel cables lost considerable strength, 90, 86, and 96 percent respectively. These decreases were all attributed to crevice corrosion of the internal wires. Many pits were also found on the individual wires away from the breaks and some broken ends were protruding from the cables prior to testing.

There was no loss in breaking strength of the three larger diameter stainless steel cables, the inside strands were chiefly metallic color with only a few localized rust spots.

Two types 304 stainless steel cables clad with a 90 percent copper-10 nickel alloy were exposed for 402 days at a depth of 2,370 feet. One cable, 1x37x7 construction with a 0.3 mil thick clad layer was covered with rust on the outside but the inside wires were uncorroded. The other cable, 7 x 7 construction with a clad layer 0.7 mil thick was covered with green corrosion products on the outside, uncorroded on the inside strands and had lost no strength.

Three aluminized steel cables (7 x 7, 1 x 19, and 1 x 19 construction) with 0.6, 0.6 and 0.7 mil thick coatings lost no strength during the 402 day exposure at a depth of 2,370 feet. The 7 x 7, 0.187 inch diameter cable was covered with white corrosion products and a few light rust stains but the inside strands were dull gray in color. The outside surfaces of the 1 x 19 construction wires (0.250 and 0.313 inch diameter) were gray in color with scattered white corrosion products covering about 50 percent of the surfaces. The inside strands were a dull gray color.

Eight wire ropes were stressed in tension equivalent to approximately 20 percent of their respective original breaking strengths. There were no stress corrosion failures after either 751 or 1,064 days of exposure. However, the breaking strength of the

Type 316 wire rope lost 40 percent of its strength after 1,064 days of exposure at a depth of 5,300 feet because of crevice corrosion of the internal wires. The breaking strength of the galvanized plow steel (0.83 oz Zn) was decreased by 17 percent. The breaking strengths of the other six wire ropes were unaffected. Although there was no loss in the breaking strength of the 18 percent chromium-14 percent manganese stainless steel rope there were quite a number of broken wires due to corrosion both on the outside and on the inside strands.

Metallic Coatings

Zinc, aluminum, sprayed aluminum and titanium-cadmium coated steel specimens were exposed at depth.

The galvanized steel (1.0 oz per sq ft) was covered with a layer of flaky red rust after 402 days of exposure at a depth of 2,370 feet. The corrosion rates were 0.9 MPY for the specimens exposed in the sea water and 0.4 MPY for the specimens partially embedded in the bottom sediment. The corrosion rate for bare steel (AISI 1010) in sea water under the same conditions was 1.2 MPY indicating that the zinc coating was removed within a short period of time 93 to 4 months). The difference in corrosion rates in the bottom sediment was 0.7 MPY which shows that the zinc coating protected the steel in the bottom sediment for at least twice as long as it did in the sea water. There was no loss in the mechanical properties of the galvanized steel.

The aluminized steel (1.03 oz per sq ft) was covered with white corrosion products, spotted with a few specks of red rust after 402 days of exposure at a depth of 2,370 feet. About 22 percent of the aluminum coating was corroded from the specimens exposed in the sea water and 40 percent was corroded from the specimens partially embedded in the bottom sediment; the underlying steel had not corroded. Therefore, it can be concluded, on a weight basis, that 1 oz per sq. ft. of aluminum will protect steel for a longer period of time than 1 oz per sq. ft. of zinc; about 4 times as long in sea water and about 2 times as long when partially embedded in the bottom sediment.

A titanium-cadmium coating on AISI 4130 steel was completely sacrificed and the steel was covered with a layer of red rust after 402 days of exposure at a depth of 2,370 feet.

A 6 mil thick, sprayed aluminum coating which had been primed and sprayed with 2 coats of clear vinyl sealer protected the underlying steel for 1,064 days of exposure at a depth of 5,300 feet. After removal from exposure the aluminum coating was dark gray in color, speckled with pin point size areas of white corrosion products.

Cast Irons

The corrosion rates for the gray, nickel, nickel-chromium, silicon, silicon-molybdenum and ductile cast irons at the two nominal depths in the Pacific Ocean are shown graphically in Figure 10 for sea water.

There was no measurable corrosion of the silicon and silicon-molybdenum cast irons at either depth.

In sea water at both depths the other cast irons behaved similarly to the steels as is clearly shown by comparing the curves in Figure 5 with those in Figure 10.

The corrosion rates of the austenitic cast irons in sea water are shown graphically in Figure 11. The corrosion rates of these alloys in sea water also decrease with time of exposure at both depths with the rates at 2,350 feet being lower than those at 5,500 feet.

The median curves for the two groups of cast irons and the alloy steels are shown in Figure 12 for sea water and in Figure 13 for bottom sediments. These curves (Figure 12) show that in sea water at a depth of 5,500 feet corrosion behavior of these three groups of alloys was the same after 750 days of exposure. There was a slight decrease in the corrosion rates of the three groups of alloys with time at a depth of 2,350 feet and the corrosion rate of each group was lower than that of its companion group at a depth of 5,500 feet. In the bottom sediments the behavior of the alloys was somewhat erratic. The lower corrosion rates after 400 days at a depth of 6,780 feet is attributed to the fact that a greater proportion of each specimen was embedded in the bottom sediment than during the other three exposure periods at the nominal depth of 5,500 feet. The corrosion rates at 2,350 feet tended to increase slightly with time for the steels and austenitic cast irons while those for the cast irons increased sharply. The type of behavior for the cast and wrought alloys can only be attributed to their proximity to the water-sediment interface or the percent embedment in the bottom sediment.

SUMMARY AND CONCLUSIONS

The purpose of this investigation was to determine the effects of deep ocean environments on the corrosion of irons, steels and cast irons. To accomplish this, specimens of 47 different alloys were exposed at nominal depths of 2,350 and 5,500 feet for periods of time varying from 123 to 1,064 days.

The corrosion rates of all the alloys, both cast and wrought, decreased asymptotically with time and became constant at rates varying between 0.5 and 1.0 MPY after three years of exposure at a nominal depth of 5,500 feet in sea water. These corrosion rates are about one-third those of wrought steels at the surface in the Atlantic Ocean at Harbor Island, North Carolina. The corrosion rates of these same alloys in sea water at a depth of 2,350 feet were lower than those at the 5,500 foot depth and decreased with time.

In general, the corrosion rates of all the alloys exposed either adjacent to or partially embedded in the bottom sediments at the 5,500 foot depth decreased asymptotically with time and became constant at rates between 0.5 and 1.0 MPY after three years of exposure. The corrosion rates of the alloys in the bottom sediments at the 2,350 feet depth tended to increase with time.

The corrosion rate of steel was not affected by nickel additions to 9 percent at either depth.

Silicon and silicon-molybdenum cast irons were immune to corrosion in deep ocean environments.

The mechanical properties of the alloys were not impaired.

The corrosion products of the alloys were composed chiefly of alpha iron oxide, ferric oxide hydrate, ferrous hydroxide and Beta iron (III) oxide-hydroxide.

Zinc (hot-dipped) (1.7 mils) and titanium-cadmium coatings failed to protect sheet steel for one year of exposure.

A hot-dipped aluminum coating (4 mils) protected sheet steel for a minimum of one year whereas a sprayed aluminum coating (6 mils, sealed) protected sheet steel for three years.

The mechanical properties of anchor chains were unimpaired. However, sea water penetrated the forged sockets of one type of chain as evidenced by corrosion at the bottoms of the sockets.

The mechanical properties of Type 304 stainless steel cables in sizes 0.094, 0.125 and 0.187 inch diameter were decreased by a minimum of 85 percent due to corrosion of the internal wires while those of the larger diameter wires were unaffected.

The breaking strength of a Type 304 stainless steel cable coated with 90 percent copper-10 percent nickel was not affected.

The breaking strengths of the aluminum coated steel wire ropes were unaffected.

The bare steel, zinc and aluminum coated steel and stainless steel wire ropes were not susceptible to stress corrosion cracking when stressed at 20 percent of their respective breaking loads. However, the Type 316 stainless steel wire rope lost 40 percent of its breaking strength due to corrosion of the internal wires.

The breaking strengths of bare steel, zinc and aluminum coated steel wire ropes, both stressed and unstressed, were unimpaired by exposure to deep ocean environments for periods of time as long as 1,064 days. However, based on visual observations zinc coatings corroded at faster rates than aluminum coatings on the wire ropes.

ACKNOWLEDGMENTS

The author wishes to acknowledge the generosity of Dr. T. P. May, Manager, Harbor Island (Kure Beach) Corrosion Laboratory, International Nickel Company, Inc. for granting permission to include his deep ocean corrosion data in this report.

REFERENCES

1. U. S. Naval Civil Engineering Laboratory Technical Note N-446: "Effects of the Deep Ocean Environment on Materials - A Progress Report" by K. O. Gray, Port Hueneme, Calif., July 1962.

2. U. S. Naval Civil Engineering Laboratory Technical Note N-657: "Environment of the Deep Ocean Test Sites (Nominal Depth 6,000 feet) Latitude 33°46'N, Longitude 120°37'W" by K. O. Gray, Port Hueneme, Calif., Feb 1965.

3. U. S. Naval Civil Engineering Laboratory, Unpublished Oceanographic Data Reports, by K. O. Gray, Port Hueneme, Calif.

4. Dr. T. P. May, unpublished data.

5. Dr. T. P. May, personal correspondence.

6. Naval Research Laboratory Report 5153, "Corrosion of Metals in Tropical Environments, Part 3 - Underwater Corrosion of Ten Structural Steels" by B. W. Forgeson, C. R. Southwell and A. L. Alexander, Washington, D. C., August 8, 1958.

7. Naval Research Laboratory Memorandum Report 1634, "Marine Corrosion Studies - Third Interim Report of Progress" by B. F. Brown and others, Washington, D. C., July 1965.

8. Naval Applied Science Laboratory Report, "Corrosion at 4,500 Foot Depth in Tongue-of-the-Ocean," SR004-03-01, Task 0589, Lab. Project 9400-72, Technical Memorandum 3, by E. Fischer & S. Finger, Brooklyn, N. Y., Mar 1966.

9. Naval Applied Science Laboratory Report, "Retrieval, Examination and Evaluation of Materials Exposed for 102 Days on NASL Deep Sea Materials Exposure Mooring No. 1" SF 099-03-01, Task 1481 and (SF-020-03-06 Task 1003) Lab. Project 9300-6, Technical Memorandum 4 (and Lab. Project 9300-7), A. Anaustasio, Brooklyn, N. Y., Nov 1965.

10. Naval Research Laboratory Report 5370, "Corrosion of Metals in Tropical Environments, Part 4 - Wrought Iron" by C. R. Southwell, B. W. Forgeson and A. L. Alexander, Washington, D. C., Oct 1959.

11. A. C. Redfield, "Characteristics of Sea Water," in Corrosion Handbook, edited by H. H. Uhlig. New York, Wiley, 1948, p. 1111.

12. F. L. LaQue, "Behavior of Metals and Alloys in Sea Water," in Corrosion Handbook, edited by H. H. Uhlig. New York, Wiley, 1948, pg. 384, pg. 390.

13. C. P. Larrabee. "Corrosion Resistance of High-strength-low-alloy Steels as Influenced by Composition and Environment," Corrosion, Vol. 9, No. 8, Aug. 1953, pp. 259-271.

14. U. S. Naval Research Laboratory. NRL Memorandum Report 1383, "Abyssal Corrosion and Its Mitigation - Part II. Results of a Pilot Exposure Test", by B. W. Forgeson, et al, Washington, D. C., Dec 1962.

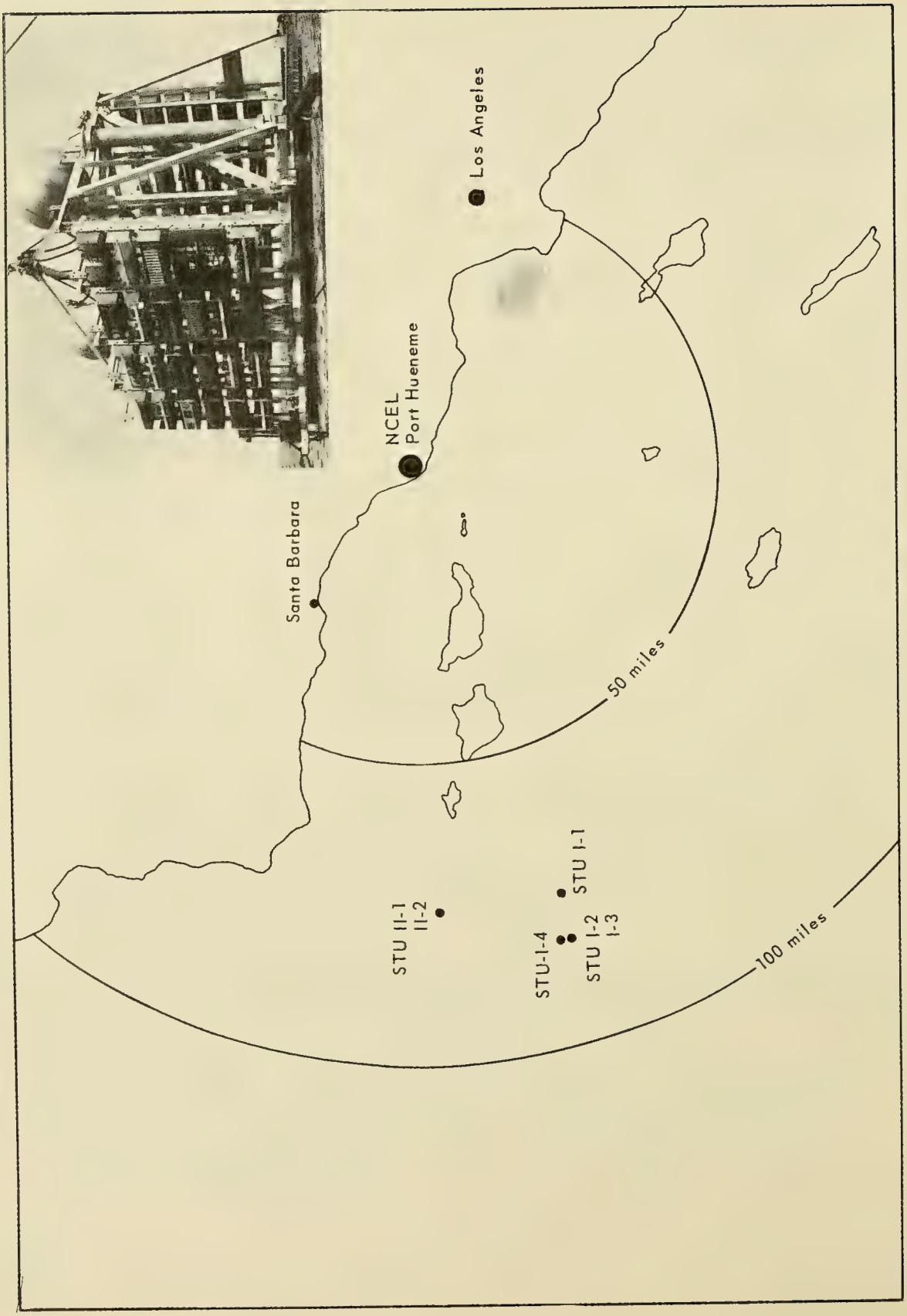

Fig. 1 - Area map showing STU sites off Pacific Coast; STU structure in inset

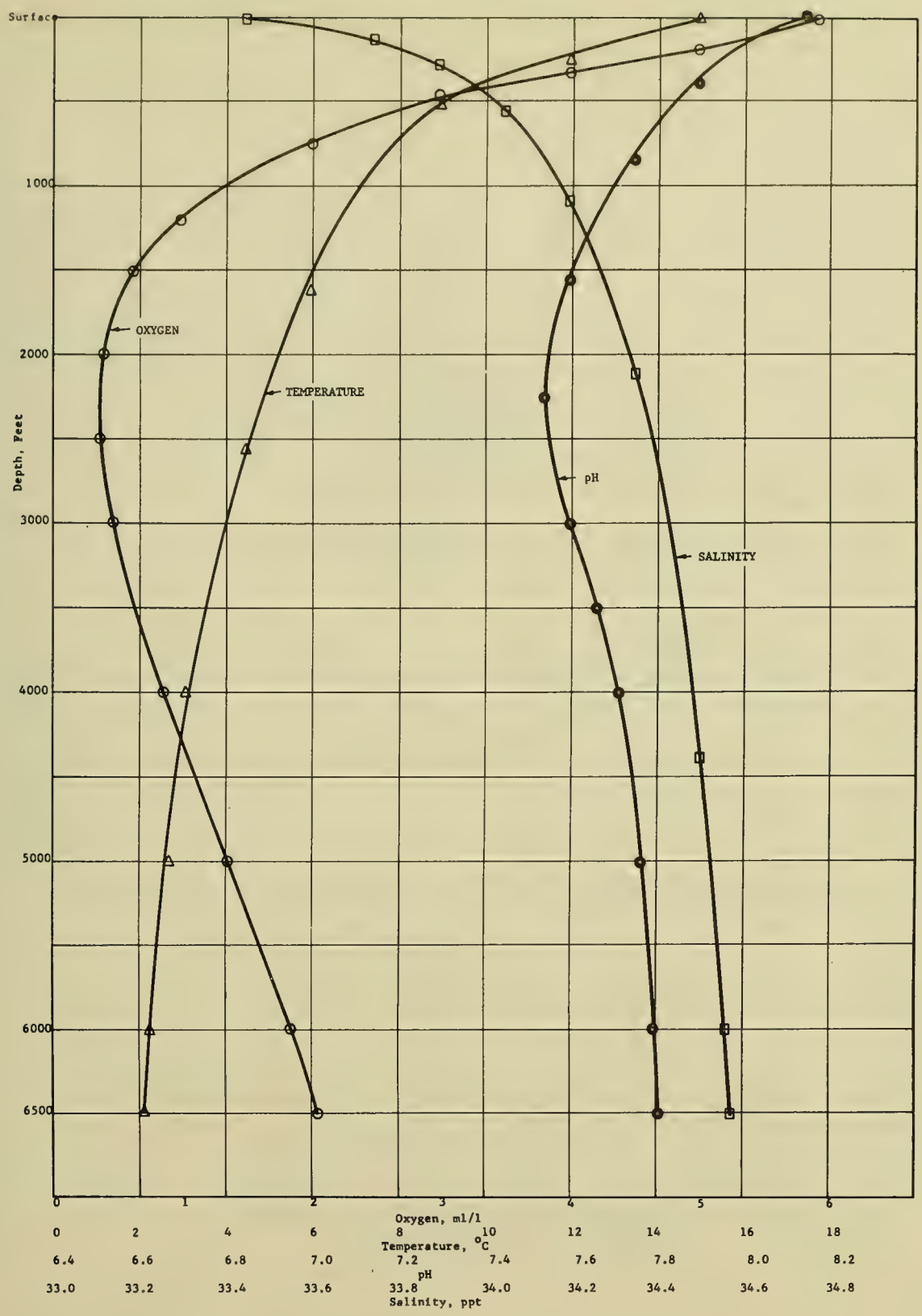

Fig. 2 - Oceanographic data at STU sites

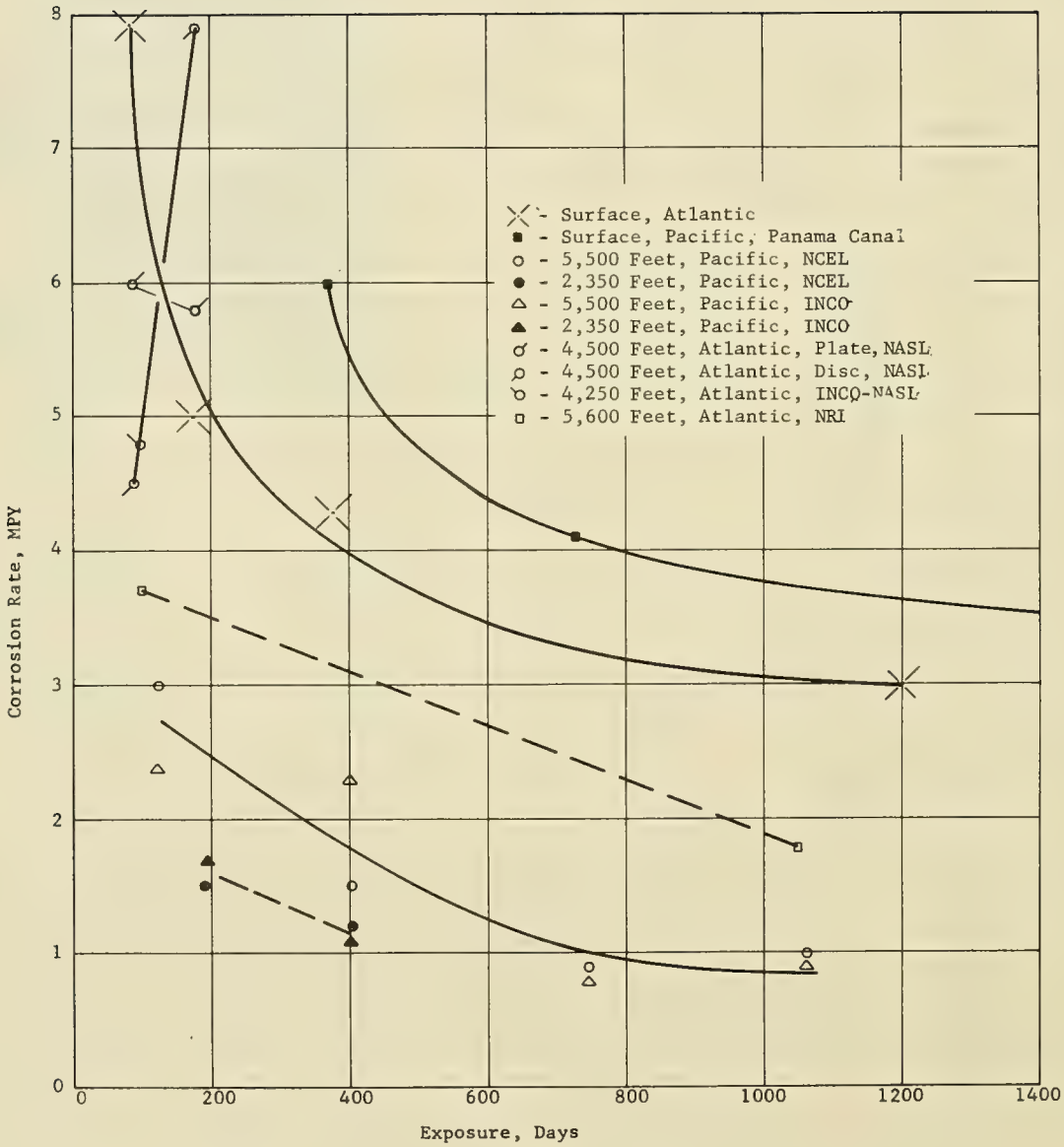

Fig. 3 - Corrosion rates of low carbon steels at various locations

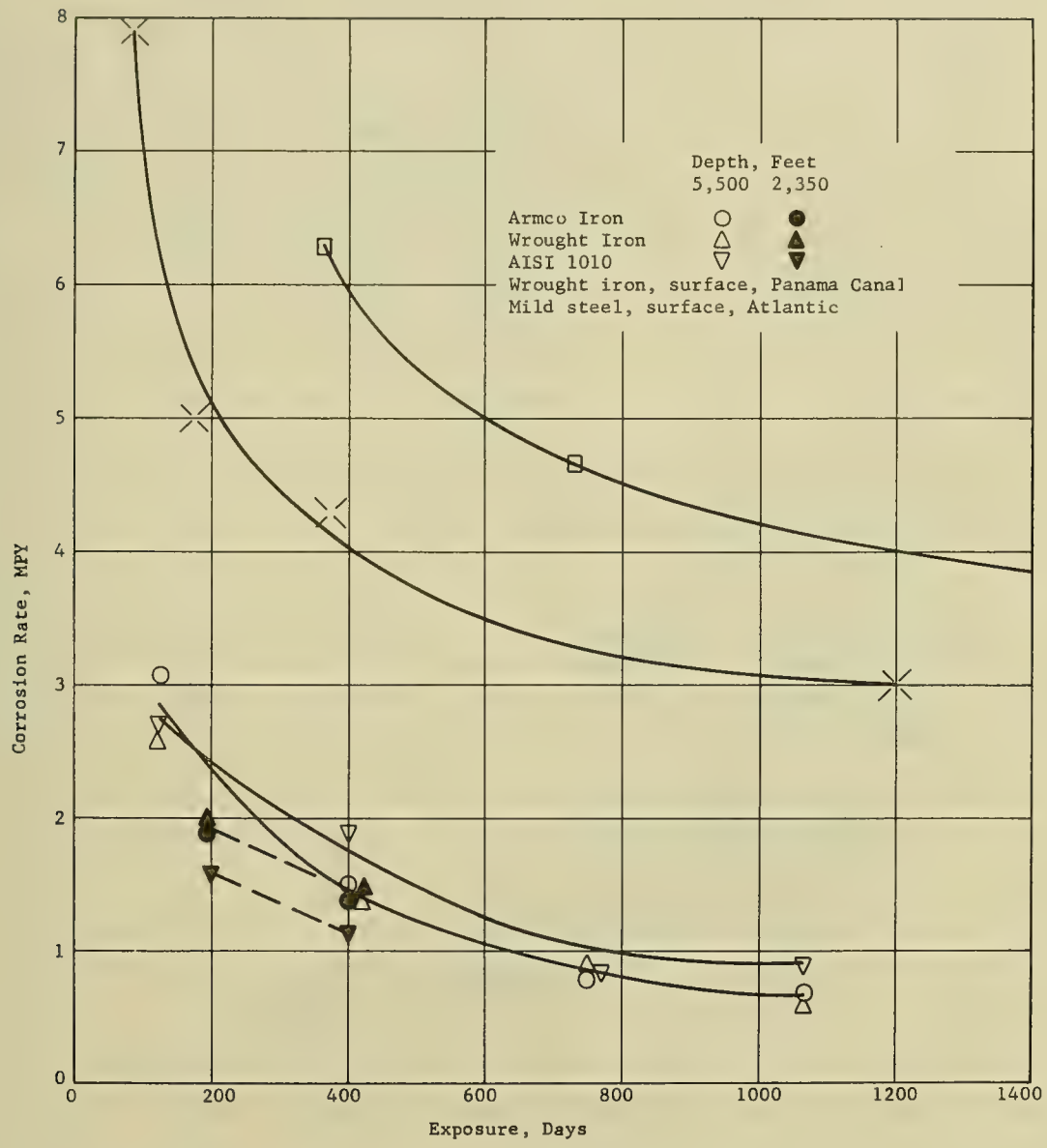

Fig. 4 - Corrosion rates of wrought ironand Armco iron

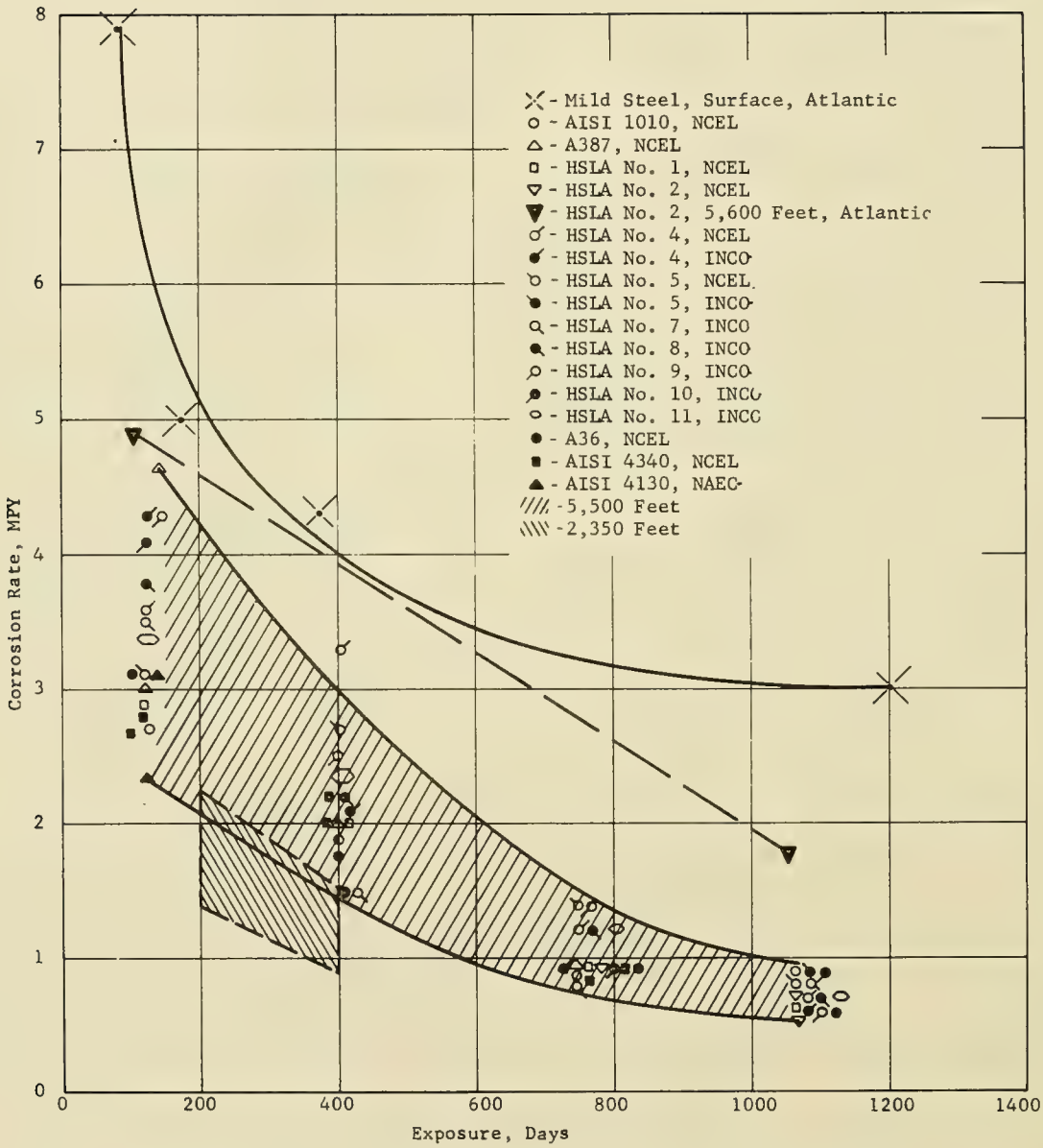

Fig. 5 - Corrosion rates of steels in sea water

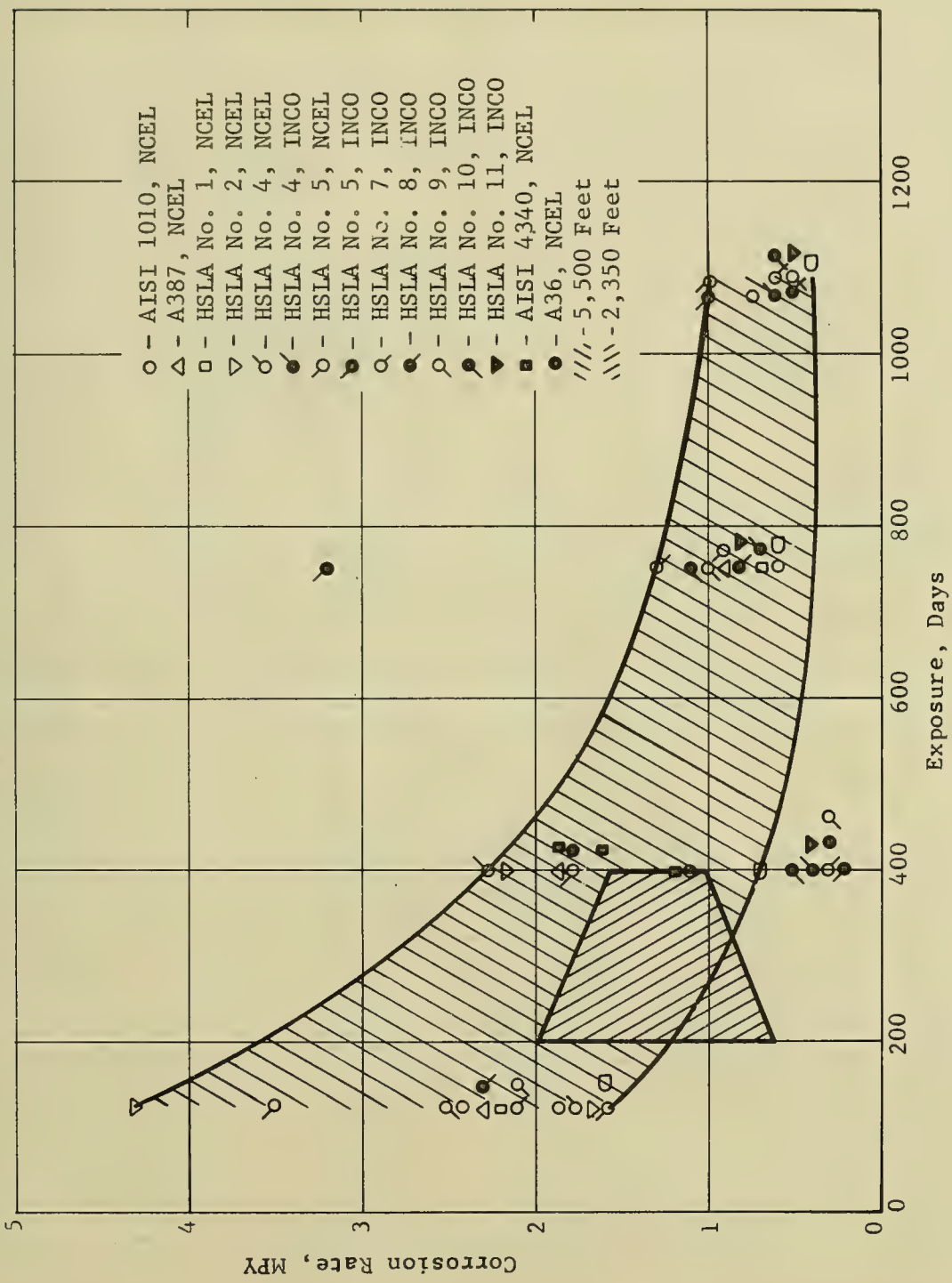

Fig. 6 - Corrosion rates of steels in the bottom sediments

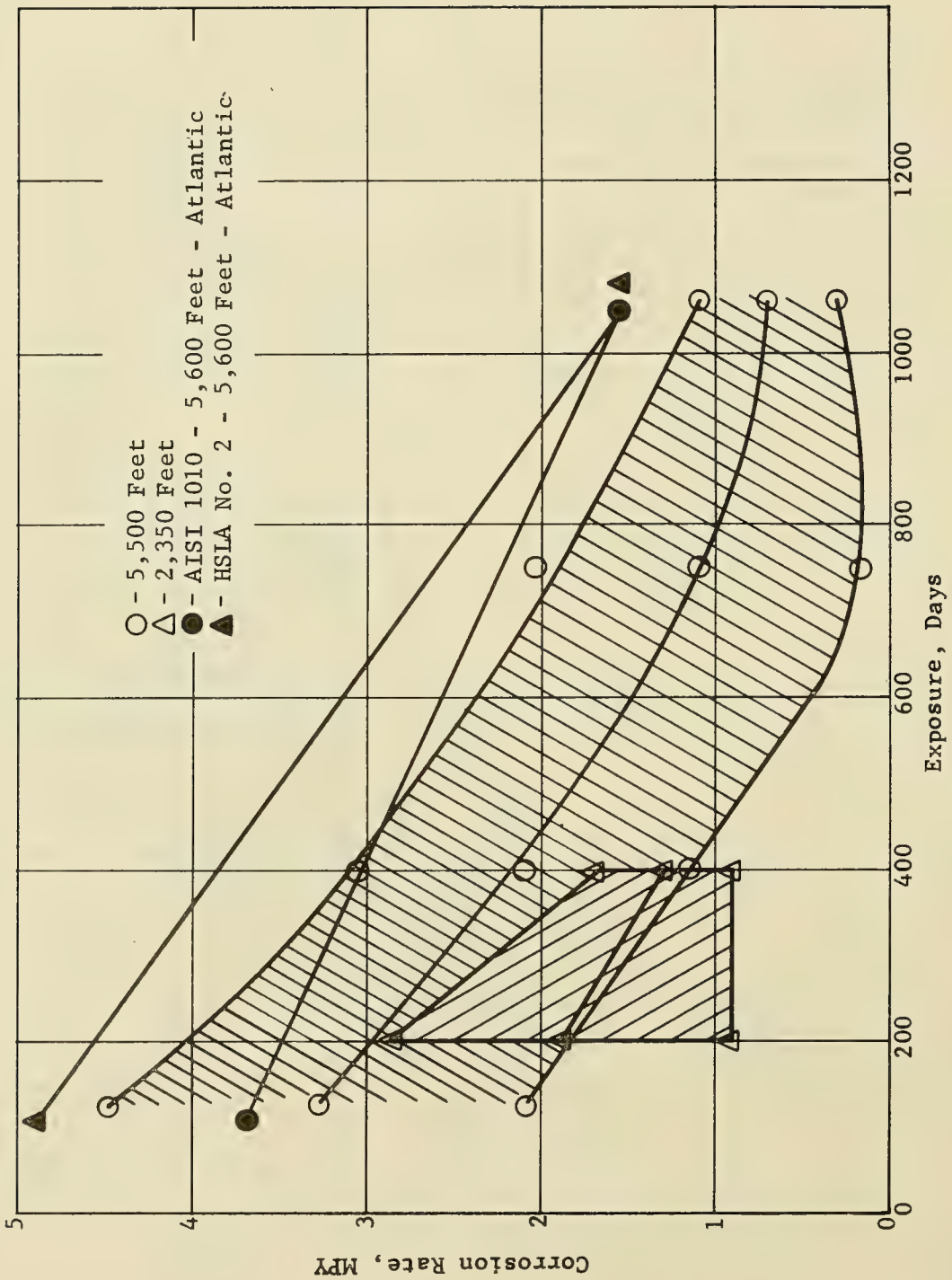

Fig. 7 - Statistical curves, 95 percent confidence limits, for steels in sea water

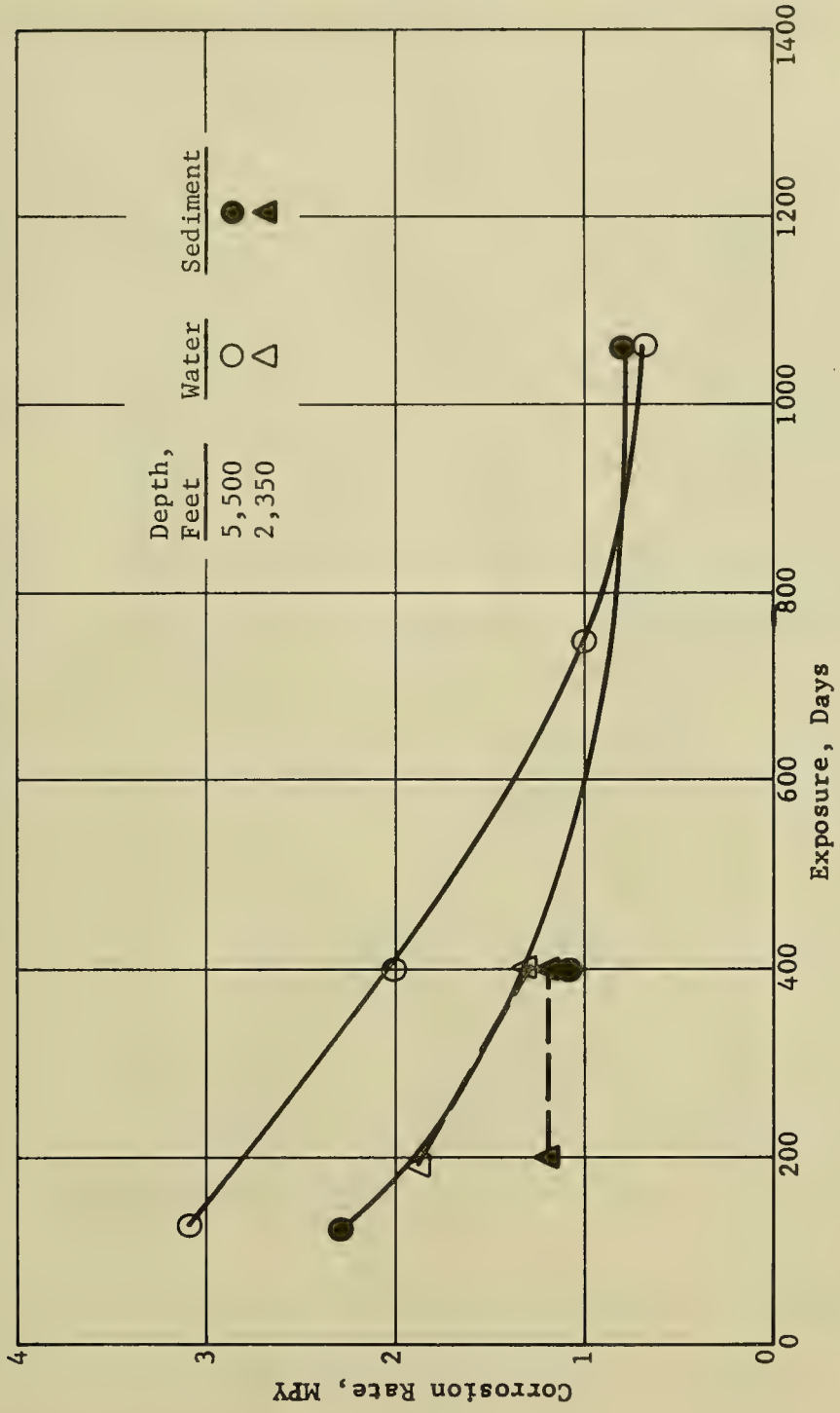

Fig. 8 - Median statistical curves for steels in sea water and in the bottom sediments

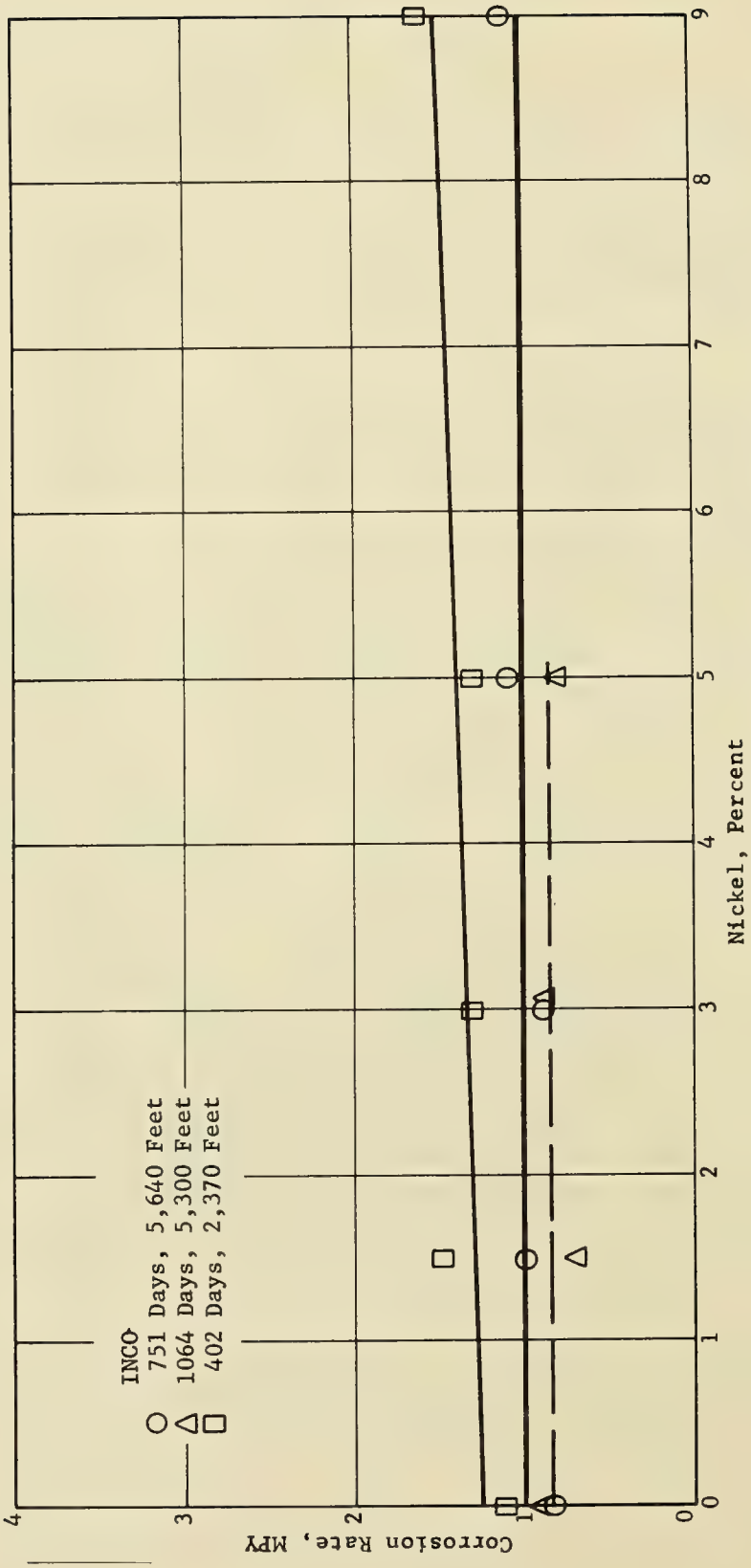

Fig. 9 - Effect of nickel on the corrosion rate of steel in sea water

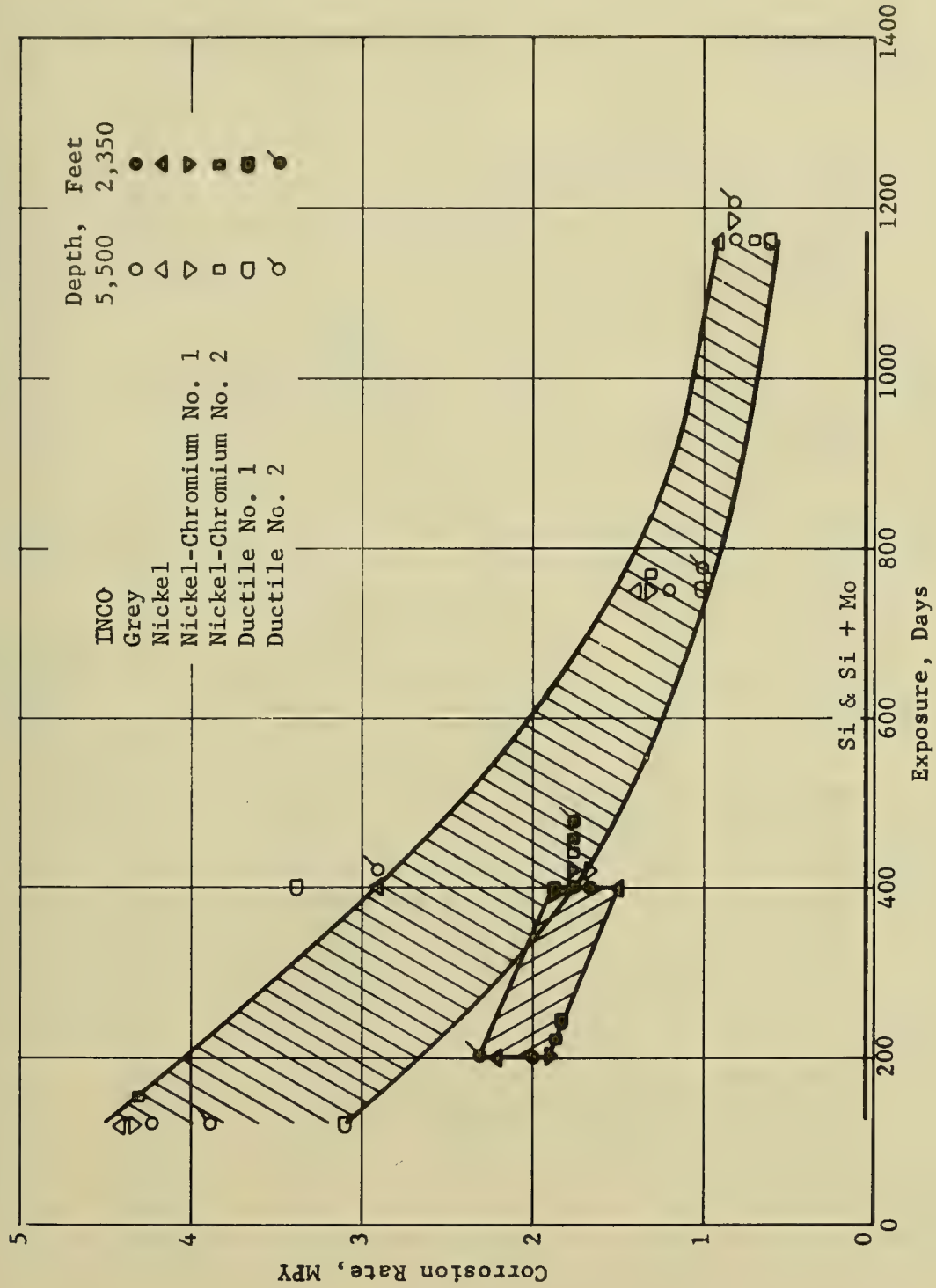

Fig. 10 - Corrosion rates of cast irons in sea water

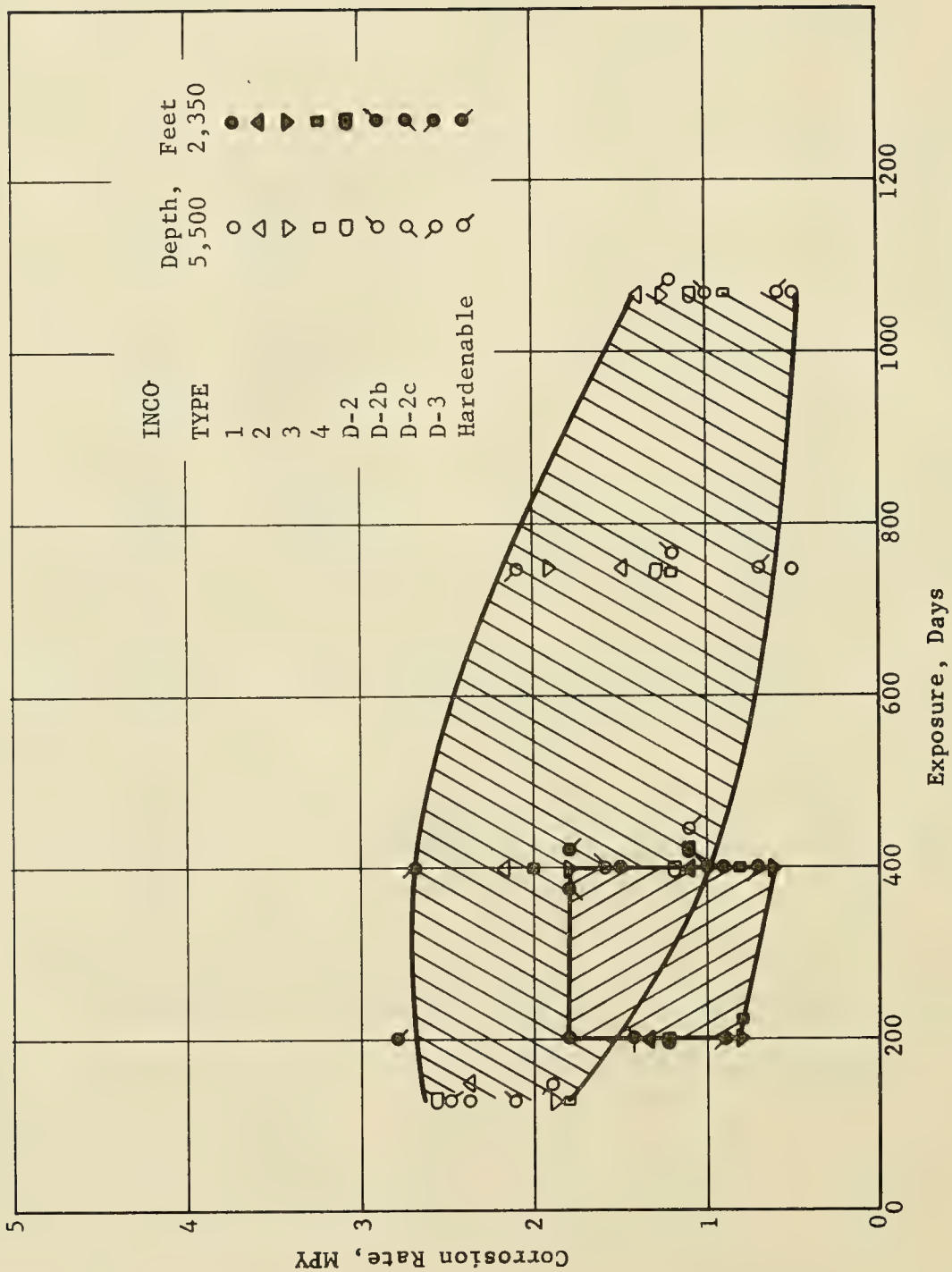

Fig. 11 - Corrosion rates of austenitic cast irons in sea water

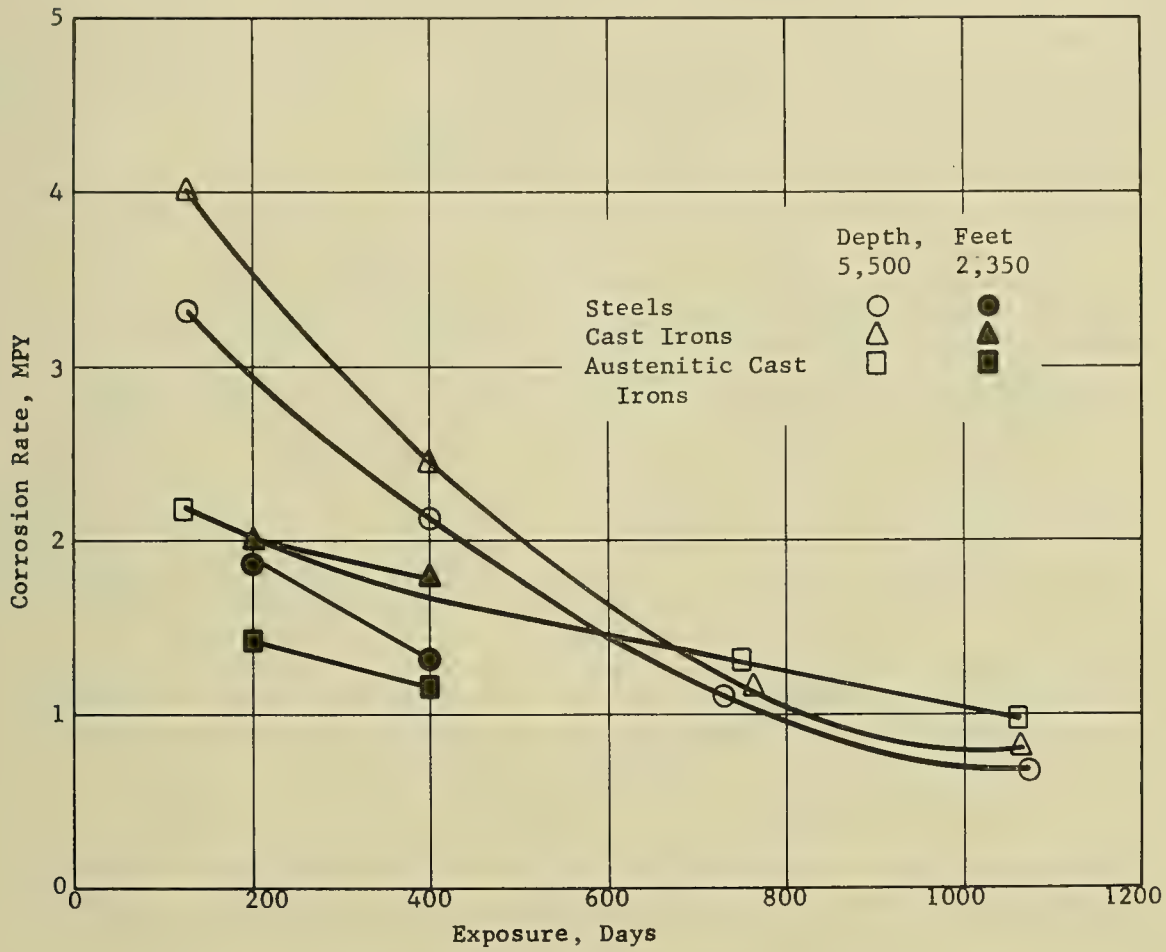

Fig. 12 - Statistical median curves for steels, cast irons and austenitic cast irons in sea water

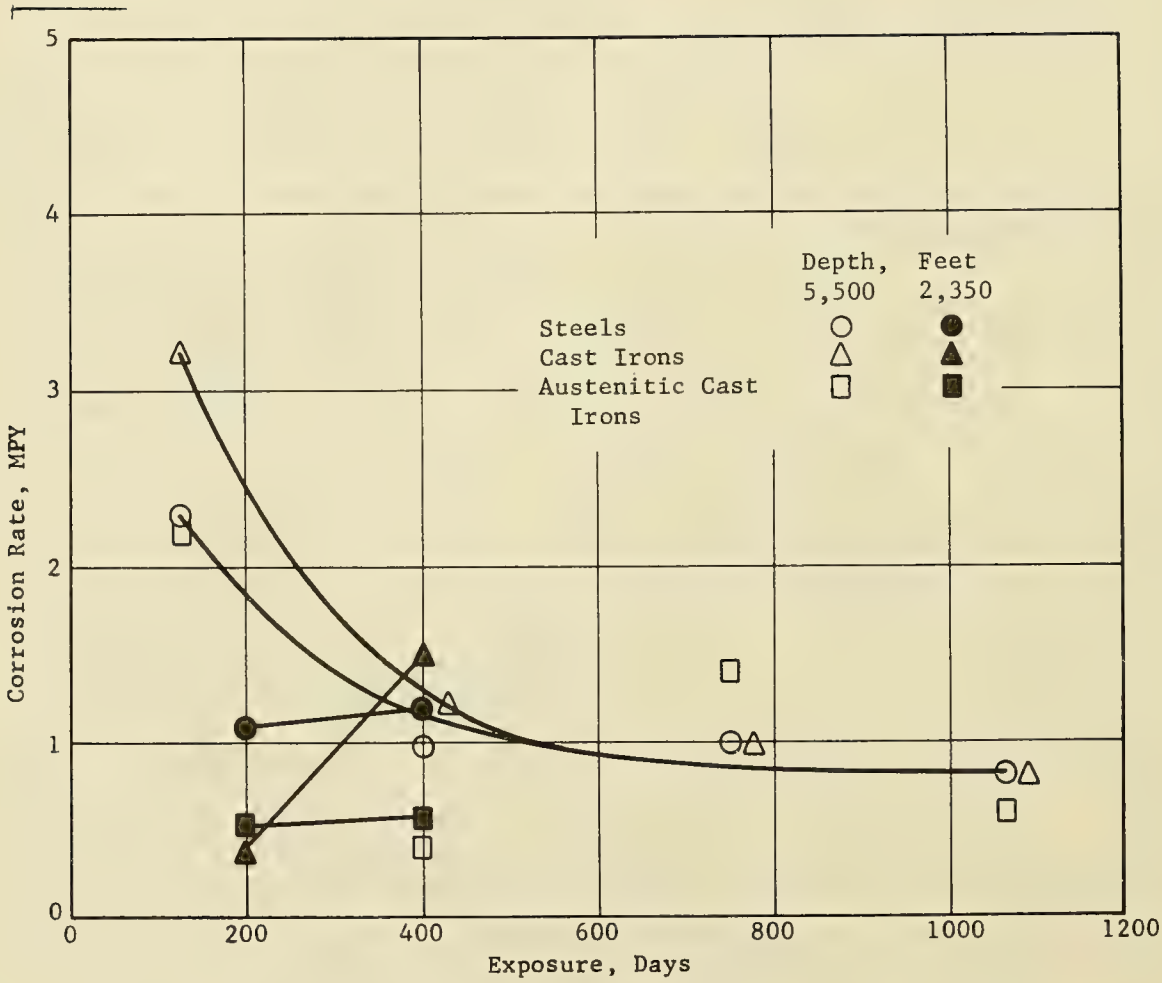

Fig. 13 - Statistical median curves for alloy steels, cast irons and austenitic cast irons in the bottom sediments

Sensors, Controls and Displays of the Deep Submergence Rescue Vehicle (DSRV)

Stanley K. Sezack
U.S. Naval Applied Science Laboratory
Brooklyn, New York 11251

The Deep Submergence Rescue Vehicle (DSRV) being developed under the cognizance of the Navy's Deep Submergence Systems Project Office will be a 50 foot submersible weighing under 60,000 pounds. The submersible will permit the evacuation of personnel from a distressed submarine under all weather conditions, under ice and at depths greater than present submarine collapse depths. Since by nature the rescue system must be a rapid response system, availing itself to any ocean area, the submersible and its support system are being designed to be both land and air transportable. Operationally the submersible will be supported by either a surface ship or a "mother" submarine which will be capable of transporting the submersible in a "piggy back" fashion. The surface support ships will be ASR's of the new catamaran class, which will transport and support two rescue submersibles simultaneously. In addition they will contain a Rescue Control Center from which a rescue operation can be monitored and controlled. Each of the nuclear "mother" submarines, which will permit under ice and all weather operations, will employ a pylon and trapeze assembly mounted above its escape hatch to facilitate transport and docking (mating) of the submersible. The sonar, navigation and sensor systems normally carried aboard the fleet "mother" submarine will, to a large extent, perform the function of the Rescue Control Center systems aboard the surface support ship.

Rescue Submersible

The hull, external effectors and life support systems of the prototype rescue submersible are being developed by the Lockheed Missiles and Space Company of Sunnyvale, California. The development and integration of sensor, ship control, and control and display systems is being accomplished by Naval laboratories, academic institutes and contractors, under the direction of the Sensors/Ship Control Branch of the Deep Submergence Systems Project Office.

The submersible is composed of three interconnecting seven foot pressure spheres which, with the external effectors, are encased in a free flooding lightweight hull. A transfer skirt will be affixed to the center sphere to facilitate mating to a submarine escape hatch. The center and rear spheres, reserved for the transfer of personnel, will be capable of accommodating up to twenty-four evacuees at one time. The forward sphere will house the pilot and co-pilot, their life support systems, an emergency battery, power converters, inverters and heat exchangers in addition to the internal sensors, controls, displays and sensor system electronics.

DSRV Sensor, Control and Display Systems

The difficult environment in which the submersible must operate, near the ocean bottom and in the proximity of a disabled submarine hull, as well as the requirement to mate to the disabled submarine escape hatch in the presence of ocean currents have imposed the need for an extensive number of sensors. The sensor, control and display subsystems, which are being integrated by the Naval Applied Science Laboratory, include the sonar, communication, optics, ship control, central processor and special device units of the submersible. Consideration has been given to the use of the submersible for secondary oceanographic research missions and its initial design has allowed for the subsequent addition of secondary mission sensors.

The optical suit consisting of camera, light and viewport optical subsystems will be used for direct short range observations as well as for recording purposes. One internal and five external TV cameras, some of which will be mounted on retractable pan or on pan and tilt mechanisms, will permit short range viewing, during inspection and final mating operations. An internal TV camera, mounted on the mating hatch viewport and two external TV cameras mounted on pan and tilt mechanisms, fore and aft of the mating skirt, will provide the operators with redundant optical systems during inspection and final mating operations. A TV camera mounted in the nose of the submersible will permit forward observation and two upper TV cameras mounted on pan mechanisms will permit surfaced observations as well as inspection in the event of underwater fouling. Still and movie cameras mounted on the pan and tilt mechanisms will provide a means of recording as well as a method of on-site evaluation of problems caused by debris obstruction. Internal viewport optics will facilitate direct observation for extended periods without the limitation caused by fatigue resulting from cramped position, direct eyeball viewing through the viewports.

The communication suit will include a long range underwater telephone, a voice and instrumentation tape recorder, a radio for surface communication and positioning, a telephone intra and intercom system and directional listening hydrophones. The hydrophones, which are merely an extension of the pilots' ears to the outer hull, will enable the operator to home in on a signal source.

The navigation suit will furnish attitude and attitude rate data as provided by gyrocompasses, a vertical gyro and rate gyros. A dead reckoning plotter will present a visual display of the submersible's motion in a horizontal plane from data furnished by the attitude indicators and a relative velocity indicator or from the doppler navigator. The doppler navigator will also furnish high accuracy rate and position data during the mating operation. A beacon navigation system which will operate with two or more transponders, deployed on the ocean bottom, will augment the dead reckoning capabilities of the submersible.

The ship control system will be a hybrid analog-digital system which will receive rate commands from the central processor or the human operator depending on the operational mode selected. In the cruise mode it will control the submersible in three degrees of freedom, however, for mating or inspection operations the necessary six degree-of-freedom control will be maintained. In order to reduce the burden on the operator, optional combinations of manual and automatic control modes will be available. Since an uncoupled response will be available in each of the six degrees-of-freedom, the operator can elect to maneuver the submersible in one degree of freedom manually while the remaining five degrees of attitude and displacement are held to their last commanded displacement.

The central processor will be a digital computer with two functional sections, a general purpose section and a digital differential analyzer section. The general purpose section will be used for low iterative random in time programs and the digital differential analyzer section will be used for high iterative continuous in time programs. The processor will service navigation, sonar, communication and ship control subsystems to provide attitude, dead reckoning, status, alarm and control functions for submersible operation.

The sonar suit will consist of horizontal and vertical obstacle avoidance sonars, an altitude and depth sonar and a short range sonar which will be used in mating operations. With the profusion of sonar units on the submersible it has been called a sonic Christmas tree. The multifold approach developed to minimize sonic cross talk is as follows:

Spatial separation - The transducers are distributed over the available surface of the vehicle and their beam patterns are directed in a manner that will cause minimal interference and still serve their intended purpose efficiently.

Functional separation - An operational plan has been devised which will ensure that only those sonars required for a specific part of the mission will be used. When not required those sonars will be secured.

Timing separation - A sonar timing coordinator has been developed that will sequence the operation of the altitude, depth, vertical obstacle avoidance and transponder interrogation sonars so as not to interfere with each other.

Frequency separation - Separate frequency bands have been allocated to the sonars so that interference between the units that must be on simultaneously will be minimized.

The controls and displays for the sensors, power supplies, vehicle effectors, manipulator and life support equipment have been integrated in a control panel located in front of the operators. Multi purpose sonar and TV displays have been incorporated in the panel for simultaneous viewing of selected sensors and for reasons of redundancy. In addition the central processor has been programmed to automate many of the control and status functions to relieve the operators of the monitoring load.

With the addition of special devices such as radiation detectors and pressure gages, the number of major Sensor/Ship Control subsystems will approach forty. To meet mission reliability requirements functional redundancy has been provided in critical areas such as obstacle avoidance, attitude reference, navigation, ship control and depth indication. With equipment redundancy, a Sensor/Ship Control subsystem reliability of 0.96 for a rescue mission sequence is considered a reasonable goal.

The developmental DSRV is scheduled for sea tests in mid 1968. Shortly thereafter the Navy will, for the first time, have a rescue capability extending to collapse depths of fleet submarines.

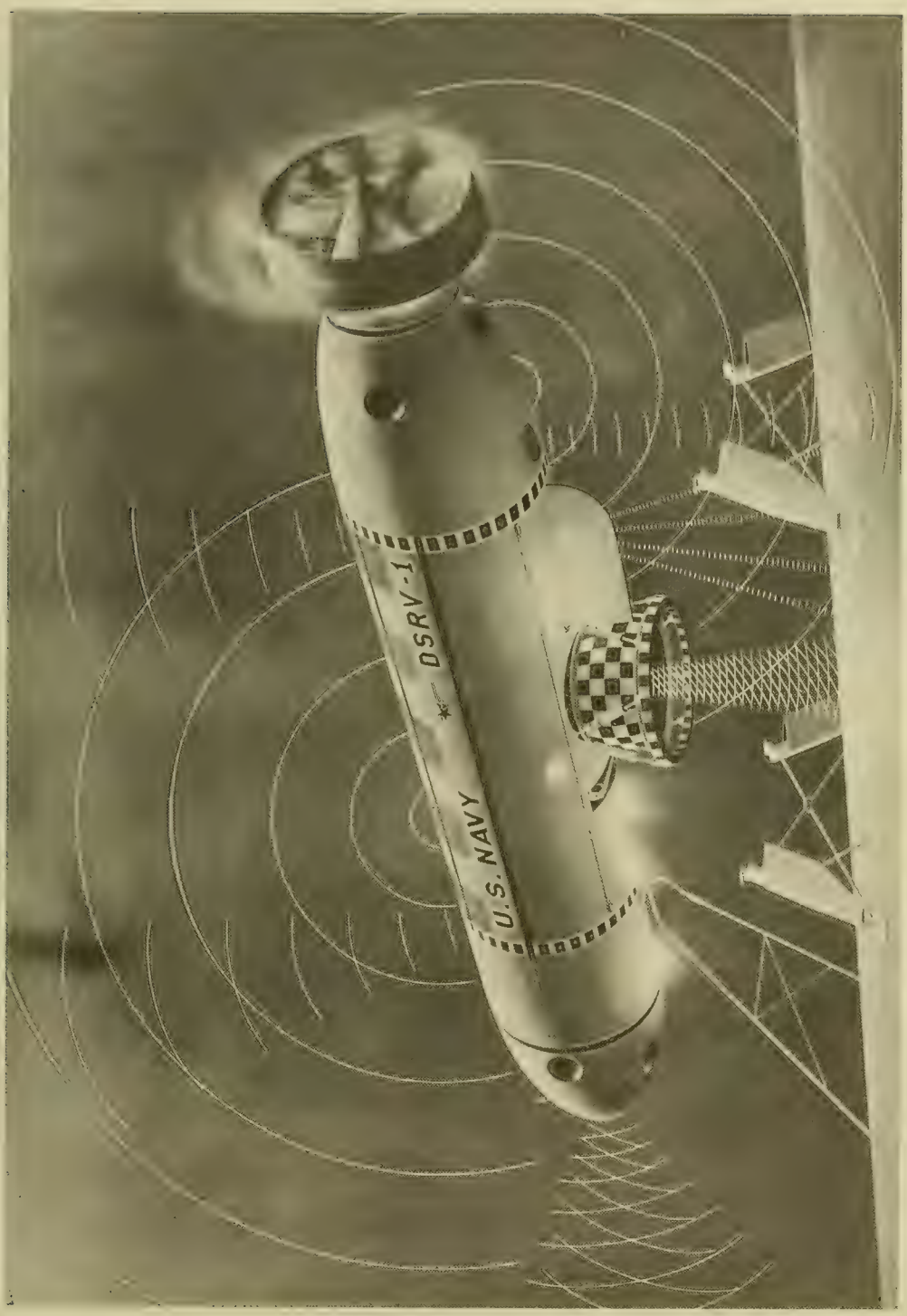

Fig. 1 - Prototype deep submergence rescue vehicle

The "Fail-Safe" Program for Prevention of Losses of Oceanographic Equipment

George L. Poudrier
U. S. Naval Weapons Laboratory
Dahlgren, Virginia

Richard L. Stewart
U. S. Naval Oceanographic Office
Washington, D. C.

Losses of oceanographic instruments over the past several years have proven expensive to the Oceanographic Office, not only because of the cost of replacing the instruments themselves, but because of the ensuing loss in ship time, failure to acquire needed data, and delays in completing programs. At the direction of the Deputy Commander for Oceanography, the "Fail-Safe" program was initiated to develop equipments and methods which would help in reducing these losses. The objective of this paper is to present the results of work to date on the program, describe developments now in progress, and identify some of the problem areas which must be approached in the future.

In first approaching this problem it became apparent that the logical steps to be followed were:

1. Determination of the causes of losses

2. Study of the cost of loss as a part of total cost of data collected.

3. Selection of areas where development was needed to provide the most immediate and rewarding solutions.

To discuss these points in the same order, determination of causes of losses was undoubtedly the most important, and unfortunately the most neglected.

An early expert on the subject once said:

> And now remains
> That we find out the cause of this effect,
> Or rather say, the cause of this defect,
> For this effect defective comes by cause.

You may recognize the quotation from Act II, Scene II, Hamlet. In the new and growing field of Reliability Engineering this is known as Failure Mode and Effect Analysis. The Aero-space and Weapons industries have developed these activities to a point far beyond that presently practiced on oceanographic instrumentation, and have developed a body of information, literature, and doctrine concerning the very real necessity of an adequate feed-back of information during design, development and field operation of their equipment. Lacking the needed failure reporting system, we were forced to rely on interviews with operating personnel and the small amount of information obtained from equipment survey reports. In many instances of equipment loss it was not possible to determine either the Failure Mode (which is the technical term used in Reliability Engineering corresponding approximately to "what happened" or the Failure Mechanism, which corresponds to why it happened. The effect was usually more apparent, i.e., the survey operation was delayed until new equipment was available, or was discontinued altogether. In a sufficient number of instances to warrant corrective action, it was determined that the Failure Mode was a parted cable, and that the Failure Mechanism was either accidental two blocking of an instrument while hoisting in or fatigue failure in the cable or terminator. The term "two-blocking" as used here is indicative of faulty semantics as well as seamanship. In its usual Naval usage it means to hoist an item until it is against the upper block. To our field survey personnel it means to hoist the item unintentionally against the block with such force that the cable is parted and hence the instrument lost.

The second step in formulating the approach was to look at the losses as a part of the total system cost, which is the cost of obtaining certain specific data. Included in this total are program planning, cost of procurement of necessary instrumentation, salaries of field and supporting personnel, cost of ship time in implanting instrument or taking data while underway, and possibly the cost of the time expended in attempting to locate and recover lost instruments. This leads naturally into a subdivision of instruments into two categories, those from which the desired data is obtained even though the instrument itself may not be retrieved, and those from which no data is obtained until the instrument is recovered. Examples of the first are instruments designed to be expendable and also those telemetering data to ship or shore stations; of the second, self contained recording current meters, etc. If the instrument is of the first type the desired mission may be completed without its recovery. The cost of recovery then becomes a separate item which may be weighed against the cost of replacement with a new instrument. If an expensive "Fail-Safe" device would be required and/or ship time used in locating the instrument a greater risk of loss can be accepted.

In the second type, more attention must be given to loss prevention and to recovery, since the total program costs may be lost unless the instrument and data are retrieved. A further subdivision of instruments would be according to method of deployment. Some are towed at

relatively shallow depths and at speeds of up to twelve knots, others are used "on station" while the ship is hove to and may be lowered to extreme depths, and some are used in conjuntion with moored buoy systems. Each of the three types requires a different approach in "fail-Safe" development, and different items of equipment now in various stages of development will be applied.

The first hardware item to be described, although not the first to be completed, is a simple mechanical device to prevent loss of instrument by two-blocking, which has been the most frequent cause of losses and probably the most costly. Some of the instruments lost in this manner have replacement costs of around $20,000, to which must be added the aforementioned attendant losses in ship time, etc. At first glance it would appear that two-blocking is inexcusable, since if the winch operator is attentive he should always stop the winch before the instrument is brought up against the block. We must remember that if an instrument has been lowered to extreme depths it may normally require an hour and a half to hoist it to the surface, but only another four seconds to hoist it from the surface to the block. Thus inattention of less than one-tenth of one percent of the hoisting time may be enough to cause loss of an expensive instrument. When we consider that the sea-state and visibility conditions are not always ideal, it is not too surprising that some instruments are two-blocked.

The solution offered is to assume that occasionally instruments will be two-blocked and cables broken, but to have ready a mechanism that will catch the instrument before it can fall back into the sea. As shown on the slide, the device which has been developed and successfully tested consists of a "V" shaped bail attached to the standard meter wheel and a special cable terminator for the cable, with the instrument itself supported by a chain about eighteen inches below the terminator. The normal position of the bail is against the wheel, where it is held by shock cords on either side. When hoisted too far, the terminator pushes the bail upward and passes through the wide part of the "V", then strikes against the top of the block. At this point the cable parts and the terminator drops back, but since the shock cords have returned the bail to its normal position, the terminator cannot pass through the small end of the "V". The instrument is caught and remains suspended by the chain. Simple, inexpensive to build, and easy to install, this device has been well received by NAVOCEANO operating personnel and is now being installed on AGOR and AGS ships. A series of tests conducted in the environmental laboratory of the NAVOCEANO Instrumentation Department and aboard USNS SANDS showed sixteen successive catches and no failures to catch a simulated 300 pound instrument package. Statistically, this indicates with a confidence of ninety percent a probability of success of eighty seven percent in actual use. Continued testing might improve this figure somewhat, but certainly it is an improvement over the former 100 percent certainty of loss of the instrument if two-blocked. The terminator tested was designed for use with 4-H-O cable (four conductor) and uses a low temperature potting solder having a melting

point of 281 degrees for potting. This low temperature does not damage the electrical insulation, and the terminator will hold the full breaking strength of the cable. In order to control the point at which the cable parts, a cutter blade is incorporated in the terminator. This may also serve to prevent damage to the meter wheel.

A smaller version of this device has been developed for use with the mechanical bathythermograph or other small instruments lowered on a solid wire of similar diameter. With this device no attempt is made to cut the cable, and the terminator is replaced with a swaged fitting of the type used on aircraft control cables. The ultimate goal of design simplicity has almost been reached here -- there is only one moving part. Preliminary tests results in the laboratory have proven completely successful, but more testing will be conducted before it will be considered ready for field installation. In view of the large number of Navy ships using mechanical BT's, the potential savings which could result from such a simple device are quite large.

The next item to be described is a recovery system for a towed acoustic transducer housing. The office has lost towed transducers used in geophysical survey operations. Cost of the transducer and housing is approximately $30,000 and a lead time of about four months required to replace a lost unit. The complete unit is nine feet long, weighs 2000 pounds in air and 800 pounds in water. It is normally towed continuously by the survey ship at a depth of about 100 feet. Failures had occurred in the terminator, the cable, and the point of attachment to the structure of the housing. The recovery system developed borrowed heavily from techniques used in recovery of exercise torpedoes. Compressed air cylinders were mounted within the body of the fish, and inflatable flotation bags mounted behind doors cut in the housing. In operation, if the "fish" drops below a preset depth an actuator mechanism opens an air valve from the bottles, an air solenoid unlatches the doors, and the flotation bags are deployed and inflated. At the same time an independent system actuates a Xenon flasher on the tail fin of the "fish" and an acoustic pinger on the bow to aid in location. This system has been field tested and performed satisfactorily.

With this system we needed an actuating device which would be reliable in operation, have long shelf life, and require a minimum amount of attention by the shipboard personnel. The solution, which is shown in the slide, consists of a cylinder having at one end a rupture disc set to break at the proper depth. When the disc breaks a compartment containing a sea-water battery is flooded and the battery energized. This in turn fires an explosive squib, which drives a piston to open the air valve. Operation of the piston is obtained in 0.6 seconds after rupture of the disc. We feel that this has been a worth while project, since several of these transducer housings are in constant use in the Marine Geophysical Survey program. It is not, however, of very general application, since it was designed for one particular instrument housing to be used in a given manner. Our attention now has turned to systems having a broader potential use with a variety of

instruments. At present, developmental work is under way on two types of flotation systems, one of which should have general application to any towed instrument used within a few hundred feet of the surface, the other for use with instrument packages which may be lowered to extreme depths, such as 20,000 feet.

While compressed gasses can be used near the surface, as the depth increases their use soon becomes impractical, since the weight of a cylinder which would contain the gas at a high enough pressure to generate buoyance becomes too great. Therefore it was necessary to investigate the use of liquids or solids which could be decomposed into gas when required.

Selection of the most practical chemical for gas generation then became the subject for investigation. The most important criterion was generation of maximum buoyancy per pound of chemical, safety, ease of initiation of reaction, etc., were also important. *The analysis is based on Van derWall's equation of state for the gases of interest. The important parameters are the molecular weight of the buoyant gas and the stiochiometry of the reacting system. The data is presented graphically as weight of chemical reagent needed per one hundred pound, water weight, of system to be lifted as a function of sea depth. Also included as parameters are the molecular weight of the buoyant gases and the gas generating efficiency of the reagent chemicals.

Again we were fortunate in being able to draw upon experience gained by the Navy in torpedo recovery systems. The Naval Ordnance Test Station in China Lake, California, was actively engaged in development of gas generators employing hydrazine (N_2H_4) for creation of buoyancy for salvage and recovery purposes, and had recovered items from depths of over 2000 feet. One of their systems had been made ready for use in the recovery of the lost nuclear bomb off Palomares. Although their systems were not directly applicable to our purposes because of the weight of the associated equipment required, it appeared that with some redesign these problems might be overcome. Financial support of the work at China Lake by the Supervisor of Salvage, Naval Ships Systems Command, was a very valuable assist, and assignment of Mr. Jay Witcher as project manager for both the salvage requirements and instrument recovery gave us immediate access to the best available experience in this area. NOTS, Pasadena had also conducted experimental work with recovery systems employing lithium hydride as a source.

At this time we have under development instrument recovery systems employing hydrazine and light metal hydrides. Prototypes of both of these systems are being tested at sea aboard USNS GILLISS in an area near Bermuda this week. The hydrazine system is designed to have a lifting capacity of 300 pounds at a depth of 20,000 feet and the light metal hydride system is incorporated in a modular housing

*Details of the analysis will be published as a U. S. Naval Weapons Laboratory Technical Memorandum.

for use with towed instruments at relatively shallow depths. Hydrazine and Hydrazine base fuel mixtures decompose in a catalyst in a gas generator to produce an exhaust gas consisting of hydrogen, nitrogen, and ammonia. These fuels are classed as corrosive liquids, with toxic vapors, and safety precautions very similar to those for handling aviation gas must be observed. Gas temperature, ranging from 200 to 2000°F, can be controlled by varying the fuel mixture and the length of the catalyst bed. Two types of catalyst pellets are used: spontaneous and non-spontaneous. Both are composed of alumina, but with different impregnated active metals. Shell 405 catalyst, developed under NASA contract, is spontaneous, but has the disadvantage of high cost. The non-spontaneous catalyst (HA-3) is low in cost but required an electric cartridge heater or a hypergolic reaction to start the decomposition, after which the reaction is self-sustaining. Our applications use a layered catalytic bed, using the 405 to initiate the reaction and the less expensive HA3 to sustain and complete it. Both types are true catalysts; that is they are not altered in the decomposition process and are indefinitely reusable.

The key to successful use of hydrazine generators for deep recovery has been the development of a suitable method of transfer of the fuel from its container to the catalytic chamber. In circumstances where system weight and size have not been critical this transfer has been made by use of compressed nitrogen or hydraulic pistons. Neither method is practical at great depths, since a pressure vessel to contain the fuel and compressed nitrogen or pumping system would add too much weight to the total instrument package. This has been overcome by storing the fuel in a rubber container, so that it is always exposed to ambient pressure. The small pressure differential needed to cause the fuel to flow from the storage container through the catalytic chamber is achieved through use of polymeric springs arranged to keep the ends of the fuel container under tension. Thus the entire system is very nearly neutrally buoyant in sea water, with only the small catalytic chamber and piping being required to withstand the ambient pressure. Feasibility of this approach was demonstrated in tests conducted in the Tongue of the Oceans in December, 1966, using a system put together from available components with a mechanical spring. The tests now being conducted use the arrangement shown on slide and will approximate an actual recovery from greater depth than previously accomplished.

It now appears that it will be possible to equip our deep instrumentation packages with a system which will bring them back to the surface in the event of cable failure. We will also need an actuating system to tell the recovery system to get to work and start generating its buoyant gas. At the moment a timer is used, and probably for most applications this will be all that is necessary. When an instrument is lowered over the side the oceanographers know within reasonable limits how long it should take to accomplish a certain operation. A timer can be set to start the recovery system if the package has not been retrieved normally within that time. Since the weight of cable

used in lowering a package to 20,000 feet is considerable, it may prove necessary to jettison the cable and recover only the instrument. This can be done by use of an explosive cutting device. Other methods of actuating the system can also be assembled, using equipment now commerically available. An acoustic command unit of the type now used on anchor release devices could be modified slightly to open a fuel valve on a hydrazine recovery system. This would also permit use of the hydrazine system for recovery of instrument which may be deliberately placed on the ocean floor for a longer period, or to provide additional life for buoyed instrument systems where the buoyancy of the supporting submerged buoy is marginal or has been impaired accidentally.

Light Metal hydrides offer another chemical source for gas generation. The basic chemicals are considerably more expensive than hydrazine, and unless properly compounded and handled can be more hazardous. Advantages are that the gas evolved is pure hydrogen, giving maximum buoyancy per pound of chemical, and that the reaction is easily started by exposure to sea water.

A wide variety of instruments are towed by survey and research ships at depths ranging from just below the surface to several hundred feet. The transducer housing described previously is one of this type, and in this case it was practical to install a complete recovery system within the housing. Since in many cases this would not be possible, it is desirable to have available a series of modular systems which can be used in conjunction with equipment such as sparker sleds, gravimeters, etc. The second recovery system now being tested aboard USNS GILLISS consists of a towed body containing the recovery system only. This will be neutrally buoyant and will be towed astern of the instrument it is intended to protect against loss. As shown in the slide, the housing consists of two fiber-glass dishes containing the flotation bag and containers of hydride. Again an overpressure mechanism will actuate the system, permitting the dishes to separate and extend the bag. The same motion will operate a lid-flipper to open the hydride containers to sea water, and hydrogen will be evolved to inflate the bag. The shape of the housing is designed to offer low drag while in the normal towing mode. When the system is actuated, the bridle separates to permit the dishes to spread apart. Weight of the instrument package is then suspended below the container, and the upper dish will act as a drogue to slow the descent of the entire assembly while the bag is filling.

Again it has been necessary to devise an actuating system, in this case to release the bridle. The same rupture disc and sea water battery used in the air operated system are employed, with the squib used to ignite an explosive wire. When this wire is burned, the cable connector is released. The slide shows a cut-away of the device, and a quick demonstration of its operation will be shown.

Although still in the prototype testing stage, this system opens the way to production of a series of modules having varying lifting capacity under various conditions of use which can be kept in stock for issue as required. Long shelf life can be obtained by careful sealing of the hydride container, and is inherent in the sea water battery-rupture disc actuator. Field personnel will need only select the unit of proper capacity and attach it to be towed astern of their instrument package.

In addition to the application of these recovery systems to prevention of instrument loss, they may have other useful applications in small object recovery. Since they are neutrally buoyant, they could be easily handled by a diver, by a small manned submersible, or CURV. We believe that the equipment developed under this project can be of very real value to the oceanographic office, and are implementing their use as rapidly as possible. The total value to the field of military oceanography is dependent upon the use that other activities can make of them. We would like to encourage the exchange of information on the subject of loss prevention, and will make available to anyone interested the details of the work presented here.

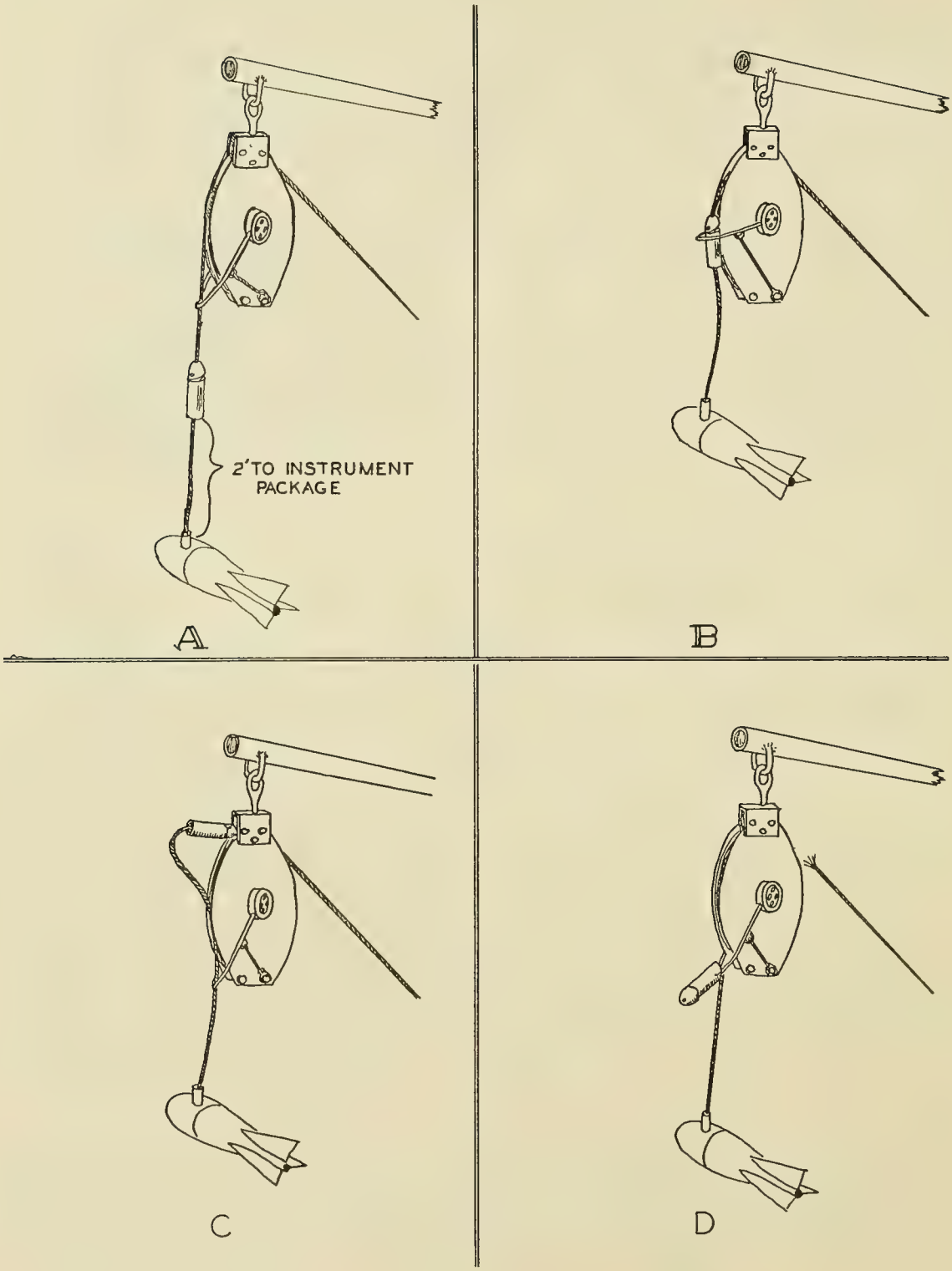

Fig. 1 - Two-blocking device

STOICHIOMETRY

$$A + bB + I \qquad hH_2 + nN_2 + cCO + R$$

REACTION EFFECIENCY

$$\text{EFF.} = \frac{gG}{hH_2 + nN_2 + cCO}$$

POUNDS OF GAS/POUND OF REACTANTS

$$X = \frac{hH_2 + nN_2 + cCO}{A + bB + I} \qquad \frac{gG}{hH_2 + nN_2 + cCO}$$

POUNDS OF REACTANTS/POUND OF GAS

$$Y = \frac{1}{X} = \frac{A + bB + I}{gG}$$

POUNDS OF GENERATOR HARDWARE/POUND OF REACTANTS

LET THIS = U

GENERATOR SYSTEM WEIGHT/POUND OF GAS

$$K = Y + YU = Y(1 + U)$$

EQUATION OF STATE

$$P = \frac{RT}{V-b} - \frac{a}{V^2}$$

VAN DER WAALS CONSTANTS

FOR MIXTURES: b LINEAR
a LINEAR SQUARE ROOT

WEIGHT OF REACTANT - (NEUTRAL BUOYANT)

$$W = Ye\left(\frac{100}{64.0 - e}\right)$$

Fig. 2 - Buoyancy equations

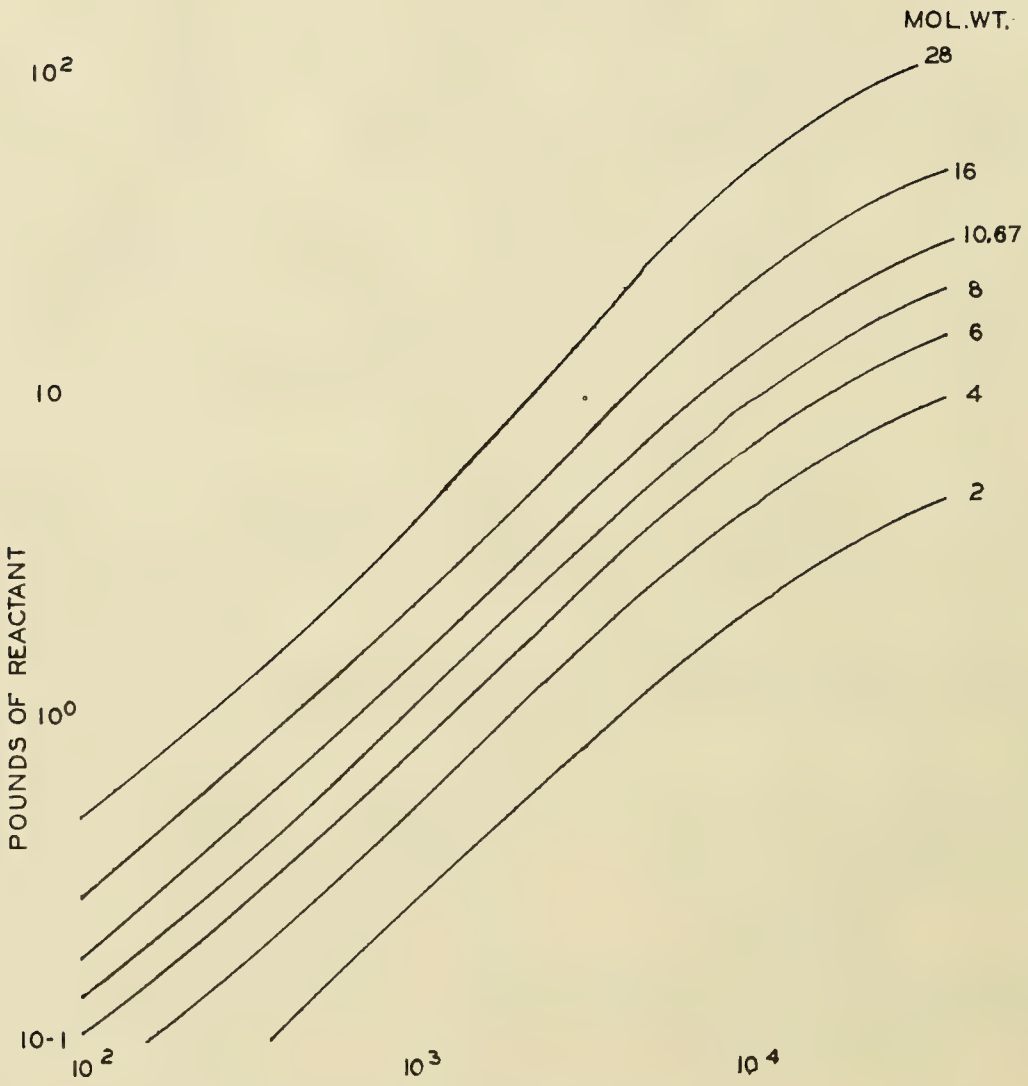

Fig. 3 - Buoyancy curves

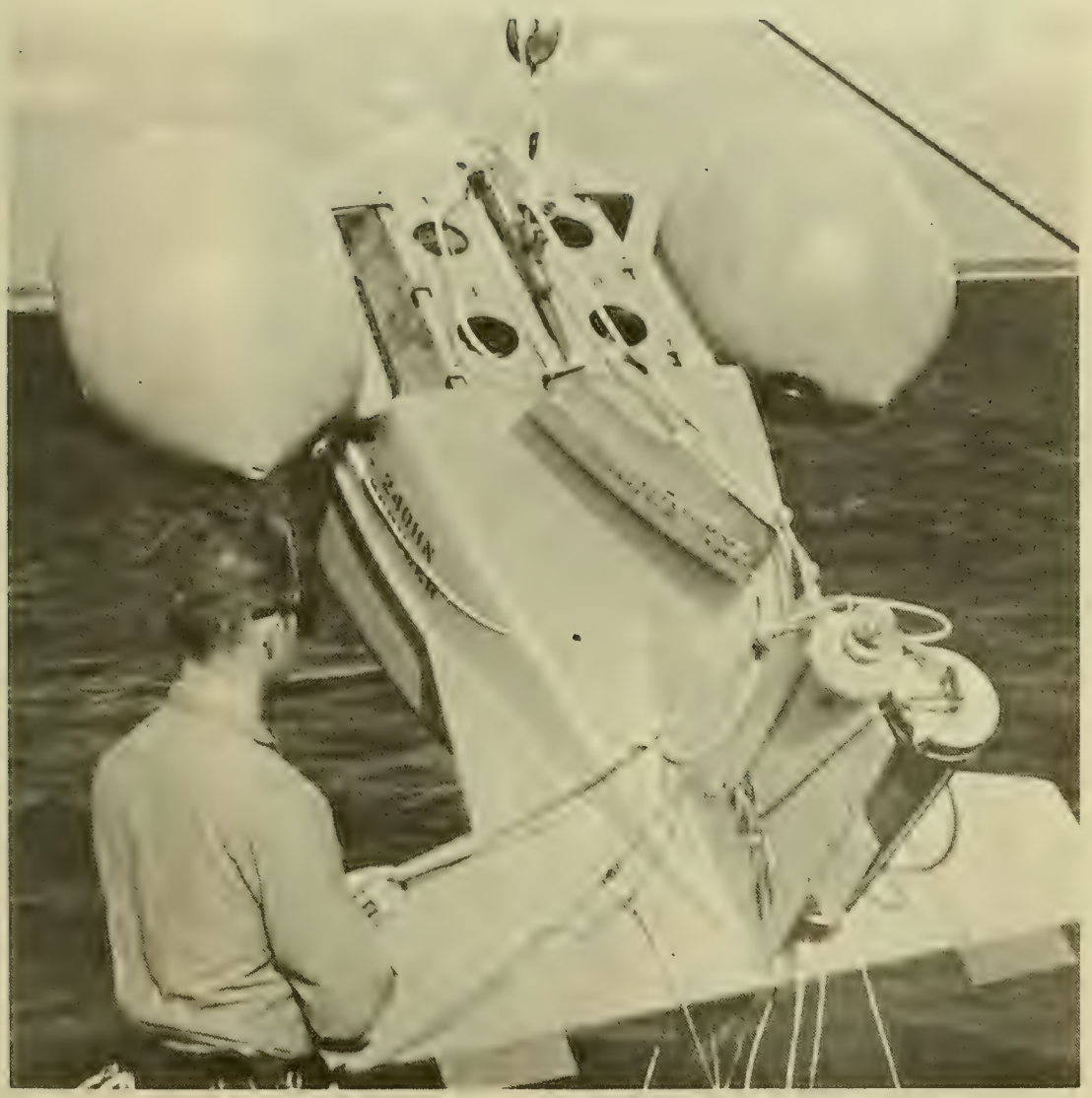

Figure 4

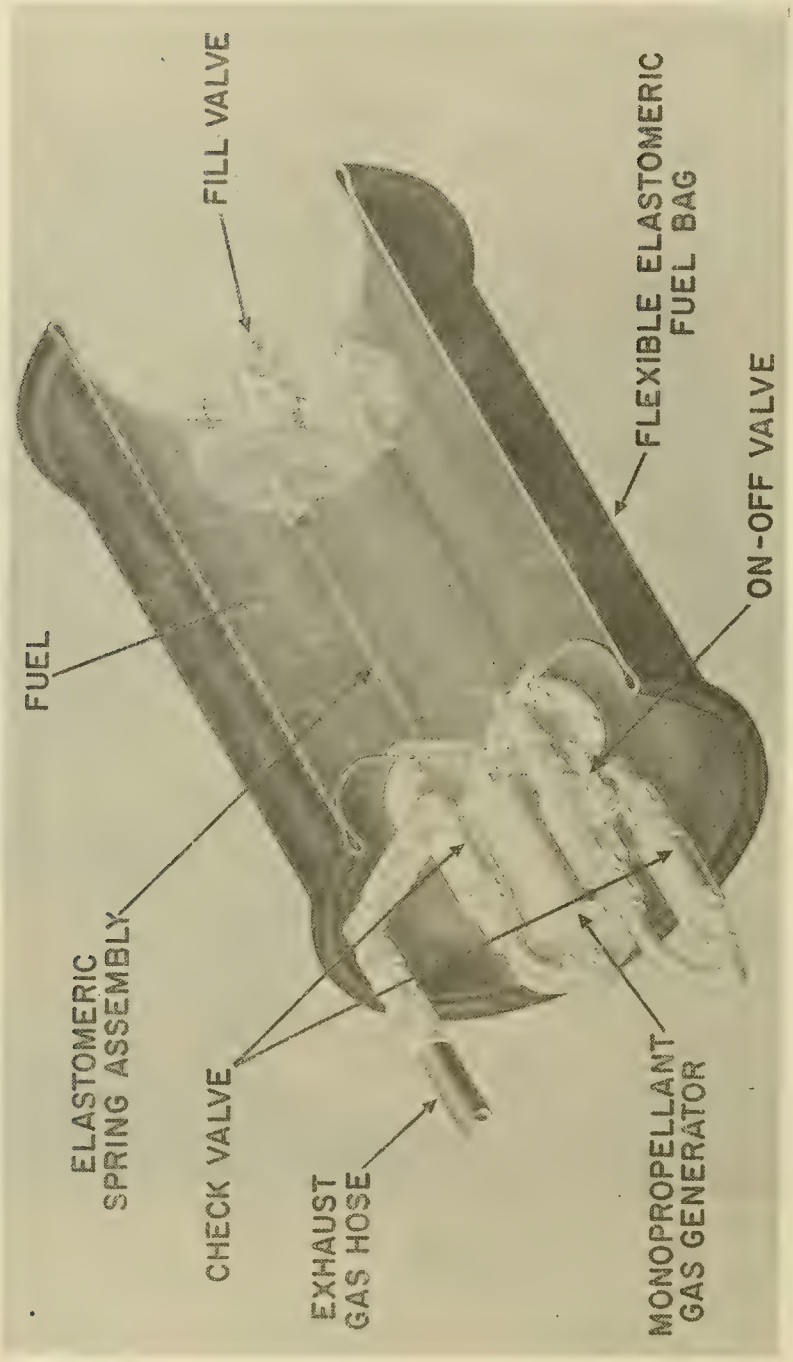

Fig. 5 - Self pressurizing fuel bag monopropellant gas generator

Session F

MARINE SCIENCES RESEARCH

Long Range Ocean Acoustics and Synoptic Oceanography
Straits of Florida Results*

John G. Clark and James R. Yarnall
Institute of Marine Science
University of Miami, Miami, Florida 33149

INTRODUCTION

The Straits of Florida acoustic-environmental measurement system (Project MIMI)** has been thoroughly described in previous publications;[1,2,3] thus only a minimum of descriptive material need be repeated here. An attempt has been made to present all of this material in Figures 1 and 2, and Table I. Figure 1a provides for geographical orientation; Figure 1b presents a bottom profile of the acoustic path with representative sound speed profiles computed from hydrographic data available at the Institute of Marine Science;[4] Figure 2 identifies the field installations of the MIMI system. Additional information regarding these installations is summarized in Table I.

By September of 1966 the system had matured sufficiently to permit the start of a long period operation which lasted until January 31, 1967. This long test has been designated "Lunar Cycle Test One" (LCT-1). Much of the data to be presented here were obtained during LCT-1. The two hydrophones given the special designations H3 and H43 in Figure 2 will be referred to frequently in the following discussions. The special designations are descriptive in that the respective ranges of the hydrophones are approximately 3 and 43 miles from the acoustic source.

Several types of acoustic signals are available for experimental use in the Straits of Florida studies;[1] this report, however, will be concerned only with the results of cw transmission at 420 Hz.

The Straits of Florida studies are transmission experiments.

---

* Contribution No. 798 from the Institute of Marine Science, University of Miami. This research was sponsored by the U.S. Office of Naval Research.

** See acknowledgements.

Such experiments are always subject to a dual interpretation. They may be viewed as a study of the medium, wherein the wave is used as a research tool or probe. In this case, a propagation model is given, and the properties of the medium are inferred from the results of the experiment. In the second case, a model for the medium is given, and the experiment becomes a study of wave propagation under prescribed conditions.

This paper is a preliminary attempt to interpret the Straits of Florida cw data from the case I viewpoint: the acoustic wave is regarded as a probe for environmental study. The nature of the experiment forces this attempt to be qualitative and speculative in many aspects. The propagation path is both acoustically and hydrodynamically complex. At 420 Hz the wave length to water depth relationships do not clearly recommend either the shallow or the deep water acoustical theoretical approach. In addition, the path transects the Florida Current in a region of high current velocity which may give rise to unusual conditions of instability in the water column. The dual nature of the experiment will be evident in what follows, and the need for a flexible approach to the analysis will be very obvious.

THE ACOUSTICAL MEASUREMENTS

For the purpose of data analysis, the techniques of the environmental measurements will require little further comment. The acoustical measurements, however, need elaboration. Figure 3 represents the design of the cw experiments, reduced to essential functional elements. The functions enclosed in dashed lines are performed by the phase coherent demodulator,[1] a key item in the cw experiments. It should be understood that a direct cable connection from the Miami laboratory to the H43 hydrophone near Bimini would make the use of matched precision oscillator "B" unnecessary. This secondary phase reference is a matter of logistics only. In the interpretation, the signals of H3 and H43 are assumed to be referred to the same phase standard. The system has been designed to have a relative phase drift of less than 360° per year at 420 Hz. A serious effort has not yet been made to obtain absolute <u>in situ</u> calibrations for H3 and H43; consequently, all amplitude measurements are relative. A calibration for phase sense has been established, as indicated in Figure 4a. The strip chart phase display extends only over 360°. For measurements which exceed this range, the total phase excursions are determined by manually accumulating multiples of 360° on a separate graph called the expanded θ display. This is shown in Figure 4b. A zero value of phase is assumed in each experiment at the time the equipment is put into operation. To clarify a potentially confusing feature of subsequent illustrations, it should be pointed out that the signal employed for cw testing is more accurately described as "interrupted cw". A basic cycle of 45 seconds of signal on, followed by 15 seconds of signal off, was most frequently used. The resulting display takes the form illustrated in Figure 4c. This

signal format is superior to straight cw in that the noise level is continuously monitored (although, with the very narrow bandwidths obtainable with the phase coherent demodulator (Fig. 3), high noise levels were rarely a problem). During the 15 seconds off period, the phase trace will either present a random smear over 360°, or display a tendency to "hang up" at 180°.

In Figure 3 the true relative angular positions of the source, H3 and H43 have been indicated. The exaggerated vertical scale in Figure 2 obviously creates a false impression. Figure 3 ignores the multipath nature of the Straits of Florida propagation path, and the complexity of the path boundaries. In this minimal form the experiment exhibits the basic geometry of one of the simplest of the wave transmission experiments--a study of forward scattering at essentially zero scattering angles. A more complete physical interpretation explicitly acknowledges the dominant influence of boundary reflections and treats the physics of the experiment with the concepts of guided wave propagation. This paper, however, is intended to emphasize techniques and data. For this purpose there is some advantage in briefly considering the ideally simple case of fully coherent forward scattering and discussing the results that would be obtained with the experimental set-up of Figure 3.

AN IDEAL EXPERIMENT

We assume a cw disturbance to be transmitted from source to receiver through a medium whose index of refraction is fluctuating sinusoidally. The experimental geometry is such that all boundary and interference effects are avoided, and the disturbance can be regarded as a single "beam" of energy. The frequency of the sinusoidal change in the medium is further assumed to be very low compared to the frequency of the propagation disturbance, and the wave length of the medium fluctuation is of sufficient length that the whole of the cw disturbance is affected. An extreme example might be the case of a plane wave sound beam passing through a body of water which is changing uniformly in temperature.*

The result of this idealized experiment is a signal at the receiver which is purely phase modulated at the medium fluctuation rate. The Fourier spectrum, amplitude, and phase of the signal might appear as in Figure 5. The phase modulation index, β, is a function of signal wave length, propagation path length, and the amplitude of the medium fluctuation.

An investigator interested in studying the medium fluctuation might choose to work directly with an "on-line" spectral analysis of the received signal. In this case the fluctuation frequency

---

* The analogous case of electromagnetic wave propagation through a fluctuating plasma is discussed with mathematical detail by Heald & Wharton (Ref. 5).

of the medium is determined from a frequency domain measurement centered at the signal frequency,[5] i.e., from the side band structure of the received signals (Fig. 5a). The experimental configuration used in the Straits of Florida studies (Fig. 3) offers an alternative approach. The time functions of the received signal amplitude and phase (Figs. 5b and 5c) are made available by the phase coherent demodulator. Since the medium itself is the phase modulator, a conversion of the phase time function, $\theta(t)$, to the frequency domain obviously provides a direct measure of the medium fluctuation frequency. In the more general case in which the index of refraction remains a slowly varying function, not necessarily sinusoidal, the spectrum of $\theta(t)$ determines the frequency content of the medium fluctuation. The phase is a linear function of the change in the medium and, in fact, provides a direct quantitative measure of this change if the proportionality constant is known. If physical phenomena are present which lead also to amplitude modulation, the spectrum of $R(t)$ is the applicable measure of the spectrum of the time varying, attenuation processes in the medium.

In this example we have been careful to specify that interference phenomena are not present. The intuitive concept of a "beam" of energy has been used to denote single path propagation. Unfortunately, as we have indicated, there is little to justify the application of this convenient concept to the Straits of Florida propagation studies. The ray path calculations to be discussed in the next section predict that the time dispersion in ray arrival times at the H43 hydrophone is very long compared with the period of the 420 Hz signal. Experimental results confirm this to be the case.[1] All studies to date leave little doubt that the H43 cw signal is the resultant of many interfering propagation paths, and we may assume that each arrival is modulated by the medium. This might lead one to the intuitive conclusion that the results of the cw experiments would, at all times, be a quite erratic display of $R(t)$ and $\theta(t)$, having little in common with the simple example of coherent forward scattering discussed in this section. Certain of the data to be discussed indicate this to be another case in which intuition fails.

THE ACOUSTIC PROPAGATION MODEL

An attempt has been made to construct a more realistic model of propagation in the Straits. This has developed into a somewhat involved exercise in ray theory and in the use of the digital computer as a research tool. The result is, of course, still highly idealized. From the theoretical standpoint, the model study has proven to be instructive in regard to the contribution of multipath effects and in regard to the physical meaning of the measure of the environment provided by the Straits of Florida acoustic data. The deficiencies of the ray theoretical approach at long ranges and low frequency cw signals are acknowledged,[6] but in the present application no precise comparisons of theoretical and experimental sound pressure are being attempted, and it will be seen that useful

qualitative results have been obtained. Only a summary of the results of the model study will be given.

The propagation model assumes that a vertical gradient in the sound speed is the single most important factor in determining the geometry of the ray paths, and that useful results are obtained by linear approximations to profiles such as those illustrated in Figure 1b. The linear profile illustrated in Figure 6 is the starting point for the computations discussed below.

An alternative theoretical description stresses the role of turbulent processes in the oceans and pictures the medium as an isotropic random distribution of thermal "patchiness". Available information indicates that this description is inappropiate for use in the present application.[7] This point is emphasized because the interpretation of some of the more interesting data to be presented is based on phenomena which occur only in a stratified fluid. Attenuation due to absorptive processes in the fluid volume has been taken to be negligible.[8]

Under the assumption of a smooth bottom, reflection loss and phase shift at bottom reflections have been simulated by means of the modified - Rayleigh plane wave reflection coefficient.[9] Details of the use of this reflection coefficient in a similar application have been provided in a previous publication.[10] Phase shifts of 180° at surface reflections and 90° at RBR ray turning points have also been incorporated.* Scattering effects within the fluid and at irregular boundaries cannot be handled by the model. It is probable that this is the most serious deficiency. There is perhaps sufficient theoretical and experimental background available to include coefficients of scattering loss for reflections at the boundaries. The work of H.W. Marsh,[11] for example, might be applied to SRBR rays at the surface. This has not yet been attempted.

The ray model will be discussed for the Fowey Rocks to Bimini (source to H43) path only. The calculations, which include spreading loss for each ray, are based on techniques recently developed by M.J. Jacobson.[12,13] These methods account analytically for all surface-reflected bottom reflected (SRBR) and all refracted-bottom reflected (RBR) rays between fixed source and receiving points (Figs. 7a and 7b). A tool is thus provided which describes analytically how the medium is "sampled" in space by the acoustic energy

* Phase shift at RBR turning points was neglected in the previous publication by Jacobson and Clark (Ref. 10). The essential theoretical conclusions of the publication appear to remain unchanged.

which reaches the receiver; i.e., all of the trajectories of energy flow are accounted for. This feature of the model, coupled with the fact that the travel time across the Straits is less than one minute (much shorter than characteristic periods of many geophysical phenomena of interest), is the theoretical basis for the claim that the received acoustic signal provides a synoptic measure of the medium along the propagation path (Fig. 7 illustrates that the aggregate pattern of either type of ray provides for substantial space coverage along the propagation path).

The use of the Jacobson approach requires that parallel surface and bottom boundaries be assumed. This is a gross over-simplification of the Fowey Rocks to Bimini path; and, in an attempt to partially overcome this deficiency, a number of models have been studied with varying depths ranging from very shallow to deep with respect to the mean depth of the actual path. These preliminary studies have resulted in the selection of the medium representation of Figure 6 and the SRBR and RBR models of Figures 7a and 7b as the best fit to all available experimental data. (Only the first four ray arrivals are shown in Figures 7a and 7b).

This "fitting" includes an independent prediction by the RBR model of both acoustic travel time and travel time dispersion, which are gratifyingly close to measured values. Project MIMI multipath studies give a measured value of roughly 750 ms for maximum signal time dispersion at H43.* The major portion of the acoustic energy appears to arrive with a time spread of 250 ms or less. The RBR model predicts a travel time dispersion for all ray arrivals of 600 ms. The first ten arrivals are time dispersed over 440 ms.

The problem of how many ray arrivals to include in a given calculation is one of the difficult questions associated with the propagation model. Jacobson's RBR analytical results [12] provide for an infinity of ray arrivals with, however, a finite travel time dispersion. Inclusion of a plane wave reflection coefficient at bottom contact eliminates, to a reasonable order of accuracy, the problem of the infinity of arrivals.[10] In practice liberal use of the digital computer permits one to sequentially "add in" ray arrivals until satisfactory resolutions are obtained, or until a decisive and physically meaningful trend is established. A total of 10 ray arrivals has been used in the simulation studies to be discussed.

A detailed comparative study of the SRBR propagation models indicates that the RBR rays will provide the dominant contribution to a cw signal. There are four reasons for this:

---

* Experimental results obtained in communication with Dr. T.G. Birdsall, University of Michigan.

1) An analytical result proves that geometrical spreading loss for all SRBR rays exceeds that of any RBR ray.[13]

2) A comparative study indicates that bottom reflection losses are greater in the SRBR model.

3) The SRBR rays will be subject to scattering losses at the surface which will not be experienced by RBR rays.

4) The RBR model provides a reasonably good fit to measured values of travel time dispersion.

A decision has been made to neglect the SRBR contribution in this discussion, and consider the signal at H43 a superposition of RBR arrivals only.

It should be noted that the model makes no provision at all for mixed rays of the type illustrated in Figure 7c.* As will be seen, the effects of the sea surface are evident in the acoustic data, but are not a dominant influence. It is necessary to emphasize that the models under discussion can make no attempt to account for the full complexities of the actual propagation path between Fowey Rocks and Bimini. Indeed, more thorough studies might lead to the conclusion that a model composed exclusively of mixed rays is the most adequate physical description possible with ray theory.

Proceeding with the RBR calculations, we are now in a position to perturb the model in various ways which will provide a simulation of certain large scale changes in the medium. Our purpose is twofold: 1) to study the acoustic response to the changes, in order to gain insight into the nature of the measure of medium variability provided by acoustic amplitude and phase, and 2) to obtain theoretical order of magnitude numbers associated with such changes, for comparison with experimental data. It is possible, for example, to simulate the effect due to tidal changes in water depth by incrementing the water depth sinusoidally, and adjusting the sound speed gradient for the effect of the pressure change at each increment.

This simulation has been studied in some detail, and has contributed to the conclusion that tidal water depth changes cannot account for the full range of observed tidally related phase variations at H43. Over a water depth change equivalent to the tidal range in the Straits the first ray arrival (N=9 in Fig. 7b) suffers negligible change in amplitude, and 260° change in phase. Subsequent

---

* These are selected rays from computer calculations performed with line segment approximations to the bottom and to the sound speed profiles (Refs. 1 and 4). The technique does not permit source to receiver calculations.

ray arrivals are also negligibly affected in amplitude, and suffer progressively smaller phase changes. A consistent trend was established in this calculation, and it may be stated that the cw resultant of any number of RBR ray arrivals suffers a phase change, due to tidal depth variation, of less than 260°.

Two additional simulations will be of interest. The first, given the descriptive designation, "sliding the profile", repeats with the propagation model the uniform sinusoidal change in the medium considered in the ideally simple experiment discussed previously. In the earlier discussion acoustic phase provided a linear measure of the change in the medium. Referring to Figure 6, we can see that a vertically uniform change in sound speed (temperature) in the acoustic path does not change the value of the sound speed gradient, g, but does slide the position of the profile along the sound speed axis. This simulates an external mode of variation in the medium, in which the stratification is undisturbed.

The second simulation of interest "swings" rather than slides the profile. This is accomplished by fixing the surface sound speed (temperature) and varying the sound speed at the bottom. Since the sound speed gradient, $g = (C_o - C_s)/H$ (where C_o = bottom sound speed, C_s = surface sound speed, H = water depth), the gradient varies linearly with the change in sound speed at the bottom. The swinging profile is as close as the propagation model can come to simulating an internal mode of variation in the medium in which the stratification is disturbed.

Returning to the sliding profile, the calculation that has been performed slides the profile sinusoidally over a peak to peak change in sound speed of 4m/sec, approximately equivalent to a 1.0°C peak to peak change in the temperature of the entire propagation path. The variation in cw resultant phase and amplitude resulting from this change in "the medium" is illustrated in Figure 8. Note that the peak to peak variation in resultant phase is about 60 cycles.

The following conclusions have been derived from the sliding profile model calculations:

1) Within the accuracy of the calculation, acoustic phase provides a linear measure of the sound speed (temperature) variation in the medium. This is identical to the result obtained in the "ideal" experiment.

2) There is negligible change in the amplitudes of the individual ray arrivals over the full variation in the medium. This implies that the calculated variation in the resultant amplitude (Fig. 8) can be interpreted strictly as a multipath interference pattern displayed in time.

Using the RBR model with "sliding profile" it is now possible to perform an interesting simulation of actual data taken at H43. The data to be simulated are cw signal phase and amplitude over a span of 12 hours, taken from an interval of exceptionally stable transmission during 27-28 November, 1966. The simulation is accomplished by sliding the profile, as a function of time, sinusoidally over a small selected range of sound speeds not far removed from those specified for the propagation model in Figure 6.

Specifically we choose:

$$C_s = 1540 + 0.34 \sin \left(\frac{2\pi}{T} t\right)$$

$$C_o = 1482 + 0.34 \sin \left(\frac{2\pi}{T} t\right)$$

The acoustic data and the results of the simulation are shown in Figure 9. The period, T, of the simulated phase change is about 26 hours.

This simulation is surprisingly consistent over the full 12 hours illustrated, but it should by no means be mistaken for a direct comparison of theory and experiment. It is, rather, a strong suggestion that the physical concepts used in constructing the propagation model are of valid application; but, at this stage, a one-sided story has been presented. The data of Figure 9 have been selected from an interval of exceptionally stable transmission. An objective approach demands representation of the opposite situation, i.e., data from an interval of unstable transmission. This will be provided, but it is instructive to first present preliminary results from the model study with swinging profile. Calculations of this kind promise eventually to be considerably more informative than the sliding profile case. Results available at this time are limited to a detailed study of a multipath effect, that was not demonstrated by the sliding profile calculations.

This effect is illustrated in Figure 10a. These results were obtained by swinging the profile of the propagation model (Fig. 6) linearly through the values of the sound speed gradient designated on the horizontal axis. Again, we are dealing with the resultant phase and amplitude of 10 RBR cw ray arrivals. The amplitudes of the individual arrivals change negligibly throughout the calculation, identifying the events illustrated in Figure 10a as deep interference nulls accompanied by very nearly discontinuous "jumps" in phase. This phenomena can be understood by recourse to a very simple phasor diagram (Fig. 10b). We picture the received multipath signal as being resolved into two phasors, approximately equal in amplitude, which are rotating either in opposite sense or at different angular rates. Since superposition applies, the existence of an interference null is a sufficient condition to justify this interpretation. If we fix ourselves in the reference frame in which one of the phasors is stationary, the stage is set for the sequence illustrated in Figure 10b.

The resultant, R, will exhibit a sharp amplitude fade and a rapid phase change of close to 180° during the time interval between diagram I and II. Figure 10a is a simulation of events commonly observed in the Straits of Florida cw data. Figure 11 is a photograph of a section of record containing several of these nulls.

Two significant observations have been derived from the model study of the swinging profile:

1) Over the range of values studied, acoustic phase can be taken as a linear measure of the change in gradient except in the vicinity of the interference nulls.

2) Over the range of values studied, the rapid phase changes at the interference nulls provide no immediate information about the variation in the medium. If our purpose is to use acoustic phase as a measure of the change in the gradient, then, as a matter of practical necessity at this stage of our understanding, we must regard these events as "noise" introduced into the measurement.

It is appropriate here to speculate briefly on the consequences of adding a true noise component to the multipath model, i.e., an influence which perturbs the multipath structure randomly. To create physical significance for this concept we might think in terms of turbulent eddies that create random nonuniformities in the medium stratification. One very likely consequence would be a random occurrence of interference nulls such as the events presented in Figure 11. However, if the "noise level" is not too high, complete incoherence of the acoustic signal will not be observed. (In Fig. 11, for example, the phase can be tracked easily through the peak occurring at 1 hour, 20 minutes, even though the continuity of the $\theta(t)$ display is interrupted by the interference nulls). Studies that have been made of the interference nulls do in fact point to a random occurrence in time, suggesting the prevalence of random rather than systematic multipath effects of this kind.

We now refer to Figure 12 which presents the counter example to the very stable transmission data of Figure 9. The "noisy" character of the phase, $\theta(t)$, and, in particular, the role played by phase discontinuities at the interference nulls can be seen. In spite of this, the expanded display of $\theta(t)$ does exhibit a recognizable trend. In Figure 12 this trend has been tracked over a time period of only about 12 hours; in the example of stable transmission (Fig. 9) the trend took the form of a half-sinusoid. Both of these data samples have been extracted from the long cw transmission test previously designated as LCT-1. It is convenient at this point to display certain of the data from this long test over its full time range from September 1966 to January 1967 (Fig. 13). Data from the thermistor string are shown, and phase at the H3 and H43 hydrophones.

The phase curve for H43 is a representation, over the full extension of the test, of the "trends" illustrated in Figures 9 and 12. These two sample periods of the phase data are identified respectively by the symbols A and B. The half-sinusoid shape of the curve during the 27-28 November period can be attributed to the tidally related phenomena to be discussed later.

The acoustic phase data appears to contain information which will be interpreted in subsequent discussion in terms of processes in the medium. One point, however, needs emphasis. In our treatment of the interference nulls we have pointed out that the phase records are a signal plus noise situation for which no quantitative assessment of the noise contribution is available. Numbers, given in the following discussion, which relate magnitude of phase change over extended periods to sound speed or temperature changes in the medium must be taken as very approximate. For the most part, discussion will be restricted to the spectral content of the phase data.

DATA ANALYSIS

The simple large scale perturbations of the medium that can be simulated with the propagation model hardly do justice to the actual processes that occur in the oceans. The ray calculations can serve only to illuminate some of the more pronounced features of the experimental results.

In practice the data analytical procedures have not been geared exclusively to large scale perturbations in the medium, but have assumed that all time varying processes which can scatter or attenuate the acoustic energy will leave spectral signatures in the phase or amplitude display of the received signal. Thus, in brief, the basic procedure has been a search for the spectra, in the acoustic phase and amplitude data, of experimentally or theoretically established geophysical phenomena which have well defined spectral characteristics. For the most part, the search has not been difficult; the signatures have been prominent in the data. It has also been possible in some cases to establish correlations with environmental measurements; this has contributed substantially to the analysis.

Most of the data will be grouped under subheadings which designate the geophysical phenomena to which the acoustic signatures are attributed. There are elements of speculation in some of these cases which will be acknowledged when the data are discussed. The following groupings have been established: a) surface wave signatures, b) short period internal wave signatures, c) tidally related signatures, d) long period signatures-atmospheric phenomena. Figure 14 has been included to schematically summarize the time scale of the signatures that have been observed in the acoustic data.

A considerable variety of data will be presented, taken at various times in the two year span from January 1965 to January 1967.

To avoid confusion Table II has been prepared which specifies the intervals of data collection, designates the geophysical categories, i.e., the headings under which data from a given interval will be discussed, and indicates previous publications which deal with some of these test intervals.

An additional source of confusion may be the wide range of time scales that must be employed to adequately illustrate phenomena with characteristic periods in the range of seconds (surface waves) to the range of weeks and months (atmospheric phenomena). The major interval of data collection, LCT-1, covers almost 5 months, and represents the longest time base on which data is to be illustrated. Certain of the data from the long test have already been introduced in Figure 13.

Signal phase at H3 and H43 were each referenced to an arbitrary starting point at the start of this long test in September. The arbitrary references were re-established after a 5-day interruption due to Hurricane Inez. In regard to the H43 phase curve, three time scales of events are resolved in this figure: the long down trend of over 250 cycles extending the full length of the test, the prominent peaks in the curve with characteristic periods on the order of days (speculatively attributed to atmospheric phenomena of the same characteristic period), and the "high frequency" fluctuation which is due to the tidally related phenomena.

On the time scale of Figure 13 it is apparent that the tidal effects have been reduced almost to the status of high frequency "noise" riding on the lower frequency spectral components of the curve. To more effectively illustrate the tidal effect, two standard techniques have been employed: selected portions of the data have been presented on an expanded time scale; high pass filtering has been employed to remove the dominant low frequency spectral components.

A further expansion of time scale is necessary to effectively illustrate the signatures of short period internal waves, which occur most frequently with characteristic periods in the range of a few minutes. The surface wave signatures, with characteristic periods in the range of seconds, appear as only an unresolved smear in all figures which illustrate lower frequency events. One additional expansion of time scale is necessary to illustrate these signatures.

Whenever practical, digital techniques have been employed for spectral analyses of the acoustic phase and amplitude fluctuations. It has been convenient to compute power spectral estimates based on the method devised by Evans, et al,[14] which corrects for limited forms of non-stationarity in the data. In the study of the tidally related effect, sharp spectral lines are involved and a power spectral estimate may not be the most efficient data analytical approach. The application of an improved technique to these spectral

lines is being investigated. Spectral estimates at the high frequency end of the fluctuation spectrum (surface wave and short period internal wave signatures) are impractical to compute over very long test periods. For example, something on the order of 10^7 data points would be required to compute surface wave estimates over the entire 140 days of LCT-1, a prohibitively expensive data load for a power spectral calculation. The data have been sufficiently "clean", however, to conduct visual studies of both surface wave and short period internal wave signatures over extended time periods, with results that are judged to be a useful spectral measure of these effects.

SURFACE WAVE SIGNATURES

The spectral signatures of wind driven surface waves are almost always present in the acoustic data from any of the hydrophones. The magnitude of the effect is relatively small and, as noted above, is seen as a high frequency "hash" or "smear" in most of the data records presented. Both signal amplitude and phase are effected and display substantially identical fluctuation spectra in the data that have been examined carefully.

A detailed visual study was made of the surface wave signatures in signal amplitude during a four day test from January 25-29, 1965. The hydrophone involved is designated as "A" in Figure 2. The signal was cw at 420 Hz, the case for all data discussed in this paper.

A random sampling of the test records for the 4-day interval showed the average peak to peak pressure variation to be about 5 dB. The maximum variation noted was 12 dB. The minimum was 1 dB, which is close to the resolution limit of the instrumentation.

The periodicity of the fluctuation was predominantly 3-4 seconds over this testing period, but did increase at times to as much as 12 seconds. The 3-4 second period was evident in the received signal throughout the test with the exception of one 10 hour interval, on 26 January, during which the period was primarily 8 seconds with some 6 second periods also present. Unfortunately, no surface wave height data were available at the time. Changes in the predominating period or in the magnitude of the amplitude variations tended to be gradual. However, it was not unusual to find several isolated cases of 5 to 7 second periods included in an interval which exhibited predominately 3-4 second fluctuations. No periods of less than 3 seconds were noted during the test.

The similarity in the spectral composition of the signal amplitude and phase fluctuation was quite apparent and no attempt was made to tabulate the periods of the phase fluctuation. The peak to peak range of the phase fluctuation varied typically from the resolution limit of about 5° up to 30 or 40°, and increased in rare case to as high as 180°.

Subsequent to the January 1965 test an opportunity was found to establish a direct environmental correlation of the acoustic signatures with wave height. The small scale "single reflection" experiment of Figure 15 was set up near the site of the Fowey Rocks projector. The inverted fathometer was employed, and a USRL type J9 transducer was used as the signal source. A typical sample of the data obtained is shown in Figure 15. In view of the periodicities observed in the visual study of the January 1965 Bimini acoustic data, little commentary is needed on the power spectral density (PSD) analyses of this special test. It should be noted, perhaps, that surface wave periods in the range of 3 to 4 seconds can be considered typical for moderate seas in the Straits.

In the light of previous studies conducted elsewhere,[15,16] these results from the Straits of Florida were not at all surprising. This is particularly so in regard to the very competent fixed-system experimental work reported by Scrimger.[16] Scrimger's data also included signal phase and amplitude and surface wave height. His experiments were performed in significantly shallower water and with smaller wave heights, but were not limited to a single frequency. Unfortunately there has not been an opportunity to make a detailed comparison of the two sets of data.

Returning briefly to the theme of the acoustic data as a synoptic measure of time varying processes in the environment, the authors are of the opinion that the term "synoptic" should be applied with caution to the surface wave signatures in the Straits of Florida data. The ray configurations illustrated in Figure 7c are obtained from computer calculations which attempted "realistic" approximations of the bottom boundary and of actual sound speed profiles. A conclusion of that study was that most surface reflections probably occur at the extreme ends of the propagation path.

It is possible that only the surface over the shallow water slopes of the propagation path are being effectively "sampled" by the acoustic energy. Comparative studies over ocean paths in which surface channel or RSR modes of propagation predominate would perhaps provide interesting contrasts with the surface data now available.

SHORT PERIOD INTERNAL WAVE SIGNATURES

Interpretation of surface wave signatures in the acoustic data has been facilitated by correlation with surface wave measurements. No correlation of environmental measurement with acoustic signatures exists for the short period internal waves. The validity of the association of signatures with short period internal waves depends upon two theoretical criteria:

1) The sinusoidal character of the signatures in the acoustic records. (Fig. 16). The signatures are similar to the surface wave effects in that they appear, for most occurrences, in both acoustic phase and amplitude.

2) The spectral distribution of the signatures lies within the range predicted for stability oscillations. Typical curves of the stability frequency (Väisälä-Brunt frequency), calculated for local conditions, appear in Figure 17.

A study of short period internal wave signatures has been undertaken for H3 hydrophone data only; we are thus concerned with processes which occur in the first 3 NM of the Fowey Rocks to Bimini acoustic path. The data are from the recent long continuous test of September 1966 through January 1967 (LCT-1).

All data records from LCT-1, as in Figure 16, were produced at a chart speed of 0.025 mm/sec, much too slow to resolve the high frequency surface wave signatures. At this chart speed, periodicities of a few seconds merely produce a widening of the trace. As a rule, surface wave effects were less prominent at H3 than at H43 and on many occasions were close to the resolution limits of the instrumentation. But many of the short period internal wave signatures were sufficiently well defined to permit determination of occurrences and an estimate of duration and characteristic period by visual inspection. These wave trains are not as persistent as those due to surface wave effects and it was necessary to establish the minimum wave train to be classified as a signature. Four clearly marked cycles of a given period appearing in either acoustic phase or amplitude were arbitrarily selected as this "minimum signature". In practice the minimum signature was not of significant occurrence. The mean "length" of the wave-trains determined by an average over all of the signatures was 12 cycles.

Distributions of the number of occurrences and the persistence in time or total duration, of observed internal wave periods are presented in Figure 18. Due to limitations of techniques employed, each designated period in these figures should be understood to contain a spread of perhaps 10% of the enumerated values. The similarity of the two distributions suggests that the persistence of a signature is more closely related to its probability of occurrence than to the length of its period. The dashed curves in Figure 18 illustrate an interesting suggestion of symmetry that appears in these data. It can be seen that minor peaks in the distribution seem to occur in the vicinity of multiples of the large peak near 3 minutes.

The distributions of Figure 18 are the result of a rather crude technique of visual analysis. At best, these are very approximate spectral descriptions of the short period internal wave signatures observed during LCT-1. The data-handling problems and the

expense of digitally computing more accurate spectral estimates were prohibitive. On-line computers are being incorporated into the MIMI system and future experiments should yield more reliable spectra.

An attempt has been made to see if the stability frequency, N(z), allows the distribution of frequencies noted in Figure 18 when its calculation is based on local conditions. Since the required knowledge of the vertical distribution of oceanographic parameters in the sound path is not available for the period of LCT-1, recourse was again made to hydrographic data obtained in 1962.[4] For a station located in the vicinity of the H3 hydrophone site, measurements of temperature and salinity at various depths were used to calculate density and sound speed. These (discontinuous) data were approximated by "least squares fit" fourth order polynomials in order to obtain equations for density, density gradient, and sound speed as functions of depth. The formula for the stability frequency calculations was obtained from Eckart.[17]

The data were inadequate in several respects for this calculation. One immediate problem was the fact that hydrographic data was available for only a portion of the full water depth at the measurement site. This effectively chopped off the lower frequency end of the calculated N(z) curve, permitting only an experimental comparison with a range of frequencies which included the maximum stability frequency.

The solutions predict a stability frequency maximum of 0.0195 Hz (period of 5.35 min) occurring at a depth of 50 m for the September (1962) data, and a maximum of 0.0190 Hz (5.50 min) at 70 m for the October data. The solutions are illustrated in Figure 17. These solutions suffer from the additional deficiency that the maximum for N(z) is quite sensitive to the value of the measured parameters near the depth of this maximum. The measured parameters were, in the first place, discrete and, in addition, were effectively smoothed by the polynomial approximation. On this basis low calculated values for the N(z) maximum might be expected. An improved representation of the density gradient would probably lead to a closer match between the predicted and the observed maximum frequency. If the density stratification in the Straits is not radically altered from year to year, the distributions of Figure 18 may be representative for this region of the Straits during the fall and winter months. (Solutions for data obtained in November, December and January of the 1962-3 study yielded curves similar to the two illustrated.)

It would be of interest to compare the spectral description provided by the acoustic data with a "point" measurement obtained from an array of environmental sensors specifically designed to measure short period internal waves.

The acoustical data evidently contains spectral signatures

of these phenomena covering a relatively broad frequency range. These signatures, however, should be interpreted with the understanding that the received signal provides a measure of disturbances in the sound speed stratification of the medium, and not a direct measure of disturbances in the density stratification. It should be expected that directivity factors are involved; e.g., the acoustic response is a function of the angle between the acoustic path and the direction of propagation of the internal wave. Also, the visual technique employed for this initial study of the signatures has limitations which are difficult to define. Even within the limitations that all of these factors impose on the analysis the acoustic probe appears to provide a measure of spectral distribution and time of occurrence of short period internal waves which may be impractical to obtain by other means.

TIDALLY RELATED SIGNATURES

Both wind driven surface waves and short period internal waves are spatially limited in their effect upon the medium. The amplitude of a surface wave, whose wavelength is small compared to water depth, decreases rapidly with depth in a manner that is well understood. Similarly, the locus of maximum disturbance for stability oscillations will be a horizontal plane at some level within the medium. On the scale of tidal phenomena, however, "long wave" behavior is to be expected, and substantially all of the water column can be involved in the motion. Under these conditions we move into a realm of large-scale, spatially coherent changes in the medium for which we might expect qualitative correspondence with previously discussed features of the propagation model.

We do, in fact, find that the most outstanding features of the propagation model are demonstrated in the data. The spectral signatures of the tidal scale processes are clearly evident in signal phase, and they display the fundamental tidal frequencies. On the other hand, signal amplitude, which provides spectral signatures of surface waves and short period internal waves at the fundamental frequencies of these phenomena, is a complex interference pattern on the time scale of tidal events and is difficult to interpret directly. These features are evident in Figure 19, which illustrates a tidally related signature. Note particularly in Figure 19 that signal amplitude, R(t), forms an almost symmetrical pattern mirrored from left to right across the valley of the phase excursion at 1400 hours. Mirror symmetry across both peaks and valleys is demonstrated by the propagation model (Fig. 8) although through a much broader range of phase excursion.

Figure 19 calls for additional discussion; it has been included primarily to be illustrative of visually transient features of the data which have been attributed to non-linear tidal harmonics (shallow water tides). The spectral lines corresponding to these effects do not show up in the tidally related phase fluctuation

spectra of LCT-1 data. This is apparently because they are of insufficient total duration in the data. They are evident to visual inspection, however, appearing as wave trains with characteristic periods in the range of 4 to 6 hours; Figure 19 presents one clearly defined period of a wave train that was visually evident for 2 days. These signatures have been manifest in the spectra of shorter test periods which preceded LCT-1.[18]

The shallow water tidal signatures appear transiently in the data, as do the signatures of short period internal waves, but they are associated with much larger phase excursions. In general the peak to peak range of all phase fluctuations on the tidal scale are one to two orders of magnitude greater than the phase fluctuations associated with surface waves and internal waves. On any record approaching a day in length they easily dominate the data display. As might be expected, the peak to peak fluctuation is progressively larger as path length to the receiving hydrophone is increased[18] e.g., substantially larger at H43 than at H3. Evidence exists that the tidal signatures are not a direct consequence of local tides as would be measured, for example, by the Miami Beach tide gauge. The reasons for this will be developed in the course of the following discussion. Steinberg[2] has suggested that these signatures are, in part, related to tidal frequency variations of the Florida Current transport. This seems a likely hypothesis but no specific attempt will be made here to identify the driving mechanisms. The remainder of this section is a discussion of direct environmental changes as possible causal agents of the tidal signatures in acoustic phase. Three possibilities will be considered: a) tidal variations in water depth (local tides), b) disturbances in the stratification of the medium which are spatially coherent over a large portion of the acoustic path (we might, for example, consider the possibility of internal tides, or a tidally resonant internal seiche). c) cross-channel (parallel to the acoustic path) current components which are oscillating at tidal frequencies, possibly associated with tidal modulations of the main stream Florida Current flow.

The consideration of local tides as a direct cause of the tidally related phase fluctuations starts with the presentation of a spectral analysis of the last 4 months of LCT-1 data. The H43 phase curve (Fig. 13), was first digitally high-pass filtered with a cutoff at a period of approximately 36 hours. The spectrum of the filtered data is presented in Figure 20. The spectrum is still under study, but the peaks marked "a" and "b" are considered reasonably reliable and are associated respectively with K_1, the dominant diurnal tidal component at Miami, and with M_2, the dominant semidiurnal component. Note that in the phase spectrum, the diurnal component is dominant with respect to the semidiurnal component. A ratio of about 5:1 is obtained for peaks a and b. This is in contrast with the spectrum of local tides which, on an amplitude squared basis, exhibits a 0.01:1 ratio between K_1 and M_2. This gross difference between the two spectra is taken as evidence that the tidally related phase signatures at H43 are not predominantly of local tidal origin.

A second factor in the argument concerns the temporal relationships between local tides and the phase fluctuation. If local tides were the dominant influence in controlling the tidally related phase fluctuation, one might expect peaks in the phase fluctuation to be coincident in time with local high or low tide. This is not observed. Figure 21* is not included to specifically illustrate this point, but to show that the filtered H43 time function ("D" hydrophone in this figure) is sufficiently "tide like" to carry out a phase comparison of this kind. (Also note the complex interference patterns formed by signal amplitude on the time scale of this figure.)

Finally we note that calculations simulating tide height variations in the RBR propagation model predict a maximum phase excursion of about 260° at hydrophone H43. Experimental maximum values are in the range of 5 to 15 full cycles. Under the assumption that pure SRBR rays dominate the resultant signal at H43, which is considered unlikely, the calculations predict about 3 cycles of phase change. These calculations and the experimental evidence presented above have been taken as sufficient to rule out the possibility that local tides are the dominant direct cause of the tidally related phase fluctuations observed at H43.

We pass on to the second possibility--disturbances in the thermal stratification which are spatially coherent over a large portion of the acoustic path. Here we have striking experimental evidence favorable to the hypothesis, but we will point out immediately that the evidence is much more convincing for the source to H3 path than for the full propagation path from source to H43. The evidence consists of a direct correlation between H3 phase and motion of the isotherms at the 100 m thermistor string. Figure 22 presents data from several days in August, 1966 which can be used to illustrate this correlation. Figure 22a is a direct comparison of H3 phase and a simultaneous temperature measurement at thermistor T3 (46 m depth). A certain amount of "eye integration" of the high frequencies in the temperature data is necessary to establish the details of the correlation; there is little doubt, however, that the correspondence of the two curves is strong on the diurnal time scale. Additional data of this kind confirms the correlation. The data of Figure 22b were taken at a later time in August when no phase information was available. These data are included to illustrate that the diurnal internal disturbance is persistent and is the dominant time varying influence upon the thermocline at the thermistor string. Thermistor T3 is being influenced here by the lower boundary of the mixed layer; T4 (which unfortunately failed prior to LCT-1 and does not appear in Figure 13) illustrates the full range of the motion. The effect appears "damped" at T5 which is located very near the bottom. The motion of isothermal

* This figure appears as No. 4 in Ref. 2.

surfaces here would be influenced by the bottom boundary.

It is tempting to extrapolate the results discussed above to the H43 propagation path, i.e., to picture a spatially coherent diurnal disturbance of the thermal structure extending completely across the Straits and accounting for the phase measurements at both H3 and H43. Such a situation could be set up by a cross-stream tidally resonant internal seiche.[20] A glance, however, at Figure 13, might generate suspicion about extrapolating results obtained for the H3 portion of the path to the complete path. There is little doubt, over the full time span of LCT-1, that dramatically different influences are dominating the signal at H3 and H43. In addition, experimental data exists in regard to the cross-channel component of current which must be taken into account at H43.

Very simple calculations involving the trajectory of a "direct ray" show that variations in the Florida Current flow component which is perpendicular to the acoustic path will produce a negligible response in acoustic phase. Cross-channel components of the flow, however, add algebraically to sound speed along the hypothetical direct ray and will have appreciable effect.

Data relating to the measured cross-channel component has been provided by Operation Strait Jacket.* Figure 23 shows four sets of depth averaged velocity measurements transecting the Straits taken in the period 24 May to 24 June, 1965.[21] The fifth curve, the dashed half-sinusoid, is a convenient approximation of the measured currents used in calculations of the acoustical effects.** The dashed curve may be understood to represent a current which is uniform from top to bottom and which peaks at 0.5 knots approximately in the center of the Straits. The calculation consists of assuming first a non-current condition and then obtaining the total acoustic phase change in the transition to a current condition represented by the dashed line. Unfortunately the propagation model is not adaptable to this calculation, and it was necessary to fall back upon the assumption of a direct ray. Since, on the average, the ratio of path length to water depth in the Straits is greater than 100:1 the calculations based on a direct ray should give useful order of magnitude values. The result of the calculation is a phase change of 2.44 cycles. For a cross-channel component, which can swing also to a maximum in the opposite direction, the peak to peak change would be 4.88 cycles. These numbers are to be compared to measured values of 5 to 15 cycles. There is order of magnitude correspondence in the results. However, in view of the approximations involved, they will be used to support

---

* Florida Current studies performed under the direction of Dr. William S. Richardson, now of Nova University, Ft. Lauderdale, Florida.

** These calculations were performed by Mr. Richard A. Altman of the University of Miami Ocean Engineering graduate program.

no more than the weak statement that cross-channel currents must remain under consideration as a possible significant contributor to the tidally related signatures in H43 phase.

If we consider the effect of the same current situation at H3 we calculate a peak to peak phase change of 0.04 cycles. This number is not comparable to measured values which are on the order of 5 cycles. There is a sufficient discrepancy to rule against a dominant cross-channel current contribution to the tidal phase fluctuation at H3.

The situation is obviously complex at both hydrophones. Rather than pursue further marginal calculations, the authors prefer to await more thorough analysis of the available data and additional experimental results. It has been a consistent theme of this discussion that the tidal signatures are related to phenomena that, to a large measure, are spatially coherent throughout the propagation path. It is perhaps on this scale of events that the synoptic "sampling" obtained along the acoustic propagation path offers the greatest promise for environmental studies. The possibilities of the acoustic probe are apparent. However, only limited conclusions can be drawn unless the acoustic measurements at H43 are "calibrated" by direct environmental measurements of the type provided by the 100 meter thermistor string for the H3 propagation path. It seems likely, at this point, that a modest increase in field instrumentation will calibrate the H3 path to the extent that certain environmental effects could be quantitatively related to the acoustic data. This premise will receive additional support in the next section of the paper. The extent to which this can be accomplished for the full path to H43 is an intriguing question that will also be considered after the long period acoustic signatures are discussed.

LONG PERIOD SIGNATURES - ATMOSPHERIC PHENOMENA

One of the most striking results of LCT-1 was the divergent behavior of signal phase at H3 and H43 (Fig. 13). At H43 the long trend was consistently downward with a net change of more than 250 cycles over the length of the test. At H3 the trend was also downward until near the end of October; at that time the trend was reversed by a series of "step function" phase advances. Similar effects are likely to be present in the H43 data, but are not of sufficient magnitude to dominate the H43 phase curve. We will confine our attention initially to the H3 data. A geophysical explanation, related to the local passage of polar fronts, can be offered for the "step function" signatures at this hydrophone. The hypothesis is supported by the evidence of the environmental data.

Local passage of an atmospheric cold front is marked by an abrupt shift to relatively strong northerly winds. The consequences for the Straits of Florida water will include:

a) A slight temperature decrease in the near-surface layer.

b) A deepening of the mixed layer.

c) A general westward drift of surface water (Ekman transport).

The westward surface current is the phenomenon that apparently controls the H3 phase in the data of LCT-1. In this regard, we note immediately that a westward transport of surface water in the Straits will bring relatively warmer water into the path of the H3 hydrophone. This is an indirect consequence of the geostrophic balance associated with the northerly flow of the Florida Current. A cross-stream surface temperature rise is an observable feature in the Straits. A value for this rise, about 1°C, can be obtained from the Institute of Marine Science hydrographic data.[4] A recent overflight with an airborne infrared thermometer yielded a surface temperature rise of 1.3°C.*

The strong control which Ekman currents can exercise over the temperature of the medium near coastlines has been discussed by several authors.[22,23,24] In general we may expect a north wind parallel to the Florida coast to set up a surface current convergence at the coastline. This will force the cold water of the local thermocline away from the coast; creating a body of water near the coast which, spatially averaged, may have a higher temperature. Given the weather pattern of the Florida coast, one can predict that this process will take place in a series of steps coincident with the southward progression of polar fronts. Available data, in fact, indicate that the step function changes in signal phase at H3 are the signatures of "impulse" surface current convergences associated with polar front passage.

The experimental evidence for this hypothesis is contained in Figures 24, 25 and 26. Figure 25 emphasizes the correlation which exists between these step signatures in the H3 phase, T5 temperature, and the northerly component of the local wind; Figure 26 lends support to the assumed cross-stream transport of warmer water.

Because of the failure of the Fowey Rocks anemometer (Fig.2, Table I) it was necessary to derive the north-south and east-west wind components (Fig. 24) from 3 hourly readings measured at the Miami International Airport.[25] Both wind components have been smoothed with a 24 hour running average. The thermistor string data in Figure 24 are repeated from Figure 13. Also in Figure 24 is the

---

* Special flight conducted on 22 March 1967 by R.B. Stone and T.R. Azarovitz of the Sandy Hook Marine Laboratory, U.S. Bureau of Sport Fisheries and Wildlife.

time distribution of the short period internal wave signatures, broken down into the indicated ranges of period. These were included in the hope of observing a relationship between the occurrence of these signatures and the environmental parameters. No obvious relationships are visible.

It will be noted in Figure 24 that the wind components have been time shifted relative to the phase and temperature curves. This is to remove the effect of the delay between the time that a north wind is established and the time the effects are felt in the H3 propagation path--a delay of about two days is assumed. We should expect that the wind must act on the water for a certain period of time before an effective volume of surface transport can be established. Several days of persistent north winds are apparently required. Figure 24 shows that the first step function increase in H3 phase, occurring on October 29, is concurrent with the first (time shifted) period of persistent north winds. Previous to that time north winds were of short duration; winds were generally from the east or southeast, and the step effect is not observed.

The correspondence of events in H3 phase, N-S wind, and thermistor T5 is most evident in the period October through December. Figure 25 provides for a direct comparison of these three parameters during this time. Subsequent to the event of October 29, the details of the visual correlation may be followed both in H3 phase and in the thermistor string data that is available. The correlation is apparently weaker in much of December and January. At the end of the test the net change in H3 phase, referred to the reference level of October 6, is a positive 8 cycles. According to the calibration of Figure 4, this suggests a spatially averaged net increase in sound speed (temperature) in the H3 propagation path from October to January.

A single event provides the most convincing direct evidence now available for cross-stream transport of surface water into the H3 path. The longest period of persistent north winds in available data occurred from 11 through 26 November. We will examine a detail of the thermistor chain data (Fig. 26) for the latter part of this period. (The detail starts at the position of the arrow in Figure 25). At the beginning of the detail the medium is thermally stratified, as indicated by the thermistor T5 curve. Subsequently, and we will assume under the action of the north wind, a complete mixed layer forms. This step is essentially completed by 23 November. Following this step the entire mixed layer at the thermistor chain rises in temperature about 0.6°C. This is the third stage in a process which requires an external source of relatively warm water. Cross-stream transport is the probable source of this warmer water.

Turning now to the data of hydrophone H43, we may suspect, from the contrasting phase behavior at H43 and H3, that the long period signatures at H43 are predominately the result of events occurring in the main stream of the Florida Current beyond H3.

We will speculate that these events are atmospheric in origin, but hasten to add that no direct correlation with environmental parameters are available at this time. Figure 27 presents a high-pass filtered spectrum of the H43 data with a filter cut-off in the period range of 24 days. This may be compared with Figure 20, the same data with cut-off at about 36 hours.

A brief comment is in order concerning the major down trend of the H43 phase. A net change of nearly 250 cycles was registered from October 6 to January 30. A large scale temperature decrease, seasonal or longer, is perhaps indicated for the waters of the Florida Straits. As a practical matter, however, there is little point in pursuing this line of thought in the absence of corroboration from direct environmental measurements. It is quite clear that the data from the 100 meter thermistor string is of very limited value in interpreting the H43 hydrophone data. It is also clear that a need exists for a similar installation in the deeper water of the Straits which will serve to "calibrate" the H43 path in the same manner that the 100 m thermistor string has helped to clarify the meaning of the phase data at H3.

CONCLUSIONS AND RECOMMENDATIONS

A spatially averaged, spectral measure of time varying processes in the ocean may be obtained from a coherently detected acoustic signal. The use of fixed source and receiver installations and experimental facilities capable of long continuous operation are required to take full advantage of the measurement technique.

In the Straits of Florida studies, measures have been obtained for events on the scale of surface waves at the high frequency end to slow changes in the medium which may be seasonal or longer. The measure provided for the short period phenomena (surface waves and short period internal waves), may be limited in space; but, on the scale of events that are tidal or longer, involving processes which are spatially coherent over the propagation path, a synoptic measure is likely provided. Quantitative determinations of spatially averaged properties of the medium (e.g., temperature and current components parallel to the acoustic path) are crude but should improve with further research. The most serious deficiency of the Straits of Florida studies is the lack of fixed, continuous environmental measurements in the central (Florida Current) regions of the Straits. Satisfactory deep water measurements from one or more fixed instrument strings would affect a substantial increase in our ability to "read" the information provided by the acoustic signal. Such measurements are a necessary "calibration" of the synoptic acoustic environmental probe.

The limited space scale of the Straits of Florida measurements would perhaps place this experiment in the category of a pilot study. It is of interest to speculate about the possibility of

similar measurements over much longer acoustic paths in the open oceans through which we may hope to study Rossby waves and other large scale phenomena not available in the Straits. Questions must be answered, however. Over longer paths it may be necessary to go to a lower frequency to obtain a usable coherent acoustic signal at the receiver--how low is perhaps the first question that must be answered.

In addition, technological and logistical problems must be faced. Highly instrumented precision measurements, carefully attended by qualified personnel, are now required. Improved instrumentation must be provided and sampling schemes devised. In the open oceans, stable, long-life fixed installations must be provided for sources and receivers.

Until our ability to interpret the information provided by the acoustic probe is improved, and the technological problems are reasonably in hand, only additional pilot studies with land-based terminal facilities can be recommended.

ACKNOWLEDGEMENTS

Project MIMI, the Straits of Florida acoustic propagation study, is a joint program under the direction of J.C. Steinberg at the University of Miami and T.G. Birdsall at the University of Michigan. The guiding influence of Dr. Steinberg and the very substantial contributions of Dr. Birdsall are gratefully acknowledged. The continued counsel of A.W. Pryce, M.L. Lasky, and A.O. Sykes (U.S. Office of Naval Research) and the sincere interest and contributions of Dr. M.J. Jacobson of Rensselaer Polytechnical Institute are also acknowledged with pleasure. Project MIMI is an interdisciplinary group effort. The creative energies of a number of scientific and technical specialists have been involved in bringing the project to its present stage of development. To our associates in the work, we will simply say that we are thankful for the opportunity to prepare this presentation of its results.

REFERENCES

1) Steinberg, J.C. and Birdsall, T.G., "Underwater Sound Propagation in the Straits of Florida", J. Acoust. Soc. Am., 39: 301-315 (1966).

2) Steinberg, J.C., "Phase Variation of Sound in the Straits of Florida", (to be published).

3) Kronengold, M. and Loewenstein, J., "Underwater Acoustic Range", Geo Marine Tech. 2(2): 21-22 (1966).

4) "A Report of Data Obtained in Florida Straits and off the West Coast of Florida", Technical Reports 62-11, 63-3, and 64-1. Inst. of Marine Science, University of Miami (unpublished manuscripts).

5) Heald, M.A. and Wharton, C.B., Plasma Diagnostics with Microwaves, ch. 6, John Wiley & Sons, New York, 1965.

6) Tolstoy, I. and Clay, C.S., Ocean Acoustics, McGraw-Hill, New York, 1966.

7) Reference 6, ch. 6.

8) Shulkin, M. and Marsh, H.W., J. Brit. IRE, 25: 493 (1963).

9) Mackenzie, K.V., "Reflection of Sound from Coastal Bottoms", J. Acoust. Soc. Am., 32: 221-231 (1960).

10) Jacobson, M.J. and Clark, J.G., "Refracted/Reflected Ray Transmission in a Divergent Channel", J. Acoust. Soc. Am., 41: 167-176 (1967).

11) Marsh, H.W., J. Acoust. Soc. Am., 33: 330-333 (1961).

12) Jacobson, M.J., "Analysis of Spreading Loss for Refracted/Reflected Rays in Constant-Velocity-Gradient Media", J. Acoust. Soc. Am., 36: 2298-2305 (1964).

13) Jacobson, M.J., "Analysis of Surface-Reflected/Bottom-Reflected Ray Transmission in Constant-Velocity-Gradient Media" J. Acoust. Soc. Am., 37: 885-893 (1965).

14) Evans, G.W., et al, "Comparison of Power Spectral Density Techniques as Applied to Digitalized Data Records of Nonstationary Processes, Part I", Technical Report 14, Stanford Research Institute, Menlo Park, California, September 1963 (unpublished manuscript).

15) Mackenzie, K.V., "Long-Range Shallow-Water Signal-Level Fluctuations and Frequency Spreading", J. Acoust. Soc. Am., 34: 67-75 (1962).

16) Scrimger, J.A., "Signal Amplitude and Phase Fluctuations Induced by Surface Waves in Ducted Sound Propagation", J. Acoust. Soc. Am., 33: 239-247 (1961).

17) Eckart, C., Hydrodynamics of Oceans and Atmospheres, Pergamon Press, New York, 1960.

18) Clark, J.G., Dann, R. and Yarnall, J.R., "Recent Results from the Straits of Florida Underwater Sound Propagation Studies", J. Acoust. Soc. Am., 40: 1195-1197 (1966).

19) Personal communication from Mr. D.C. Simpson, Tide & Tidal Current Predictions Section, ESSA.

20) Stommel, H., The Gulf Stream, p. 68, University of California Press, Los Angeles, 1965.

21) "A Preliminary Report on Operation Strait Jacket", Inst. of Mar. Science, University of Miami, Technical Report 66-1 (unpublished manuscript).

22) Sverdrup, H.U., Oceanography for Meteorologists, Prentice-Hall, New York, 1942.

23) Cairns, J.L. and LaFond, E.C., "Prediction of Summer Thermocline Depth off Mission Beach", Proc. U.S. Navy Sym. Mil. Oceanog., 1: 113-132 (1965).

24) Longard, J.R. and Banks, R.E., "Wind-Induced Vertical Movement of the Water on an Open Coast", Trans. Am. Geophys. Un. 33: 377-380 (1952).

25) "Local Climatological Data", International Airport, Miami, Fla., ESSA, Sept. 1966 - Jan. 1967.

TABLE Ia

Field Instruments of MIMI Acoustic-Environmental Measurement System - Western Side

INSTRUMENT	LOCATION	REMARKS
Anemometer	Wind spd. & direct.,mounted on FRLH* 60 m above sea level	Frequent failures--data in text obtained from Miami International Airport
Inverted Fathometer **	Wave hgt. and tide, 0.4 km east of FRLH, at 16 m depth	Surface wave studies - "single reflection" experiment
Projector	Signal source, 0.6 km east of FRLH, axis of beam 21 m below surface	Source for all tests except "single reflection" experiment
Current Meter	Current spd. & direct. at proj. site	
Therm. TX	Temperature at projector site	
Monitor Hydro F3	20 m from source at 21 m	
Thermistor String	Vertical sensor array anchored 2.0 km in front of source provides:	Max. inclin. from vertical is 6° in 4 knot curr. (calc.)
	pressure at 21 m	Therm. resolution - $0.3^{o}C$
**	temp. at 21 m (T1)	Press. gauge failed 8/5/66
**	" " 29 m (T2)	T4 failed 9/2/66 (Fig. 22 only)
**	" " 46 m (T3)	Entire string failed 12/9/66
**	" " 69 m (T4)	
**	" " 100 m (T5)	
Hydro F4	4.5 km from source at 180 m	
Hydro F5 **	5.9 km from source at 300 m	Hydrophone "H3"

TABLE Ib

Field Instruments of MIMI Acoustic-Environmental System - Eastern Side

INSTRUMENT		LOCATION	REMARKS
Hydro B		77.7 km from source at 360 m	
Hydro D	**	79.5 km from source at 23 m	Hydrophone "H43"
Spar Buoy		Array of sensors 79.5 km from source provides: wind spd. & direct. at 5 m above surface surface wave height temperature at 3 m " "18 m " "33 m current spd. & direct. at 12 m	Developed under sponsorship of U.S. Navy Ship Systems Command
Hydro A	**	79.5 km from source at 20 m	Visual study of surface wave signatures
Tide Gauge		Western shore of Bimini	Instrument operated by ESSA

* Fowey Rocks Light House

** A source of data discussed in text

TABLE II

Major cw Tests with the MIMI Acoustic-Environmental System

START	END	DURATION	MAJOR OBSERVATIONS	SECTION	REFS
25 Jan 65	29 Jan 65	4 days	First observation of tidally-related signatures and surface-wave effects	a,c	1
19 Aug 65	20 Aug 65	1 day	Time and frequency domain study of surface-wave signatures	a	
17 Mar 66	19 Mar 66	2 days	Observed growth of tidal signatures with increasing range from source	c	18
16 Jul 66	21 Jul 66	5 days	Low frequency signature, period ≥5 days, evident in data from both sides of the Straits	c,d	
11 Aug 66	23 Aug 66	10 days	Direct correlation between phase at 3 mile hydrophone and water temperature at depth of 46 m	b,c	2
7 Sep 66	31 Jan 67	140 days	Developed in text	b,c,d	2

a surface wave signatures
b short period internal wave signatures
c tidally-related signatures
d long period signatures-atmospheric phenomena

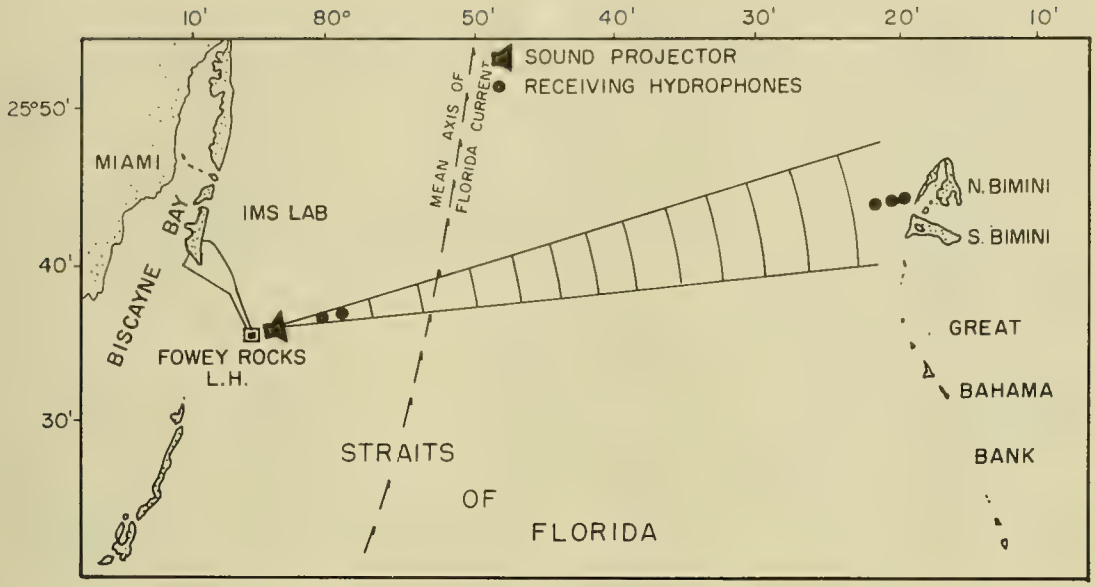

a) LOCATION OF SYSTEM

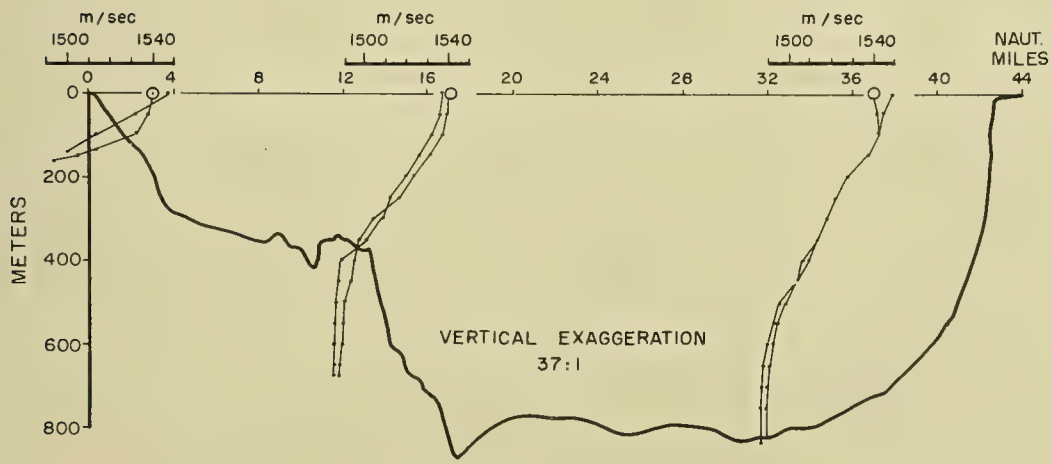

b) BOUNDARIES OF PROPAGATION PATH AND REPRESENTATIVE SOUND SPEED PROFILES

Fig. 1 - Straits of Florida propagation path

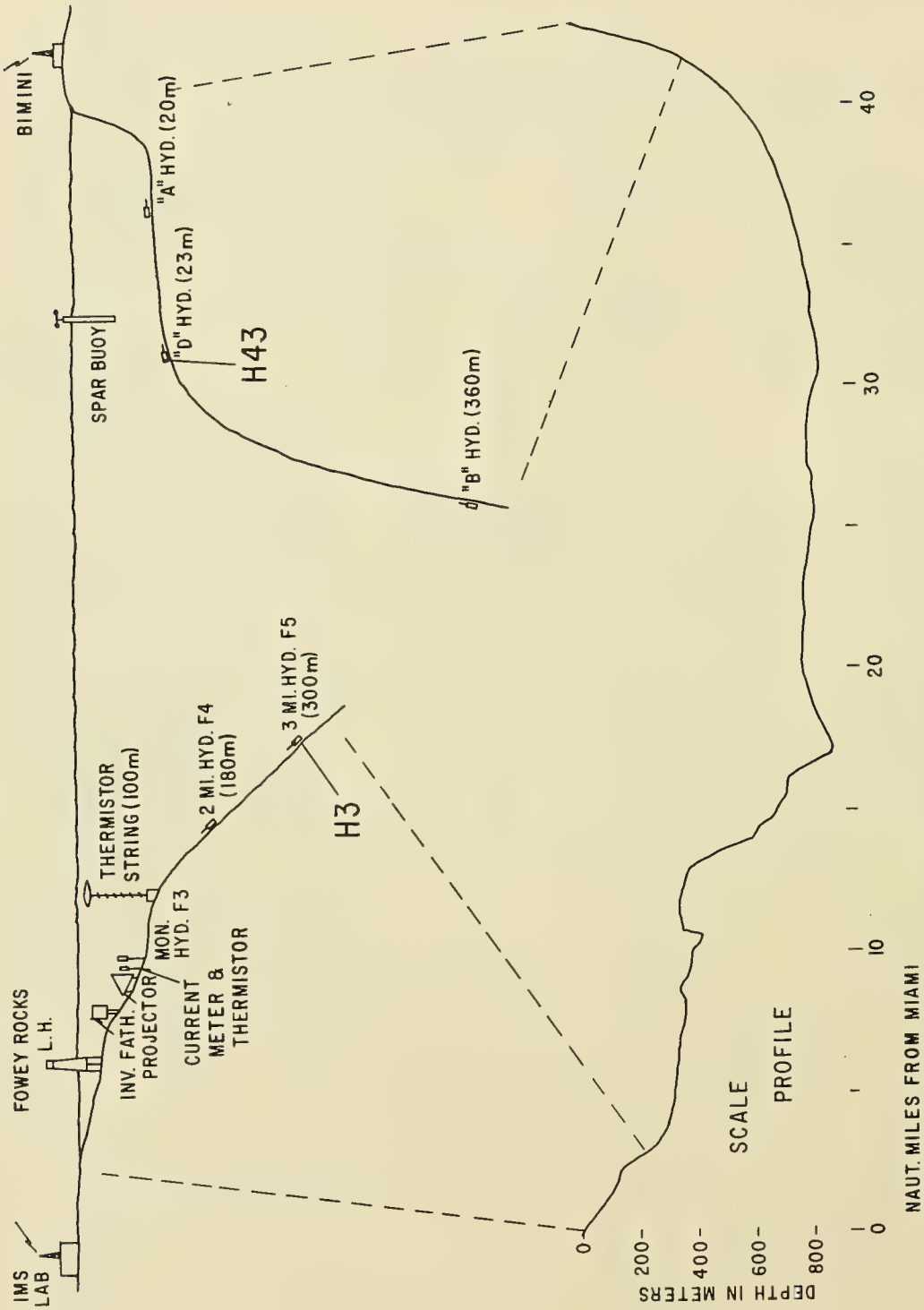

Fig. 2 - Elements of acoustic-environmental system

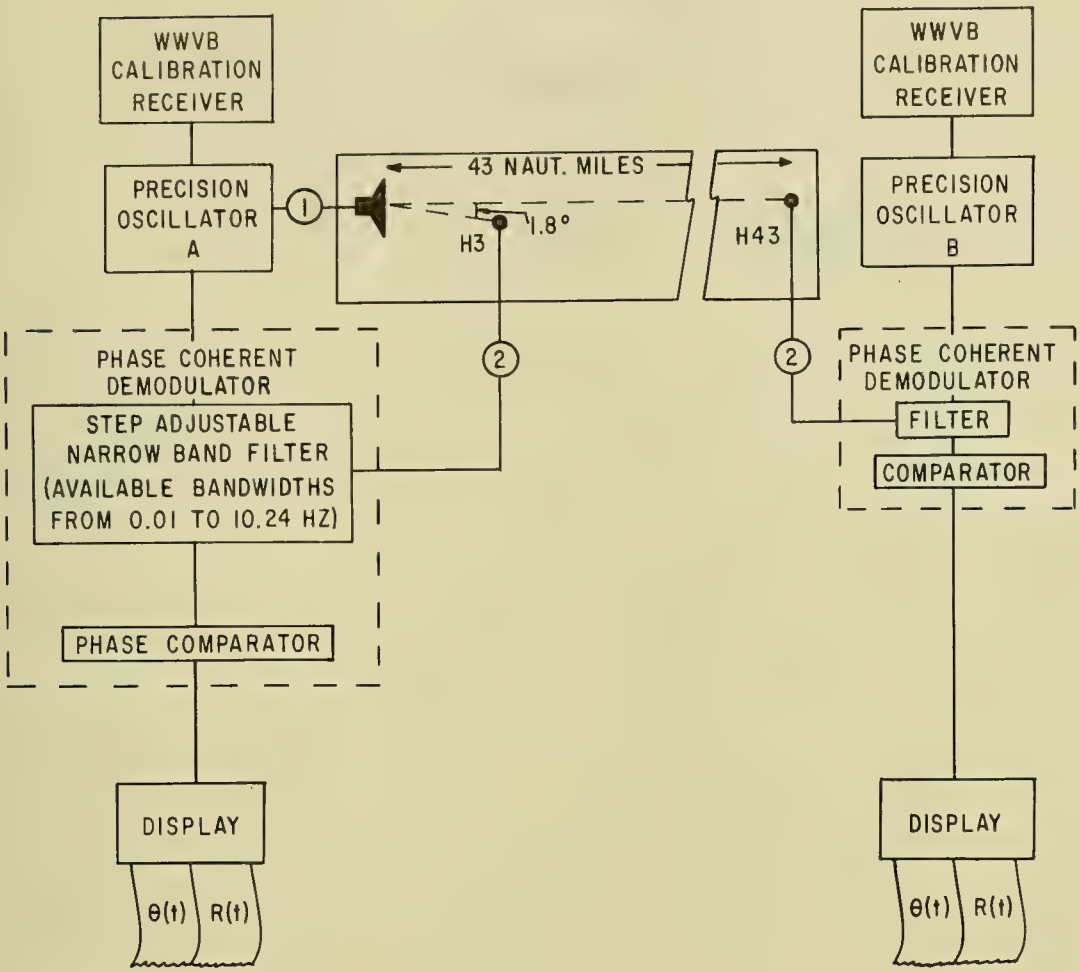

(1) Transmitted signal is of form: $A \cos \omega_0 t$.

(2) Received signal is of form: $R(t) \cos \left[\omega_0 t - \theta(t)\right]$, where $R(t)$ and $\theta(t)$ are functions of time-varying processes in the medium.

Fig. 3 - Functional elements of acoustic measurement system

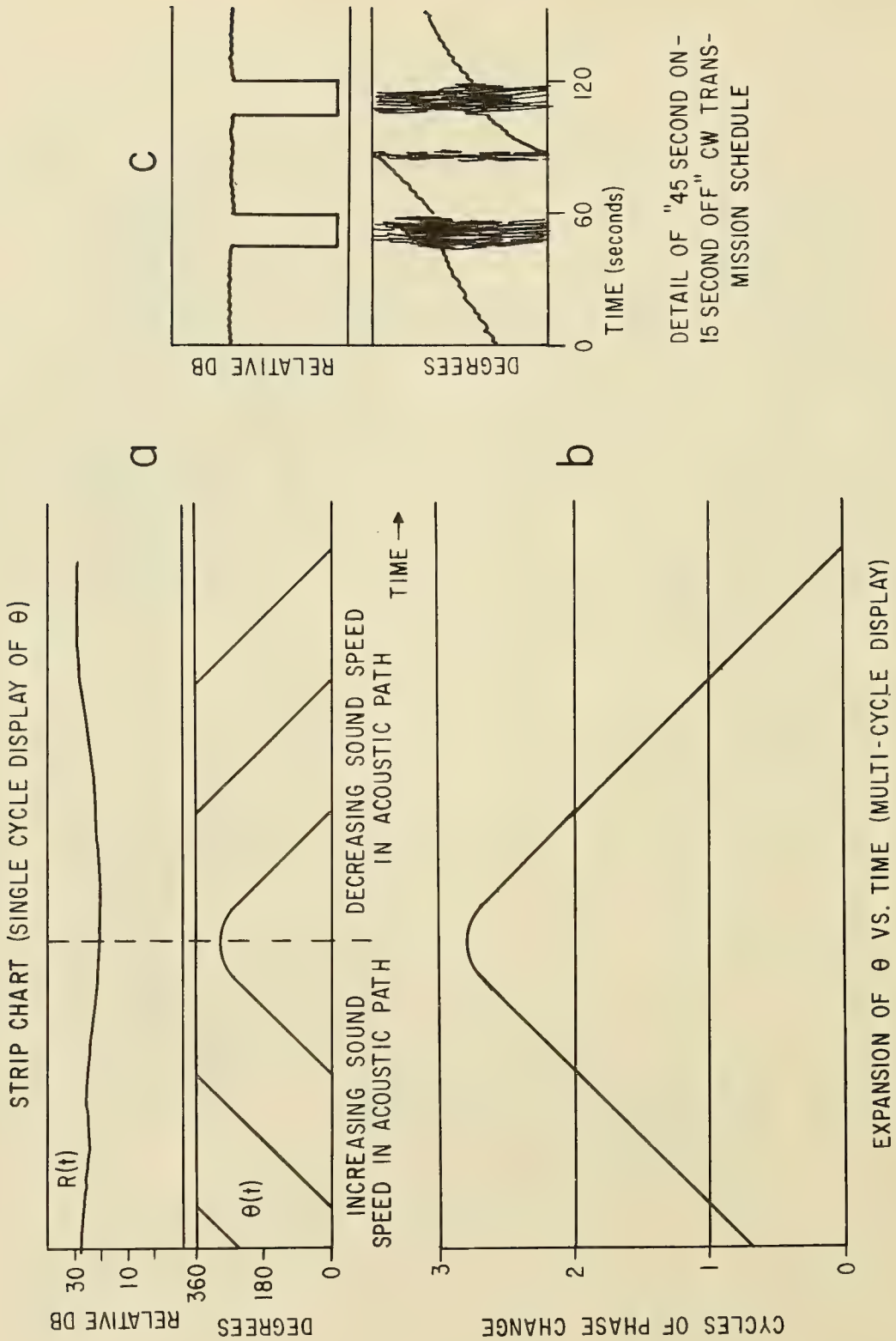

Fig. 4 - Details of acoustic display and phase calibration

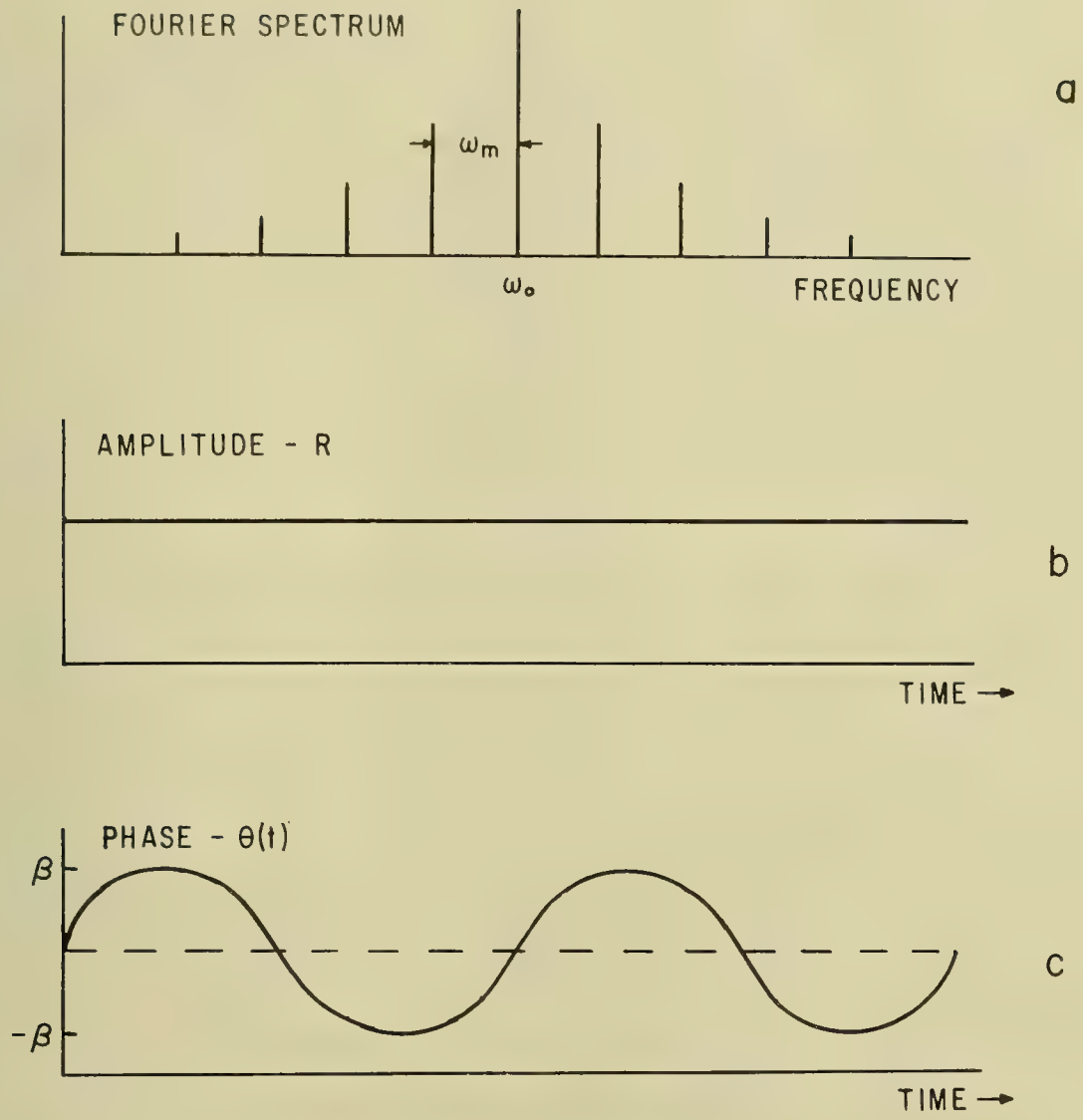

Received signal of form $R\cos\left[\omega_o t - \theta(t)\right]$, where

$\theta(t) = \beta \sin \omega_m t, \quad \beta << 1.$

Fig. 5 - Ideal experiment

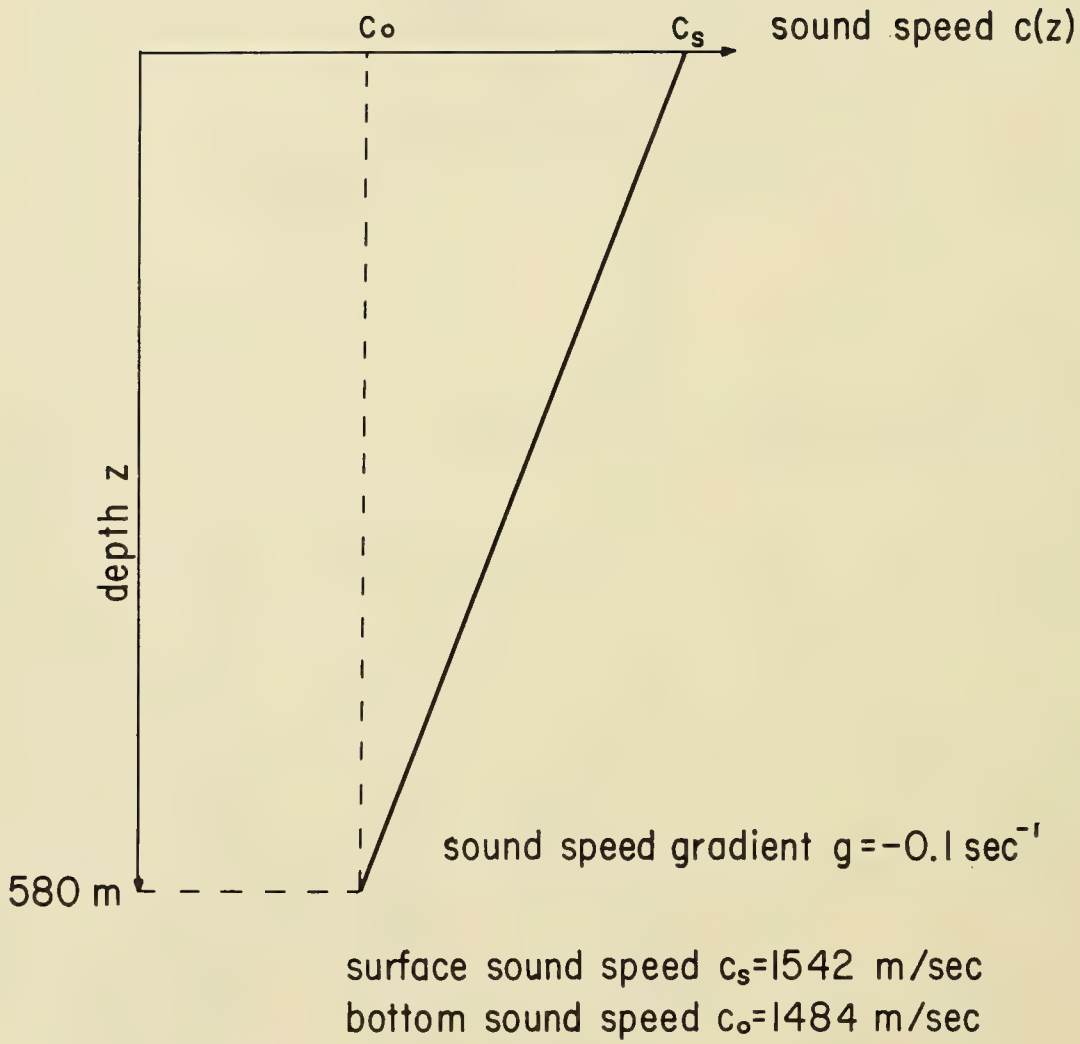

Fig. 6 - Medium representation - propagation model

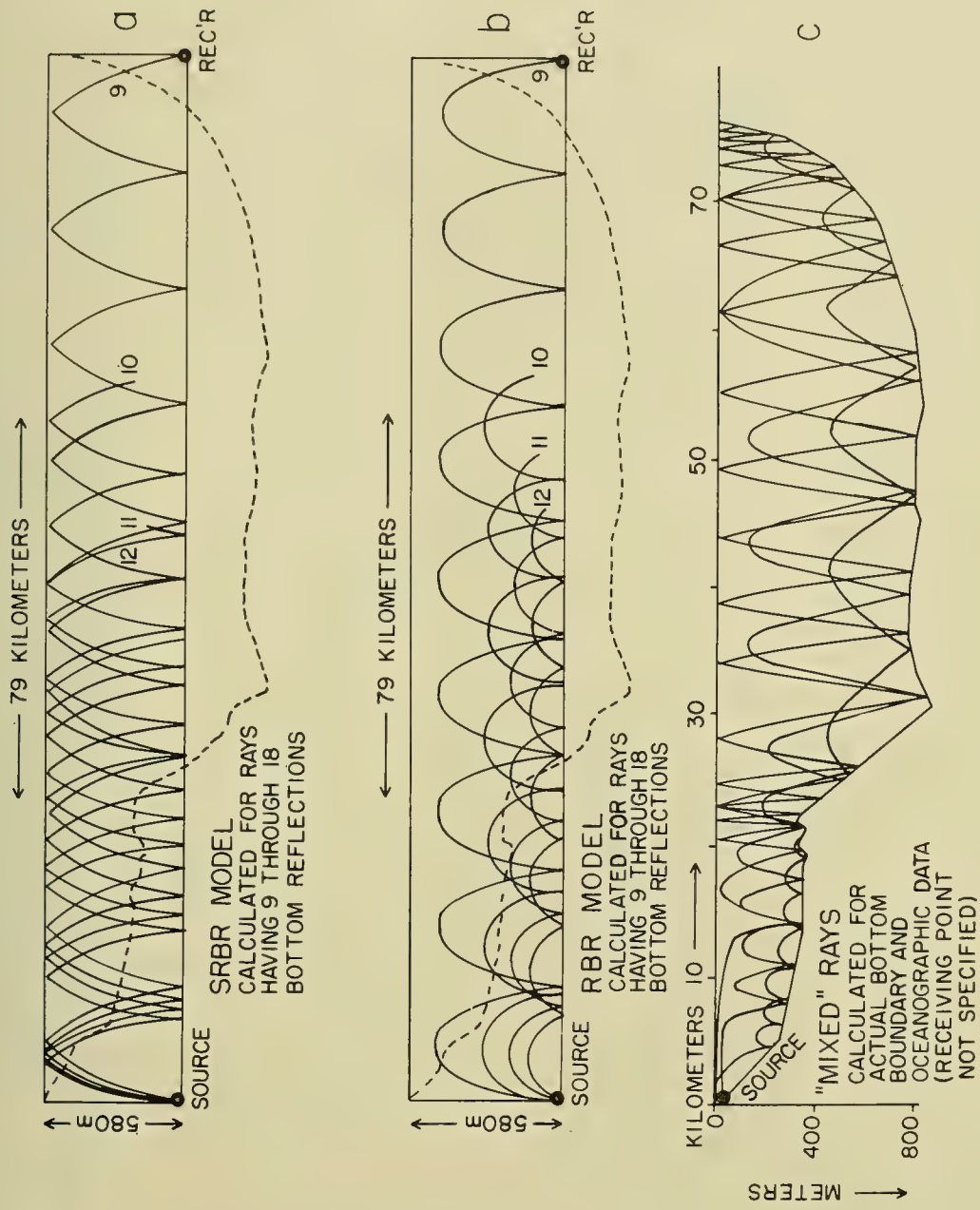

Fig. 7 - Representative rays

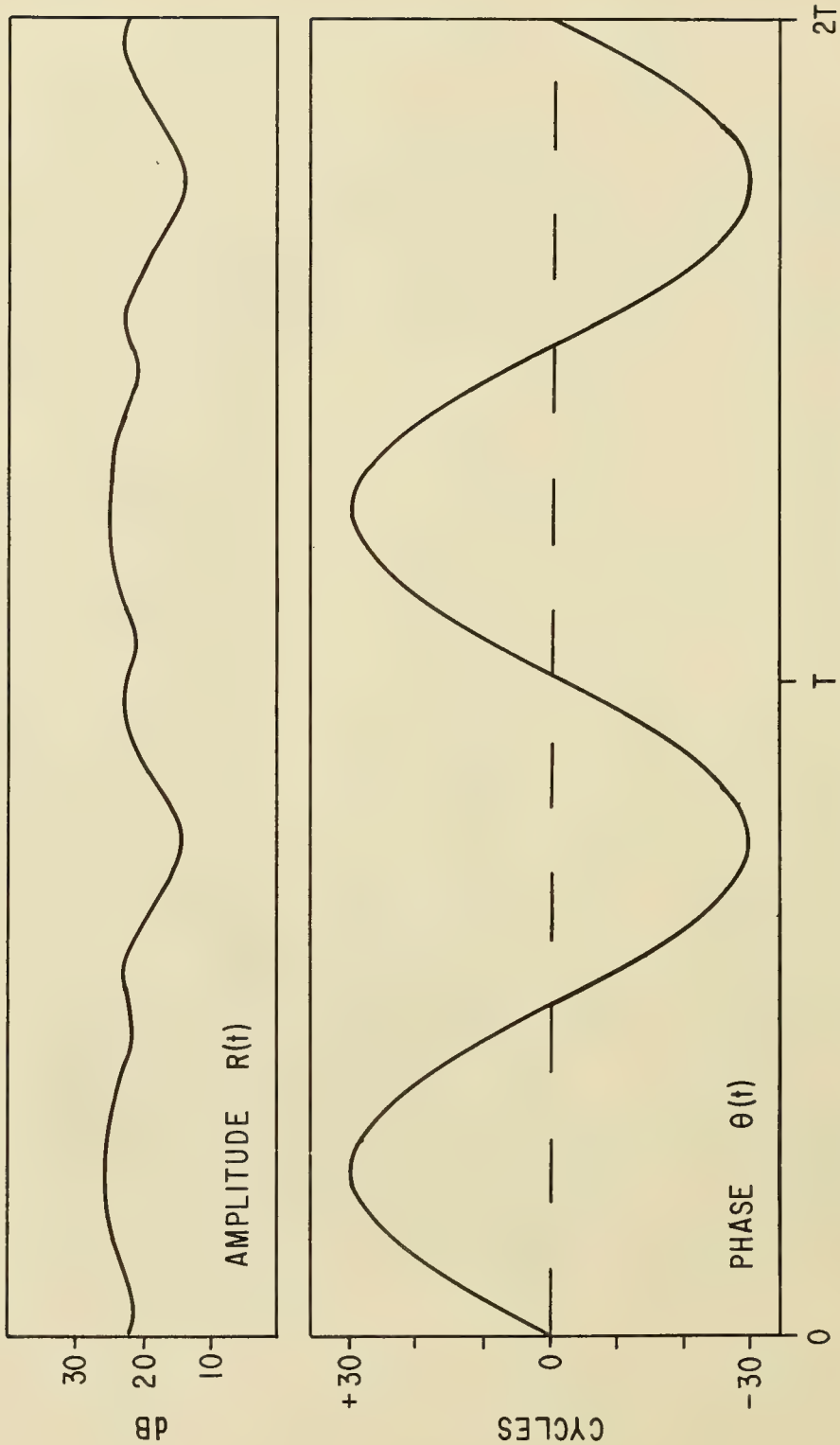

Fig. 8 - Results of "sliding profile" calculations - RBR model

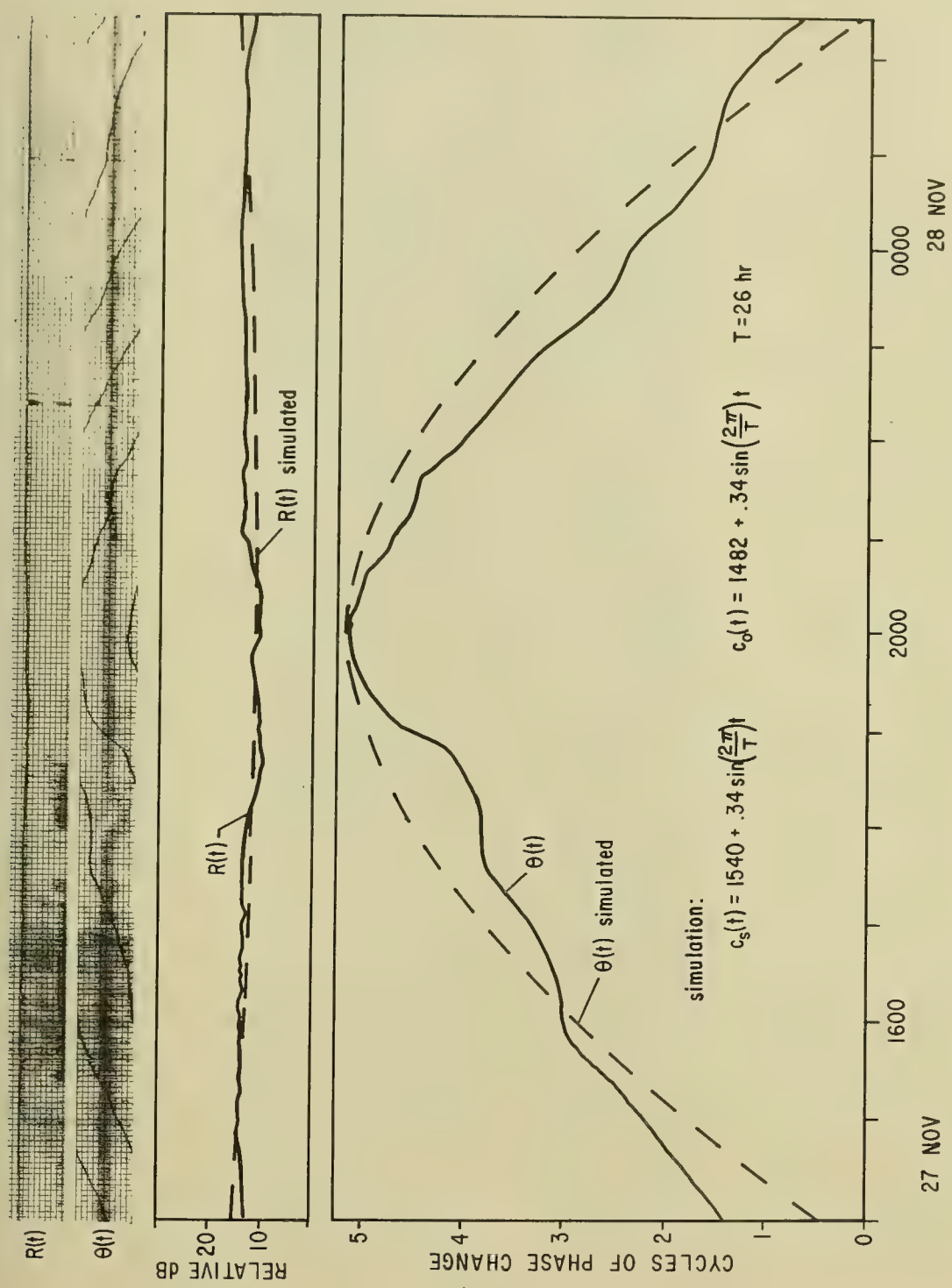

Fig. 9 - "Sliding profile" simulation of stable transmission data

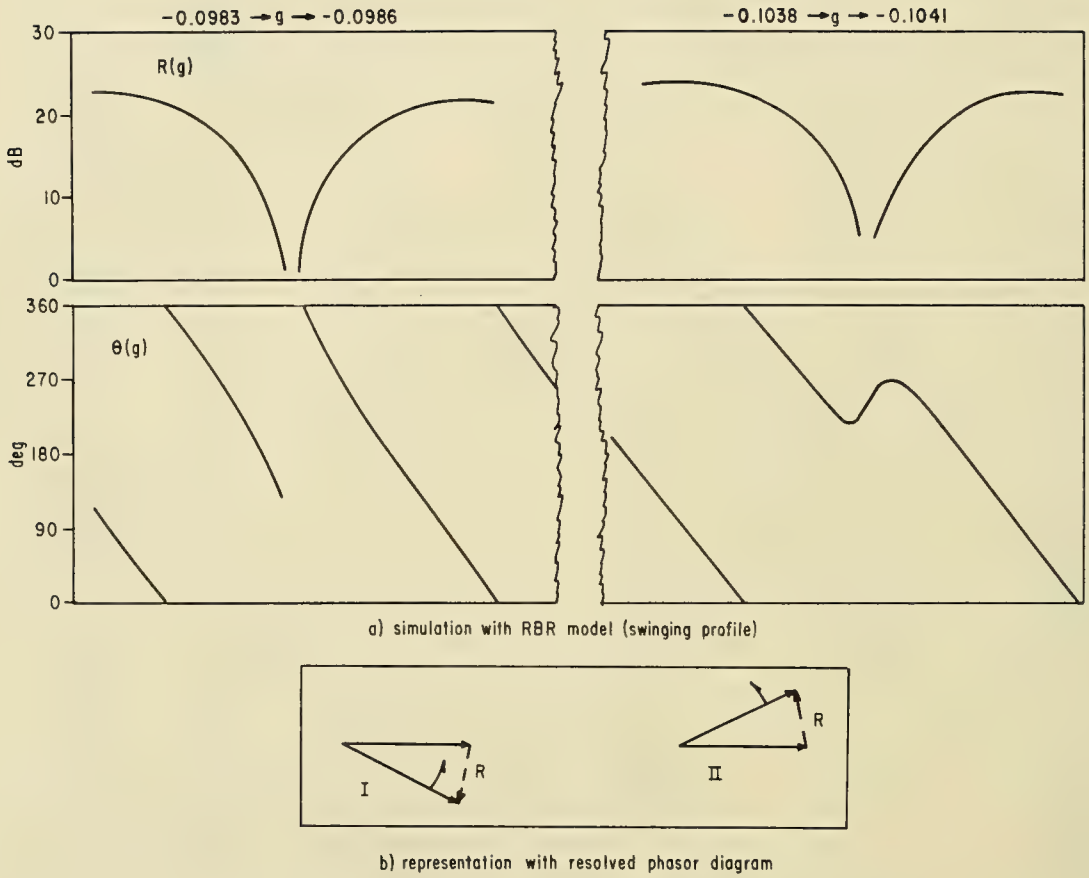

Fig. 10 - Interpretation of "interference nulls"

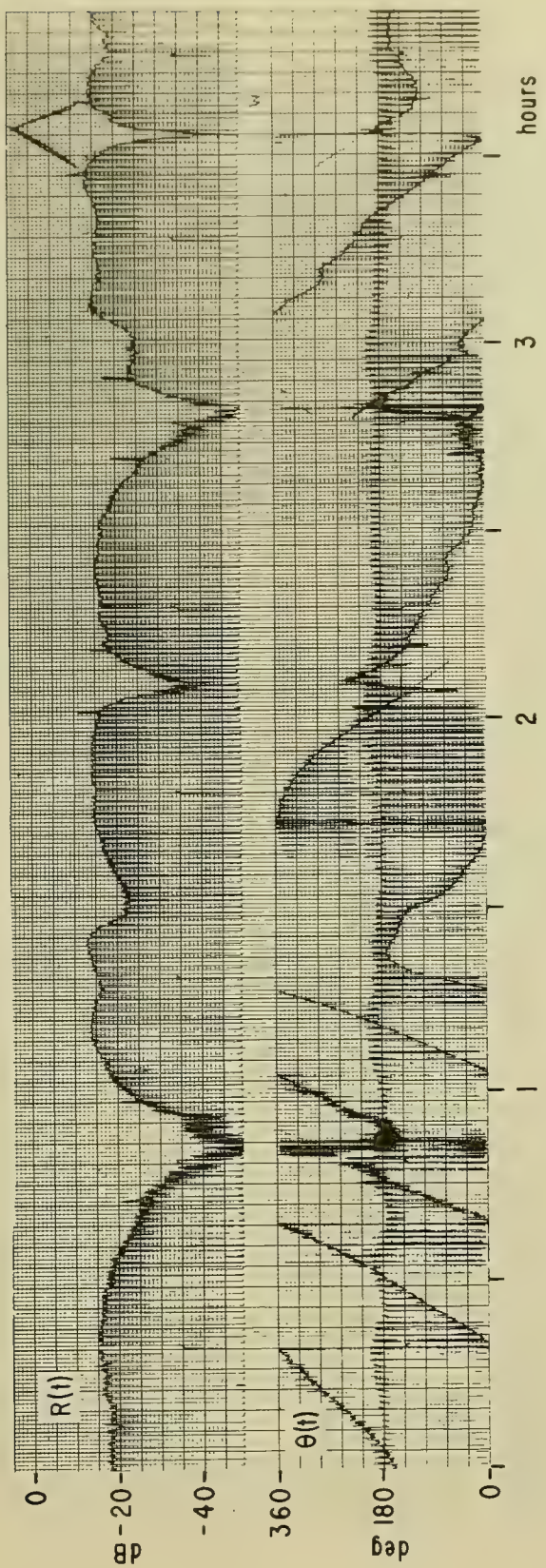

Fig. 11 - Interference nulls in data record

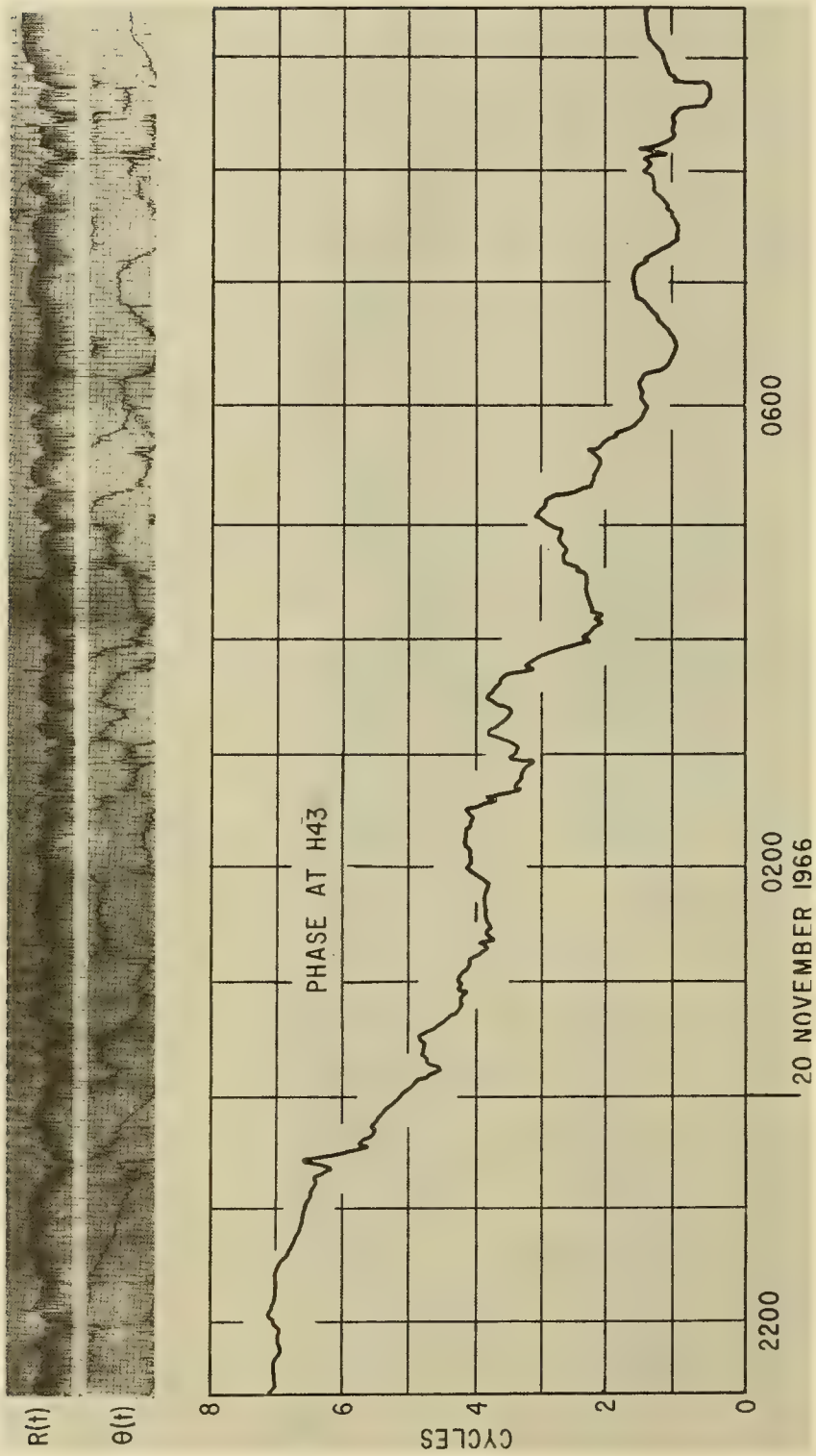

Fig. 12 - Unstable transmission data

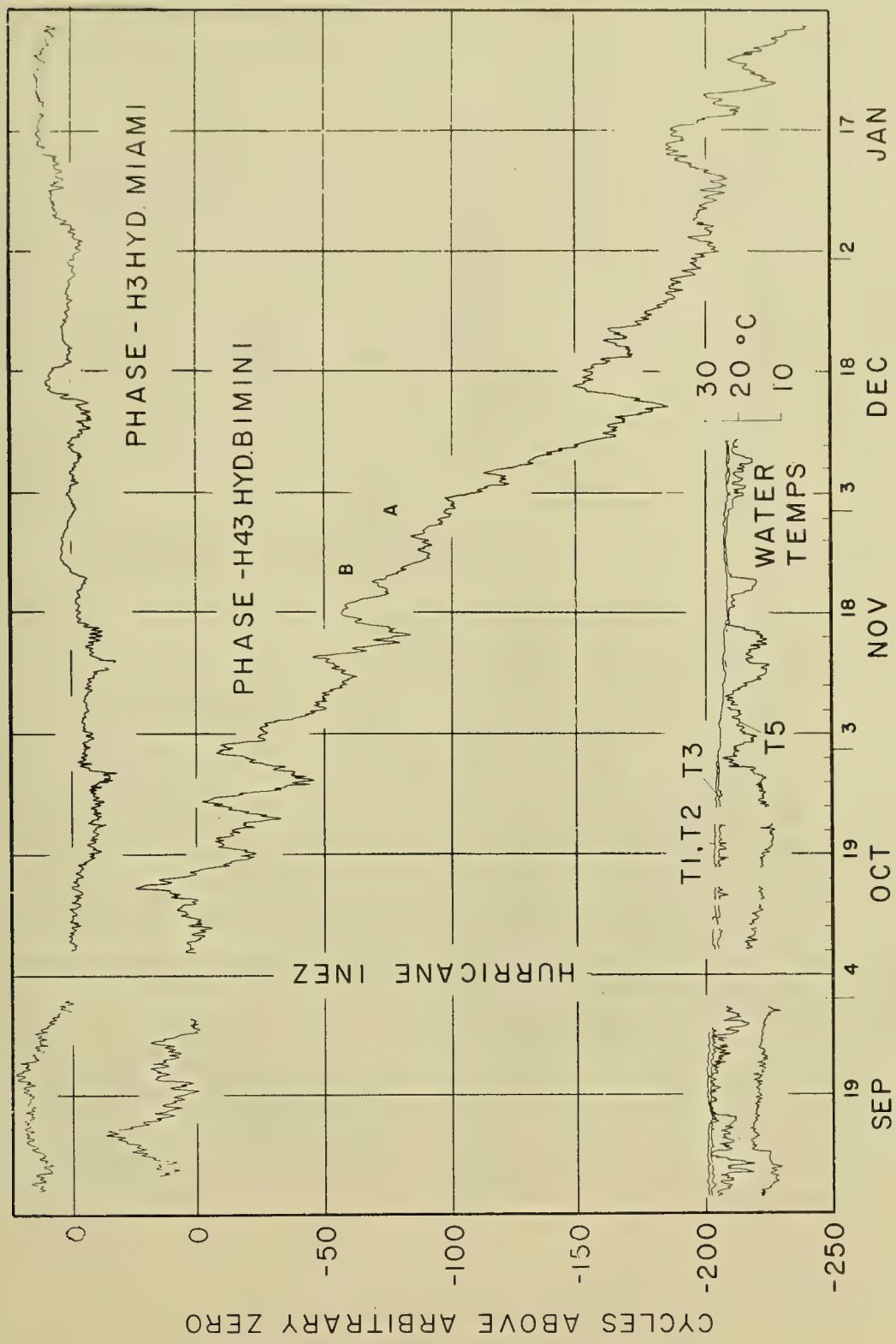

Fig. 13 - Areas marked A and B are detailed in Figs. 9 and 12

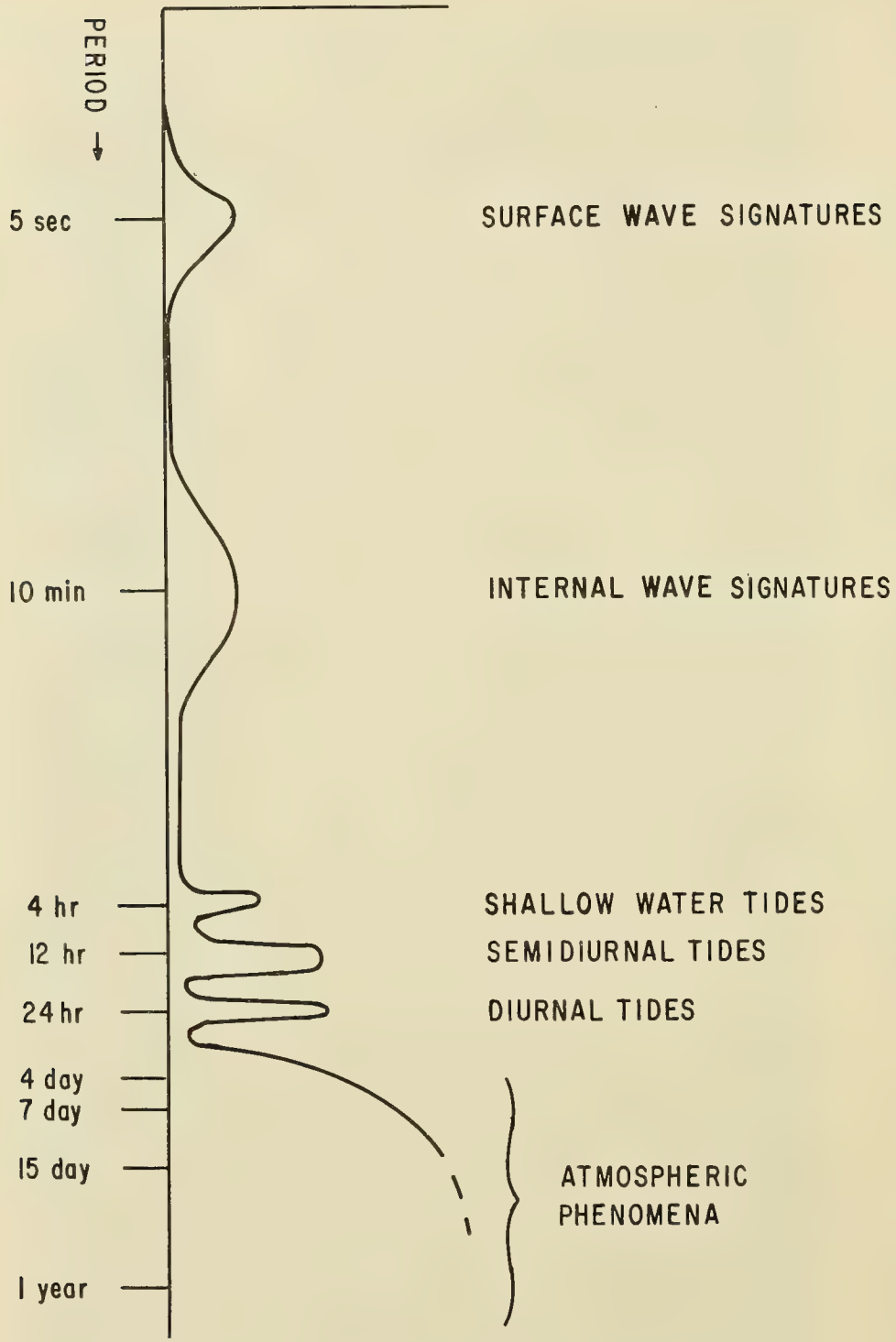

Fig. 14 - Time scale of periodicities observed in acoustic data

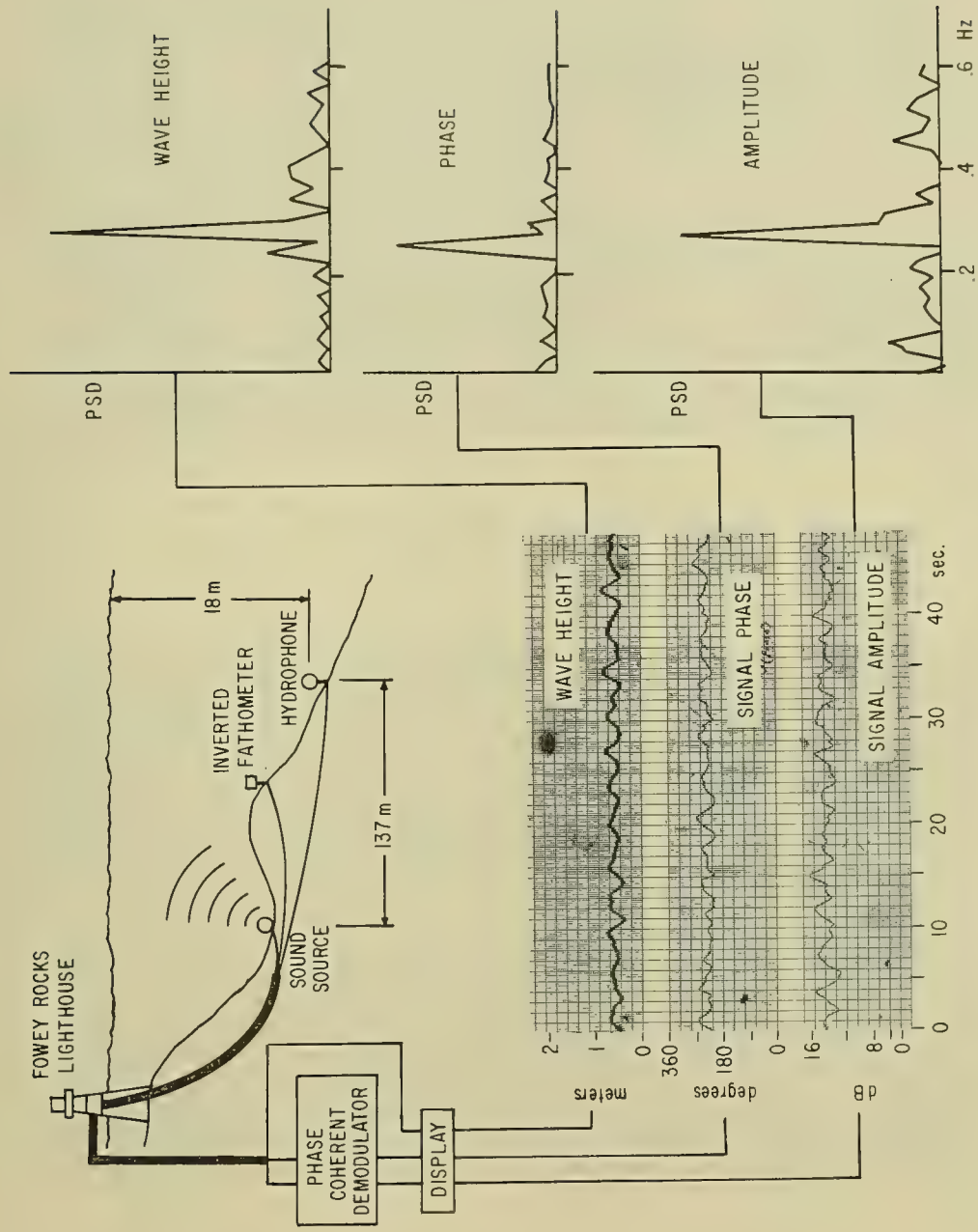

Fig. 15 - "Single reflection" surface wave experiment

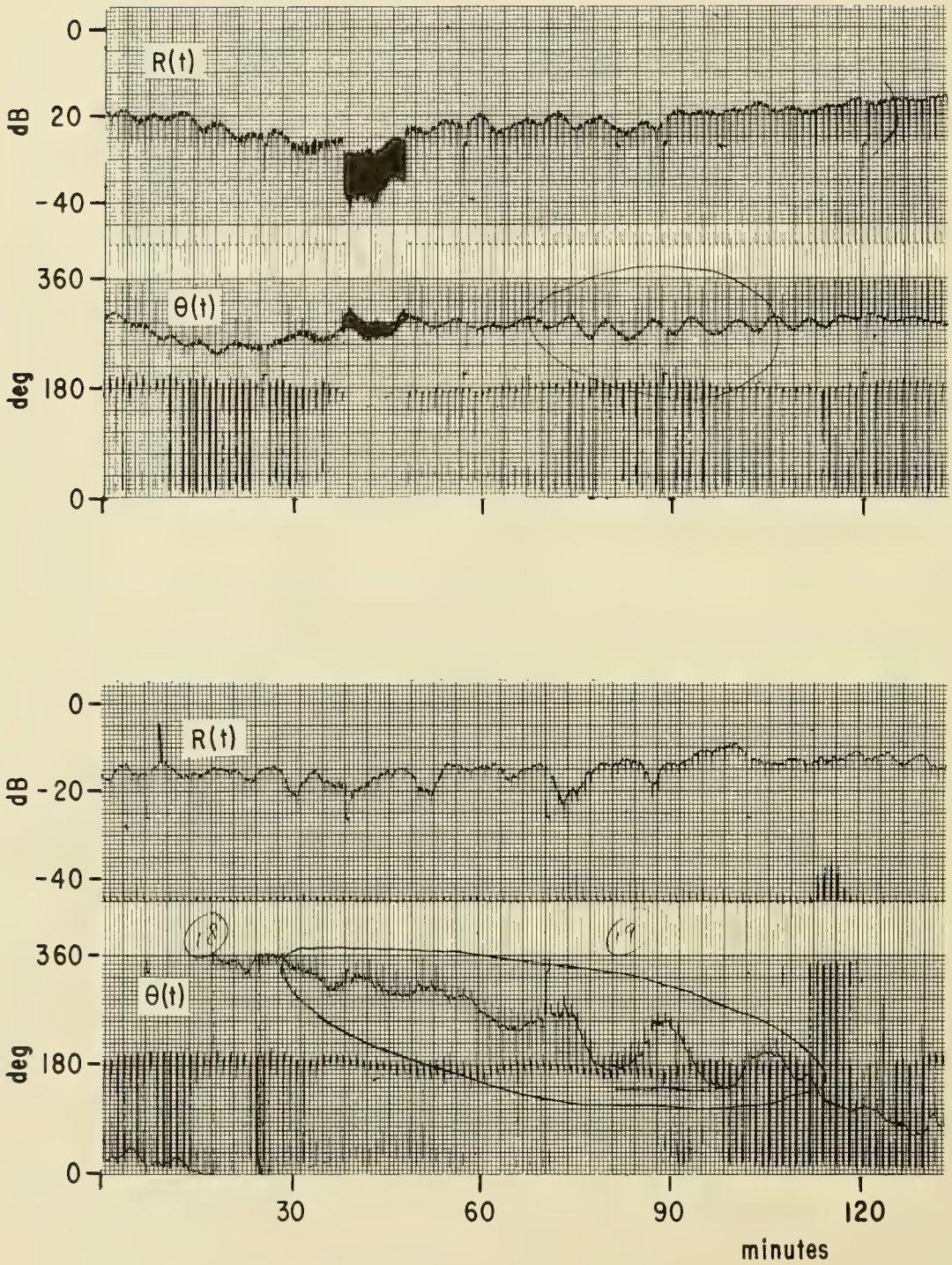

Fig. 16 - Internal wave signatures

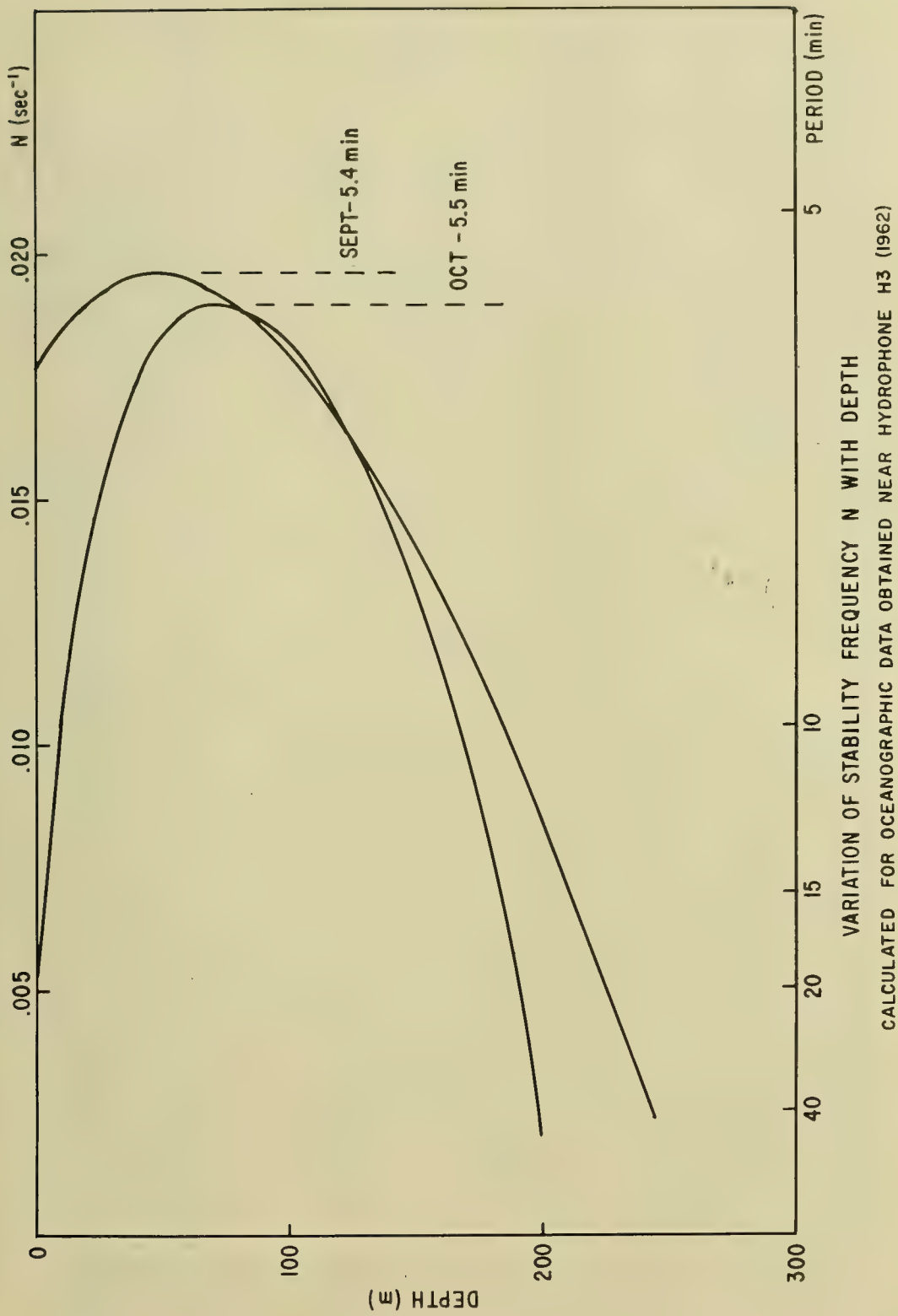

Fig. 17 - Variation of stability frequency N with depth. Calculated for oceanographic data obtained near hydrophone H3 (1962)

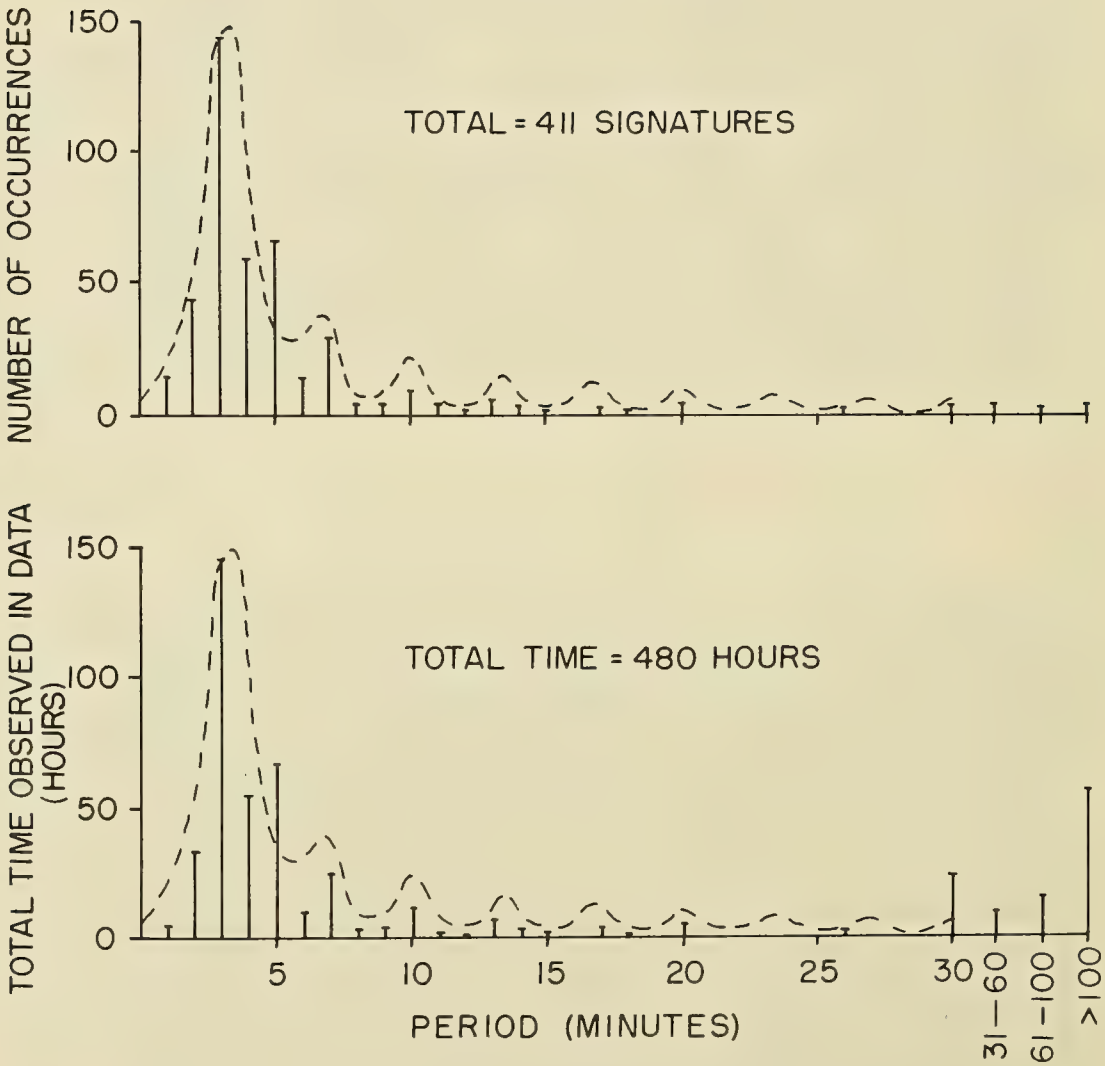

Fig. 18 - Distributions of internal wave signatures

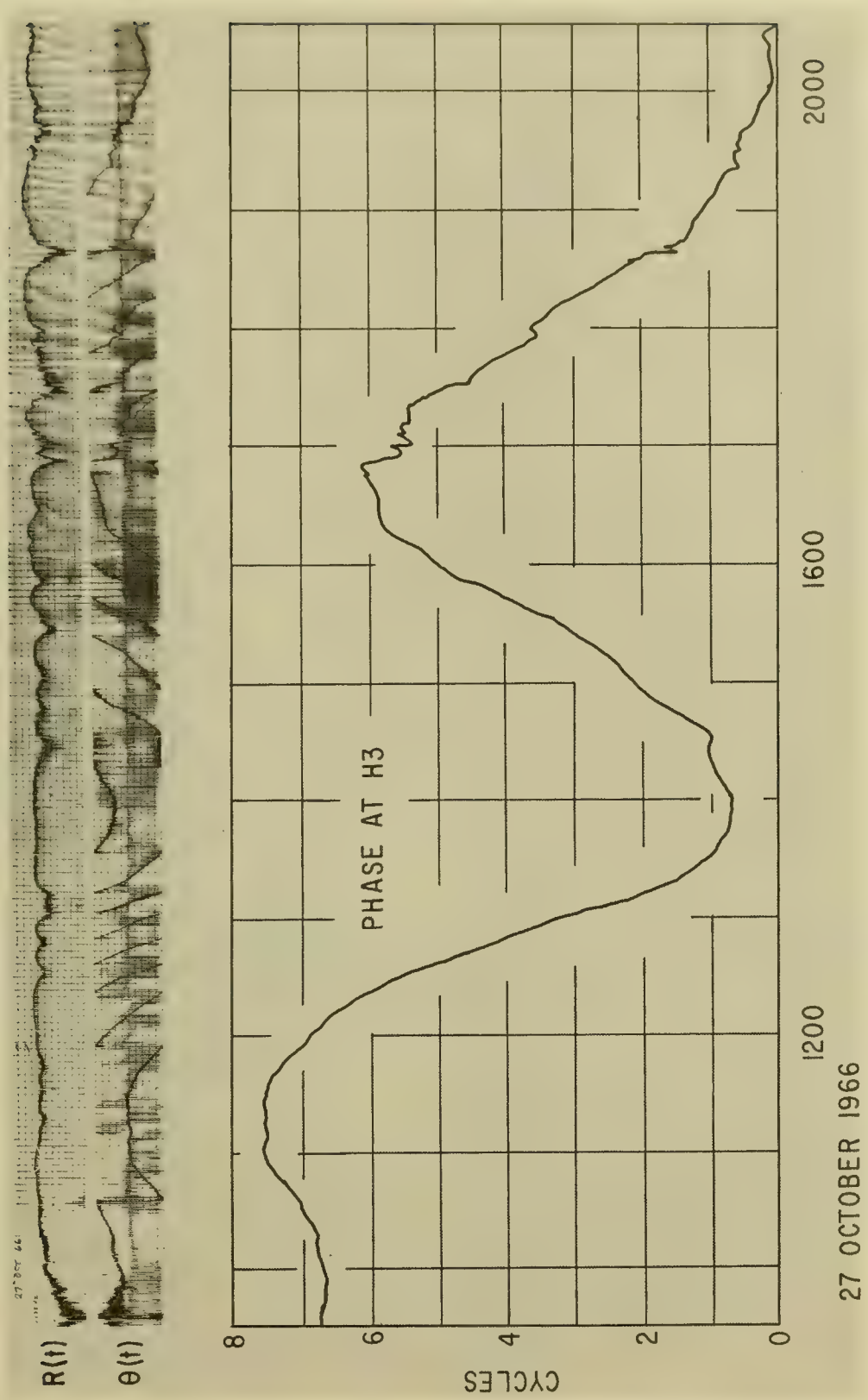

Fig. 19 - Shallow water tidal signature

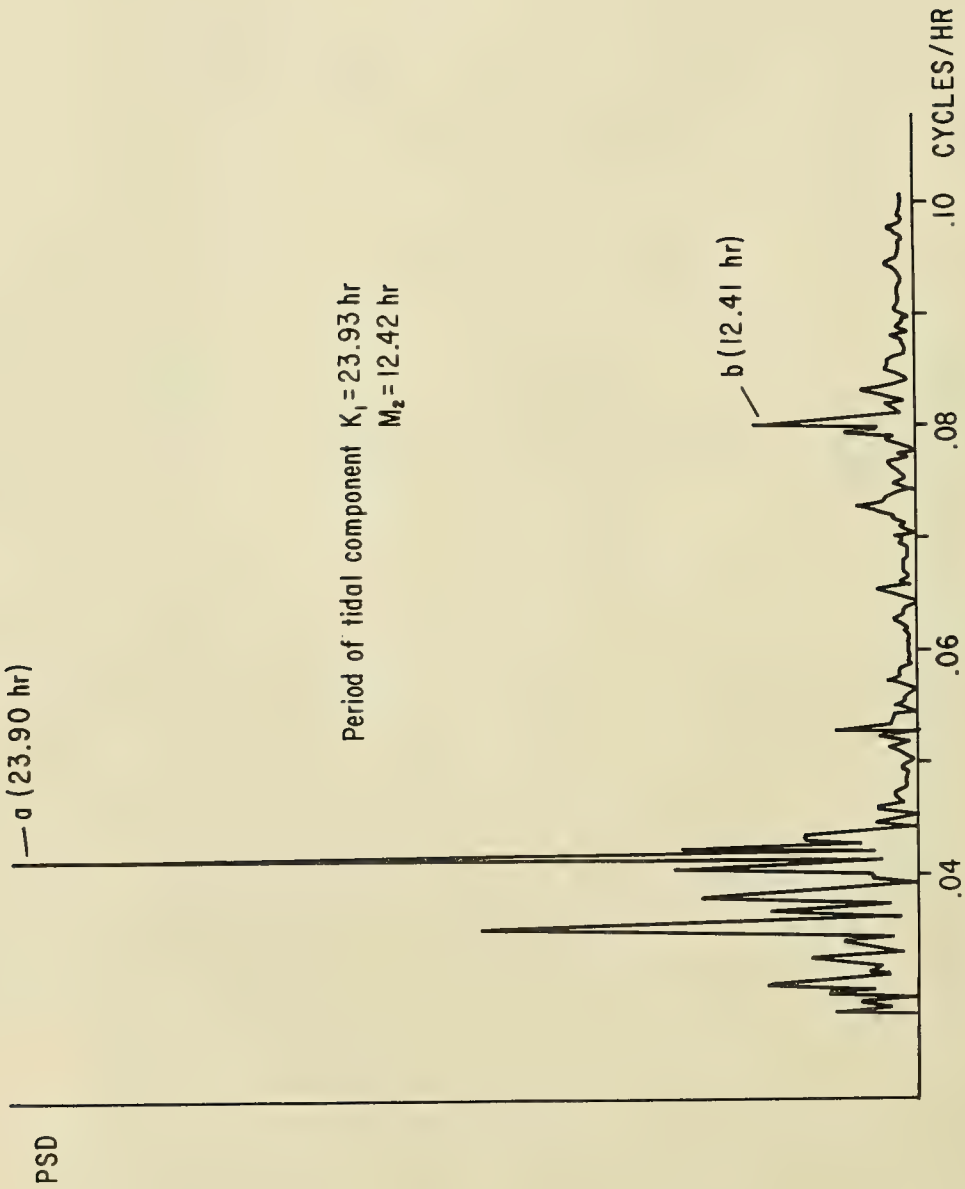

Fig. 20 - Spectrum of tidally-related phase fluctuations at hydrophone H43 (LCT-1)

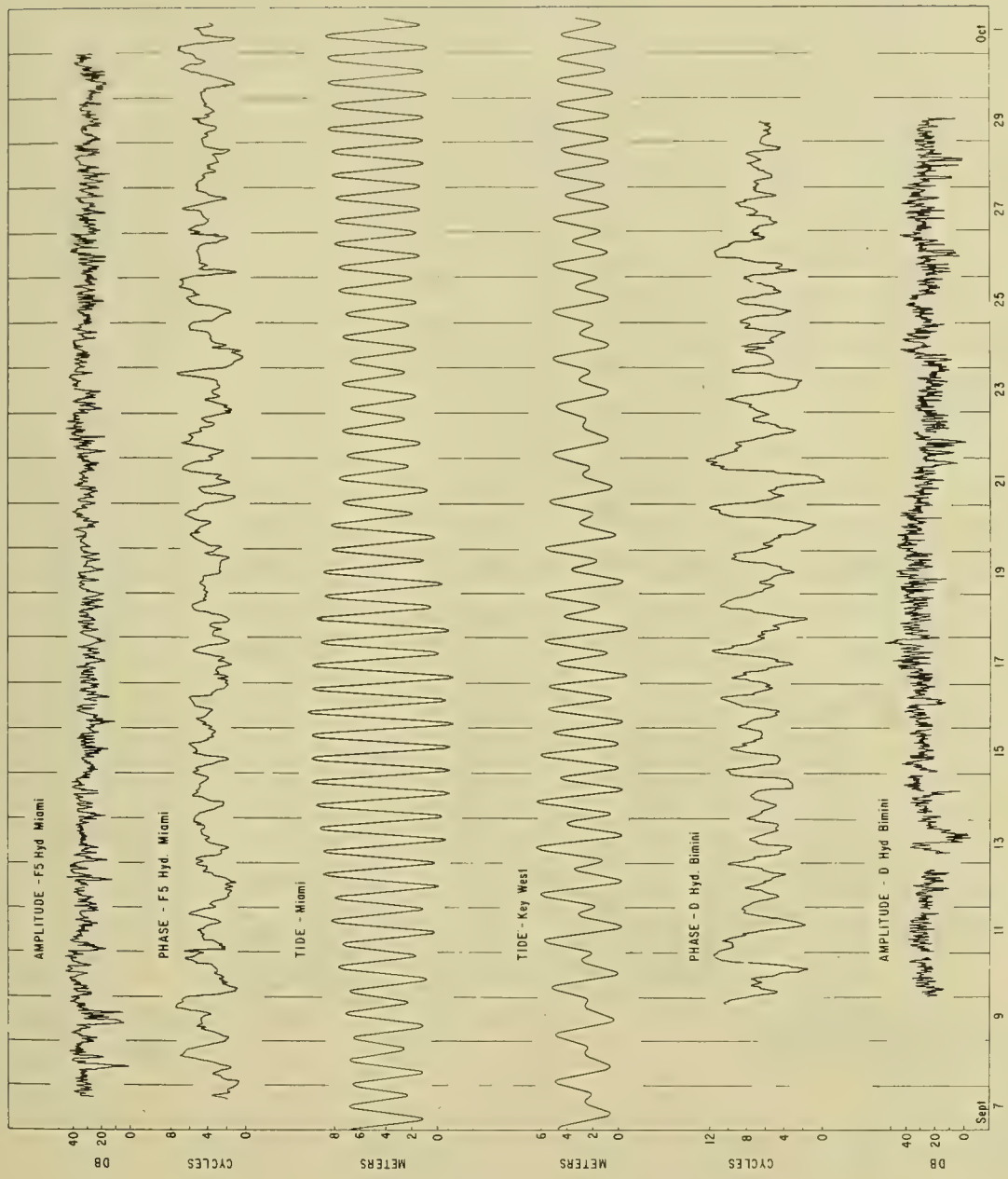

Fig. 21 - Tide, amplitude, and filtered phase patterns - September 1966

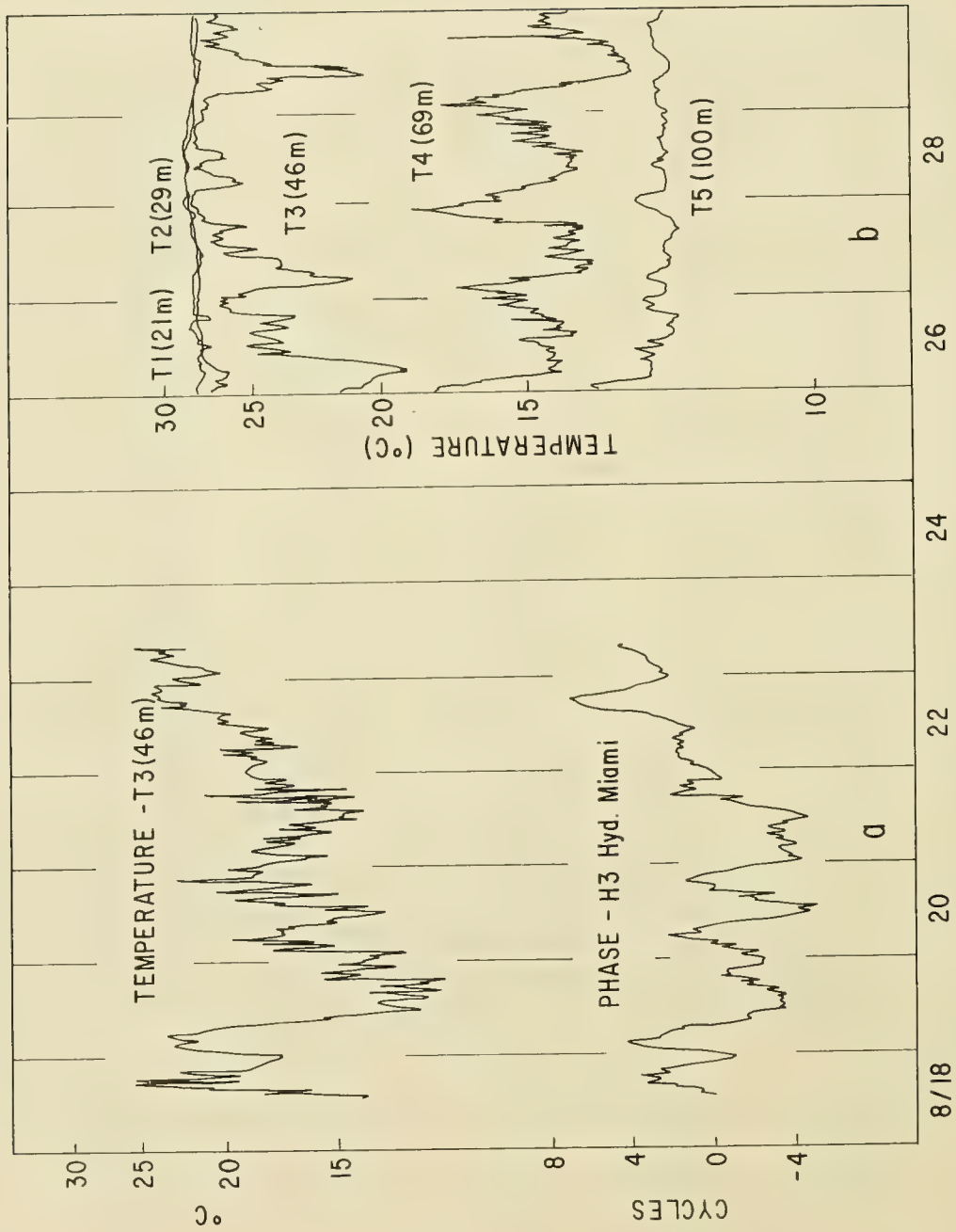

Fig. 22 - Phase and temperature patterns, August 1966

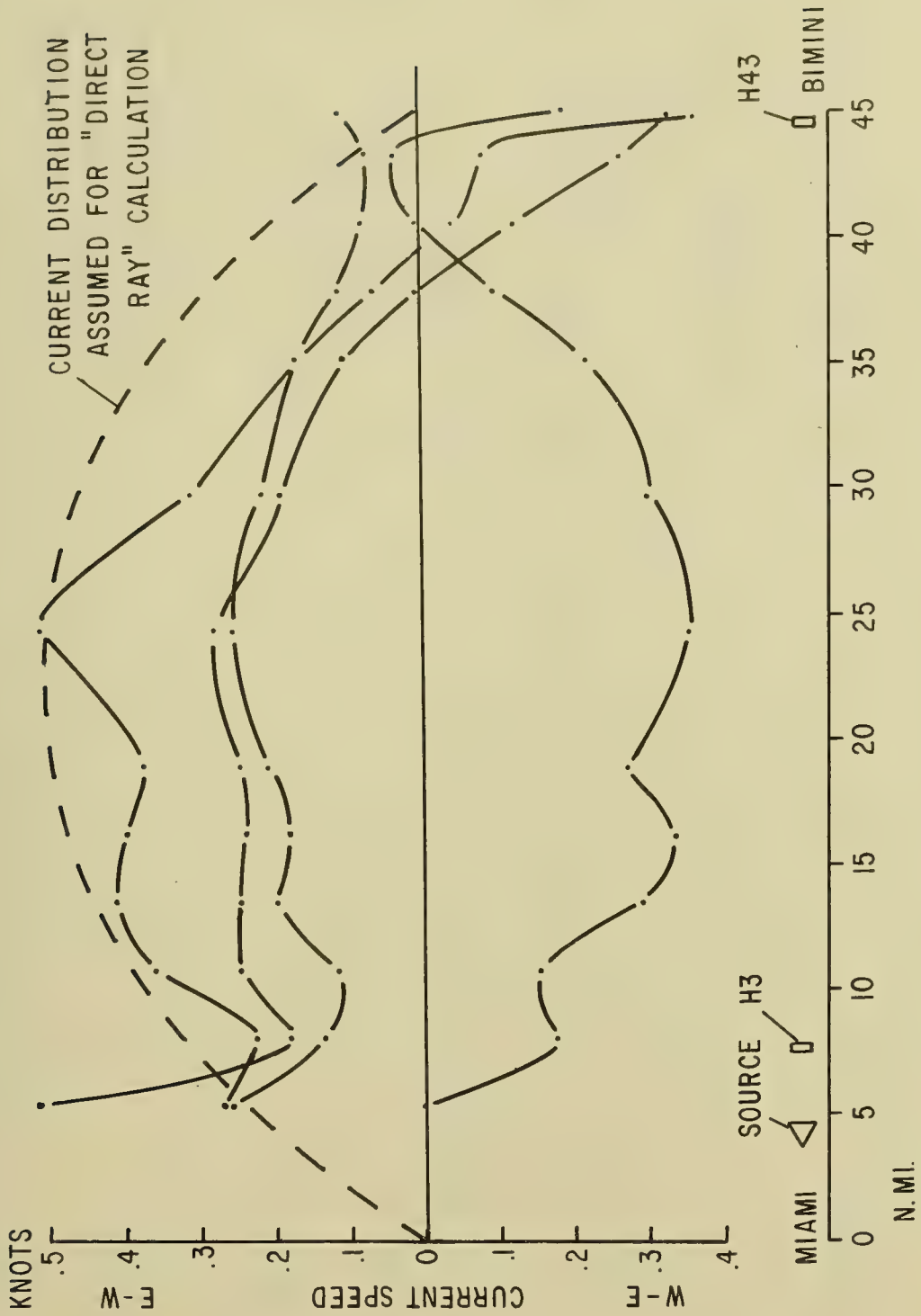

Fig. 23 - Cross-stream current components

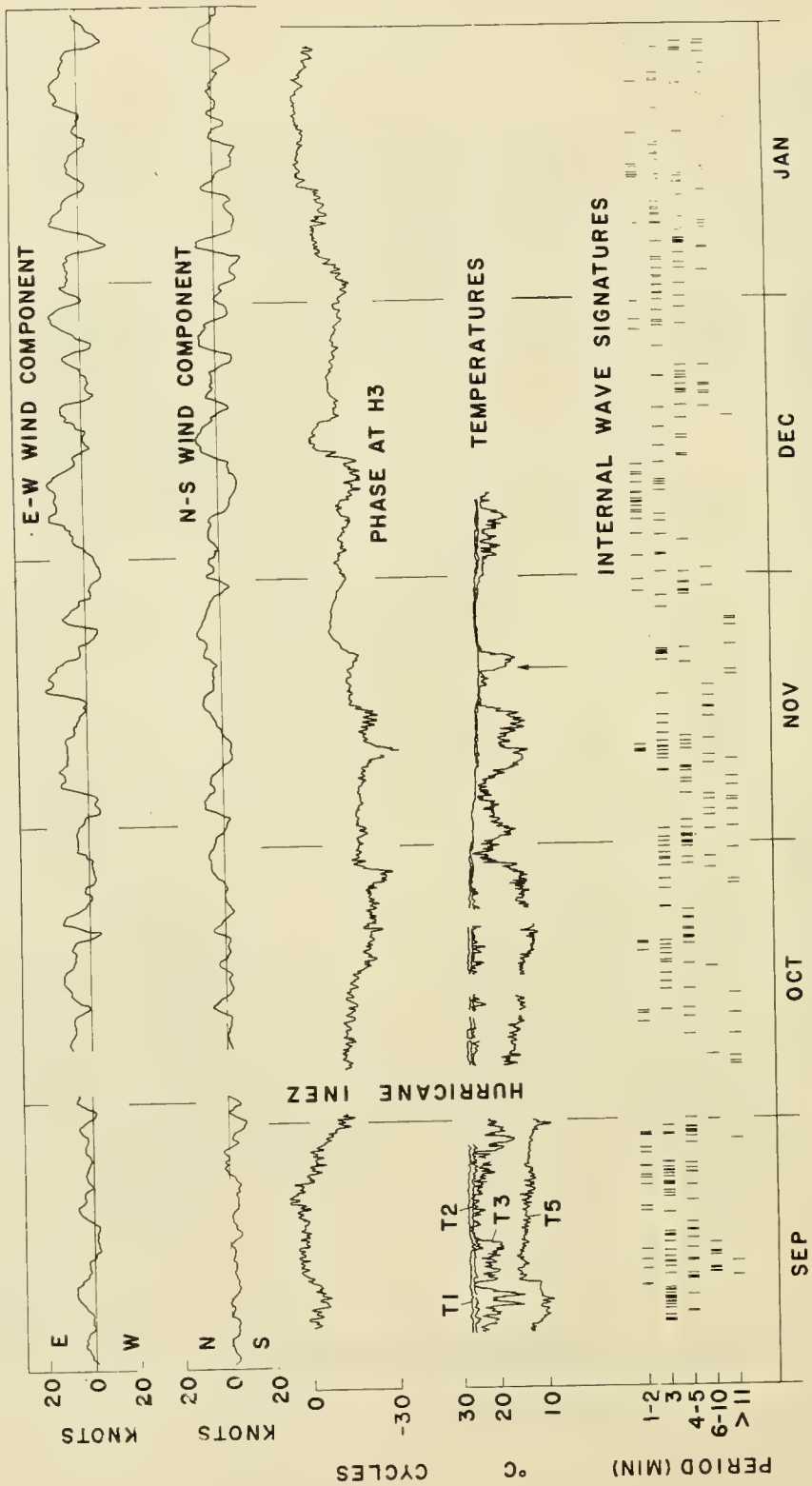

Fig. 24 - Hydrophone H3 phase-environmental relationships

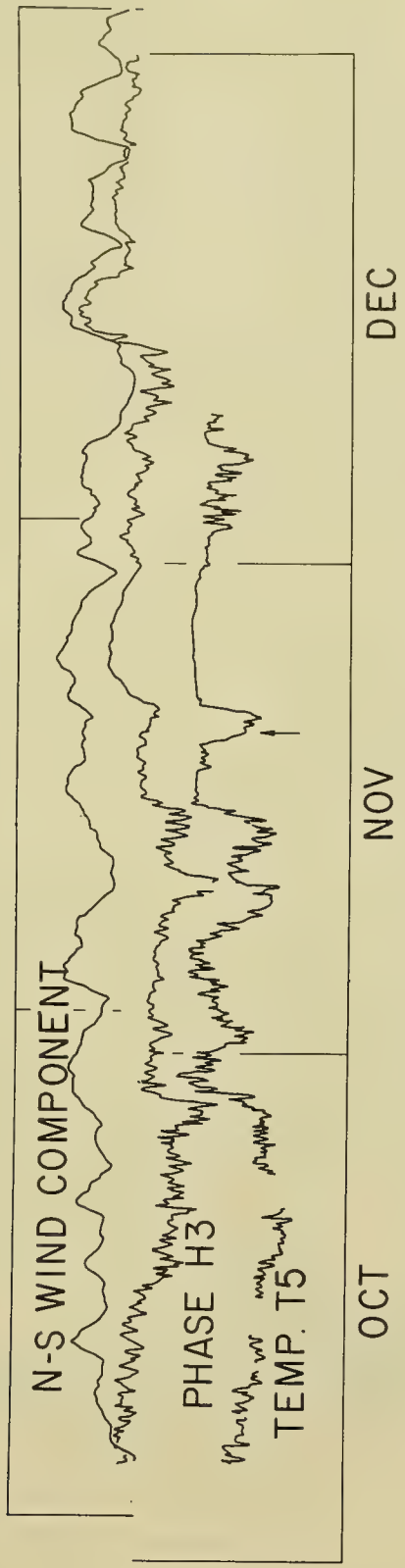

Fig. 25 - Comparison of phase and environmental parameters

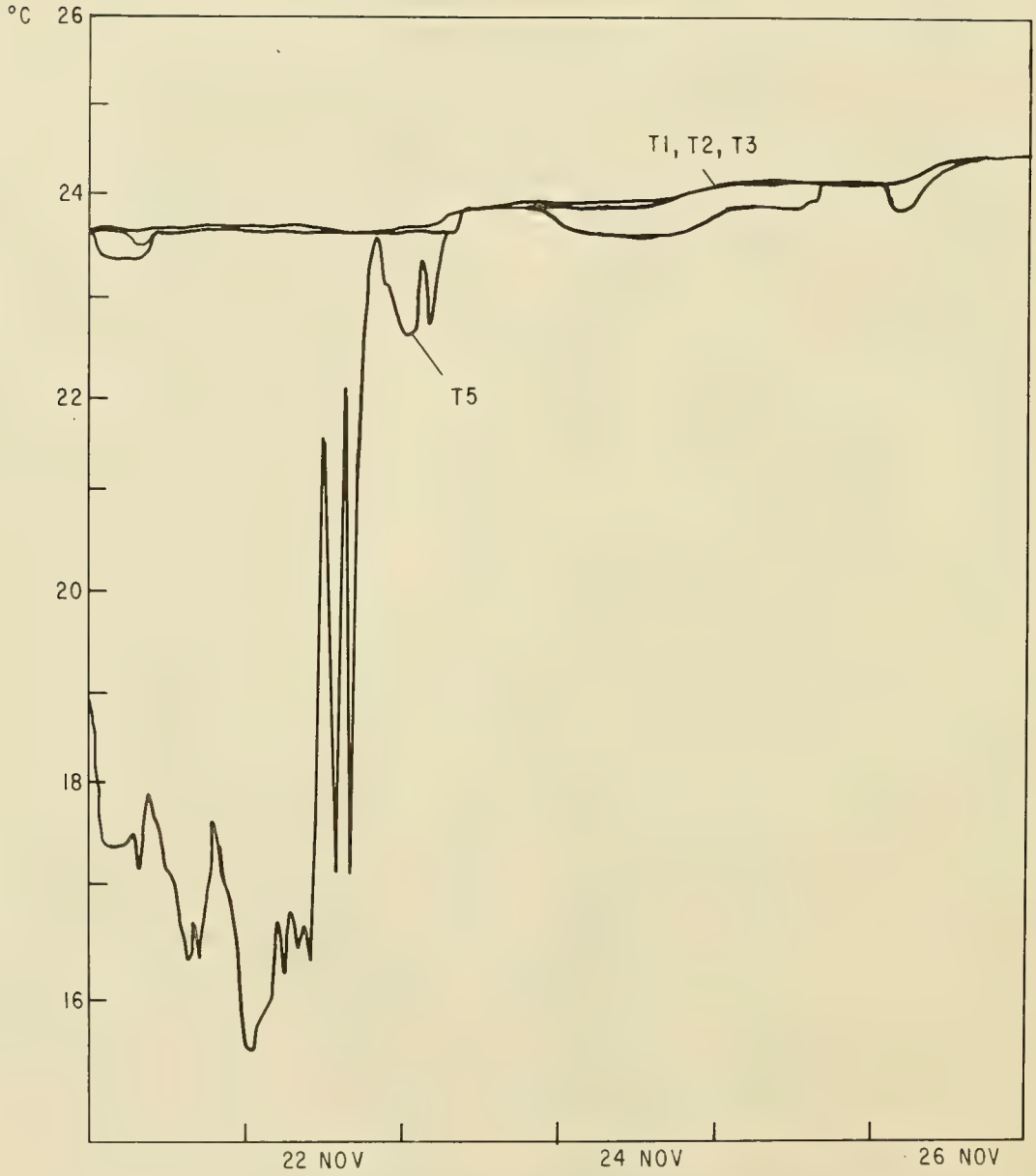

Fig. 26 - Temperature detail. Evidence of cross-stream surface transport.

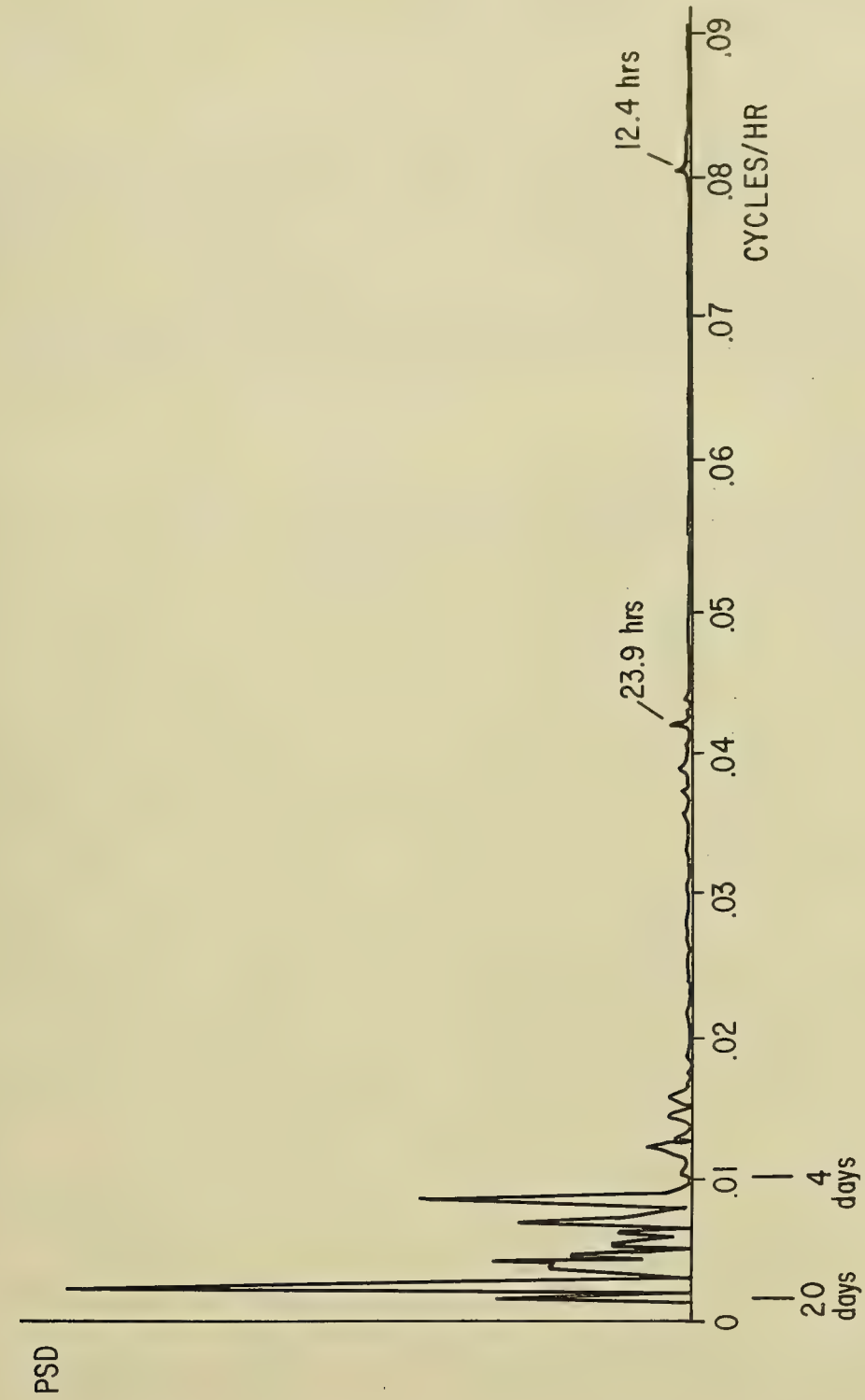

Fig. 27 - Spectrum of phase fluctuations at hydrophone H43. Contribution of atmospheric phenomena

OCEANIC TURBULENCE AND AMPLITUDE FLUCTUATIONS IN ACOUSTIC SIGNALS

Laurence C. Breaker
U. S. Naval Oceanographic Office
Washington, D. C. 20390

William D. O'Neil, Jr.
The Bissett-Berman Corporation
Santa Monica, California 90404

INTRODUCTION

This paper deals with an experiment in the fluctuations in transmission loss for underwater acoustic signals. There are considerable gaps in our empirical knowledge of these fluctuations and this in itself might be considered sufficient reason to conduct such an experiment. This experiment, however, proceeded out of a particular theory of the origin and nature of transmission-loss fluctuations. A certain knowledge of this theory (which will be glossed, not altogether accurately, as the "turbulence induced" theory of fluctuation in transmission loss or amplitude) is necessary if one is to understand why the experiment was planned, executed, and analyzed in the manner about to be described. Moreover, this theory (to the extent to which it may actually be valid) offers a means to predict some operationally significant sonar-performance parameters.

Thus this paper will open with a survey of the theoretical background to the experiment. Next will come sections dealing with the experiment itself, the planning which preceded it, and the data reduction which followed. As data reduction and analysis is not, at this writing, complete, report of results and conclusions must await a later occasion. Persons having especial interest in these matters, however, are invited to correspond with the authors.

THEORETICAL BACKGROUND

Suppose an omnidirectional source is placed some distance below the surface of the ocean and a number of hydrophones are arrayed about it, each at a different depth but all at a common slant range. Now a very short pulse is transmitted from the source. If in a typical case one observes the amounts of energy received by the various hydrophones over direct paths (i.e., excluding any boundary reflections) it will be found that they differ significantly one

from another. This phenomenon has been observed by virtually everyone who has ever worked in underwater acoustics and has long been known to be largely due to spatial variations in the local acoustic-propagation velocity within the ocean.

Another familiar phenomenon is the fluctuation over time in the amplitude of a signal observed at a hydrophone whose position, with respect to the source, is constant. This temporal fluctuation is less well understood than the spatial variation but it has long been felt by many that they were related (see, for instance, Ref. 1). For suppose that the structure of local acoustic-propagation velocities itself fluctuated over time; might this not cause variation in constant-geometry received amplitudes very much like that seen when the propagation-velocity structure is fixed while the geometry is varied slightly? (Ref. 2 provides direct empirical evidence that this is, in fact, the case.)

In passing from this idea to a definite model of transmission-loss fluctuation one is faced with two chief problems. The first is to learn what sort of fluctuations in the structure of propagation-velocities might be expected in the ocean while the second is to predict the effects of these fluctuations on acoustic propagation. The first problem, clearly, is especially formidable theoretically and complex empirically. The difficulty of solving the second problem would seem to depend upon the answer to the first.

The velocity of sound in the ocean increases regularly with pressure. More important, for our purposes, is that it also varies with water temperature and salinity. If a patch of warmer (or more saline) water happens to occur within a body of colder (or less saline) water then in the absence of outside influences, hydrodynamic forces will eventually break it up and disperse it throughout the "host" body. In the ocean, with its constant but spatially and temporally irregular receipts and drains of heat and salts, such "patches" are continually being generated.

This breakup and dispersion process can be viewed in terms of the particle-velocity field generated by the hydrodynamic forces. (This field within a region is to be distinguished from the net average velocity of the region as a whole due to large-scale currents, etc.) In seawater, with its low kinematic viscosity, these particle velocities are generally non-zero and random for scales greater than a centimeter. Such random motion is of course described as turbulent.

Any fluid will have an inner scale of turbulence ℓ_o, set by the scale at which viscosity tends to strongly damp fluid motion, and an outer scale of turbulence L_o, set by the geometry of the fluid as a whole and generally of the same order as the minimum of the dimensions of the body of fluid. (Of course, unless $\ell_o \ll L_o$ turbulence of the sort we are about to discuss cannot occur.) For

regions whose scale lies well within this range the velocity field of the turbulence will (in consequence of what we mean by ℓ_0 and L_0) be locally homogeneous and isotropic. That is, if R is such a region, v(p) is the velocity vector at point p, and p_1 and p_2 lie within R, then the probability distribution of velocity differences $v(p_1)-v(p_2)$ depends only upon the distance between the points $r=|p_1-p_2|$ and not at all on their positions within the region or their orientation with respect to one another. Thus the mean square velocity differences, or structure functions can be written,

$$D_{rr}(r)=\mathrm{Avg}\left[\left(V_r(p_1)-V_r(p_2)\right)^2\right]$$

$$D_{tt}(r)=\mathrm{Avg}\left[\left(V_t(p_1)-V_t(p_2)\right)^2\right]$$

D_{rr}, the longitudinal structure function, is taken along the line connecting p_1 and p_2 while D_{tt}, the transverse structure function is taken across the line.

If the fluid can be regarded as incompressible then it can be shown, from purely dimensional considerations, that

$$D_{rr}(r)=C(\epsilon r)^{2/3} \qquad \ell_0 << r << L_0$$

$$D_{tt}(r)=\tfrac{4}{3}C(\epsilon r)^{2/3} \qquad \ell_0 << r << L_0$$

where C is a dimensionless constant of order unity and ϵ is the energy dissipation rate. From these may be determined the statistics of the concentration of a conservative (with respect to position changes) and passive (with respect to the turbulence mechanism) "additive" to the fluid, such as heat or salt. In fact, if $\theta(p)$ is the concentration of such an additive at point p, then

$$D_\theta(r)=C_\theta^2\, r^{2/3} \qquad r >> \ell_0 \tag{1}$$

where C_θ is a physical constant depending upon the fluid and the additive.

As one would expect, the index of refraction structure also follows a two-thirds law,

$$D_n(r)=C_n^2\, r^{2/3} \tag{2}$$

C_n, the refraction-index structure constant, is (in the ocean) essentially directly proportional in the usual case to C_T, the temperature structure constant of equation (1).

Finally, it has been found that such fluctuations in the index of refraction will indeed give rise to significant fluctuations in acoustic amplitudes. Suppose a wave, initially plane and orthogonal to the x axis, is traveling along the x axis through a body of seawater whose index of refraction structure is as described above. If the wave's transit time is short with respect to the time

required for the pattern of the turbulence to shift appreciably and if the decibel level (with the average power as a reference) is observed, in a plane orthogonal to the x axis, the mean square level is found to be,

$$\chi^2 = 197.10\, C_n^2\, \lambda^{-7/6}\, L^{11/6}\,, \qquad \sqrt{\lambda L} \gg \ell_0 \tag{3}$$

where λ is the acoustic wave length and L is the range. Moreover, one can find the two dimensional spectrum of the level fluctuations in the plane as*

$$F_A(\kappa,0) = 2.4896\pi C_n^2 K^2 L \left(1 - \frac{K}{\kappa^2 L}\sin\frac{\kappa^2 L}{K}\right)\kappa^{-11/3} \tag{4}$$

where k is the wave number of the acoustic wave ($k=2\pi/\lambda$), κ_2 is the wave number of the fluctuation in the y direction, κ_3 that in the z direction, and, in consequence of the isotropy assumption, $\kappa^2 = \kappa_2^2 + \kappa_3^2$.

The case of practical interest is that in which one is moving along some line in the plane x = constant with velocity v_n. This could represent either actual movement of the receiver with respect to the source or displacement of the water (e.g., by a current with velocity v_n) across the x axis. (Velocity components along the x axis, unless very large, will have little effect upon the fluctuations.) If the turbulence structure may be regarded as "frozen-in" the fluid (see below), then the total variance observed will still be represented by Eq. (4) but the (one-dimensional) spectrum of the fluctuations in level will be

$$W(f) = \frac{8\pi}{V_n}\int_0^\infty F_A\left(\sqrt{\kappa^2 + \frac{4\pi^2 f^2}{V_n^2}}, 0\right) d\kappa$$

where f is the frequency of fluctuation. This may be reduced to the dimensionless quantity,

$$P(f) = \frac{f\,W(f)}{\sigma^2} = 1.35\,u \int_0^\infty \left[1 - \frac{\sin(t^2+u^2)}{t^2+u^2}\right](t^2+u^2)^{-11/6}\, dt \tag{5}$$

---

*To aid in interpreting $F_A(\kappa,0)$, recall that the spectrum P(f) of an ordinary one-dimensional time-random variable, x(t), records the contribution made to the variance (or mean-square fluctuation) of x by frequencies near f. Since the wave numbers, κ_2 and κ_3 may be interpreted as spatial (angular) frequencies F_A simply gives the contribution made to the variance of the fluctuation by spatial frequencies lying in a small "area" near κ_2 and κ_3. Isotropy allows one to pick any κ_2 and κ_3 lying on a circle $\kappa_2^2 + \kappa_3^2$ = constant and get the same result, so F_A can be formally expressed as a function of one variable, κ .

where

$$f_0 = \frac{V_n}{2\pi}\sqrt{\frac{K}{L}} = \frac{V_n}{\sqrt{2\pi\lambda L}}, \quad u = f/f_0 \tag{6}$$

P(f) can be computed by numerical integration and is plotted in Fig. 1.

While it was not possible to consider phase effects in this experiment it is of interest to note that this same theory predicts significant phase fluctuations as well. In fact, the two-dimensional phase-fluctuation spectrum analogous to Eq. (4) is

$$F_s(\kappa,0) = 0.033\pi\, C_n^2 K^2 L\left(1 + \frac{K}{\kappa^2 L}\sin\frac{\kappa^2 L}{K}\right)\kappa^{-11/3} \tag{7}$$

From this may be derived phase fluctuation and difference spectra along a line, analogous to Eq. (5).

The physical interpretation of the foregoing is fairly straightforward. The turbulence takes the form of nested eddies of all scales from ℓ_0 to the largest scale of the fluid body (often $> L_0$). The largest eddies (of scale near L_0) are anisotropic while the smallest (near ℓ_0) are affected by viscosity. These eddies produce corresponding inhomogeneities with respect to temperature and salinity and, thus, with respect to the refraction index. It is the inhomogenities with scales near $\sqrt{\lambda L}$ which account for the fluctuations in the acoustic signal. These inhomogeneities do not evolve rapidly and may be regarded as "frozen-in" the fluid when $\sqrt{\lambda L} \ll L_0$. Comparing Eq. (4) we see that the theory should be valid for $\ell_0 \ll \sqrt{\lambda L} \ll L_0$.

All of the foregoing is discussed in detail in Tatarski's book (Ref. 3). (Generally his approach and notation have been used here although our numerical constants differ because we will work in decibels.) Briefer summaries occur in References 4 and 5. The validity of the theory is well established for acoustic (and electromagnetic) waves in the atmosphere.

But there are certainly reasons to wonder whether it applies equally well in the ocean. This is especially so when one reflects that the relatively stable vertical stratification of the ocean due to buoyancy forces must seriously limit the scales over which truly isotropic turbulence can exist. This implies that L_0 would be small and thus that our condition $\sqrt{\lambda L} \ll L_0$ might not be satisfied for interesting values of λ or L. (Still further limitations might be expected near the surface where wave motions may strongly modify the turbulent velocity field.)

Dunn, Ref. 4, reports evidence for isotropy but his data extend to scales only up to about 5 meters. This problem of the scale of isotropic turbulence in the ocean was taken up in 1965 by a group of Bissett-Berman Corporation personnel headed by

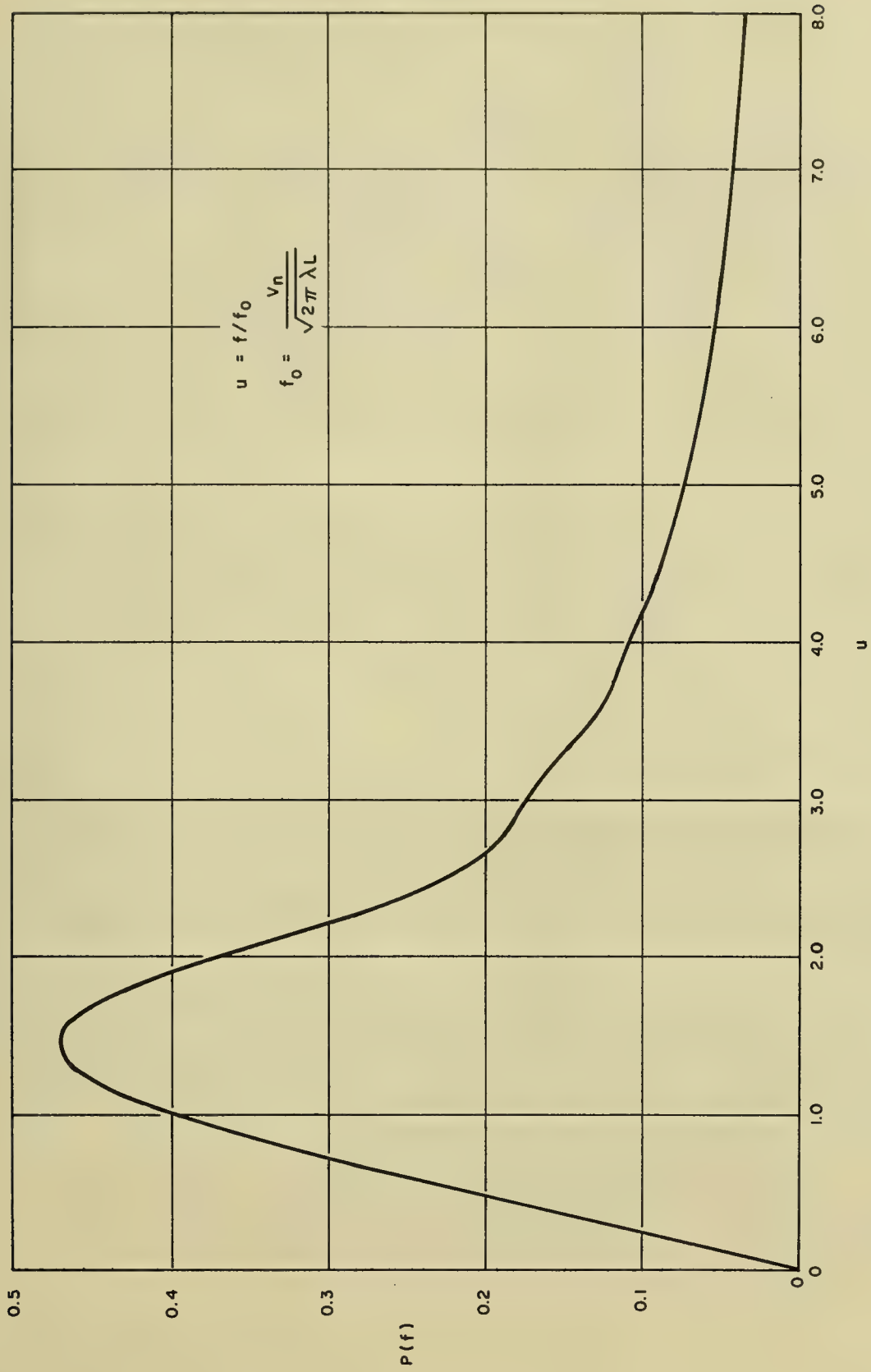

Fig. 1 - Normalized spectrum

Dr. C. F. Black (presently with RAND Corporation). The structure function, $D_T(r)$ was computed along horizontal lines at various depths out to a range of 35000 meters using NEL thermistor-chain data. The slopes of these horizontal structure functions, when plotted against range on log-log scales, were generally just slightly in excess of the 2/3 predicted by Eq. (1), indicating that ocean turbulence "looks" nearly isotropic in the horizontal plane. With vertical temperature data, however, obtained using a Bissett-Berman STD unit, the structure functions had slopes of about 1.8 over scales from 50 to 500 meters. Thus, ocean turbulence is significantly anisotropic at least for scales greater than 50 meters but seems nearly isotropic to one traveling in a horizontal line at least out to scales of 35000 meters. (This work is reported in Ref. 5.) When one reflects that sonar-to-target geometries are typically such that the energy is transmitted very largely in the horizontal it seems likely that, anisotropy notwithstanding, the fluctuations in signal level may actually follow Eqs. (4) and (6) rather closely.

Previous work has often attributed observed fluctuations to such causes as motion of source and/or receiver, non-uniform beam patterns, and variations in source level, etc. These effects may well overshadow turbulence effects at the short ranges usually employed. However, since turbulence effects are cumulative with range, fluctuations arising from turbulence should control the structure of fluctuations at longer ranges.

PLANNING AND EXECUTION OF EXPERIMENT

In October of 1966, the Naval Oceanographic Office conducted an experiment to determine whether the turbulence-induced theory of transmission-loss fluctuation was, in fact, valid for values of $\sqrt{\lambda L}$ typical of those experienced in sonar operation. Bissett-Berman, under contract to the Oceanographic Office, assisted in the planning of the experiment and the reduction and analysis of the resulting data.

The geometry selected for the experiment is shown in Figure 2. The receiving hydrophone was suspended from a moored vessel while the transmitting projector was towed in a circle about the receiving ship. The radius of the circle is L and v_n is one-half of the transmitting ship's speed (if that is sufficiently large that currents may be neglected by comparison).

The experiment was conducted in the Tongue of the Ocean during the period 11 to 15 October 1966. The R. V. PAUL LANGEVIN served as the receiving vessel and the USS LITTLEHALES (AGSC-15) towed the projector.

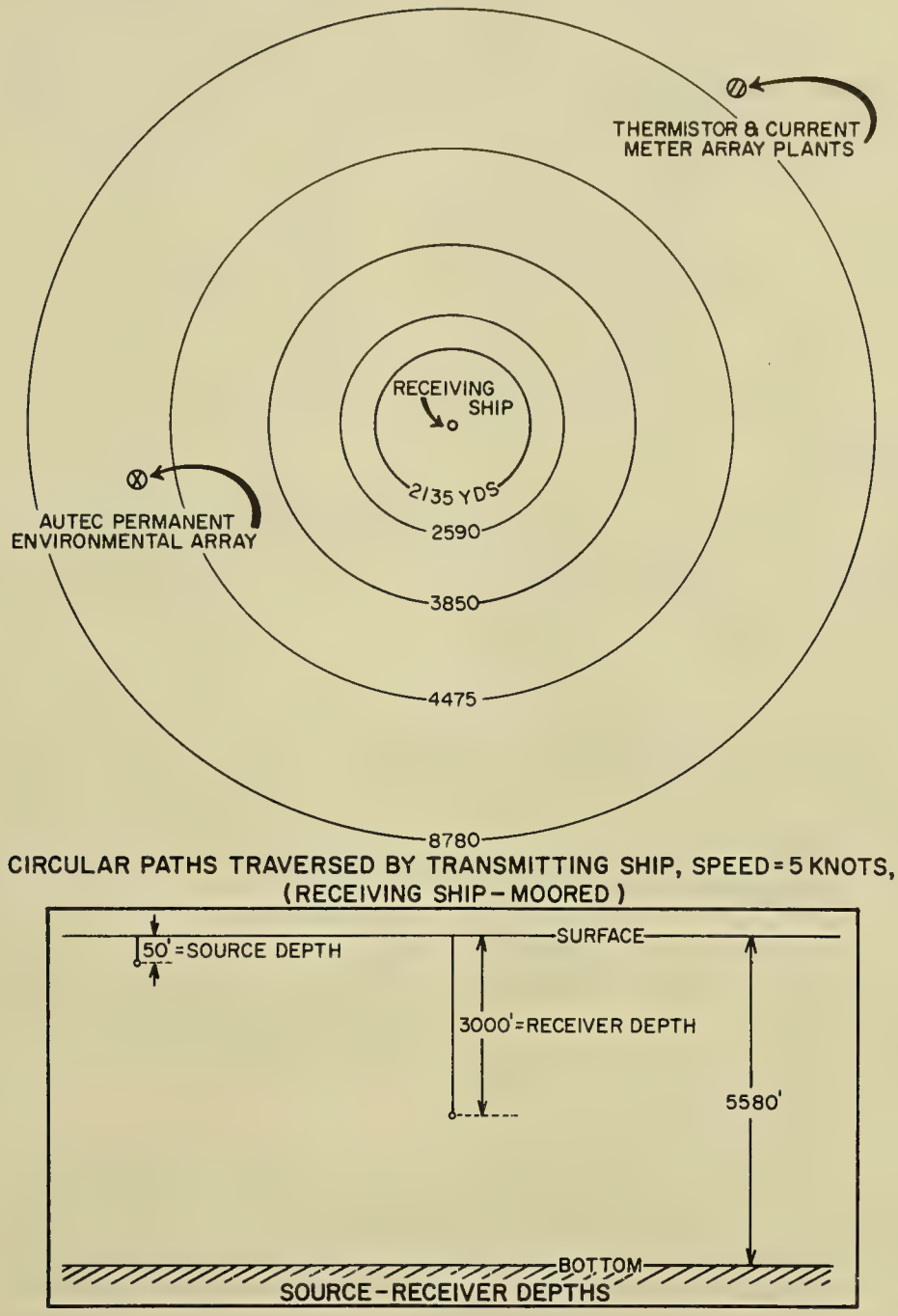

Fig. 2 - Experiment geometries

The projector was a USRD Type G31 transducer produced by the Underwater Sound Reference Division of the Naval Research Laboratory. It was mounted in an Ocean Research Equipment, Inc. towed body. The transmitted frequencies were 1.3, 3.0, 5.3, and 9.0 kHz (determined by the resonant peaks in transducer output). USRD Calibrated the transducer as mounted in the body and obtained the following sound pressure levels at 1 meter from the transducer face, measured in dB//1 μ bar:

Frequency	Level
1.3 kHz	91 dB
3.0	88
5.3	93
9.0	80

Transmitting beamwidths were found to be very broad, even at high frequencies.

A NUS Model LM-2 Deep Sea Hydrophone was used on the receiving end, suspended at a depth of approximately 3000 feet. The signal was passed through a filter, set to a one octave band centered at the transmitter frequency, amplified, and recorded on magnetic tape at 7-1/2 i.p.s.

It can be seen from Eq. (6) and Figure 1 that the effective width of P(f) and hence the amount of data which must be collected to obtain satisfactory resolution of the shape of the spectrum is proportional to v_n. It was decided that a v_n = 1.3 m/sec, corresponding to a ship speed of 5 knots, represented a satisfactory compromise between ship and towed body capabilities on the one hand and data-taking time on the other.

Ten different "events" or subexperiments were undertaken. Table 1 displays the important features of these events arranged in order of increasing values of $\sqrt{\lambda L}$ and decreasing acoustic frequency. The durations were chosen according to the methods outlined in Ref. 6 to give equally good resolution and stability for each event's sample estimate of the spectrum P(f).

After consideration of the propagation-velocity data available for the TOTO area, it was decided that a 2-second keying interval would provide adequate insurance against overlap of bottom reflections with the succeeding direct pulse. This, of course, fixed the effective sampling rate and thus the Nyquist (or folding) frequency for the spectral estimates. In the worst case (Event 10),

$$f_0 = \frac{1.3 \text{ m/sec}}{\sqrt{2\pi} \cdot 20\text{m}} = .026 \text{ Hz} \quad ,$$

Event No.	Acoustic Frequency	λ	L	$\sqrt{\lambda L}$	Duration
10	9.0 KHZ	0.1675m. = 0.5531 ft.	2,370m. = 2,590 yd.	20 m.	2.7 Hr.
7	5.3 KHZ	0.2863m. = 0.9388 ft.	2,010m. = 2,200 yd.	24 m.	3.4 Hr.
8	5.3 KHZ	0.2865m. = 0.9399 ft.	3,560m. = 3,895 yd.	32 m.	4.3 Hr.
6	3.0 KHZ	0.5055m. = 1.6585 ft.	2,020m. = 2,210 yd.	32 m.	4.3 Hr.
9	5.3 KHZ	0.2887m. = 0.9462 ft.	8,030m. = 8,780 yd.	48 m.	6.5 Hr.
2	3.0 KHZ	0.5070m. = 1.6627 ft.	4,550m. = 4,975 yd.	48 m.	6.5 Hr.
5	1.3 KHZ	1.1680m. = 3.8271 ft.	1,970m. = 2,135 yd.	48 m.	6.5 Hr.
3	3.0 KHZ	0.5100m. = 1.6718 ft.	8,080m. = 8,835 yd.	64 m.	8.5 Hr.
1	1.3 KHZ	1.1690m. = 3.8320 ft.	3,500m. = 3,850 yd.	64 m.	8.5 Hr.
4	1.3 KHZ	1.1750m. = 3.8566 ft.	7,870m. = 8,605 yd.	96 m.	12.8 Hr.
					64.0 Hr.

Table 1. Characteristics of the "Events"

so that the Nyquist frequency of $f_N = 1/(2 \cdot 2 \text{ sec}) = .25$ HZ corresponds to a u of 9.6. Figure 1 shows this to be adequate to prevent serious problems with aliasing (P(f) is monotone decreasing for $u > 1.38$).

In no case was it possible to tow the projector at depths greater than 50 feet. This of course raised the problem of the surface reflection. A pulse length of 10 milliseconds was felt to be the minimum necessary to permit reliable pulse detection. Thus, considerable direct-transmission/surface-reflected-transmission overlay was inevitable.

Two unanticipated noise problems were encountered about which little could be done, given the time constraints of the experiment. The first was simply that the weather was worse than is usual in the Tongue of the Ocean. Sea states rose as high as three late in the experiment, and rain squalls occasionally blotted out transmission altogether. The other problem was noise leakage to the receiving amplifiers and recorder from the ship's ground circuit.

On the whole, however, the experiment went well. It produced a total of 124 reels of magnetic tape containing 64 hours (real-time) of analogue data. During this time approximately 115,000 pulses had been transmitted.

REDUCTION AND ANALYSIS OF DATA

At this time, the reduction and analysis has not been completed. The work which has been completed, however, will be described, while a sketch will be given of the work planned.

Because pulsed signals were used the data were inherently suited better to digital than to analogue processing, but the quantity of analogue data tapes, their noisiness, and the relatively high acoustic frequencies all presented serious problems in converting the data to digital form.

Direct digitization of the analogue tapes was felt to be infeasible due to the volume of data. Moreover, only about 0.5% of the total tape time was devoted to data of interest (i.e., 10 ms/2 sec) so that many hours of computer time would have been required to sift the output tapes for pulses.

Figure 3 is a block diagram of the system (designed by Dr. M. F. Gordon of Bissett-Berman) developed to deal with this problem. It detects pulses and digitizes the pulse envelopes. These are recorded in computer-compatible format on tape, one pulse

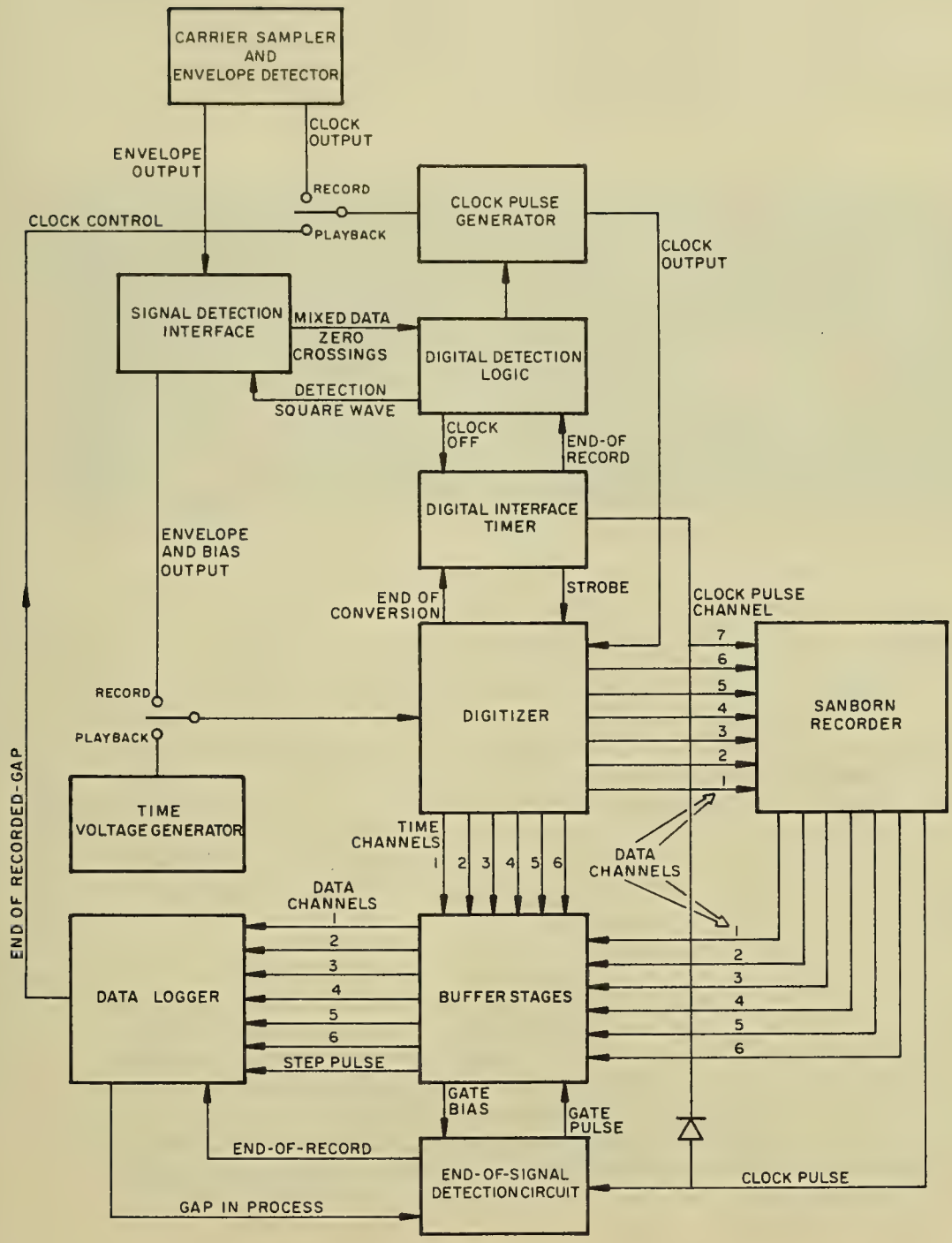

Fig. 3 - Block diagram of digitizing system

to a record, together with the time of the pulse. The speed of this process is still limited by the rate at which the digital data logger can record the final computer-compatible tape--500 frames per second. To reduce digitizing time the 5.3 kHz tapes are sampled only at 2.65 kHz and the 9.0 kHz tapes at 3.0 kHz. Even so, a total of more than 500 hours of digitization time will be required from first to last.

Pulses are detected by a modified zero-crossing method. A high-frequency detection square wave, of sufficient amplitude to exceed the average analogue-tape noise level, is added to the analogue data. Changes in the high frequency zero-crossing pattern signal a detection. As presently set, this system will accept virtually all "good" data pulses but will also let some noise and bottom-reflected pulses through. These are later eliminated by the computer, making use of the constant 2-second keying interval. The program uses a pushdown-list sieve to select subsequences of records having a constant 2-second separation. These methods have worked very well with the short and medium-range events. Further refinements may be necessary to deal with the long-range events, however.

After this rejection of noise and bottom-bounce pulses, the pulse amplitudes are computed. Figure 4 shows two actual pulse envelopes and one schematized version of a pulse envelope. "D" is the portion due only to direct transmission, and "I" is the portion due to the interference between surface-reflected and direct transmission. Where "D" is sufficiently broad and well defined one can calculate the height of a hypothetical direct-transmission pulse by using only those envelope points falling within "D". At long ranges, however, "D" becomes very narrow. Moreover, pulse distortion becomes more serious and S/N ratios become worse at these ranges. Thus, especially at lower frequencies, estimation of a "direct" pulse height may become sheer guesswork. Only the height of the whole D+I+S pulse can be computed.

Although this is inconvenient, information about the purely turbulence-caused fluctuations may still be extracted from such data. Clearly the lag between direct and surface-reflected arrivals can be small only if the paths lie very close together. Since the reflection at the surface should not (for the low sea states encountered and the frequencies used) cause any significant change in the structure or frequency of the pulse the surface-reflected pulse should be affected by turbulence very much as its direct brother is. That is, the "D heights" and the "S heights" should have virtually identical distributions and spectra.

Because of the relatively short wavelengths used, however,

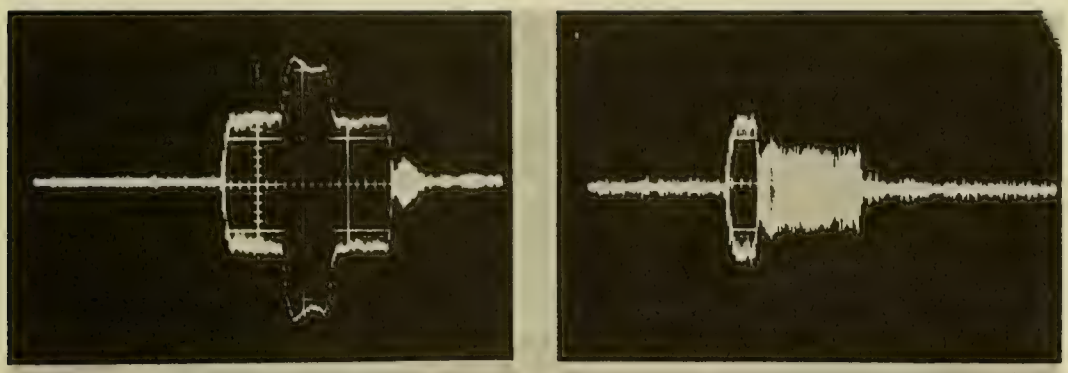

5.3 KHz - 2200 YARDS

5.3 KHZ - 3895 YARDS

(a)

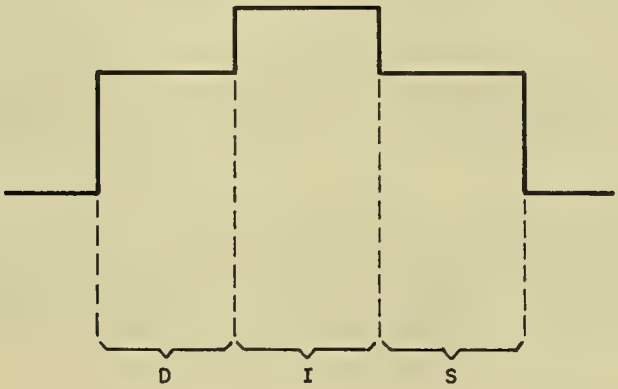

(b)

Fig. 4 - (a) Oscilloscope photographs of received pulse envelopes showing direct signal duration and surface arrival interference effects, and (b) schematic representation of pulse

the phase angle difference between the two should be essentially uniformly distributed from $-\pi$ to π, with no pulse-to-pulse correlation. Thus, including the "I height" merely introduces a white noise which will have no effect upon the shape of the spectra.

The next step in data reduction then is to compute the "D heights" where possible and "D+I+S heights" for each pulse in the event. The logarithms of these are taken and the average log is later subtracted off to give the fluctuation. (In order to save on multiplications the factor of 20, necessary to convert the units to dB/s, is applied only to the final estimates.) The variance is computed in the usual manner.

Sample estimates of the normalized power spectrum, P(f), are next computed. The statistical procedures of Ref. 6 will be followed but the mechanics of computing the "raw" estimates will differ significantly. The computational methods of Ref. 6, involving calculation of the sample autocorrelation function followed by Fourier transformation to obtain the sample spectrum, would be most time consuming for so large an accumulation of data. Instead, a modification of the "fast Fourier transform method" of Ref. 7 will be employed to compute the raw spectral estimate directly from the data, using the relation

$$\Phi(f) = \lim_{T\to\infty} \frac{1}{T} \left| \int_{-T/2}^{T/2} x(t) e^{2\pi i f t}\, dt \right|^2$$

Certain precautions will have to be observed in "grading" the data much as one does in analogue spectral analysis. The spectral analysis has not yet begun, but the necessary computer programs are complete.

Temperature and current-velocity data taken near the experiment site will be used to provide independent estimates of C_n^2, via Eq. (3). For the period of each event the estimate of the structure function, $D_T(r)$, will be computed directly from the definition,

$$D_T(r) = \mathrm{Avg}_y \left[\left(T(y) - T(y-r) \right)^2 \right]$$

where the ergodic hypothesis plus our "frozen-in" assumption will be used to translate the time intervals between temperature observations at the array's fixed position plus the mean local current velocity into an equivalent value of r. This has not yet been undertaken due to some technical problems with the records.

Estimates of the average wavelengths have been computed (they are shown in Table 1) using available environmental data together with a ray-plotting program to determine the relative times spent in each layer. Sensitivity analysis indicates that no more than very slight deviations are to be expected.

Finally, the actual average ranges and error-variances will be computed from radar-log data kept during the experiment. (The values of L shown in Table 1 are nominal, as are the $\sqrt{\lambda L}$.)

Final results and conclusions will be available after 15 June 1967.

REFERENCES

Liebermann, L., The Effect of Temperature Inhomogeneities in the Ocean on the Propagation of Sound, Journal of the Acoustical Society of America, Vol. 23, No. 5, May 1951.

Leiss, W. J. and Whitmarsh, D. C., Effect of Velocity-Profile Simplification upon Measured Fluctuation of Sound Propagation in Water, 72nd Meeting of the Acoustical Society of America, Nov. 1966.

Tatarski, V. I., Wave Propagation in a Turbulent Medium, McGraw-Hill, QC, 157,T313, 1961.

Dunn, D. J., Turbulence and its Effects Upon the Transmission of Sound in Water, Journal of Sound and Vibration, Vol. 2, No. 3, 1965.

Black, C. F., The Turbulent Distribution of Temperature in the Ocean, MJO 1049, The Bissett-Berman Corp., Dec. 1965.

Blackman, R. B. and Tukey, J. W., The Measurement of Power Spectra, BTL, Inc., Dover Publications, 1958.

Cooley, J. W. and Tukey, J. W., An Algorithm for the Machine Calculation of Complex Fourier Series, Mathematics of Computations, Vol. 19, 1965.

SIPHONOPHORES AND THEIR RELEASED BUBBLES AS ACOUSTIC TARGETS WITHIN THE DEEP SCATTERING LAYER*

G. V. Pickwell
U. S. Navy Electronics Laboratory
San Diego, California

INTRODUCTION

In studies on the Deep Scattering Layer (DSL) a central concept, long favored, has been the resonant bubble theory.[1,2] This theory holds that return signals from many scattering layers in the sea are obtained largely from gas-filled cavities resonating in response to the particular sonic frequency being used. Until recently the swimbladders of various mesopelagic fishes were thought to be the main, if not the sole, contributors to resonant sound scattering.[3,4,5,6]

Since the observations by Barham from various deep submersible vehicles it has become clear that in addition to fishes with swimbladders, certain types of siphonophores residing at DSL depths also possess gas-filled structures.[7,8,9] These colonial coelenterates, particularly of the suborder, Physonectae, maintain inflated floats, or pneumatophores, at the apex of the colony by production of carbon monoxide gas from specialized gas glands within the pneumatophore.[10]

Species of the physonectae have been observed to congregate in comparatively large numbers at the daytime depths of the DSL and to migrate vertically with the DSL on a twice-daily basis.[7,8,9] Freshly captured specimens of the pneumatophores of one physonect species, Nanomia bijuga (Delle Chiaje), are obtainable from net hauls through the DSL over the San Diego Trough. These isolated individuals, although broken off from the remainder of the colony, have been observed to manufacture fresh gas[11] and to voluntarily extrude bubbles of this gas through a pore in the float tip.[12]

The possibilities for resonant gas-filled cavities arising from siphonophores in the DSL are thus increased to include not only the

*The material presented in this paper is extracted from a larger body of data which appears in a forthcoming NEL Research Report (see reference 12).

gelatinous pneumatophores themselves, but also their released bubbles. The potential significance to resonant sound scattering at various frequencies from these two sources is the subject of this report.

METHODS

Siphonophore floats were collected with the NEL Tucker net[4,13] towed through the DSL at 4 to 5 knots for periods of one-half to 2 hours. Upon removal from the cod-end bucket by means of forceps, the floats were placed in dishes for sorting. Those not used immediately were placed in a refrigerator at 7° C, the approximate temperature at the daytime depth of the DSL.[12]

Measurements of floats and expelled bubbles were accomplished using an ocular micrometer in a dissecting microscope at 12 to 15X. Volume of floats was calculated as a regular prolate spheroid. Volume of bubbles was calculated as a sphere, hemisphere or cylinder, depending on whether the bubbles were measured freely in the sorting dish, within a glass syringe where they adhered to the sides, or within the tip of an analyzer pipette.

Close-up photographs of pneumatophores in the act of voluntarily extruding bubbles were obtained with a single-lens, reflex camera equipped with lens extension tubes. Additional photos of bubble expulsion were obtained with a camera mounted on a compound microscope. All observations and photographs were made at temperatures from 21 to 25° C. All work reported in this paper was performed aboard ship with the exception of observations made from the Westinghouse deep submersible vehicle, DEEPSTAR DS-4000. Five dives were made in this vehicle for the primary purpose of observing and photographing physonect siphonophores at close range.[14,15] Additional observations on their relative abundance within the DSL and at depths above and below it were obtained during slow, controlled descents made with the observation lights on continuously.[15] Photographs of the siphonophores were obtained with the DEEPSTAR 70-mm still camera and strobe flash.

RESULTS

A typical sequence in the expulsion of a single bubble is shown in Fig. 1. The time required for expulsion of an individual bubble from the moment it first appears until it breaks free from the float may be as little as 30 seconds. Bubble expulsion from the pneumatophore is often associated with the appearance of bubbles of freshly-produced gas in the basal gas-gland region of the float, but this is not invariably the case.[10,12]

Virtually no muscular contraction has been observed during production of bubbles, but application of concentrated magnesium sulfate to the sea water serves to "freeze" the extruding bubble in a partially protruding condition as shown in Fig. 2. Once stopped in this manner

the bubbles remain thus exposed for long periods, neither protruding further, nor retracting.

Correlation of bubble size with increasing float size is possible only within very broad limits as shown in Fig. 3. The range in size of expelled bubbles for a single pneumatophore may be greater than an order of magnitude. The total observed number of expelled bubbles and of pneumatophores within arbitrarily chosen increments of size is presented in Fig. 4. The maximum observed number of bubbles expelled by a single float was 9.

Close observations from DEEPSTAR at mid-morning, mid-afternoon, and in the early morning during October, November, and December, 1966, have shown the pneumatophores of intact colonies of Nanomia bijuga to be inflated whenever observed. It is presumed that the float is fully inflated at all times and, therefore, always a potentially effective sound scatterer.

An inflated pneumatophore, although small, is also an effective light reflector. This is clearly seen in Fig. 5 where an intact colony of Nanomia bijuga is shown in a characteristic feeding position with tentacles extended. The glistening float is situated at the uppermost terminus of the colony where it serves as a sort of gas-filled trim tank providing neutral buoyancy for the motionless colony.

DISCUSSION

The standard means of determining resonant frequency, f_r, for a bubble of known radius, R, at any given depth is by the formula

$$f_r = \frac{1}{2\pi R}\left(\frac{3\gamma P_o}{\rho}\right)^{\frac{1}{2}} \qquad (1)$$

where f_r is in cycles per second, R is in centimeters, γ is the ratio of specific heat of the gas at constant pressure to its specific heat at constant volume (this equals 1.4 for both air and carbon monoxide), P_o is the static pressure of the gas within the bubble in dynes/cm^2, and ρ is the specific gravity of the medium, usually taken to be 1.025 gm/cm^3 for sea water.[16]

Equation (1) may be reduced to the more convenient, approximate form

$$f_r = \frac{(d + 10)^{\frac{1}{2}}}{R} \qquad (2)$$

where f_r is in kc/s, d is the depth in meters, and the radius, R, is in mm.

Recently the Russians, Andreyeva and Chindinova,[17] when dealing with fish swimbladders, have added the shear factor of Lebedeva,[18] μ_o, to equation (1) to give

$$f_r = \frac{1}{2\pi R}\left(\frac{3\gamma P_o + 4\mu_o}{\rho}\right)^{\frac{1}{2}} \tag{3}$$

where μ_o is said to be generally in the range of 10^5 to 10^7 dynes/cm^2, and R is stated to equal the radius of a sphere of volume equivalent to that of the swimbladder in question. These authors transform equation (3) to the approximate form

$$f_r = 1.5\frac{\sqrt{H + 30}}{\sqrt[3]{V}} \tag{4}$$

where f_r is in kc/s, H is the depth in meters, and V, the volume of the gas phase, in mm^3.

An important difference thus appears to arise in computing resonant frequencies since in equation (2) the radius, R, is the critical dimension while in equation (4) the volume, V, is the critical dimension. Experiments have yet to be conducted to assess the relative importance of these two approaches; particularly to assess the significance of μ_o as it relates to resonance by siphonophore floats.

However, the work of Strasberg[19] indicates that the frequency of vibration of a sphere and that of a spheriod of equal volume differs only slightly until the ratio of major-to-minor axes of the spheroid becomes greater than 4. This again suggests that the volume is the most important quantity relating to resonance by gas-bladders as well as by free bubbles.

Accordingly, both equations (2) and (4) have been employed in Table 1 to determine the theoretical resonant frequency for the smallest and largest pneumatophores measured and for an arbitrarily chosen pneumatophore of "median" dimensions. Equation (2) is also employed to determine f_r for a similar range in voluntarily expelled bubbles.

The data presented in Figs. 3 and 4 and Table 1 suggest that siphonophores may be expected to contribute to resonant scattering to some degree at any frequency from somewhat less than 10 kc/s to greater than 100 kc/s. The contribution from expelled bubbles will probably be amplified during upward migration since expanding gases must be periodically released to avoid rupture of the pneumatophore. However, observations by Jacobs[20] indicate that intact nanomians may regularly release bubbles and resecrete new gas on an approximately hourly basis. It seems possible that this type of behavior at depth, as well as upward vertical migration, could lead to a continuous, though diffuse, screen of rising bubbles. Some of these would pass through a size critical for resonance at a particular frequency as they expanded or dissolved.

Finally, it is necessary to point out that in order for bubbles released at depth to be comparable in size to those observed at ambient pressure (1 atm), an additional mass of gas must be present within the bubble. This is almost certain to be the case since the pneumatophore, in maintaining relatively constant volume, must secrete additional gas. For example, at a hydrostatic pressure of 30 atmospheres (300 m depth), a float of 1 mm^3 volume must secrete a total of 31 mm^3 of CO to maintain this volume. The range in initial size of released bubbles is thus probably comparable to that given in Figs. 3 and 4.

SUMMARY

1. Physonectid siphonophores are potentially responsible for resonant scattering from the DSL partly due to their gelatinous, gas-filled floats, and partly due to bubbles expelled from these floats.

2. Voluntary expulsion of bubbles by siphonophore floats has been observed and photographed. Range in volume of expelled bubbles was 0.03 mm^3 to 2.51 mm^3. Range in volume of pneumatophores observed to expel bubbles was 0.25 mm^3 to 12.55 mm^3.

3. Observations on siphonophores from a deep submersible vehicle at the depths of the DSL revealed their pneumatophores to be inflated at all times observed. They are thus continuously potential sound scatterers.

4. Range in theoretical resonant frequencies based on the initial size of the expelled bubbles at 100 and 400 meters depth was 57 to 111 kc/s for the smallest and 12 to 24 kc/s for the largest. A similar range for bubble expelling pneumatophores was 27 to 50 kc/s for the smallest and 7 to 13 kc/s for the largest when calculated on the basis of float volume.

BIBLIOGRAPHY

1. National Defense Research Committee (NDRC), Division 6, Summary Technical Report, v. 7, Principles of Under Water Sound, C. Eckart, ed., Part I, "Basic Principles of Underwater Sound," p. 100-102 et seq., 1946

2. Raitt, R. W., "Sound of Scatterers in the Sea," Journal of Marine Research, v. 7, p. 393-409, 1948

3. Marshall, N. B., "Bathypelagic Fishes as Sound Scatterers in the Ocean," Journal of Marine Research, v. 10, p. 1-17, 1951

4. Tucker, G. H., "Relation of Fishes and Other Organisms to the Scattering of Underwater Sound," Journal of Marine Research, v. 10, p. 215-238, 1951

5. Hersey, J. B. and Backus, R. H., "New Evidence that Migrating Gas Bubbles, Probably the Swimbladders of Fish, are Largely Responsible for Scattering Layers on the Continental Rise South of New England," Deep-Sea Research, v. 1, p. 190-191, 1954

6. Hersey, J. B., Backus, R. H. and Hellwig, J., "Sound-Scattering Spectra of Deep Scattering Layers in the Western North Atlantic Ocean," Deep-Sea Research, v. 8, p. 196-210, 1962

7. Barham, E. G., "Siphonophores and the Deep Scattering Layer," Science, v. 140, p. 826-828, 1963

8. Barham, E. G., "Deep Scattering Layer Migration and Composition: Observations from a Diving Saucer," Science, v. 151, p. 1399-1403, 1966

9. Barham, E. G. and Davies, I. E., "Bio-Acoustics," p. 31-38 in NEL Deep Submergence Log No. 1, August 1966, and subsequent logs

10. Pickwell, G. V., Barham, E. G. and Wilton, J. W., "Carbon Monoxide Production by a Bathypelagic Siphonophore," Science, v. 144, p. 860-862, 1964

11. Pickwell, G. V., "Physiological Dynamics of Siphonophores from Deep Scattering Layers," USNEL Research and Development Report 1369, p. 1-50, 20 April 1966

12. Pickwell, G. V., "Gas and Bubble Production by Siphonophores," USNEL Research and Development Report, in press

13. Davies, I. E. and Barham, E. G., "An Automatic Opening-Closing Net for Collection of Pelagic Organisms," in manuscript

14. Davies, I. E., Barham, E. G. and Pickwell, G. V., "Bio-Acoustics," p. 47-52 in NEL Deep Submergence Log No. 3, February 1967

15. Adams, R. L., "Bio-Acoustic Scattering Measurements," p. 53-56 in NEL Deep Submergence Log No. 3, February 1967

16. National Defense Research Committee (NDRC), Division 6, Summary Technical Report, v. 8, Physics of Sound in the Sea, L. Spitzer, Jr., ed., Part IV, "Acoustic Properties of Wakes," p. 462, 1946

17. Andreyeva, I. B. and Chindonova, Y. G., "On the Nature of Sound-Scattering Layers," Okeanologiya, v. 4, p. 112-124, 1964

18. Lebedeva, L. P., "Measurement of the Dynamic Complex Shear Modulus of Animal Tissues," Soviet Physics - Acoustics, v. 11, p. 163-165, 1965

19. Strasberg, M., "The Pulsation Frequency of Nonspherical Gas Bubbles in Liquids," Journal of the Acoustical Society of America, v. 25, p. 536-537, 1953

20. Jacobs, W., "Beobachtungen über das Schweben der Siphonophoren," Zeitschrift fur Vergleichende Physiologie, v. 24, p. 583-601, 1937

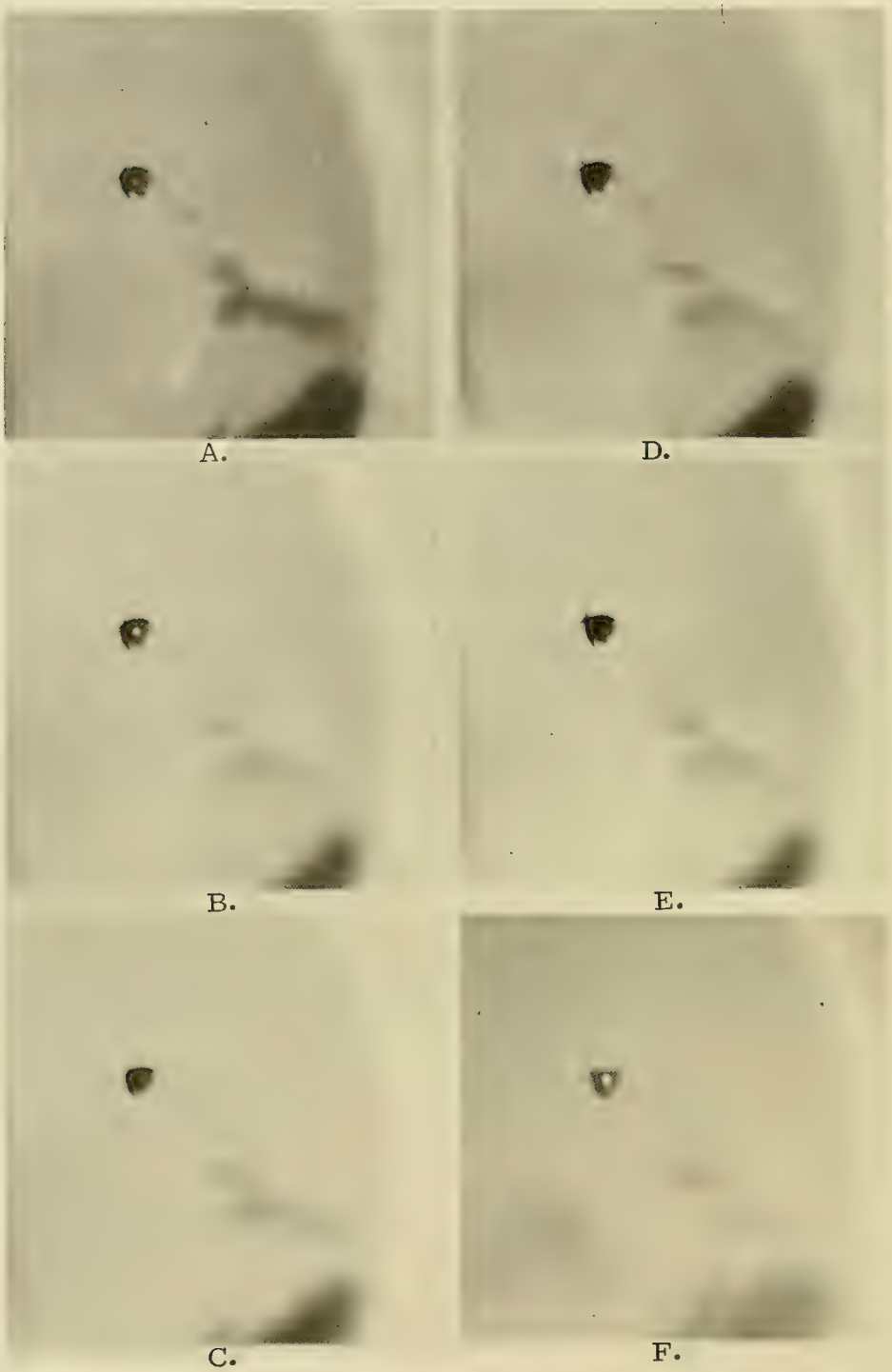

Fig. 1 - Continuous stages in the expulsion of a single bubble by a pneumatophore of Nanomia bijuga (X5). The entire sequence required approximately 30 seconds.

Fig. 2 - A partially expelled bubble "frozen" in place by application of magnesium sulfate to the surrounding sea water. The chemical apparently relaxes the muscles within the pneumatophore responsible for extruding the bubble (X60).

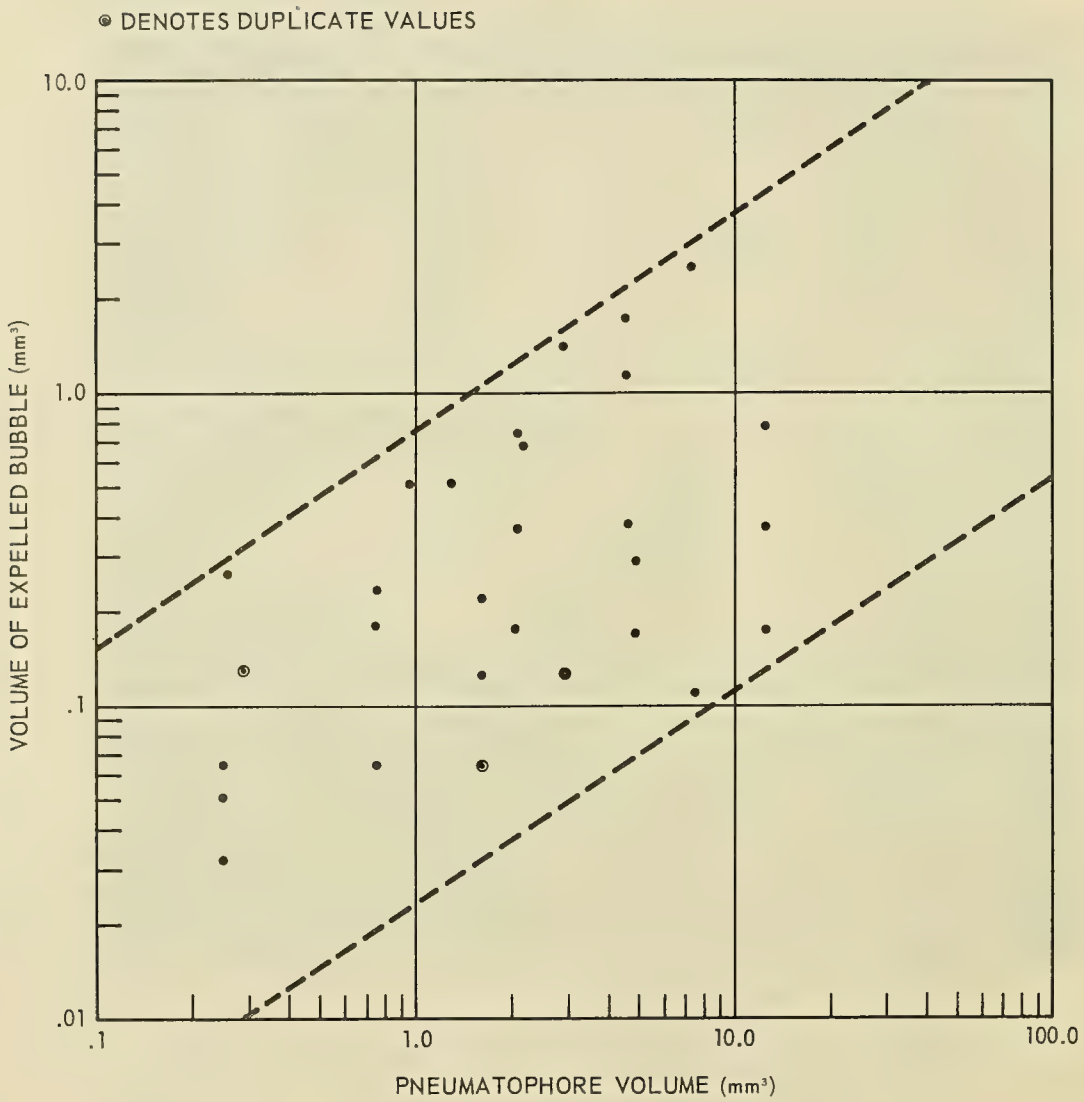

Fig. 3 - Relationship of expelled bubble volume to float volume. Dashed lines arbitrarily denote limits. Points vertically in line represent bubbles emitted from the same float.

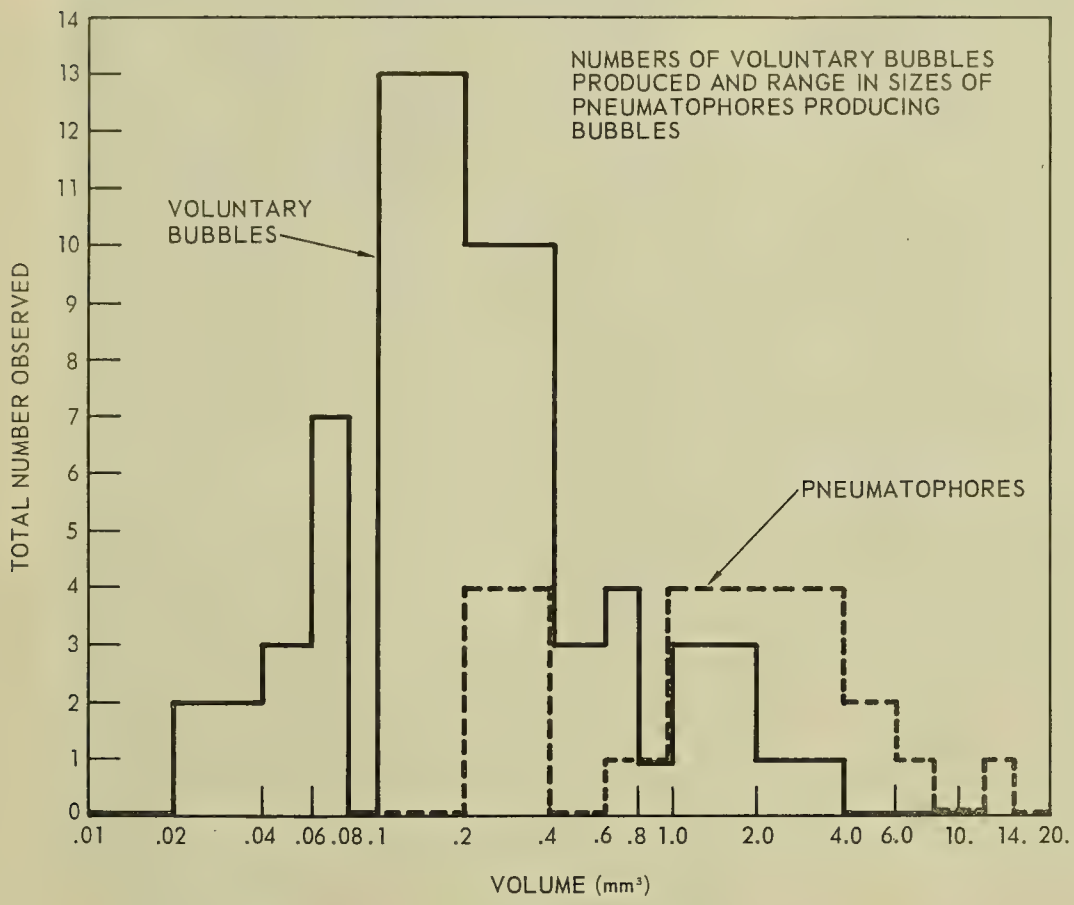

Fig. 4 - Frequency distribution of voluntarily expelled bubbles and of pneumatophores in arbitrary increments of size

Fig. 5 - A living, intact colony of Nanomia bijuga, photographed in an extended feeding position at the daytime depths of the Deep Scattering Layer from the submersible vehicle, DEEPSTAR 4000. Estimated length 60 cm.

TABLE 1

THEORETICAL RESONANT FREQUENCIES FOR VOLUNTARILY RELEASED BUBBLES AND FOR BUBBLE-RELEASING PNEUMATOPHORES

		Minimum			Arbitrary "Median"			Maximum		
	Depth (m)	R (cm)	f_{ri}* (kc/s)	f_{rs}** (kc/s)	R (cm)	f_{ri} (kc/s)	f_{rs} (kc/s)	R (cm)	f_{ri} (kc/s)	f_{rs} (kc/s)
Voluntary Bubbles	100	0.018	57		0.040	26		0.084	12	
	200	0.018	79		0.040	36		0.084	17	
	300	0.018	96		0.040	44		0.084	21	
	400	0.018	111		0.040	51		0.084	24	
Pneumatophores	100	0.039***	27	27†	0.079***	13	13††	0.145***	7	7†††
	200	0.039	37	36	0.079	18	18	0.145	10	10
	300	0.039	45	43	0.079	22	21	0.145	12	12
	400	0.039	52	50	0.079	26	24	0.145	14	13

*f_{ri} = resonant frequency for an ideal bubble

$$= \frac{(d + 10)^{\frac{1}{2}}}{R}$$

***R = radius of a sphere of volume equal to that of the spheroid.

†V = 0.25 mm^3, total pneumatophore gas phase.

††V = 2.07 mm^3. †††V = 12.55 mm^3.

**f_{rs} = resonant frequency for a real bubble including consideration of a shear factor

$$= 1.5 \frac{\sqrt{H + 30}}{\sqrt[3]{V}}$$

MIGRATION AND TEMPERATURE STRUCTURE OF EDDIES ON THE LEEWARD SIDE OF THE HAWAIIAN ISLANDS

Edward L. Smith
U. S. Navy Electronics Laboratory
San Diego, California

INTRODUCTION

This paper discusses the variability of the oceanographic environment in the lee of the Hawaiian Islands caused by cyclonic and anticyclonic eddies in their wake. The paper presents new data acquired in the eddy region by means of the U. S. Navy Electronics Laboratory Thermistor Chain.

The chain was used during two cruises in the eddy region, Cruise 29 in August 1964, and Cruise 36 (made in conjunction with the Marine Physical Laboratory and based on the results of Cruise 29) in July 1966. During Cruise 29 a cyclonic eddy 125 miles in diameter was located. During Cruise 36, in the same region that had been investigated in 1964, two smaller eddies were found. One was cyclonic and near shore, the second was anticyclonic and west of the first. In both studies two independent methods were used to define the areas occupied by the respective vortices: internal temperature structure as profiled by the thermistor chain, and relative currents determined from ducted current meters attached to the chain.

The data and results for each cruise are presented here separately. From the collective results some conclusions are drawn with regard to the expected variation in environmental parameters caused by the eddies.

EQUIPMENT

The internal temperature structure was plotted during both cruises using the towed thermistor chain which provides a profile of the temperature distribution to an average depth of 750 feet. Thirty-four thermistors, spaced at 25-foot intervals along the chain, sense the temperature, and their electrical output is transmitted to the ship's laboratory. An analog computer determines the depth of

each whole-degree Celsius isotherm and prints the results every 12 seconds on a continuous 19-inch-wide tape. At the normal towing speed of 6 knots, the printout is equivalent to a temperature-depth cross section every 120 feet. The thermistor outputs are also recorded in digital form every 12 seconds on magnetic and paper tape.

Marine Advisors Model B-7C Ducted Current Meters (fig. 1) attached to the thermistor chain were used to determine current speed and direction (Christensen, 1966). The B-7C meter operates on the pulse rate generated by the alternate opening and closing of a reed relay by a magnetic slug in the tip of each impeller blade. Meters C_1, C_2, C_3, and C_4 (fig. 1) provide continuous relative water-motion observations at 43, 259, 505, and 750 feet (usual maximum depth of the chain), respectively.* The output of each meter is recorded continuously on a chart recorder. Constant instrument errors in the data are eliminated by towing the current meters in a square pattern and averaging the readings from oppositely directed tow legs (fig. 1). This procedure allows for the resolution of the two orthogonal components of the relative current vector at the level of each meter and, subsequently, for determination of the relative current vector itself. The square pattern usually involves 5 minutes on each side after the chain becomes mechanically stable following each 90-degree course change. Several time intervals have been used but 5 minutes has proved to be adequate. Stability is recognized from a steady output from the pressure sensor at the bottom of the chain and steady pulse rates from the current meters.

In order for current vectors measured this way to have any validity, a reasonable estimate of ship's speed over the ground must be made. When considering currents in deep oceans it is usually assumed that horizontal pressure gradients vanish at some intermediate depth. Geostrophic flow calculations have been made using this assumption in areas of eddies and, in general, agree well with direct current observations (Reid, 1963). However, the level at which motion vanishes remains controversial. Wind-driven currents in the ocean decrease in strength very rapidly with depth (Ekman, 1905). At the normal depth of current meter C_4, 750 feet, the wind effect is negligible under usual oceanic conditions, and currents referenced to this level will be nearly equal to their true values. Errors in this method of reference-level selection could arise near the eddy centers where "domes" and "dishes" in the structures are most pronounced and differences may exist between the true current and the current relative to 750 feet; the peripheral current measurements are more reliable, however.

Another apparent problem is determining the direction of flow through the ducted meters. Ocean currents are rarely as great as 6 knots, the towing speed of the chain. The chord-to-thickness ratio of the current meter fairing is 15 and that of the other fairings is 9. The fairings will align themselves with the ship; therefore, the flow

*In the 1964 study only meters C_1 and C_4 were used; in 1966 all four meters were used.

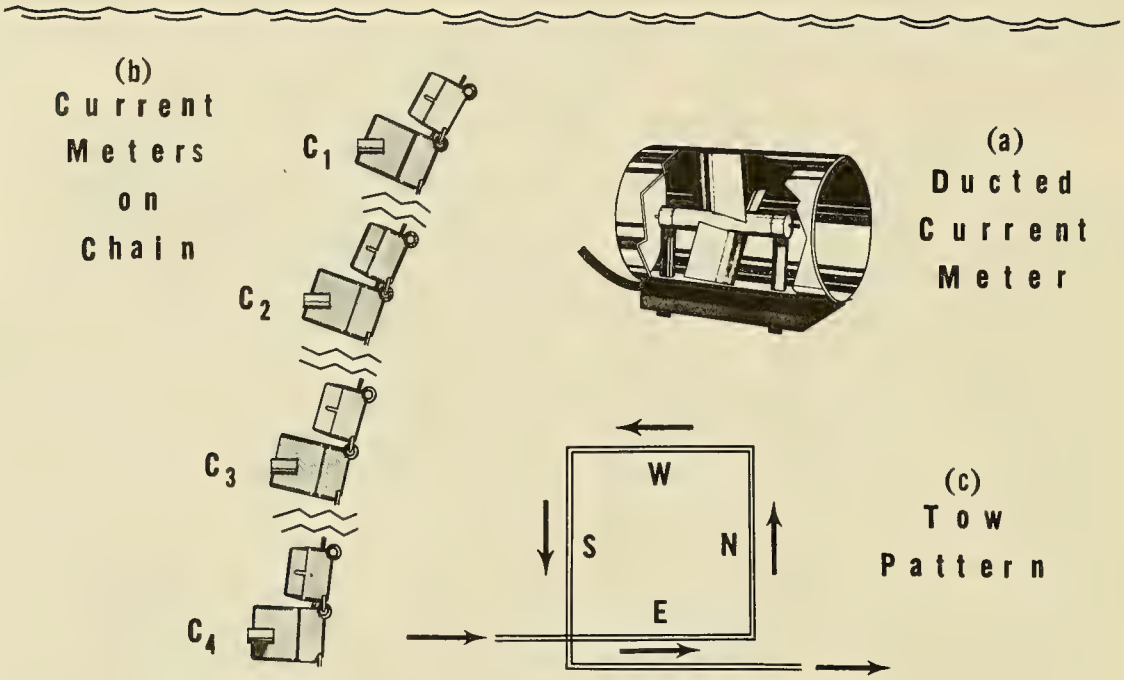

Fig. 1 - (a) Cutaway view of ducted current meter, (b) Current meters mounted on thermistor chain, and (c) Tow pattern for current determinations

through the meter will always be opposite the direction of the ship's travel. Summarizing current measurement considerations: C_4 at 750 feet will give the ship's speed over the ground, and the ship's speed is always much greater than the current speed; and the eddy center is an area of possible error.

CRUISE 29, 1964

In this cruise, two types of measurements were used to define the eddy boundaries: water properties (internal temperature structure and surface density distribution) and relative currents. In the area south of Oahu, a cyclonic eddy 125 miles in diameter, centered 70 miles off the west coast of the island of Hawaii, was located.

The average depths of the 25° C and 23° C isotherms were contoured after low-pass filtering the detailed analog temperature records (figs. 2 and 3). The doming apparent in the temperature structure is indicative of counterclockwise eddy rotation in the northern hemisphere. The eddy appears somewhat elliptical in shape in both figures. The 25° C depth contours show a trough or possibly a parisitic eddy near shore (fig. 2). This feature is not present at the depths of the 23° C isotherm (fig. 3). The temperature structure for the leg that passes nearest the eddy center (leg H to I) is shown in figure 4. The dome in the structure is obvious,

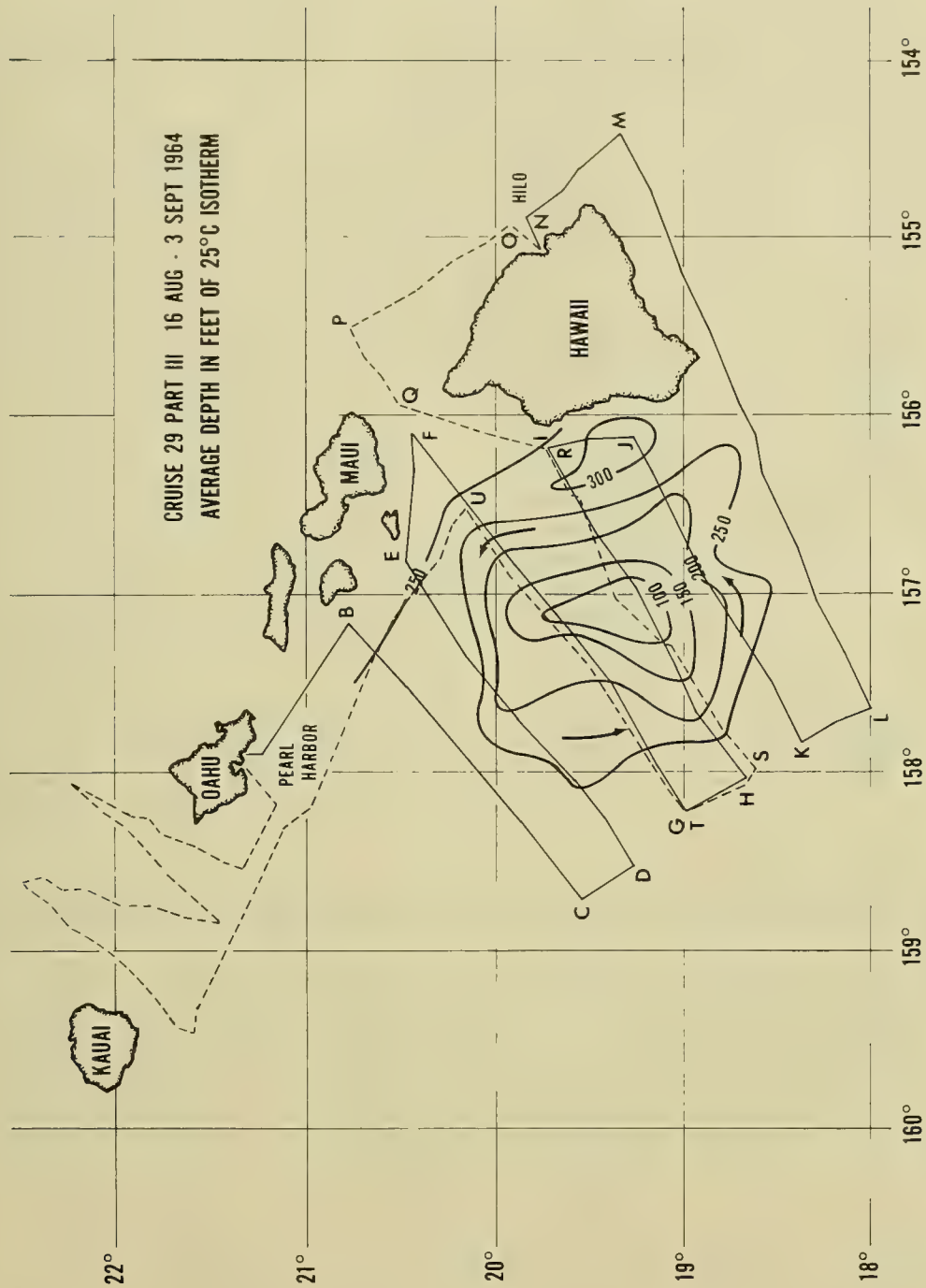

Fig. 2 - Cyclonic eddy located during Cruise 29 depicted by the depth contours of the 25°C isotherm

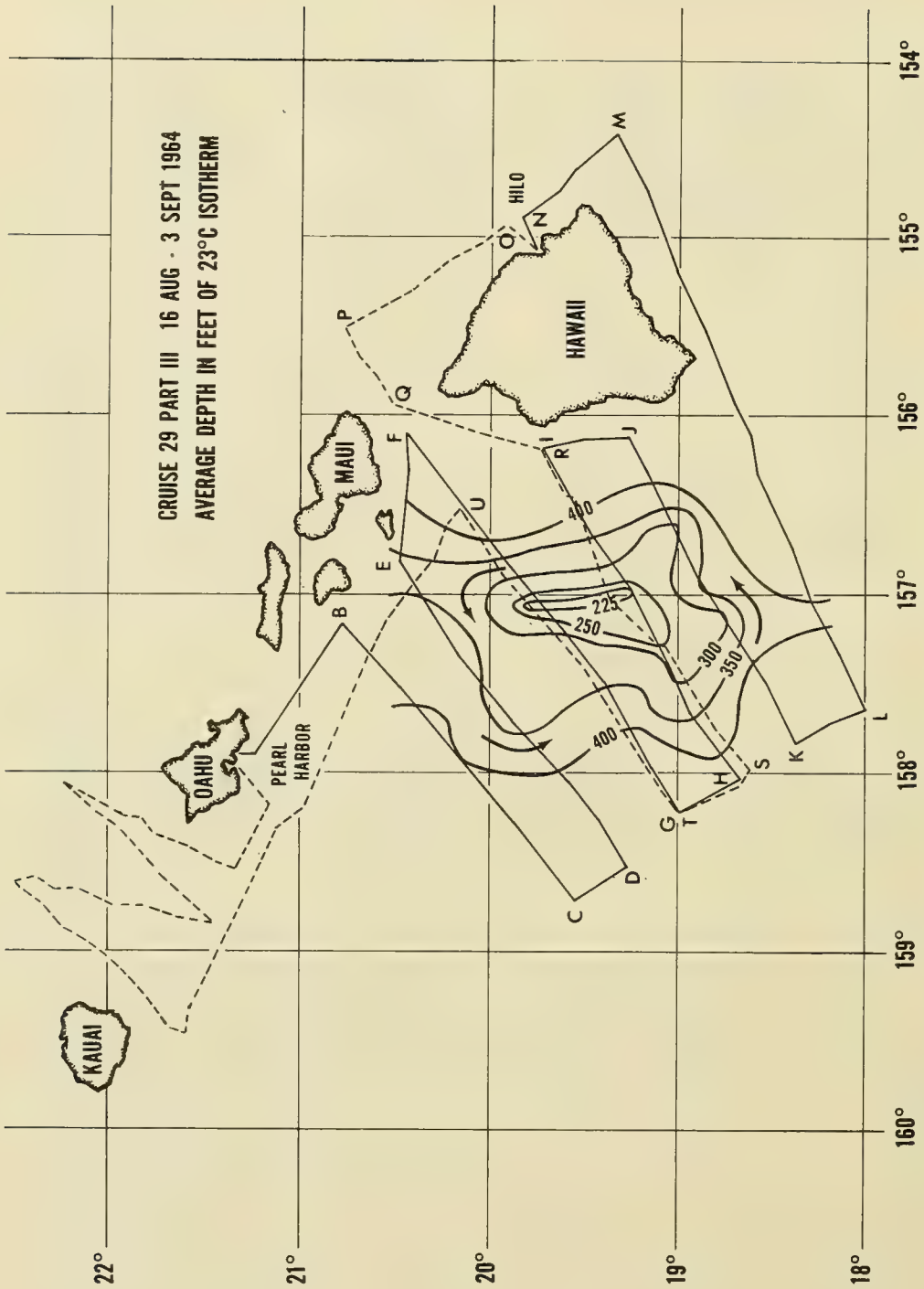

Fig. 3 - Cyclonic eddy located during Cruise 29 depicted by the depth contours of the 23°C isotherm

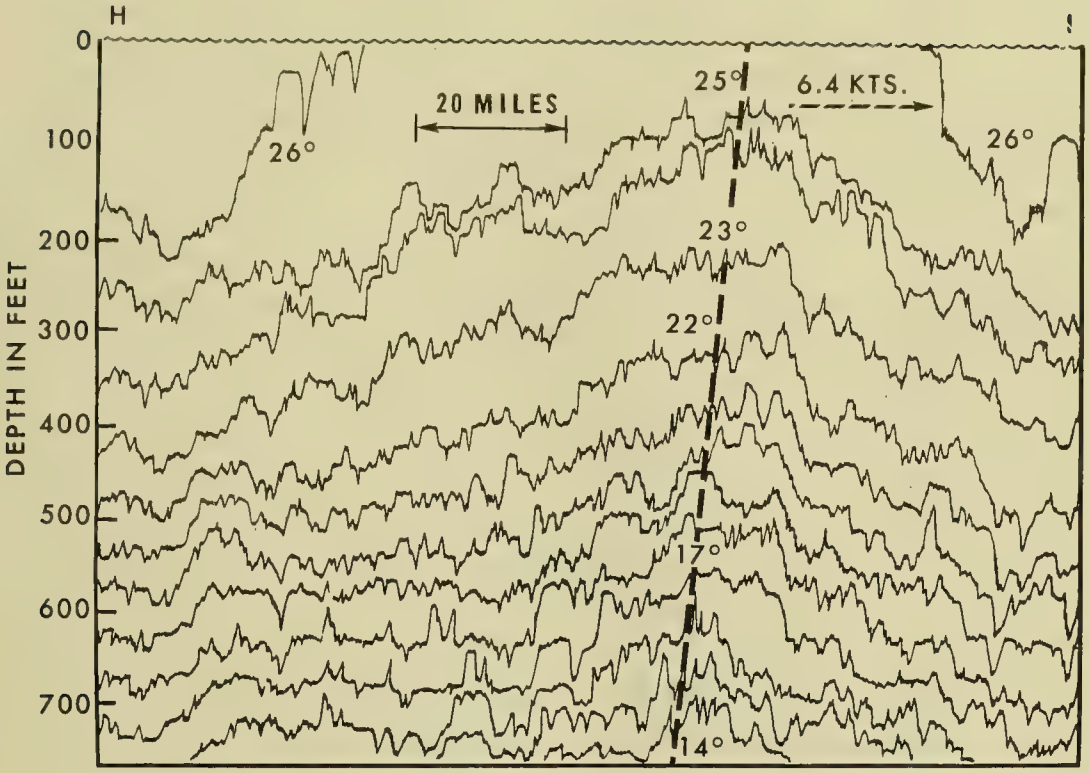

Fig. 4 - Temperature structure as recorded by the NEL Thermistor Chain between points H and I (Figs. 2 and 3) during 1964 eddy study. Dashed line shows asymmetry and eastward trend of eddy apex.

but appears asymmetric about a vertical center. The vertical axis of the dome points eastward. The average isotherm slope is steeper to the east and, hence, the horizontal temperature gradient is stronger to the east than to the west. The 26° C isotherm is forced to the surface on each side of the dome and further displays asymmetry. The small-scale vertical variations in this temperature structure are somewhat masked because of the necessary horizontal scale compression. However, most vertical variations in these temperature structure data are 20 to 30 feet with wavelengths of 0.5 to 1.5 miles. This type of structure has been shown to be common for this region and other areas of the ocean (Smith, 1967).

The thermal structures along the two center legs of the track (F to G and H to I) were measured again (R to S and T to U) 10½ days later. For comparison with track leg H to I, figure 5 shows the temperature structure for track leg R to S. It can be seen that the dome in the structure is better developed and is more symmetric about a vertical center. The most important feature is the migration

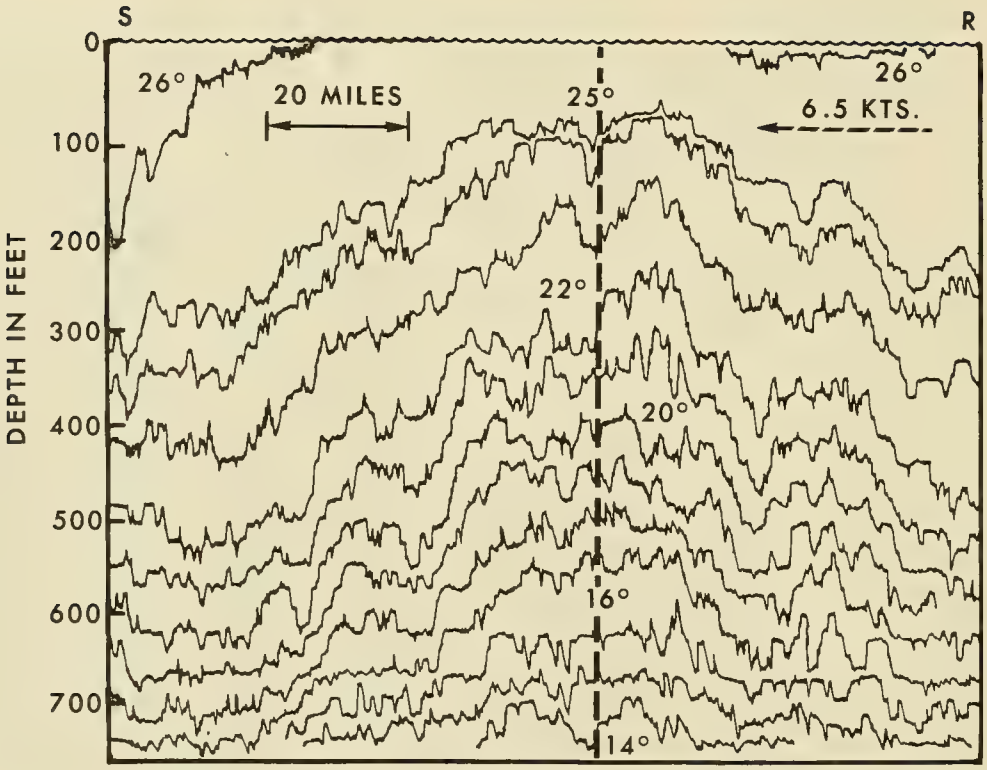

Fig. 5 - Temperature structure between points R and S (Figs. 2 and 3) 10-1/2 days after points H to I were recorded. Dashed line shows better symmetry and migration from east to west of the eddy.

of the dome apex from east to west during the elapsed time. From the east-to-west change in position of the average depth of isotherms, it appears that the eddy moved in a westerly direction at the rate of 0.6 mile per day during the period of observation. This rate of migration is quite slow when compared to that of a cyclonic eddy, 50 miles in diameter and southeast of Oahu, which moved westward in 1963 at about 7 miles per day (Barkley, et al., 1965).

Another method was used to study the eddy. Surface water samples and bucket thermometer temperatures were taken at intervals that varied from one to six hours, dependent upon the position in the track. The eddy position as derived from the surface density (σ_t) distribution (fig. 6) agrees well with the position derived from the isotherm depth contours. Upwelling of dense water at the eddy center is clearly demonstrated, and the direction of eddy rotation can be established. In the northern hemisphere, the light water is to the right of the observer when facing the direction of flow (Sverdrup, et al., 1942).

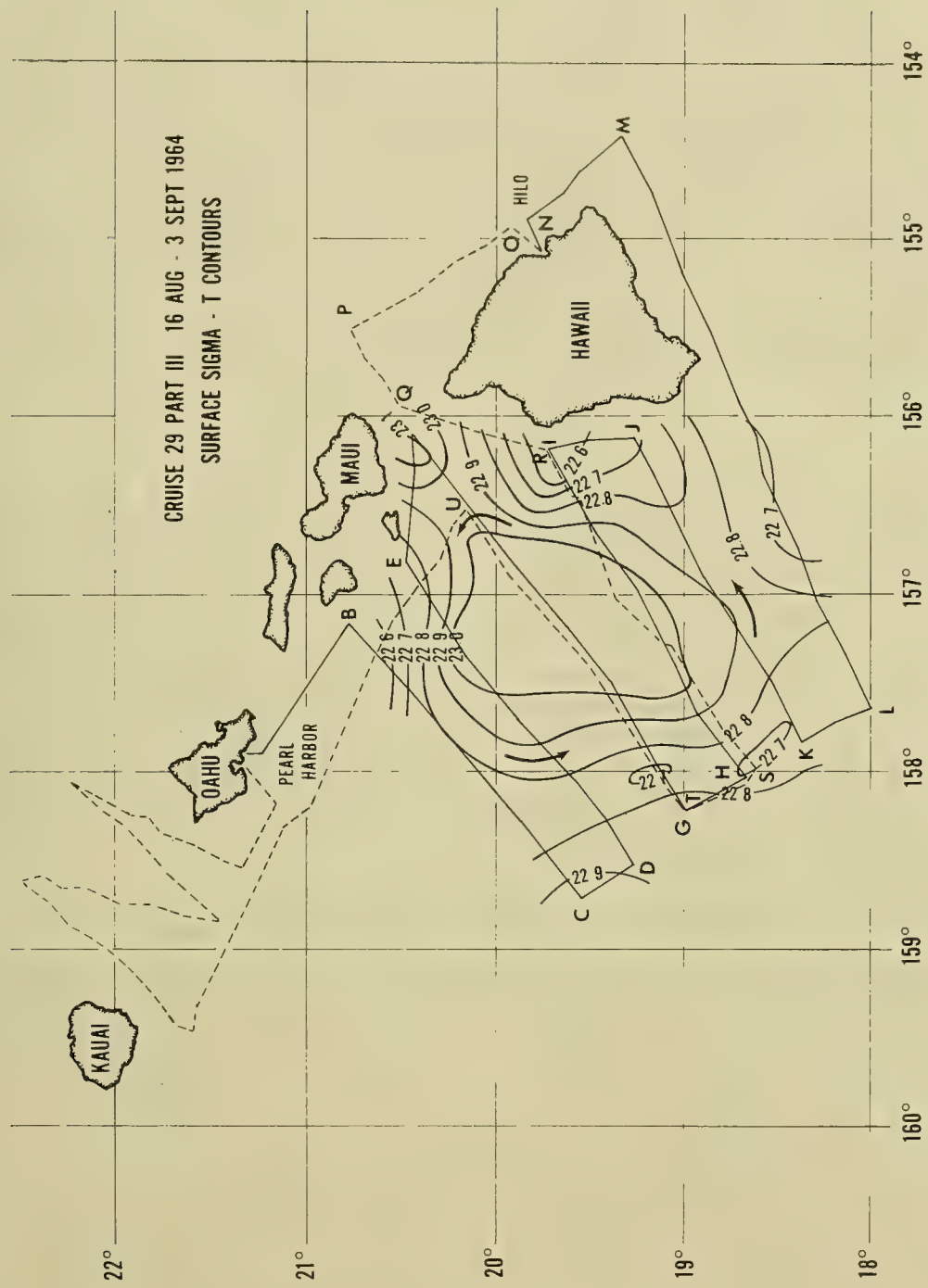

Fig. 6 - Cyclonic eddy of Cruise 29 depicted by the surface density distribution (σ_t contours)

Tow patterns for current determinations were scheduled for changes and at the leg mid-points but because of some equipment problems in this first attempt to use current meters mounted on the chain, not all schedules were kept. Figure 7 shows current vectors at 43 feet referenced to 750 feet in the region of the cyclonic eddy. The 250-foot depth contour of the 25° C isotherm shows the relative position of the eddy. The current velocity is the greatest nearshore (1. 0 knot). This is probably caused by the addition of the eddy tangential velocity and the velocity of the water flowing northward along the obstruction after breaking off from the main westerly flow. The average peripheral current, at 60-mile radius, is 0. 6 knot. At distances slightly greater than 60 miles from the center, the tangential velocity is about 0. 3 knot. Near the eddy center, 15-mile radius, the current is about 0. 3 knot also. Therefore, the velocity distributions are similar to those of a Rankine vortex which has a velocity (v) proportional to a distance, r, in an inner region and to r^{-1} in an outer region (Lamb, 1945).

CRUISE 36, 1966

In July 1966, again the thermal structure profile was recorded and direct current observations were made in the area southwest of Alenuihaha Channel (Maui-Hawaii). In the region that had been occupied by a single cyclonic eddy in 1964, two smaller eddies were found, one cyclonic near shore and the second anticyclonic and west of the first. Both eddies were elliptical in shape as shown by the average depth contours of the 25° C and 23° C isotherms of figures 8 and 9, respectively. The anticyclonic eddy is typified by the "dish" or depression in the temperature structure, which is indicative of clockwise rotation in the northern hemisphere. The major axis of this eddy is about 90 miles, and the minor axis about 60 miles. The cyclonic eddy is slightly smaller, major and minor axes being about 80 miles and 50 miles respectively.

The temperature structure for the track leg E to F (fig. 10) clearly shows the "dome" and "dish" generated by the counter-rotating eddies. A strong horizontal temperature gradient, 0. 2° C/mile, at 300 feet persists for more than 20 miles in the region of eddy confluence. The rotation effects of the eddies reach to depths greater than 750 feet at the eddy centers. The 26° C isotherm is forced to the surface by the upwelling of the colder water at the center of the cyclonic eddy, but the same isotherm is drawn down to more than 400 feet by the convergence of warm water at the center of the anticyclonic eddy. Hence, a depth change of 400 feet for the 26° C isotherm occurs over 50 miles to the east and 30 miles to the west of the area of confluence. A small pocket of 26° C water can be seen shoreward of the dome. Both eddies appear symmetric about a vertical center. The small-scale vertical variations are of about the same dimensions as those observed in 1964. A few intermediate-scale vertical variations are evident in the structure. Coherent depth changes of isotherms can be observed throughout

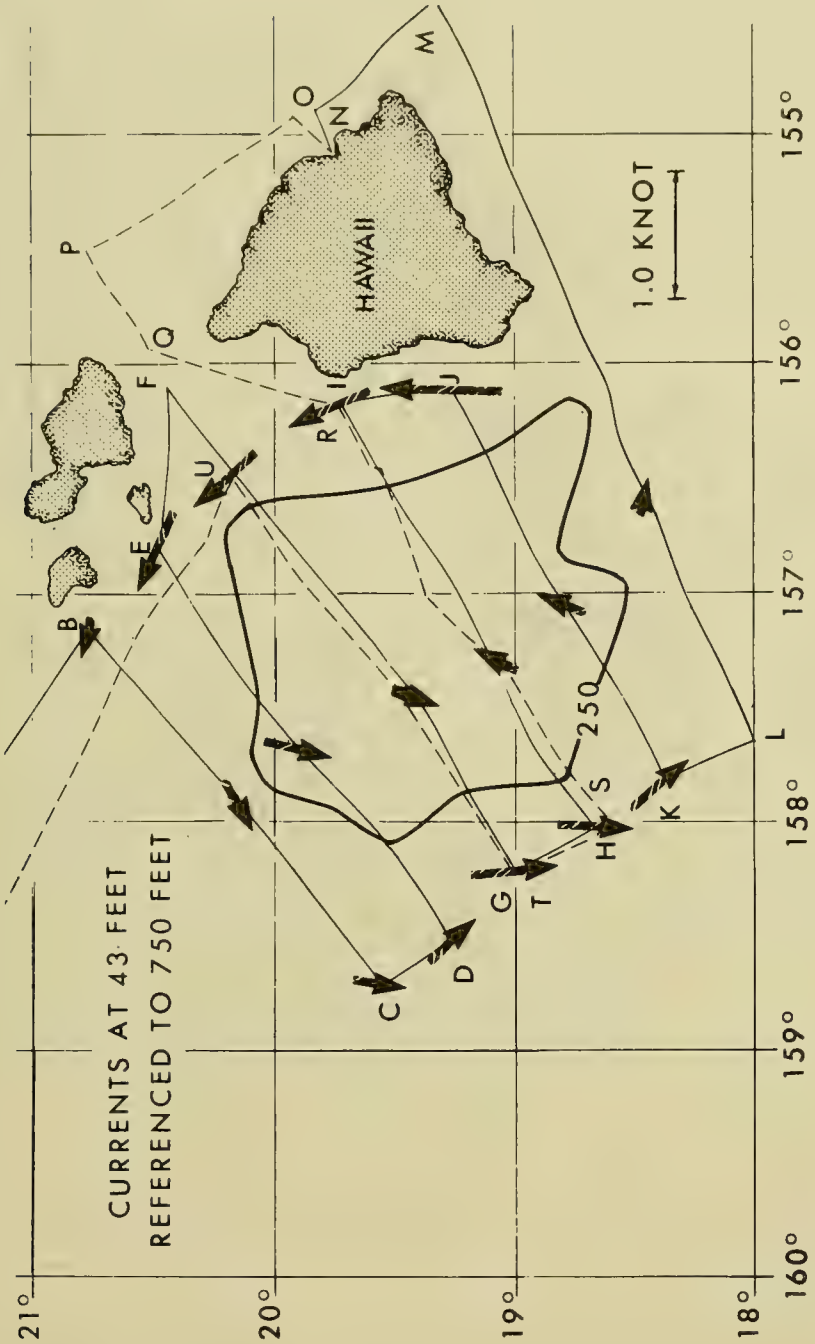

Fig. 7 - Relative currents at 43 feet associated with 1964 cyclonic eddy. Solid line is the depth contour of 25 C isotherm

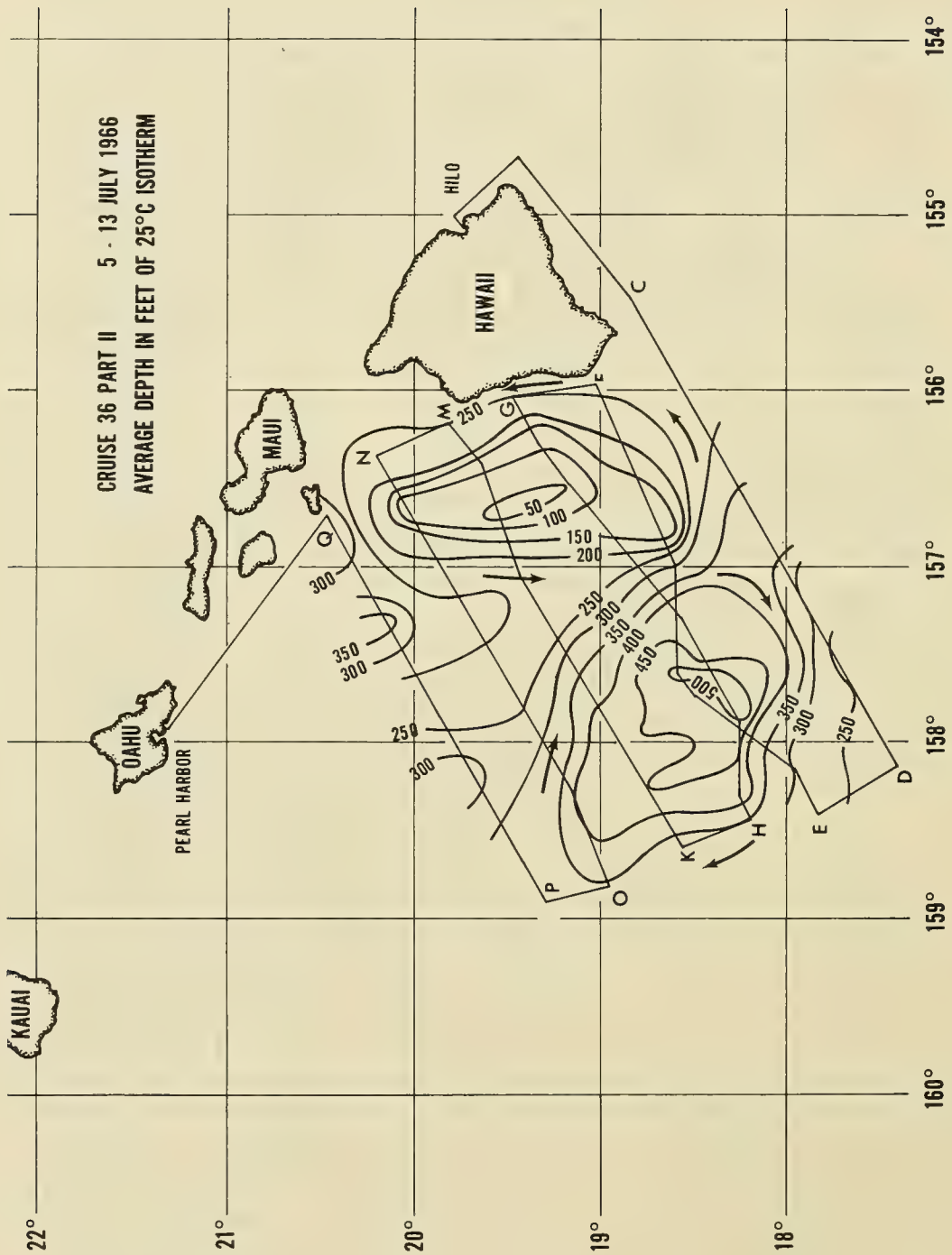

Fig. 8 - Counter-rotating eddies located during Cruise 36 depicted by the depth contours of the 25° isotherm

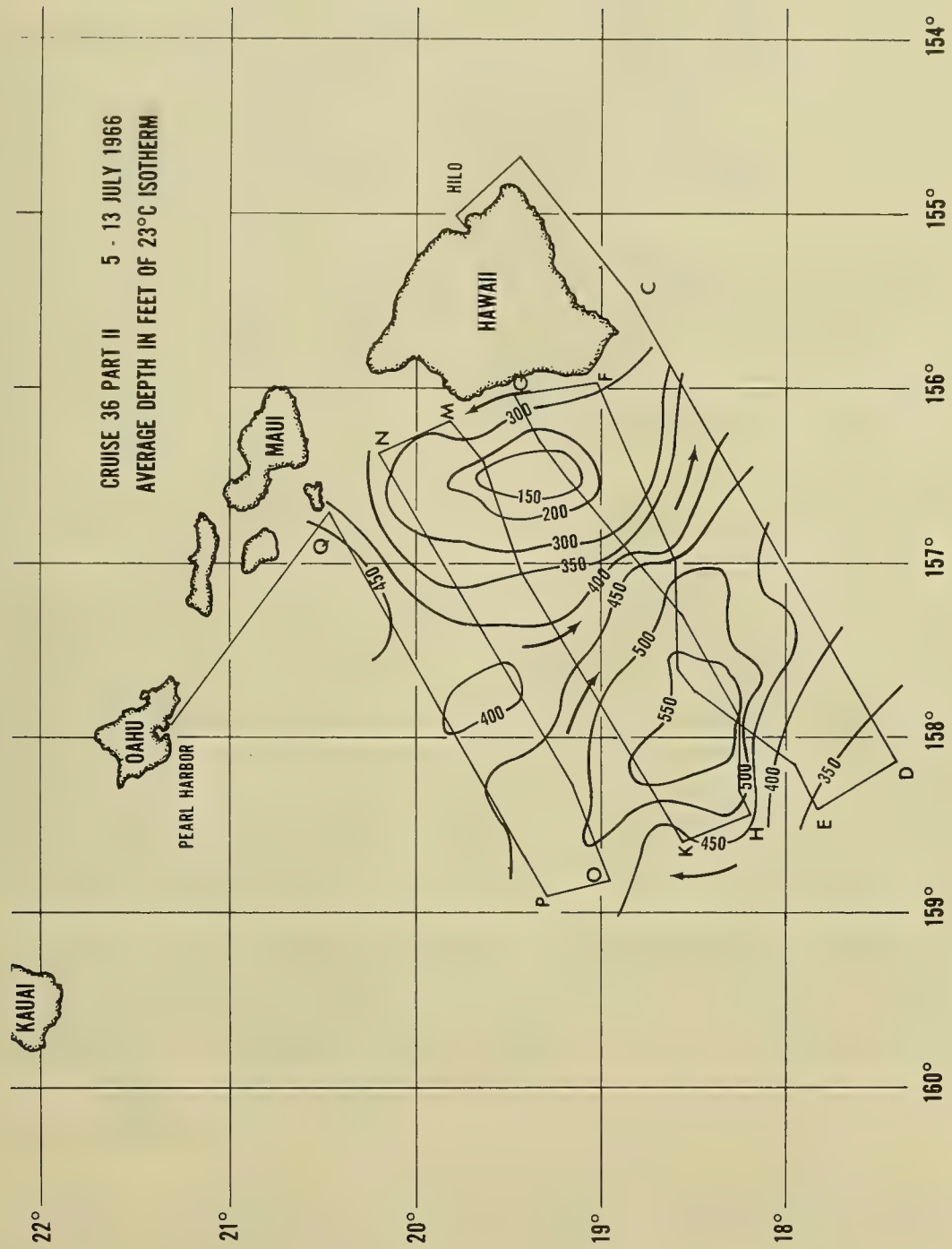

Fig. 9 - Location of counter-rotating eddies during Cruise 36, depicted by the depth contour of 23°C isotherm

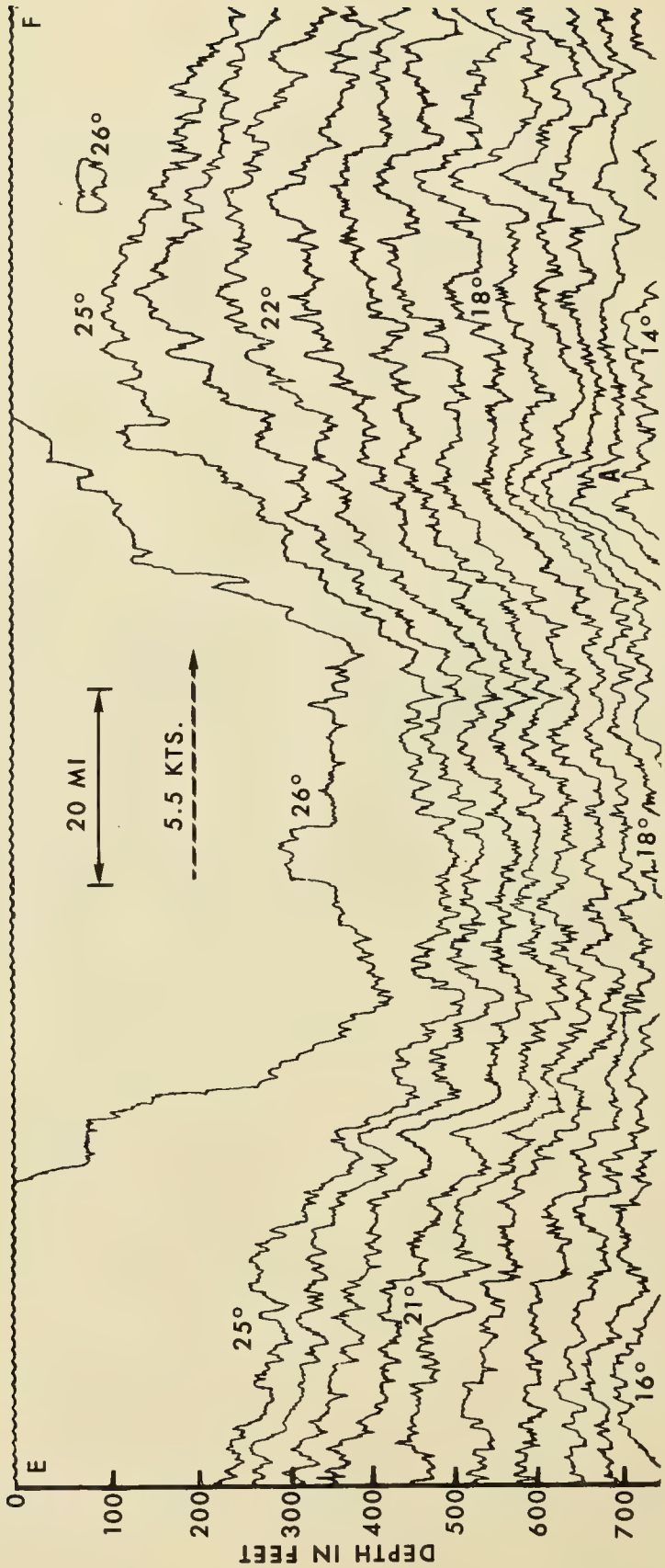

Fig. 10 - Temperature structure as recorded by the NEL Thermistor Chain between points E and F (Figs. 8 and 9) during 1966 eddy study

the temperature structure, but the most striking is on the seaward side of the cyclonic eddy where the 14° C to 18° C isotherms at 650 feet exhibit a depth change of 125 feet (Area A, fig. 10).

Direct current measurements were made in the same manner as in 1964. Square tow patterns for current determinations were scheduled for the ends of each track leg and for each leg center. The current pattern at the middle of leg P-Q and point Q were deleted because of equipment failure. The midleg pattern of leg K-M was omitted in order to obtain an uninterrupted digital temperature recording to be used in a separate study.

Figures 11, 12, and 13 display the circulation referenced to 750 feet for depths of 43, 259, and 505 feet, respectively. The 200- and 400-foot depth contours of the 25° C isotherm are included in each figure to better show the region of confluence of the counter-rotating eddies. At each depth the converging currents near the center of track leg E-F are the greatest, where the proximity of the two eddies is the smallest. Here currents, referenced to 750 feet, were 1.4, 1.8, and 1.3 knots at the respective depths.

As would be expected, the near-surface (43 feet) currents (fig. 11) for the general area are the strongest and range from 0.3 to 1.4 knots. Although it is not conclusive, some evidence of water leaving the main westerly flow west of point C and flowing northward along the west coast of the flow obstruction, as in 1964, can be seen. Figures 11, 12, and 13 present similar circulation patterns, with the velocities decreasing with depth in all areas except one. In the area of eddy convergence, as described by the middle of track legs C-D, E-F, and G-H, the current at 259 feet is greater than that above or below it. It should be pointed out that the current directions for this area at depths 259 and 505 feet are more easterly than that at 43 feet. Transient wind effects may cause the current at 43 feet to have a more westerly direction and could effectively reduce the eddy tangential current velocity.

No current measurements were made near the eddy centers. Hence, speculation on a vortex type is not possible on the basis of variation of tangential velocities with respect to distance from the center. However, the position and the counter-rotation of the eddies resemble Karman vortices in the wake of the island of Hawaii. Several similar eddies could exist downstream to the west.

DISCUSSION

The current in the region of the Hawaiian Islands generally flows toward the west but sometimes has a northerly or southerly component, dependent basically upon the position of the Eastern North Pacific High (Sverdrup, et al., 1942).

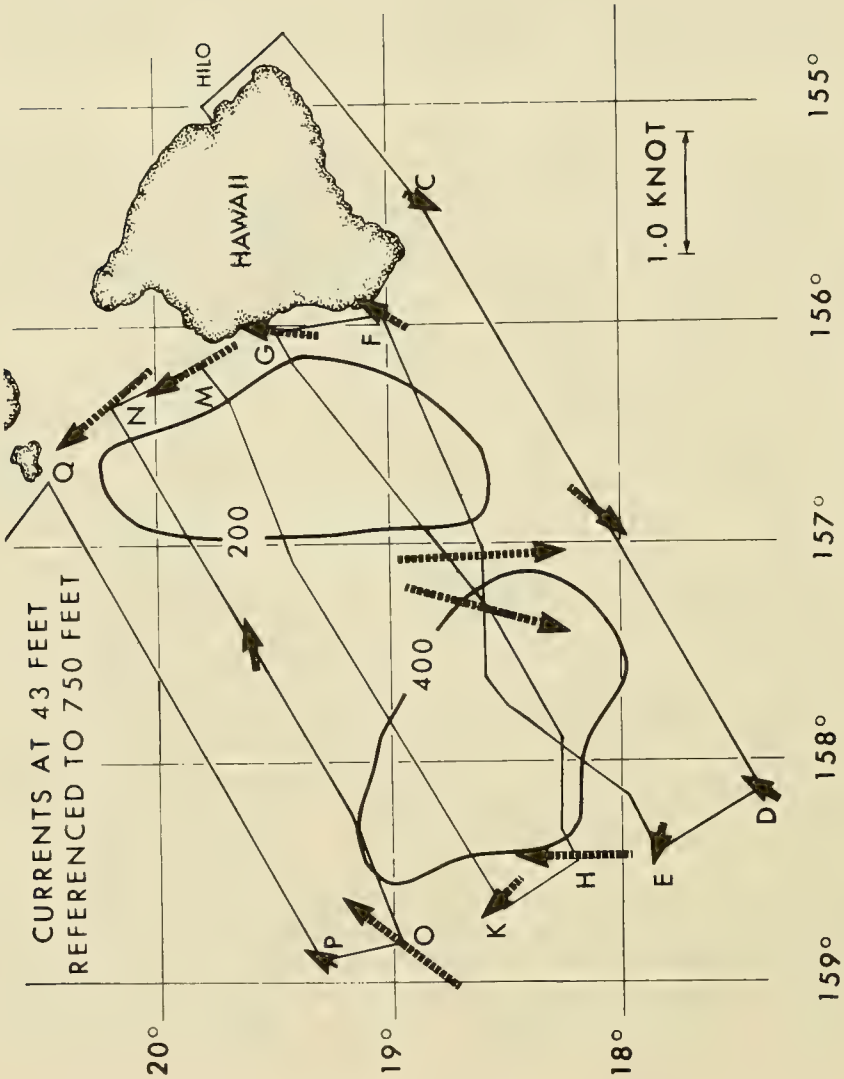

Fig. 11 - Relative currents at 43 feet associated with 1966 counter-rotating eddies. Solid line is the depth contour of 25°C isotherm.

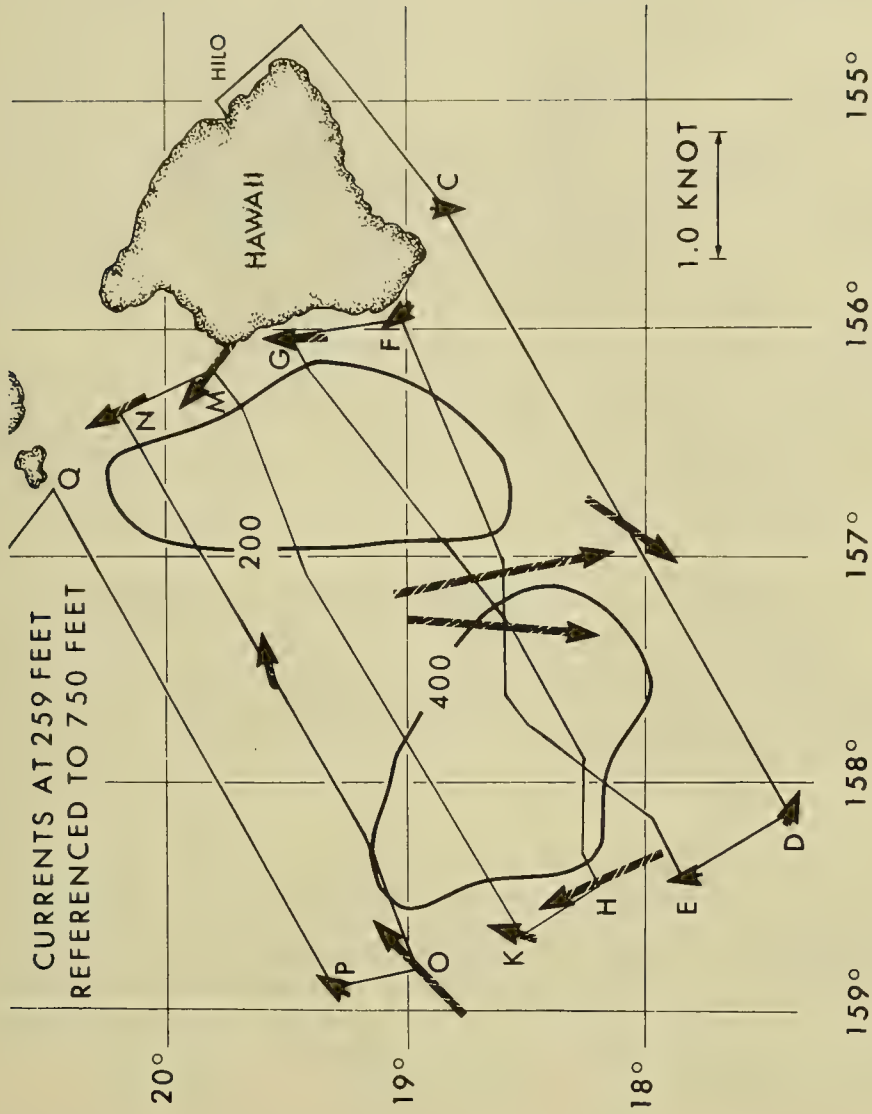

Fig. 12 - Relative currents at 259 feet associated with 1966 counter-rotating eddies. Solid line is the depth contour of 25°C isotherm.

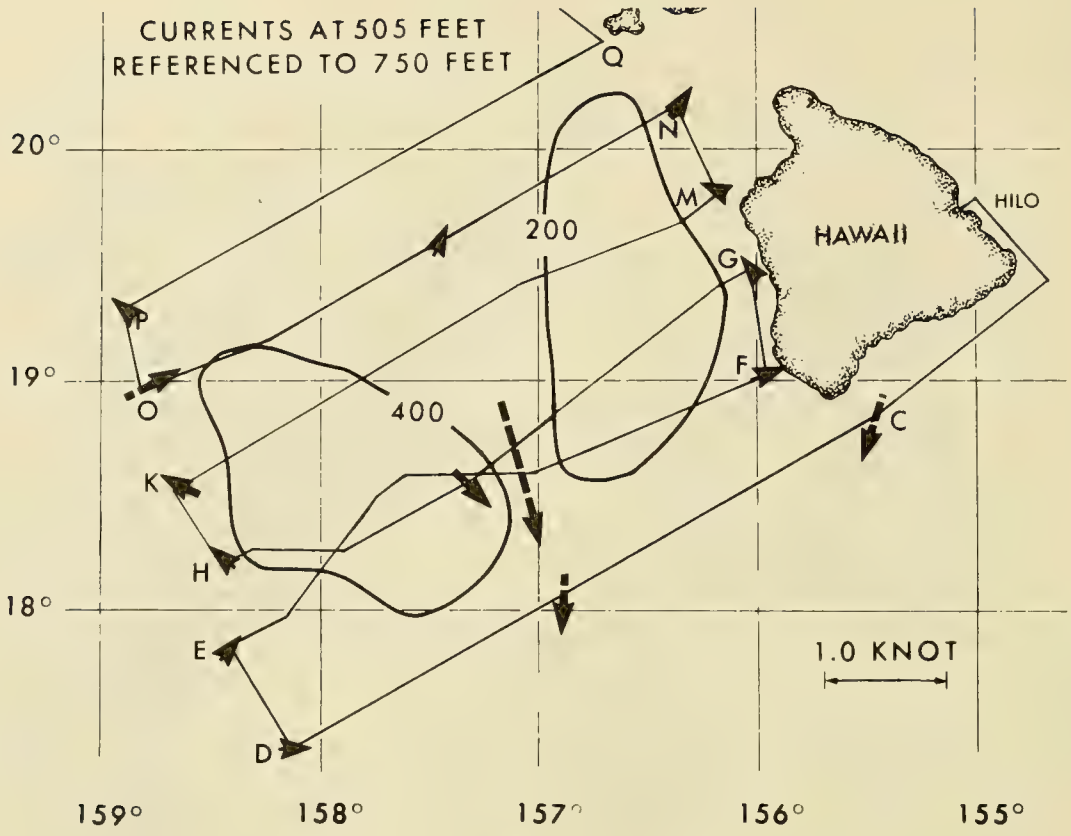

Fig. 13 - Relative currents at 505 feet associated with 1966 counter-rotating eddies. Solid line is the depth contour of 25°C isotherm.

The Hawaiian Archipelago liès in a southeast to northwest arc, and presents a nearly solid barrier to any impinging ocean currents. Only two of the four openings in the island barrier have sill depths greater than 1000 fathoms; namely, the Kauai Channel (Kauai-Oahu), 1800 fathoms, and the Alenuihaha Channel (Maui-Hawaii), 1100 fathoms. These deeper openings, to the north and south of the island barrier can pass a large volume of water and probably cause a jet stream effect (similar to that of a jet or wake discharged into a fluid at rest (Rossby, 1936). The remaining openings are Kaiwi Channel (Oahu-Molokai) and Pailolo Channel (Molokai-Maui) with sill depths of 300 fathoms and 40 fathoms, respectively. These shallow openings, in the middle of the island group, although allowing the passage of some water, in effect act as a quasi-solid barrier to fluid flow. In theory, this effect is similar to stream flow along a lamina (Lamb, 1945) and flow past a barrier in a rotating spherical shell (Long, 1952). Consequently, eddies in the lee of the Hawaiian Islands can be generated in several ways.

In addition to the eddies reported here, cyclonic and anticyclonic eddies, 50 to 100 miles in diameter, have been reported on the leeward side of the island chain during all seasons of the year (McGary, 1955, and Sechel, 1955). Some of the eddies migrated and some were stationary during the periods of observation. Eddies of about this same size have been observed northeast of Oahu during the winter months (Sechel, 1955).

CONCLUSION

The oceanographic environment on the leeward side of the Hawaiian Islands is highly variable because of eddies. The eddies are present consistently and to maintain individual eddy histories would require a formidable number of observations. Therefore, any reliable long-term prediction of underwater sound-propagation parameters in this area is unlikely at the present time.

The region discussed here is used as an exercise area by surface and subsurface vessels of the U. S. Navy. Environmental parameters such as spreading, adsorption, and reflection must be known for reliable and efficient operation of advanced sonar systems. Since each of these variables can be density-dependent, predictions made in an area of migrating eddies might be valid for short periods only.

In view of the environmental variability of the area and the technological requirements of advanced underwater sound systems, it is the opinion of the author that another area, perhaps east of the Hawaiian Islands, should be considered for initial testing and evaluation of such systems. After reliable operation is achieved in a stable and more predictable environment, the island wake area could be used.

REFERENCES

Barkley, R. A. and staff, 1965, "Progress in 1962-63," U. S. Bureau of Commercial Fisheries, Hawaii Area Biological Laboratory, Circular 206.

Christensen, N., 1966, "Determination of Currents From Instruments Attached to the NEL Thermistor Chain," U. S. NEL Tech. Memo. No. 974, pp 15.

Ekman, V. W., 1905, "On the Influence of the Earth's Rotation on Ocean Currents," Akr. Mat. Astr. Fys., 2, 11: 52 pp.

Lamb, H., 1945, Hydrodynamics, Dover Publications.

Long, R. R., 1952, "The Flow of a Fluid Past a Barrier in a Rotating Spherical Shell," Jour. of Meteorology, Vol. 9, No. 3, pp. 187-199.

McGary, J. W., 1955, "Mid-Pacific Oceanography, Part VI, Hawaiian Offshore Waters, December 1949-November 1951," U. S. Fish and Wildlife Service, Spec. Sci. Rep.: Fish. No. 152.

Reid, J. L., Jr., R. A. Schwartzlose, and D. M. Brown, 1963, "Direct Measurements of a Small Surface Eddy off Northern Baja California," J. Mar. Res., 21, 3: 205-218.

Rossby, C. G., 1936, "Dynamics of Steady Ocean Currents in the Light of Experimental Fluid Mechanics," Papers in Physical Oceanography and Meteorology, Vol. V, No. 1, pp 43.

Seckel, G. R., 1955, "Mid-Pacific Oceanography, Part VII, Hawaiian Offshore Waters, September 1952-August 1953," U. S. Fish and Wildlife Service, Spec. Sci. Rep.: Fish. No. 164.

Smith, Edward L., 1967, "A Predictive Horizontal-Temperature-Gradient Model of the Upper 750 feet of the Ocean," NEL Report 1445 (in press).

Sverdrup, H. U., M. W. Johnson, and R. H. Fleming, 1942, The Oceans, New York, Prentice-Hall, Inc. 1087 pp.

POSITIONING OF THE GULF STREAM BY MEANS OF AERIAL INFRARED RADIATION THERMOMETER MEASUREMENTS

J. C. Wilkerson
U.S. Naval Oceanographic Office
Washington, D.C. 20390

INTRODUCTION

Fluctuations of the position and shape of the Gulf Stream can be examined by three methods. One method consists of tracking the path of the Stream by ship with a temperature sensor towed at a depth of 200 meters (Fuglister and Voorhis, 1965). By steering the ship along the 15°C isotherm, which characterizes the horizontal temperature gradient of the Gulf Stream's inner edge at 200 meters, the position and shape of the Stream can be charted over long distances. The second method is to fly along the length of the current guided by radiometric observations of the sea surface structure. Stommel et al. (1953), von Arx and Richardson (1953), and von Arx, Bumpus, and Richardson (1955) developed the technique and conducted repeated aerial surveys of the Gulf Stream boundary. Aerial observations, made with an airborne radiation thermometer, position the inshore boundary of the Gulf Stream at points of sudden change in characteristics of the contrast in surface temperature between the Gulf Stream and adjacent slope water. The Gulf Stream boundary can be followed by positioning of the aircraft at frequent intervals and by steering the aircraft so as to intersect the line of sudden temperature change at the sea surface. The third method of examining the Gulf Stream is observation of the thermal emission of the sea surface by satellite with a high resolution infrared radiometer such as those used aboard the NIMBUS II meteorological spacecraft. In the absence of clouds, the contrast in surface temperature between the Gulf Stream and colder slope water (as much as 10°C in several hundred meters) is clearly visible in infrared imagery (Wilkerson, 1967). The inshore boundary of the Gulf Stream can be tracked for distances of 1000 km seaward from the east coast of the United States by means of repeated satellite observations under cloud-free conditions.

The relationship between the frontal position detected from ships and aircraft has been studied by Strack (1953), who found that the frontal outcrop at the surface is closely associated with the

strongest horizontal temperature gradients at depths of 100 to 200 meters during winter. In late spring and summer, warming of the surface layer tends to blur and obscure their relationship.

Using this accumulation of knowledge, the Naval Oceanographic Office early in 1966 began a series of tracking flights over the Gulf Stream with an oceanographic research aircraft fitted with an airborne radiation thermometer (Pickett and Wilkerson, 1966). Knowledge of the fluctuations of position and shape of the Gulf Stream was required for making more accurate ocean environment forecasts for the Antisubmarine Warfare Environmental Prediction Services (ASWEPS) of the Oceanographic Office.

This paper presents the results of a series of ASWEPS oceanographic aircraft (Figure 1) tracking missions made for detecting changes in the shape and position of the Gulf Stream between September 1966 and January 1967.

TECHNIQUE OF MEASUREMENT

The principal value of the aircraft in Gulf Stream studies is the speed and endurance of the aircraft. An aerial survey of the Gulf Stream boundary from Cape Hatteras to 60°W, requiring about 8 hours to complete, results in collection of very nearly synoptic data and virtually eliminates the time changes inherent in ship tracking data. Clouds over the Gulf Stream which would obscure the view from satellite altitudes is generally not a problem in aircraft observation. The cloud base over the Gulf Stream is normally above 300 meters.

Once the boundary has been observed the pilot, guided by radiometric observation, steers the aircraft left or right along the boundary to cross and recross the zone of abrupt temperature change. A sample surface temperature recording taken as the aircraft crossed the Gulf Stream inshore boundary is shown in Figure 2.

The characteristically abrupt change in surface temperature (in this case 5°C in about 300 meters) is clearly recorded.

Normally, a boundary crossing can be made every minute so that a position fix of the aircraft is also necessary each minute. With Loran A the location of the boundary can be determined to within about 2 n.m. from Cape Hatteras out to 63°W, and to within about 4 n.m. between 59°W and 63°W.

RESULTS OF MEASUREMENTS

On 30 September 1966 the ASWEPS aircraft completed the boundary tracking flight shown in Figure 3. The survey started at Cape Hatteras and continued to 63°W, a distance of about 1,000 km. The data showed two principal meanders in the Stream, one positioned at

about 69°W and the second at 73°W. The western edges of both meanders are aligned very nearly north-south along 70°30'W and 73°30'W. The meanders have heights of about 100 km and 140 km and describe a wave length of about 400 km.

Figure 4 shows the position of the boundary during October as observed from ship by tracking the 15°C isotherm at a depth of 200 meters. The data were collected by a Coast and Geodetic Survey ship of the Environmental Science Services Administration (ESSA) (Hansen, 1967) and are included for continuity, since no aircraft data were available for October. The ship completed two tracking operations between 13 and 22 October. The first from 13 to 17 October (solid line) and the second from 18 to 22 October (broken line). The position of the boundary was shifting toward the east with a translational speed of about 3 n.m. per day or 6 cm/sec. The shape of the boundary is similar to the aircraft boundary data of September.

The wavelength of about 400 km is unchanged and the two meanders are still evident with change in heights of both. The smaller meander, now centered at about 72°W, has decreased in height to about 35 km while the height of the larger meander has increased to about 200 km.

Figure 5 shows the northern boundary as observed by aircraft on 14 November 1966. A continued shift of the boundary position toward the east was observed between Cape Hatteras and 64°30'W. The two meanders can still be identified. The smaller of the two is now centered at about 71°W, and the principal meander is centered at about 68°30'W. Note that the western edge of the larger meander has moved eastward more rapidly than the eastern edge, changing its shape and causing a decrease in wavelength from 400 km to about 300 km.

Figure 6 shows the Gulf Stream boundary as observed by aircraft on 15 December 1966. The change in position and shape is apparent from the continued shift of the two meanders toward the east and of the changes in their height. The principal meander, now centered at about 66°W, has increased in height to about 300 km; the smaller has increased to about 100 km. The wavelength remains about 300 km.

Figure 7 shows boundary data on 13 January 1967. The significant change from December is seen in the eastward shift of the larger meander, whereas the smaller meander has remained nearly stationary. The shift has increased the described wavelength to about 500 km.

CONCLUSIONS

Figure 8 presents the five monthly boundary positions, four from aircraft (solid line) and one from ship data (broken line) in a form that lends itself nicely to an examination of the change in both shape and position of the Gulf Stream frontal boundary. The vertical separation of the data according to time is such that a 45-degree

slope of the phase progression line connecting meanders (dashed lines) corresponds to a phase speed of 6 n.m. per day or 13 cm/sec. The eastward translation of the meanders is neither uniform nor constant during this five month period. From September through November the smaller of the two meanders moved eastward at a speed of about 2 to 3 n.m. per day or about 5 to 9 cm/sec, while the larger meander moved somewhat slower toward the east at about 1 to 1.5 n.m. per day or about 2.5 cm/sec.

From November to January, the translational speed increases for the larger meander to about 4 n.m. per day or about 10 cm/sec. The speed of the smaller meander decreased to about 1 n.m. per day and appears to have regressed slightly westward.

In summary the shape of the northern boundary of the Gulf Stream between 30 September 1966 and 13 January 1967 is described by two meanders which moved eastward at speeds of 1 to 4 n.m. per day (2.5 to 10 cm/sec) with a wavelength of 300 to 500 km. The height of the meanders generally increased with distance from Cape Hatteras and ranged from 35 to 100 km between Cape Hatteras and 70°W, and from about 200 to 300 km between 60°W and 70°W.

REFERENCES

FUGLISTER, F.C. and VOORHIS, A.D. (1965), A New Method of Tracking the Gulf Stream. Limnology and Oceanography, 10 (Supplement: Readfield Anniversary Volume).

HANSEN, D.V. (1966), Personal Communication. Environmental Science Services Administration (ESSA).

PICKETT, R.L. and WILKERSON, J.C. (1966), Airborne IR tracking of Gulf Stream. Geo-Marine Technology 2(5): 8-11.

STOMMEL, HENRY, von ARX, W.S., PARSON, D. and RICHARDSON, W.S. (1953), Rapid aerial survey of Gulf Stream with camera and radiation thermometer. Science, 117 (3049): 639-640.

STRACK, S.L. (1953), Surface temperature gradients as indicators of the position of the Gulf Stream. Woods Hole Oceanogr. Inst. Tech. Rept., Ref. 53-53 (unpublished manuscript).

von ARX, W.S. and RICHARDSON, W.S. (1953), Aerial reconnaissance of the surface outcrop of the Gulf Stream front. Woods Hole Oceanogr. Inst. Tech. Rept., Ref. 53-24 (unpublished manuscript).

von ARX, W.S., BUMPUS, D.F. and RICHARDSON, W.S. (1955), On the fine-structure of the Gulf Stream front. Deep Sea Research, 3: 46-65.

WILKERSON, J.C. (1967), Gulf Stream from Space. Oceanus, 13(4).

Fig. 1 - The ASWEPS oceanographic aircraft

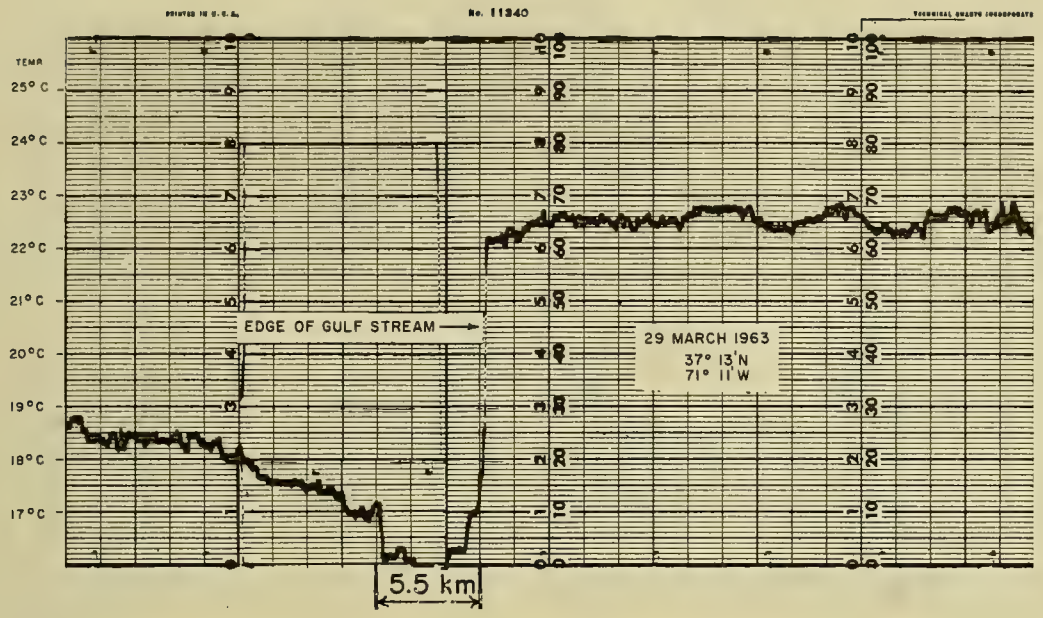

Fig. 2 - Sea surface temperature record - airborne radiation thermometer

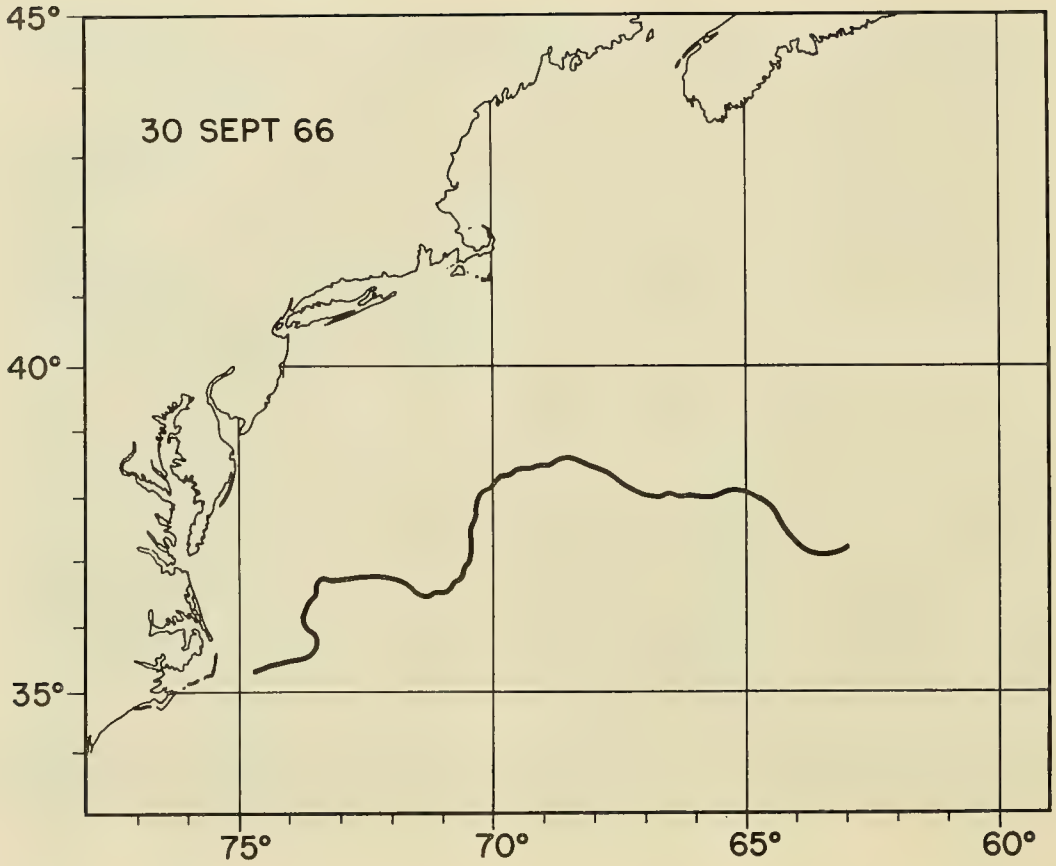

Fig. 3 - Gulf Stream northern boundary as indicated by airborne radiation thermometer during flight of 30 September 1966

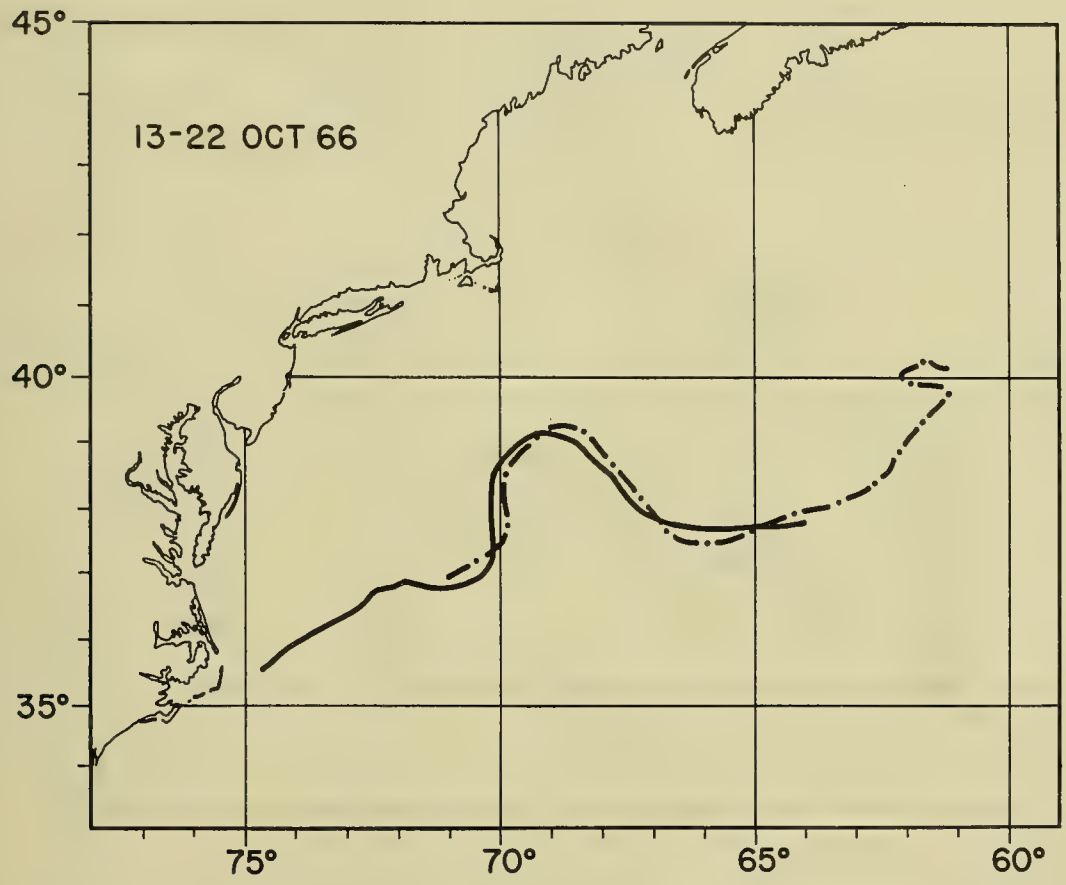

Fig. 4 - Gulf Stream northern boundary as indicated by the 15°C isotherm at 200 meter depth. Environmental Science Services Administration (ESSA) Cruise for October 1966

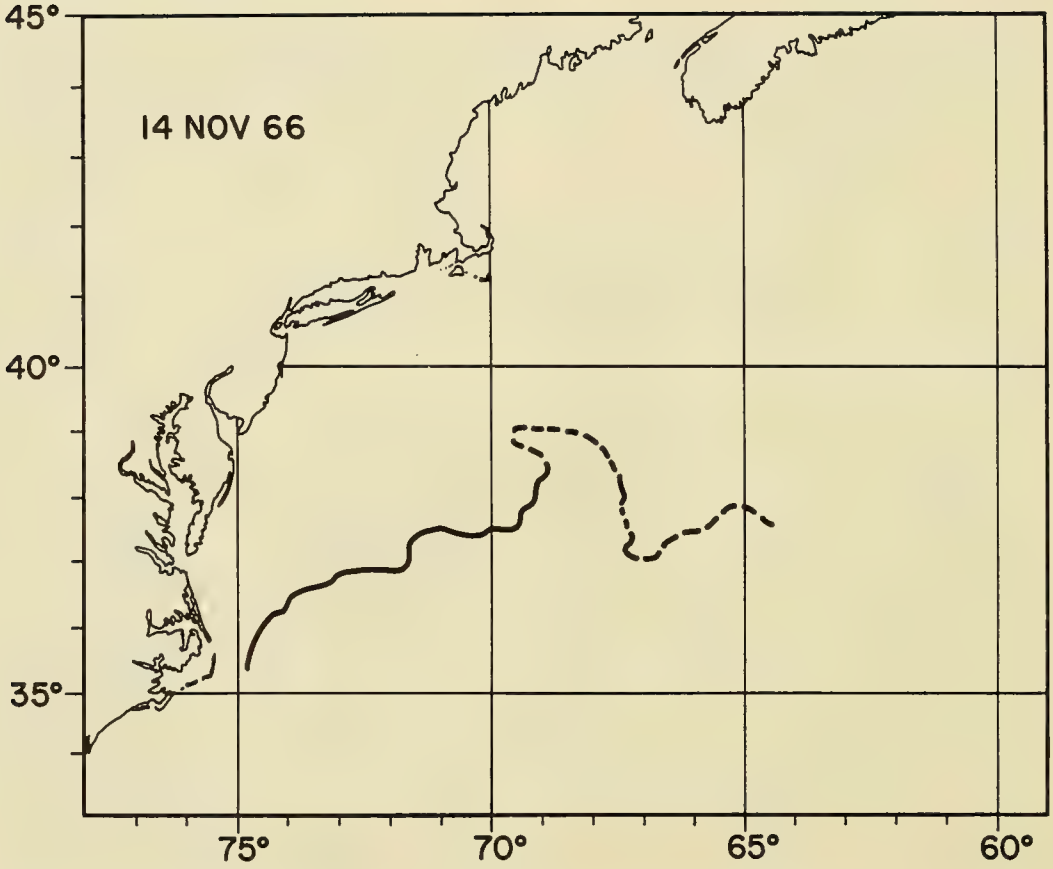

Fig. 5 - Gulf Stream northern boundary as indicated by airborne radiation thermometer during flight of 14 November 1966

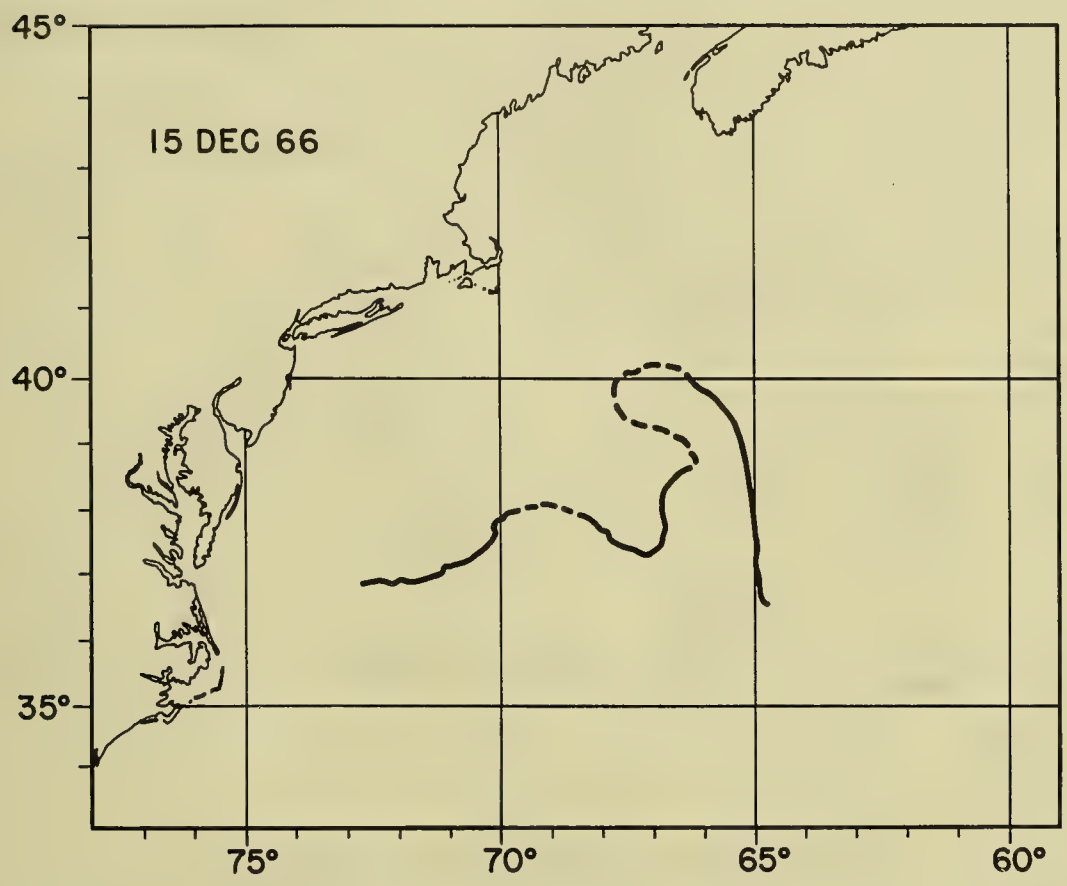

Fig. 6 - Gulf Stream northern boundary as indicated by airborne radiation thermometer during flight of 15 December 1966

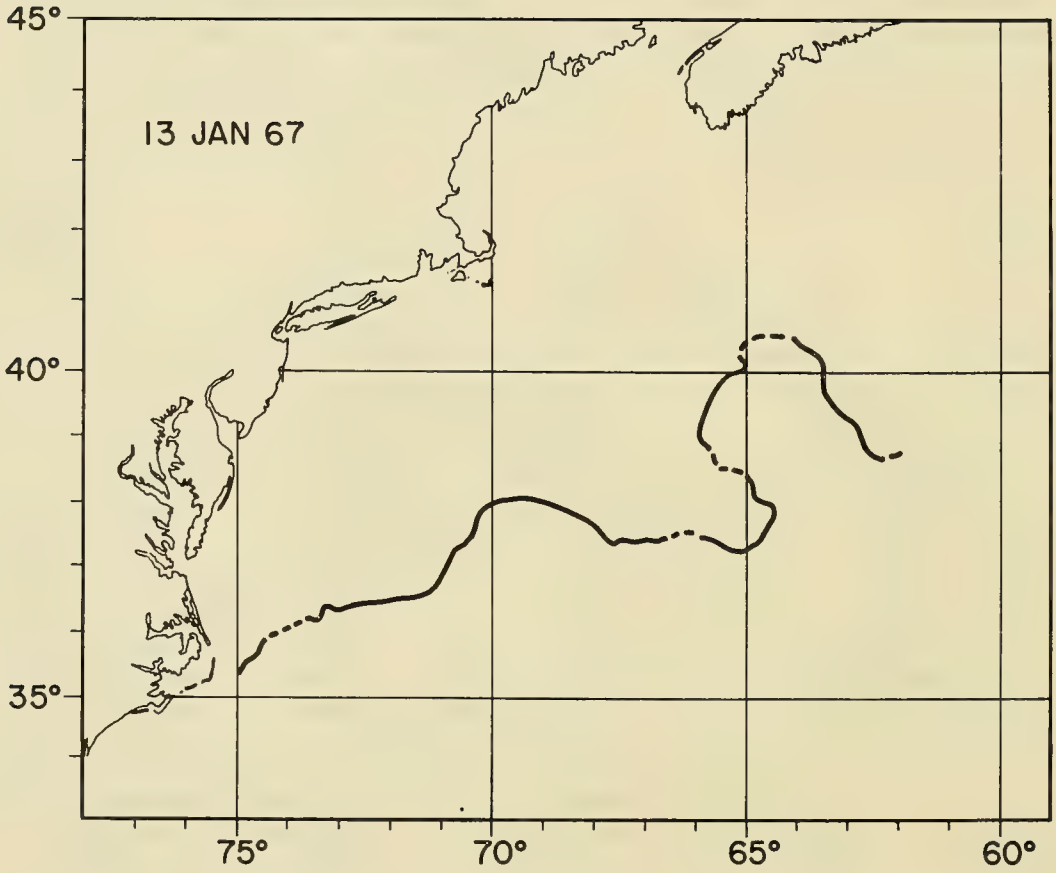

Fig. 7 - Gulf Stream northern boundary as indicated by airborne radiation thermometer during flight of 13 January 1967

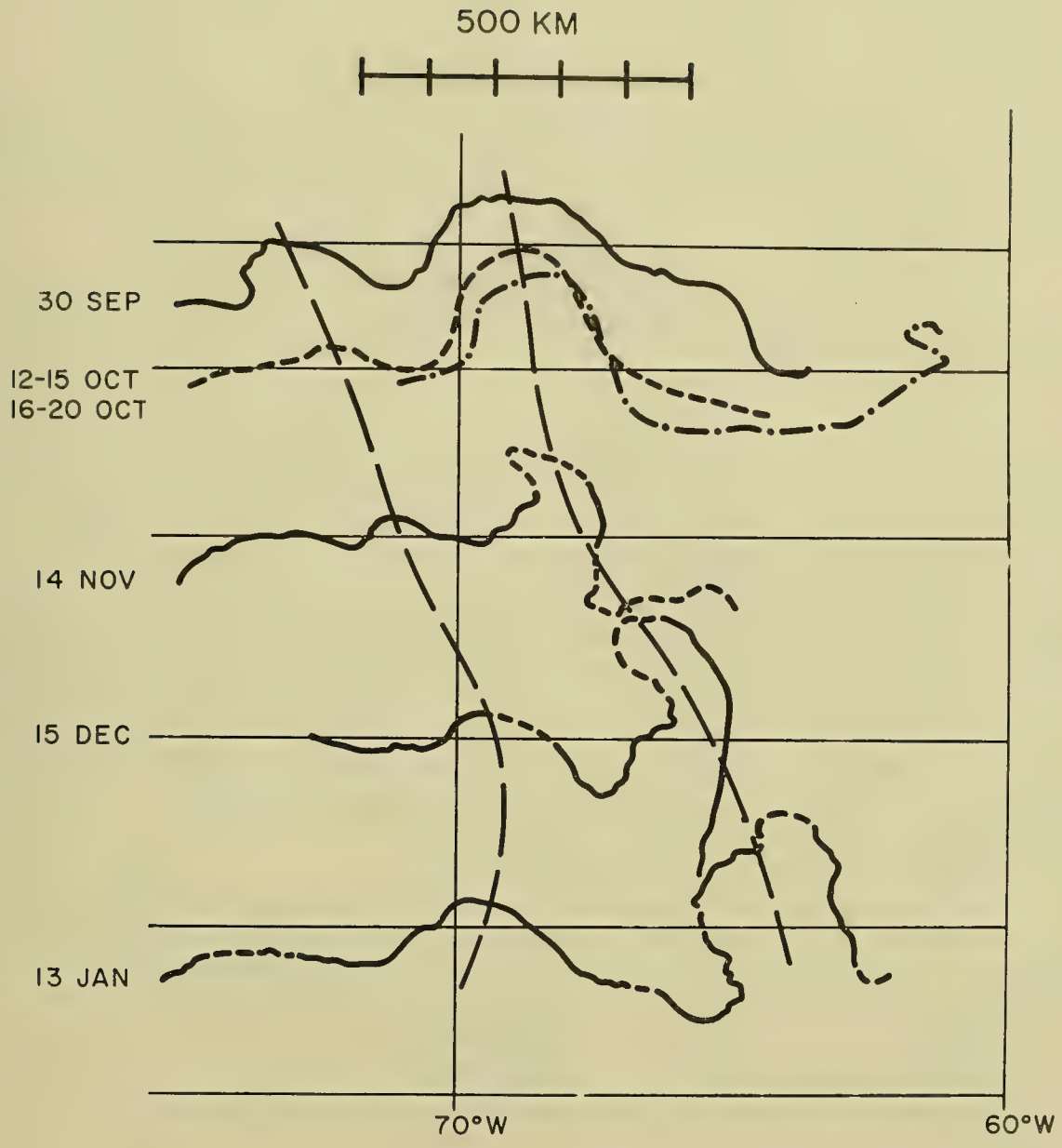

Fig. 8 - Phase progression of Gulf Stream meanders
September 1966 to January 1967

Comparison of Minimum Detectable Light Levels and the Level of Stimulated Marine Bioluminescence in Ocean Waters

Steve Neshyba
Oregon State University
Corvallis, Oregon

The development of the Laser light source has given new impetus to the study of ways by which man might extend his visual reconnaissance of the oceans. One factor in the design of a Light Detection and Ranging (Lidar) system for use in the marine environment is that bioluminescence can be a spurious signal; further, this luminescence may itself be altered in the presence of laser transmissions. The engineer designing underwater lidar should recognize that the optical receiver must obtain information while immersed in a biologically active source field. Such a factor is wholly absent in the design of atmospheric radar; its analogy could be that of a sky full of tiny, floating, organically live transmitters whose output level changes when the radar attempts to "look through" them.

The Stimulated Bioluminescent Field

Measurements have been made of the *in situ* bioluminescent field when the organisms are subjected to trains of vari-colored light pulses. A photomultiplier bathyphotometer and a Xenon flashtube, both controlled from a deck recorder unit, comprised the *in situ* device which was lowered to a depth of 700 meters. The flashtube was commanded to emit trains of 1 millisecond pulses, through selectable color filters, at repetition rates of from 6 to 25 ppm, and the luminescent response recorded on deck. Details of the apparatus, along with a discussion of the measured response to the several colors and rates of stimuli, are given by Neshyba (1967, in press). In general, the response is positive to trains whose repetition rate is at least 6 ppm, with maximum response to green, blue, and white light stimuli. Figure 1 shows the type of response usually measured. The response to stimuli above the threshold rate usually reaches a peak at 1.5 to 2.0 seconds following the stimulus but decays at a slower rate. Such response is readily distinguished from the normal

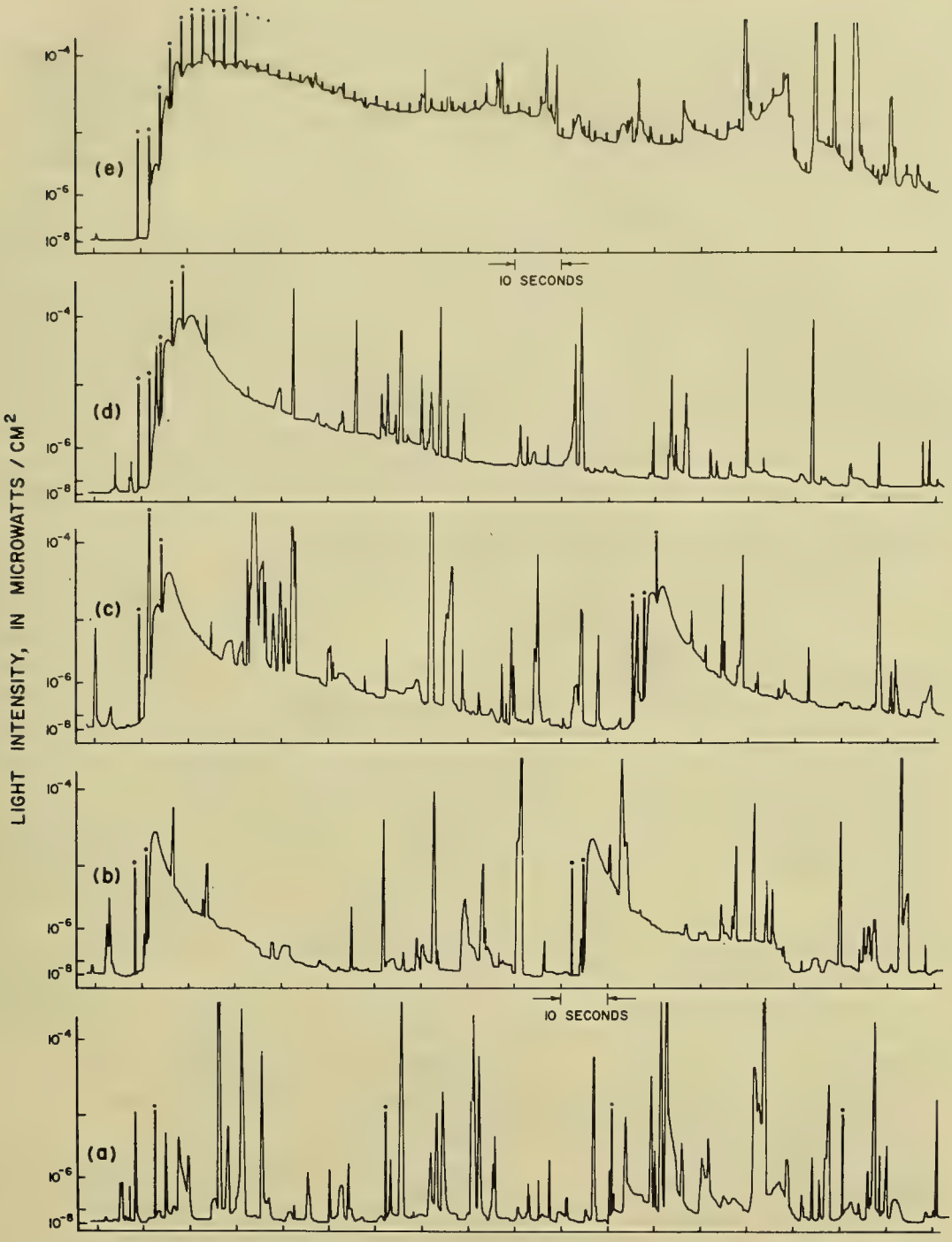

Fig. 1 - Traces of bioluminescence recorded in the presence of pulsed white light stimuli, 28 April 1965 at 2100 PDST, at an instrument depth of 700 meters. (a) is a recording for single-pulse stimuli spaced 50 sec. apart; (b) double-pulse stimuli spaced 2.5 sec. (c) three-pulse stimuli spaced 2.5 sec. (d) five-pulse stimuli spaced 2.5 sec., and (e) continuous train of pulses spaced 2.5 sec. apart. The recording of the stimulus itself is a spike, here shown with superposed dot.

luminescent flash. Of importance to this discussion is the fact that for rapid stimuli the response builds up, following the onset of the train, to a level as much as 10,000 times as intense as the normal background level (Fig. 1e). This enhanced background level may be sustained for several minutes, and decays slowly following cessation of stimuli.

The engineer in designing underwater lidar will treat differently the two phenomena of flashes and of increase in background level. For instance, the high intensity flashes may be discriminated by either pulse width gating or by other "false alarm" type circuitry. The background level is probably discriminated only through the use of narrow band filters, and represents a more severe limitation to receiver performance. In the following sections, the effect of these noise-like sources upon the available range of a typical underwater laser-powered optical device is examined.

Specifications of a Model Underwater Lidar

Consider a model lidar designed for use in ocean water, having the general specifications:

TRANSMITTER	
Type	Q switched laser
Transmission	Pulse
Pulse rate	At least 1000 pulses/second
Peak pulse power	1 megawatt
Pulse length	Dependent upon type: 2×10^{-9} seconds for Q-switched laser, others not specified
Wavelength	470 millimicrons
Power spectrum	Monochromatic
Antenna	6" telescope
Beamwidth	0.4 milliradians, circular
Resolution	20 cm. diameter @ 500 meters
Scan method	Strip map
Scanning angle	$\pm$ 40° vertical angle
Strip scan rate	40°/second
Velocity scan rate	8 cm per second ground speed
RECEIVER	
Type	Photomultiplier
Wavelength	Dependent upon photocathode material For S-11 phosphor, the wavelength of peak response is 440 millimicrons

Bandwidth	
Unfiltered	330-600 millimicrons (S-11)
Filtered	1 millimicron, centered at 470 millimicrons
Dark Current	0.002 microamperes
Antenna	5" telescope
Beamwidth	0.5 milliradians, circular
Effective Aperture	1.26×10^{-2} square meters

Such a system might be used to map the ocean floor, employing a scanning technique similar to that used in side-looking aircraft radar, or by side-looking sonar mounted in a submersible.

Noise Considerations

In an optical receiver employing a photomultiplier tube, statistical fluctuations in the mean rate of electron emission from the photocathode surface are a noise source. In the absence of extraneous radiation, the thermionic emission, commonly called dark current, limits receiver sensitivity. The noise power depends upon the work function of the cathode emissive surface and represents an inherent limit to system performance.

The background radiation field results from the natural and stimulated bioluminescence and from near field backscatter from the transmitter. The latter source is usually eliminated by gating the receiver to the actual target return.

For any radar system, there exists a minimum useful value of the signal-to-noise ratio, S/N, at the receiver. The probability of detection of a target is the probability of the signal-plus-noise exceeding some threshold. This is a statistical value based upon

(a) the mean rate of thermionic emission from the cathode;

(b) the mean rate of photon arrival, at the photomultiplier cathode, of both the signal and the radiation background.

The problem has been treated in the literature, a good example being that given by Flint (1964). For mapping radar, a usually selected minimum useful signal-to-noise ratio is one.

Minimum Detectable Signal

For a receiver employing a photomultiplier sensor, the inherent receiver noise is that noise generated by dark level emission from the photocathode. The dark current of the typical RCA 6199 is 2×10^{-9} amperes and the gain is 6×10^{5}. The mean rate of photocathode emission due to dark current is given by

$$\overline{N} = \frac{id}{g\epsilon} \quad sec^{-1} \tag{1}$$

where i_d = dark durrent in amperes,
g = gain, and
ϵ = electronic charge in coulombs.

Typical values yield $N = 2.08 \times 10^4$ electrons/sec.

For the S-11 phosphor, quantum efficiency at 470 millimicrons is 12%. Therefore, the mean rate of photon capture by the photocathode equivalent to the mean rate of photocathode emission above is given by

$$\frac{2.08 \times 10^4}{.12} = 1.73 \times 10^5 \ \frac{\text{photons}}{\text{second}} \tag{2}$$

The area of the 6199 photocathode is 7.75 cm^2. Therefore, the mean rate of photon capture per cm^2 is given by

$$\frac{1.73 \times 10^5}{7.75} = 2.23 \times 10^4 \ \frac{\text{photons}}{cm^2 \text{ second}} \tag{3}$$

By translating the photon density rate into a power density, one then arrives at the noise power density equivalent to the dark level noise in the receiver. This quantity, called anode dark current equivalent noise power density, ENPD, exists at the illuminated surface of the photocathode and is given by

$$ENPD = \frac{h\,c\,p}{t\lambda \times 10^{-7}} \quad watts/cm^2, \tag{4}$$

where t = one second,
h = Planck's constant = 6.624×10^{-27},
c = speed of light = 3×10^{14} microns/sec,
p = number of photons/cm^2/second, and
λ = wavelength, in microns.

Typical values thus yield

$$ENPD = 9.4 \times 10^{-15} \text{ watts}/cm^2$$
$$= 9.4 \times 10^{-9} \text{ microwatts}/cm^2$$

At a minimum usable signal-to-noise ratio of 1, the noise power density given in equation (4) also becomes the minimum detectable signal at the photocathode, in the absence of noise radiation background.

Propagation Factors and the Range Equation

The computation of maximum operating range for the lidar follows the methods used in microwave radar studies (Povejsil, et al., 1961). Perhaps the one unusual factor is that the narrow beamwidth of the lidar means that all targets are beam-filling targets; thus, the signal returned to the receiver obeys the inverse

square law rather than the inverse fourth power law.

The power density at range of a target in an absorbing and scattering medium, for the model lidar, is given by

$$P.D._{target} = \frac{P_t G_t e^{-\alpha R}}{4\pi R^2} \tag{5}$$

where P_t = transmitted power, 1 megawatt peak
G_t = transmitter gain factor, 10^8 for the 6" telescope
α = attenuation coefficient, 5×10^{-4} at 470μ, and
R = range to target in cms.

Let r be the diffuse reflectance of the target, here taken as 10%. The target area within the field of view is given by

$$A = \frac{\pi}{4} \phi^2 R^2 \ cm^2$$

where ϕ = the beamwidth in milliradians

The total power reflected by the target is then

$$P_{refl} = (P.D.)_{Target} \times Area_{Target} \times r . \tag{7}$$

Taking into account that this power is reflected into a solid angle of 2π steradians, and accounting for the total attenuation encountered during signal return, the power density at the receiver is then

$$P.D._{Rcvr} = \frac{P_t G_t e^{-2\alpha R}}{4 R^2} \cdot \frac{\pi\phi^2 R^2}{4} \cdot \frac{r}{2\pi} \tag{8}$$

Considering now the numerical values from the specifications, the power density at the receiver aperture is computed and plotted as curve (a) in Fig. 2 as a function of target range.

Minimum Detectable Signal at Receiver Aperture

Consider now that the energy intercepted by the receiving aperture above is focused so as to illuminate the total active photocathode surface of the 6199 receiver tube, i.e., 7.75 cm^2. From equation (4) the minimum detectable signal at the photocathode surface is 9.4×10^{-9} microwatts/cm^2. For the receiver with 5" telescopic aperture, the minimum detectable signal level at the aperture can now be found by

$$M.D.S._{Aperture} = M.D.S._{Cathode} \times \frac{\text{Area of Cathode}}{\text{Area of Aperture}} \tag{9}$$
$$= 5.78 \times 10^{-10} \text{ microwatts/cm}^2$$

For an allowable signal-to-noise ratio of one, the maximum useful mapping range for this value of minimum detectable signal is shown as point n on curve (a), Fig. 2. This is about 250 meters,

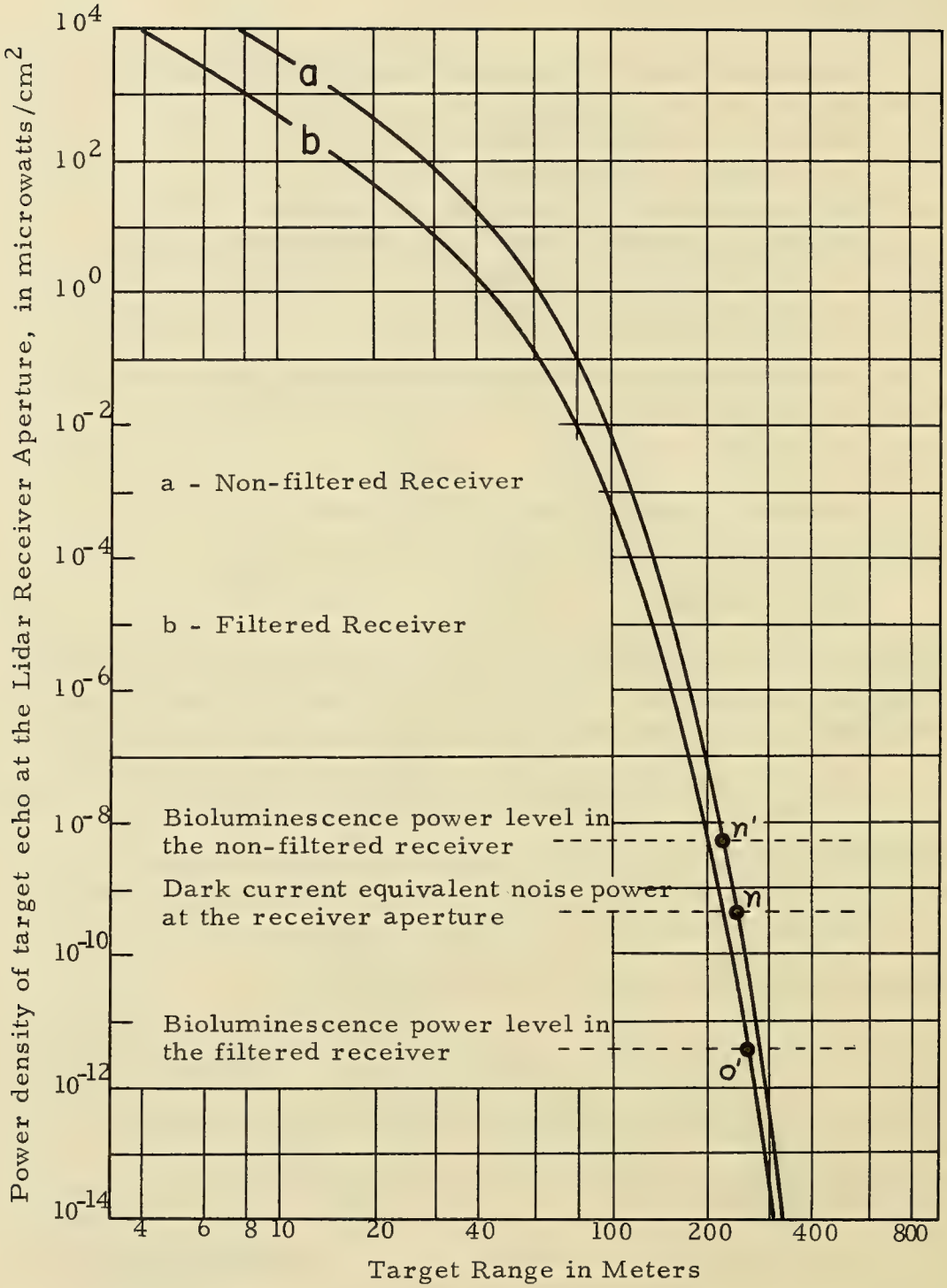

Fig. 2 - Range performance of a model Lidar Mapper in clear ocean water ($\alpha = 0.05 m^{-1}$)

and is the range obtainable in the absence of external noise.

Comparison of Laser Beam Scatter and Bioluminescent Stimulation Lamp Intensity

A question naturally posed is whether the Xenon stimulation light intensity used in the luminescence experiments is equivalent to the intensity of light scattered into a similar volume of water by a laser mapper. Clarke and Hubbard (1959) have concluded that flashes from organisms at ranges greater than about 8 meters are not recorded by a photomultiplier photometer of the type used. The following computations of the laser scatter are made for a point 10 meters off laser axis, as shown in Figure 3.

The intensity of light scattered in a direction Θ from the propagation axis of a light beam is given by

$$J(\Theta) = HV\,\sigma(\Theta) \tag{10}$$

Where $J(\Theta)$ is the intensity of scattered light in the direction Θ, in microwatts per steradian,

H is the laser beam flux per unit area on the volume V; for the model lidar, this is 5.9×10^{12} microwatts/cm^2 at a point 10 meters from source.

V is the volume of the laser beam path element from which scatter is computed; for the model lidar, this is taken as 1 cm^3.

$\sigma(\Theta)$ is the volume scattering coefficient; a typical value of $\sigma(90°)$ at 470 millimicrons for ocean water is 2×10^{-6} cm^{-1} steradian^{-1}.

Total scatter intensity in the direction p is found by integration over all such scatter volumes in the laser beam. A rough approximation to the integral, considering that

(a) $\sigma(\Theta)$ is constant and conservatively taken as $\sigma(90°)$,

(b) only scatter in the first 20 meters of laser path is significant, then

$$J_{total,\,p} = \int_{\Theta_1}^{\Theta_2} J(\Theta)\,d\Theta \doteq 2.4 \times 10^{10} \text{ microwatts/steradian.} \tag{11}$$

An analogous computation for the light intensity at p in the field of the Xenon flash lamp is also sketched in Figure 3. For a lamp output of 2×10^6 lumens peak and a reflector gain of 6, the intensity is

$$J_{p,\,xenon} = 1 \times 10^{10} \text{ microwatts/steradian} \tag{12}$$

One concludes that a laser pulse would provide an equivalent volumetric stimulation coverage to that used in the luminescence experiments. Since this volume coverage envelopes the instrument, so

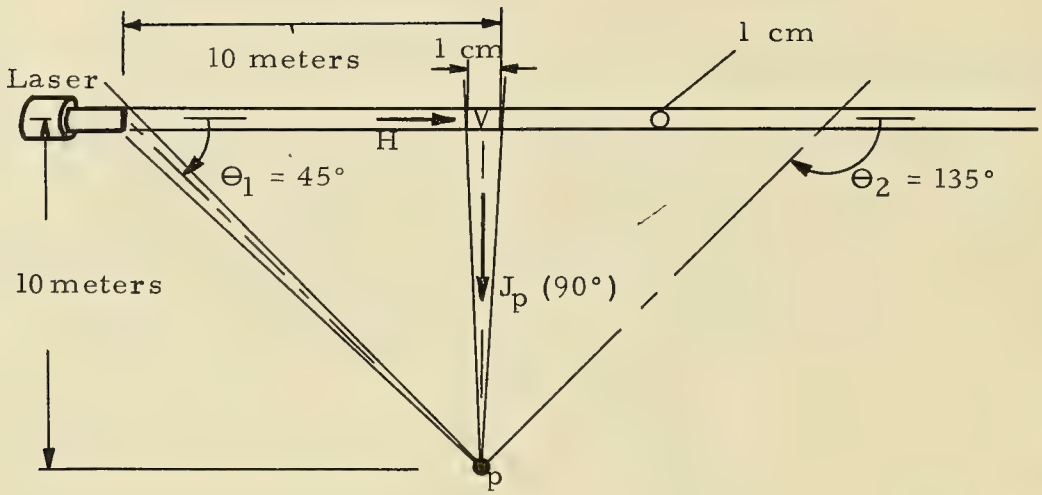

(a)

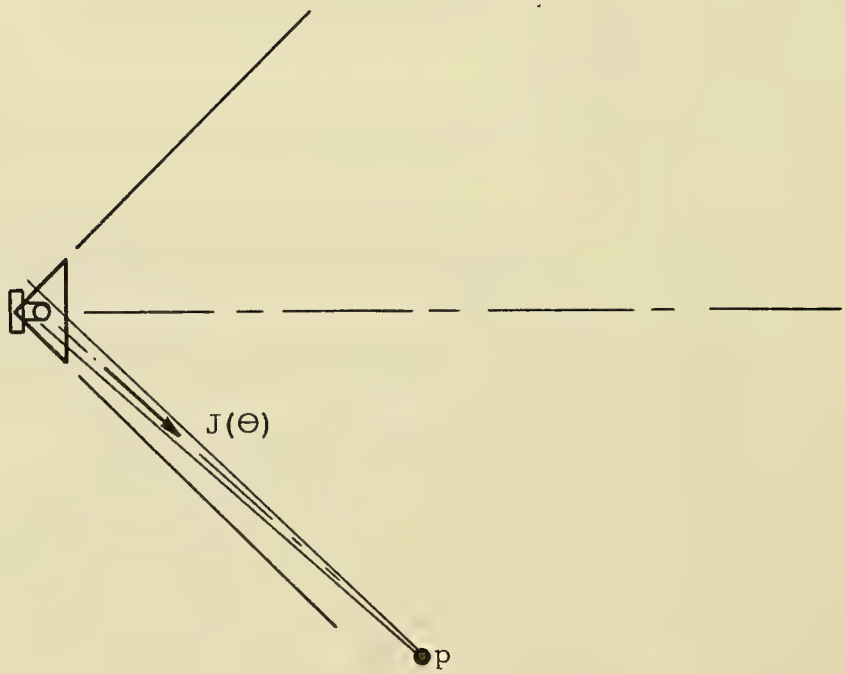

(b)

Fig. 3 - (a) Scattering out of the laser beam, and (b) light intensity in the xenon flash tube field

to speak, the case is strong that the optical receiver will record the bioluminescent response to such stimulation. If the velocity scan speed of the submersible exceeded 10 meters per 1.5 to 2.0 seconds, the receiver would then pass out of effective range of the luminescent organisms before they achieved their peak response. Such speeds would be feasible for a bottom mapping lidar only if the pulse repetition rates for the laser could be at least 80,000 pps. Lasers having this high a pulse repetition rate at one megawatt peak pulse power have not yet been built.

Effective Bioluminescent Radiation in the Mapping Receiver Aperture

It is assumed that the biological organisms responsible for the stimulated response are uniformly distributed. The lidar receiver at any one instant will see only a portion of the volume from which the background radiation emanates. Computations have been made which show that the volume coverage by the mapping receiver is only about 7×10^{-4} of the volume sampled during the bioluminescent experiments. Considering that the maximum bioluminescent median background power density obtained during blue-green stimulation (Neshyba, 1967, in press) is 1×10^{-5} microwatts/cm^2, then the power density effective as noise background at the receiver optical aperture is

$$(1 \times 10^{-5}) \times (7 \times 10^{-4}) = 7 \times 10^{-9} \text{ microwatts/cm}^2 \qquad (13)$$

Useful Mapping Range in the Presence of Stimulated Bioluminescence

In Figure 2, the effective bioluminescent noise power density is plotted as point n' on curve (a). It is concluded that the useful mapping range of the lidar system is now limited by the stimulated noise background, and not by the inherent noise internal to the lidar itself, to about 230 meters.

Use of a Narrow-Band Filter in the Receiver Optics

Since the bioluminescent spectrum is broad, it is worthwhile to examine whether range performance can be bettered by incorporating a narrow band-pass filter in the receiver optics. A filter having a 10 Angstrom (1 millimicron) pass band centered at 470mμ, and a transmittance of 10% is selected here; the corresponding range curve for the modified receiver is shown as curve (b) in Figure 2.

Bioluminescent spectra are not well known. Clarke (1962) states that the lantern fish emit 80% of their energy in the range 450-550 millimicrons. Assuming their energy uniformly distributed in this band, the spectral irradiance of bioluminescence is then given by

$$Q = \frac{0.8\, M_{\Delta\lambda}}{\Delta\lambda} \tag{14}$$

where $M_{\Delta\lambda}$ = median energy flux over the band, taken as 7×10^{-9} μw/cm^2 (equation 13),

$\Delta\lambda$ = 80 % bandwidth of the luminescent spectra, i.e. 100mμ.

These typical values yield a spectral irradiance of 5.6×10^{-11} microwatts/cm^2/millimicron. Accounting for the 10% transmittance of the filter reduces spectral irradiance to 5.6×10^{-12}. For the one millimicron filter pass band, this also becomes the bioluminescent energy flux background in the filtered receiver, and is plotted as point o' on curve (b) of Figure 2.

One concludes that for the filter-modified receiver, range performance is limited by receiver noise rather than by the luminescent background. However, due to the loss in the inserted filter, no additional gain in range has been achieved.

Summary

It is shown that the stimulated bioluminescent field can be the factor that limits the maximum useful mapping range of an underwater lidar. This limitation can be circumvented only at the expense of sophistication in the system design, namely, the incorporation of a low-loss, narrow pass-band optical filter. Finally, it should be stated that the field of stimulated bioluminescence will not be everywhere the same; extensive measurements of the field near the ocean bottom have not been reported.

References

Neshyba, S. 1967. In Situ Stimulation of Marine Bioluminescence by Pulsed Light, Limnology and Oceanography, in press.

Flint, G. W. 1964. Analysis and Optimization of Laser Ranging Techniques, IEE Trans. on Mil. Elect., Vol. MIL-8, Jan. 1964.

Povejsil, D. J., Roven, R. S., and Waterman, P. 1961. Airborne Radar. D. Van Nostrand Co., New York. 823 pp.

Clarke, G. L., and Hubbard, C. J. 1959. Quantitative Records of the Luminescent Flashing of Oceanic Animals at Great Depths. Limn. & Ocean., Vol. 4.

Clarke, G. L., and Denton, E. J. 1962. Light and Animal Life, The Sea, Vol. I, Interscience, New York, 1962.

GPO 929-050